frontiers | Research Topics

Plant molecular farming for biopharmaceutical production and beyond

Edited by
Kevin Wang and Yongfeng Guo

Published in
Frontiers in Plant Science

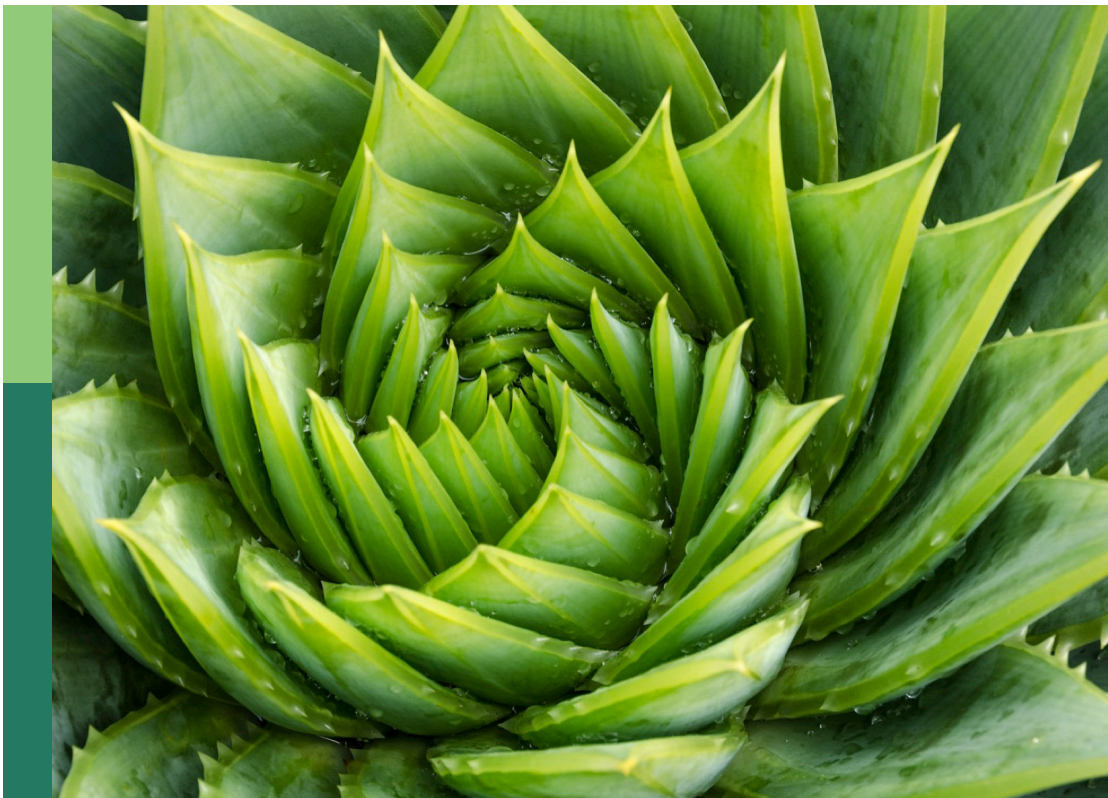

ISSN 1664-8714
ISBN 978-2-8325-7363-1
DOI 10.3389/978-2-8325-7363-1

Generative AI statement
Any alternative text (Alt text) provided alongside figures in the articles in this ebook has been generated by Frontiers with the support of artificial intelligence and reasonable efforts have been made to ensure accuracy, including review by the authors wherever possible. If you identify any issues, please contact us.

About Frontiers

Frontiers is more than just an open access publisher of scholarly articles: it is a pioneering approach to the world of academia, radically improving the way scholarly research is managed. The grand vision of Frontiers is a world where all people have an equal opportunity to seek, share and generate knowledge. Frontiers provides immediate and permanent online open access to all its publications, but this alone is not enough to realize our grand goals.

Frontiers journal series

The Frontiers journal series is a multi-tier and interdisciplinary set of open-access, online journals, promising a paradigm shift from the current review, selection and dissemination processes in academic publishing. All Frontiers journals are driven by researchers for researchers; therefore, they constitute a service to the scholarly community. At the same time, the *Frontiers journal series* operates on a revolutionary invention, the tiered publishing system, initially addressing specific communities of scholars, and gradually climbing up to broader public understanding, thus serving the interests of the lay society, too.

Dedication to quality

Each Frontiers article is a landmark of the highest quality, thanks to genuinely collaborative interactions between authors and review editors, who include some of the world's best academicians. Research must be certified by peers before entering a stream of knowledge that may eventually reach the public - and shape society; therefore, Frontiers only applies the most rigorous and unbiased reviews. Frontiers revolutionizes research publishing by freely delivering the most outstanding research, evaluated with no bias from both the academic and social point of view. By applying the most advanced information technologies, Frontiers is catapulting scholarly publishing into a new generation.

What are Frontiers Research Topics?

Frontiers Research Topics are very popular trademarks of the *Frontiers journals series*: they are collections of at least ten articles, all centered on a particular subject. With their unique mix of varied contributions from Original Research to Review Articles, Frontiers Research Topics unify the most influential researchers, the latest key findings and historical advances in a hot research area.

Find out more on how to host your own Frontiers Research Topic or contribute to one as an author by contacting the Frontiers editorial office: frontiersin.org/about/contact

Plant molecular farming for biopharmaceutical production and beyond

Topic editors

Kevin Wang — University of Pikeville, United States

Yongfeng Guo — Tobacco Research Institute, Chinese Academy of Agricultural Sciences, China

Citation

Wang, K., Guo, Y., eds. (2026). *Plant molecular farming for biopharmaceutical production and beyond*. Lausanne: Frontiers Media SA.

doi: 10.3389/978-2-8325-7363-1

Table of contents

frontiers | Frontiers in Plant Science

TYPE Editorial
PUBLISHED 05 January 2026
DOI 10.3389/fpls.2025.1765245

OPEN ACCESS

EDITED AND REVIEWED BY
James Lloyd,
Stellenbosch University, South Africa

*CORRESPONDENCE
Kevin Yueju Wang
kevinwang@upike.edu
Yongfeng Guo
guoyongfeng@caas.cn

RECEIVED 10 December 2025
ACCEPTED 11 December 2025
PUBLISHED 05 January 2026

CITATION
Wang KY and Guo Y (2026) Editorial: Plant molecular farming for biopharmaceutical production and beyond.
Front. Plant Sci. 16:1765245.
doi: 10.3389/fpls.2025.1765245

Editorial: Plant molecular farming for biopharmaceutical production and beyond

Kevin Yueju Wang[1]* and Yongfeng Guo[2]*

[1]Division of Math and Natural Sciences, University of Pikeville, Pikeville, KY, United States, [2]Tobacco Research Institute, Chinese Academy of Agricultural Sciences, Qingdao, China

KEYWORDS

biopharmaceuticals, CRISPR/Cas9, plant molecular farming, plant-biotechnology, PMF

Editorial on the Research Topic
Plant molecular farming for biopharmaceutical production and beyond

Plant Molecular Farming (PMF) continues to advance as a multidisciplinary field at the intersection of biotechnology, agriculture, and therapeutic development, yet challenges such as limited expression efficiency, protein instability, and scalability continue to shape its translational landscape. Recent studies have shown promising advancements in plant genetic engineering and novel expression systems, which have significantly improved the yield, purity, and functionality of plant-derived pharmaceuticals (Eidenberger et al., 2023; Akher et al., 2025). However, there remains a need for comprehensive research to address regulatory, economic, and ethical considerations, as well as to explore the successful commercialization and global impact of these plant-made pharmaceuticals. The articles in this Research Topic illustrate how platforms including *Nicotiana benthamiana*, *Arabidopsis thaliana*, moss, and chloroplast-based systems are evolving into flexible and scalable biomanufacturing hosts for therapeutics, metabolic products, and nanomaterials.

Several studies across this Research Topic highlight the continual refinement of *N. benthamiana* as a host for improved recombinant protein production. Suppressing the defense-associated genes Nb-SABP2 and Nb-COI1 markedly increased transient expression efficiency by reducing immune responses that normally limit heterologous protein accumulation, offering a practical strategy for enhancing yield without affecting plant growth (Kopertekh). Yang et al. also characterized the papain-like cysteine protease (PLCP) gene family and identified specific proteases that degrade recombinant proteins, revealing targets whose suppression can further improve protein stability in planta. Additional refinement comes from Kaur et al. (2025) employed multiplex CRISPR/Cas9 editing to disrupt all seven core glycosyltransferase genes responsible for plant-specific N-glycan motifs, generating stable, Cas9-free *N. benthamiana* lines completely lacking α-1,3-fucosyltransferase and β-1,2-xylosyltransferase activities. These glycoengineered plants grew normally and formed a robust platform for producing biotherapeutics with human-compatible glycosylation profiles.

Glyco-optimization remains central to enabling therapeutic-grade protein production in plants. Göritzer et al. demonstrated that modifying amino acids adjacent to the conserved Asn297 site, particularly through the Y300L variant, markedly increases N-glycan occupancy in plant-produced IgG1 and enhances Fc receptor binding and thermal stability, thereby reducing functional differences between plant- and mammalian-derived antibodies. Moss systems offer

an additional avenue for controlled glycan engineering. Jonner et al. showed that introducing *Spodoptera frugiperda* mannosidase III and hexosaminidase into *Physcomitrium patens*, together with promoter tuning and targeted subcellular localization, enables production of recombinant human lysosomal acid α-glucosidase (Repleva GAA, RPV-002) enriched with paucimannosidic (MM) glycans. The engineered moss lines retained normal growth and achieved up to 43.5% of MM glycans, offering a practical strategy for improving mannose receptor–mediated uptake of therapeutic proteins.

Several articles in this Topic highlight the production of functional therapeutic molecules in plant systems. Yu et al. demonstrated that expression of an epidermal growth factor (EGF)–transdermal peptide fusion in *A. thaliana* yields a recombinant protein capable of penetrating the skin, and topical application markedly improves skin barrier repair in mice, illustrating the potential of plants for dermatological biologics. Melendez et al. reported that *N. benthamiana* can rapidly produce a monoclonal antibody targeting the extracellular enveloped virion (EV) form of Monkeypox virus; the plant-derived antibody bound the MPXV A35 antigen and neutralized EV particles, demonstrating that plant-based systems can generate antibodies with functional antiviral activity against this clinically important virion form. Wang et al. also compared the expression of full-length and mature nattokinase, revealing that the full-length precursor induces rapid leaf necrosis, whereas the mature enzyme accumulates efficiently and retains strong fibrinolytic activities, supporting its feasibility as a plant-produced therapeutic enzyme.

Viral nanoparticle technologies represent another major thematic area in this Research Topic. Ljumović et al. developed an innovative foliar spray infection method for producing Tomato Bushy Stunt Virus (TBSV)-derived viral nanoparticles in *N. benthamiana*, offering a simple and scalable alternative to syringe or vacuum infiltration and demonstrating compatibility with vertical farming systems. This advance is paired with a detailed description of a GMP-compliant manufacturing facility for producing clinical-grade plant-made nanomaterials, which outlines upstream cultivation, downstream purification, and regulatory considerations and provides a practical blueprint for industrial-scale nanoparticle production Pivotto et al. Vater et al. also demonstrated that *N. benthamiana* can produce functional human Galectin-1 (hGAL1) with correct folding, glycan binding, and immunomodulatory activities, reinforcing the suitability of plant systems for generating active immunotherapeutic proteins.

The Research Topic features significant contributions in metabolic engineering and agricultural biotechnology. Gerasymenko et al. demonstrated that co-expression of specialized isoprenyl diphosphate synthases (IDSs) and substrate-producing enzymes in *N. benthamiana* enables efficient biosynthesis of irregular monoterpene malonyl glucosides that are otherwise difficult to obtain, illustrating the versatility of plant systems for generating structurally diverse metabolites with pharmaceutical potential. Qi et al. reviewed advances in RNA interference as a precise and environmentally sustainable strategy for crop protection, highlighting developments in delivery platforms, regulatory considerations, and pathways for integration into large-scale agricultural practice. Schubert et al. utilized multilayered zein-based protein bodies in *N. benthamiana* to encapsulate both wild-type and hypoallergenic parvalbumin, enhancing resistance to gastrointestinal digestion and enabling controlled release. These engineered protein bodies were efficiently internalized by intestinal epithelial cells, establishing a promising plant-derived bioencapsulation platform for oral administration.

Together, these studies reflect a field moving rapidly toward technical maturity, translational relevance, and manufacturing readiness. We thank all contributing authors and reviewers for advancing the scientific and practical foundations of this evolving field, and we hope this Research Topic will inspire continued innovation across molecular farming applications.

Author contributions

KW: Funding acquisition, Writing – review & editing, Validation, Writing – original draft. YG: Writing – review & editing, Writing – original draft, Funding acquisition, Validation.

Funding

The author(s) declared that financial support was received for this work and/or its publication. This work was supported by China National Tobacco Corporation (110202102026) and the Agricultural Science and Technology Innovation Program (ASTIP-TRIC02). Additional support was provided in part by the National Institute of General Medical Sciences of the National Institutes of Health under award number P20GM103436-24.

Conflict of interest

The author(s) declared that this work was conducted in the absence of any commercial or financial relationships that could be construed as a potential conflict of interest.

The author(s) declared that YG were an Associate Editor of Plant Abiotic Stress, at the time of submission. This had no impact on the peer review process and the final decision.

The author(s) declared that this work received funding from China National Tobacco Corporation. The funder was not involved in the study design, collection, analysis, interpretation of data, the writing of this article or the decision to submit it for publication.

Generative AI statement

The author(s) declared that generative AI was not used in the creation of this manuscript.

Any alternative text (alt text) provided alongside figures in this article has been generated by Frontiers with the support of artificial intelligence and reasonable efforts have been made to ensure accuracy, including review by the authors wherever possible. If you identify any issues, please contact us.

Publisher's note

References

Akher, S. A., Wang, K. Y., Hall, K., Hunpatin, O. S., Shan, M., Zhang, Z., et al. (2025). Harnessing transient expression systems with plant viral vectors for the production of biopharmaceuticals in nicotiana benthamiana. *Int. J. Mol. Sci.* 26, 5510. doi: 10.3390/ijms26125510

Eidenberger, L., Kogelmann, B., and Steinkellner, H. (2023). Plant-based biopharmaceutical engineering. *Nat. Rev. Bioeng.* 1, 426–439. doi: 10.1038/s44222-023-00044-6

Kaur, C., Song, H., Lee, M., Kim, S.-Y., Seo, D.-H., Kang, H., et al. (2025). Multiplex CRISPR/cas9-mediated editing of seven glycosyltransferase homologs in nicotiana benthamiana to produce stable, cas9-free, glycoengineered plants. *Front. Plant Sci.* doi: 10.3389/fpls.2025.1701668

frontiers | Frontiers in Plant Science

TYPE Original Research
PUBLISHED 09 September 2024
DOI 10.3389/fpls.2024.1453930

OPEN ACCESS

EDITED BY
Kevin Yueju Wang,
University of Pikeville, United States

REVIEWED BY
Jinping Zhao,
Texas A and M University, United States
Beatriz Xoconostle-Cázares,
National Polytechnic Institute of Mexico (CINVESTAV), Mexico

*CORRESPONDENCE
Lilya Kopertekh
lilya.kopertekh@julius-kuehn.de

RECEIVED 24 June 2024
ACCEPTED 12 August 2024
PUBLISHED 09 September 2024

CITATION
Kopertekh L (2024) Improving transient expression in *N. benthamiana* by suppression of the *Nb-SABP2* and *Nb-COI1* plant defence response related genes.
Front. Plant Sci. 15:1453930.
doi: 10.3389/fpls.2024.1453930

Improving transient expression in *N. benthamiana* by suppression of the *Nb-SABP2* and *Nb-COI1* plant defence response related genes

Lilya Kopertekh*

Institute for Biosafety in Plant Biotechnology, Julius Kühn-Institut (JKI) - Federal Research Centre for Cultivated Plants, Quedlinburg, Germany

Currently transient expression is one of the preferred plant-based technologies for recombinant protein manufacturing, particularly in respect to pharmaceutically relevant products. Modern hybrid transient expression systems combine the features of *Agrobacterium tumefaciens* and viral vectors. However, host plant reaction to Agrobacterium-mediated delivery of gene of interest can negatively affect foreign protein accumulation. In this study, we investigated whether the modulation of plant immune response through knockdown of the *Nb-SABP2* and *Nb-COI1 N. benthamiana* genes could improve recombinant protein yield. In plants, the SABP2 and COI1 proteins are involved in the salicylic acid and jasmonic acid metabolism, respectively. We exemplified the utility of this approach with the green fluorescence (GFP) and β nerve growth factor (βNGF) proteins: compared to the tobacco mosaic virus (TMV)-based vector the *Nb-SABP2* and *Nb-COI1*-suppressed plants provided an increased recombinant protein accumulation. We also show that this strategy is extendable to the expression systems utilizing potato virus X (PVX) as the vector backbone: the enhanced amounts of βNGF were detected in the *Nb-SABP2* and *Nb-COI1*-depleted leaves co-infiltrated with the PVX-*βNGF*. These findings suggest that modulating host plant reaction to agrodelivery of expression vectors could be useful for improving transient foreign protein production in *N. benthamiana*.

KEYWORDS

***Nicotiana benthamiana*, *Nb-COI1*, *Nb-SABP2*, plant defense response, recombinant proteins, transient expression**

Introduction

Transient expression in *N. benthamiana* is an advanced technology, which has turned plants into commercial platform for recombinant protein production (Lomonossoff and D'Aoust, 2016; Schillberg et al., 2019; Schillberg and Finnern, 2021). This method uses the ability of *Agrobacterium tumefaciens* to transfer T-DNA carrying the expression vector with the gene of interest into plant cells (Kapila et al., 1997; Fischer et al., 1999). The major advances in this technique have centered on the development of hybrid expression systems combining features of *A. tumefaciens* and viral vectors (Gleba et al., 2005; Peyret and Lomonossoff, 2015). With a few exceptions the modern viral expression vectors rely on sequences of RNA (tobacco mosaic virus (TMV), potato virus X (PVX), cowpea mosaic virus (CPMV)) and DNA (bean yellow dwarf virus (BeYDV)) viruses (Gleba et al., 2007; Peyret and Lomonossoff, 2015). Among different species that have been tested for transient expression *Nicotiana benthamiana* is the preferred host due to a short life cycle, fast growth rate, suitable for massive infiltration leaf anatomy and a partly defective RNA silencing system (Goodin et al., 2008; Bally et al., 2018). Current research in the field of *N. benthamiana*-based transient expression is focused on the improvement of vector delivery systems and fine-tuning of plant expression host. A number of strategies have been developed to design plant cell conditions supporting foreign protein production. The first one is based on co-expression of cell cycle regulatory genes. In particular, several research groups reported about positive impact of virus- and plant-derived cell-cycle regulators on recombinant protein accumulation in *N. benthamiana* (Norkunas et al., 2018; Kopertekh and Reichardt, 2021, 2022). Another experimental approach of plant cell engineering has been described in publication of Wang et al. (2023). The authors showed that the application of a semi-dominant negative gain-of-function mutant form of plasmodesmata located protein 5 (PDLP) from *Arabidopsis thaliana* facilitated TMV-based vector movement and enhanced foreign protein production. One of the recent reports demonstrated that the depletion of the NbCORE receptor perceiving the cold shock protein of *A. tumefaciens* improves agroinfiltration productivity in *N. benthamiana* (Dodds et al., 2023). Finally, the attenuation of plant defense response against microbial components of transient vector delivery system has been also addressed to design a supportive cell environment for increased foreign protein accumulation. There are several examples in the literature showing that downregulation of endogenous plant genes involved in post-transcriptional gene silencing (PTGS) process can elevate recombinant protein accumulation in *N. benthamiana* host. Particularly, this approach has been shown to be feasible for the *DCL2*, *DCL4* (Matsuo and Matsumura, 2017; Matsuo, 2022), *RDR6* (Matsuo and Atsumi, 2019) and *Arg2* (Ludman et al., 2017) genes encoding Dicer-like 2, Dicer-like 4, RNA-dependent RNA polymerase 6 and Argonaut 2 proteins, respectively.

One of the essential components of the plant pathogen response is the regulatory network of phytohormones. Salicylic acid (SA), jasmonic acid (JA) and ethylene (ET) are major plant hormones that orchestrate defense reaction (Li et al., 2019; Ngou et al., 2022). The phytohormones involved in plant response to biotic stress have been shown to play an essential role in both Agrobacterium- and virus-plant interactions. In respect to plant-Agrobacterium pathosystem it was demonstrated that the defective in SA accumulation *Arabidopsis thaliana* and *N. bethamiana* plants were more susceptible to infection, whereas mutants overproducing SA were relatively resistant (Yuan et al., 2007; Anand et al., 2008). It was suggested that SA shuts down the expression of the Vir regulon by the attenuation of the VirA protein kinase activity (Yuan et al., 2007). The role of JA and SA in plant-virus interaction has also been reported. For example, the exogenous application of SA and JA improved plant resistance to RNA viruses (Lee et al., 2011; Shang et al., 2011). Inversely, suppression of the SA and JA biosynthetic and signaling genes accelerated development of symptoms and accumulation of virus titters (Liu et al., 2004; Pacheco et al., 2012; García-Marcos et al., 2013; Zhu et al., 2014). Considering the negative impact of plant defense response on microbial component of transient vector delivery system, we supposed that the attenuation of defense reaction might have positive effect on agroinfiltration efficiency and subsequent recombinant protein accumulation. To proof our hypothesis we modulated pathogen defense in *N. benthamiana* by silencing two endogenous genes, *Nb-SABP2* and *Nb-COI1*, which are involved in SA and JA metabolism, respectively. The *Nb-SABP2* gene encodes a SA-binding protein 2 termed SABP2, which is essential for establishing systemic acquired resistance (SAR) (Kumar and Klessig, 2003; Forouhar et al., 2005). The SABP2 is involved in the conversion of biologically inactive methyl salicylate (MeSA) into active SA leading to activation of the SA-dependent defense response (Park et al., 2007). The coronatine insensitive 1 (*COI1*) gene encodes an F-box COI1 protein that determines the substrate specificity of the E3 ubiquitin ligase SCF^{COI1} complex. This complex targets repressors of the JA-induced genes for degradation inducing their expression (Xie et al., 1998; Xu et al., 2002; Chini et al., 2009).

We report here that transient downregulation of the *Nb-SABP2* and *Nb-COI1* genes facilitated accumulation of viral vector and target protein transcripts, and resulted in enhanced recombinant protein production in *N. benthamiana*. These findings indicate that the attenuation of plant host response against biotic stress could have value in improving transient expression technology.

Materials and methods

Plasmid constructs

The pLH-*35S-COI1-INT-COI1* and pLH-*35S-SABP2-INT-SABP2* constructs were designed in several steps. The 186 bp region of the *Nb-COI1* gene was amplified from *N. benthamiana* cDNA using two primer combinations, NcoI-COI1-forw/COI1-BamHI-rev and SpeI-COI1forw/COI1-XhoI-rev. The 230 bp fragment of the *Nb-SABP2* gene was amplified from the same cDNA sample as for the *Nb-COI1* gene by two primer pairs: the NcoI-SABP2-forw/SABP2-HindIII-rev and the XbaI-SABP2-forw/SABP2-SalI-rev. The second intron (IV2) of the potato *ST-LS1* gene

was amplified from the p35S-creINT plasmid (Mlynárová and Nap, 2003) by PCR using the BglII-ST-LS1-INT-forw/ST-LS1-INT-SalI-rev and HindIII-ST-LS1-INT-forw/STLS1-INT-SalI-rev primer combinations. The amplified fragments were cloned in pGEM-T Easy (Promega, Walldorf, Germany) vector and sequenced. The primers can be found in Supplementary Table S1. Next, the sense and antisense gene fragments together with the separating hairpin loop sequence were introduced between the 35S promoter and terminator in the pCK-*GFP* plasmid (Reichel et al., 1996). The pCK-*35S-COI1-INT-COI1* construct was generated by the ligation of the *Nco*I-*Xba*I digested pCK-*GFP* with three restriction fragments, NcoI-COI1-BamHI, BglII-ST-LS1-INT-SalI and SpeI-COI1-XhoI, derived from the pGEM-*NcoI-COI1-BamHI*, pGEM-*BglII-ST-LS1-INT-SalI* and pGEM-*SpeI-COI1-XhoI* plasmids, respectively. The restriction enzymes used for cloning are defined at 5' and 3' ends of the restriction fragments. Finally, the Nb-COI1 RNAi cassette from the pCK-*35S-COI1-INT-COI1* plasmid was cloned into *Pst*I restriction site of the pLH7000 binary vector (Töpfer et al., 1993) resulting in the pLH-*35S-COI1-INT-COI1* (*Nb-COI1hpc*).

Ligation of the *Nco*I/*Xba*I digested pCK-*GFP* plasmid with three restriction fragments, NcoI-SABP2-HindIII, HindIlI-ST-LS1-INT-SalI and XbaI-SABP2-SalI, yielded the pCK-*35S-SABP2-INT-SABP2* plasmid. For the *Nb-SABP2* gene, the NcoI-SABP2-HindIII, HindIlI-ST-LS1-INT-SalI and XbaI-SABP2-SalI restriction fragments were obtained from the pGEM-*NcoI-SABP2-HindIII*, pGEM-*HindIlI-ST-LS1-INT-SalI* and pGEM-*XbaI-SABP2-SalI* plasmids. Next, the silencing expression cassette from the pCK-*35S-SABP2-INT-SABP2* intermediate construct was released by *Pst*I and ligated to *Nsi*I digested pLH7000 resulting in the pLH-*35S-SABP2-INT-SABP2* (*Nb-SABP2-hpc*) final plasmid.

To design the pLH-*TMV-GFP* expression construct the *Hind*III-*Kpn*I digested pLH-Δbar-*Pac*I (Kopertekh et al., 2004) plasmid was ligated with three restriction fragments, namely, *Kpn*I-*Nco*I fragment of pICH17344, *Nco*I-*Spe*I fragment of pICH17344, and *Spe*I-*Hind*III fragment of pICH17344. The pLH-*TMV-GFP* was subsequently used to prepare the pLH-*TMV-βNGF*. At first, the *βNGF* gene containing *Xho*I and *Swa*I restriction sites at 5' and 3' ends, respectively, was synthesized by BioCat (Heidelberg, Germany). Then, *Xho*I-*β-NGF-SwaI* sequence digested with *Xho*I and *Swa*I enzymes was introduced into identical cloning sites of the pLH-*TMV-GFP* construct.

The pLH-*PVX-βNGF* expression vector was constructed as follows. At first, the *βNGF* gene containing *Nhe*I restriction site at the 5' of the start codon and *Sal*I restriction site at the 3' end of the stop codon was synthesized by BioCat (Heidelberg, Germany). Following *Nhe*I-*Sal*I restriction the *βNGF* sequence was ligated into equally digested p*PVX201* (Chapman et al., 1992) producing the p*PVX-βNGF*. To transfer the *PVX-βNGF* sequence into the pLH-*Δbar-PacI* plasmid the p*PVX-βNGF* was linearized with *Sph*I and, following removal of the single stranded termini with T4 polymerase digested with *Ehe*I. The *Sph*I-*Ehe*I DNA fragment containing the *PVX-βNGF* sequence was ligated to pLH-*Δbar-PacI* plasmid restricted with *Stu*I. The final plasmid was designated as pLH-*PVX-βNGF*.

The pLH7000, pLH-35S-*COI1-INT-COI1*, pLH-*35S-SABP2-INT-SABP2*, pLH-*TMV-GFP*, pLH-*TMV-βNGF* and pLH-*PVX-βNGF* expression vectors were introduced into *A. tumefaciens* (recently renamed to *Rhizobium radiobacter*) strain C58C1 by the freeze-thaw method (Holsters et al., 1978).

Agroinfiltration of *N. benthamiana*

A. tumefaciens cultures (strain C58C1) containing the expression vectors were grown overnight in LB medium supplemented with appropriate antibiotics (100 mg/L spectinomycin, 300 mg/L streptomycin, 50 mg/L rifampicin, 100 mg/L carbenicillin), pelleted by centrifugation and resuspended in agroinfiltration buffer (10 mM MES, 10 mM $MgCl_2$, 150 μM acetosyringone, pH 5.6). The final optical density of *A. tumefaciens* cultures carrying the pLH-*TMV-GFP*, pLH-*TMV-βNGF* and pLH-*PVX-βNGF* vectors was adjusted to OD600 of 0.1, whereas the *A. tumefaciens* cultures carrying the pLH7000, pLH-*35S-COI1-INT-COI1* and pLH-*35S-SABP2-INT-SABP2* plasmids were brought to a final OD600 of 0.3. Agrobacterium suspensions were infiltrated into expanded leaves of 5-6 week-old *N. benthamiana* plants using a syringe without a needle. *N. benthamiana* plants were grown in the greenhouse at 24/22 ^{0}C day/night temperature with a 16 h light and 8 h dark photoperiod.

Gene expression analysis

Expression of the *Nb-SABP2*, *Nb-COI1*, TMV, *GFP* and *βNGF* was estimated by qPCR analysis. To this end, RNA from the agroinfiltrated and non-agroinfiltrated *N. benthamiana* plants was isolated using the BioSELL RNA Mini Kit (Bio&SELL, Feucht, Germany). One μg of RNA was used to synthesize cDNA by the random hexamer primer and Maxima Reverse Transcriptase according to the manufacturer's protocol (Thermo Scientific, Waltham, USA). The qPCR has been carried out with the Nb-SABP2-forw/Nb-SABP2-rev, Nb-COI-forw/NbCOI-rev, gfp-forw/gfp-rev, βNGF-forw/βNGF-rev and TMV-CP-forw/TMV-CP-rev primers specific to the *Nb-SABP2* (JX317629.1), *Nb-COI1* (AY547493.1), *GFP* (KX458.181.2), *βNGF* (KF057035.1) and TMV coat protein (M34077.1) genes, respectively. The qPCR reactions were accomplished in Mastercycler® EP realplex (Eppendorf, Hamburg, Germany) utilizing Maxima SYBR Green qPCR Master Mix (Thermo Scientific, Waltham, USA). Relative quantifications were performed based on the ΔCT method using cyclophilin (*cyp*) (AY368274.1) gene as an internal standard. Primer sequences for target and reference genes are listed in Supplementary Table S1.

In total samples from 6-8 plants were subjected to RNA analysis. Each sample was pooled from three middle leaves of one plant. The number of samples is designated in figure legends as n. Three technical replicates were performed for each probe. The Mann-Whitney U test was applied to test if there were differences between wild type and silenced plants.

GFP imaging

For visual detection of GFP fluorescence *N. benthamiana* leaves were illuminated with a handheld UV lamp and photographed with the Canon digital camera EOS 300D.

Protein quantification

The GFP and βNGF proteins were quantified by specific ELISA. Plant samples were collected from the middle agroinfiltrated leaves at 3, 5 and 7 dpi. The description of the GFP quantification can be found in Kopertekh and Reichardt (2021). The amounts of the βNGF protein in *N. benthamiana* leaves were determined as follows. Leaf material (300 mg) was harvested, homogenized in two volumes (w/v) of TBS buffer (50 mM Tris, 150 mM NaCI, 0.05% Tween-20, pH 7.4) and clarified by centrifugation for 10 min at 4 °C. ELISA plates were coated overnight with capture antibody diluted in carbonate buffer (0.1 M $NaHCO_3$, 0.1 M Na_2CO_3, pH 9.5). After incubation, the plates were washed three times with TBS buffer and blocked with blocking solution (TBS buffer supplemented with 1% BSA) for 1 h at room temperature. Following washing step as described above the plates were coated with the fresh prepared plant extracts and incubated overnight at 4 °C. Subsequently, the washing with TBS was repeated and a biotin anti-human NGF antibody in TBS buffer containing 1% BSA was added and incubated for 1 h at room temperature. After washing step performed as described, an avidine alkaline phosphatase was added and incubated for 30 minutes at room temperature. Finally, the plates were developed for 30 min with p-nitrophenyl phosphate as substrate and optical density was measured at 405 nm in a SUNRISE™ microplate reader (Tecan, Männedorf, Switzerland). All plates contained control βNGF protein diluted in TBS buffer for a standard curve.

Recombinant protein accumulation was analyzed in 6-8 biological and three technical replicates. The biological replicate represents a pooled sample from three middle leaves of one plant. The Mann-Whitney U test was performed to test if there were differences in recombinant protein accumulation between agroinfiltrated wild type and silenced plants.

Results

Expression of the *Nb-SABP2* and *Nb-COI1* genes in agroinfiltrated *N. benthamiana* leaves

To examine the involvement of the *Nb-SABP2* and *Nb-COI1* genes in *N. benthamiana* defense response to Agrobacterium-mediated delivery of virus-based expression vector the expression profile of these genes was investigated in agroinoculated leaf tissue. Following agroinfiltration of *N. benthamiana* plants with *A. tumefaciens* cultures carrying the pLH7000 and pLH-TMV-GFP (Figure 1) constructs the *Nb-SABP2* and *Nb-COI1* transcripts were quantified by qPCR at 2, 5 and 7 days after inoculation (dpi) and compared to that of non-treated plants. This analysis showed that the *Nb-SABP2* gene was upregulated in response to *A. tumefaciens* (pLH7000) and TMV (pLH-*TMV-GFP*) at early infection stage, 2 dpi (Figure 2A). In the *N. benthamiana* leaves treated only with *A. tumefaciens* the accumulation of the *Nb-SABP2* RNA was increased with a significant fold change value of 5.9 at 2 dpi, 6.3 at 5 dpi and 4.8, at 7 dpi. In presence of the pLH-*TMV-GFP* virus vector the *Nb-SABP2* expression increased at levels 8.9, 8.7 and 6-fold of the means for the non-treated plant at 2, 5 and 7 dpi, respectively. These results suggest that the *Nb-SABP2* gene is involved in *N. benthamiana* defense reaction against both components of transient gene delivery system, Agrobacterium and virus vector, and its upregulation starts at the early infection stage.

The expression profile of the *Nb-COI1* gene differed from that of the *Nb-SABP2* gene (Figure 2B). In comparison to non-inoculated control, no significant differences in the *Nb-COI1* transcript accumulation were observed in agroinfiltrated *N. benthamiana* leaves at 2 and 5 dpi. The upregulation of the *Nb-COI1* gene expression in treated leaves started late in the infection, at 7 dpi, achieving a 1.6-fold increase for Agrobacterium (pLH7000) and 2.4-fold increase for TMV (pLH-*TMV-GFP*). Therefore, the *Nb-COI1* gene is also involved in plant defense response against Agrobacterium-mediated delivery of the TMV-based vector.

Downregulation of the *Nb-SABP2* and *Nb-COI1* genes facilitated TMV and foreign protein transcript accumulation

To determine whether downregulation of the *Nb-SABP2* and *Nb-COI1* endogenous genes can influence the TMV and foreign protein RNA accumulation the pLH-*35S-COI1-INT-COI1* and pLH-*35S-SABP2-INT-SABP2* constructs have been designed. Both construct are based on the pLH7000 vector backbone and utilize the CaMV 35S promoter and terminator to control the dsRNA expression unit. The *Nb-SABP2* dsRNA expression cassette in the pLH-*35S-SABP2-INT-SABP2* vector includes the *Nb-SABP2* DNA fragment of 230 bp in sense and antisense orientation separated by the second intron of the potato *ST-LS1* gene (Figure 1A). The pLH-*35S-COI1-INT-COI1* silencing construct contained a 186 bp fragment of the *Nb-COI1* gene in direct and indirect orientation and the same splitting intron sequence as in the case of the pLH-*35S-SABP2-INT-SABP2* plasmid (Figure 1B).

The functionality of the pLH-*35S-SABP2-INT-SABP2* and pLH-*35S-COI1-INT-COI1* constructs has been tested for two vectors, pLH-*TMV-GFP* and pLH-*TMV-βNGF* (Figure 1C). For each expression vector *N. bethamiana* plants were agroinfiltrated with the *A. tumefaciens* cultures in following combinations: (i) pLH-*TMV-GOI*, (ii) pLH-*TMV-GOI*/pLH-*35S-COI1-INT-COI1*, (iii) pLH-*TMV-GOI*/pLH-*35S-SABP2-INT-SABP2*, (iv) pLH-*TMV-GOI*/pLH-*35S-SABP2-INT-SABP2*/pLH-*35S-COI1-INT-COI1*. The *GOI* designates the *GFP* and *βNGF* encoding sequences. The levels of the *Nb-SABP2*, *Nb-COI1*, TMV, *GFP* and *βNGF* transcripts were determined by qPCR analysis in the *Nb-SABP2* and *Nb-COI1* silenced leaves and compared with those of plants treated only with the pLH-*TMV-GOI* vector. The qPCR results for

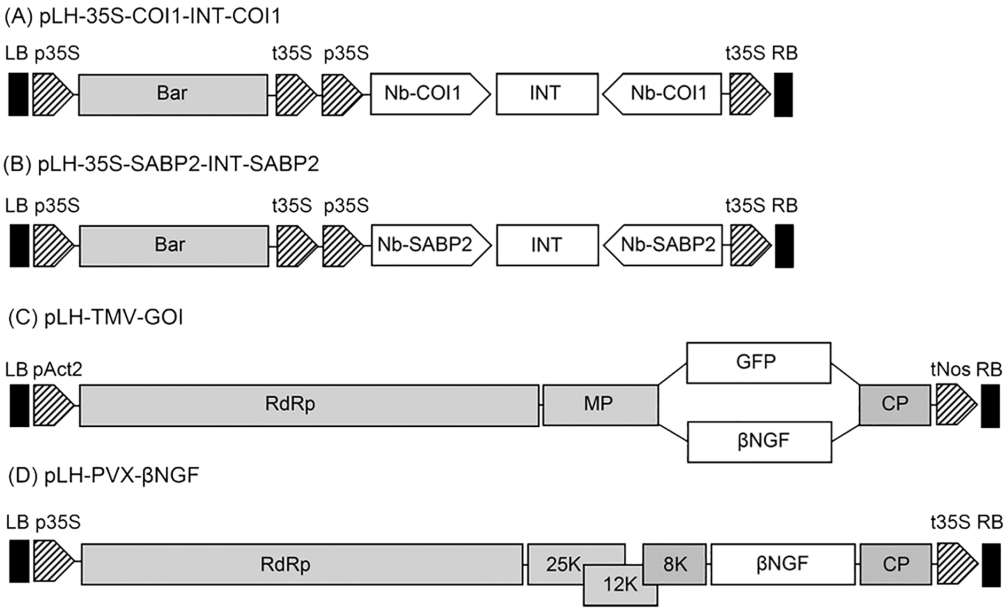

FIGURE 1
Schematic representation of expression constructs used in this study. **(A)** The pLH-*35S-COI1-INT-COI1* RNAi construct. The pLH-*35S-COI1-INT-COI1* plasmid contains the *bar* and *Nb-COI1* RNAi expression cassettes. The components of the pLH-*35S-COI1-INT-COI1* are designated as follows: *bar*, *bar* gene; *Nb-COI1*, the 186 bp fragment of the *Nb-COI1* gene in sense and antisense orientation; INT, the second intron (*IV2*) of the potato *ST-LS1* gene. **(B)** The pLH-*35S-SABP2-INT-SABP2* RNAi construct. The pLH-*35S-SABP2-INT-SABP2* plasmid contains the *bar* and *Nb-SABP2* RNAi expression cassettes. The components of the pLH-*35S-SABP2-INT-SABP2* are designated as follows: bar, *bar* gene; Nb-SABP2, the 230 bp fragment of the *Nb-SABP2* gene in sense and antisense orientation; INT, the second intron (*IV2*) of the potato *ST-LS1* gene. **(C)** The pLH-*TMV-GOI* expression vector. Features are as follows: RdRp, RNA-dependent RNA polymerase; MP, movement protein; genes of interest (GOI): *βNGF* (βNGF) and *GFP* (GFP); CP, coat protein encoding sequence; **(D)** The pLH-*PVX-βNGF* expression vector. Features are as follows: RdRp, RNA-dependent RNA polymerase; 25K, 12K, 8K, triple gene block; βNGF, *βNGF* gene; CP, coat protein encoding sequence. All expression constructs are based on the pLH7000 vector backbone. The regulatory elements used in expression vectors are pAct2, Act2 promoter from *A thaliana*; tNos, nopaline synthase terminator, p35S, CaMV 35S promoter; t35S, CaMV 35S terminator. LB, RB, left and right border of T-DNA, respectively.

the pLH-*TMV-GFP* virus vector demonstrated that the *Nb-SABP2* mRNA levels were reduced to 91% and 90% in the pLH-*TMV-GFP*/pLH-*35S-SABP2-INT-SABP2*, and pLH-*TMV-GFP*/pLH-*35S-SABP2-INT-SABP2*/pLH-*35S-COI1-INT-COI1* agroinfiltrated leaves, respectively (Figure 3). The presence of the pLH-*35S-COI1-INT-COI1* dsRNA construct resulted in the downregulation of the *Nb-COI1* gene by 57% for the pLH-*TMV-GFP*/pLH-*35S-COI1-INT-COI1* combination and by 68% for the *TMV-GFP*/pLH-*35S-SABP2-INT-SABP2*/pLH*35S-COI1-INT-COI1* mixture of *A. tumefaciens* cultures. The content of TMV RNA elevated by 7, 9 and 6-fold in the *Nb-COI1, Nb-SABP2* and *Nb-COI1*/*Nb-SABP2*-silenced plants, respectively. The accumulation of the *GFP* transcripts correlated with that of the TMV: it was increased by 5, 6 and 4-fold for the pLH-*TMV-GFP*/pLH-*35S-COI1-INT-COI1*, pLH-*TMV-GFP*/pLH-*35S-SABP2-INT-SABP2*, and pLH-*TMV-GFP*/pLH-*35S-SABP2-INT-SABP2*/pLH*35S-COI1-INT-COI1* samples, correspondingly.

The qPCR data for the TMV vector carrying the *βNGF* coding sequence are shown in Figure 4. Similar to the pLH-*TMV-GFP* virus vector the *Nb-SABP2* expression was reduced by 90% in leaves agroinfiltrated with the pLH-*TMV-βNGF*/pLH-*35S-SABP2-INT-SABP2* culture mixture and by 86% in leaves agroinfiltrated with the pLH-*TMV-βNGF*/pLH-*35S-SABP2-INT-SABP2*/pLH-*35S-COI1-INT-COI1* culture mixture. In leaves agroinfiltrated with the pLH-*TMV-βNGF*/pLH-*35S-COI1-INT-COI1* and pLH-*TMV-βNGF*/pLH-*35S-SABP2-INT-SABP2*/pLH-*35S-COI1-INT-COI1* combinations the *Nb-COI1* mRNA levels were reduced by 60% and 59%, correspondingly. Downregulation of the *Nb-SABP2* and *Nb-COI1* genes resulted in increased accumulation of the TMV RNA at 3 fold in all tested combinations of constructs.

Positive correlation was also found between the accumulation of viral and βNGF RNA. The *βNGF* gene showed significant fold change values of 3.6, 4.2 and 3.3 in the pLH-*TMV-βNGF*/pLH-*35S-COI1-INT-COI1*, pLH-*TMV-βNGF*/pLH-*35S-SABP2-INT-SABP2* and pLH-*TMV-βNGF*/pLH-*35S-SABP2-INT-SABP2*/pLH-*35S-COI1-INT-COI1* samples, respectively. These results suggest that the RNAi constructs for the *Nb-SABP2* and *Nb-COI1* are functional in a transient assay and the suppression of these genes has positive effect on foreign protein transcript accumulation.

Downregulation of the *Nb-SABP2* and *Nb-COI1* genes enhanced transient recombinant protein accumulation

Having identified the beneficial effect of the *Nb-SABP2* and *Nb-COI1* gene suppression on transient gene delivery system at RNA level (Figures 3, 4), we assessed the recombinant protein

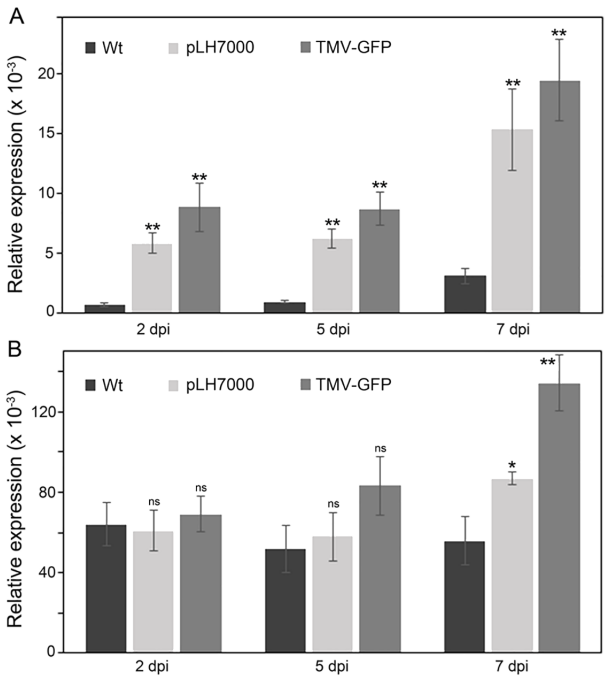

FIGURE 2
Expression of the *Nb-SABP2* and *Nb-COI1* genes in agroinfiltrated *N. benthamiana* leaves. *N. benthamiana* plants were agroinfiltrated with *A. tumefaciens* cultures carrying the pLH7000 and pLH-*TMV-GFP* expression vectors. The total RNA was isolated from leaf samples collected on 2, 5 and 7 dpi and subjected to qPCR analysis. The levels of the *Nb-SABP2* **(A)** and *Nb-COI1* **(B)** mRNA were quantified by gene-specific primers and normalized to *cyp* gene. Values represent the means with SE (n=8). Asterisks indicate significance as determined by the Mann-Whitney test, with *and ** denoting $p < 0.05$ and $p < 0.01$, respectively. Not significant values are determined as ns.

accumulation. Investigation of *N. benthamiana* leaves agroinfiltrated with the pLH-*TMV-GFP* under UV light revealed stronger GFP fluorescence in the presence of the *Nb-SABP2* and *Nb-COI1* RNAi silencing constructs (Figure 5A). Following a visual observation, the expression of GFP recombinant protein was analyzed over time in *N. benthamiana* leaves by specific ELISA. This analysis showed that the GFP accumulation increased steadily from day 3 to 7 and reached a peak on day 7 (Figure 5B). Compared to samples agroinfiltrated with the pLH-*TMV-GFP* alone, higher recombinant protein amounts were detected in leaf tissue co-infiltrated with the *A. tumefaciens* cultures containing the pLH-*TMV-GFP* and RNAi expression vectors. Production of GFP increased by 2.4-fold for the pLH-*TMV-GFP*/pLH-*35S-COI1-INT-COI1* combination of expression constructs, by 2.6-fold for the pLH-*TMV-GFP*/pLH-*35S-SABP2-INT-SABP2* combination of expression constructs and by 2.2-fold for the pLH-*TMV-GFP*/pLH-*35S-SABP2-INT-SABP2*/pLH-*35S-COI1-INT-COI1* combination of expression constructs. The highest GFP accumulation level 560 ± 30 μg/g fresh weight was detected at 7 dpi in the *N. benthamiana* leaves co-infiltrated with the pLH-*35S-SABP2-INT-SABP2* RNAi construct.

The expression profile of βNGF protein was similar to that of the GFP protein with the accumulation peak at 7 dpi (Figure 5C). The ELISA data revealed that co-expression of the pLH-*TMV-βNGF*/pLH-*35S-COI1-INT-COI1*, pLH-*TMV-βNGF*/pLH-*35S-SABP2-INT-SABP2* and pLH-*TMV-βNGF*/pLH-*35S-SABP2-INT-SABP2*/pLH-*35S-COI1-INT-COI1* constructs increased βNGF accumulation over the pLH-*TMV-βNGF* control in 1.8, 2.2 and 1.6-folds, respectively. The highest βNGF production 91 ± 10 ng/g fresh weight was observed at 7 dpi when the pLH-*TMV-βNGF* and pLH-*35S-SABP2-INT-SABP2* were combined.

To investigate whether RNAi-mediated suppression of the *Nb-SABP2* and *Nb-COI1* plant defense related genes can facilitate the accumulation of βNGF delivered by the PVX-based expression vector *N. benthamiana* plants were agroinfiltrated with the *A. tumefaciens* cultures carrying following constructs: the pLH-*PVX-βNGF*/pLH-*35S-COI1-INT-COI1*, pLH-*PVX-βNGF*/pLH-*35S-SABP2-INT-SABP2* and pLH-*PVX-βNGF*/pLH-*35S-SABP2-INT-SABP2*/pLH-*35S-COI1-INT-COI1*. Five days after inoculation the agroinfiltrated leaves were examined using ELISA assay to determine the βNGF production. The results of this analysis are shown in Figure 6. In line with the results obtained for the pLH-*TMV-βNGF* expression vector knockdown of the *Nb-SABP2* and *Nb-COI1* genes had positive impact on the βNGF accumulation. Co-infiltration of the pLH-*35S-COI1-INT-COI1* caused 2.6-fold enhancement of the βNGF amount. Combination of the pLH-*PVX-βNGF* and pLH-*35S-SABP2-INT-SABP2* led to 3.3-fold increase in βNGF content. Finally, simultaneous suppression of *Nb-SABP2* and *Nb-COI1* gene expression by the corresponding RNAi constructs resulted in 2.4 fold increase in βNGF accumulation. The best performing combination (pLH-*PVX-βNGF*/pLH-*35S-SABP2-INT-SABP2*) yielded 129 ± 25 ng/g fresh weight of βNGF.

The size and relative abundance of GFP and βNGF were estimated using Western blot analysis in total protein extracts from agroinfiltrated plant tissue. In the *Nb-SABP2* and *Nb-COI1* downregulated plants as well as in the control plants agoinfiltrated only with the pLH-*PVX-βNGF* and pLH-*TMV-GFP* the produced proteins had the expected size of 27 kDa for GFP and 35-37 kDa for βNGF (Supplementary Figure S1).

Discussion

The success of transient expression depends on both host plant and expression vector delivery component. Recent overview of the molecular changes in agroinfiltrated *N. benthamiana* leaves demonstrated that hybrid expression systems consisting of *A. tumefaciens* and binary vector trigger the plant defense response

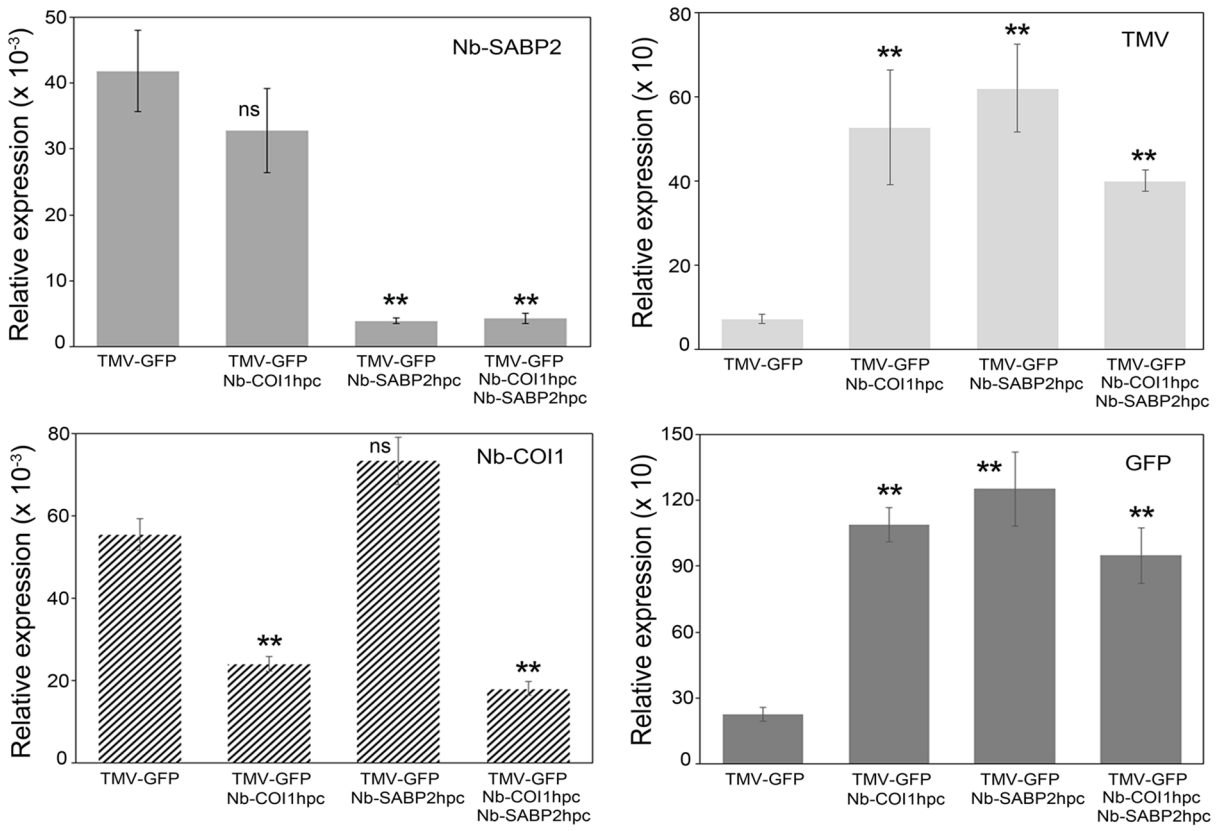

FIGURE 3
TMV and GFP RNA accumulation in *Nb-COI1* and *Nb-SABP2*-silenced *N. benthamiana* leaves. *N. benthamiana* leaves were agroinfiltrated with four combinations of *A. tumefaciens* cultures, namely, pLH-*TMV-GFP*, pLH-*TMV-GFP*/pLH-*35S-COI1-INT-COI1*, pLH-*TMV-GFP*/pLH-*35S-SABP2-INT-SABP2*, pLH-*TMV-GFP*/pLH-*35S-SABP2-INT-SABP2*/pLH-*35S-COI1-INT-COI1*. Leaf samples for RNA isolation were collected at 6 dpi. RNA levels were quantified by qPCR using primers specific to the *Nb-SABP2*, *Nb-COI1*, TMV and *GFP*. Values represent the means with SE (n=6). Asterisks indicate significance as determined by the Mann-Whitney test, with ** denoting $p < 0.01$. Not significant values are determined as ns.

and this can limit the recombinant protein yield (Hamel et al., 2023). In this study we suppressed *N. benthamiana* immunity through knockdown of endogenous genes involved in plant hormone metabolism. The expression pattern of the *Nb-SABP2* and *Nb-COI1* genes assessed by qPCR analysis revealed that both genes were upregulated upon agroinfiltration conferring their involvement in plant immune reaction. The association of the SABP2 with SA-dependent plant defense response to biotic stress has been shown by several research groups. In *Nicotiana tabacum* the *Nt-SABP2* gene expression was induced after TMV inoculation (Kumar and Klessig, 2003). Similarly, the functional homologs of the *Nt-SABP2* gene from *A. thaliana*, *At-MES1*, *At-MES7* and *At-MES9* were transcriptionally upregulated during infection with *Pseudomonas syringae* (Vlot et al., 2008). Our data are also consistent with the experiments demonstrating the positive role of a key regulator of JA signaling COI1 in plant defense. For example, in *Sacharum sp* the expression levels of the *Ss-COI1–4b* and *Ss-COI1–3b* genes were increased in smut-resistant cultivar YC05–179 and downregulated in smut-susceptible cultivar ROC22 (Sun et al., 2022). Similarly, the higher *Ta-COI1* transcript amounts were observed during early response to *Blumeria graminis* in resistant *Triticum aestivum* variety in comparison to susceptible one (Liu et al., 2018).

To examine whether suppression of plant immune system can facilitate the TMV multiplication we targeted the *Nb-SABP2* and *Nb-COI1* genes with corresponding dsRNAs. Downregulation of these genes increased susceptibility to TMV virus carrying *GFP* and *βNGF* sequences, which was manifested by the enhanced viral RNA accumulation in agroinfiltrated leaves. Our data are in agreement with the previous reports demonstrating that SA functions as a positive regulator of TMV resistance. For instance, Kumar and Klessig (2003) showed that the *Nt-SABP2*-silenced *N. tabacum* plants accumulated higher levels of TMV coat protein in comparison to control plants. In *N. benthamiana* knockdown of

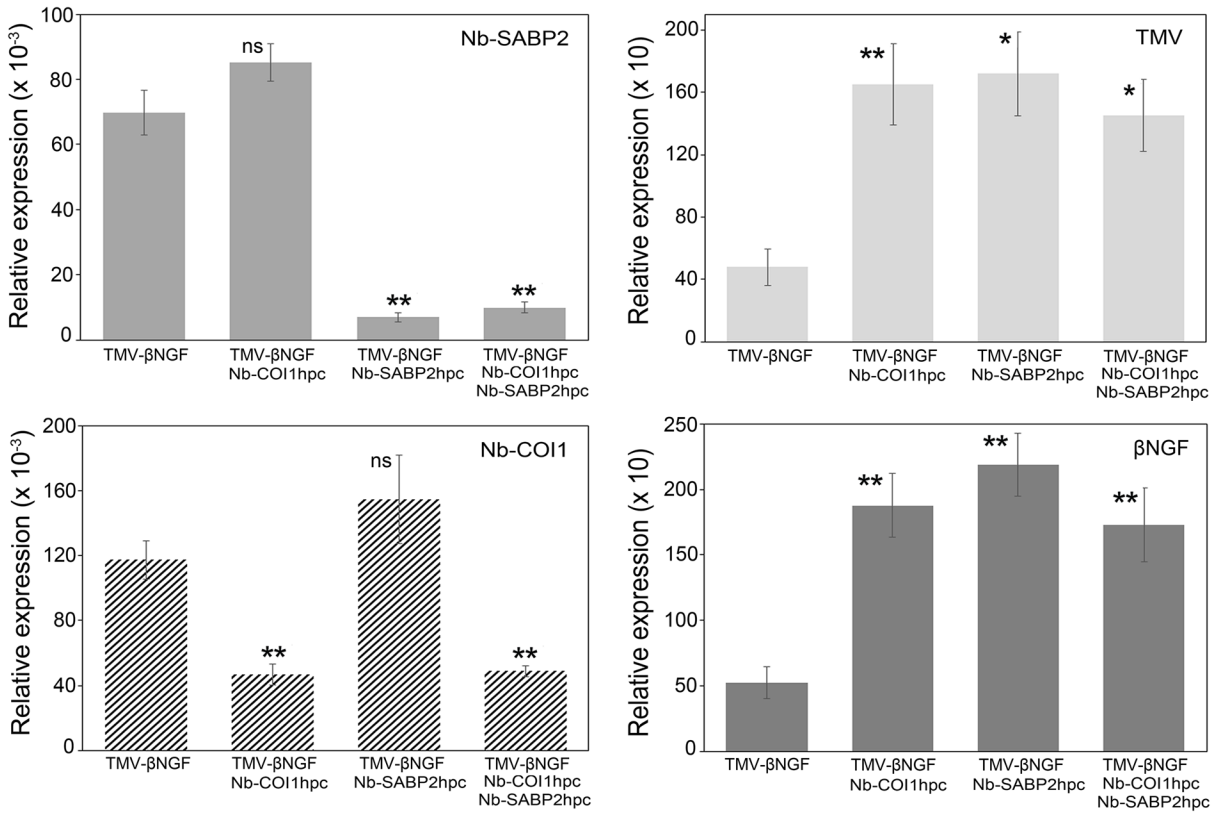

FIGURE 4
TMV and βNGF RNA accumulation in *Nb-COI1* and *Nb-SABP2*-silenced *N. benthamiana* leaves. *N. benthamiana* leaves were agroinfiltrated with four combinations of *A. tumefaciens* cultures, namely, pLH-*TMV-βNGF*, pLH-*TMV-βNGF*/pLH-*35S-COI1-INT-COI1*, pLH-*TMV-βNGF*/pLH-*35S-SABP2-INT-SABP2*, pLH-*TMV-βNGF*/pLH-*35S-SABP2-INT-SABP2*/pLH-*35S-COI1-INT-COI1*. Leaf samples for RNA isolation were collected at 6 dpi. RNA levels were quantified by qPCR using primers specific to the *Nb-SABP2*, *Nb-COI1*, TMV and *βNGF*. Values represent the means with SE (n=6). Asterisks indicate significance as determined by the Mann-Whitney test, with * and ** denoting $p < 0.05$ and $p < 0.01$, respectively. Not significant values are determined as ns.

SA-metabolism-related genes including *Nb-SABP2*, *Nb-ICS1* (isochorismate synthase), *Nb-NPR1* (non-expresser of PR gene 1), *Nb-SAMT* (SA methyl transferase) strongly increased susceptibility to TMV (Zhu et al., 2014). The role of JA in TMV resistance has not been fully clarified. Our data are in accordance with the report showing the positive role of the JA biosynthetic and signaling genes in antiviral response: downregulation of the *Nb-COI1*, *Nb-OPR3* (12-oxo-phytodienoic acid reductase), *NbJMT* (jasmonic acid carboxyl methyltransferase) genes boosted accumulation of TMV (Zhu et al., 2014). In contrast, Oka and co-workers demonstrated that silencing of the JA receptor COI1 resulted in resistance against TMV in tobacco containing N gene (Oka et al., 2013). These authors suggested that the JA signaling is indirectly responsible for TMV susceptibility through modification of SA-dependent and SA-independent resistance pathways.

The usefulness of strategy based on plant defense response modification for biotechnological purposes was demonstrated for GFP and βNGF recombinant proteins: the enhanced accumulation of TMV correlated with the increased amounts of GFP and βNGF transcripts. Furthermore, ELISA investigation confirmed this observation at protein level. For TMV-based expression vector, the downregulation of the *Nb-SABP2*, *Nb-COI1* and *Nb-SABP2*/*Nb-COI1* genes enhanced GFP accumulation by 2.4, 2.6 and 2.2 fold, respectively. Co-expression of the pLH-*TMV-βNGF* and RNAi constructs increased βNGF yield by 1.8-fold for the pLH-*TMV-βNGF*/pLH-*35S-COI1-INT-COI1* combination, 2.2-fold for the pLH-TMV-*βNGF*/pLH-*35S-SABP2-INT-SABP2* combination and 1.6-fold for the pLH-*TMV-βNGF*/pLH-*35S-SABP2-INT-SABP2*/pLH-*35S-COI1-INT-COI1* combination. These results are in content with data that have been reported for a number of

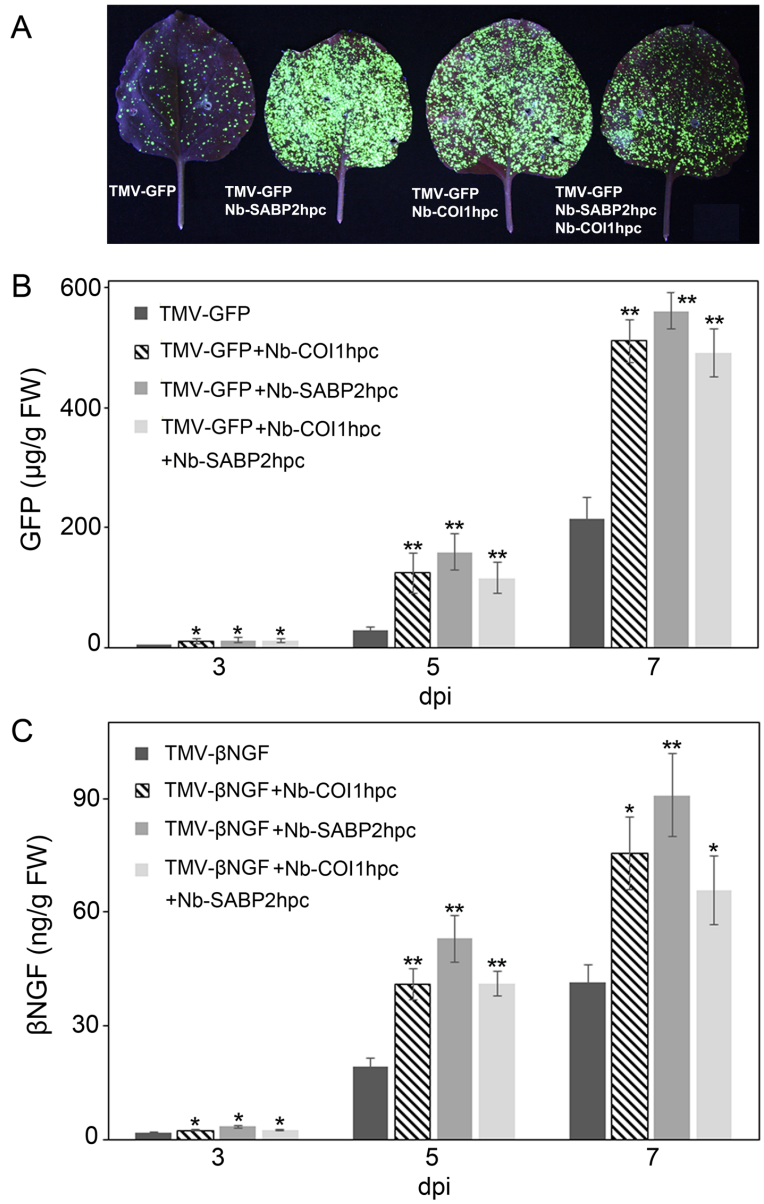

FIGURE 5
Transient production of GFP and βNGF recombinant proteins in *Nb-COI1* and *Nb-SABP2*-silenced *N. benthamiana* leaves. **(A)** GFP visualization in agroinfiltrated leaves. *N. benthamiana* plants were co-agroinfiltrated with *Nb-COI1* and *Nb-SABP2* RNAi silencing constructs and pLH-*TMV-GFP*. Images were taken at 5 dpi. The representative leaves coinfiltrated with the pLH-*TMV-GFP* (1), pLH-*TMV-GFP*/pLH-*35S-SABP2-INT-SABP2* (2), and pLH-*TMV-GFP*/pLH-*35S-COI1-INT-COI1* (3), pLH-*TMV-GFP*/pLH-*35S-SABP2-INT-SABP2*/pLH-*35S-COI1-INT-COI1* (4) are shown. **(B)** Time course analysis of GFP production. The leaves of *N. benthamiana* plants co-agroinfiltrated with the pLH-*TMV-GFP*, pLH-*TMV-GFP*/pLH-*35S-SABP2-INT-SABP2* and pLH-*TMV-GFP*/pLH-*35S-COI1-INT-COI1*, pLH-*TMV-GFP*/pLH-*35S-SABP2-INT-SABP2*/pLH-*35S-COI1-INT-COI1 A. tumefaciens* cultures were sampled at 3, 5 and 7 dpi and analysed by specific ELISA for GFP accumulation. **(C)** Time course analysis of βNGF production. The leaves of *N. benthamiana* plants co-infiltrated with the pLH-*TMV-βNGF*, pLH-*TMV-βNGF*/pLH-*35S-COI1-INT-COI1*, pLH-*TMV-βNGF*/pLH-*35S-SABP2-INT-SABP2*, pLH-*TMV-βNGF*/pLH-*35S-SABP2-INT-SABP2*/pLH-*35S-COI1-INT-COI1 A. tumefacines* cultures were sampled at 3, 5 and 7 dpi and analysed by specific ELISA for βNGF accumulation. Values represent the means with SE (n=8). Asterisks indicate significance as determined by the Mann-Whitney test, with * and ** denoting $p < 0.05$ and $p < 0.01$, respectively.

strategies for plant host optimization. In particular, transient co-delivery of virus-derived cell cycle regulator genes elevated GUS accumulation about 2-3 fold (Norkunas et al., 2018). Similar increase in production of GFP and scFv-TM43-E10 antibody fragment was observed in *N. benthamiana* leaves, which were co-infiltrated with the At-CycD2 and At-CDC27a plant cell regulators and TMV-based vector containing the *GFP* and *scFvTM43-E10* sequences (Kopertekh and Schiemann, 2019). Modification of gene

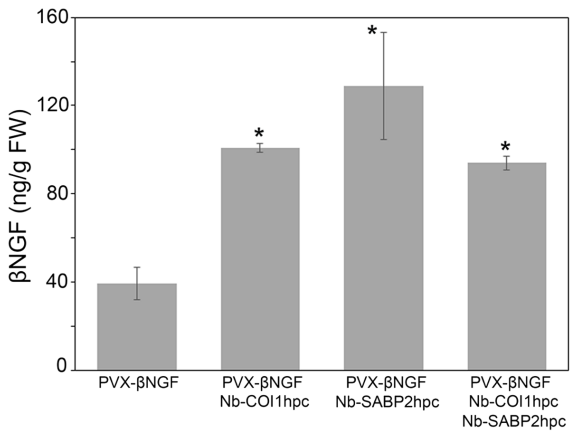

FIGURE 6
Transient production of the βNGF recombinant protein delivered by the PVX-based vector in the *Nb-COI1* and *Nb-SABP2*-silenced *N. benthamiana* leaves. The leaves of *N. benthamiana* plants co-infiltrated with the pLH-*PVX-βNGF*, pLH-*PVX-βNGF*/pLH-*35S-COI1-INT-COI1*, pLH-*PVX-βNGF*/pLH-*35S-SABP2-INT-SABP2*, pLH-*PVX-βNGF*/pLH-*35S-SABP2-INT-SABP2*/pLH-*35S-COI1-INT-COI1 A. tumefacines* cultures were sampled at 5 dpi and analyzed by specific ELISA for βNGF accumulation. Values represent the means with SE (n=6). Asterisks indicate significance as determined by the Mann-Whitney test, with * denoting $p < 0.05$.

silencing machinery through simultaneous knockout of *Nb-DCL2* and *Nb-DCL4* genes using CRISPR/Cas9 technology enhanced the production of human fibroblast growth factor by 9 fold (Matsuo, 2022). In the same manner, the CRISPR/Cas9-mediated editing of the *Nb-RDR6* gene elevated GFP accumulation in *N. benthamiana* by 2.5-fold (Matsuo and Atsumi, 2019).

A combined downregulation of multiple genes may have an additive effect to maximize the recombinant protein yield in transient expression. The simultaneous silencing of the *Nb-SABP2* and *Nb-COI1* genes did not result in synergistic effect compared to the suppression of the *Nb-SABP2* and *Nb-COI1* alone: we observed lower RNA and protein accumulation levels for TMV, GFP and βNGF in double-silenced plants. Data reported in several papers indicated the importance of the crosstalk between JA and SA to determine the degree of TMV resistance (Oka et al., 2013; Zhu et al., 2014). It can be suggested that in the *Nb-SABP2/Nb-COI1*-suppressed leaves the balance between endogenous JA and SA did not provide the superior cellular conditions for TMV infection in comparison to the individual silencing of the *Nb-SABP2* and *Nb-COI1* genes. Therefore, separated knockdown of the *Nb-SABP2* and *Nb-COI1* genes is more effective for enhanced recombinant protein production.

In summary, we demonstrated in this study that the components of Agrobacterium-mediated vector delivery system upregulate the *Nb-SABP2* and *Nb-COI1* genes, which take part in SA and JA-mediated plant defense response. The suppression of plant immunity through silencing of these genes improved recombinant protein yield as was exemplified by the full TMV-based expression vector. We suppose that this strategy can be useful for several commercial transient expression systems including GENEWARE® (Shivprasad et al., 1999), TRBO (Lindbo, 2007), magnICON® (Gleba et al., 2007), TMV launch vector (Musiychuk et al., 2007) utilizing TMV as the vector backbone. This approach might be extended to other virus-based expression vectors given that other plant-virus-based expression systems are limited by the SA- and JA-mediated virus resistance. Indeed, we demonstrated the increased βNGF production in the presence of the *Nb-SABP2* and *Nb-COI1* RNAi silencing constructs when the *βNGF* encoding sequence was delivered by the PVX-based virus vector.

It is important to note that this strategy is might be incompatible with the application of expression vectors containing strong suppressors of gene silencing such as P19 protein of Tomato bushy stunt virus (TBSV) (Scholthof, 2006). However, the commercial plant virus-based expression vectors listed above do not utilize strong silencing suppressors.

Data availability statement

The raw data supporting the conclusions of this article will be made available by the author, without undue reservation.

Author contributions

LK: Writing – review & editing.

Funding

The author(s) declare financial support was received for the research, authorship, and/or publication of this article. This research was financed in frame of the self-funded JKI project by the German Federal Ministry of Food and Agriculture (BMEL).

Acknowledgments

The technical support of Cornelia Freyer and Dominik Meindl is greatly acknowledged.

Conflict of interest

The author declares that the research was conducted in the absence of any commercial or financial relationships that could be construed as a potential conflict of interest.

Publisher's note

All claims expressed in this article are solely those of the authors and do not necessarily represent those of their affiliated organizations, or those of the publisher, the editors and the reviewers. Any product that may be evaluated in this article, or claim that may be made by its manufacturer, is not guaranteed or endorsed by the publisher.

Supplementary material

The Supplementary Material for this article can be found online at: https://www.frontiersin.org/articles/10.3389/fpls.2024.1453930/full#supplementary-material

References

Anand, A., Uppalapati, S. R., Ryu, C. M., Allen, S. N., Kang, L., Tang, Y., et al. (2008). Salicylic acid and systemic acquired resistance play a role in attenuating crown gall disease caused by *Agrobacterium tumefaciens*. *Plant Physiol.* 146, 703–715. doi: 10.1104/pp.107.111302

Bally, J., Jung, H., Mortimer, C., Naim, F., Philips, J. G., Hellens, R., et al. (2018). The rise and rise of *Nicotiana benthamiana*: a plant for all reasons. *Annu. Rev. Phytopathol.* 56, 405–426. doi: 10.1146/annurev-phyto-080417050141

Chapman, S., Kavanagh, T., and Baulcombe, D. (1992). Potato virus X as a vector for gene expression in plants. *Plant J.* 2, 549–557. doi: 10.1046/j.1365-313x.1992.t01-24-00999.x

Chini, A., Boter, M., and Solano, R. (2009). Plant oxylipins: COI1/JAZs/MYC2 as the core jasmonic acid-signalling module. *FEBS J.* 276, 4682–4692. doi: 10.1111/j.1742-4658.2009.07194.x

Dodds, I., Chen, C., Buscaill, P., and van der Hoorn, R. A. L. (2023). Depletion of the NbCORE receptor drastically improves agroinfiltration productivity in older *Nicotiana benthamiana* plants. *Plant Biotechnol. J.* 21, 1103–1105. doi: 10.1111/pbi.14037

Fischer, R., Vaquero-Martin, C., Sack, M., Drossard, J., Emans, N., and Commandeur, U. (1999). Towards molecular farming in the future: transient protein expression in plants. *Biotechnol. Appl. Biochem.* 30, 113–116. doi: 10.1111/j.1470-8744.1999.tb00900.x

Forouhar, F., Yang, Y., Kumar, D., Chen, Y., Fridman, E., Park, S. W., et al. (2005). Structural and biochemical studies identify tobacco SABP2 as a methyl salicylate esterase and implicate it in plant innate immunity. *Proc. Natl. Acad. Sci. U. S. A.* 102, 1773–1778. doi: 10.1073/pnas.0409227102

García-Marcos, A., Pacheco, R., Manzano, A., Aguilar, E., and Tenllado, F. (2013). Oxylipin biosynthesis genes positively regulate programmed cell death during compatible infections with the synergistic pair potato virus X-potato virus Y and Tomato spotted wilt virus. *J. Virol.* 87, 5769–5783. doi: 10.1128/JVI.03573-12

Gleba, Y., Klimyuk, V., and Marillonnet, S. (2005). Magnifection - a new platform for expressing recombinant vaccines in plants. *Vaccine* 23, 2042–2048. doi: 10.1016/j.vaccine.2005.01.006

Gleba, Y., Klimyuk, V., and Marillonnet, S. (2007). Viral vectors for the expression of proteins in plants. *Curr. Opin. Biotechnol.* 18, 134–141. doi: 10.1016/j.copbio.2007.03.002

Goodin, M. M., Zaitlin, D., Naidu, R. A., and Lommel, S. A. (2008). *Nicotiana benthamiana:* its history and future as a model for plant-pathogen interactions. *Mol. Plant Microbe Interact.* 2, 1015–1026. doi: 10.1094/MPMI-21-8-1015

Hamel, L. P., Tardif, R., Poirier-Gravel, F., Rasoolizadeh, A., Brosseau, C., Giroux, G., et al. (2023). Molecular responses of agroinfiltrated *Nicotiana benthamiana* leaves expressing suppressor of silencing P19 and influenza virus-like particles. *Plant Biotechnol. J.* 22, 1078–1100. doi: 10.1111/pbi.14247

Holsters, M., de Waele, D., Depicker, A., Messens, E., van Montagu, M., and Schell, J. (1978). Transfection and transformation of *A. tumefaciens*. *Mol. Gen. Genet.* 163, 181–187. doi: 10.1007/BF00267408

Kapila, J., De Rycke, R., Van Montagu, M., and Angenon, G. (1997). An Agrobacterium-mediated transient gene expression system for intact leaves. *Plant Sci.* 122, 101–108. doi: 10.1016/S0168-9452(96)04541-4

Kopertekh, L., Jüttner, G., and Schiemann, J. (2004). PVX-Cre-mediated marker gene elimination from transgenic plants. *Plant Mol. Biol.* 55, 491–500. doi: 10.1007/s11103-004-0237-8

Kopertekh, L., and Reichardt, S. (2021). At-CycD2 enhances accumulation of above-ground biomass and recombinant proteins in transgenic *Nicotiana benthamiana* plants. *Front. Plant Sci.* 12, 712438. doi: 10.3389/fpls.2021.712438

Kopertekh, L., and Reichardt, S. (2022). Effect of the *At-CDC27a* gene on *Nicotiana benthamiana* phenotype and accumulation of recombinant proteins. *Front. Plant Sci.* 13, 1042446. doi: 10.3389/fpls.2022.1042446

Kopertekh, L., and Schiemann, J. (2019). Enhanced foreign protein accumulation in *Nicotiana benthamiana* leaves co-infiltrated with a TMV vector and plant cell cycle regulator genes. *Transgenic Res.* 28, 411–417. doi: 10.1007/s11248-019-00128-3

Kumar, D., and Klessig, D. F. (2003). High-affinity salicylic acid-binding protein 2 is required for plant innate immunity and has salicylic acid-stimulated lipase activity. *Proc. Natl. Acad. Sci. U. S. A.* 100, 16101–16106. doi: 10.1073/pnas.0307162100

Lee, W. S., Fu, S. F., Verchot-Lubicz, J., and Carr, J. P. (2011). Genetic modification of alternative respiration in *Nicotiana benthamiana* affects basal and salicylic acid-induced resistance to potato virus X. *BMC Plant Biol.* 11, 41. doi: 10.1186/1471-2229-11-41

Li, N., Han, X., Feng, D., Yuan, D., and Huang, L.-J. (2019). Signaling crosstalk between salicylic acid and ethylene/jasmonate in plant defense: Do we understand what they are whispering? *Int. J. Mol. Sci.* 20, 671. doi: 10.3390/ijms20030671

Lindbo, J. A. (2007). TRBO: a high-efficiency tobacco mosaic virus RNA-based overexpression vector. *Plant Physiol.* 145, 1232–1240. doi: 10.1104/pp.107.106377

Liu, X., Wang, J., Fan, B., Shang, Y., Sun, Y., Dang, C., et al. (2018). A COI1 gene in wheat contributes to the early defence response against wheat powdery mildew. *J. Phytopathol.* 166, 116–122. doi: 10.1111/jph.12667

Liu, Y., Schiff, M., and Dinesh-Kumar, S. P. (2004). Involvement of MEK1 MAPKK, NTF6 MAPK, WRKY/MYB transcription factors, COI1 and CTR1 in N-mediated resistance to tobacco mosaic virus. *Plant J.* 38, 800–809. doi: 10.1111/j.1365-313X.2004.02085.x

Lomonossoff, G. P., and D'Aoust, M. A. (2016). Plant-produced biopharmaceuticals: A case of technical developments driving clinical deployment. *Science* 353, 1237–1240. doi: 10.1126/science.aaf6638

Ludman, M., Burgyán, J., and Fátyol, K. (2017). Crispr/Cas9 mediated inactivation of argonaute 2 reveals its differential involvement in antiviral responses. *Sci. Rep.* 7, 1010. doi: 10.1038/s41598-017-01050-6

Matsuo, K. (2022). CRISPR/Cas9-mediated knockout of the DCL2 and DCL4 genes in *Nicotiana benthamiana* and its productivity of recombinant proteins. *Plant Cell Rep.* 41, 307–317. doi: 10.1007/s00299-021-02809-y

Matsuo, K., and Atsumi, G. (2019). CRISPR/Cas9-mediated knockout of the *RDR6* gene in *Nicotiana benthamiana* for efficient transient expression of recombinant proteins. *Planta* 250, 463–473. doi: 10.1007/s00425-019-03180-9

Matsuo, K., and Matsumura, T. (2017). Repression of the *DCL2* and *DCL4* genes in *Nicotiana benthamiana* plants for the transient expression of recombinant proteins. *J. Biosci. Bioeng.* 124, 215–220. doi: 10.1016/j.jbiosc.2017.02.019

Mlynárová, L., and Nap, J. P. (2003). A self-excising Cre recombinase allows efficient recombination of multiple ectopic heterospecific lox sites in transgenic tobacco. *Transgenic Res.* 12, 45–57. doi: 10.1023/a:1022112221427

Musiychuk, K., Stephenson, N., Bi, H., Farrance, C. E., Orozovic, G., Brodelius, M., et al. (2007). A launch vector for the production of vaccine antigens in plants. *Influenza other Respir. viruses* 1, 19–25. doi: 10.1111/j.1750-2659.2006.00005.x

Ngou, B. P. M., Jones, J. D. G., and Ding, P. (2022). Plant immune networks. *Trends Plant Sci.* 27, 255273. doi: 10.1016/j.tplants.2021.08.012

Norkunas, K., Harding, R., Dale, J., and Dugdale, B. (2018). Improving agroinfiltration-based transient gene expression in *Nicotiana benthamiana*. *Plant Methods* 14, 71. doi: 10.1186/s13007-018-0343-2

Oka, K., Kobayashi, M., Mitsuhara, I., and Seo, S. (2013). Jasmonic acid negatively regulates resistance to Tobacco mosaic virus in tobacco. *Plant Cell Physiol.* 54, 1999–2010. doi: 10.1093/pcp/pct137

Pacheco, R., García-Marcos, A., Manzano, A., de Lacoba, M. G., Camañes, G., García-Agustín, P., et al. (2012). Comparative analysis of transcriptomic and hormonal responses to compatible and incompatible plant-virus interactions that lead to cell death. *Mol. Plant Microbe Interact.* 25, 709–723. doi: 10.1094/MPMI-11-11-0305

Park, S. W., Kaimoyo, E., Kumar, D., Mosher, S., and Klessig, D. F. (2007). Methyl salicylate is a critical mobile signal for plant systemic acquired resistance. *Science* 318, 113–116. doi: 10.1126/science.1147113

Peyret, H., and Lomonossoff, G. P. (2015). When plant virology met Agrobacterium: the rise of the deconstructed clones. *Plant Biotechnol. J.* 13, 1121–1135. doi: 10.1111/pbi.12412

Reichel, C., Mathur, J., Eckes, P., Langenkemper, K., Koncz, C., Schell, J., et al. (1996). Enhanced green fluorescence by the expression of an *Aequorea victoria* green fluorescent protein mutant in mono- and dicotyledonous plant cells. *Proc. Natl. Acad. Sci. U. S. A.* 93, 5888–5893. doi: 10.1073/pnas.93.12.5888

Schillberg, S., and Finnern, R. (2021). Plant molecular farming for the production of valuable proteins - Critical evaluation of achievements and future challenges. *J. Plant Physiol.* 258-259, 153359. doi: 10.1016/j.jplph.2020.153359

Schillberg, S., Raven, N., Spiegel, H., Rasche, S., and Buntru, M. (2019). Critical analysis of the commercial potential of plants for the production of recombinant proteins. *Front. Plant Sci.* 10. doi: 10.3389/fpls.2019.00720

Scholthof, H. B. (2006). The Tombusvirus-encoded P19: from irrelevance to elegance. *Nat. Rev. Microbiol.* 4, 405–411. doi: 10.1038/nrmicro1395

Shang, J., Xi, D. H., Xu, F., Wang, S. D., Cao, S., Xu, M. Y., et al. (2011). A broad-spectrum, efficient and nontransgenic approach to control plant viruses by application of salicylic acid and jasmonic acid. *Planta* 233, 299–308. doi: 10.1007/s00425-010-1308-5

Shivprasad, S., Pogue, G. P., Lewandowski, D. J., Hidalgo, J., Donson, J., Grill, L. K., et al. (1999). Heterologous sequences greatly affect foreign gene expression in tobacco mosaic virus-based vectors. *Virology* 255, 312–323. doi: 10.1006/viro.1998.9579

Sun, T., Meng, Y., Cen, G., Feng, A., Su, W., Chen, Y., et al. (2022). Genome-wide identification and expression analysis of the coronatine-insensitive 1 (COI1) gene family in response to biotic and abiotic stresses in Saccharum. *BMC Genomics* 23, 38. doi: 10.1186/s12864-021-08255-0

Töpfer, R., Maas, C., Horicke-Grandpierre, C., Schell, J., and Steinbiss, H. H. (1993). Expression vectors for high-level gene expression in dicotyledonous and monocotyledonous plants. *Meth. Enzymol.* 217, 67–87. doi: 10.1016/0076-6879(93)17056-b

Vlot, A. C., Liu, P. P., Cameron, R. K., Park, S. W., Yang, Y., Kumar, D., et al. (2008). Identification of likely orthologs of tobacco salicylic acid-binding protein 2 and their role in systemic acquired resistance in *Arabidopsis thaliana*. *Plant J.* 56, 445–456. doi: 10.1111/j.1365-313X.2008.03618.x

Wang, X., Prokhnevsky, A. I., Skarjinskaia, M., Razzak, M. A., Streatfield, S. J., and Lee, J. Y. (2023). Facilitating viral vector movement enhances heterologous protein production in an established plant system. *Plant Biotechnol. J.* 21, 635–645. doi: 10.1111/pbi.13977

Xie, D. X., Feys, B. F., James, S., Nieto-Rostro, M., and Turner, J. G. (1998). COI1: an Arabidopsis gene required for jasmonate-regulated defense and fertility. *Science* 280, 1091–1094. doi: 10.1126/science.280.5366.1091

Xu, L., Liu, F., Lechner, E., Genschik, P., Crosby, W. L., Ma, H., et al. (2002). The SCF (COI1) ubiquitin-ligase complexes are required for jasmonate response in Arabidopsis. *Plant Cell.* 14, 1919–1935. doi: 10.1105/tpc.003368

Yuan, Z. C., Edlind, M. P., Liu, P., Saenkham, P., Banta, L. M., Wise, A. A., et al. (2007). The plant signal salicylic acid shuts down expression of the vir regulon and activates quormone-quenching genes in Agrobacterium. *Proc. Natl. Acad. Sci. U. S. A.* 104, 11790–11795. doi: 10.1073/pnas.0704866104

Zhu, F., Xi, D. H., Yuan, S., Xu, F., Zhang, D. W., and Lin, H. H. (2014). Salicylic acid and jasmonic acid are essential for systemic resistance against tobacco mosaic virus in *Nicotiana benthamiana*. *Mol. Plant Microbe Interact.* 27, 567–577. doi: 10.1094/MPMI-11-130349-R

frontiers | Frontiers in Plant Science

TYPE Original Research
PUBLISHED 01 November 2024
DOI 10.3389/fpls.2024.1481452

OPEN ACCESS

EDITED BY
Kevin Yueju Wang,
University of Pikeville, United States

REVIEWED BY
Bhabesh Borphukan,
Washington State University, United States
Md Salik Noorani,
Jamia Hamdard University, India
Balamurugan Shanmugaraj,
Chulalongkorn University, Thailand

*CORRESPONDENCE
Qiang Chen
qiang.chen.4@asu.edu

†These authors have contributed equally to this work

RECEIVED 15 August 2024
ACCEPTED 10 October 2024
PUBLISHED 01 November 2024

CITATION
Melendez JA, Sun H, Bonner J and Chen Q (2024) Characterization of a plant-derived monoclonal antibody targeting extracellular enveloped virions of Monkeypox virus. *Front. Plant Sci.* 15:1481452. doi: 10.3389/fpls.2024.1481452

Characterization of a plant-derived monoclonal antibody targeting extracellular enveloped virions of Monkeypox virus

Jennifer A. Melendez[1,2†], Haiyan Sun[1†], James Bonner[1,2] and Qiang Chen[1,2*]

[1]Biodesign Institute, Arizona State University, Tempe, AZ, United States, [2]School of Life Sciences, Arizona State University, Tempe, AZ, United States

In 2022, the global outbreak of monkeypox virus (MPXV) with increased human-to-human transmission triggered urgent public health interventions. Plant-derived monoclonal antibodies (mAbs) are being explored as potential therapeutic strategies due to their diverse mechanisms of antiviral activity. MPXV produces two key infectious particles: the mature virion (MV) and the extracellular enveloped virion (EV), both essential for infection and spread. Effective therapies must target both to halt replication and transmission. Our prior research demonstrated the development of a potent neutralizing mAb against MPXV MV. This study focuses on developing a plant-derived mAb targeting MPXV EV, which is critical for viral dissemination within the host and generally resistant to antibody neutralization. Our findings reveal that the mAb (H2) can be robustly produced in *Nicotiana benthamiana* plants via transient expression. The plant-made H2 mAb effectively targets MPXV EV by binding specifically to the A35 MPXV antigen. Importantly, H2 mAb shows notable neutralizing activity against the infectious MPXV EV particle. This investigation is the first to report the development of a plant-derived anti-EV mAb for MPXV prevention and treatment, as well as the first demonstration of anti-MPXV EV activity by an mAb across any production platform. It highlights the potential of plant-produced mAbs as therapeutics for emerging infectious diseases, including the MPXV outbreak.

KEYWORDS

Monkeypox virus (MPXV), extracellular enveloped virion (EV), monoclonal antibody, plant-made biologics, plant-made antibody

Introduction

Monkeypox virus (MPXV) is a zoonotic double-stranded DNA virus belonging to the *Orthopoxvirus* genus and shares close genetic and structural similarities with other genus members including Vaccinia virus (VACV), Variola virus (VARV, the causative agent of smallpox), and ectromelia virus (ECTV) (Lum et al., 2022). Endemic to central and western

Africa for decades, MPXV experienced a global resurgence in 2022 through human-to-human transmission, leading to 109,699 confirmed cases worldwide and prompting an international health emergency declaration by the World Health Organization (WHO, 2024). MPXV exists in two infectious forms that facilitate infection: the mature virion (MV) and the extracellular enveloped virion (EV), each of which is responsible for the inter-host and intra-host dissemination, respectively (Schmidt et al., 2012).

Transmission of MPXV occurs through bodily fluids, respiratory droplets, direct contact with infected skin lesions, or contaminated fomites (Lum et al., 2022). The incubation period ranges from 5 to 21 days, and symptoms can include headache, fever, lymph node swelling, and muscle aches. Within 3 days of infection, a rash develops at the infection site, spreading to other bodily areas and resulting in papules or blisters (Lum et al., 2022). Currently, there are no specific approved treatments for MPXV. Antiviral therapies for other orthopoxviruses can be administered to treat MPXV infection under compassionate use policies (Siegrist and Sassine, 2022), although the clinical outcomes and risk-benefit ratio remain uncertain. Smallpox vaccines can also provide cross-protection against MPXV. However, due to the global eradication of smallpox in 1980, the vaccine is no longer routinely used (Gruber, 2022). Ongoing research and development efforts are focused on MPXV-specific treatments, underscoring the critical need for prophylactics and post-exposure therapeutics to protect immunocompromised individuals and those with severe allergic reactions to orthopoxvirus vaccines.

In the past few decades, monoclonal antibodies (mAbs) have emerged as promising protein-based biologics for combating a wide range of diseases due to their high specificity, versatility, and efficacy (Pantaleo et al., 2022). mAbs can be engineered to precisely target specific pathogens or cells, leading to better efficacy and fewer side effects compared to traditional therapies. Given the demonstrated effectiveness of neutralizing antibodies in protecting animals and humans from orthopoxvirus infections (Belyakov et al., 2003; Edghill-Smith et al., 2005; Sang et al., 2023), mAbs present a promising class of therapeutic candidates for combating the re-emerging MPXV epidemic. Our previous research demonstrated the development of a mAb that has potent neutralizing activity against the MV form of MPXV to curb the inter-host transmission (Esqueda et al., 2023). In contrast, there is still a need to develop more efficacious mAbs against the EV form of MPXV as it is generally more resistant to antibody neutralization due to the extra membrane that EVs possess (Vanderplasschen et al., 1998; Law and Smith, 2001). As a result, developing mAbs that can effectively target and neutralize the EV form of MPXV is crucial for achieving comprehensive protection and treatment of MPXV infection. The major viral antigens displayed by the EV of MPXV are A35 and B6, which are homologous to the VACV EV antigens of A33 and B5, respectively (Manes et al., 2008; Wang et al., 2023; Zhao et al., 2024). A35/A33 is particularly noteworthy for its role in viral dissemination within the host and anti-A33 antibodies have demonstrated protective efficacy in susceptible mice against lethal ECTV and VACV infections. Additionally, anti-A33 antibodies have been shown to reduce ECTV viral load in infected organs (Payne, 1980; Cohen et al., 2011; Tamir et al., 2024). Recently, a mAb (H2) has been isolated from A33-specific memory B cells of a volunteer vaccinated against smallpox over 40 years ago (Gu et al., 2022). The H2 mAb has been shown to bind to the A33 antigen of both VACV and ECTV, inhibit ECTV replication, and protect mice from VACV infection (Gu et al., 2022). However, the neutralizing activity of H2 mAb and other anti-A33/A35 mAbs against the EV form of MPXV has not been extensively characterized.

Currently, more than 100 mAbs are approved for therapeutic use (Mullard, 2021). The predominant platform for producing these biologics is based on mammalian cell culture systems, particularly Chinese hamster ovary (CHO) cells. CHO cells are favored for their ability to produce mAbs with high efficiency and human-like glycosylation patterns, which are crucial for antibody efficacy (Dahodwala and Lee, 2019). However, this production platform has several drawbacks, including high production costs and potential risks of contamination by mammalian pathogens. Furthermore, the glycosylation patterns in proteins produced by CHO cells can be heterogeneous, potentially hindering the development of mAbs with optimal effector functions (Sumit et al., 2019). Plants have emerged as a promising alternative platform for the production of mAbs (Chen, 2022). Utilizing plants as expression systems leverages their inherent capacity for rapid growth and biomass accumulation, which can significantly shorten production time and lower production costs compared to traditional mammalian cell culture methods (Chen and Davis, 2016; Nandi et al., 2016). Plant-based production of biologics also reduces the chance of introducing human pathogens during the manufacturing process (Chen, 2011). Furthermore, plant glycoengineering enables the generation of mAbs with a homogenous glycosylation profile, offering the capacity to modulate antibody Fc effector functions such as antibody-dependent cellular cytotoxicity (ADCC) activity and complement-dependent cytotoxicity (CDC) (Chen, 2016; Eidenberger et al., 2023; Esqueda and Chen, 2023).

In this study, we characterized a mAb H2, which was expressed in a glycoengineered *Nicotiana benthamiana* plant line (Strasser et al., 2008), targeting specifically the EV form of MPXV. The H2 mAb was successfully expressed and purified from *N. benthamiana* plants, achieving robust protein expression levels within 5-6 days post infiltration (DPI). Our findings reveal that plant-produced H2 mAb (p-H2 mAb) exhibits strong and specific binding to both MPXV-infected cells and its target antigen. Importantly, H2 mAb also demonstrated neutralizing activity against the EV form of MPXV. These results collectively suggest that plant-produced H2 mAb may be an effective candidate for eliminating MPVX EV virions, highlighting its potential therapeutic application in combating MPXV infections.

Materials and methods

Expression vector design and *Agrobacterium tumefaciens* infiltration

The heavy chain (HC) and light chain (LC) of the H2 mAb (Gu et al., 2022) were synthesized by Azenta Life Sciences (Burlington. MA, USA). For targeting the H2 mAb to the apoplast of leaf cells, the

calreticulin signal peptide from *Nicotiana plumbaginifolia* (Giritch et al., 2006) was added to the N-terminus of both the LC and HC, without including any ER retention signals in either construct. Full sequences for the LC and HC can be found in the Supplementary Data Sheet 1. The synthesized HC and LC fragments were initially cloned into pBluescript KS^+ and were then cloned into the one-module plant expression vector pBYR11eK2Md as described previously (Jugler et al., 2022a). Positive clones were verified by colony PCR using primers detailed in the Supplementary Material and were electroporated into *Agrobacterium tumefaciens* strain EHA105 (Esqueda and Chen, 2021). The EHA105 strain containing the H2 mAb construct was agroinfiltrated into the leaves of glycoengineered *N. benthamiana* plants using a needleless syringe as previously described (Leuzinger et al., 2013; Chen and Lai, 2014). Plants were grown in 65% humidity, at 25°C, with a 16-hour light and 8-hour dark cycle as described previously (Lai and Chen, 2012; Goulet et al., 2019).

H2 mAb extraction and purification

Leaves of glycoengineered *N. benthamiana* (~ 200 g per batch) were harvested at 5 DPI and homogenized in a buffer containing 1x phosphate-buffered saline (PBS) at pH 5.2, 10 mg/mL Sodium L-ascorbate, 1 mM ethylenediaminetetraacetic acid (EDTA), and 2 mM phenylmethylsulfonyl fluoride (PMSF) as previously described (Fulton et al., 2015; Jugler et al., 2020). The homogenate was filtered through a cheesecloth. The plant protein extract was centrifuged twice 15,000 x g at 4°C for 30 minutes and the pH of the supernatant was adjusted to 5.2 using 0.5N HCl. The protein extract was then incubated at 4°C overnight to precipitate host proteins. Following incubation, the plant extract was clarified by centrifuging three times at 15,000 x g at 4°C for 30 minutes. The pH of the clarified extract was adjusted to 7.0 using 0.5M NaOH and filtered using a 0.2-micron vacuum filter. The p-H2 mAb from plant extract was then purified using Protein A (MabSelect, Cytiva, Marlborough, MA, USA) affinity chromatography using a protocol provided by the manufacturer as we reported previously (Lai et al., 2010; Jugler et al., 2020). At least five batches of H2 mAb purification were conducted.

SDS-PAGE and western blot analysis

For SDS-PAGE analysis, purified p-H2 mAb was separated under both reducing and non-reducing conditions using 4-20% acrylamide gels and protein bands were visualized with Coomassie Blue R-250 staining as previously described (Jugler et al., 2022b). The purity of the H2 mAb was determined by imaging and quantifying Coomassie blue-stained protein bands on SDS-PAGE using a densitometer as described previously (Jugler et al., 2020). Western blot analysis was performed as previously described (Jugler et al., 2023). Briefly, total leaf soluble proteins were subjected to SDS-PAGE under reducing condition with 10% (v/v) β-mercaptoethanol and non-reducing condition on 4-12% or 12% acrylamide gels. The proteins were then transferred to PVDF membranes at 90 V for 90 minutes) in 1x transfer buffer (25mM Tris, 192 mM glycine, 10% Methanol, pH8.3). The membranes were blocked with 5% milk in 1X PBS containing 0.1% Tween-20 (PBS-T) and incubated for 1 hour at room temperature with goat anti-human kappa conjugated to horseradish peroxidase (HRP) for detecting the LC (Southern Biotech, Birmingham, AL, USA, 1:3,000 dilution) or goat anti-human gamma-HRP for the HC (Southern Biotech, Birmingham, AL, USA. 1:5,000 dilution). Detection was carried out using Pierce Western Blotting Substrate (Thermo Scientific, Waltham, MA, USA) for 5 minutes. Membranes were washed five times with 1X PBS-T at 5-minute intervals, and images were captured using the ImageQuant imaging system (Cytiva, Marlborough, MA, USA).

ELISA

1. P-H2 Binding to MPXV A35 Antigen

An ELISA was conducted to measure the specific binding of p-H2 mAb to the A35 antigen. The coding sequence of the antigen protein was cloned into the pET28a vector and expressed in *E. coli* strain BL21 as described previously (Fang et al., 2006; Yang et al., 2017). The soluble fraction of A35 was purified using immobilized metal affinity chromatography (IMAC) with Ni^{2+} resin, following the manufacturer's instructions (Thermo Fisher Scientific, Waltham, MA, USA). Purified A35 (200 µl at 1µg/ml) was then coated onto a 96-well plate and incubated at 4°C overnight. The plate was blocked with 5% milk and followed by generic human IgG (SeraCare Life Sciences Inc., Milford, CT, USA, 50µg/ml). The plate was then incubated with p-H2 mAb (5µg/ml) conjugated to HRP using EZ-Link Plus Activated Peroxidase Kit (Thermo Fisher Scientific, Waltham, MA, USA). Detection of p-H2 mAb was performed using an HRP substrate (TMB, SeraCare Life Sciences Inc., Milford, CT, USA), after which the reaction was stopped with 1M H_2SO_4. The plate was then read on a spectrophotometer at 450 nm (Biotek Powerwave, Agilent Technologies., Santa Clara, CA, USA) and results were calculated and graphed using GraphPad Prism 10.2.2 (GraphPad, San Diego, CA, USA). The binding ELISA was conducted six times with technical triplicates.

2. Time Course of H2 mAb expression in plants

An ELISA that detects the fully assembled mAb was performed to investigate the temporal expression patten of H2 mAb in plants as described (Lai et al., 2014). Glycoengineered *N. benthamiana* plant leaves (at least 20 leaves per time point) were agroinfiltrated (OD_{600} = 0.2) with the expression vector of H2 mAb. Leaves were harvested at 4-9 DPI and stored at -80°C. Once all samples were collected, the leaves were ground for 5 minutes using a chilled mortar and pestle. Protein extracts from each DPI were isolated, clarified using the same extraction buffer and procedure as described in the "H2 mAb Extraction and Purification" section above. Throughout the isolation process, buffers, containers, and procedures were pre-chilled at 4°C and conducted at 4°C to ensure the stability of the H2 mAb. The extracts were then assayed on a 96-well plate coated with the capture antibody (goat anti-human HC, Southern Biotech, Birmingham, AL, USA, 200 µl at 2µg/ml). After 1 hour of incubation at 37°C, the plate was incubated with the detection antibody (a goat anti-human kappa IgG labeled with

HRP, Southern Biotech, Birmingham, AL, USA, 0.25µg/ml) for 1 hour at 37°C. The plate was then developed using an HRP substrate (TMB, SeraCare Life Sciences Inc., Milford, CT, USA) and read on a spectrophotometer at 450 nm (Biotek Powerwave, Agilent Technologies., Santa Clara, CA, USA). For each ELISA, serial dilutions of an isotype IgG with known concentrations were included as standards to generate a standard curve, which we used to calculate the concentration of the H2 mAb in the leaves (µg of mAb per gram of fresh leaf weight, FLW). The H2 concentration was then graphed using GraphPad Prism 10.2.2 (GraphPad, San Diego, CA, USA). The time-course experiments were repeated three times. Proteins isolated from each experiment were assayed using ELISA, which was conducted at least twice with technical replicates.

Virus propagation and cell culture

MPXV strain WRAIR 7-61 (BEI Resources, NR-58622, Rockville, MD, USA) was propagated by infecting T175 cm^2 flasks of BSC40 cells (American Type Culture Collection (ATCC) CRL-2761, Manassas, VA, USA) at a multiplicity of infection (MOI) of 0.01 for one hour at 37°C in Eagle's Minimal Essential Medium (MEM) containing 2% fetal bovine serum (FBS) (ThermoFisher, Waltham, MA, USA). After infection, the cells were overlaid with Dulbecco's Modified-Minimal Essential Medium (DMEM) (ThermoFisher, Waltham, MA, USA) supplemented with 5% FBS. Upon observing viral cytopathic effect (CPE) in 75-100% of cells (approximately 3-4 days post-infection), the virus was harvested by scraping cells into media, centrifuging at 1,000 x g for 10 minutes, and resuspending the pellet in 10 mM Tris, pH 8.0. Crude viral stocks were prepared by freeze-thaw cycles (-80°C, thawed on ice for 30 minutes, then at 37°C for 10 minutes), removing cellular debris by centrifugation at 1,000 x g for 10 minutes, and collecting and aliquoting the supernatant. These crude viral stocks were titrated by infecting confluent monolayers of BSC40 cells with serial dilutions of the viral stock, staining the cells with 0.1% crystal violet in 20% ethanol (MilliporeSigma, Burlington, MA, USA) three days after infection, and then counting plaques. VACV strain Copenhagen (COP) VC2 (kindly provided by Virogenetics) (Jentarra et al., 2008) was prepared similarly as described for MPXV but cultivated in BHK21 cells (ATCC, CCL-10) in MEM with 5% FBS. Additionally, the virus was purified by centrifugation on a 36% sucrose pad at 18,000 x g for one hour at 4°C. Like MPXV, VACV stocks were titrated using BSC40 cells.

Immunofluorescence staining

BSC40 cells were seeded into a 96-well plate at 50% confluency, infected in triplicate with different dilutions of MPXV or VACV stocks, then fixed with 4% Paraformaldehyde (ThermoFisher, Waltham, MA, USA) in PBS for 15 minutes at room temperature by 24 or 48 hours post infection, respectively. After fixation, the cells were permeabilized with 0.1% Saponin (MilliporeSigma, Burlington, MA, USA) in PBS and stained with 5 µg/ml p-H2 mAb at 4°C overnight. The next day, cells were washed three times with PBS and stained with Alexa488 goat anti-human IgG Kappa (Southern Biotech, Birmingham, AL, USA) at a 1:500 dilution for 1.5 hours at room temperature. Images were captured using the EVOS Cell Imaging System (Thermo Fisher Scientific, Waltham, MA, USA). Experiments were independently repeated three times for both MPXV and VACV.

Preparation of extracellular enveloped virions

EVs were isolated by infecting a confluent monolayer of BSC40 cells in a 60 mm dish with the indicated virus (MPXV or VACV) at an MOI of 5. The monolayer was washed twice to remove input IMVs, and the cell media supernatant was collected 18-24 hours post-infection. The supernatant was centrifuged twice at 1,000 x g for 10 minutes to remove infected cells. This approach is comparable to, if not more stringent than, previously published protocols for EV isolation (Benhnia Mohammed et al., 2009b). EV stocks were used immediately or stored overnight at 4°C prior to subsequent neutralization assays.

MPXV and VACV neutralization assay

MPXV EVs were neutralized by diluting fresh MPXV and VACV EV stocks by 10^{-3} and 10^{-5}, respectively, and then adding the appropriate volume of antibody or PBS to each dilution. The mixtures of diluted EVs and antibody/PBS were incubated at 37°C for one hour and then applied to confluent monolayers of BSC40 cells in a volume of 0.1mL for an additional hour at 37°C, with rocking every ten minutes. After the one-hour infection, monolayers were washed twice with fresh cell media and then incubated in cell media. MPXV and VACV-infected cells were stained with crystal violet 48 hours (VACV) and 72 hours (MPXV) post-infection. Percent (%) plaque reduction was calculated as: [(number of plaque per well without mAb) – (number of plaque per well with diluted mAb)/(number of plaque per well without mAb) × 100].

Statistical analyses

Statistical analyses were performed using GraphPad Prism software version 10.2.2. First, the data distribution was assessed using the D'Agostino & Pearson normality test, confirming a Gaussian distribution for all neutralization data. Subsequently, T-tests were employed to compare the neutralization activity of the p-H2 mAb against MPXV and VACV with data from at least two independent experiments with technical triplicates. A p-value of less than 0.05 was considered statistically significant.

Results

Expression of H2 mAb in *Nicotiana benthamiana*

The coding sequences of H2 mAb HC and LC were cloned into the plant expression vector and agroinfiltrated into leaves of a glycoengineered line of *N. benthamiana* plants that forgo the attachment of plant-specific xylose and fucose on their complex N-glycans (Strasser et al., 2008). Western blot analysis validated the expression of H2 mAb in plants, showing detection of the HC and LC at the expected molecular weights of 50kDa and 25 kDa respectively (Figure 1). Results obtained under non-reducing conditions indicated that p-H2 assembled into its tetrameric IgG format (Supplementary Figure S1), although there were minor, not-fully-assembled fragments that shared a similar banding pattern with the pharmaceutical-grade IgG isotype control (Supplementary Figure S1). Furthermore, the temporal expression pattern of p-H2 mAb was investigated by an ELISA that detects only the assembled form of IgG. Our results indicate that the fully assembled mAb accumulated quickly in plants with its peak expression (~ 150 µg of mAb per gram FLW) occurred at 5-6 DPI (Figure 2). These results indicate the robust production and assembly of p-H2 mAb in plants.

Assembly and purification of plant-produced H2 mAb

p-H2 mAb was purified by a two-step purification protocol previously developed in our laboratory. SDS-PAGE analysis of purified p-H2 mAb demonstrated that the mAb can be purified to greater than 90% homogeneity by this purification method, which is comparable to that of the control mAb produced in CHO cells (Figure 3). No significant degradation products were detected for either LC or HC (Figure 3, Lane 1), indicating the integrity of p-H2 mAb. Furthermore, p-H2 mAb was detected as a major band of approximately 170 kDa (Figure 3, Lane 3), confirming the assembly of the mAb as indicated by the western blot and ELISA results.

p-H2 mAb specifically binds to the target Monkeypox virus antigen

The specific recognition of p-H2 mAb to its cognate antigen was investigated by two independent methods. We first measured its binding to the specific MPXV antigen displayed on the authentic virus. Our results demonstrated that p-H2 mAb exhibits targeted binding to MPXV-infected BSC40 cells (Figure 4A), but with no

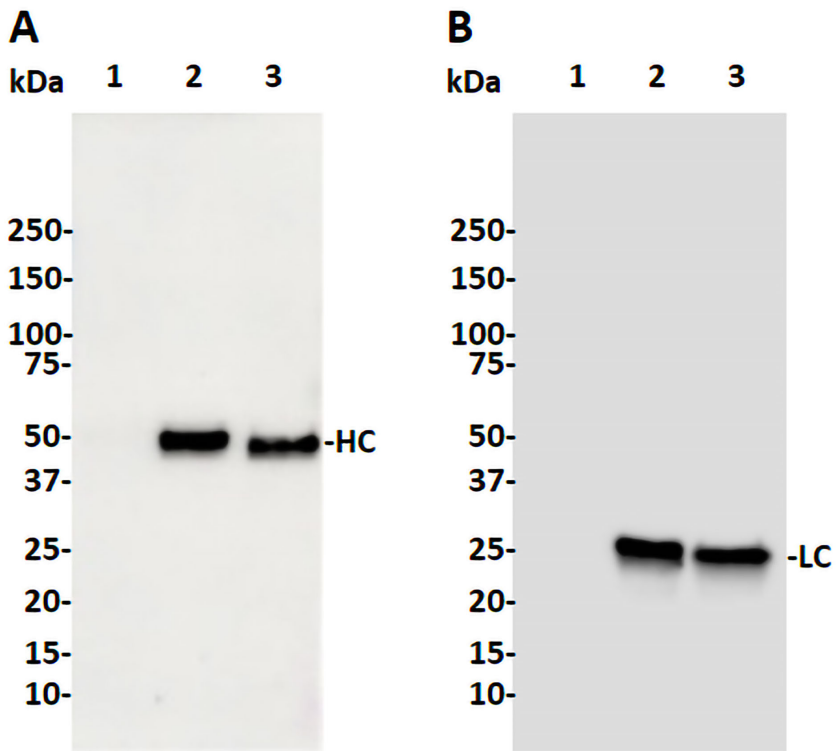

FIGURE 1
Western blot analysis of the H2 mAb produced in glycoengineered *N. benthamiana* plant. Total proteins were extracted from *N. benthamiana* leaves infiltrated with either the H2 mAb construct or buffer. Proteins were then separated by SDS-PAGE under reducing condition and transferred to PVDF membranes. Immunodetection was performed under reducing condition using antibodies against human gamma HC **(A)** or human kappa LC **(B)**. Lane 1: 20 µg of total proteins from buffer-infiltrated leaves, serving as a negative control. Lane 2: 20 ng of isotype IgG, serving as both a positive control and a loading control. Lane 3: 20 µg of proteins from leaves infiltrated with the H2 mAb construct. One representative blot from multiple experiments is shown.

10.3389/fpls.2024.1481452

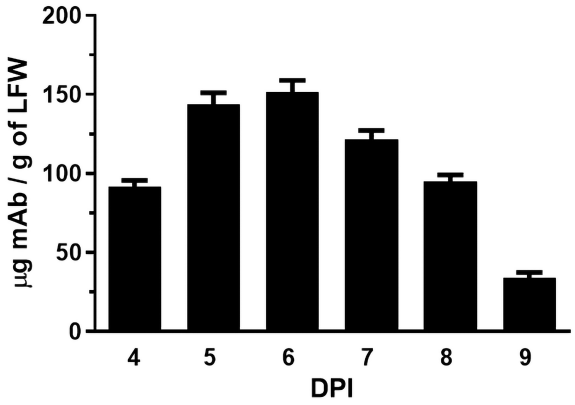

FIGURE 2
Time course of H2 mAb expression in *N. benthamiana*. Total protein was extracted from glycoengineered *N. benthamiana* leaves agroinfiltrated with the H2 mAb construct at 4, 5, 6, 7, 8, and 9 days post-infiltration. The Levels of H2 mAb were quantified by an ELISA that specifically detects assembled IgG. The data presented are derived from three independent infiltration experiments, with each ELISA repeated twice with technical replicates.

binding observed to uninfected cells (Figure 4B) or cells detected with only the secondary antibody (Figure 4C). As shown in Figures 4D–F, similar cell numbers and distributions were observed under bright-field settings, regardless of whether the cells were infected, uninfected, stained sequentially with primary and secondary antibodies, or stained with only the secondary antibody. Similarly, the p-H2 mAb also demonstrated specific binding to cells infected with the closely related VACV (Figure 5). To confirm that p-H2 mAb specifically recognized its target antigen (A35) displayed on MPXV EV, an ELISA was performed with purified A35. As shown in Figure 6, p-H2 mAb indeed showed specific binding to A35 antigen. These results demonstrated that p-H2 mAb displayed Fab domains with authentic conformation that can recognize its target antigen in purified form as well as when displayed on the surface of the virion.

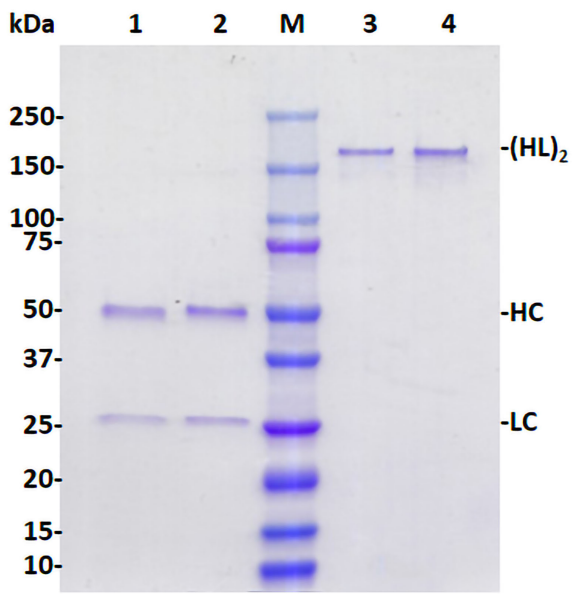

FIGURE 3
Assembly and purification of plant-produced H2 mAb. The p-H2 mAb was extracted from leaves of glycoengineered *N. benthamiana* plants and purified using Protein A affinity chromatography. Purified p-H2 mAb was analyzed by SDS-PAGE under both reducing (Lanes 1 and 2) and non-reducing conditions (Lanes 3 and 4), and subsequently stained with Coomassie blue. Lanes 1 (3 µg protein) and 3 (1 µg protein) show the plant-produced H2 mAb, while Lanes 2 (3 µg protein) and 4 (1 µg protein) show the Isotype IgG reference produced in CHO cells, serving as both a positive control and a loading control. A single representative result from multiple experiments is presented.

p-H2 mAb neutralizes extracellular enveloped Monkeypox virion

The neutralization potential of p-H2 mAb against the EV virion of MPXV was investigated by a plaque assay as described previously (Denzler et al., 2011; Arndt et al., 2016). As shown in Figure 7A, treatment with p-H2 mAb resulted in significant neutralization of MPXV compared to the negative control achieving a 56% plaque reduction (p = 0.0001 compared to the negative control). Additionally, the p-H2 mAb also exhibited significant neutralizing activity against VACV, which is similar to that of MPXV (p = 0.14 compared to MPXV), resulting in a 45% plaque reduction when treated with p-H2 mAb (p < 0.0001 compared to the negative control) (Figure 7B). These results indicate that p-H2 mAb are functional *in vitro* against the EV form of MPXV as well as that of VACV.

Discussion

The global MPXV outbreak in 2022 was the largest and most widespread in history, with a significant increase in human-to-human transmission highlighting the urgent need for prophylactics and therapeutics (Lum et al., 2022). These measures are critical to prevent further virus spread and to protect and treat individuals who are allergic to existing MPXV vaccines or unable to mount a protective response to vaccination, especially given the current lack of an FDA-approved therapy specifically for MPXV. mAbs are promising candidates for treating MPXV infection, as their protective efficacy against related orthopoxviruses has been demonstrated in animal models, although research on MPXV remains limited (Belyakov et al., 2003; Edghill-Smith et al., 2005). MPXV produces two distinct types of infectious particles: the MV and the EV. MV, characterized by a single lipid membrane, is predominantly released from infected cells upon cell lysis (Roberts and Smith, 2008; Lum et al., 2022). In contrast, EV buds off from infected cells, acquiring an additional outer lipid envelope that confers resistance to the host's immune responses, facilitates more efficient viral spread within the host, and helps the virus evade immune detection (Payne, 1980; Schmidt et al., 2012). Consequently, MVs primarily establish initial infection and facilitate host-to-host transmission, while EVs are crucial for viral spread and immune evasion within the host (Schmidt et al., 2012).

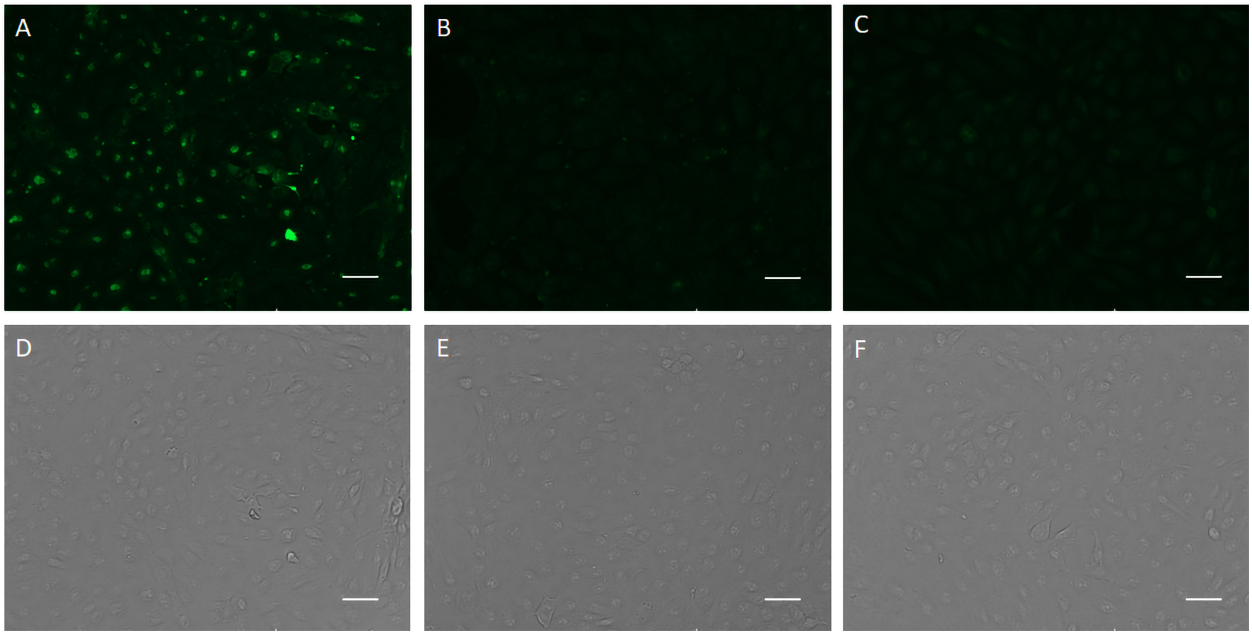

FIGURE 4
Recognition of viral antigen in MPXV-infected BSC40 cells by p-H2 mAb using immunofluorescence microscopy. MPXV-infected **(A, D)** or uninfected [**(B, E)**, negative control] BSC40 cells in a 96-well plate were fixed and permeabilized, then incubated with p-H2 mAb and subsequently stained with Alexa488-conjugated goat anti-human IgG Kappa. Panels **(C, F)** show MPXV-infected BSC40 cells stained directly with Alexa488-conjugated goat anti-human IgG Kappa, serving as a secondary-antibody-only negative control. Images were captured using an EVOS Cell Imaging System with the EVOS AlexaFluor 488 light cube filter **(A–C)** or under white light settings **(D–F)**. Scale bar represents 50 µm.

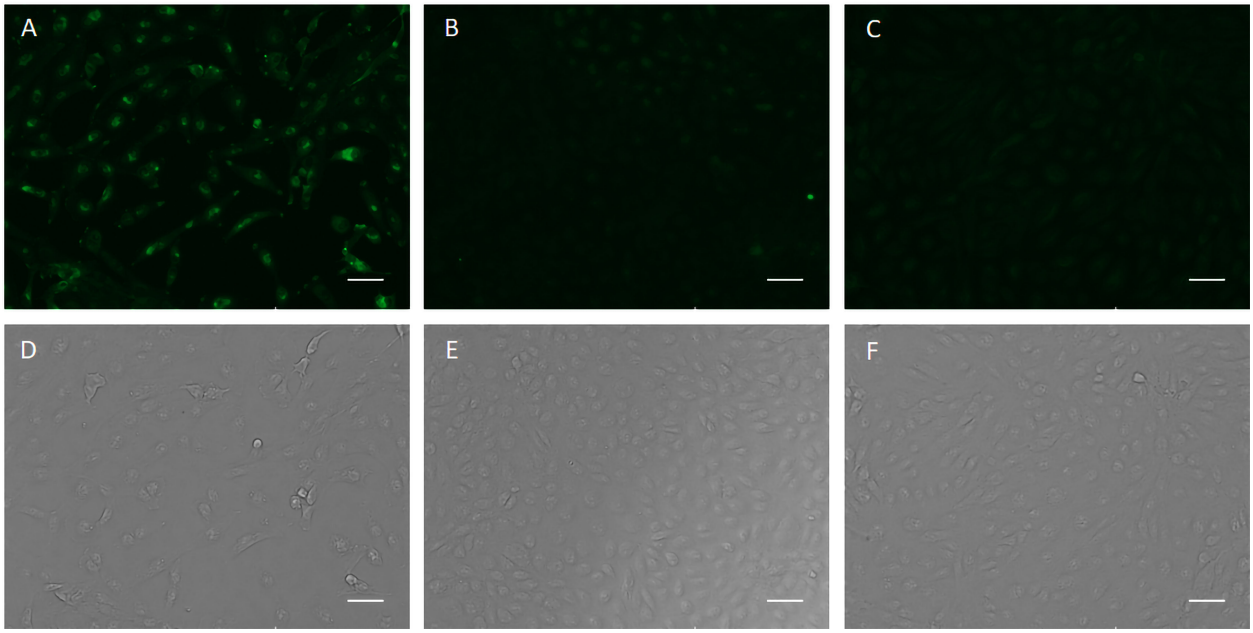

FIGURE 5
p-H2 mAb recognizes viral antigen in VACV-infected BSC40 cells. BSC40 cells infected with VACV were stained sequentially with p-H2 mAb and the secondary antibody Alexa488-conjugated goat anti-human IgG Kappa **(A, D)** or with the secondary antibody only [**(C, F)**, negative control]. Uninfected BSC40 cells stained with p-H2 mAb and Alexa488-conjugated goat anti-human IgG Kappa **(B, E)** served as an additional negative control. Immunostained images are shown in panels **(A–C)**, with corresponding bright field images in panels **(D–F)**.

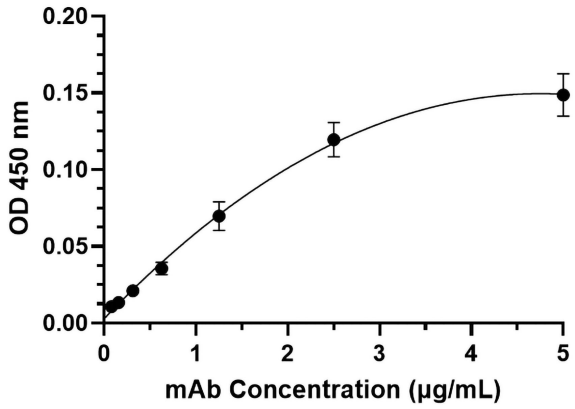

FIGURE 6
Specific binding of p-H2 mAb to the MPXV A35 antigen. MPXV A35 antigen was immobilized on ELISA plates. After blocking with 5% milk and generic human IgG, the plates were incubated with serial dilutions of HRP-conjugated p-H2 mAb. The mean and standard deviation of absorbance values at 450 nm were measured from six independent experiments, each with technical triplicates, and the data were plotted using GraphPad Prism 10.2.2.

Accordingly, a successful mAb-based therapy for MPXV should target both MVs and EVs to ensure effective virus neutralization during early infection stages and control viral spread within the host. Failure to target both forms may result in incomplete viral containment, leading to ongoing viral replication and transmission.

Previously, we developed a mAb with potent neutralizing activity against the MV form of MPXV, aimed at preventing inter-host transmission (Esqueda et al., 2023). In this study, we sought to characterize an EV-specific mAb to inhibit viral spreading within the infected host, focusing on the EV-specific antigen A35 from MPXV. The A35 antigen, a homolog of VACV A33, is an envelope glycoprotein, contributing to the formation of action-containing microvilli and facilitating the effective viral dissemination within the host (Perdiguero and Blasco, 2006; Wang et al., 2023). We specifically selected the H2 mAb for further evaluation as a candidate against MPXV EV due to its demonstrated ability to inhibit VACV infection and its recognition of a conserved epitope on both VACV A33 and MPXV A35 (Gu et al., 2022; Yefet et al., 2023). Here, we demonstrated that H2 mAb was rapidly expressed in glycoengineered *N. benthamiana* plants, reaching an accumulation level of approximately 150 µg/gram FLW within 5-6 days post-gene delivery. This expression level is comparable to that of other plant-expressed mAbs driven by the same expression vector (Jugler et al., 2021; Sun et al., 2023). However, further yield enhancement of p-H2 mAb in plants can be achieved through several strategies, such as employing improved expression vectors (Klimyuk et al., 2014) or co-expressing H2 mAb with chaperones (Margolin et al., 2020). Our results also confirm that p-H2 mAb correctly assembled into the expected IgG structure and was purified to a high degree of homogeneity, with no detectable degradation or truncation occurring during its accumulation or purification from plants. We validated the specific binding of p-H2 mAb using two distinct assays. First, we assessed its binding to the MPXV antigen on the authentic virus and found that p-H2 mAb specifically bound to MPXV-infected cells. Similarly, it bound to cells infected with VACV. To further confirm that p-H2 mAb recognizes its target antigen on MPXV EV, we conducted an ELISA using purified A35 EV antigen. The results confirmed that p-H2 mAb specifically binds to the A35 antigen, indicating proper folding and recognition of its target antigen in both purified form and on the surface of the virion. Importantly, p-H2 mAb exhibits neutralization activity against both live MPXV and VACV, with comparable potency to each other and to that reported for ECTV (Gu et al., 2022). Given that the mammalian cell-produced H2 mAb has shown significant protective efficacy against lethal VACV infection in mice (Gu et al., 2022), the similar neutralizing potency against MPXV suggests that p-H2 mAb may also be effective

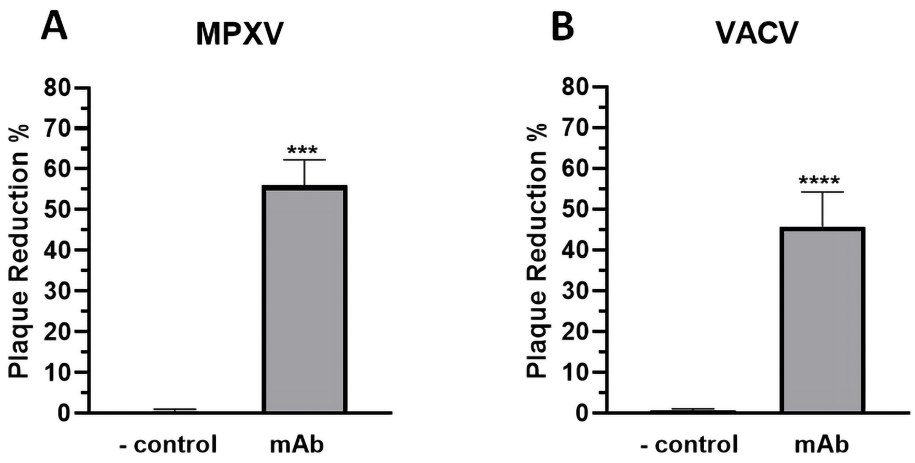

FIGURE 7
Neutralization of extracellular virion of MPXV and VACV by p-H2 mAb. EVs of MPXV **(A)** or VACV **(B)** were incubated with either PBS (negative control) or p-H2 mAb (25 µg/ml) before being added to BSC40 cells. MPXV- or VACV-infected cells were stained with crystal violet three days or two days later, respectively. Plaque numbers were counted, and plaque reduction percentage (%) was calculated. The results represent data from at least two independent experiments with technical triplicates. *** and **** indicate p values of 0.0001 and < 0.0001, respectively, from T test analysis.

in vivo as a prophylactic or therapeutic agent for preventing or treating MPXV infection.

Neutralizing MPXV EV with antibodies is challenging primarily due to the EV's additional outer lipid envelope. Studies with VACV have shown that direct antibody neutralization of EVs is inefficient even at high antibody concentrations (Vanderplasschen et al., 1998; Galmiche et al., 1999; Law and Smith, 2001; Bell et al., 2004; Viner and Isaacs, 2005). However, further studies reveal that anti-EV antibodies can provide protection through mechanisms beyond neutralization, such as Fc effector functions. For example, polyclonal antibodies against A33 and B5 have been shown to engage the complement system, eliminating VACV EVs via CDC activity through opsonization and virolysis (Lustig et al., 2004; Cohen et al., 2011). Additionally, Fc receptor engagement and ADCC activity of anti-EV antibodies have been documented (Benhnia Mohammed et al., 2009a, Benhnia Mohammed et al., 2009b; Cohen et al., 2011). Given that Fc effector functions depend on the N-glycosylation of the antibody's Fc domain (Kellner et al., 2017; Steffen et al., 2020), this evidence suggests that our plant-based system may provide an opportunity to enhance the efficacy of anti-MPXV EV mAbs. Plant glycoengineering has enabled the production of mAbs with a homogeneous N-glycosylation profile, a level of uniformity that current mammalian-cell-based systems cannot achieve (Chen, 2016). Since p-H2 mAb was produced in the glycoengineered GnGn plant line, it is expected to exhibit the same uniform GnGn N-glycosylation structure as other mAbs produced in this line of *N. benthamiana* (Jugler et al., 2022a, Jugler et al., 2023; Sun et al., 2023). Afucosylated GnGn glycoforms have been shown to enhance CDC and ADCC activity via increased binding to Fc-gamma receptors (Sun et al., 2019; Yu et al., 2021; Yang et al., 2023). Thus, p-H2 mAb may offer additional mechanisms of MPXV elimination *in vivo* in addition to neutralization, supporting the hypothesis that p-H2 mAb might have better *in vivo* efficacy compared to mammalian cell-produced H2 mAb due to enhanced Fc effector functions. While plant host engineering has produced plant lines with several advantages over mammalian systems for producing mAbs with defined human N-glycans, challenges remain. One such challenge is underglycosylation, which is occasionally observed in plant-produced IgGs (Chen, 2016). This issue can be addressed by co-expressing oligosaccharyltransferases—enzymes that transfer preassembled oligosaccharides to polypeptides in the endoplasmic reticulum (Chen, 2016). Additionally, as a relatively new production platform, there has been uncertainty regarding regulatory hurdles in approving glycoprotein biologics made in plants. Fortunately, results from human clinical trials of plant-made glycoproteins have shown that they are not particularly immunogenic, and even the presence of plant-specific glycans does not induce any unwanted side effects (Shaaltiel and Tekoah, 2016; Rup et al., 2017).

This study is the first to report the development of an anti-EV mAb in plants for preventing and treating MPXV infection, as well as the first demonstration of anti-MPXV EV activity by an mAb across any production platform. In the next phase of the study, we plan to perform comparative analyses of the CDC and ADCC activities of various H2 mAb glycovariants, including those produced in mammalian cells, and assess their efficacy in animal models. These studies will provide valuable insights into the full potential of plant-produced H2 mAb. It would also be worthwhile to investigate potential synergistic effects with a therapeutic cocktail comprising p-H2 anti-EV mAb and anti-MV mAb against MPXV. These analyses could provide valuable insights into how different viral proteins dictate the requirements for the host to eliminate the virus using various mechanisms and how Fc effector functions contribute to protection *in vivo*. As H2 mAb was isolated from a volunteer vaccinated with the VARV vaccine and has demonstrated inhibitory activity against both VACV and ECTV, our findings on its activity against MPXV further expand its effectiveness against another orthopoxvirus, supporting its potential as a broad-spectrum, pan-orthopoxvirus therapeutic. In August of 2024, the WHO re-declared that the MPXV epidemic a Public Health Emergency of International Concern. As MPXV outbreaks continue, up to 90% of cases occur in people with human immunodeficiency virus (HIV) (Saldana et al., 2023), who experience in more severe symptoms than those without HIV (Chastain et al., 2023). Therefore, it is crucial to monitor emerging mutants and quickly develop effective therapeutics against them. We propose that the plant-based system may be one of the best platforms to rapidly develop therapeutic mAbs that maintain efficacy against potential mutants via Fc effector functions and quickly screen for mAb cocktails with synergistic interactions. In summary, this study demonstrates the potential of using anti-EV mAbs as therapeutics against MPXV infection and highlights the utility of plant biotechnology in developing biologics against viral infections.

Data availability statement

The original contributions presented in the study are included in the article/Supplementary Material. Further inquiries can be directed to the corresponding author/s.

Author contributions

JM: Writing – original draft, Methodology, Investigation, Formal analysis, Data curation. HS: Writing – review & editing, Supervision, Methodology, Investigation, Formal analysis, Data curation. JB: Writing – review & editing, Methodology, Investigation, Formal analysis, Data curation. QC: Writing – original draft, Supervision, Funding acquisition, Conceptualization.

Funding

The author(s) declare financial support was received for the research, authorship, and/or publication of this article. This research was supported in part by a grant (FP00019102) from Greenbio to QC.

Acknowledgments

The authors would like to thank Dr. Herta Steinkellner at the University of Natural Resources and Life Sciences, Vienna (BOKU),

for providing the seeds of the GnGn plant line. Additionally, we acknowledge Daniel Tran for his assistance with the maintenance of *N. benthamiana*.

Conflict of interest

The authors have no conflicts of interest to disclose concerning this manuscript. Q.C is a shareholder of Greenbio, a biotechnology company. However, he has no conflict of interest pertaining to the research conducted or the results discussed in this article.

The author(s) declared that they were an editorial board member of Frontiers, at the time of submission. This had no impact on the peer review process and the final decision.

Publisher's note

Supplementary material

The Supplementary Material for this article can be found online at: https://www.frontiersin.org/articles/10.3389/fpls.2024.1481452/full#supplementary-material

References

Arndt, W. D., White, S. D., Johnson, B. P., Huynh, T., Liao, J., Harrington, H., et al. (2016). Monkeypox virus induces the synthesis of less dsRNA than vaccinia virus, and is more resistant to the anti-poxvirus drug, IBT, than vaccinia virus. *Virology* 497, 125–135. doi: 10.1016/j.virol.2016.07.016

Bell, E., Shamim, M., Whitbeck, J. C., Sfyroera, G., Lambris, J. D., and Isaacs, S. N. (2004). Antibodies against the extracellular enveloped virus B5R protein are mainly responsible for the EEV neutralizing capacity of vaccinia immune globulin. *Virology* 325, 425–431. doi: 10.1016/j.virol.2004.05.004

Belyakov, I. M., Earl, P., Dzutsev, A., Kuznetsov, V. A., Lemon, M., Wyatt, L. S., et al. (2003). Shared modes of protection against poxvirus infection by attenuated and conventional smallpox vaccine viruses. *Proc. Natl. Acad. Sci.* 100, 9458–9463. doi: 10.1073/pnas.1233578100

Benhnia Mohammed, R.-E.-I., Mccausland Megan, M., Laudenslager, J., Granger Steven, W., Rickert, S., Koriazova, L., et al. (2009a). Heavily isotype-dependent protective activities of human antibodies against vaccinia virus extracellular virion antigen B5. *J. Virol.* 83, 12355–12367. doi: 10.1128/JVI.01593-09

Benhnia Mohammed, R.-E.-I., Mccausland Megan, M., Moyron, J., Laudenslager, J., Granger, S., Rickert, S., et al. (2009b). Vaccinia virus extracellular enveloped virion neutralization *in vitro* and protection *in vivo* depend on complement. *J. Virol.* 83, 1201–1215. doi: 10.1128/JVI.01797-08

Chastain, D. B., Motoa, G., Ortiz-Martínez, Y., Gharamti, A., and Henao-Martínez, A. F. (2023). Characteristics and clinical manifestations of monkeypox among people with and without HIV in the United States: a retrospective cohort. *Aids* 37, 611–616. doi: 10.1097/QAD.0000000000003449

Chen, Q. (2011). "Expression and manufacture of pharmaceutical proteins in genetically engineered horticultural plants," in *Transgenic Horticultural Crops: Challenges and Opportunities - Essays by Experts*. Eds. B. Mou and R. Scorza (Taylor & Francis, Boca Raton), 83–124.

Chen, Q. (2016). Glycoengineering of plants yields glycoproteins with polysialylation and other defined N-glycoforms. *Proc. Natl. Acad. Sci.* 113, 9404–9406. doi: 10.1073/pnas.1610803113

Chen, Q. (2022). Development of plant-made monoclonal antibodies against viral infections. *Curr. Opin. Virol.* 52, 148–160. doi: 10.1016/j.coviro.2021.12.005

Chen, Q., and Davis, K. (2016). The potential of plants as a system for the development and production of human biologics. *F1000Research* 5. doi: 10.12688/f11000research.18010.12681

Chen, Q., and Lai, H. (2014). Gene delivery into plant cells for recombinant protein production. *BioMed. Res. Int.* 2014, 10. doi: 10.1155/2015/932161

Cohen, M. E., Xiao, Y., Eisenberg, R. J., Cohen, G. H., and Isaacs, S. N. (2011). Antibody against extracellular vaccinia virus (EV) protects mice through complement and Fc receptors. *PLoS One* 6, e20597. doi: 10.1371/journal.pone.0020597

Dahodwala, H., and Lee, K. H. (2019). The fickle CHO: a review of the causes, implications, and potential alleviation of the CHO cell line instability problem. *Curr. Opin. Biotechnol.* 60, 128–137. doi: 10.1016/j.copbio.2019.01.011

Denzler, K. L., Schriewer, J., Parker, S., Werner, C., Hartzler, H., Hembrador, E., et al. (2011). The attenuated NYCBH vaccinia virus deleted for the immune evasion gene, E3L, completely protects mice against heterologous challenge with ectromelia virus. *Vaccine* 29, 9691–9696. doi: 10.1016/j.vaccine.2011.09.108

Edghill-Smith, Y., Golding, H., Manischewitz, J., King, L. R., Scott, D., Bray, M., et al. (2005). Smallpox vaccine-induced antibodies are necessary and sufficient for protection against monkeypox virus. *Nat. Med.* 11, 740–747. doi: 10.1038/nm1261

Eidenberger, L., Kogelmann, B., and Steinkellner, H. (2023). Plant-based biopharmaceutical engineering. *Nat. Rev. Bioengineering* 1, 426–439. doi: 10.1038/s44222-023-00044-6

Esqueda, A., and Chen, Q. (2021). Development and expression of subunit vaccines against viruses in plants. *Methods Mol. Biol.* 2225, 25–38. doi: 10.1007/978-1-0716-1012-1_2

Esqueda, A., and Chen, Q. (2023). "Producing biologics with defined N-glycosylation in plants," in *Chemokine-Glycosaminoglycan Interactions: Methods and Protocols*. Ed. A. R. Lucas (Springer US, New York, NY), 235–250.

Esqueda, A., Sun, H., Bonner, J., Lai, H., Jugler, C., Kibler, K. V., et al. (2023). A monoclonal antibody produced in glycoengineered plants potently neutralizes monkeypox virus. *Vaccines* 11, 1179. doi: 10.3390/vaccines11071179

Fang, M., Cheng, H., Dai, Z., Bu, Z., and Sigal, L. J. (2006). Immunization with a single extracellular enveloped virus protein produced in bacteria provides partial protection from a lethal orthopoxvirus infection in a natural host. *Virology* 345, 231–243. doi: 10.1016/j.virol.2005.09.056

Fulton, A., Lai, H., Chen, Q., and Zhang, C. (2015). Purification of monoclonal antibody against Ebola GP1 protein expressed in Nicotiana benthamiana. *J. Chromatogr. A* 1389, 128–132. doi: 10.1016/j.chroma.2015.02.013

Galmiche, M. C., Goenaga, J., Wittek, R., and Rindisbacher, L. (1999). Neutralizing and protective antibodies directed against vaccinia virus envelope antigens. *Virology* 254, 71–80. doi: 10.1006/viro.1998.9516

Giritch, A., Marillonnet, S., Engler, C., Van Eldik, G., Botterman, J., Klimyuk, V., et al. (2006). Rapid high-yield expression of full-size IgG antibodies in plants coinfected with noncompeting viral vectors. *Proc. Natl. Acad. Sci. United States America* 103, 14701–14706. doi: 10.1073/pnas.0606631103

Goulet, M.-C., Gaudreau, L., Gagné, M., Maltais, A.-M., Laliberté, A.-C., Éthier, G., et al. (2019). Production of biopharmaceuticals in nicotiana benthamiana—Axillary stem growth as a key determinant of total protein yield. *Front. Plant Sci.* 10. doi: 10.3389/fpls.2019.00735

Gruber, M. F. (2022). Current status of monkeypox vaccines. *NPJ Vaccines* 7, 94. doi: 10.1038/s41541-022-00527-4

Gu, X., Zhang, Y., Jiang, W., Wang, D., Lu, J., Gu, G., et al. (2022). Protective human anti-poxvirus monoclonal antibodies are generated from rare memory B cells isolated by multicolor antigen tetramers. *Vaccines (Basel)* 10. doi: 10.3390/vaccines10071084

Jentarra, G. M., Heck, M. C., Youn, J. W., Kibler, K., Langland, J. O., Baskin, C. R., et al. (2008). Vaccinia viruses with mutations in the E3L gene as potential replication-competent, attenuated vaccines: Scarification vaccination. *Vaccine* 26, 2860–2872. doi: 10.1016/j.vaccine.2008.03.044

Jugler, C., Grill, F. J., Eidenberger, L., Karr, T. L., Grys, T. E., Steinkellner, H., et al. (2022a). Humanization and expression of IgG and IgM antibodies in plants as potential diagnostic reagents for Valley Fever. *Front. Plant Sci.* 13. doi: 10.3389/fpls.2022.925008

Jugler, C., Joensuu, J., and Chen, Q. (2020). Hydrophobin-protein A fusion protein produced in plants efficiently purified an anti-west nile virus monoclonal antibody from plant extracts via aqueous two-phase separation. *Int. J. Mol. Sci.* 21, 2140. doi: 10.3390/ijms21062140

Jugler, C., Sun, H., and Chen, Q. (2021). SARS-CoV-2 spike protein-induced interleukin 6 signaling is blocked by a plant-produced anti-interleukin 6 receptor monoclonal antibody. *Vaccines* 9, 1365. doi: 10.3390/vaccines9111365

Jugler, C., Sun, H., Grill, F., Kibler, K., Esqueda, A., Lai, H., et al. (2022b). Potential for a plant-made SARS-CoV-2 neutralizing monoclonal antibody as a synergetic cocktail component. *Vaccines* 10. doi: 10.3390/vaccines10050772

Jugler, C., Sun, H., Nguyen, K., Palt, R., Felder, M., Steinkellner, H., et al. (2023). A novel plant-made monoclonal antibody enhances the synergetic potency of an antibody cocktail against the SARS-CoV-2 Omicron variant. *Plant Biotechnol. J.* 21, 549–559. doi: 10.1111/pbi.13970

Kellner, C., Otte, A., Cappuzzello, E., Klausz, K., and Peipp, M. (2017). Modulating cytotoxic effector functions by fc engineering to improve cancer therapy. *Transfus Med. Hemother* 44, 327–336. doi: 10.1159/000479980

Klimyuk, V., Pogue, G., Herz, S., Butler, J., and Haydon, H. (2014). Production of recombinant antigens and antibodies in Nicotiana benthamiana using 'magnifection' technology: GMP-compliant facilities for small- and large-scale manufacturing. *Curr. Top. Microbiol. Immunol.* 375, 127–154. doi: 10.1007/82_2012_212

Lai, H., and Chen, Q. (2012). Bioprocessing of plant-derived virus-like particles of Norwalk virus capsid protein under current Good Manufacture Practice regulations. *Plant Cell Rep.* 31, 573–584. doi: 10.1007/s00299-011-1196-6

Lai, H., Engle, M., Fuchs, A., Keller, T., Johnson, S., Gorlatov, S., et al. (2010). Monoclonal antibody produced in plants efficiently treats West Nile virus infection in mice. *Proc. Natl. Acad. Sci. United States America* 107, 2419–2424. doi: 10.1073/pnas.0914503107

Lai, H., He, J., Hurtado, J., Stahnke, J., Fuchs, A., Mehlhop, E., et al. (2014). Structural and functional characterization of an anti-West Nile virus monoclonal antibody and its single-chain variant produced in glycoengineered plants. *Plant Biotechnol. J.* 12, 1098–1107. doi: 10.1111/pbi.2014.12.issue-8

Law, M., and Smith, G. L. (2001). Antibody neutralization of the extracellular enveloped form of vaccinia virus. *Virology* 280, 132–142. doi: 10.1006/viro.2000.0750

Leuzinger, K., Dent, M., Hurtado, J., Stahnke, J., Lai, H., Zhou, X., et al. (2013). Efficient agroinfiltration of plants for high-level transient expression of recombinant proteins. *J. Visualized Experiments* 77. doi: 10.3791/50521

Lum, F.-M., Torres-Ruesta, A., Tay, M. Z., Lin, R. T. P., Lye, D. C., Rénia, L., et al. (2022). Monkeypox: disease epidemiology, host immunity and clinical interventions. *Nat. Rev. Immunol.* 22, 597–613. doi: 10.1038/s41577-022-00775-4

Lustig, S., Fogg, C., Whitbeck, J. C., and Moss, B. (2004). Synergistic neutralizing activities of antibodies to outer membrane proteins of the two infectious forms of vaccinia virus in the presence of complement. *Virology* 328, 30–35. doi: 10.1016/j.virol.2004.07.024

Manes, N. P., Estep, R. D., Mottaz, H. M., Moore, R. J., Clauss, T. R., Monroe, M. E., et al. (2008). Comparative proteomics of human monkeypox and vaccinia intracellular mature and extracellular enveloped virions. *J. Proteome Res.* 7, 960–968. doi: 10.1021/pr070432+

Margolin, E., Oh, Y. J., Verbeek, M., Naude, J., Ponndorf, D., Meshcheriakova, Y. A., et al. (2020). Co-expression of human calreticulin significantly improves the production of HIV gp140 and other viral glycoproteins in plants. *Plant Biotechnol. J.* 18, 2109–2117. doi: 10.1111/pbi.v18.10

Mullard, A. (2021). FDA approves 100th monoclonal antibody product. *Nat. Rev. Drug Discovery* 20, 491–495. doi: 10.1038/d41573-021-00079-7

Nandi, S., Kwong, A. T., Holtz, B. R., Erwin, R. L., Marcel, S., and Mcdonald, K. A. (2016). Techno-economic analysis of a transient plant-based platform for monoclonal antibody production. *mAbs* 8, 1456–1466. doi: 10.1080/19420862.2016.1227901

Pantaleo, G., Correia, B., Fenwick, C., Joo, V. S., and Perez, L. (2022). Antibodies to combat viral infections: development strategies and progress. *Nat. Rev. Drug Discovery* 21, 676–696. doi: 10.1038/s41573-022-00495-3

Payne, L. G. (1980). Significance of extracellular enveloped virus in the *in vitro* and *in vivo* dissemination of vaccinia. *J. Gen. Virol.* 50, 89–100. doi: 10.1099/0022-1317-50-1-89

Perdiguero, B., and Blasco, R. (2006). Interaction between vaccinia virus extracellular virus envelope A33 and B5 glycoproteins. *J. Virol.* 80, 8763–8777. doi: 10.1128/JVI.00598-06

Roberts, K. L., and Smith, G. L. (2008). Vaccinia virus morphogenesis and dissemination. *Trends Microbiol.* 16, 472–479. doi: 10.1016/j.tim.2008.07.009

Rup, B., Alon, S., Amit-Cohen, B. C., Brill Almon, E., Chertkoff, R., Tekoah, Y., et al. (2017). Immunogenicity of glycans on biotherapeutic drugs produced in plant expression systems-The taliglucerase alfa story. *PLoS One* 12, e0186211. doi: 10.1371/journal.pone.0186211

Saldana, C. S., Kelley, C. F., Aldred, B. M., and Cantos, V. D. (2023). Mpox and HIV: a narrative review. *Curr. HIV/AIDS Rep.* 20, 261–269. doi: 10.1007/s11904-023-00661-1

Sang, Y., Zhang, Z., Liu, F., Lu, H., Yu, C., Sun, H., et al. (2023). Monkeypox virus quadrivalent mRNA vaccine induces immune response and protects against vaccinia virus. *Signal Transduction Targeted Ther.* 8, 172. doi: 10.1038/s41392-023-01432-5

Schmidt, F. I., Bleck, C. K. E., and Mercer, J. (2012). Poxvirus host cell entry. *Curr. Opin. Virol.* 2, 20–27. doi: 10.1016/j.coviro.2011.11.007

Shaaltiel, Y., and Tekoah, Y. (2016). Plant specific N-glycans do not have proven adverse effects in humans. *Nat. Biotech.* 34, 706–708. doi: 10.1038/nbt.3556

Siegrist, E. A., and Sassine, J. (2022). Antivirals with activity against mpox: A clinically oriented review. *Clin. Infect. Dis.* 76, 155–164. doi: 10.1093/cid/ciac622

Steffen, U., Koeleman, C. A., Sokolova, M. V., Bang, H., Kleyer, A., Rech, J., et al. (2020). IgA subclasses have different effector functions associated with distinct glycosylation profiles. *Nat. Commun.* 11, 120. doi: 10.1038/s41467-019-13992-8

Strasser, R., Stadlmann, J., Schahs, M., Stiegler, G., Quendler, H., Mach, L., et al. (2008). Generation of glyco-engineered Nicotiana benthamiana for the production of monoclonal antibodies with a homogeneous human-like N-glycan structure. *Plant Biotechnol. J.* 6, 392–402. doi: 10.1111/j.1467-7652.2008.00330.x

Sumit, M., Dolatshahi, S., Chu, A. A., Cote, K., Scarcelli, J. J., Marshall, J. K., et al. (2019). Dissecting N-glycosylation dynamics in chinese hamster ovary cells fed-batch cultures using time course omics analyses. *iScience* 12, 102–120. doi: 10.1016/j.isci.2019.01.006

Sun, H., Yang, M., Lai, H., Neupane, B., Teh, A. Y.-H., Jugler, C., et al. (2023). A dual-approach strategy to optimize the safety and efficacy of anti-zika virus monoclonal antibody therapeutics. *Viruses* 15, 1156. doi: 10.3390/v15051156

Sun, P., Williams, M., Nagabhushana, N., Jani, V., Defang, G., and Morrison, B. J. (2019). NK cells activated through antibody-dependent cell cytotoxicity and armed with degranulation/IFN-γ Production suppress antibody-dependent enhancement of dengue viral infection. *Sci. Rep.* 9, 1109. doi: 10.1038/s41598-018-36972-2

Tamir, H., Noy-Porat, T., Melamed, S., Cherry-Mimran, L., Barlev-Gross, M., Alcalay, R., et al. (2024). Synergistic effect of two human-like monoclonal antibodies confers protection against orthopoxvirus infection. *Nat. Commun.* 15, 3265. doi: 10.1038/s41467-024-47328-y

Vanderplasschen, A., Mathew, E., Hollinshead, M., Sim, R. B., and Smith, G. L. (1998). Extracellular enveloped vaccinia virus is resistant to complement because of incorporation of host complement control proteins into its envelope. *Proc. Natl. Acad. Sci.* 95, 7544–7549. doi: 10.1073/pnas.95.13.7544

Viner, K. M., and Isaacs, S. N. (2005). Activity of vaccinia virus-neutralizing antibody in the sera of smallpox vaccinees. *Microbes infection* 7, 579–583. doi: 10.1016/j.micinf.2005.02.004

Wang, Y., Yang, K., and Zhou, H. (2023). Immunogenic proteins and potential delivery platforms for mpox virus vaccine development: A rapid review. *Int. J. Biol. Macromolecules* 245, 125515. doi: 10.1016/j.ijbiomac.2023.125515

WHO. (2024). *2022-2024 Monkeypox Outbreak: Global Trends*. Available online at: https://worldhealthorg.shinyapps.io/mpx_global/ (Accessed October 10, 2024).

Yang, M., Dent, M., Lai, H., Sun, H., and Chen, Q. (2017). Immunization of Zika virus envelope protein domain III induces specific and neutralizing immune responses against Zika virus. *Vacccine* 35, 4287–4294. doi: 10.1016/j.vaccine.2017.04.052

Yang, M., Sun, H., Lai, H., Neupane, B., Bai, F., Steinkellner, H., et al. (2023). Plant-produced anti-zika virus monoclonal antibody glycovariant exhibits abrogated antibody-dependent enhancement of infection. *Vaccines* 11, 755. doi: 10.3390/vaccines11040755

Yefet, R., Friedel, N., Tamir, H., Polonsky, K., Mor, M., Cherry-Mimran, L., et al. (2023). Monkeypox infection elicits strong antibody and B cell response against A35R and H3L antigens. *iScience* 26, 105957. doi: 10.1016/j.isci.2023.105957

Yu, L., Liu, X., Ye, X., Su, W., Zhang, X., Deng, W., et al. (2021). Monoclonal Antibodies against Zika Virus NS1 Protein Confer Protection via Fcγ Receptor-Dependent and -Independent Pathways. *mBio* 12. doi: 10.1128/mbio.03179-03120

Zhao, R., Wu, L., Sun, J., Liu, D., Han, P., Gao, Y., et al. (2024). Two noncompeting human neutralizing antibodies targeting MPXV B6 show protective effects against orthopoxvirus infections. *Nat. Commun.* 15, 4660. doi: 10.1038/s41467-024-48312-2

frontiers | Frontiers in Plant Science

TYPE Review
PUBLISHED 24 December 2024
DOI 10.3389/fpls.2024.1502015

OPEN ACCESS

EDITED BY
Yongfeng Guo,
Tobacco Research Institute, Chinese Academy of Agricultural Sciences, China

REVIEWED BY
Ming Wang,
Chinese Academy of Sciences (CAS), China
Gothandapani Sellamuthu,
Czech University of Life Sciences Prague, Czechia

*CORRESPONDENCE
Dan Wang
wangdan_star@163.com
Dongfei Han
dongfeihan@usts.edu.cn

RECEIVED 26 September 2024
ACCEPTED 27 November 2024
PUBLISHED 24 December 2024

CITATION
Qi H-Y, Zhang D-D, Liu B, Chen J-Y, Han D and Wang D (2024) Leveraging RNA interference technology for selective and sustainable crop protection.
Front. Plant Sci. 15:1502015.
doi: 10.3389/fpls.2024.1502015

Leveraging RNA interference technology for selective and sustainable crop protection

Hong-Yue Qi[1], Dan-Dan Zhang[1,2], Binhui Liu[3], Jie-Yin Chen[1,2], Dongfei Han[4]* and Dan Wang[5]*

[1]The State Key Laboratory for Biology of Plant Diseases and Insect Pests, Institute of Plant Protection, Chinese Academy of Agricultural Sciences, Beijing, China, [2]Western Agricultural Research Center, Chinese Academy of Agricultural Sciences, Changji, China, [3]Key Laboratory of Crop Drought Resistance Research of Hebei Province/Institute of Dryland Farming, Hebei Academy of Agriculture and Forestry Sciences, Hengshui, China, [4]School of Environmental Science and Engineering, Suzhou University of Science and Technology, Suzhou, China, [5]State Key Laboratory of Subtropical Silviculture, School of Forestry and Biotechnology, Zhejiang A & F University, Hangzhou, China

Double-stranded RNA (dsRNA) has emerged as key player in gene silencing for the past two decades. Tailor-made dsRNA is now recognized a versatile raw material, suitable for a wide range of applications in biopesticide formulations, including insect control to pesticide resistance management. The mechanism of RNA interference (RNAi) acts at the messenger RNA (mRNA) level, utilizing a sequence-dependent approach that makes it unique in term of effectiveness and specificity compared to conventional agrochemicals. Two primary categories of small RNAs, known as short interfering RNAs (siRNAs) and microRNAs (miRNAs), function in both somatic and germline lineages in a broad range of eukaryotic species to regulate endogenous genes and to defend the genome from invasive nucleic acids. Furthermore, the application of RNAi in crop protection can be achieved by employing plant-incorporated protectants through plant transformation, but also by non-transformative strategies such as the use of formulations of sprayable RNAs as direct control agents, resistance factor repressors or developmental disruptors. This review explores the agricultural applications of RNAi, delving into its successes in pest-insect control and considering its broader potential for managing plant pathogens, nematodes, and pests. Additionally, the use of RNAi as a tool for addressing pesticide-resistant weeds and insects is reviewed, along with an evaluation of production costs and environmental implications.

KEYWORDS

small interfering RNA, microRNA, gene silencing, crop protection, RNA interference

1 Introduction

The phenomenon of RNA-induced gene silencing (RNAi) gained prominence following its disclosed mechanism in pests, but it was in tobacco (*Nicotiana tabacum*) plants that this phenomenon was initially documented and published as early as 1928 (Wingard, 1928). This groundbreaking discovery has revolutionized our understanding of gene regulation and its implications for various biological processes, particularly gene silencing via RNAi. Harnessing this process has shown promise in diverse applications, including gene knock down, disease treatment, and crop improvement. Over the last decade, substantial efforts have been made to exploit RNAi for the development of novel crop protection methods. Moreover, RNAi technology has facilitated the creation of genetically modified crops with enhanced traits such as increased yield, improved nutritional content, and prolonged shelf life (Kumar et al., 2020).

Sustainable agriculture entails the development and implementation of environmentally friendly technologies and practices that are readily accessible and advantageous to farmers in terms of crop improvement and productivity (Fletcher et al., 2020). To minimize the adverse effects of synthetic pesticides on health and the environment, there has been a shift towards employing bio-based alternatives. This shift aims to promote agricultural sustainability, leading to the adoption of more environmentally friendly and innovative crop protection strategies by the scientific community. Plant genetic engineering has emerged as a promising avenue to address food shortage and mitigate the impact of plant stresses. Notably, the development of transgenic crops employing advanced biotechnological techniques, including RNAi, has been a significant contribution in this regard. Transgenic RNAi crops are still regarded as GM crops. Provided that Double-stranded RNA (dsRNA)-based products contain no GM organisms (e.g., bacteria for dsRNA production), they are not regarded as genetically modified organisms (GMOs). Interestingly, recent developments using exogenous dsRNA spray to control pathogens and pests have provided a non-transgenic alternative to GMOs (Rajam, 2020; Rodrigues and Petrick, 2020). Furthermore, RNAi induces the silencing of target genes, which is more advantageous than genome editing tools (Arpaia et al., 2020). These distinctive features of RNAi have made it a popular and effective strategy for crop enhancement and protection (Arpaia et al., 2020; Rajam, 2020).

In this review, we explained the mechanism of RNAi-mediated gene silencing and furnished a comprehensive report of the role of RNAi in protecting crops against diverse biotic stresses. Furthermore, we have directed attention towards the potential of RNAi as an innovative and potent alternative for global crop protection strategy, as well as its application in the development of futuristic smart crops resilient to various biotic stresses.

2 The functional basis of RNA interference

The ability of RNAi to specifically inhibit gene expression arises from the design 21-25 bp dsRNAs, ensuring only the intended target gene is silenced. The specificity grants RNAi a wide range of potential applications for genetic studies and agriculture, including the protection of beneficial insects against viruses and parasites (San-Miguel and Scott, 2016; Mehlhorn et al., 2021), novel and highly specific insect and parasites control, and traditional plant-incorporated protectants (PIPs: i.e. transgenic plants/RNAi-based plant traits) (Walawage et al., 2013). Another crucial aspect of RNAi is its conservation across different species, indicating its versatile use in manipulating gene expression not only within an organism but also for the organism's survival and adaptation.

RNAi regulates gene expression through small noncoding RNAs (sRNAs) (Rajam, 2020) (Figure 1). These sRNAs identify the target messenger RNA (mRNA) via homology-based binding and facilitate its degradation with effector proteins. Within the RNAi pathway, there are two primary classes of sRNAs: short-interfering RNAs (siRNAs) and micro-RNAs (miRNAs) (Margis et al., 2006; Borges and Martienssen, 2015; Mamta and Rajam, 2018). While the basic pathway for sRNA biogenesis involves trimming long dsRNAs to form sRNAs, the type of sRNA present is determined by the source of the dsRNA (Parker and Barford, 2006). The application of RNA-based products for insect management requires dsRNA longer than 50 bp but not sRNAs (Ivashuta et al., 2015; Yoshida et al., 2023; Chi et al., 2023), although some studies have shown that sRNA can trigger gene silencing (Gong et al., 2013; Liu S. et al., 2021). In contrast, fungi and plants take up both dsRNAs and sRNAs (Wang and Jin, 2017; Subha et al., 2023; McLaughlin et al., 2023), suggesting different uptake mechanisms for these organisms (Wang and Jin, 2017).

siRNAs were originally observed during transgene- and virus-induced silencing in plants (Mello and Conte, 2004). They are generally formed from the dsRNA obtained from various sources, including viruses, transposons, transgenes, aberrant mRNAs, and inverted repeats (IRs), among others (Preall and Sontheimer, 2005; Matranga and Zamore, 2007; Golden et al., 2008; Wilson and Doudna, 2013). In addition to siRNAs, a multitude of miRNAs have been identified in various eukaryotes, and their sequences are available online. miRNAs are short, endogenous, single-strand RNAs, typically 21-24 nucleotides long, derived from hairpin transcripts. They play a regulatory role in gene expression in animals and plants (Bartel, 2009; Feng and Riddle, 2020). Furthermore, multiple miRNAs can regulate the same gene (Samad et al., 2021). The miRNA pathway operates at the post-transcriptional level and is involved in a range of physiological and pathophysiological processes (Ambros, 2004; Yu et al., 2017). Even though siRNAs and miRNAs were first found in separate research studies, these two small RNAs are closely connected in their biological functions, formation of RNA-protein complexes, and capacity to regulate gene transcription negatively (Meister and Tuschl, 2004). Both siRNA and miRNA molecules are initially generated from dsRNAs processed by the ribonuclease III enzyme Dicer into 20-30 nucleotide duplexes (Margis et al., 2006).

In plants, whereas for the miRNAs, the related endogenous genes are transcribed into long primary microRNAs (pri-miRNAs) under the action of RNA Polymerase II (Pol II) (Wassenegger and Krczal, 2006). These pri-miRNAs, which are single-stranded and polyadenylated RNA molecules, form hairpin-like structures.

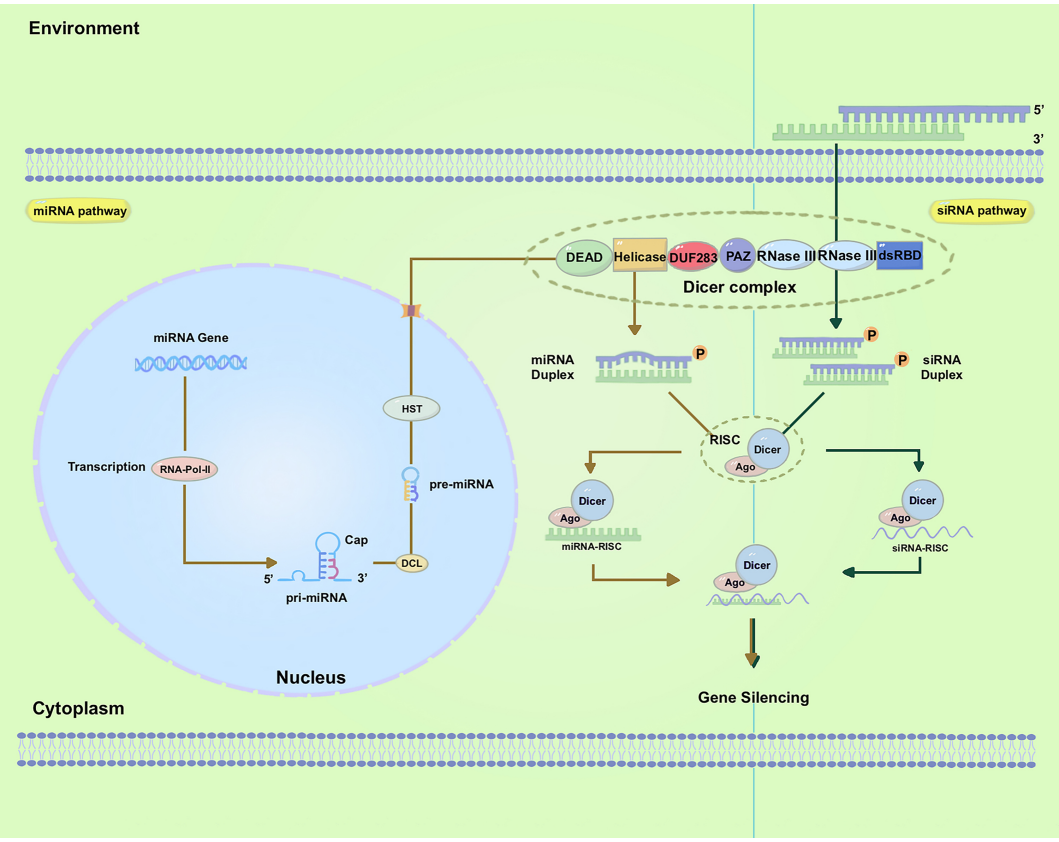

FIGURE 1
Biogenesis of small RNAs and mechanism of gene silencing. The left panel demonstrates miRNA biogenesis and gene silencing. The right panel shows siRNA biogenesis and gene silencing; Abbreviations used in the figures: dsRNA, double-stranded RNA; siRNA, small-interfering RNA; RISC, RNAi-induced silencing complex; mRNA, messenger RNA; AGO, Argonaute; RNA Pol II, RNA polymerase II; PAZ, PIWI/ARGONAUTE/ZWILLE; DUF283, domain of unknown function 283; dsRBD, dsRNA-binding domain; pre-miRNAs, precursor microRNAs; HST, HASTY.

Dicer-Like1 (DCL1) cleaves the pri-miRNAs, generating precursor microRNAs (pre-miRNAs) which undergo further processing by DCL1 (Zotti and Smagghe, 2015). This leads to the production of mature miRNA duplexes consisting of the active miRNA strand and its complementary strand miRNA*. The pre-miRNAs are subsequently transported to the cytoplasm through HASTY (HST), the ortholog of human exportin-5, where they undergo further processing by the cytoplasmic RNase III Dicer to produce approximately 22-nucleotide miRNAs duplexes (Figure 1, Left). The export of pre-miRNAs is facilitated by HST (Cambiagno et al., 2021).

For siRNAs, these RNAi-triggering dsRNAs are formed in the nucleus through several mechanisms (Figure 1, Right). The 21/22-nt sRNAs are primarily associated with mRNA cleavage and are involved in posttranscriptional gene silencing (PTGS) (Hamilton and Baulcombe, 1999). The 24-nt sRNAs are primarily associated with RNA-directed DNA methylation (RdDM) and transcriptional gene silencing (Henderson et al., 2006; Hamilton et al., 2015). Both metazoan and plant Dicer-Like proteins display domains such as DEAD-box, helicase-C, domain of unknown function 283 (DUF283), PIWI/Argonaute/Zwille (PAZ), RNase-III, and dsRNA-binding domain (dsRBD) domains (Parker et al., 2005). These sRNAs, which consist of 21-24 nucleotide duplexes, are subsequently incorporated into the RNA-induced silencing complex (RISC). With the RISC, they undergo unwinding (Borges and Martienssen, 2015). Following this step, an Argonaute (AGO) protein cleaves the passenger (sense) strand, while retaining the guide (antisense) strand within RISC (Kedde et al., 2007; Ketting, 2011; Gong, 2021). The guide strand of the sRNA then directs RISC to target mRNA through Watson-Crick base pairing, resulting in the cleavage of the target mRNA by the AGO protein and subsequent degradation. This degradation of the target mRNA leads to specific post-transcriptional gene silencing (Huvenne and Smagghe, 2010; Borges and Martienssen, 2015; Tyagi et al., 2019; Kaur et al., 2020). The AGO protein Nrde-3, which is necessary for nuclear RNAi in *Caenorhabditis elegans*, was identified through a genetic screen and found to reside in the cytoplasm until siRNA binding induced its translocation to the nucleus (Guang et al., 2008). The dynamic localization of RNAi factors suggests a highly regulated and adaptable system for gene regulation in cells, allowing for efficient targeting and silencing of specific genes or transcripts.

Beyond these classical miRNAs and siRNAs, other classes of RNA are continually being discovered, participating in a wide range of pathways and regulatory mechanisms. Recent research has uncovered further intricacies within the RNAi machinery. For example, the involvement of long non-coding RNAs (lncRNAs)

in plant immunity, the mechanisms of lncRNA action in various stages of immunity, and different interactions between plants, microbes and insects (Wu et al., 2020; Statello et al., 2020). Additionally, a study found that aphids translocated a lncRNA into plants, which functioned as lncRNA virulence factors by enhancing aphid fecundity (Chen et al., 2020).

3 RNAi application in crop protection

The RNAi mechanism operates at the mRNA level through a sequence-dependent mode of action, rendering it unique in potency and selectivity compared to regular agrochemicals. One advantage of RNAi, whether through transformative or non-transformative approaches, is its potential to enable farmers to target pathogens, nematodes, and pests more specifically. The technology can be designed by using RNA sequences that match specific gene sequences in the target pathogens, nematodes, and pests, thereby minimizing harm to other species. Careful selection of unique regions of insect genes results in highly targeted effects, while avoiding unintended consequences. RNAi in crop protection can be achieved through plant transformation via PIPs, such as transgenic plants, or through non-transformative strategies employing a spray-induced gene silencing (SIGS) process. Exogenously applied dsRNA can be taken up by two means: pathogenic cells directly uptake dsRNAs to evoke RNAi in pathogens. On the other hand, exogenously applied dsRNAs can be taken up by plant cells and then transferred to interacting pathogens to induce RNAi responses. Irrespective of the delivery strategy, the use of RNA-based products to provide plant protection against pests and pathogens represents a potential alternative to conventional pesticides. Moreover, these dsRNAs can function as resistance repressors for resistant insect and weed strains. In this category of non-PIPs, dsRNA-containing end-use products (dsRNA-EPs) are anticipated to enter the market in four categories: (i) direct control agents; (ii) resistance factor repressors; (iii) development disruptors; and (iv) growth enhancers (Zotti and Smagghe, 2015; San-Miguel and Scott, 2016). This review will focus exclusively on developments related to crop protection (Figure 2).

The RNAi strategy, known as host-induced gene silencing (HIGS), has been successfully employed in transgenic plants to protect crops from specific insects (Head et al., 2017; Rodriguez Coy et al., 2022; Darlington et al., 2022), plant pathogens (Ray et al., 2022; McLaughlin et al., 2023), viruses (Tenllado and Díaz-Ruíz, 2001; Khalid et al., 2017), and nematodes (Sikandar et al., 2021; Morozov et al., 2019), as reviewed recently. The use of transgene-expressed dsRNA for inducing virus resistance and gene silencing in plants has proven to be effective against various viral infections and pests (Waterhouse et al., 1998). Scientists have successfully enhanced the natural defenses of plants by targeting specific genes involved in pathogen defense or insect resistance pathways, thus eliminating the need for chemical pesticides. However, approval from various regulatory agencies is required for crops that express dsRNA due to laws and regulations concerning genetically modified organisms. These factors complicate broader applications of HIGS worldwide, despite undeniable practicality and efficiency of HIGS strategies. Furthermore, the spray application of exogenous dsRNA or sRNA has initiated an era of RNAi-based fungicide strategies for controlling crop disease (Wang and Jin, 2017; Islam and Sherif, 2020). Table 1 summarizes some examples of successful application of HIGS and SIGS through RNAi-based approaches in insects or fungi.

Research efforts are underway to explore non-transformative approaches to control insects, diseases, nematodes, and weeds. It is anticipated that RNAi-based products will soon be available on the market as sprays for foliar application, trunk injection, root dipping, or seed treatment to directly employ as controlling agents. Since the discovery of RNAi and its regulatory potential, scientists have been investigating diverse applications of this powerful tool in insect control. The immense potential of RNAi lies in its capacity to selectively target and suppress genes responsible for insect survival and reproduction. An important advantage of utilizing RNAi in insect control is its distinct mode of action in comparison to traditional chemical pesticides (Kupferschmidt, 2013; Cagliari et al., 2019). RNAi-based products can be designed to selectively target particular pests while sparing non-target species. This targeted approach not only minimizes environmental impact but also mitigates the risk of pest resistance development.

dsRNA-based products, such as RNAi therapeutics or RNAi-based pesticides, utilize this mechanism to selectively suppress disease-causing genes or pest-specific genes. By designing dsRNA molecules that are complementary to the target gene's mRNA, researchers can effectively shut down the expression of the target gene, potentially leading to the treatment of genetic disorders or enhanced crop protection. One of the earliest studies in the use of sprayable RNA molecules to control insect pests involved the application of siRNA, which led to effective RNAi silencing in the diamondback moth (*Plutella xylostella*). When larvae were fed with *Brassica* spp. leaves sprayed with chemically synthesized siRNAs targeting the acetylcholine esterase gene *AchE2*, mortality rates of about 60% were observed (Gong et al., 2013).

Moreover, the use of RNA to target pathogen resistance to conventional fungicides is currently in development (Song et al., 2018). *Botrytis cinerea* transfers small RNAs into plant cells, which then bind to the plant's AGO1 to suppress host genes essential for plant immunity (Weiberg et al., 2013). This application is sprayed onto the surface of fruits (such as tomato, strawberry, and grape), and vegetables (such as lettuce and onion), resulting in a significant inhibition of grey mold disease development (Wang et al., 2016).

Recent advances in nanoparticle technology have significantly improved the potential applications for plant protection. To address issues related to dsRNA stability, double-layered hydroxide (LDH) nanoparticles were developed and combined with dsRNA molecules to produce "BioClay" (Mitter et al., 2017; Dubrovina and Kiselev, 2019; Yong et al., 2021; Jha et al., 2023). Nanoparticles are particles with diameters ranging from 1 to 100 nanometres (nm), with high stability and transport in plants (Cheng et al., 2024). LDH also degrades safely under mildly acidic conditions, thereby minimizing risk of the excessive persistence of dsRNA in the environment (Abd El-Monaem et al., 2023). Foliar spraying of LDH-dsRNA could disrupt *Bemisia tabaci* at multiple whitefly developmental stages by enhancing the delivery of dsRNA to cotton leaves (Jain et al., 2022).

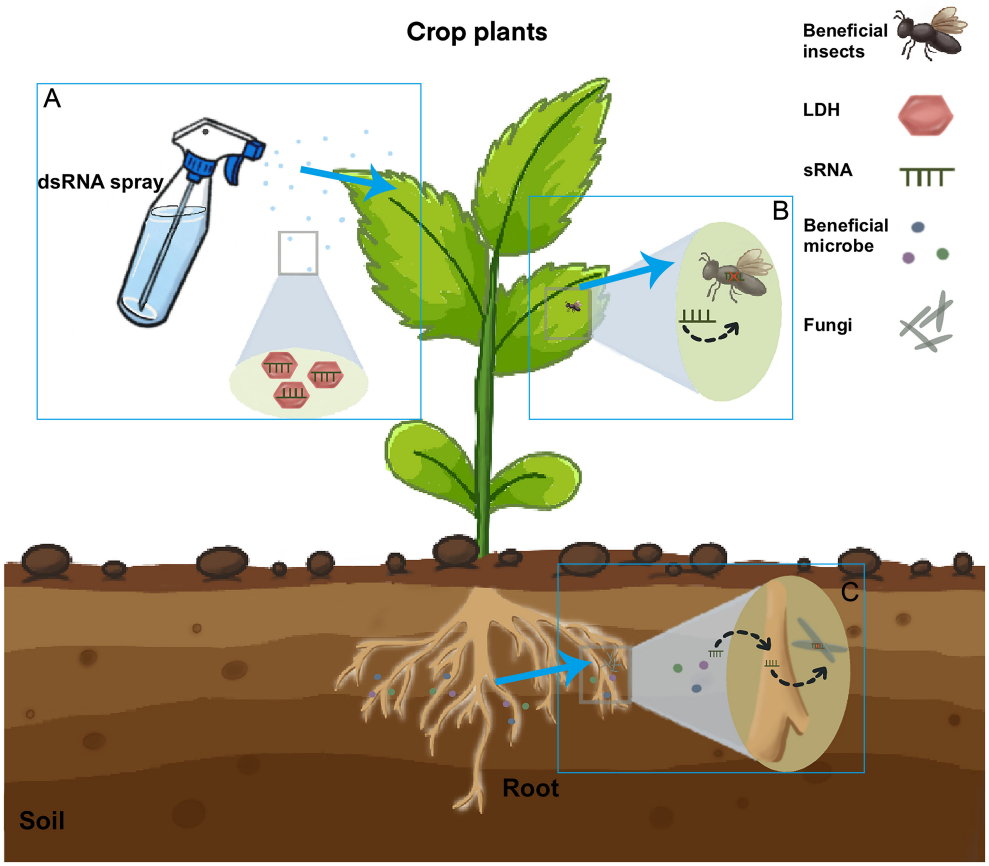

FIGURE 2
The pathway of silencing insect and fungal genes induced by sprays of sRNAs. Insects and fungi directly take up sprayed RNAs. Externally applied sRNAs are taken up by plant cells **(A)** and then transferred into insect **(B)** or Fungal cells **(C)**. In beneficial microbe process, the sRNA from the beneficial microbe would be first transferred to the host plant and then to the pathogen (Wen et al., 2023). sRNAs can be loaded onto layered double hydroxide (LDH) clay nanosheets, which are designer, non-toxic, degradable, and layered. Once loaded, the dsRNA remains on the LDH and exhibits sustained release. LDH has been developed to increase sprayed RNA stability and target delivery. Current RNA spray applications are based on mature small RNAs for spray-induced gene silencing against fungal pathogens. RNAi is also efficient for the control of plant pathogens (Joga et al., 2016). RNAi-based products can be used to suppress virus infection in pests either by administering a sugar water solution containing dsRNA or through large-scale field treatments. Future applications may be extended to mRNAs to produce inhibiting peptides inside fungi and pests.

Additionally, optimizing nanostructures for agricultural use enhances the stability of RNA-based treatments, boosting control effectiveness and minimizing environmental impact (Wang et al., 2023).

Up to now, RNA-based molecules (dsRNA or siRNA) commonly utilized in insect and disease management studies have been expensive synthetic molecules or have been produced through time-consuming, laborious procedures. To address the limitations of these methods, the potential of delivering dsRNA expressed in bacteria has been investigated, providing an alternative method for large-scale target gene screening. For instance, the *Escherichia coli* HT115 (DE3) strain has been used to produce large quantities of dsRNA due to its lack of the enzyme RNase III which degrades dsRNA (Ahn et al., 2019; Figueiredo-Prates et al., 2023). Nanomaterials derived from plant viruses offer a promising alternative to synthetic nanoparticles. Unlike synthetic nanoparticles, plant viruses offer a higher environmental biocompatibility and degradability, yet they are exceptionally robust in the harsh environment. And most importantly, they are non-infections to mammals. Indeed, some of the most widely used plant viruses have been cowpea mosaic virus (CPMV) (Beatty and Lewis, 2019; Ortega-Rivera et al., 2021) and tobacco mild green mosaic virus (TMGMV) (Caparco et al., 2023). Practical applications of RNAi have rapidly advanced with transgene-expressed dsRNA employed not only for inducing virus resistance and gene silencing in plants but also for enhancing crop traits such as yield improvement and nutritional enhancement. Although the precise mechanism of external RNA recognition, uptake, and transport is yet to be determined, recent studies demonstrated that exogenous RNA application is a promising strategy for the regulation of plant properties, indicating the need for further research.

4 Overcome barriers to foliar uptake of sRNAs

Indeed, efficient methods to facilitate the uptake of exogenous dsRNA for RNAi-mediated crop protection are essential for practical applications. In recent years, there has been a growing

10.3389/fpls.2024.1502015

TABLE 1 Examples of RNA-mediated gene silencing in phytopathogenic fungi/pests via different applications to plants.

Croup	Target Organism	Target Gene(s)	Species	Application Method	Silencing Outcome	Reference
Insects	*Radopholus similis*	*Chs-2, Unc-87, Pat-10, Eng1a*	Banana	Host induced gene silencing via transgenic plants)	Reduction in nematode multiplication and root damage	Mwaka et al., 2023
	Helicoverpa armigera	Chitinase	Tomato and tobacco		Detrimental effects on larval growth and survival	Mamta et al., 2016
	Bemisia tabaci	*Trehalose-6-phosphate synthase 1 and 2*	*Nicotiana tabacum*		90% mortality and decreased the fecundity in whitefly adults	Gong et al., 2022
	Myzus persicae	*ATPD, ATPG*	Oilseed rape	Spraying	nanocarrier-delivered RNA pesticides affected insect survival	Ma et al., 2023
	Sogatella furcifera	Vacuolar-type (H+)-ATPase	Rice		More than 97% insect mortality	Ma et al., 2024
	Sitobian avenae	Salivary sheath protein	*Hordeum vulgare*		60% reduction in disease resistance	Biedenkopf et al., 2020
Fungi	*Aspergillus flavus*	*Alk*	Maize	Host induced gene silencing via transgenic plants)	84% reduction in aflatoxin accumulation and reduced fungal biomass	Omolehin et al., 2021
	Fusarium oxysporum	*Chs*	Soybean		Reduction in lesion size & fungal biomass	Kong et al., 2022
	Fusarium graminearum	*SGE1, PP1, STE12*	Wheat		Reduction in fungal infection structures, inhibition of DON biosynthesis	Wang et al., 2020
	Magnaporthe oryzae	*DES1*	Rice	Spraying	25-60% reduction in disease symptoms	Sarkar and Roy-Barman, 2021
	Sclerotinia sclerotiorum	*VPS51, DCTN1, SAC1, DCL1, DCL2*	Lettuce Collard green		Reduction in disease symptoms and lesion size	Qiao et al., 2021
	Botryotiania fuckeliana	*Chitin synthase class III, DCL 1, DCL2*	*Fragaria ananassa*		75% reduction in biomass accumulation	Islam et al., 2021

interest in the market for dsRNA, promoting both established companies and startups to focus on enhancing production efficiency and developing stable delivery systems. With the potential of dsRNA for crop protection, many companies and academic researchers are exploring cost-efficient methods for large-scale dsRNA production. It is speculated that externally applied synthetic dsRNA and siRNA may enter plant tissues and cells through natural mechanisms similar to those used by extracellular nucleic acids from plant microbial pathogens, insects, or viruses (Tatematsu et al., 2018; Dubrovina and Kiselev, 2019; Dad et al., 2021; Liu G. et al., 2021). However, the existing literature offers limited insight into the natural mechanisms responsible for the recognition, uptake, and translocation of exogenous nucleic acids in plant tissues.

Environmental risks associated with chemical and microbial pesticides are typically evaluated using a tiered approach (Pathak et al., 2022). This approach often involves testing the maximum hazard dose of known environmental exposure concentration using non-target indicator species from different ecological guilds such as pollinators, predators, and parasitoids (Lundgren and Duan, 2013). Predicting toxic effects and designing maximum hazard assays for the numerous potentially exposed organisms is a challenging task. It has been reported that foliar applied transgene-encoding dsRNA was detectable in RNA probes obtained from treated *Arabidopsis* leaves at 1 day and 7 days post-treatment, but its presence sharply decreased after 14 days (Lundgren and Duan, 2013). The "RNAgri" agricultural industry has developed microbial fermentation technology for large-scale production of dsRNA, utilizing a protein to bind the desired RNAs and protect them against degradation. The resulting dsRNA products are considered safer to use and more stable than naked dsRNA (Numata et al., 2014). Additionally, bacterial minicells have shown promise as a technology for both the production and encapsulation of dsRNA (Islam et al., 2021). If successful, this technology could provide improved shielding and slow, sustained release of dsRNA for agricultural purposes under open-field conditions. It is important to note that siRNAs might exhibit off-target binding in the genome of non-target species. However, considerations for microbial production of dsRNA include potential by-products from fermentation and the additional concern of GMOs (Figueiredo-Prates et al., 2023). In addition to the standard quality control measures aimed at ensuring dsRNA purity, bacterial production

systems require meticulous attention to exclude potential contaminants and living GMOs. Longer dsRNA (>200 nt) yields many siRNAs after cleavage, enhancing RNAi response and reducing resistance (Darlington et al., 2022). Transgenic plants, with continuous dsRNA, increase selection pressure and resistance. RNAi resistance may come from reduced cellular uptake (Khajuria et al., 2018), mRNA mutations, RNAi suppressor production (Tayler et al., 2019), target gene overexpression, silencing machinery gene downregulation (Timani et al., 2023), increased nuclease activity, or behavioral changes (Spit et al., 2017; Kadoić-Balaško et al., 2020). Recently, cell-free platforms for dsRNA synthesis have been established, allowing for cost-effective, GMO-free production of significant quantities of dsRNA suitable for use in agricultural applications. The efficiency of RNAi naturally varies among the target species, life stage, and delivery strategy. Choosing appropriate combination of these factors can significantly expedite research and conservation of resources. Regardless of the delivery strategy or target species, the successful implementation of a non-transformative RNAi strategy hinges on the identification of unique regions within essential target genes. This ensure that even minor changes in expression levels will elicit substantial consequences.

4.1 Uptake efficiency

Broad translational success of RNAi technology depends on effective delivery approaches. In order to access the plant RNAi machinery for small RNA production, dsRNA needs to penetrate the cytoplasm. The plasma membrane, composed of different components than the cell wall, serves as a highly selective barrier that restricts the entry of extracellular particles.

The cell membrane is a negatively charged lipid bilayer with transmembrane channels and transporters that regulate the movement of small molecules across membranes through active transport, osmosis, and diffusion. Recent reports emphasize the importance of extracellular vesicles (EVs) in facilitating the transport of various plant defense and virulence factors between the plant and the pathogen (Bahar et al., 2016; Mordukhovich and Bahar, 2017; Yang et al., 2020; Tran et al., 2022). EVs are heterogenous phospholipid bilayer membrane-bound spherical structures that carry biologically active cargo such as liposomes, proteins, and nucleic acids (Liu G. et al., 2021). They have been implicated in cell-to-cell communication and biomolecules transfer (Colombo et al., 2014; Mathieu et al., 2019; Gurunathan et al., 2021). The topical application of exogenous nanoparticle-dsRNA complexes on plants can also improve the absorption efficiency of dsRNA into pathogens. Recent advances in RNA-based products have utilized liposomes and synthetic spherical lipid-based nanoparticles for sRNA delivery (Yan et al., 2021; Komarova et al., 2023; Qiao et al., 2023).

4.2 Stability on plant surfaces

RNAi efficacy is impacted by the persistence and stability of topically applied dsRNA before entering the plant. As foliar uptake of dsRNA is not instant, longer leaf-surface retention ensures a stable supply of dsRNA. Environmental elements such as rain, ultraviolet (UV) radiation, and microbial degradation can degrade dsRNA and diminish its effectiveness. Therefore, the development of a delivery system that shields dsRNA from degradation is crucial for practical field applications. Recent studies have revealed that formulating dsRNA with nanocarriers can protect it from UV and nuclease degradation (Schwartz et al., 2020; Zhang et al., 2022; Ijaz et al., 2023). Additionally, the use of nanoparticles has also demonstrated increased persistence of sprayed dsRNA on leaf surfaces even after rinsing (Vatanparast and Kim, 2017; Nitnavare et al., 2021). These approaches showed that when dsRNA is complexed with layered BioClay, it tends to remain on leaves, while unprotected dsRNA is readily washed off. Furthermore, nanoparticles have the potential to improve foliar and cellular uptake of sprayed dsRNA (Golestanipour et al., 2018; Wu et al., 2023; Mat-Jalaluddin et al., 2023). For instance, it has been demonstrated that BioClay delivered dsRNA can prolong protection against *B. cinerea* on tomato leaves and fruit, as well as on mature chickpea plants (Niño-Sánchez et al., 2022). Specifically, BioClay increased the protection duration from 1 to 3 weeks on tomato leaves and from 5 to 10 days on tomato fruits when compared with naked dsRNA.

In summary, while RNAi as a foliar spray exhibits potential for insect control, there are challenges to be addressed for successful field applications. Continued research and development efforts are essential to overcome these challenges and fully harness the potential of this technology in agriculture.

4.3 Delivery scalability

Nanotechnology-mediated RNAi provides new approaches for the control strategies of plant diseases and insect pests. Delivery scalability must be considered when dsRNA is exogenously applied to crops. Utilizing RNAi as a foliar spray in large-scale agricultural fields necessitates efficient and cost-effective delivery systems. The successful cellular uptake and subsequent initiation of target gene silencing by exogenous dsRNA are influenced by various factors that can influence their effectiveness (Das and Sherif, 2020). One such factor is the length of the dsRNA utilized. Studies have indicated that shorter dsRNA tend to be more effective in gene silencing compared to longer ones, as they can more readily penetrate cells and interact with their target genes (Numata et al., 2014; Dalakouras et al., 2016; Dubrovina and Kiselev, 2019). sRNAs can move short and long distances within plant cells. Primary siRNAs can spread over short distances (10-15 cells) through the symplastic route without producing secondary siRNAs (Han et al., 2019). Systemic spreading of RNA silencing via the phloem has been reported in studies using plant transformation (David-Schwartz et al., 2008; Liu and Chen, 2018). Long-distance movement or systemic silencing is phloem-mediated and requires the amplification of silencing signals by RNA-dependent RNA polymerases (RDRPs) (Cuperus et al., 2010; Bally et al., 2016; Dalakouras et al., 2018; Uslu et al., 2020). It has been documented in several studies that the phloem-mediated transport of systemic sRNA signals from source to sink (Qiao et al., 2018; Yan and Ham, 2022). Furthermore, the concentration of applied dsRNA also

plays a crucial role in its efficacy. Higher concentrations may enhance cellular uptake, but excessive amounts can potentially cause off-target effects or even toxicity (Willow et al., 2021). Therefore, finding an optimal concentration is essential for achieving successful gene silencing without adverse effects.

It is worth noting that the effectiveness of exogenous dsRNA-induced RNAi in plant-microbe interactions can vary depending on factors such as the delivery method, targeting strategy, and the specific organisms involved. Ongoing research aims to further optimize and understand the potential of this approach for sustainable agriculture and crop protection (Yan et al., 2020).

5 Mitigation and avoidance of risks associated with RNAi-based products

RNAi is an emerging technology that offers new opportunities for innovative insect control strategies and the development of desired traits in genetically modified plants. The next generation of RNAi-based products will harness dsRNA to induce gene suppression in insect species, either through *in planta* production or application via plant spraying. Regulatory agencies for biotechnological products, such as the U.S. Environmental Protection Agency (US-EPA) and the European Food Safety Authority (EU-EFSA), have extensive experience in assessing ecological risk associated with newly introduced PIPs, the unique mode of action of dsRNA may necessitate a distinct assessment framework, as indicated by several years of crop assessments (Devos et al., 2014; Papadopoulou et al., 2020). To fully harness the potential of RNAi-based products, effective communication among agricultural consumers, RNAi-based product users (farmers), RNA pesticides producers, and public institutions will be essential to ensure accurate information exchange and mutual understanding. This should be firmly rooted in scientific evidence pertaining to RNAi-based products. Additionally, the implementation of appropriate management, oversight, and legislation, along with safety evaluation and approval processes, will be imperative for the successful adoption and regulation of RNAi-based products.

5.1 Regulatory concerns

The utilization of RNAi-based products in agriculture may provoke regulatory concerns regarding their safety, potential off-target effects, and long-term impacts on ecosystems (Paces et al., 2017; Christiaens et al., 2018; Dávalos et al., 2019). Adhering to regulatory guidelines and requirements is vital for the development and approval of RNAi-based products. Close collaboration with regulatory authorities throughout the development process helps early identify potential risks and effective resolution (Arpaia et al., 2020). It is important to consider, for the risk assessment purposes, that RNAi-based products might take longer to demonstrate efficacy compared to conventional pesticides (Romeis and Widmer, 2020; Fletcher et al., 2020). Globally, the legislative status of dsRNA pesticides varies, which reflects diverse regulatory approaches.

In the USA, biochemical pesticides still need to be registered by the US EPA before manufacture, transport, and sale (Leahy et al., 2014). The EPA approves them under the Federal Insecticide, Fungicide, and Rodenticide Act (FIFRA) and the Federal Food, Drug, and Cosmetic Act (FFDCA), basing the approval on a risk/benefit standard. While no specific data requirements for sprayable or externally applied dsRNA-based pesticides are available, the EPA requires that the active ingredient as well as the final product must be evaluated (Wozniak et al., 2024).

Australia has an advanced and efficient agricultural industry, focusing on developing innovative systems through research and design to enhance food production and sustainability. In terms of RNAi-based products, Australia has been a pioneer in establishing a legal structure for approving these crop protection products. By October 8, 2019, topically applied dsRNA-based products for protecting plants against pests (insects, fungi, and viruses) are defined as agricultural chemical products. Previously, the office of the gene technology regulator (OGTR) and the Australian Pesticides and Veterinary Medicines Authority (APVMA) regulated these products. However, the OGTR's review indicated that applying RNA to an organism for the induction of temporary RNAi is not GMOs. So, SIGS-applications are not under OGTR regulation and should be regulated based on risk. Currently, there are no specific guidelines regarding data requirements for the registration of RNAi-based agricultural products. However, at a minimum, data related to chemistry, manufacturing, human health, worker health and safety, environmental fate and toxicity, efficacy, and crop safety are required. In Australia, the APVMA will keep providing regulatory supervision for topically applied RNAi-based products. And the APVMA must be ensure that the safety, trade, and efficacy requirements related to the specific active ingredient or product are fulfilled. On February 9, 2021, the Food Standards Australia New Zealand (FSANZ) approved the RNAi-based herbicide-tolerant and insect-resistant corn product DP23211 for food. This transgenic corn simultaneously expresses the ds*DvSSJ1* and IPD072Aa proteins for the control of corn rootworms (*Diabrotica* spp.). In addition, multiple transgenic plants based on RNAi technology have been approved for commercial cultivation. In 2014, JR Simplot's InnateÔ (SPS-ØØE12-8 (E12)) potato was approved for cultivation in the United States and subsequently approved in many countries such as Malaysia, Canada, Mexico, Japan, Australia, and New Zealand (James, 2014).

In the EU, any plant protection product (PPP), which is a pesticide safeguarding crops or other valuable plants, must receive authorization before being place on market. The legal framework for this process is defined in Regulation (EC) No. 1107/2009 (EC, 2009). The authorization process consists of approving the active substance and subsequently authorizing the PPP. The authorization of a PPP is conditional upon the approval of the active substance by the EU Commission, based on a risk assessment conducted by the EFSA. A PPP containing an approved active substance is then assessed and authorized by the Member States (MS). To streamline the authorization process, the EU is divided into three zones, the Northern, Central, and Southern (EC, 2009). The risk assessment of a PPP is conducted by one Member State for the entire zone, with the Additional Member States in the same zone must accepting the results and decision of the assessing state. However, they can make claims based on national ecological or agricultural specificities to

determine their risk management options. The European Medicines Agency (EMA) mandates an extensive risk assessment process for novel therapeutic approaches such as RNA interference (Hines et al., 2020; Talap et al., 2021). This assessment includes evaluating potential off-target effects on non-target genes that could lead to adverse events. RNAi is mechanism that relies on sequence homology. Several studies have indicated that siRNA is not always specific and can lead to off-target effects (Carthew and Sontheimer, 2009). RNAi have the potential to impact unintended organisms when the target gene share homologous sequences with non-target organisms, thus resulting in unintended environmental consequences and affecting beneficial organisms. The efficiency of RNAi as a foliar spray is influenced by several factors. First, the selection of target gene is critical. Identifying genes that are essential for insect survival or reproduction increases the likelihood of successful RNAi-mediated suppression (Ghosh et al., 2017; Mamta and Rajam, 2017). Second, it is important to design dsRNA molecules that are specific to the target gene and can be efficiently taken up by the pests.

To ensure the safety, efficacy, and quality of RNAi-based products, it is essential for companies to strictly adhere to regulatory guidelines. Distinguishing regulatory studies as either risk-driven or advocacy-driven would help dispel the public's misconception that extensive and intricate regulations for products developed through modern breeding techniques solely aimed at addressing higher safety risks (Auer and Frederick, 2009; Qaim, 2020). This suggestion assumes that assessing potential safety concerns is more important than promoting consumer acceptance of these technologies and products. Utilizing bioinformatics could assist in identifying off-target sequences and potential effects in non-target species. These guidelines are established by regulatory authorities such as the Food and Drug Administration (FDA) in the United States or EMA in Europe (Hokaiwado et al., 2008; Mohr and Perrimon, 2012; Setten et al., 2019). Compliance with these guidelines allows companies to demonstrate that their products meet all necessary standards before they can be approved for use. For instance, it was reported that siRNA resulting from Dicer-2 processing can have a variable length (20-22 nt) in different insect species (Christiaens et al., 2018).

5.2 Post market surveillance

After a product receives market approval, continuous monitoring and surveillance are necessary to identify any potential safety concerns that may arise post-commercialization. Encouraging professionals to report any adverse events helps ensure timely identification and mitigation of risks. When assessing the environmental risks associated with the use of dsRNA-based pesticides, it is crucial to consider the distribution, stability, and persistence of dsRNA in the environment following product application (OECD, 2020). It has shown a rapid decline in the concentration of foliar-applied dsRNA under field conditions with a 95% reduction after 3 days (Bachman et al., 2020). Recent studies have indicated that the decrease of dsRNA in soil is attributed to both adsorption to soil and chemical and microbial degradation (Dubelman et al., 2014; Parker et al., 2019). The flag bearer here is the global giant Monsanto whose brand "Biodirect" is already developing RNA-based biopesticides to control pests, followed by other multinationals such as Bayer, Syngenta, and others (Abdellatef et al., 2021).

While RNAi-based technologies offer evident safety advantages compared to numerous current crop protection products, unintended impacts on human health (OECD, 2023) and the environment cannot be completely ruled out (OECD, 2020). It is important for researchers and regulatory agencies to continue studying and monitoring the potential effects of RNAi-based technologies order to ensure their safe use in agriculture (Auer and Frederick, 2009). Additionally, public awareness and education about these technologies can help address any concerns or misconceptions surrounding their impact on human health. It is considered unlikely for dsRNA to pose a significant risk to human health in a sequence-specific manner, because of the difficulty in achieving successful systemic delivery (Chen et al., 2018). Systemic exposure following consumption of plants containing dsRNA that mediate RNAi is limited in higher organisms by extensive physical and biochemical barrier (Jay et al., 2013). The approach involves comparing regions of the dsRNA with gene orthologs in databases for non-target species in different agroecosystems, to avoid off-target effects as siRNA. Non-coding RNAs in biological fluids are unstable due to enzymes and kidney removal (Moreno et al., 2021). Environmental dsRNA without protection would have similar issues. Introduced dsRNA must be similar enough to endogenous transcripts for degradation, but their impact may still be minimal due to delivery constraints. RNAi-based insect pest control is not extremely effective in various pests because the dsRNA degrades quickly and the insects don't take it up or process it efficiently. In addition, dsRNA can be degraded by nucleases in nucleic acid digestion in the insect midgut guts as has for example been reported for Liu et al. (2012). To counter unintended impacts on closely related beneficial species, an understanding of the setting in which the RNAi technology will be applied is key. Overall, a balanced approach that considers both the benefits and potential risks of RNAi-based technologies is necessary for their responsible implementation in crop protection.

6 Conclusions

In conclusion, the utilization of exogenous dsRNA-induced RNAi technology holds great potential for revolutionizing various aspects of agriculture and crop management. By harnessing this innovative approach, we can pave the way for more eco-friendly and sustainable practices in gene regulation. By targeting genes related to plant diseases, exogenous dsRNA-induced RNAi offers a promising solution for combating plant pathogens, potentially reducing reliance on chemical pesticides and minimizing their harmful effects on human health and the environment (OECD, 2020; 2023). This technology also benefits crop improvement by selectively targeting specific genes involved in desirable traits such as drought tolerance or insect resistance, thus accelerating breeding programs, and developing new varieties with enhanced resilience and productivity (Jothi et al., 2023). However, before exogenous dsRNA-induced RNAi can be widely adopted in agricultural practices at large-scale levels such as greenhouses and fields, several essential considerations

need to be addressed. One critical aspect is production technologies-optimizing methods for synthesizing quantities of high-quality dsRNA molecules efficiently will be essential to meet the demands of commercial applications. Additionally, cost-effectiveness plays a vital role in determining whether this technology becomes economically viable on a larger scale. Research efforts should focus on finding ways to reduce production costs while maintaining efficacy. Enhancing the stability of dsRNA is critically significant because it directly impacts the effectiveness of applications. In challenging environmental conditions, dsRNA is susceptible to degradation, resulting in diminished efficacy. Advancements in dsRNA delivery mechanisms are essential. Currently, the available methods exhibit low efficiency and poor targeting capabilities. In agricultural applications, encapsulating dsRNA within liposomes can facilitate better adherence to plant foliage and enable timely release, thus allowing for precise action against pests and enhancing pest management efficiency. The development of novel carriers or the optimization of existing delivery system parameters can further enhance the effectiveness of dsRNA.

7 Future directions

The United Nations Environment Programme (UNEP) and the Food and Agriculture Organization (FAO) have recognized the crucial necessity of rehabilitating degraded ecosystems. They claim that the required restoration efforts are indispensable for attaining sustainability goals, including food and water supply security, biodiversity preservation, poverty alleviation, and climate change mitigation. Comprehensive risk assessments are necessary to ensure environmental safety when deploying exogenous dsRNA-induced RNAi technology extensively. When adequate conservation biocontrol strategies are implemented in combination with RNAi technology, the effectiveness of sustainable crop protection can be greatly enhanced. This is especially significant considering that RNAi products have relatively lower environmental risks compared to traditional pesticides.The U.S. EPA has officially approved the innovative RNA-based biopesticide Ledprona by Greenlight Biosciences to combat the increasingly severe destructive pest, the Colorado potato beetle (CPB, *Leptinotarsa decemlineata*) (Kadoić-Balaško et al., 2020; Rodrigues et al., 2021). The EPA emphasizes that RNA-based biopesticides provide farmers with additional tools to address the challenges of climate change and contribute to resistance management. In summary, while there are still challenges ahead regarding production technologies and cost-effectiveness issues surrounding exogenous dsRNA-induced RNAi technology's implementation in large-scale agricultural settings like greenhouses and open fields, continued research efforts will play a pivotal role in realizing its potential to achieve more sustainable farming practices worldwide.

Author contributions

H-YQ: Writing – original draft. D-DZ: Writing – review & editing. BL: Writing – review & editing. J-YC: Writing – review & editing. DH: Writing – review & editing. DW: Writing – review & editing.

Funding

The author(s) declare financial support was received for the research, authorship, and/or publication of this article. This study was supported by the National Key R&D Program of China (2023YFD1401200), the National Natural Science Foundation of China (32302327), the Gusu Innovation and Entrepreneurship Talent Program (ZXL2024372) grant to DH, the Jiangsu Provincial Science and Technology Planning Project (BK20231516) grant to DH, Suzhou Science and Technology Development Project (SNG2023018) to DH.

Conflict of interest

The authors declare that the research was conducted in the absence of any commercial or financial relationships that could be construed as a potential conflict of interest.

Generative AI statement

The authors declare that no Generative AI was used in the creation of this manuscript.

Publisher's note

References

Abdellatef, E., Kamal, N. M., and Tsujimoto, H. (2021). Tuning beforehand: a foresight on RNA interference (RNAi) and in *vitro*-derived dsRNAs to enhance crop resilience to biotic and abiotic stresses. *Int. J. Mol. Sci.* 22, 7687. doi: 10.3390/ijms22147687

Abd El-Monaem, E. M., Elshishini, H. M., Bakr, S. S., El-Aqapa, H. G., Hosny, M., Andaluri, G., et al. (2023). A comprehensive review on LDH-based catalysts to activate persulfates for the degradation of organic pollutants. *NPJ Clean Water* 6, 34. doi: 10.1038/s41545-023-00245-x

Ahn, S. J., Donahue, K., Koh, Y., Martin, R. R., and Choi, M. Y. (2019). Microbial-based double-stranded RNA production to develop cost-effective RNA interference application for insect pest management. *Int. J. Insect Sci.* 11, 1179543319840323. doi: 10.1177/1179543319840323

Ambros, V. (2004). The functions of animal microRNAs. *Nature* 431, 350–355. doi: 10.1038/nature02871

Arpaia, S., Christiaens, O., Giddings, K., Jones, H., Mezzetti, B., Moronta-Barrios, F., et al. (2020). Biosafety of GM crop plants expressing dsRNA: data requirements and EU regulatory considerations. *Front. Plant Sci.* 11. doi: 10.3389/fpls.2020.00940

Auer, C., and Frederick, R. (2009). Crop improvement using small RNAs: applications and predictive ecological risk assessment. *Trends Biotechnol.* 27, 644–651. doi: 10.1016/j.tibtech.2009.08.005

Bachman, P., Fischer, J., Song, Z., Urbanczyk-Wochniak, E., and Watson, G. (2020). Environmental fate and dissipation of applied dsRNA in soil, aquatic systems, and plants. *Front. Plant Sci.* 11. doi: 10.3389/fpls.2020.00021

Bahar, O., Mordukhovich, G., Luu, D. D., Schwessinger, B., Daudi, A., Jehle, A. K., et al. (2016). Bacterial outer membrane vesicles induce plant immune responses. *Mol. Plant Microbe Interact.* 29, 374–384. doi: 10.1094/MPMI-12-15-0270-R

Bally, J., McIntyre, G. J., Doran, R. L., Lee, K., Perez, A., Jung, H., et al. (2016). In-plant protection against *helicoverpa armigera* by production of long hpRNA in chloroplasts. *Front. Plant Sci.* 7. doi: 10.3389/fpls.2016.01453

Bartel, D. P. (2009). MicroRNAs: target recognition and regulatory functions. *Cell* 136, 215–233. doi: 10.1016/j.cell.2009.01.002

Beatty, P. H., and Lewis, J. D. (2019). Cowpea mosaic virus nanoparticles for cancer imaging and therapy. *Adv. Drug Delivery Rev.* 145, 130–144. doi: 10.1016/j.addr.2019.04.005

Biedenkopf, D., Will, T., Knauer, T., Jelonek, L., Alexandra-Charlotte-Ursula, F., Busche, T., et al. (2020). Systemic spreading of exogenous applied RNA biopesticides in the crop plant Hordeum vulgare. *ExRNA* 2, 12. doi: 10.1186/s41544-020-00052-3

Borges, F., and Martienssen, R. A. (2015). The expanding world of small RNAs in plants. *Nat. Rev. Mol. Cell Biol.* 16, 727–741. doi: 10.1038/nrm4085

Cagliari, D., Dias, N. P., Galdeano, D. M., Dos-Santos, E. Á., Smagghe, G., and Zotti, M. J. (2019). Management of pest insects and plant diseases by non-transformative RNAi. *Front. Plant Sci.* 10. doi: 10.3389/fpls.2019.01319

Cambiagno, D. A., Giudicatti, A. J., Arce, A. L., Gagliardi, D., Li, L., Yuan, W., et al. (2021). HASTY modulates miRNA biogenesis by linking pri-miRNA transcription and processing. *Mol. Plant* 14, 426–439. doi: 10.1016/j.molp.2020.12.019

Caparco, A. A., Gonzalez-Gamboa, I., Hays, S. S., Pokorski, J. K., and Steinmetz, N. F. (2023). Delivery of nematicides using TMGMV-derived spherical nanoparticles. *Nano Lett.* 23, 5785–5793. doi: 10.1021/acs.nanolett.3c01684

Carthew, R. W., and Sontheimer, E. J. (2009). Origins and mechanisms of miRNAs and siRNAs. *Cell* 136, 642–655. doi: 10.1016/j.cell.2009.01.035

Chen, X., Mangala, L. S., Rodriguez-Aguayo, C., Kong, X., Lopez-Berestein, G., and Sood, A. K. (2018). RNA interference-based therapy and its delivery systems. *Cancer Metastasis Rev.* 37, 107–124. doi: 10.1007/s10555-017-9717-6

Chen, Y., Singh, A., Kaithakottil, G. G., Mathers, T. C., Gravino, M., Mugford, S. T., et al. (2020). An aphid RNA transcript migrates systemically within plants and is a virulence factor. *Proc. Natl. Acad. Sci. U.S.A.* 117, 12763–12771. doi: 10.1073/pnas.1918410117

Cheng, X., Zhou, Q., Xiao, J., Qin, X., Zhang, Y., Li, X., et al. (2024). Nanoparticle LDH enhances RNAi efficiency of dsRNA in piercing-sucking pests by promoting dsRNA stability and transport in plants. *J. Nanobiotechnol.* 22, 544. doi: 10.1186/s12951-024-02819-4

Chi, X., Wang, Z., Wang, Y., Liu, Z., Wang, H., and Xu, B. (2023). Cross-kingdom regulation of plant-derived miRNAs in modulating insect development. *Int. J. Mol. Sci.* 24, 7978. doi: 10.3390/ijms24097978

Christiaens, O., Dzhambazova, T., Kostov, K., Arpaia, S., Joga, M. R., and Urru, I. (2018). Literature review of baseline information on RNAi to support the environmental risk assessment of RNAi-based GM plants. *EFSA Support* 15, EN–1424. doi: 10.2903/sp.efsa

Colombo, M., Raposo, G., and Théry, C. (2014). Biogenesis, secretion, and intercellular interactions of exosomes and other extracellular vesicles. *Annu. Rev. Cell Dev. Biol.* 30, 255–289. doi: 10.1146/annurev-cellbio-101512-122326

Cuperus, J. T., Carbonell, A., Fahlgren, N., Garcia-Ruiz, H., Burke, R. T., Takeda, A., et al. (2010). Unique functionality of 22-nt miRNAs in triggering RDR6-dependent siRNA biogenesis from target transcripts in Arabidopsis. *Nat. Struct. Mol. Biol.* 17, 997–1003. doi: 10.1038/nsmb.1866

Dad, H. A., Gu, T. W., Zhu, A. Q., Huang, L. Q., and Peng, L. H. (2021). Plant exosome-like nanovesicles: emerging therapeutics and drug delivery nanoplatforms. *Mol. Ther.* 29, 13–31. doi: 10.1016/j.ymthe.2020.11.030

Dalakouras, A., Jarausch, W., Buchholz, G., Bassler, A., Braun, M., Manthey, T., et al. (2018). Delivery of hairpin RNAs and small RNAs into woody and herbaceous plants by trunk injection and petiole absorption. *Front. Plant Sci.* 9. doi: 10.3389/fpls.2018.01253

Dalakouras, A., Wassenegger, M., McMillan, J. N., Cardoza, V., Maegele, I., Dadami, E., et al. (2016). Induction of silencing in plants by high-pressure spraying of in *vitro*-synthesized small RNAs. *Front. Plant Sci.* 7. doi: 10.3389/fpls.2016.01327

Darlington, M., Reinders, J. D., Sethi, A., Lu, A. L., Ramaseshadri, P., Fischer, J. R., et al. (2022). RNAi for western corn rootworm management: lessons learned, challenges, and future directions. *Insects* 13, 57. doi: 10.3390/insects13010057

Das, P. R., and Sherif, S. M. (2020). Application of exogenous dsRNAs-induced RNAi in agriculture: challenges and triumphs. *Front. Plant Sci.* 11. doi: 10.3389/fpls.2020.00946

Dávalos, A., Henriques, R., Latasa, M. J., Laparra, M., and Coca, M. (2019). Literature review of baseline information on non-coding RNA (ncRNA) to support the risk assessment of ncRNA-based genetically modified plants for food and feed. *EFSA Support* 16, EN–1688. doi: 10.2903/sp.efsa

David-Schwartz, R., Runo, S., Townsley, B., Machuka, J., and Sinha, N. (2008). Long-distance transport of mRNA via parenchyma cells and phloem across the host-parasite junction in *Cuscuta*. *New Phytol.* 179, 1133–1141. doi: 10.1111/j.1469-8137.2008.02540.x

Devos, Y., Aguilera, J., Diveki, Z., Gomes, A., Liu, Y., Paoletti, C., et al. (2014). EFSA's scientific activities and achievements on the risk assessment of genetically modified organisms (GMOs) during its first decade of existence: looking back and ahead. *Transgenic Res.* 23, 1–25. doi: 10.1007/s11248-013-9741-4

Dubelman, S., Fischer, J., Zapata, F., Huizinga, K., Jiang, C., Uffman, J., et al. (2014). Environmental fate of double-stranded RNA in agricultural soils. *PloS One* 9, e93155. doi: 10.1371/journal.pone.0093155

Dubrovina, A. S., and Kiselev, K. V. (2019). Exogenous RNAs for gene regulation and plant resistance. *Int. J. Mol. Sci.* 20, 2282. doi: 10.3390/ijms20092282

EC (2009). *Regulation (EC) no 1107/2009 of the European parliament and of the council of 21 October 2009 concerning the placing of plant protection products on the market and repealing council directives 79/117/EEC and 91/414/EEC.* (Luxembourg: European Union). 309, 1–50.

Feng, J. X., and Riddle, N. C. (2020). Epigenetics and genome stability. *Mamm. Genome* 31, 181–195. doi: 10.1007/s00335-020-09836-2

Figueiredo-Prates, L. H., Merlau, M., Rühl-Teichner, J., Schetelig, M. F., and Häcker, I. (2023). An optimized/scale up-ready protocol for extraction of bacterially produced dsRNA at good yield and low costs. *Int. J. Mol. Sci.* 24, 9266. doi: 10.3390/ijms24119266

Fletcher, S. J., Reeves, P. T., Hoang, B. T., and Mitter, N. (2020). A perspective on RNAi-based biopesticides. *Front. Plant Sci.* 11. doi: 10.3389/fpls.2020.00051

Ghosh, S. K., Hunter, W. B., Park, A. L., and Gundersen-Rindal, D. E. (2017). Double strand RNA delivery system for plant-sap-feeding insects. *PloS One* 12, e0171861. doi: 10.1371/journal.pone.0171861

Golden, D. E., Gerbasi, V. R., and Sontheimer, E. J. (2008). An inside job for siRNAs. *Mol. Cell.* 31, 309–312. doi: 10.1016/j.molcel.2008.07.008

Golestanipour, A., Nikkhah, M., Aalami, A., and Hosseinkhani, S. (2018). Gene delivery to tobacco root cells with single-walled carbon nanotubes and cell-penetrating fusogenic peptides. *Mol. Biotechnol.* 60, 863–878. doi: 10.1007/s12033-018-0120-5

Gong, P. (2021). Structural basis of viral RNA-dependent RNA polymerase nucleotide addition cycle in picornaviruses. *Enzymes* 49, 215–233. doi: 10.1016/bs.enz.2021.06.002

Gong, L., Chen, Y., Hu, Z., and Hu, M. (2013). Testing insecticidal activity of novel chemically synthesized siRNA against *Plutella xylostella* under laboratory and field conditions. *PloS One* 8, e62990. doi: 10.1371/journal.pone.0062990

Gong, C., Yang, Z., Hu, Y., Wu, Q., Wang, S., Guo, Z., et al. (2022). Silencing of the *BtTPS* genes by transgenic plant-mediated RNAi to control *Bemisia tabaci* MED. *Pest Manag. Sci.* 78, 1128–1137. doi: 10.1002/ps.6727

Guang, S., Bochner, A. F., Pavelec, D. M., Burkhart, K. B., Harding, S., Lachowiec, J., et al. (2008). An argonaute transports siRNAs from the cytoplasm to the nucleus. *Science.* 321, 537–541. doi: 10.1126/science.1157647

Gurunathan, S., Kang, M. H., Qasim, M., Khan, K., and Kim, J. H. (2021). Biogenesis, membrane trafficking, functions, and next generation nanotherapeutics medicine of extracellular vesicles. *Int. J. Nanomed.* 16, 3357–3383. doi: 10.2147/IJN.S310357

Hamilton, A. J., and Baulcombe, D. C. (1999). A species of small antisense RNA in posttranscriptional gene silencing in plants. *Science* 286, 950–952. doi: 10.1126/science.286.5441.950

Hamilton, A., Voinnet, O., Chappell, L., and Baulcombe, D. (2015). Two classes of short interfering RNA in RNA silencing. *EMBO J.* 34, 2590. doi: 10.15252/embj.201570050

Han, X., Huang, L. J., Feng, D., Jiang, W., Miu, W., and Li, N. (2019). Plasmodesmata-related structural and functional proteins: the long sought-after secrets of a cytoplasmic channel in plant cell walls. *Int. J. Mol. Sci.* 20, 2946. doi: 10.3390/ijms20122946

Head, G. P., Carroll, M. W., Evans, S. P., Rule, D. M., Willse, A. R., Clark, T. L., et al. (2017). Evaluation of smartstax and smartstax PRO maize against western corn rootworm and northern corn rootworm: efficacy and resistance management. *Pest Manag. Sci.* 73, 1883–1899. doi: 10.1002/ps.4554

Henderson, I. R., Zhang, X., Lu, C., Johnson, L., Meyers, B. C., and Green, P. J. (2006). Dissecting *Arabidopsis thaliana* DICER function in small RNA processing, gene silencing, and DNA methylation patterning. *Nat. Gen.* 38, 721–725. doi: 10.1038/ng1804

Hines, P. A., Gonzalez-Quevedo, R., Lambert, A. I. O. M., Janssens, R., Freischem, B., Torren-Edo, J., et al. (2020). Regulatory science to 2025: an analysis of stakeholder responses to the European medicines agency's strategy. *Front. Med. (Lausanne)* 7. doi: 10.3389/fmed.2020.00508

Hokaiwado, N., Takeshita, F., Banas, A., and Ochiya, T. (2008). RNAi-based drug discovery and its application to therapeutics. *IDrugs* 11, 274–278.

Huvenne, H., and Smagghe, G. (2010). Mechanisms of dsRNA uptake in insects and potential of RNAi for pest control: A review. *J. Insect Physiol.* 56, 227–235. doi: 10.1016/j.jinsphys.2009.10.004

Ijaz, M., Khan, F., Ahmed, T., Noman, M., Zulfiqar, F., Rizwan, M., et al. (2023). Nanobiotechnology to advance stress resilience in plants: current opportunities and challenges. *Mater. Today Bio.* 22, 100759. doi: 10.1016/j.mtbio.2023.100759

Islam, M. T., Davis, Z., Chen, L., Englaender, J., Zomorodi, S., Frank, J., et al. (2021). Minicell-based fungal RNAi delivery for sustainable crop protection. *Microb. Biotechnol.* 14, 1847–1856. doi: 10.1111/1751-7915.13699

Islam, M. T., and Sherif, S. M. (2020). RNAi-based biofungicides as a promising next-generation strategy for controlling devastating gray mold diseases. *Int. J. Mol. Sci.* 21, 2072. doi: 10.3390/ijms21062072

Ivashuta, S., Zhang, Y., Wiggins, B. E., Seshadri, P. R., Segers, G. C., Johnson, S., et al. (2015). Environmental RNAi in herbivorous insects. *RNA.* 21, 840–850. doi: 10.1261/rna.048116.114

Jain, R. G., Fletcher, S. J., Manzie, N., Robinson, K. E., Li, P., Lu, E., et al. (2022). Foliar application of clay-delivered RNA interference for whitefly control. *Nat. Plants* 8, 535–548. doi: 10.1038/s41477-022-01152-8

James, C. (2014). *Global Status of Commercialized Biotech/GM Crops: 2014. ISAAA Brief No. 49* (Ithaca, NY: ISAAA).

Jay, S., Petrick-Brent, B. T., Aimee, L., and Jackson-Larry, D. K. (2013). Safety assessment of food and feed from biotechnology-derived crops employing RNA-mediated gene regulation to achieve desired traits: A scientific review. *Regul. Toxicol. Pharmacol.* 2, 167–176. doi: 10.1016/j.yrtph.2013.03.008

Jha, U. C., Nayyar, H., Chattopadhyay, A., Beena, R., Lone, A. A., Naik, Y. D., et al. (2023). Major viral diseases in grain legumes: designing disease resistant legumes from plant breeding and OMICS integration. *Front. Plant Sci.* 14. doi: 10.3389/fpls.2023.1183505

Joga, M. R., Zotti, M. J., Smagghe, G., and Christiaens, O. (2016). RNAi efficiency, systemic properties, and novel delivery methods for pest insect control: what we know so far. *Front. Physiol.* 7. doi: 10.3389/fphys.2016.00553

Jothi, K. B., Ramaswamy, A., Lincy, K. B., Sowbiya, M., and Muthu-Arjuna, S. P. (2023). Recent trends and advances of RNA interference (RNAi) to improve agricultural crops and enhance their resilience to biotic and abiotic stresses. *Plant Physiol. Biochem.* 194, 600–618. doi: 10.1016/j.plaphy.2022.11.035

Kadoić-Balaško, M., Mikac, K. M., Bažok, R., and Lemic, D. (2020). Modern techniques in Colorado potato beetle (*leptinotarsa decemlineata* say) control and resistance management: history review and future perspectives. *Insects* 11, 581. doi: 10.3390/insects11090581

Khajuria, C., Ivashuta, S., Wiggins, E., Flagel, L., Moar, W., Pleau, M., et al. (2018). Development and characterization of the first dsRNA-resistant insect population from western corn rootworm, *Diabrotica virgifera virgifera* LeConte. *PloS One* 13, e0197059. doi: 10.1371/journal.pone.0197059

Kaur, R., Bhunia, R. K., and Rajam, M. V. (2020). MicroRNAs as potential targets for improving rice yield via plant architecture modulation: Recent studies and future perspectives. *J. Biosci.* 45, 116. doi: 10.1007/s12038-020-00084-9

Kedde, M., Strasser, M. J., Boldajipour, B., Oude-Vrielink, J. A., Slanchev, K., le-Sage, C., et al. (2007). RNA-binding protein Dnd1 inhibits microRNA access to target mRNA. *Cell* 131, 1273–1286. doi: 10.1016/j.cell.2007.11.034

Ketting, R. F. (2011). The many faces of RNAi. *Dev. Cell.* 20, 148–161. doi: 10.1016/j.devcel.2011.01.012

Khalid, A., Zhang, Q., Yasir, M., and Li, F. (2017). Small RNA based genetic engineering for plant viral resistance: application in crop protection. *Front. Microbiol.* 8. doi: 10.3389/fmicb.2017.00043

Komarova, T., Ilina, I., Taliansky, M., and Ershova, N. (2023). Nanoplatforms for the delivery of nucleic acids into plant cells. *Int. J. Mol. Sci.* 24, 16665. doi: 10.3390/ijms242316665

Kong, L., Shi, X., Chen, D., Yang, N., Yin, C., Yang, J., et al. (2022). Host-induced silencing of a nematode chitin synthase gene enhances resistance of soybeans to both pathogenic *Heterodera glycines* and *Fusarium oxysporum*. *Plant Biotechnol. J.* 20, 809–811. doi: 10.1111/pbi.13808

Kumar, K., Gambhir, G., Dass, A., Tripathi, A. K., Singh, A., Jha, A. K., et al. (2020). Genetically modified crops: current status and future prospects. *Planta* 251, 91. doi: 10.1007/s00425-020-03372-8

Kupferschmidt, K. (2013). A lethal dose of RNA. *Science* 341, 732–733. doi: 10.1126/science.341.6147.732

Leahy, J., Mendelsohn, M., Kough, J., Jones, R., and Berckes, N. (2014). "Biopesticide oversight and registration of the U.S. Environmental Protection Agency," in *Biopesticides: State of Art and Future Opportunities*. Eds. A. Gross, J. R. Coats, S. O. Duke and J. N. Seiber (ACS Publications, Washington, DC), 1–16. doi: 10.1021/bk-2014-1172.ch001

Liu, L., and Chen, X. (2018). Intercellular and systemic trafficking of RNAs in plants. *Nat. Plants* 4, 869–878. doi: 10.1038/s41477-018-0288-5

Liu, S., Geng, S., Li, A., Mao, Y., and Mao, L. (2021). RNAi technology for plant protection and its application in wheat. *aBIOTECH* 2, 365–374. doi: 10.1007/s42994-021-00036-3

Liu, G., Kang, G., Wang, S., Huang, Y., and Cai, Q. (2021). Extracellular vesicles: emerging players in plant defense against pathogens. *Front. Plant Sci.* 12. doi: 10.3389/fpls.2021.757925

Liu, J., Swevers, L., Iatrou, K., Huvenne, H., and Smagghe, G. (2012). Bombyx mori DNA/RNA non-specific nuclease: expression of isoforms in insect culture cells, subcellular localization and functional assays. *J. Insect Physiol.* 58, 1166–1176. doi: 10.1016/j.jinsphys.2012.05.016

Lundgren, J. G., and Duan, J. J. (2013). RNAi-based insecticidal crops: potential effects on nontarget species. *BioScience* 63, 657–665. doi: 10.1525/bio.2013.63.8.8

Ma, Z. Z., Zhang, Y. H., Li, M. S., Chao, Z. J., Du, X. G., Yan, S., et al. (2023). A first greenhouse application of bacteria-expressed and nanocarrier-delivered RNA pesticide for *Myzus persicae* control. *J. Pest Sci.* 96, 181–193. doi: 10.1007/s10340-022-01485-5

Ma, Y. F., Zhao, Y. Q., Zhou, Y. Y., Feng, H. Y., Gong, L. L., Zhang, M. Q., et al. (2024). Nanoparticle-delivered RNAi-based pesticide target screening for the rice pest white-backed planthopper and risk assessment for a natural predator. *Sci. Total Environ.* 926, 171286. doi: 10.1016/j.scitotenv.2024.171286

Mamta, B., and Rajam, M. V. (2018). RNA Interference: A Promising Approach for Crop Improvement. *Biotechnologies of Crop Improvement*. (Cham: Springer International Publishing AG) 2, 41–65. doi: 10.1007/978-3-319-90650-8_3

Mamta,, Reddy, K. R., and Rajam, M. V. (2016). Targeting chitinase gene of Helicoverpa armigera by host-induced RNA interference confers insect resistance in tobacco and tomato. *Plant Mol. Biol.* 90, 281–292. doi: 10.1007/s11103-015-0414-y

Mamta, B., and Rajam, M. V. (2017). RNAi technology: a new platform for crop pest control. *Physiol. Mol. Biol. Plants.* 23, 487–501. doi: 10.1007/s12298-017-0443-x

Margis, R., Fusaro, A. F., Smith, N. A., Curtin, S. J., Watson, J. M., Finnegan, E. J., et al. (2006). The evolution and diversification of Dicers in plants. *FEBS Lett.* 580, 2442–2450. doi: 10.1016/j.febslet.2006.03.072

Mathieu, M., Martin-Jaular, L., Lavieu, G., and Théry, C. (2019). Specificities of secretion and uptake of exosomes and other extracellular vesicles for cell-to-cell communication. *Nat. Cell Biol.* 21, 9–17. doi: 10.1038/s41556-018-0250-9

Mat-Jalaluddin, N. S., Asem, M., Harikrishna, J. A., and Ahmad-Fuaad, A. A. H. (2023). Recent progress on nanocarriers for topical-mediated RNAi strategies for crop protection-a review. *Molecules* 28, 2700. doi: 10.3390/molecules28062700

Matranga, C., and Zamore, P. D. (2007). Small silencing RNAs. *Curr. Biol.* 17, 789–793. doi: 10.1016/j.cub.2007.07.014

McLaughlin, M. S., Roy, M., Abbasi, P. A., Carisse, O., Yurgel, S. N., and Ali, S. (2023). Why do we need alternative methods for fungal disease management in plants? *Plants (Basel)* 12, 3822. doi: 10.3390/plants12223822

Mehlhorn, S., Hunnekuhl, V. S., and Geibel, S. (2021). Establishing RNAi for basic research and pest control and identification of the most efficient target genes for pest control: a brief guide. *Front. Zool.* 18, 60. doi: 10.1186/s12983-021-00444-7

Meister, G., and Tuschl, T. (2004). Mechanisms of gene silencing by double-stranded RNA. *Nature* 431, 343–349. doi: 10.1038/nature02873

Mello, C. C., and Conte, D. Jr. (2004). Revealing the world of RNA interference. *Nature* 431, 338–342. doi: 10.1038/nature02872

Mitter, N., Worrall, E. A., Robinson, K. E., Xu, Z. P., and Carroll, B. J. (2017). Induction of virus resistance by exogenous application of double-stranded RNA. *Curr. Opin. Virol.* 26, 49–55. doi: 10.1016/j.coviro.2017.07.009

Mohr, S. E., and Perrimon, N. (2012). RNAi screening: new approaches, understandings, and organisms. *Wiley Interdiscip. Rev. RNA* 3, 145–158. doi: 10.1002/wrna.110

Mordukhovich, G., and Bahar, O. (2017). Isolation of outer membrane vesicles from phytopathogenic *Xanthomonas campestris* pv. *campestris*. *Bio Protoc.* 7, e2160. doi: 10.21769/BioProtoc.2160

Moreno, J. A., Hamza, E., Guerrero-Hue, M., Rayego-Mateos, S., García-Caballero, C., Vallejo-Mudarra, M., et al. (2021). Non-Coding RNAs in kidney diseases: The long and short of them. *Int. J. Mol. Sci.* 22, 6077. doi: 10.3390/ijms22116077

Morozov, S. Y., Solovyev, A. G., Kalinina, N. O., and Taliansky, M. E. (2019). Double-stranded RNAs in plant protection against pathogenic organisms and viruses in agriculture. *Acta Naturae* 11, 13–21. doi: 10.32607/20758251-2019-11-4-13-21

Mwaka, H. S., Bauters, L., Namaganda, J., Marcou, S., Bwesigye, P. N., Kubiriba, J., et al. (2023). Transgenic East African highland banana plants are protected against *Radopholus similis* through Host-delivered RNAi. *Int. J. Mol. Sci.* 24, 12126. doi: 10.3390/ijms241512126

Niño-Sánchez, J., Sambasivam, P. T., Sawyer, A., Hamby, R., Chen, A., Czislowski, E., et al. (2022). BioClay™ prolongs RNA interference-mediated crop protection against *Botrytis cinerea*. *J. Integr. Plant Biol.* 64, 2187–2198. doi: 10.1111/jipb.13353

Nitnavare, R. B., Bhattacharya, J., Singh, S., Kour, A., Hawkesford, M. J., and Arora, N. (2021). Next generation dsRNA-based insect control: success so far and challenges. *Front. Plant Sci.* 12. doi: 10.3389/fpls.2021.673576

Numata, K., Ohtani, M., Yoshizumi, T., Demura, T., and Kodama, Y. (2014). Local gene silencing in plants via synthetic dsRNA and carrier peptide. *Plant Biotechnol. J.* 12, 1027–1034. doi: 10.1111/pbi.12208

OECD (2020). Considerations for the environmental risk assessment of the application of sprayed or externally applied dsRNA-based pesticides. *Series on Pesticides and Biocides* (Paris: Paris). No. 104, ENV/JM/MONO 26. doi: 10.1787/576d9ebb-en

OECD (2023). *Considerations for the human health risk assessment of externally applied dsRNA-based pesticides*. (Paris: OECD), ENV/CBC/MONO 2023. doi: 10.1787/54852048-en

Omolehin, O., Raruang, Y., Hu, D., Han, Z. Q., Wei, Q., Wang, K., et al. (2021). Resistance to aflatoxin accumulation in maize mediated by host-induced silencing of the aspergillus flavus alkaline protease (alk) gene. *J. Fungi (Basel)* 7, 904. doi: 10.3390/jof7110904

Ortega-Rivera, O. A., Shukla, S., Shin, M. D., Chen, A., Beiss, V., Moreno-Gonzalez, M. A., et al. (2021). Cowpea mosaic virus nanoparticle vaccine candidates displaying peptide epitopes can neutralize the severe acute respiratory syndrome coronavirus. *ACS Infect. Dis.* 7, 3096–3110. doi: 10.1021/acsinfecdis.1c00410

Paces, J., Nic, M., Novotny, T., and Svoboda, P. (2017). Literature review of baseline information to support the risk assessment of RNAi-based GM plants. *EFSA Support* 14, EN–1246. doi: 10.2903/sp.efsa.2017.EN-1246

Papadopoulou, N., Devos, Y., Álvarez-Alfageme, F., Lanzoni, A., and Waigmann, E. (2020). Risk assessment considerations for genetically modified RNAi plants: EFSA's activities and perspective. *Front. Plant Sci.* 11. doi: 10.3389/fpls.2020.00445

Parker, J. S., and Barford, D. (2006). Argonaute: A scaffold for the function of short regulatory RNAs. *Trends Biochem. Sci.* 31, 622–630. doi: 10.1016/j.tibs.2006.09.010

Parker, K. M., Barragán-Borrero, V., van-Leeuwen, D. M., Lever, M. A., Mateescu, B., and Sander, M. (2019). Environmental fate of RNA interference pesticides: adsorption and degradation of double-stranded RNA molecules in agricultural soils. *Environ. Sci. Technol.* 53, 3027–3036. doi: 10.1021/acs.est.8b05576

Parker, J., Roe, S., and Barford, D. (2005). Structural insights into mRNA recognition from a PIWI domain-siRNA guide complex. *Nature* 434, 663–666. doi: 10.1038/nature03462

Pathak, V. M., Verma, V. K., Rawat, B. S., Kaur., B., Babu, N., Sharma, A., et al. (2022). Current status of pesticide effects on environment, human health and it's eco-friendly management as bioremediation: A comprehensive review. *Front. Microbiol.* 13. doi: 10.3389/fmicb.2022.962619

Preall, J. B., and Sontheimer, E. J. (2005). RNAi: RISC gets loaded. *Cell* 123, 543–545. doi: 10.1016/j.cell.2005.11.006

Qaim, M. (2020). Role of new plant breeding technologies for food security and sustainable agricultural development. *Appl. Econ. Perspect. Policy* 42, 129–150. doi: 10.1002/aepp.13044

Qiao, L., Lan, C., Capriotti, L., Ah-Fong, A., Nino-Sanchez, J., Hamby, R., et al. (2021). Spray-induced gene silencing for disease control is dependent on the efficiency of pathogen RNA uptake. *Plant Biotechnol. J.* 19, 1756–1768. doi: 10.1111/pbi.13589

Qiao, W., Medina, V., Kuo, Y. W., and Falk, B. W. (2018). A distinct, non-virion plant virus movement protein encoded by a crinivirus essential for systemic infection. *mBio* 9, e02230-18. doi: 10.1128/mBio.02230-18

Qiao, L., Niño-Sánchez, J., Hamby, R., Capriotti, L., Chen, A., Mezzetti, B., et al. (2023). Artificial nanovesicles for dsRNA delivery in spray-induced gene silencing for crop protection. *Plant Biotechnol. J.* 21, 854–865. doi: 10.1111/pbi.14001

Rajam, M. V. (2020). RNA silencing technology: A boon for crop improvement. *J. Biosci.* 45, 118. doi: 10.1007/s12038-020-00082-x

Ray, P., Sahu, D., Aminedi, R., and Chandran, D. (2022). Concepts and considerations for enhancing RNAi efficiency in phytopathogenic fungi for RNAi-based crop protection using nanocarrier-mediated dsRNA delivery systems. *Front. Fungal Biol.* 3. doi: 10.3389/ffunb.2022.977502

Rodrigues, T. B., Mishra, S. K., Sridharan, K., Barnes, E. R., Alyokhin, A., Tuttle, R., et al. (2021). First sprayable double-stranded RNA-based biopesticide product targets proteasome subunit beta type-5 in colorado potato beetle (*Leptinotarsa decemlineata*). *Front. Plant Sci.* 18. doi: 10.3389/fpls.2021.728652

Rodrigues, T. B., and Petrick, J. S. (2020). Safety considerations for humans and other vertebrates regarding agricultural uses of externally applied RNA molecules. *Front. Plant Sci.* 11. doi: 10.3389/fpls.2020.00407

Rodriguez Coy, L., Plummer, K. M., Khalifa, M. E., and MacDiarmid, R. M. (2022). Mycovirus-encoded suppressors of RNA silencing: Possible allies or enemies in the use of RNAi to control fungal disease in crops. *Front. Fungal Biol.* 3. doi: 10.3389/ffunb.2022.965781

Romeis, J., and Widmer, F. (2020). Assessing the risks of topically applied dsRNA-based products to non-target arthropods. *Front. Plant Sci.* 11. doi: 10.3389/fpls.2020.00679

Samad, A. F. A., Kamaroddin, M. F., and Sajad, M. (2021). Cross-kingdom regulation by plant microRNAs provides novel insight into gene regulation. *Adv. Nutr.* 12, 197–211. doi: 10.1093/advances/nmaa095

San-Miguel, K., and Scott, J. G. (2016). The next generation of insecticides: dsRNA is stable as a foliar-applied insecticide. *Pest Manag. Sci.* 72, 801–809. doi: 10.1002/ps.4056

Sarkar, A., and Roy-Barman, S. (2021). Spray-induced silencing of pathogenicity gene MoDES1 via exogenous double-stranded RNA can confer partial resistance against fungal blast in Rice. *Front. Plant Sci.* 12. doi: 10.3389/fpls.2021.733129

Schwartz, S. H., Hendrix, B., Hoffer, P., Sanders, R. A., and Zheng, W. (2020). Carbon dots for efficient small interfering RNA delivery and gene silencing in plants. *Plant Physiol.* 184, 647–657. doi: 10.1104/pp.20.00733

Setten, R. L., Rossi, J. J., and Han, S. P. (2019). The current state and future directions of RNAi-based therapeutics. *Nat. Rev. Drug Discovery* 18, 421–446. doi: 10.1038/s41573-019-0017-4

Sikandar, A., Khanum, T. A., and Wang, Y. (2021). Biodiversity and community analysis of plant-parasitic and free-living nematodes associated with maize and other rotational crops from Punjab, Pakistan. *Life (Basel)* 11, 1426. doi: 10.3390/life11121426

Song, X. S., Gu, K. X., Duan, X. X., Xiao, X. M., Hou, Y. P., Duan, Y. B., et al. (2018). A myosin5 dsRNA that reduces the fungicide resistance and pathogenicity of *Fusarium asiaticum*. *Pestic. Biochem. Physiol.* 150, 1–9. doi: 10.1016/j.pestbp.2018.07.004

Spit, J., Philips, A., Wynant, N., Santos, D., Plaetinck, G., and Vanden Broeck, J. (2017). Knockdown of nuclease activity in the gut enhances RNAi efficiency in the Colorado potato beetle, *Leptinotarsa decemlineata*, but not in the desert locust, *Schistocerca gregaria*. *Insect Biochem. Mol. Biol.* 81, 103–116. doi: 10.1016/j.ibmb.2017.01.004

Statello, L., Guo, C. J., Chen, L. L., and Huarte, M. (2020). Gene regulation by long non-coding RNAs and its biological functions. *Nat. Rev. Mol. Cell Biol.* 22, 96–118. doi: 10.1038/s41580-020-00315-9

Subha, D., AnuKiruthika, R., Sreeraj, H., and Tamilselvi, K. S. (2023). Plant exosomes: nano conveyors of pathogen resistance. *Discovery Nano*. 18, 146. doi: 10.1186/s11671-023-03931-4

Talap, J., Zhao, J., Shen, M., Song, Z., Zhou, H., Kang, Y., et al. (2021). Recent advances in therapeutic nucleic acids and their analytical methods. *J. Pharm. BioMed. Anal.* 206, 114368. doi: 10.1016/j.jpba.2021.114368

Tatematsu, M., Funami, K., Seya, T., and Matsumoto, M. (2018). Extracellular RNA sensing by pattern recognition receptors. *J. Innate Immun.* 10, 398–406. doi: 10.1159/000494034

Tayler, A., Heschuk, D., Giesbrecht, D., Park, J. Y., and Whyard, S. (2019). Efficiency of RNA interference is improved by knockdown of dsRNA nucleases in tephritid fruit flies. *Open Biol.* 9, 190198. doi: 10.1098/rsob.190198

Tenllado, F., and Díaz-Ruíz, J. R. (2001). Double-stranded RNA-mediated interference with plant virus infection. *J. Virol.* 75, 12288–12297. doi: 10.1128/JVI.75.24.12288-12297.2001

Timani, K., Bastarache, P., and Morin, P. J. (2023). Leveraging RNA interference to impact insecticide resistance in the Colorado potato beetle, *Leptinotarsa decemlineata*. *Insects* 14, 418. doi: 10.3390/insects14050418

Tran, T. M., Chng, C. P., Pu, X., Ma, Z., Han, X., Liu, X., et al. (2022). Potentiation of plant defense by bacterial outer membrane vesicles is mediated by membrane nanodomains. *Plant Cell.* 34, 395–417. doi: 10.1093/plcell/koab276

Tyagi, S., Sharma, S., Ganie, S. A., Tahir, M., Mir, R. R., and Pandey, R. (2019). Plant microRNAs: biogenesis, gene silencing, web-based analysis tools and their use as molecular markers. *3 Biotech.* 9, 413. doi: 10.1007/s13205-019-1942-y

Uslu, V. V., Bassler, A., Krczal, G., and Wassenegger, M. (2020). High-pressure-sprayed double stranded RNA does not induce RNA interference of a reporter gene. *Front. Plant Sci.* 11. doi: 10.3389/fpls.2020.534391

Vatanparast, M., and Kim, Y. (2017). Optimization of recombinant bacteria expressing dsRNA to enhance insecticidal activity against a lepidopteran insect, *Spodoptera exigua*. *PloS One* 12, e0183054. doi: 10.1371/journal.pone.0183054

Walawage, S. L., Britton, M. T., Leslie, C. A., Uratsu, S. L., Li, Y., and Dandekar, A. M. (2013). Stacking resistance to crown gall and nematodes in walnut rootstocks. *BMC Genomics* 14, 668. doi: 10.1186/1471-2164-14-668

Wang, M., and Jin, H. (2017). Spray-induced gene silencing: a powerful innovative strategy for crop protection. *Trends Microbiol.* 25, 4–6. doi: 10.1016/j.tim.2016.11.011

Wang, M., Weiberg, A., Lin, F. M., Thomma, B. P., Huang, H. D., and Jin, H. (2016). Bidirectional cross-kingdom RNAi and fungal uptake of external RNAs confer plant protection. *Nat. Plants* 2, 16151. doi: 10.1038/nplants.2016.151

Wang, M., Wu, L., Mei, Y., Zhao, Y., Ma, Z., Zhang, X., et al. (2020). Host-induced gene silencing of multiple genes of *Fusarium graminearum* enhances resistance to *Fusarium* head blight in wheat. *Plant Biotechnol. J.* 18, 2373–2375. doi: 10.1111/pbi.13401

Wang, Y., Yan, Q., Lan, C., Tang, T., Wang, K., Shen, J., et al. (2023). Nanoparticle carriers enhance RNA stability and uptake efficiency and prolong the protection against *Rhizoctonia solani*. *Phytopathol. Res.* 5, 2. doi: 10.1186/s42483-023-00157-1

Wassenegger, M., and Krczal, G. (2006). Nomenclature and functions of RNA-directed RNA polymerases. *Trends Plant Sci.* 11, 142–151. doi: 10.1016/j.tplants.2006.01.003

Waterhouse, P. M., Graham, M. W., and Wang, M.-B. (1998). Virus resistance and gene silencing in plants can be induced by simultaneous expression of sense and antisense RNA. *Proc. Natl. Acad. Sci. U. S. A.* 95, 13959–13964. doi: 10.1073/pnas.95.23.13959

Weiberg, A., Wang, M., Lin, F. M., Zhao, H., Zhang, Z., Kaloshian, I., et al. (2013). Fungal small RNAs suppress plant immunity by hijacking host RNA interference pathways. *Science* 342, 118–123. doi: 10.1126/science.1239705

Wen, H. G., Zhao, J. H., and Zhang, B. S. (2023). Microbe-induced gene silencing boosts crop protection against soil-borne fungal pathogens. *Nat. Plants* 9, 1409–1418. doi: 10.1038/s41477-023-01507-9

Willow, J., Soonvald, L., Sulg, S., Kaasik, R., Silva, A. I., Taning, C. N. T., et al. (2021). RNAi efficacy is enhanced by chronic dsRNA feeding in pollen beetle. *Commun. Biol.* 4, 444. doi: 10.1038/s42003-021-01975-9

Wilson, R. C., and Doudna, J. A. (2013). Molecular mechanisms of RNA interference. *Annu. Rev. Biophys.* 42, 217–239. doi: 10.1146/annurev-biophys-083012-130404

Wingard, S. A. (1928). Hosts and symptoms of ring spot, a virus disease of plants. *J. Agric. Res.* 37, 127–153.

Wozniak, C. A., McClung, G., Gagliardi, J., Segal, M., and Matthews, K. (2024). "Regulation of genetically engineered microorganisms under FIFRA, FFDCA and TSCA," in *Regulation of Agricultural Biotechnology: The United States and Canada*. Eds. C. A. Wozniak and A. McHughen (Springer, Heidelberg), 57–94. doi: 10.1007/978-94-007-2156-2_4

Wu, K., Xu, C., Li, T., Ma, H., Gong, J., Li, X., et al. (2023). Application of nanotechnology in plant genetic engineering. *Int. J. Mol. Sci.* 24, 14836. doi: 10.3390/ijms241914836

Wu, L., Liu, S., Qi, H., Cai, H., and Xu, M. (2020). Research progress on plant long non-coding RNA. *Plants (Basel).* 9, 408. doi: 10.3390/plants9040408

Yan, Y., and Ham, B. K. (2022). The mobile small RNAs: Important messengers for long-distance communication in plants. *Front. Plant Sci.* 13. doi: 10.3389/fpls.2022.928729

Yan, S., Qian, J., Cai, C., Ma, Z. Z., Li, J. H., Yin, M. Z., et al. (2020). Spray method application of transdermal dsRNA delivery system for efficient gene silencing and pest control on soybean aphid *Aphis glycines*. *J. Pest Sci.* 93, 449–459. doi: 10.1007/s10340-019-01157-x

Yan, S., Ren, B. Y., and Shen, J. (2021). Nanoparticle-mediated double-stranded RNA delivery system: A promising approach for sustainable pest management. *Insect Sci.* 28, 21–34. doi: 10.1111/1744-7917.12822

Yang, J., Hwang, I., Lee, E., Shin, S. J., Lee, E. J., Rhee, J. H., et al. (2020). Bacterial outer membrane vesicle-mediated cytosolic delivery of flagellin triggers host NLRC4 canonical inflammasome signaling. *Front. Immunol.* 11. doi: 10.3389/fimmu.2020.581165

Yong, J. X., Zhang, R., Bi, S. N., Li, P., Sun, L. Y., Mitter, N., et al. (2021). Sheet-like clay nanoparticles deliver RNA into developing pollen to efficiently silence a target gene. *Plant Physiol.* 2, 886–899. doi: 10.1093/plphys/kiab303

Yoshida, K., Suehiro, Y., Dejima, K., Yoshina, S., and Mitani, S. (2023). Distinct pathways for export of silencing RNA in *Caenorhabditis elegans* systemic RNAi. *iScience* 26, 108067. doi: 10.1016/j.isci.2023.108067

Yu, Y., Jia, T., and Chen, X. (2017). The 'how' and 'where' of plant microRNAs. *New Phytol.* 216, 1002–1017. doi: 10.1111/nph.14834

Zhang, H., Goh, N. S., Wang, J. W., Pinals, R. L., González-Grandío, E., Demirer, G. S., et al. (2022). Nanoparticle cellular internalization is not required for RNA delivery to mature plant leaves. *Nat. Nanotechnol.* 17, 197–205. doi: 10.1038/s41565-021-01018-8

Zotti, M. J., and Smagghe, G. (2015). RNAi technology for insect management and protection of beneficial insects from diseases: lessons, challenges and risk assessments. *Neotrop. Entomol.* 44, 197–213. doi: 10.1007/s13744-015-0291-8

frontiers | Frontiers in Plant Science

TYPE Original Research
PUBLISHED 22 January 2025
DOI 10.3389/fpls.2024.1531710

OPEN ACCESS

EDITED BY
Kevin Yueju Wang,
University of Pikeville, United States

REVIEWED BY
Kazuhito Fujiyama,
Osaka University, Japan
Marcos Oggero,
Centro Biotecnológico del Litoral, Argentina

*CORRESPONDENCE
Kathrin Göritzer
kathrin.goeritzer@boku.ac.at

RECEIVED 20 November 2024
ACCEPTED 20 December 2024
PUBLISHED 22 January 2025

CITATION
Göritzer K, Ruocco V, Vavra U, Izadi S, Bolaños-Martínez OC, Phetphoung T, Pisuttinusart N, Phoolcharoen W and Strasser R (2025) Improving the *N*-glycosylation occupancy of plant-produced IgG1 by engineering the amino acid environment at Asn297.
Front. Plant Sci. 15:1531710.
doi: 10.3389/fpls.2024.1531710

Improving the *N*-glycosylation occupancy of plant-produced IgG1 by engineering the amino acid environment at Asn297

Kathrin Göritzer[1]*, Valentina Ruocco[1], Ulrike Vavra[1], Shiva Izadi[1], Omayra C. Bolaños-Martínez[1], Thareeya Phetphoung[2], Nuttapat Pisuttinusart[2], Waranyoo Phoolcharoen[2] and Richard Strasser[1]

[1]Department of Applied Genetics and Cell Biology, BOKU University, Vienna, Austria, [2]Department of Pharmacognosy and Pharmaceutical Botany, Faculty of Pharmaceutical Sciences, Chulalongkorn University, Bangkok, Thailand

Monoclonal antibodies are crucial recombinant biopharmaceuticals, with *N*-glycosylation at Asn297 essential for their functionality. Plants are increasingly used for antibody production, achieving high expression levels and enabling glycoengineering to produce homogenous human-like *N*-glycan structures. However, plant-produced human IgG1 often shows significant underglycosylation with potential adverse effects for immune functions and stability. This study addressed this limitation of the widely used plant-based expression platform *Nicotiana benthamiana* by employing protein engineering to enhance *N*-glycosylation occupancy in plant-produced IgG1. This was achieved through an amino acid mutation near the conserved glycosylation site in the CH2 domain of the heavy chain. The transient expression of trastuzumab and SARS-CoV-2 neutralizing IgG1 antibody COVA2-15 in *N. benthamiana*, with mutations such as Y300L, resulted in a notable improvement in glycosylation occupancy. While the structural integrity and monodispersity of the IgG1 variant remained unaltered, an improvement in thermal stability was observed. Furthermore, functional assays showed that antigen binding and human hFcRn interaction were unaffected, while FcγRIIIa binding affinity increased. These findings demonstrate the potential of protein-engineering to enhance the quality and functionality of plant-produced IgG1 antibodies, making them comparable to mammalian-produced counterparts.

KEYWORDS

monoclonal antibodies, *Nicotiana benthamiana*, IgG1, *N*-glycosylation, glycosylation efficiency

1 Introduction

Monoclonal antibodies represent the most important and fastest-growing class of recombinant biopharmaceuticals, utilized in various therapeutic settings (Crescioli et al., 2024). The conserved *N*-glycosylation at Asn297 of human IgG1 is crucial for its proper folding and functionality, particularly in terms of receptor interaction. Consequently, glycosylation is considered a critical quality attribute of recombinant antibodies, necessitating tight control to ensure effective antibody functions, avoid unwanted side effects, and facilitate the development of biosimilars (Reusch and Tejada, 2015).

Plants are increasingly being used for the production of recombinant biopharmaceuticals and have successfully expressed various classes of highly effective recombinant antibodies against viruses and human antigens (Ruocco and Strasser, 2022; Shanmugaraj et al., 2022; Eidenberger et al., 2023; Göritzer et al., 2024a). Expression levels of more than 1 g/kg for IgG antibodies are frequently achieved by transient expression in *Nicotiana benthamiana* plants, making this system economically attractive (Bendandi et al., 2010; Ridgley et al., 2023). Host glycoengineering enables the production of functional IgG antibodies with human-like complex *N*-glycan structures that lack core fucose residues, resulting in increased functional activities (Strasser et al., 2008; Forthal et al., 2010; Zeitlin et al., 2011; Stelter et al., 2020).

However, it has been demonstrated that the transient expression of recombinant human IgG1 antibodies in *Nicotiana benthamiana* leaves results in significant underglycosylation at Asn297 in the Fc domain, which is likely influenced by the local amino acid environment adjacent to the *N*-glycosylation site (Murray et al., 2015; Castilho et al., 2018). In contrast, recombinant IgG1 antibodies produced in mammalian cells are typically more than 99% glycosylated at Asn297 (Stadlmann et al., 2008). The observed underglycosylation at the conserved *N*-glycosylation site increases the heterogeneity of recombinant IgG1 antibodies, potentially leading to adverse effects on immune effector functions. Non-glycosylated (i.e., both heavy chains in the assembled antibody lack *N*-glycans) or hemi-glycosylated (i.e., one heavy chain is non-glycosylated while the other is glycosylated) IgG1 antibodies typically display reduced effector functions (Ha et al., 2011; Ju and Jung, 2014).

To address this issue, several strategies have been employed to increase *N*-glycosylation occupancy in plant-produced proteins. One approach involves the co-expression of oligosaccharyltransferase (OST) subunits from *Leishmania* such as LmSTT3D or LdOST to compensate limitations of the plant endogenous OST complex (Castilho et al., 2018; Beihammer et al., 2023). Here, we aimed to address the issue of underglycosylation in plant-produced IgG1 by exploring an alternative strategy to enhance *N*-glycosylation occupancy. We focused on mutating amino acids adjacent to the *N*-glycosylation site to improve glycosylation efficiency. We generated various variants of the monoclonal IgG1 antibody trastuzumab, which targets the breast cancer antigen HER2, as well as the SARS-CoV-2 neutralizing monoclonal IgG1 antibody COVA2-15 (Claret and Vu, 2012; Brouwer et al., 2020; Göritzer et al., 2024a). This was achieved by mutating single amino acids near the *N*-glycosylation sequon to resemble sequences found in other IgG isotypes, such as human IgG2, IgG3, IgG4, and mouse IgG2, which have been previously approved for human therapy. To verify the broader applicability, we analyzed the glycosylation status, structural integrity, thermal stability, and receptor binding properties of the mutated IgG1 glycosylation variants.

2 Material and methods

2.1 IgG1 expression vectors

The codon-optimized genes of the heavy chain (OP892522.1) and light chain (OP892523.1) required for expression of trastuzumab IgG1 in *N. benthamiana* were synthesized by GeneArt (Thermo Fisher Scientific, USA). Sequences for expression in *N. benthamiana* were flanked with the signal peptide from barley alpha-amylase (AAA98615) and the restriction sites XhoI and AgeI. The synthesized DNA was then amplified by PCR with the primers "Strings_7F (CTTCCGGCTCGTTTGACCGGTATG)/Strings_8R (AAAAACCCTGGCGCTCGAG)", and the constructs were separately cloned into the AgeI/XhoI sites of the binary vector pEAQ-HT (Sainsbury et al., 2009).

Construction of expression vectors for pEAQ-COVA2-15 heavy chain and light chain have been described previously (Göritzer et al., 2024a).

To generate IgG1 variants, point mutations were introduced using QuikChange site-directed mutagenesis kit (Agilent Technologies) according to manufacturer's protocols using the primes described in Supplementary Table S1.

For expression in leaf epidermal cells of *N. benthamiana*, the plasmids were introduced into *Agrobacterium tumefaciens* strain UIA143 (Strasser et al., 2008).

Mammalian cell produced trastuzumab IgG1 was kindly provided by Alois Jungbauer (da Silva et al., 2019).

2.2 Plant material and agroinfiltration

N. benthamiana plants were grown at 23°C under long-day conditions (i.e., 16 h light/8 h dark). Infiltration into leaves of 5-week-old *N. benthamiana* was done as previously described (Göritzer et al., 2017). Briefly, the respective *Agrobacteria* were grown in LB-medium overnight at 29°C. Bacteria were centrifuged, resuspended in infiltration buffer (10 mM $MgSO_4$, 10 mM MES and 0.1 mM acetosyringone) and the suspension was used for infiltration. Agrobacteria suspensions of heavy-chain plasmids were infiltrated with a OD_{600} of 0.15, while Agrobacteria suspension with light-chain plasmids were infiltrated with an OD_{600} of 0.1. Recombinant proteins were expressed *in N. benthamiana* glycosylation mutant plants (ΔXT/FT) (Strasser et al., 2008). Infiltrated leaves were harvested 5 days post infiltration (dpi) and used for protein extraction as previously described (Göritzer et al., 2024a).

2.3 Antibody purification

Clarified leaf extracts were passed through columns packed with Pierce Protein A resin (Thermo Fisher, USA). Proteins were eluted with 0.1 M glycine pH 3.5, followed by the immediate addition of 10% (v/v) 1 M Tris-HCl pH 9.0 to neutralize the pH. Fractions containing the protein of interest were pooled and dialyzed against 1xPBS pH 7.4 at 4°C overnight using a dialyzing cassette with 10-kDa molecular weight cutoff (MWCO; Slide-A-Lyzer, Thermo Scientific, USA). Pooled and dialyzed protein fractions were concentrated using Amicon centrifugal filters with an MWCO of 30 kDa (Merck Millipore) and subjected to SEC on a HiLoad 16/600 Superdex 200 pg column (GE Healthcare, USA) equilibrated with 1xPBS pH 7.4 connected to an ÄKTA pure (GE Healthcare, USA) fast protein LC system.

2.4 Mass spectrometric analysis

For mass spectrometric analysis of IgG1 glycopeptides, 20 µg of purified protein was S-alkylated with iodoacetamide and digested in solution with trypsin (Promega, Austria). The digested samples were loaded on a nanoEase C18 column (nanoEase M/Z HSS T3 Column, 100Å, 1.8 µm, 300 µm × 150 mm, Waters), detected with an Orbitrap MS (Exploris 480, Thermo Fisher Scientific, Austria) and the obtained data analyzed using Skyline Version 22.2 software.

For intact protein analysis, around 2 µg of the protein solution was directly injected to a LC-ESI-MS system (LC: Agilent 1290 Infinity II UPLC). A gradient from 15 to 80% acetonitrile in 0.1% formic acid (using a Waters BioResolve column (2.1 x 5 mm) at a flow rate of 400 µL/min was applied (9 minutes gradient time). Detection was performed with a Q-TOF instrument (Agilent Technologies 6230B LC- TOFMS) equipped with the Jetstream ESI source in positive ion, MS mode (range: 100-3200 Da). Instrument calibration was performed using ESI calibration mixture (Agilent). Data was processed using MassHunter BioConfirm B.08.00 (Agilent) and the spectrum was deconvoluted by MaxEnt. Two blank runs (injection of 5 µL MS-grade water) were performed prior to the injection of the samples and a blank run was performed in between each sample in order to reduce carry-over from previous measurements/samples.

2.5 SDS-PAGE

For reducing or nonreducing SDS-PAGE a total of 5 µg of purified protein was loaded on a 10% gel and visualized with Coomassie Brilliant Blue staining.

2.6 Differential scanning fluorimetry

Differential scanning fluorimetry (DSF) was conducted using a CFX real-time PCR instrument (Bio-Rad Laboratories, Hercules, CA, USA) in 1×PBS buffer at pH 7.4 as previously described (Göritzer et al., 2024b). In short, monoclonal antibodies were diluted to a concentration of 1 mg/mL in the formulation buffer. SYPRO Orange Fluorescent Dye (Thermo Fisher Scientific, Waltham, MA, USA) was diluted 1000-fold from a 5000× concentrated stock to prepare the working dye solution in the formulation buffer before addition to the antibody samples. Thermal denaturation was initiated by gradually increasing the temperature from 25 to 95°C at a rate of 0.05°C/s. Fluorescence intensity measurements were recorded using the FRET channel. Automated data processing of thermal denaturation curves involved truncating the dataset to eliminate post-peak quenching effects. The first derivative approach to calculate *T*m was used. In this method, *T*m is the temperature corresponding to the maximum value of the first derivative of the DSF melting curve.

2.7 Dynamic light scattering

DLS measurements were performed as described previously with protein concentrations of 500 µg/mL in 1×PBS pH 7.4 supplemented with 0.05% Tween on a Malvern Zetasizer nano-ZS (Malvern Panalytical, Malvern, UK) in a 12 mL quartz cuvette (Göritzer et al., 2024b). Samples were measured at 25.0°C, and the LS was detected at 173° and collected in automatic mode. The mean values and SDs of the number weighted diameter were calculated from three measurements for each sample, and each reported value is an average.

2.8 OMNISEC

SEC-LS was used to characterize the recombinant expressed proteins in solutions relating to their purity, native oligomers or aggregates, and molecular weights as previously described (Göritzer et al., 2024a). Analyses were performed on an OMNISEC multidetector gel permeation chromatography (GPC)/SEC system equipped with a refractive index detector, a right-angle LS detector, a low-angle LS detector and a UV/visible light photodiode array detector (Malvern Panalytical, Malvern, UK). A Superdex 200 Increase 10/300 GL column (Cytiva, Marlborough, MA, USA) was used and equilibrated with Dulbecco's PBS without Ca and Mg, P04-361000 (PAN-Biotech, Germany), as running buffer. Experiments were performed at a flow rate of 0.5 mL min−1 at 25°C and analyzed using OMNISEC software version 11.40 (Malvern Panalytical, Malvern, UK). Proper performance of the instrument was ensured by calibration and verification using the 200 mg Pierce BSA standard (Thermo Fisher Scientific). Before analysis, samples were centrifuged (16,000× g, 10 min) and filtered through 0.2 mm Durapore PVDF centrifugal filter(s) (MilliporeSigma, Burlington, MA, USA). A 100 µL volume of each sample was injected at a concentration of 1 mg/mL.

2.9 Antigen-binding ELISA

To determine the binding of the purified recombinant IgG1 to the antigens HER2 and SARS-CoV-2 RBD, ELISA plates coated with 100 ng/well purified RBD-His or 250 ng/well purified HER2 (kindly provided by Elisabeth Laurent, BOKU University, Vienna)

as previously described (Göritzer et al., 2017; Göritzer et al., 2024a). For detection HRP-labeled anti-human IgG antibody was used (W4031, Promega, Austria). The EC_{50} was calculated in GraphPad Prism 9.0.

2.10 Receptor binding by surface plasmon resonance spectroscopy

Binding of IgG glycosylation variants to human FcRn was determined by surface plasmon resonance (SPR) in three replicates, using the Biacore T200 system (Cytiva) at 25°C. A Biacore CM5 Sensor Chip (Cytiva) was directly coated with 2.5 µg/mL of hFcRn (R&D Systems, 8639-FC-050, P55899) using an amine coupling kit (Cytiva, BR-1000-50) to approximately 80 response units (RU). PBS pH 6 supplemented with 0.05% Tween-20 was used as running buffer. Recombinant IgG1 were injected at 25-400 nM for 60 s and allowed to dissociate for 60 s. The chip was regenerated in PBS pH 7.4. The binding kinetics, k_{on} (1/Ms), k_{off} (1/s) and K_D (nM) were calculated from global fittings using a 1:1 binding model (BIAcore T2 Evaluation software).

For *in vitro* binding experiments to the extracellular domain (amino acids 17-208) of FcγRIIIa/CD16a was performed using a Biacore T200 (Cytiva), first the sensor chip surface was captured with anti-His antibody with the His Capture Kit (Cytiva) to a CM5 chip as described in the manufacturers' protocol. The capturing of anti-His antibody reached 32000 RU. Secondly, immobilization of the His-tagged FcγRIIIa (V158 allotype, AcroBiosystems) on the chip surface was performed for 60s with a concentration of 1 µg/mL and a flow rate of 10 µL/min in HEPES-EP running buffer. 40 RU units were achieved. The immobilization step was previously optimized to avoid avidity effects using lower concentration of FcγRIIIa. Flow cell 2 remained unmodified and served as a reference cell for the subtraction of systematic instrument noise and drift. IgG binding curves were generated in multi-cycle kinetic experiments at five different concentrations in three independent runs ranging from 31.25 nM to 500 nM with 180 seconds association and 480 seconds dissociation time at a flow rate of 10 µL/min. After each run, surface regeneration was accomplished using 10 mM glycine, pH 1.7, for 120 seconds at a flow rate of 30 µL/min. The binding kinetics, k_{on} (1/Ms), k_{off} (1/s) and K_D (nM) were calculated from global fittings using a 1:1 binding model (BIAcore T2 Evaluation software).

3 Results

3.1 Mutating amino-acids adjacent to the *N*-glycosylation site improves site-occupancy in plant-produced human IgG1

We transiently expressed the monoclonal IgG1 antibody trastuzumab ("Tz") in the glyco-engineered plant line *Nicotiana benthamiana* ΔXT/FT, which is almost completely devoid of β1,2-xylose- and α1,3-fucose-carrying *N*-glycans (Strasser et al., 2008). To investigate the role of the amino acid adjacent to the *N*-glycosylation sequon in glycosylation efficiency in plants, we generated various trastuzumab variants by mutating single amino acids near the *N*-glycosylation sequon of IgG1. These variants were designed to resemble sequences commonly found in other IgG isotypes, such as human IgG2, IgG3, IgG4, and mouse IgG2 (Figure 1A).

After transient expression of all IgG variants in *N. benthamiana* and small-scale purification from at least three pooled biological replicates, their glycosylation status was investigated. LC-ESI-MS analysis of the proteolytically digested heavy chain (HC) showed that, in contrast to commercially available trastuzumab produced in a mammalian cell line ("Tz-IgG_Ctrl"), considerable amounts of the non-glycosylated peptide are present in plant-produced wild-type IgG1 (~ 30%) and these amounts were further increased in the variant Q295D (~ 40%, Figures 1B, C). Other variants, including Y300F, Y296F and Y296F/Y300F, showed a notable reduction in the non-glycosylated peptide (~10-20%), with variant Y300L performing the best, which carries the mouse IgG2 sequence in close proximity to the sequon, exhibiting the most pronounced effect, with almost non-detectable amounts of non-glycosylated peptide. The reduction of underglycosylation was further demonstrated by immunoblotting of total soluble protein extracts under reducing conditions showing the presence of a double band representing the glycosylated (~ 53 kDa) and underglycosylated (~ 50 kDa) HC (Supplementary Figure S1), with a shift towards a single band for variant Y300L. This shift is caused by a higher degree of *N*-glycosylation occupancy as confirmed by Pngase F digestion followed by visualization by immunoblotting of Tz-IgG1 and variants Y300F and Y300L produced in *N. benthamiana* ΔXT/FT, which are not carrying α-1,3 linked core-fucose and can be cleaved by PngaseF in contrast to wild-type produced IgG1 (Supplementary Figure S2).

Besides the *N*-glycosylation efficiency of the different hosts, mammalian and plant-based systems also differ tremendously in terms of structural composition of attached *N*-glycans. The *N*-glycans found on plant-produced IgG1 variants showed a highly homogeneous profile, with biantennary complex-type GlcNAc2Man3GlcNAc2 (GnGn) as major glycoform. Mammalian cell-line produced trastuzumab glycan profiles are more complex and include high levels of galactosylation and sialylation, incomplete processing of branches and the possible modification with bisecting GlcNAc and core α1,6-fucosylation. Notably, the very homogenous glycosylation profile consisting of mostly GnGn type *N*-glycans of plant-produced IgG1 did not change by mutating amino-acids close to the *N*-glycosylation site demonstrating that the local amino acid environment does not affect complex *N*-glycan processing.

To further quantify and characterize the *N*-glycosylation occupancy of plant-produced IgG variants, we carried out an additional mass-spectrometry analysis by examining intact, fully assembled IgG (Figures 1D, E). While mammalian cell-line produced trastuzumab exhibits nearly complete *N*-glycosylation occupancy, intact MS measurements of the plant-produced wild-type IgG1 confirmed the presence of considerable amounts of non-glycosylated (0xGnGn) and the presence of hemi-glycosylated (1xGnGn) trastuzumab which is only glycosylated in one of the two HCs (together 24%). These values were significantly reduced in

10.3389/fpls.2024.1531710

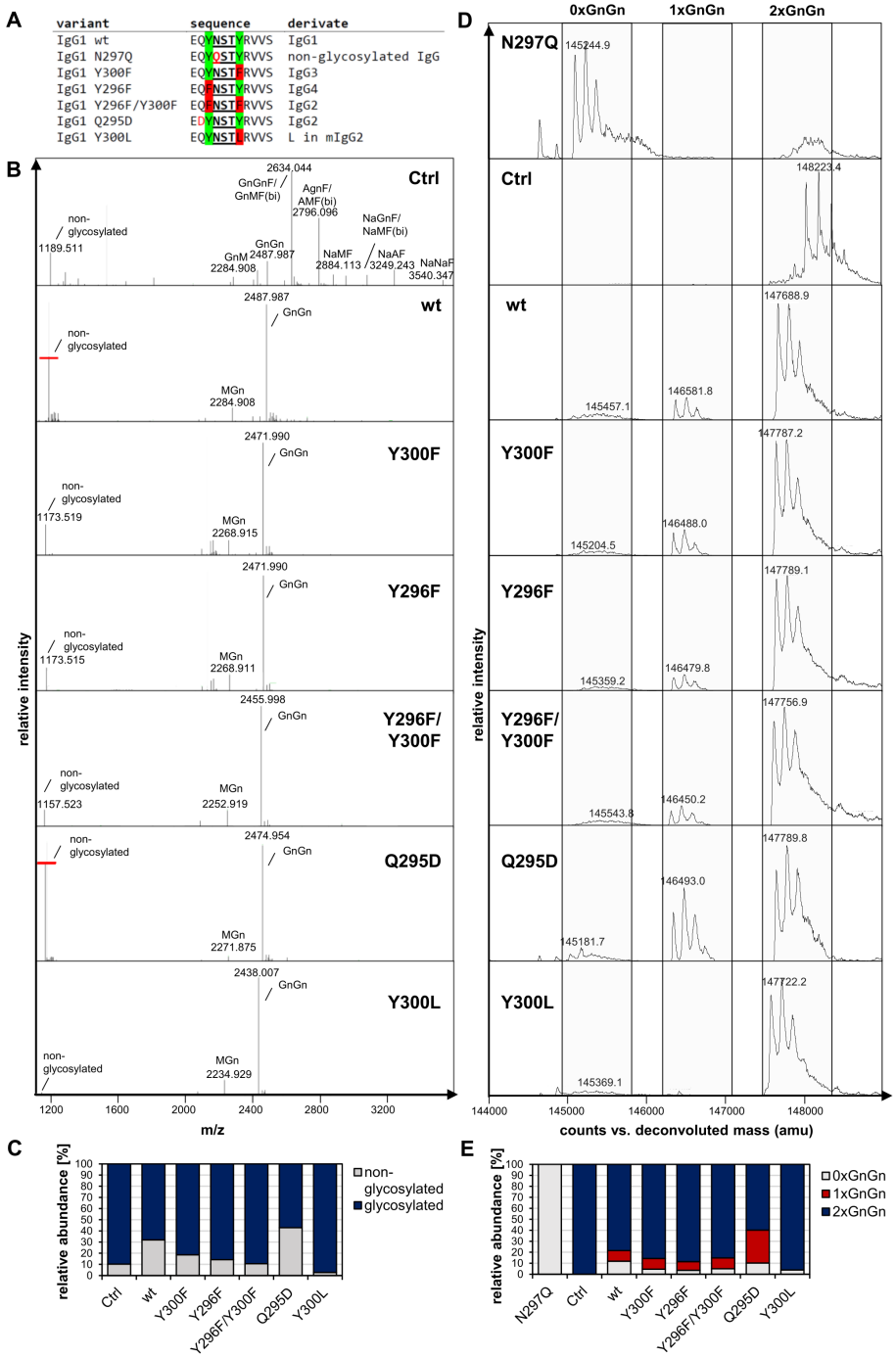

FIGURE 1
N-glycosylation analysis of trastuzumab (Tz) IgG1 variants produced in *N. benthamiana* ΔXT/FT. **(A)** Overview of the introduced amino acid sequence changes close to the conserved *N*-glycosylation site at position Asn297 of human IgG1. **(B)** LC-ESI-MS mass spectrometry spectra of tryptic peptide of Tz-IgG1 variants (wt:"EEQYNSTYR", $(M+2H)^{2+}$). Major glycoforms are labeled with abbreviations according to the ProGlycAn system (www.proglycan.com). **(C)** Quantification of the non-glycosylated glyco-peptide of Tz-IgG1 variants from LC-ESI-MS. **(D)** The *N*-glycan site occupancy of fully assembled intact Tz-IgG1 variants was determined using LC-ESI-MS. The peaks corresponding to non-glycosylated (0xGnGn), hemi-glycosylated (1xGnGn) and fully glycosylated (2xGnGn) IgG1 are highlighted. Multiple peaks represent different glycoforms and variations in the clipping of C-terminal lysine. **(E)** Quantification of the peaks from **D**.

all variants, except for Q295D. Variant Y300L displayed the most favorable outcome, with up to 98% of the assembled antibodies being fully glycosylated (2xGnGn).

To verify whether the Y300L mutation is also beneficial in terms of *N*-glycosylation occupancy in other monoclonal IgG1 antibodies, we generated a mutated variant of the SARS-CoV-2 neutralizing IgG1 antibody COVA2-15 (Figure 2). After transient expression in *N. benthamiana* and purification, wild-type and Y300L COVA2-15 IgG1 were analyzed via LC-ESI-MS of tryptic glycopeptides and subjected to intact mass spectrometry as described above.

Glycopeptide analysis (Figures 2A, B) showed the presence of high amounts of non-glycosylated peptide in wild-type COVA2-15 IgG1. Intact MS measurements (Figures 2C, D) confirmed that underglycosylation is mostly the hemiglycosylated type (1xGnGn, ~22%). However, the Y300L mutation significantly improved *N*-glycosylation, reducing underglycosylation to approximately 5%.

3.2 IgG1 glycosylation variants exhibit similar overall structural integrity, but differ in thermal stability

In the next step, we scaled up the recombinant production of trastuzumab and COVA2-15 IgG1 variants in *N. benthamiana* to enable downstream analysis of the mutations' effects and increased *N*-glycan occupancy on conformation and structural integrity. All variants were successfully expressed and purified, yielding amounts consistent with previously reported values (~100 mg/kg leaf fresh weight) (Kallolimath et al., 2020; Göritzer et al., 2024a). SDS-PAGE analysis of affinity- and SEC-purified IgG1 under reducing conditions showed predominant bands at the expected sizes of 53 kDa for the HC and 25 kDa for the light chain (LC) in all variants, except COVA2-15 IgG1. The latter displayed an additional minor band at around 40 kDa, corresponding to a commonly observed degradation product for this IgG1 variant in plants, likely due to proteolytic cleavage in the variable domain of the HC within the apoplast (manuscript under preparation; Figure 3A). Under non-reducing conditions all variants also showed characteristic bands at ~150 kDa corresponding to the fully assembled IgG1 antibody.

Size-exclusion chromatography coupled with light scattering revealed single, monodisperse peaks for all variants, with molecular sizes in the expected range of 149-151 kDa, confirming proper conformational integrity (Figure 3B; Table 1) and the absence of high molecular weight aggregates or additional degradation products. The high homogeneity of the variants was further supported by dynamic light scattering, which demonstrated a narrow particle size distribution. Notably, the Y300L mutants exhibited a significantly reduced polydispersity index (PDI < 0.05), indicating improved sample monodispersity compared to wild-type IgG1 produced *in planta* and in mammalian cell lines (Figure 3C). The non-glycosylated N297Q variant was not analyzed because it displayed a very high tendency to aggregate.

We next performed differential scanning fluorimetry to assess the thermal stability of IgG1 variants. Thermal unfolding of all antibodies revealed two distinct transitions, corresponding to the unfolding of the Fc domain (Tm_1) and the Fab domain (Tm_2) (Figure 3D; Supplementary Table S2). While all variants showed similar Tm_2 values to wild-type of around 80°C and 72°C for trastuzumab and COVA2-15, respectively, Tm_1 varied significantly among the variants. Commercial trastuzumab exhibited the highest Tm_1 (69.25°C), whereas the plant-produced non-glycosylated IgG1 (N297Q) displayed a 10°C reduction in

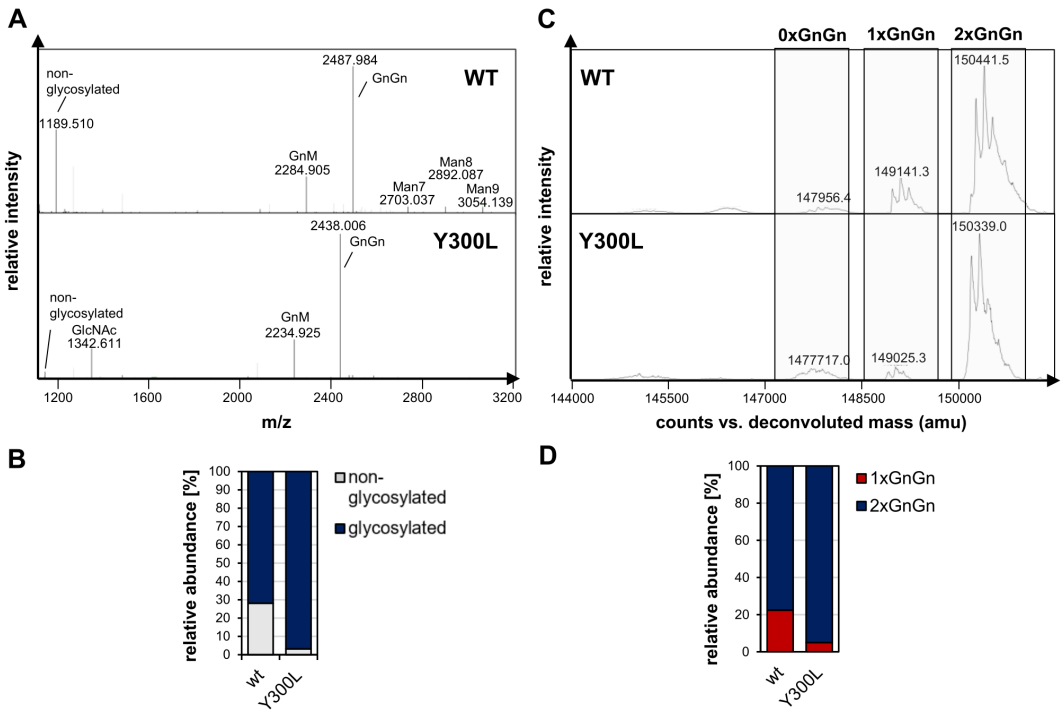

FIGURE 2
N-glycosylation analysis of COVA2-15 (CoV) IgG1 variants produced in *N. benthamiana* ΔXT/FT. **(A)** LC-ESI-MS mass spectrometry spectra of tryptic peptide of CoV-IgG variants (wt:"EEQYNSTYR", $(M+2H)^{2+}$). Major glycoforms are labeled with abbreviations according to the ProGlycAn system (www.proglycan.com). **(B)** Quantification of the non-glycosylated glyco-peptide of CoV-IgG variants from LC-ESI-MS from **A**. **(C)** The *N*-glycan site occupancy of fully assembled intact CoV-IgG variants was determined using LC-ESI-MS. The peaks corresponding to unglycosylated, hemi-glycosylated (1xGnGn) and fully glycosylated (2xGnGn) are highlighted. Multiple peaks represent different glycoforms and variations in the clipping of C-terminal lysine. **(D)** Quantification of the peaks from **C**.

10.3389/fpls.2024.1531710

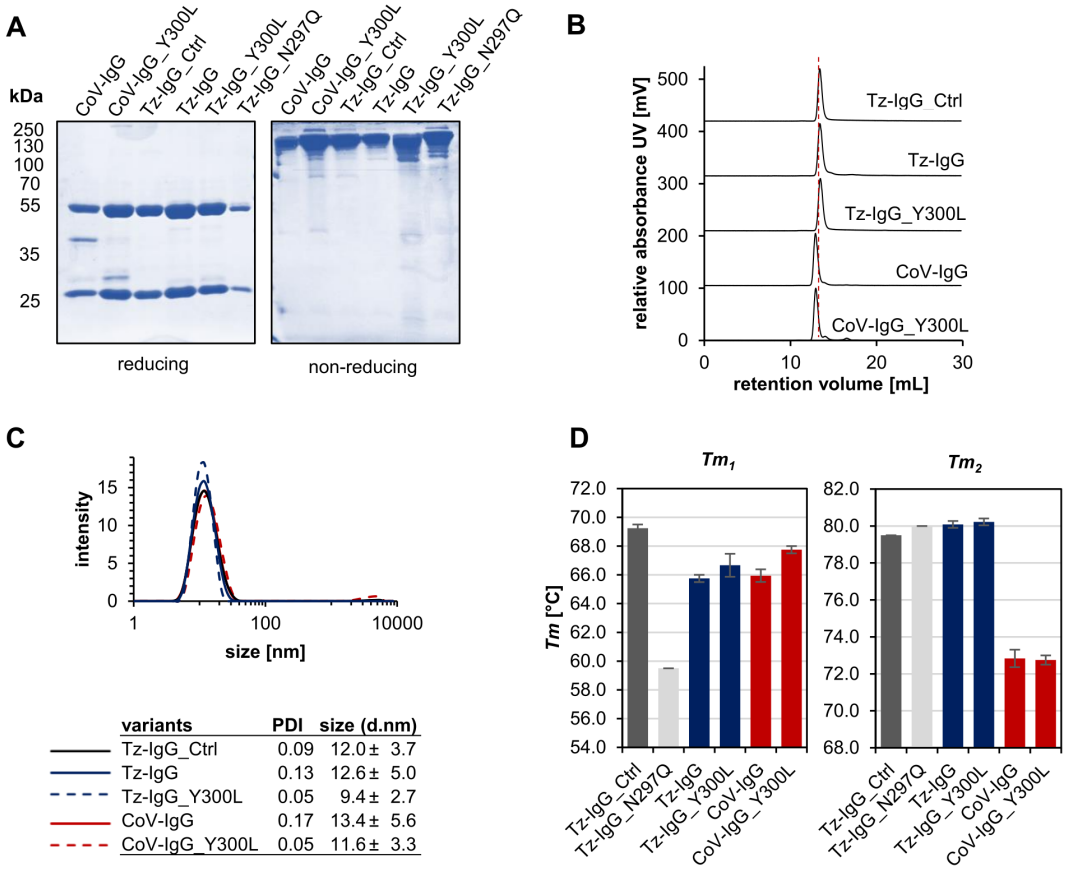

FIGURE 3
Characterization of purified recombinant IgG1 variants. **(A)** SDS-PAGE and Coomassie Brilliant Blue (CBB) staining of affinity and size-exclusion purified trastuzumab (Tz) and COVA2-15 (CoV) IgG1 variants from *N. benthamiana* ΔXT/FT. **(B)** Normalized size-exclusion chromatograms (A280) of affinity-purified and gel-filtration purified Tz- and CoV-IgG1 variants (A280 nm). **(C)** Dynamic light scattering (DLS) of Tz- and CoV-IgG1 variants. The mean diameter (size) and the homogeneity (PDI) were measured using a Malvern Zetasizer nano-ZS at 25°C. Each sample was measured in triplicates. **(D)** Thermal unfolding of Tz- and CoV-IgG variants was determined by differential scanning fluorimetry (DSF) in 1xPBS buffer pH 7.4. Experiments were performed at 1 mg/mL. Represented values are the mean ± SD of three technical repeats of three independent experiments.

thermal stability, consistent with previous reports highlighting the critical role of the Asn297 *N*-glycan in maintaining the IgG Fc domain's conformation (Kiyoshi et al., 2017). Plant-produced wild-type trastuzumab IgG1 exhibited a Tm_1 value 4°C lower than that of the commercial mammalian-produced version, emphasizing the role of not only the presence but also the composition of attached *N*-glycans for thermal stability of IgG1. Notably, the Y300L mutation improved the thermal stability of both trastuzumab and COVA2-15 IgG1, with an increase in Tm_1 of up to 2°C compared to their wild-type counterparts further approaching values of mammalian produced IgG1.

TABLE 1 Molecular weight (MW) and retention volume (RV) of recombinant IgG1 variants determined by SEC-LS.

	RV (mL)	MW (g/mol)
Tz-IgG_Ctrl	13.40	150539.5 ± 3889.4
Tz -IgG	13.41	148917.3 ± 4217.9
Tz -IgG_Y300L	13.47	149475.9 ± 3302.4
CoV -IgG	12.94	150851.8 ± 2384.0
CoV-IgG_Y300L	12.90	149559.1 ± 2099.3

Commercial trastuzumab (Tz-IgG_Ctrl) and *N. benthamiana* produced IgG1 variants were subjected to OMNISEC and molecular weight was determined with OMNISEC software v11.40 software.

3.3 Altered Fc glycosylation occupancy does not alter binding to antigens and has a minor impact on binding to the neonatal Fc receptor

We tested the functionality of the IgG1 glycosylation variants in terms of antigen-binding and receptor binding. Binding of trastuzumab and COVA2-15 IgG1 to the antigen HER2 and SARS-CoV-2 RBD, respectively, was unaffected by Fc-domain modifications (Figure 4; Supplementary Table S3). This is in accordance to previous reports that showed only minor cross-talk between the IgG1 Fc domain and antigen-binding capacities (Ha et al., 2011).

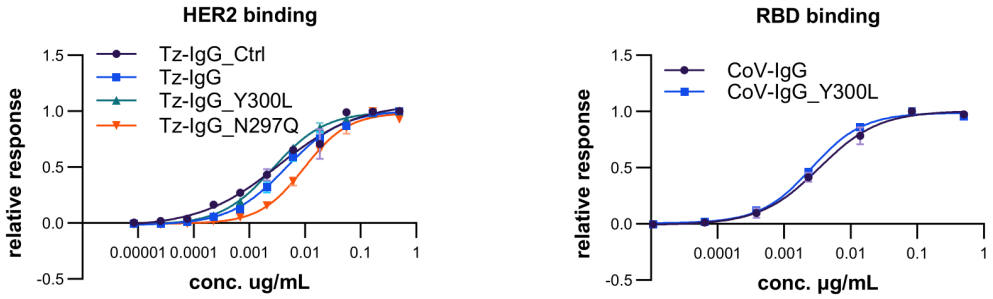

FIGURE 4
Antigen binding of different trastuzumab (Tz) and COVA2-15 (CoV) IgG1 variants. EC_{50} of binding of commercial trastuzumab (Tz-IgG_Ctrl) and recombinant Tz-IgG1 variants (Tz-IgG, Tz-IgG_N297Q, Tz-IgG_Y300L), as well as COVA2-15 IgG1 variants (CoV-IgG, CoV-IgG_Y300L) produced in *N. benthamiana* ΔXF plants to the respective antigens HER2 and SARS-COV-2 RBD was determined by ELISA. Each value is the mean ± SD from three independent measurements with two technical repeats and are depicted in detail in Supplementary Table S3.

The human FcRn is a key determinant in extending the plasma half-life of antibodies by recycling them through transcytosis pathways (Pyzik et al., 2019). Binding of IgG glycosylation variants to FcRn was assessed using surface plasmon resonance (SPR). A Biacore CM5 sensor chip was coated with recombinant FcRn, and IgG variants were injected at concentrations ranging from 25 to 400 nM. Binding kinetics were analyzed using a 1:1 binding model to determine kinetic parameters, including the association rate constant (k_{on}), dissociation rate constant (k_{off}), and equilibrium dissociation constant (K_D). Additionally, affinity was determined by steady-state kinetics (Table 2; Supplementary Figure S3A).

The interaction was characterized by fast association and very fast dissociation constants. Commercial trastuzumab (Tz-IgG_Ctrl) exhibited the highest k_{on}, indicating rapid binding to FcRn, and the lowest K_D, reflecting the highest affinity for FcRn. The association of plant-produced IgG variants was generally lower but improved with the introduction of the Y300L mutation. The dissociation constants were very fast for all variants and hence were challenging to fit in a 1:1 binding model. Therefore, affinity constants were also determined by steady-state. These K_D values were generally higher than values determined by kinetic measurements and may be more reliable due to the rapid association and dissociation of the complex. Affinity determined by steady-state kinetics showed very similar FcRn binding of commercial and plant-produced trastuzumab, even when the Y300L mutation was introduced (Table 2; Supplementary Table S5).

The affinity of COVA2-15 IgG1 wild-type to FcRn was generally lower than the trastuzumab counterpart and was similar to the N297Q variant. Introduction of the Y300L mutation with increased *N*-glycosylation occupancy significantly improved FcRn binding, reaching the same affinity as commercial trastuzumab. The primary interaction between IgG1 and FcRn is mediated by the protein-protein interface involving the CH2 and CH3 domains of the Fc region, rather than directly by the *N*-glycans at Asn297. However, glycosylation at Asn297 contributes to the overall structural integrity and stability of the Fc region, which may indirectly influence binding. Indeed, the relatively low RU_{max} of the N297Q variant and the slightly reduced RU_{max} of COVA2-15 wild-type IgG1 compared to commercial trastuzumab (Supplementary Table S4) indicates the presence of aggregated or non-functional protein under the tested conditions, which is in accordance with the importance of the Asn297 *N*-glycan for the structural integrity of IgG1.

3.4 Improved *N*-glycan occupancy increases the binding to FcγRIIIa

It has been extensively shown that the *N*-glycan at position Asn297 significantly influences the binding affinity of IgG1 to Fcγ receptors (Reusch and Tejada, 2015; Golay et al., 2022). In this study, we investigated the binding of IgG1 variants to FcγRIIIa (CD16a, V158) using SPR (Table 3; Supplementary Figure S3B). An anti-His antibody was immobilized on a CM5 sensor chip, followed by the capture of FcγRIIIa and the injection of monoclonal antibodies at concentrations ranging from 31.25 to 500 nM. Binding kinetics were analyzed using a 1:1 binding model to determine kinetic parameters. For the interaction of IgG1 with FcγRIIIa, also a fast association and dissociation were characteristic, whereas better fits of the 1:1 model were achieved compared to binding interactions with FcRn as described above. Commercial trastuzumab exhibited the lowest affinity (K_D=295.38 ± 4.31 nM), while plant-produced IgG1 variants showed a 3- to 4-fold increase in affinity to FcγRIIIa. This is in accordance with previous reports demonstrating the role of the α1,6-linked core fucose in the *N*-glycan at position Asn297 of mammalian-produced IgG1 in reducing the affinity to FcγRIIIa, which is significantly improved when this glycan moiety is removed, as in IgG1 produced in glyco-engineered *N. benthamiana* plants (Stelter et al., 2020). Improving the *N*-glycan occupancy through the Y300L mutation further increased binding affinity to FcγRIIIa for COVA2-15 IgG1 and to a lower extend for Trastuzumab IgG1 (Supplementary Table S6).

4 Discussion

The production of recombinant IgG1 antibodies in plants, particularly in *Nicotiana benthamiana*, has been shown to result in significant underglycosylation at the conserved Asn297 site. This phenomenon has been consistently observed in both transiently

TABLE 2 Kinetic parameters of recombinant IgG1 binding to human FcRn determined by surface plasmon resonance (SPR) spectroscopy.

	k_{on} (1/Ms)	k_{off} (1/Ms)	K_D (nM)	steady-state K_D (nM)
Tz-IgG_Ctrl	1579899.1 ± 2.8x10^5	0.084 ± 0.015	53.07 ± 0.77	195.31 ± 17.98
Tz-IgG_N297Q	124391.3 ± 2.9x10^4	0.011 ± 0.001	93.47 ± 28.7	309.12 ± 33.87
Tz-IgG	701727.1 ± 8.9x10^3	0.093 ± 0.042	94.00 ± 3.08	212.24 ± 1.49
Tz-Y300L	813348.6 ±1.5x10^4	0.100 ± 0.051	84.21 ± 2.56	209.28 ± 4.62
CoV-IgG	389378.1 ± 9.6x10^3	0.076 ± 0.001	195.57 ± 2.51	344.19 ± 28.14
COV-IgG_Y300L	170333.4 ± 2.4x10^4	0.012 ± 0.001	74.36 ± 14.35	209.63 ± 9.82

Values for kinetic constants k_{on}, k_{off} and K_D, as well as K_D obtained by steady-state analysis represent means ± SD from three independent experiments at 5 different concentrations.

produced IgG1 in *N. benthamiana* leaves and in stably expressed antibodies derived from various tissues and species (Rademacher et al., 2008; Vamvaka et al., 2016; Castilho et al., 2018; Jansing et al., 2019; Eidenberger et al., 2022). In contrast, mammalian cell-derived recombinant IgG1 is typically fully glycosylated at this site (Stadlmann et al., 2008).

The high expression levels achieved through viral vectors in plants can lead to an overload of the endogenous plant OST machinery, resulting in reduced *N*-glycosylation (Eidenberger et al., 2022). The limitation of the plant OST complex appears to be specific to distinct sites like Asn297 and is likely influenced by the local amino acid environment adjacent to the *N*-glycosylation site (Murray et al., 2015). While overexpression of the entire OST complex or individual subunits, such as LdOST or LmSTT3D, has been shown to increase *N*-glycan occupancy on recombinant glycoproteins expressed in plants, these approaches occasionally resulted in unwanted side effects (Castilho et al., 2018; Göritzer et al., 2020; Beihammer et al., 2023). For instance, the overexpression of LmSTT3D led to increased amounts of incompletely processed *N*-glycan structures, likely due to mislocalization to the Golgi apparatus and interference with other cellular processes (Castilho et al., 2018). LdOST seemed to be better suited and displayed only ER localization and did not lead to unwanted alterations of the overall *N*-glycan profile when co-expressed with recombinant antibodies (Beihammer et al., 2023).

To date, LdOST has only been employed for transient co-expression with plant-produced recombinant glycoproteins. For robust industrial-scale production of human IgG1 in *N. benthamiana*, the use of a stable engineered line expressing LdOST or, alternatively, the engineered Y300L IgG1 HC variants would be advantageous.

Our study aimed to address the issue of underglycosylation in plant-produced IgG1 by exploring strategies to enhance *N*-glycosylation occupancy through target protein engineering. We focused on mutating amino acids adjacent to the *N*-glycosylation site to investigate the role of the amino-acid sequence around the *N*-glycosylation sequon for glycosylation efficiency of the endogenous plant OST. We chose human sequences and sequences from murine immunoglobulins because human sequences are unlikely to cause adverse side effects, and several murine IgG1 and IgG2 antibodies, such as Ibritumomab tiuxetan, have been approved for human therapy (Grillo-López, 2002). The results demonstrated that mutating specific amino acids near the *N*-glycosylation sequon significantly improved glycosylation efficiency, while not changing the composition of attached glycans. Notably, the Y300L mutation resulted in almost non-detectable amounts of non-glycosylated peptide, indicating a substantial improvement in glycosylation occupancy.

Our findings suggest that protein engineering of the target protein, specifically through amino acid mutations adjacent to the *N*-glycosylation site, can lead to increased glycosylation efficiency. The Y300L mutation not only improved glycosylation occupancy, but also enhanced thermal stability of the IgG1 antibodies. This is consistent with previous studies that reported reduced thermal stability of non-glycosylated IgG1, primarily affecting the CH2 domain (Garber and Demarest, 2007).

While as expected antigen-binding was not affected, increased glycosylation of IgG1 also resulted in improved glycosylation-

TABLE 3 Kinetic parameters of recombinant IgG1 binding to FcγRIIIa determined by SPR.

	k_{on} (1/Ms)	k_{off} (1/Ms)	K_D (nM)	steady-state K_D (nM)
Tz-IgG_Ctrl	131348.0 ± 462.7	0.0388 ± 0.0005	295.38 ± 4.31	501.92 ± 8.18
Tz-IgG	362784.9 ± 3811.0	0.0296 ± 0.0007	81.69 ± 2.21	166.80 ± 6.85
Tz-IgG_Y300L	425111.5 ± 1365.1	0.0325 ± 0.0002	76.47 ± 0.29	152.31 ± 6.02
CoV-IgG	306487.9 ± 2456.5	0.0388 ± 0.0007	126.74 ± 2.93	258.65 ± 17.57
CoV-IgG_Y300L	367319.4 ± 14973.9	0.0358 ± 0.0005	97.62 ± 5.49	194.99 ± 6.26

Values for kinetic constants k_{on}, k_{off} and K_D, as well as K_D obtained by steady-state analysis represent means ± SD from three independent experiments at 5 different concentrations.

dependent activities, such as enhanced FcγRIIIa binding affinities. These results align with previous studies that reported decreased FcγRIIIa binding of hemi-glycosylated IgG1 (Ha et al., 2011). The recycling of human IgG1 via interaction with FcRn is a crucial factor in determining the serum half-life. It is established that FcRn interacts with specific amino acid residues located within the CH2 and CH3 domains, which are distant from the conserved *N*-glycosylation site (Ying et al., 2014). However, FcRn affinity chromatography showed differences between glycoengineered IgG1 variants with reduced binding of partially or fully deglycosylated variants (Cymer et al., 2017). The non-glycosylated trastuzumab variant displayed a reduced affinity for FcRn by SPR. Furthermore, a distinction in binding was identified between COVA2-15 IgG1 and the Y300L variant with increased *N*-glycosylation. Although the observed discrepancies in binding could be ascribed to variations in the aggregation propensity of the non-glycosylated IgG1 variants, it is conceivable that the glycans exert a more direct influence on FcRn binding.

Increasing the glycosylation occupancy in plant-produced IgG, combined with well-established glyco-engineering approaches in plants to produce monoclonal IgG antibodies with human-like *N*-glycosylation, can significantly enhance the performance of therapeutic plant-based IgG antibodies. These well-established approaches include producing *N*-glycans without core-fucose and with either terminal galactose or sialic acid, which are essential for enhancing the effector function and circulatory half-life of monoclonal antibodies (Strasser et al., 2009; Forthal et al., 2010; Castilho et al., 2015; Kogelmann et al., 2024).

In conclusion, our study demonstrates that targeted amino acid mutations near the *N*-glycosylation site can significantly enhance glycosylation efficiency in plant-produced IgG1 antibodies. This approach not only improves the structural integrity and thermal stability of the antibodies but also enhances their functional activities, such as receptor binding. These findings provide valuable insights into the optimization of plant-based expression systems for the production of high-quality recombinant antibodies.

Data availability statement

The original contributions presented in the study are included in the article/Supplementary Material. Further inquiries can be directed to the corresponding author.

Author contributions

KG: Conceptualization, Data curation, Formal analysis, Investigation, Methodology, Supervision, Writing – original draft. VR: Formal analysis, Investigation, Writing – review & editing. UV: Formal analysis, Investigation, Writing – review & editing. SI: Formal analysis, Investigation, Writing – review & editing. OB-M: Formal analysis, Investigation, Writing – review & editing. TP: Formal analysis, Investigation, Writing – review & editing. NP: Formal analysis, Investigation, Writing – review & editing. WP: Supervision, Writing – review & editing. RS: Conceptualization, Funding acquisition, Methodology, Project administration, Supervision, Writing – review & editing.

Funding

The author(s) declare financial support was received for the research, authorship, and/or publication of this article. This work was funded by the Austrian Science Fund FWF (P31920/Grant DOI: 10.55776/P31920, Doctoral Program BioToP-Biomolecular Technology of Proteins, W1224-B09) and Schrödinger Fellowship J4583). Research reported in this publication was jointly supported by the ASEAN-European Academic University Network (ASEAUNINET), the Austrian Federal Ministry of Education, Science and Research (BMBWF). The authors declare that this study received funding from OeAD-GmbH -Austria's Agency for Education and Internationalisation -project: ASEA 2023 24/BOKU/2. The funder was not involved in the study design, collection, analysis, interpretation of data, the writing of this article or the decision to submit it for publication.

Acknowledgments

We thank Elisabeth Laurent for conducting SEC-LS, as well as Daniel Maresch, Clemens Grünwald-Gruber and Rudolf Figl (all BOKU University, Vienna) for MS analysis. The OMNISEC multidetector GPC/SEC system (Malvern Panalytical), Zetasizer Nano ZSP (Malvern Panalytical), and MS equipment were kindly provided by the EQ-BOKU VIBT GmbH, and the project was supported by the BOKU Core Facility Biomolecular & Cellular Analysis and BOKU Core Facility Mass Spectrometry.

Conflict of interest

The authors declare that the research was conducted in the absence of any commercial or financial relationships that could be construed as a potential conflict of interest.

Publisher's note

Supplementary material

The Supplementary Material for this article can be found online at: https://www.frontiersin.org/articles/10.3389/fpls.2024.1531710/full#supplementary-material

References

Beihammer, G., König-Beihammer, J., Kogelmann, B., Ruocco, V., Grünwald-Gruber, C., D'Aoust, M. A., et al. (2023). An oligosaccharyltransferase from Leishmania donovani increases the N-glycan occupancy on plant-produced IgG1. *Front. Plant Sci.* 14. doi: 10.3389/fpls.2023.1233666

Bendandi, M., Marillonnet, S., Kandzia, R., Thieme, F., Nickstadt, A., Herz, S., et al. (2010). Rapid, high-yield production in plants of individualized idiotype vaccines for non-Hodgkin's lymphoma. *Ann. Oncol.* 21, 2420–2427. doi: 10.1093/annonc/mdq256

Brouwer, P. J. M., Caniels, T. G., van der Straten, K., Snitselaar, J. L., Aldon, Y., Bangaru, S., et al. (2020). Potent neutralizing antibodies from COVID-19 patients define multiple targets of vulnerability. *Science* 369, 643–650. doi: 10.1126/science.abc5902

Castilho, A., Beihammer, G., Pfeiffer, C., Göritzer, K., Montero-Morales, L., Vavra, U., et al. (2018). An oligosaccharyltransferase from Leishmania major increases the N-glycan occupancy on recombinant glycoproteins produced in Nicotiana benthamiana. *Plant Biotechnol. J.* 16, 1700–1709. doi: 10.1111/pbi.12906

Castilho, A., Gruber, C., Thader, A., Oostenbrink, C., Pechlaner, M., Steinkellner, H., et al. (2015). Processing of complex N-glycans in IgG Fc-region is affected by core fucosylation. *MAbs* 7, 863–870. doi: 10.1080/19420862.2015.1053683

Claret, F. X., and Vu, T. T. (2012). Trastuzumab: updated mechanisms of action and resistance in breast cancer. *Front. Oncol.* 2. doi: 10.3389/fonc.2012.00062

Crescioli, S., Kaplon, H., Chenoweth, A., Wang, L., Visweswaraiah, J., and Reichert, J. M. (2024). Antibodies to watch in 2024. *mAbs* 16, 2297450. doi: 10.1080/19420862.2023.2297450

Cymer, F., Schlothauer, T., Knaupp, A., and Beck, H. (2017). Evaluation of an FcRn affinity chromatographic method for IgG1-type antibodies and evaluation of IgG variants. *Bioanalysis* 9, 1305–1317. doi: 10.4155/bio-2017-0109

da Silva, G. F. L., Plewka, J., Tscheließnig, R., Lichtenegger, H., Jungbauer, A., and Dias-Cabral, A. C. M. (2019). Antibody binding heterogeneity of protein A resins. *Biotechnol. J.* 14, e1800632. doi: 10.1002/biot.201800632

Eidenberger, L., Eminger, F., Castilho, A., and Steinkellner, H. (2022). Comparative analysis of plant transient expression vectors for targeted N-glycosylation. *Front. Bioeng Biotechnol.* 10. doi: 10.3389/fbioe.2022.1073455

Eidenberger, L., Kogelmann, B., and Steinkellner, H. (2023). Plant-based biopharmaceutical engineering. *Nat. Rev. Bioeng* 1, 426–439. doi: 10.1038/s44222-023-00044-6

Forthal, D. N., Gach, J. S., Landucci, G., Jez, J., Strasser, R., Kunert, R., et al. (2010). Fc-glycosylation influences Fcγ receptor binding and cell-mediated anti-HIV activity of monoclonal antibody 2G12. *J. Immunol.* 185, 6876–6882. doi: 10.4049/jimmunol.1002600

Garber, E., and Demarest, S. J. (2007). A broad range of Fab stabilities within a host of therapeutic IgGs. *Biochem. Biophys. Res. Commun.* 355, 751–757. doi: 10.1016/j.bbrc.2007.02.042

Golay, J., Andrea, A. E., and Cattaneo, I. (2022). Role of fc core fucosylation in the effector function of igG1 antibodies. *Front. Immunol.* 13. doi: 10.3389/fimmu.2022.929895

Göritzer, K., Goet, I., Duric, S., Maresch, D., Altmann, F., Obinger, C., et al. (2020). Efficient N-glycosylation of the heavy chain tailpiece promotes the formation of plant-produced dimeric igA. *Front. Chem.* 8. doi: 10.3389/fchem.2020.00346

Göritzer, K., Groppelli, E., Grünwald-Gruber, C., Figl, R., Ni, F., Hu, H., et al. (2024a). Recombinant neutralizing secretory IgA antibodies for preventing mucosal acquisition and transmission of SARS-CoV-2. *Mol. Ther.* 32, 689–703. doi: 10.1016/j.ymthe.2024.01.025

Göritzer, K., Maresch, D., Altmann, F., Obinger, C., and Strasser, R. (2017). Exploring site-specific N-glycosylation of HEK293 and plant-produced human igA isotypes. *J. Proteome Res.* 16, 2560–2570. doi: 10.1021/acs.jproteome.7b00121

Göritzer, K., Strasser, R., and Ma, J. K. (2024b). Stability engineering of recombinant secretory igA. *Int. J. Mol. Sci.* 25, 6856. doi: 10.3390/ijms25136856

Grillo-López, A. J. (2002). Zevalin: the first radioimmunotherapy approved for the treatment of lymphoma. *Expert Rev. Anticancer Ther.* 2, 485–493. doi: 10.1586/14737140.2.5.485

Ha, S., Ou, Y., Vlasak, J., Li, Y., Wang, S., Vo, K., et al. (2011). Isolation and characterization of IgG1 with asymmetrical Fc glycosylation. *Glycobiology* 21, 1087–1096. doi: 10.1093/glycob/cwr047

Jansing, J., Sack, M., Augustine, S. M., Fischer, R., and Bortesi, L. (2019). CRISPR/Cas9-mediated knockout of six glycosyltransferase genes in Nicotiana benthamiana for the production of recombinant proteins lacking beta-1,2-xylose and core alpha-1,3-fucose. *Plant Biotechnol. J.* 17, 350–361. doi: 10.1111/pbi.12981

Ju, M. S., and Jung, S. T. (2014). Aglycosylated full-length IgG antibodies: steps toward next-generation immunotherapeutics. *Curr. Opin. Biotechnol.* 30, 128–139. doi: 10.1016/j.copbio.2014.06.013

Kallolimath, S., Hackl, T., Gahn, R., Grünwald-Gruber, C., Zich, W., Kogelmann, B., et al. (2020). Expression profiling and glycan engineering of igG subclass 1-4 in nicotiana benthamiana. *Front. Bioeng Biotechnol.* 8. doi: 10.3389/fbioe.2020.00825

Kiyoshi, M., Tsumoto, K., Ishii-Watabe, A., and Caaveiro, J. M. M. (2017). Glycosylation of IgG-Fc: a molecular perspective. *Int. Immunol.* 29, 311–317. doi: 10.1093/intimm/dxx038

Kogelmann, B., Melnik, S., Keshvari, T., Bogner, M., Lavoie, P. O., MA, D. A., et al. (2024). An industrial-grade Nicotiana benthamiana line for the production of glycoproteins carrying fucose-free galactosylated N-glycans. *N Biotechnol.* 85, 23–30. doi: 10.1016/j.nbt.2024.11.007

Murray, A. N., Chen, W., Antonopoulos, A., Hanson, S. R., Wiseman, R. L., Dell, A., et al. (2015). Enhanced aromatic sequons increase oligosaccharyltransferase glycosylation efficiency and glycan homogeneity. *Chem. Biol.* 22, 1052–1062. doi: 10.1016/j.chembiol.2015.06.017

Pyzik, M., Sand, K. M. K., Hubbard, J. J., Andersen, J. T., Sandlie, I., and Blumberg, R. S. (2019). The neonatal fc receptor (FcRn): A misnomer? *Front. Immunol.* 10. doi: 10.3389/fimmu.2019.01540

Rademacher, T., Sack, M., Arcalis, E., Stadlmann, J., Balzer, S., Altmann, F., et al. (2008). Recombinant antibody 2G12 produced in maize endosperm efficiently neutralizes HIV-1 and contains predominantly single-GlcNAc N-glycans. *Plant Biotechnol. J.* 6, 189–201. doi: 10.1111/j.1467-7652.2007.00306.x

Reusch, D., and Tejada, M. L. (2015). Fc glycans of therapeutic antibodies as critical quality attributes. *Glycobiology* 25, 1325–1334. doi: 10.1093/glycob/cwv065

Ridgley, L. A., Falci Finardi, N., Gengenbach, B. B., Opdensteinen, P., Croxford, Z., Ma, J. K., et al. (2023). Killer to cure: Expression and production costs calculation of tobacco plant-made cancer-immune checkpoint inhibitors. *Plant Biotechnol. J.* 21, 1254–1269. doi: 10.1111/pbi.14034

Ruocco, V., and Strasser, R. (2022). Transient expression of glycosylated SARS-coV-2 antigens in nicotiana benthamiana. *Plants (Basel)* 11. doi: 10.3390/plants11081093

Sainsbury, F., Thuenemann, E. C., and Lomonossoff, G. P. (2009). pEAQ: versatile expression vectors for easy and quick transient expression of heterologous proteins in plants. *Plant Biotechnol. J.* 7, 682–693. doi: 10.1111/j.1467-7652.2009.00434.x

Shanmugaraj, B., Malla, A., Bulaon, C. J. I., Phoolcharoen, W., and Phoolcharoen, N. (2022). Harnessing the potential of plant expression system towards the production of vaccines for the prevention of human papillomavirus and cervical cancer. *Vaccines (Basel)* 10. doi: 10.3390/vaccines10122064

Stadlmann, J., Pabst, M., Kolarich, D., Kunert, R., and Altmann, F. (2008). Analysis of immunoglobulin glycosylation by LC-ESI-MS of glycopeptides and oligosaccharides. *Proteomics* 8, 2858–2871. doi: 10.1002/pmic.200700968

Stelter, S., Paul, M. J., Teh, A. Y., Grandits, M., Altmann, F., Vanier, J., et al. (2020). Engineering the interactions between a plant-produced HIV antibody and human Fc receptors. *Plant Biotechnol. J.* 18, 402–414. doi: 10.1111/pbi.13207

Strasser, R., Castilho, A., Stadlmann, J., Kunert, R., Quendler, H., Gattinger, P., et al. (2009). Improved virus neutralization by plant-produced anti-HIV antibodies with a homogeneous beta1,4-galactosylated N-glycan profile. *J. Biol. Chem.* 284, 20479–20485. doi: 10.1074/jbc.M109.014126

Strasser, R., Stadlmann, J., Schahs, M., Stiegler, G., Quendler, H., Mach, L., et al. (2008). Generation of glyco-engineered Nicotiana benthamiana for the production of monoclonal antibodies with a homogeneous human-like N-glycan structure. *Plant Biotechnol. J.* 6, 392–402. doi: 10.1111/j.1467-7652.2008.00330.x

Vamvaka, E., Twyman, R. M., Murad, A. M., Melnik, S., Teh, A. Y., Arcalis, E., et al. (2016). Rice endosperm produces an underglycosylated and potent form of the HIV-neutralizing monoclonal antibody 2G12. *Plant Biotechnol. J.* 14, 97–108. doi: 10.1111/pbi.12360

Ying, T., Ju, T. W., Wang, Y., Prabakaran, P., and Dimitrov, D. S. (2014). Interactions of igG1 CH2 and CH3 domains with fcrn. *Front. Immunol.* 5. doi: 10.3389/fimmu.2014.00146

Zeitlin, L., Pettitt, J., Scully, C., Bohorova, N., Kim, D., Pauly, M., et al. (2011). Enhanced potency of a fucose-free monoclonal antibody being developed as an Ebola virus immunoprotectant. *Proc. Natl. Acad. Sci. U.S.A.* 108, 20690–20694. doi: 10.1073/pnas.1108360108

frontiers | Frontiers in Plant Science

TYPE Original Research
PUBLISHED 04 April 2025
DOI 10.3389/fpls.2025.1573193

OPEN ACCESS

EDITED BY
Kevin Yueju Wang,
University of Pikeville, United States

REVIEWED BY
Zenglin Zhang,
Chinese Academy of Agricultural Sciences, China
Thilaga D.,
Saveetha Dental College And Hospitals, India

*CORRESPONDENCE
Nuo Xu
20160125@wzu.edu.cn
Yunpeng Wang
wangypbio@cjaas.com

RECEIVED 08 February 2025
ACCEPTED 14 March 2025
PUBLISHED 04 April 2025

CITATION
Yu G, Lin S, Huang X, Gao S, Song C, Khalilov F, Chen Q, Issaro N, Xiao J, Xu X, Wang J, Zhao W, Wang Y and Xu N (2025) Expression of an epidermal growth factor-transdermal peptide fusion protein in *Arabidopsis thaliana* and its therapeutic effects on skin barrier repair.
Front. Plant Sci. 16:1573193.
doi: 10.3389/fpls.2025.1573193

Expression of an epidermal growth factor-transdermal peptide fusion protein in *Arabidopsis thaliana* and its therapeutic effects on skin barrier repair

Guangdong Yu[1,2], Shisheng Lin[1,2], Xulong Huang[1], Shuang Gao[3], Chengyang Song[1], Farid Khalilov[1], Qiongzhen Chen[1], Nipatha Issaro[4], Jiali Xiao[1,2], Xiashun Xu[1,2], Junchao Wang[3], Wengang Zhao[1], Yunpeng Wang[2]* and Nuo Xu[1,5]*

[1]College of Life and Environmental Sciences, Wenzhou University, Wenzhou, China, [2]Institute of Agricultural Biotechnology, Jilin Academy of Agricultural Sciences (Northeast Agricultural Research Center of China), Changchun, China, [3]Technology Development Department, Zhejiang Tianqu Beiben Instrument Technology Co., Ltd, Wenzhou, China, [4]Institute of Agricultural Biotechnology, Jilin Academy of Agricultural Sciences (Northeast Agricultural Research Center of China), Chonburi, Thailand, [5]Technology Development Department, Zhejiang Tianqu Beiben Instrument Technology Co., Ltd., Wenzhou, China

Epidermal growth factor (EGF) is recognized for its role in regulating keratinocyte proliferation and differentiation, thereby facilitating the restoration of impaired skin barriers. Nevertheless, challenges related to the penetration and safety of EGF remain to be resolved. In this study, we evaluated the efficacy of TDP1, a transdermal peptide, in enhancing the penetration of EGF through murine skin, utilizing EGF expressed in *A. thaliana*. The coding sequences of the TDP1 and EGF genes were cloned as a fusion construct into a plant expression vector. The resulting plasmid, pGM3301-TDP1-EGF, was introduced into *A. thaliana* via the floral dip method. Positive clones were identified using polymerase chain reaction (PCR). High-expression strains were selected through Western-blot analysis and enzyme-linked immunosorbent assay (ELISA). Homozygotes plants were obtained through self-pollination. The impact of the TDP1-EGF fusion protein on the restoration of a compromised epidermal barrier was assessed using dermatoscopy. Keratinocyte (KC) proliferation was examined via hematoxylin and eosin (H&E) staining, while KC differentiation, lipid synthesis, and inflammatory factors were analyzed using reverse transcription quantitative PCR (RT-qPCR) and immunohistochemistry. Compared to other expression systems, the *A. thaliana* system utilized for TDP1-EGF expression offers the advantages of being devoid of toxicity from endogenous plant substances, rendering it both safe and suitable for scalable production of the recombinant protein. The yield of the TDP1-EGF fusion protein expressed in *A. thaliana* accounted for 0.0166% of the total soluble protein. EGF conjugated with TDP1 displayed enhanced transdermal activity compared to unconjugated EGF, as evidenced by the Franz diffusion cell assay. Furthermore, the biological efficacy of the TDP1-EGF

fusion protein surpassed that of EGF alone in ameliorating epidermal barrier damage in a murine skin injury model. This research has the potential to revolutionize the development and delivery of skincare products and establishes a foundation for the application of molecular farming in skin health.

KEYWORDS

epidermal growth factor, transdermal peptide, fusion protein, a. thaliana expression system, skin barrier damage repair

1 Introduction

The skin barrier is a regular structure composed of the stratum corneum and intercellular lipids in a "brick and mortar" arrangement, and its main function is to protect the skin against mechanical, physical, chemical, and biological external stimuli and maintain the stability of the internal environment of the body (Montero-Vilchez et al., 2021; Panzuti et al., 2020). It is the first line of defense against external factors that may harm the body (Xu et al., 2019; Goverman, 2014). The skin barrier is formed by the basal layer keratinocytes proliferating and differentiating in an orderly manner as they migrate upward to form the spinous layer, granular layer, and eventually the stratum corneum (Segre, 2006; Joly-Tonetti et al., 2021). A healthy skin barrier is one that undergoes a continuous process of self-renewal (Labarrade et al., 2015; Hänel et al., 2013; Candi et al., 2005; Lim, 2021). When the structure of the skin barrier is damaged, harmful substances and pathogens from the external environment can invade the skin and disrupt its internal homeostasis (Yosipovitch et al., 2019). This will then hinder the differentiation of keratinocytes, leading to abnormal proliferation and an inability to form a healthy skin barrier, eventually giving rise to a series of skin problems (Wikramanayake et al., 2014; Lee et al., 2006). Thus, regulating keratinocyte proliferation and differentiation is essential for preserving skin barrier integrity and safeguarding skin health.

Epidermal growth factor (EGF) is the first discovered growth factor, and it is a 53-amino acid peptide that plays an important role in regulating cell growth, proliferation, and differentiation (Liou et al., 1997). EGF promotes the phosphorylation of AKT/PI3K, thereby activating the AKT/PI3K signaling pathway. The AKT/PI3K signaling pathway represents a critical intracellular signaling network that plays a pivotal role in regulating diverse physiological processes, including cell metabolism, proliferation, survival, and migration, eventually resulting in elevated expression of differentiation markers (e.g., filaggrin) in keratinocytes (KC) (Oda et al., 2005; Haase et al., 2003). Thus, its function is also to promote the differentiation of keratinocytes, and such a function can facilitate the repair of damaged epidermal barriers (Zhang et al., 2014; Chen et al., 2022b; Li et al., 2021). However, the transdermal efficacy of EGF is rather low because the large size of EGF (6,045 Da) makes it difficult for the peptide to effectively penetrate the membrane of KC (Adamson and Rees, 1981). The transdermal peptide (TDP1), a short peptide consisting of 11 polar amino acids, served as a carrier to facilitate the transdermal delivery of protein therapeutics to the dermal layer. Studies have shown that simply mixing transdermal peptide with insulin and applying it to the skin of diabetic rats can effectively lower their blood glucose levels (Chen et al., 2006). A study demonstrated that fusing TDP1 with EGF enhances the efficacy of EGF in repairing compromised skin barriers.

TDP1 is derived from TD1, a bacteriophage-derived transdermal peptide, through codon optimization for plant-based expression. Plant bioreactors offer the advantage of performing post-translational modifications on eukaryotic proteins, a capability absent in prokaryotic expression systems (Webster and Thomas, 2012). Expressing the TDP1-EGF fusion protein would ensure that the structure and function are very close to those of the natural protein, thus guaranteeing the efficacy of both TDP1 and EGF (Huang and McDonald, 2012). Plant bioreactors do not contain pyrogens, endotoxins, or other allergenic substances, thus reducing the potential risk of allergenicity and pathogenicity that may contaminate the exogenously expressed proteins (Moustafa et al., 2016; Ren et al., 2018). The plant bioreactor system can stably express exogenous proteins with lower costs, making it easier to achieve industrial application (Ma et al., 2003). Although the expression level of foreign proteins in *A. thaliana* is below 0.1% of total protein—a concentration necessary for commercial applications—the use of a whole-plant expression strategy renders this approach viable. This approach not only can boost the bioaccumulation of the foreign proteins but also ensure stable inheritance and significantly reduce labor costs (Zhang et al., 2021). However, some plant expression systems are not suitable for expressing skin care products; for example, studies have shown that nicotine can affect protein composition and damage organelles, particularly disrupting mitochondrial and peroxisomal reactive oxygen species (ROS) homeostasis in the 3D human skin model EpiDerm (Pozuelos et al., 2022). These alterations may aggravate skin infections, impede wound healing, and promote oxidative damage in skin cells. Consequently, due to safety concerns, *Nicotiana tabacum* is deemed unsuitable for producing skin care products. In contrast, more suitable plant candidates for such applications include *Arabidopsis thaliana*, legumes, fruits, and

vegetables. As a model plant, *A. thaliana* possesses several advantageous traits compared to other species, including high transformation efficiency, robust adaptability, rapid growth, a short life cycle, and substantial biomass (Vasseur et al., 2018; Koenig and Weigel, 2015). Furthermore, *A. thaliana* is distinguished by its elevated anthocyanin content (Kovinich et al., 2014), which may synergistically augment the skin care benefits of the TDP1-EGF fusion protein. Moreover, Arabidopsis extract is officially recognized and registered as a cosmetic raw material in the International Nomenclature of Cosmetic Ingredients (INCI) catalog. The expressing TDP1-EGF in *A. thaliana* offers several advantages over its expression in bacterial system. Foremost among these is the enhanced safety of the final product, a critical consideration given its intended future application in humans. Additionally, plant-based expression eliminates the need for extensive protein purification, as the target protein can be utilized as a crude extract of total protein, thereby simplifying the process and substantially reducing costs associated with protein drug preparation (Michalak, 2023). However, the efficacy of using a crude protein extract—subjected only to centrifugation to isolate the soluble fraction—depends on achieving a sufficiently high expression level of the target protein. In this study, TDP1 and EGF were co-expressed as a fusion protein to enhance the transdermal delivery of EGF. The coding sequence of this fusion gene was optimized for expression in *A. thaliana* to improve safety and preserve the functionality of the fusion protein. Subsequently, A murine model of skin barrier impairment was employed to assess the safety and efficacy of the fusion protein. The primary goal was to establish to a feasible strategy for repairing skin barrier damage and treating associated skin disorders while evaluating the practicality of plant-based expression systems for fusion protein production. These findings offer valuable insights into the therapeutic potential of EGF in skin health and provide a foundation for investigating the mechanisms underlying fusion protein-mediated skin barriers repair and for developing novel skincare raw materials.

2 Materials and methods

2.1 Construction plant expression vector

The TDP1 gene was amplified from the plasmid pET-15b-TDP1 via PCR using gene-specific primers: 5'-ATGCCCATGGGTCATATGGCGTGCAG-3' (forward) and 5'-ATGGGGTACCACCGCCACCGCC-3' (reverse). Similarly, the EGF gene was amplified from pET-15b-EGF using primers 5'-ATGGGGTACCAACAGCGACT-3' (forward) and 5'-ATCGGGTAACCCAGGATCCTTAGC-3' (reverse). The resulting PCR products were cloned into the pEASY®-T1 vector as a fusion construct, generating pEASY-TDP1-EGF, which was subsequently transformed into *Escherichia coli*. Positive clones were identified through PCR screening and confirmed by DNA sequencing. The pEASY-TDP1-EGF plasmid was extracted from a verified clone, digested with *NcoI* and *BstEII*, and the TDP1-EGF DNA fragment was ligated into the *NcoI*/*BstEII*-digested plant expression vector pGM3301, yielding pGM3301-TDP1-EGF. Cleavage sites are detailed in Supplementary Table S1. The ligation product was transformed into Trans-T1 *E. coli*, and positive clones were selected via PCR and DNA sequencing. The plasmid isolated from one positive clone was then introduced into *Agrobacterium tumefaciens* strain EHA105. The recombinant *A. tumefaciens* EHA105 was subsequently used to transform *A. thaliana* for TDP1-EGF expression.

2.2 Transformation of arabidopsis strains and screening of transgenic plants

YEP medium was utilized to culture *Agrobacterium* until an OD600 of 0.8-1.0 was achieved, after which the cells were harvested by centrifugation at 4,000 × g/for 20 minutes at 4°C. The cells were resuspended in transformation solution (50 g/L of sucrose, 2.2g/L of ½ MS, 200 µL/L of surfactant, pH 5.8) and then used to infect *A. thaliana*, performed according to a previous study (Harrison et al., 2006; Purwantoro et al., 2023). After infection, the plants were incubated darkness for 48 hours, then cultivated under a 16-hour light/8-hour dark photoperiod with a light intensity of 50-100 µmol m^{-2} s^{-1}. Seeds from the T1 generation were harvested, and positive clones were initially screened for growth on solid MS medium (Murashige and Skoog medium) supplemented with 11 mg/mL glufosinate. MS medium, a foundational formulation, is widely utilized in plant tissue culture. In this study, solid MS medium was utilized primarily for the germination and development of *Arabidopsis thaliana* seeds. To screen for transgenic *A. thaliana* seedlings, the medium was supplemented with glufosinate (1 L MS formulation: 2.2 g MS salt mix, 10 g sucrose, PH 5.7, 6.5 g plant agar). Plants exhibiting normal growth were transplanted into individual soil-filled pots, with one plant per pot, and seeds were harvested from each plants to obtain the T2 generation. Based on the T2 segregation ratio, heterozygous plants carrying a single copy of the recombinant gene were selected to generate the T3 generation, yielding homozygous plants for the recombinant gene.

2.3 RT-qPCR analysis of transgene expression in transgenic arabidopsis

To confirm the integration of the TDP1-EGF fusion gene into the *A. thaliana* genome, transgenic plants from the T3 generation were initially screened via PCR. Genomic DNA was extracted from whole plant and subjected to PCR analysis using gene-specific primers: 5'-AACAGCGACTCTGAATGCCCGC-3' (forward) and 5'-GCGCAGTTCCCACCACTTCAGGTC-3' (reverse). Following verification, seeds from these plants were germinated to produce additional plants for gene expression analysis. Total RNA was isolated from distinct tissues (roots, stems, leaves, and flowers), and RNA concentrations was quantified. For each sample, 1 µg of total RNA was reverse transcribed using the PrimeScript RT reagent Kit (Takara, Dalian, China). Quantitative real-time PCR (qPCR) was conducted on a LightCycler 96 system (Roche, Basel,

Switzerland) with SYBR Green Master Mix (Applied Biosystems, Foster City, CA, USA) and gene-specific primers: 5'-ATGGCGTGCAGCAGTAGCCCGAG-3' (forward) and 5'-AACAGCGACTCTGAATGCCCGC-3' (reverse). Total RNA was extracted from various *A. thaliana* tissues (roots, stems, leaves, and flowers) using the pBiozol Plant Total RNA Kit (BioFLUX-Pion Inc., USA), and TDP1-EGF mRNA expression levels in these tissues were quantified via RT-qPCR. Total protein was extracted from positive clones and analyzed by SDS-PAGE using Tricine gel. The TDP1-EGF band was detected by Western blot with an anti-EGF antibody. The yield of TDP1-EGF, expressed as a percentage of total plant protein, was determined using an ELISA kit (MEIMIAN, China, MM-0184H1), and plants exhibiting high expression levels were selected for subsequent protein production experiments.

2.4 Hydrogel preparation

To formulate a hydrogel for topical application, 1.2 g of carbomer, 10 g of glycerin, and 6 g of propylene glycol were combined with 20 g of water and stirred slowly to achieve a homogeneous mixture. Subsequently, 1.2 g of triethanolamine was added, and the mixture was stirred gently until a hydrogel matrix formed. The hydrogel matrix was sterilized by autoclaving at 1214°C for 15 minutes, and after cooling to room temperature, supplemented with a sterile TDP1-EGF solution to a final concentration of 35 ng/mL hydrogel. The resulting TDP1-EGF hydrogel was stored in a refrigerator at 4°C until use. A Hydrogel containing only EGF was prepared following the same procedure.

2.5 Transdermal absorption of the fusion protein TDP1-EGF

Six male mice were randomly assigned to three groups, with two mice per group. To assess the transdermal penetration of TDP1-EGF and EGF, the dorsal skin of two mice from each group was depilated. A 3 cm × 3 cm area of the dorsal skin was secured over the mouth of a conical flask filled with normal saline, ensuring the inner skin surface contacted the saline. Hydrogel containing either TDP1-EGF or EGF was uniformly applied to the depilated skin. The saline was continuously agitated using a magnetic stirrer, and 1 mL samples were collected hourly, stored at 4°C, with the volume replenished by adding 1 mL of normal saline. Concentrations of TDP1-EGF and EGF in each sample were quantified using an ELISA kit.

2.6 Animal model and treatments

To establish a murine model of skin barrier damage, the dorsal skin of mice was initially shaved with a razor. Subsequently, the hairless dorsal region was treated with Veet depilatory cream (Hubei, China) for 90 seconds and then cleaned with a pad moistened with warm, sterile water. Given that depilatory cream may induce mild skin irritation, a 24-hour interval was observed post-depilation before subjecting the skin to physical disruption through repeated adhesive tape stripping. Accordingly, 24 hours after depilation, the dorsal skin of the mice was stripped multiple times using adhesive tape (3M600 Scotch Tape, 3M Corporation, USA). The degree of barrier impairment was evaluated by measuring transepidermal water loss (TEWL), with a VapoMeter (Delfin Technologies, Finland). A TEWL value of greater than 35 $mg/cm^2/h$ was considered adequate damage in this model (Jing et al., 2024; Fusté et al., 2019). Subsequently, the mice were randomly allocated into five groups, with five mice per group. The control group remained untreated. The remaining groups underwent tape stripping were then treated with either hydrogel alone (vehicle group), hydrogel containing the soluble protein fraction from wild-type *Arabidopsis thaliana* (Arabidopsis group), hydrogel with purified EGF (EGF group), or hydrogel containing the soluble protein fraction from TDP1-EGF transgenic *A. thaliana* (TDP1-EGF group). The condition of the dorsal skin was assessed every 12 hours through photography, dermoscopy, and TWEL measurements.

2.7 Histology examination

To evaluate the efficacy of TPD1-EGF in promoting skin barrier repair, changes in epidermal thickness of the dorsal skin of mice were assessed following treatment. Initially, dorsal skin tissue was soaked in 4% paraformaldehyde for 24-48 hours and subsequently rinsed with running tap water for 4-6 hours. The tissue samples were then immersed in 70% ethanol overnight and dehydrated through a graded series of ethanol solutions (80%, 95%, and 100%), followed by 100% xylene. Subsequently, the samples were sectioned into 6 μm-thick slices, deparaffinized in xylene, and rehydrated using a descending ethanol gradient (95%, 90%, 80%, 70%, 0%). The rehydrated sections were stained with hematoxylin and eosin (HE; Solarbio, Beijing, China) and examined under a DM3000 microscope (Leica, Wetzlar, Germany) to measure epidermis thickness. To examine the impact of TPD1-EGF on skin cell differentiation, two differentiation-related proteins, involucrin and loricrin, were selected for analysis. Initially, rehydrated tissue sections were immersed in sodium citrate antigen retrieval solution (Solarbio, Beijing, China). Subsequently, the sections were treated dropwise with either a 1:500 dilution of anti-involucrin antibody (Proteintech, Wuhan, China) or a 1:200 dilution of anti-loricrin antibody (Absin, Shanghai, China), and incubated overnight at 4°C. The sections were then washed three times with PBS and incubated with a horseradish peroxidase (HRP)-conjugated secondary antibody at 37°C for 4 hours. Following this, 3,3'-diaminobenzidine (DAB) chromogen was applied, and the sections were counterstained with hematoxylin. The stained sections were then examined under a DM3000 microscope (Leica, Wetzlar, Germany) to evaluate histological changes.

2.8 Immunofluorescence analysis

Following antigen retrieval with sodium citrate solutions as described in Section 3.7, tissue sections were incubated with either a 1:200 dilution of anti-PCNA antibody (Cat. No. 2586; RRID: AB_2160343; Cell Signaling Technology, Beverly, MA, USA) or a 1:200 dilution of anti-K16 antibody (Cat. No. 2586; RRID: AB_2160343; Cell Signaling Technology, Beverly, MA, USA) at 4°C overnight. The sections were then washed three times with PBS and incubated with an Alexa Flour 568-conjugated secondary antibody for 1 hour at 37°C. Subsequently, the sections were mounted using an antifade medium containing DAPI (Invitrogen, Life Technologies, Carlsbad, CA, USA) and examined using a Ti2-E & CSU-W1 confocal fluorescence microscope (Nikon, Tokyo, Japan).

2.9 Statistical analysis

Data analysis and statistical procedures adhered to the guidelines and requirements outlined by *Frontiers in Plant Science* for experimental design and analysis. Mice were randomly and blindly allocated to groups, with each group consisting of an equal number of mice. Technical replicates were averaged prior to statistical analysis and excluded from calculation of variance parameters. Differences between pairs of groups were evaluated using an unpaired Student's t-test. Statistical analyses were performed using GraphPad Prism 6.01 (GraphPad Software, San Diego, CA, USA). Multicomponent data and multiple group comparisons were assessed via one-way analysis of variance (ANOVA) followed by Dunnett's test. Statistical significance was determined at an F-value corresponding to $P < 0.05$ in the one-way ANOVA. The reported group size represents the number of independent values (n = 4) before being statistically analyzed. All quantitative data are presented as the mean ± standard error of the mean (SEM).

3 Results

3.1 Distribution of TDP1-EGF in transgenic arabidopsis thaliana

To assess the expression levels of the TDP1-EGF fusion gene in *A. thaliana*, genomic DNA was extracted from glufosinate-resistant plants for molecular analyses. Initial PCR screening confirmed the integration of the TDP1-EGF gene into the *A. thaliana* genome (Figure 1A). The expression of TDP1-EGF in the transgenic *A. thaliana* plants was further evaluated using RT-qPCR. Total RNA was extracted from the roots, leaves, stems, and flowers of transgenic plants and subjected to RT-qPCR to quantify TDP1-EGF transcript levels. Results indicated the presence of TDP1-EGF transcripts across all examined tissues, with significantly elevated levels in stems compared to other tissues (Figure 1B). RT-qPCR Primer sequences are provided in Supplementary Table S2. From the transgenic lines analyzed, four exhibiting high TDP1-EGF transcript abundance were selected for protein expression analysis. Total protein extracted from whole plants revealed a band of approximately 8.2 kDa via SDS-PAGE and Western blot analysis using an anti-EGF antibody, aligning with the predicted molecular mass of the TDP1-EGF fusion protein (Figure 1C). The TDP1-EGF fusion protein constituted approximately 0.016% of the total soluble protein extracted from transgenic plants (Figure 1D). The transdermal properties of TDP1-EGF were assessed using a Franz diffusion cell assay relative to an EGF standard, demonstrating a time-dependent increase in fusion protein accumulation in the receiver compartment, with the fusion protein consistently exhibiting significantly greater transdermal efficacy than the EGF standard across all time points (Figure 1E).

3.2 Cultivation of homozygous fusion protein arabidopsis thaliana

To establish homozygous and genetically stable positive plants, a substantial quantity of seeds was harvested. These seeds were cultivated on MS basal medium supplemented with 11 mg/L glufosinate (Figure 2A). Following Mendelian inheritance principles, T2 seeds were collected from individual transgenic *A. thaliana* plants (Supplementary Figure S3B). Heterozygote (Aa) = 3:1 was identified through screening of T2 seeds (Figure 2B). Subsequently, homozygote (AA) = 1:0 was selected from T3 generation seeds (Figure 2C).

3.3 TDP1-EGF enhances epidermal barrier repair

To assess the therapeutic efficacy of TDP1-EGF in epidermal barrier recovery, a standardized murine model of skin barrier damage was established via tape stripping, utilizing transepidermal water loss (TEWL) as the primary measure of barrier function. The TDP1-EGF-treated group demonstrated superior wound healing properties compared to other experimental groups. At 24 hours post-injury, this group displayed earlier scab formation and significantly reduced scab areas. By 36 hours, distinct white marginal spots, slight bulging, and initial signs of shedding were observed in the TDP1-EGF, EGF, and *Arabidopsis* groups, in contrast to the vehicle group. Notably, while the vehicle, *Arabidopsis*, and EGF groups showed minimal changes in scab area between 36 and 60 hours, the TDP1-EGF group demonstrated progressive white edge formation and scab detachment. At 72 hours, the TDP1-EGF group exhibited a substantial reduction in scab area, with emerging stratum corneum in shed regions, though vascular network development remained incomplete. By 84 hours, unlike the delayed and less pronounced scab detachment in other groups, the TDP1-EGF group demonstrated significant scab reduction, accompanied by clear neovascularization in previously shed areas, approximating normal skin morphology (Figure 3A). TEWL measurements, conducted at 12-hour intervals, consistently indicated enhanced epidermal barrier recovery in the

10.3389/fpls.2025.1573193

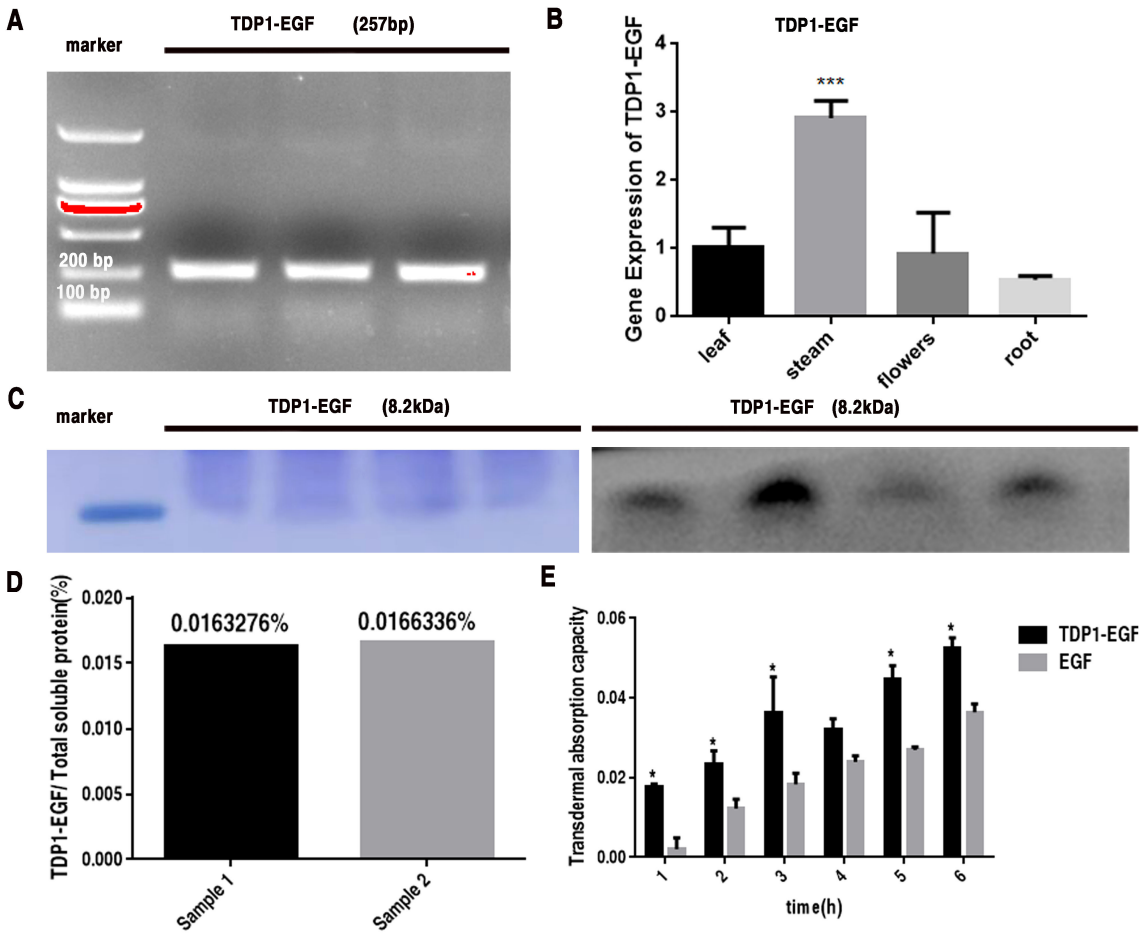

FIGURE 1
Analysis of TDP1-EGF Expression in *Arabidopsis thaliana*. **(A)** PCR detection of the TDP1-EGF DNA fragment in positive transgenic plants. **(B)** RT-qPCR analysis of TDP1-EGF transcript levels across various tissues of positive transgenic plants. **(C)** SDS-PAGE and Western blot analysis of total protein extracted from positive transgenic plants. **(D)** ELISA-based quantification of TDP1-EGF protein within the total soluble protein extracted from whole transgenic plants. **(E)** Franz diffusion cell assay assessing the transdermal activity of TDP1-EGF from total protein extracts compared to an EGF standard. All graphical data are presented as mean ± SEM from two or three independent experiments. Statistical significance is denoted by '*' ($P < 0.05$) and '**' ($P < 0.01$).

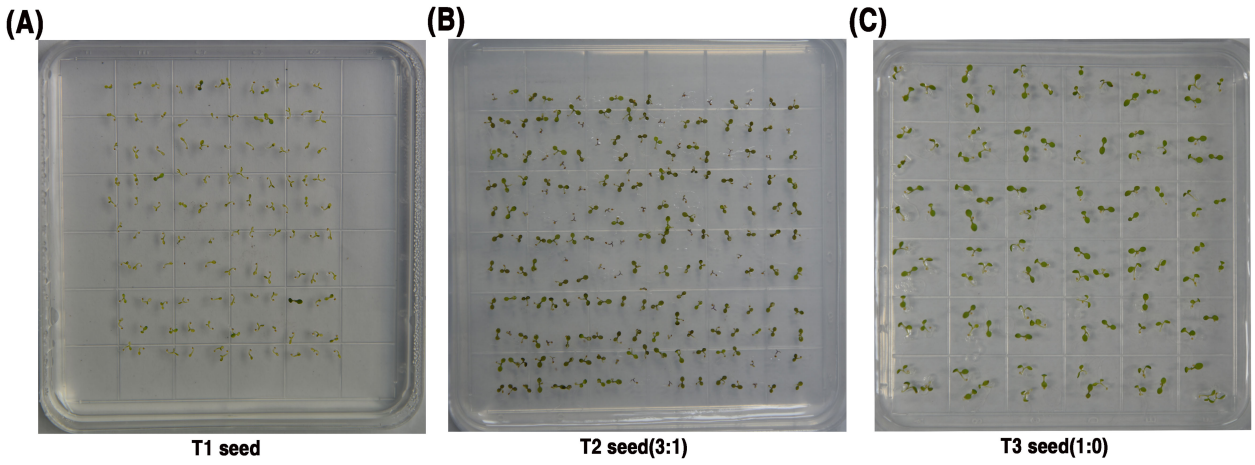

FIGURE 2
Selection of Transgenic Arabidopsis thaliana Plants Homozygous for the TDP1-EGF Gene. **(A)** Screening T1 transgenic seedlings; **(B)** Screening of T2 generation transgenic seedlings; **(C)** Screening T3 transgenic seedlings

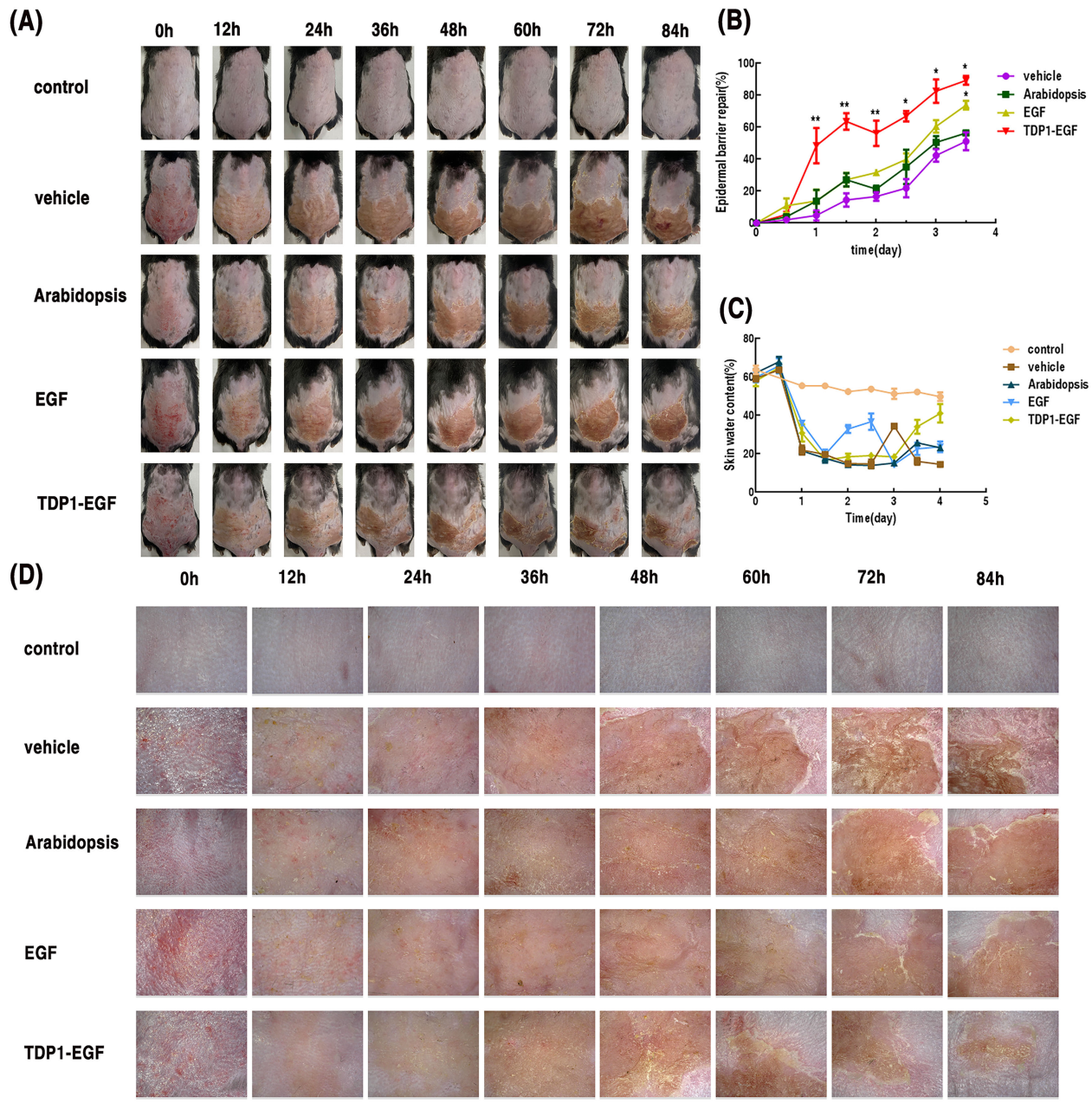

FIGURE 3
Effects of TDP1-EGF on epidermal barrier repair in mice. **(A)** Photographs of damaged dorsal skin area at various time points. **(B)** Assessment of skin barrier damage via transepidermal water loss (TEWL, mg/cm^2/h). Barrier repair rate was calculated as: [(TEWL value after molding – TEWL value at a specific time point)/(TEWL value after molding – TEWL value before molding)] ×100%. **(C)** Skin hydration levels measured using a skin moisture analyzer. **(D)** Dermoscopic observation of the damaged murine skin barrier across multiple time points. Data are presented as mean ± SEM (n = 5). Statistical significance is denoted by '*' ($P < 0.01$) and '**' ($P < 0.001$).

TDP1-EGF group, with notably faster recovery rates than other groups prior to 72 hours (Figure 3B). Skin hydration analysis at 84 hours revealed significantly elevated moisture content in the TDP1-EGF group (Figure 3C). Dermoscopic analysis identified early pigmented spots and hyperkeratosis in the vehicle and *Arabidopsis* groups at 24 hours. Whereas the TDP1-EGF group developed characteristic red and white spots at 36 hours, followed by progressive crust shedding and new cuticle formation at 60 and 72 hours, culminating in neovascularization by 84 hours (Figure 3D). Collectively, these findings highlight TDP1-EGF's substantial therapeutic potential, suppressing excessive keratinocyte differentiation and scar formation while accelerating wound healing through enhanced scab detachment, stratum corneum regeneration, and neovascularization.

3.4 TDP1-EGF modulates keratinocyte proliferation in a murine model of epidermal barrier damage

To evaluate the impact of TDP1-EGF on epidermal hyperplasia in mice, skin sections from each treatment group were examined using H&E staining and immunofluorescence. H&E staining revealed no significant differences in epidermal thickness between the TDP1-EGF and EGF groups or between the vehicle and *Arabidopsis* groups. However, the TDP1-EGF group displayed significantly thinner epidermis compared to the vehicle and *Arabidopsis* groups (Figure 4A). To further determine whether TDP1-EGF suppresses aberrant epidermal proliferation, immunofluorescence analysis was conducted to evaluate the expression of proliferation markers K16 and PCNA. The TDP1-EGF-treated group exhibited markedly reduced K16 and PCNA expression levels compared to the vehicle, *Arabidopsis*, and EGF groups. Strikingly, TDP1-EGF exerted a more potent inhibition of K16 and PCNA expression than EGF alone, with statistically significant differences. These results suggest that, while TDP1-EGF and EGF share similar biological functions in alleviating epidermal hyperplasia, TDP1-EGF's enhanced transdermal efficacy—attributable to TDP1's properties—confers a more pronounced regulatory effect on proliferation marker expression (Figures 4B, C).

3.5 Effects of TDP1-EGF on cell differentiation and lipid synthesis

To elucidate TDP1-EGF's role in epidermal barrier recovery, its effects on cell differentiation and lipid synthesis were assessed.

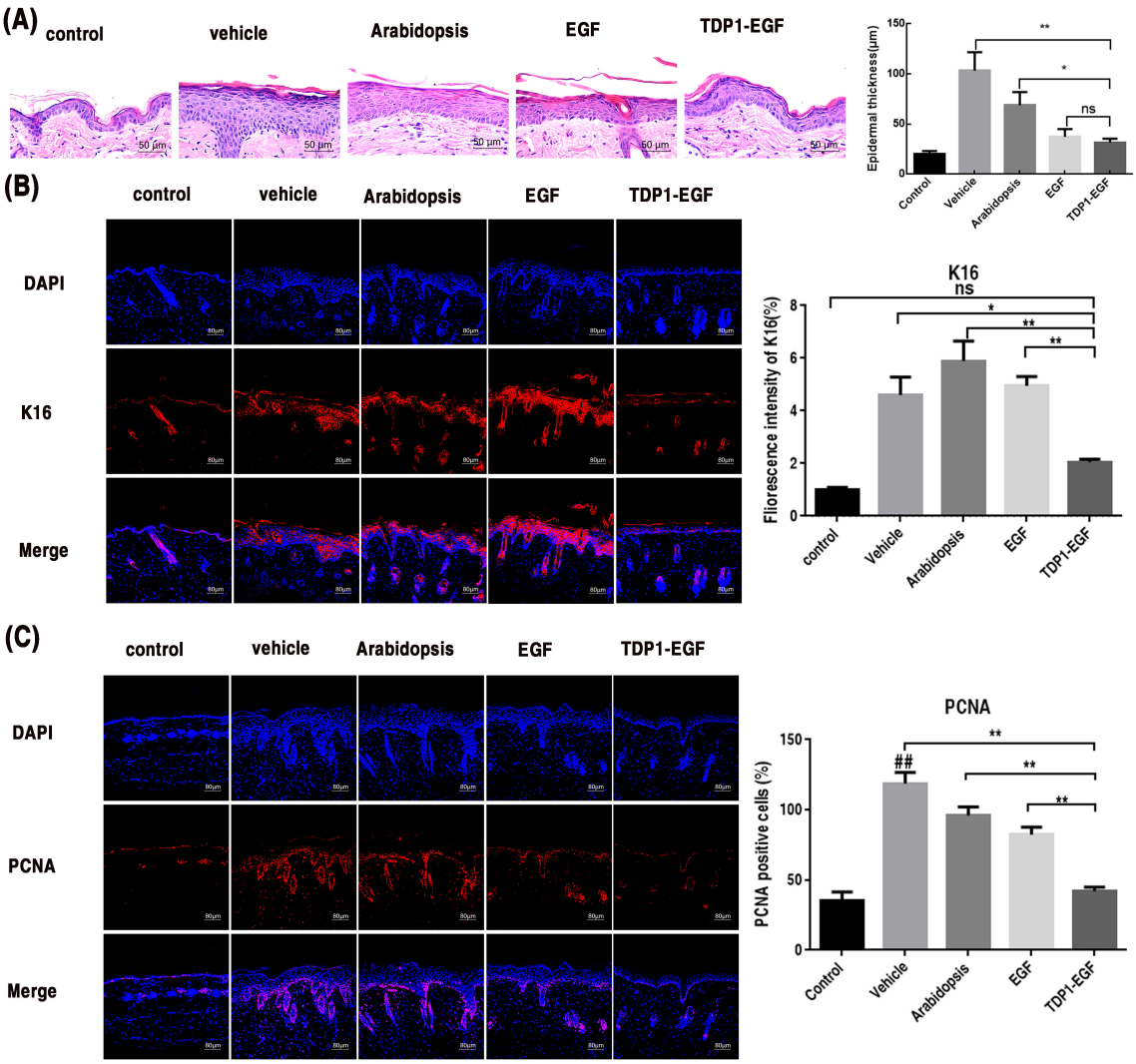

FIGURE 4
TDP1-EGF alleviates epidermal hyperplasia in mice. **(A)** Epidermal thickness alterations in dorsal skin assessed via hematoxylin and eosin (H&E) staining. **(B)** Keratin 16 (K16) expression levels in epidermal sections evaluated by immunofluorescence analysis. **(C)** Proliferating cell nuclear antigen (PCNA) expression levels in epidermal sections evaluated by immunofluorescence analysis. All graphical data are presented as mean ± SEM from four independent experiments. Statistical significance is denoted by '##' ($P < 0.01$ vs. control), '*' ($P < 0.05$ vs. vehicle), and '**' ($P < 0.01$ vs. vehicle).

Immunohistochemical analysis revealed that markedly elevated loricrin expression in the TDP1-EGF-treated group compared to the vehicle, *Arabidopsis*, and EGF groups, alongside a significantly thinner epidermis. Notably, loricrin in the TDP1-EGF group displayed a highly organized arrangement, in contrast to the reduced and disordered expression observed in the vehicle, *Arabidopsis*, and EGF groups (Figure 5A). Elongation of very long-chain fatty acids 1 (ELOVL-1), a key enzyme in the fatty acid elongation pathway, is essential for synthesizing ultra-long-chain fatty acids that serve as critical precursors for ceramide production. Serine Palmitoyltransferase (SPT), the rate-limiting enzyme in sphingolipid biosynthesis, catalyzes the initial step of sphingolipid synthesis, indirectly influencing ceramide generation. Fatty acid synthase (FAS), a multifunctional enzyme complex, drives the *de novo* fatty acids synthesis, providing fundamental components for ceramides, cholesterol esters, and other complex lipids. Collectively, these enzymes form an integrated network underpinning the synthesis of lipids vital for epidermal barrier integrity and function. Real-time quantitative PCR (RT-qPCR) analysis further demonstrated significantly elevated transcript levels of *SPT*, *FAS*, and *ELOVL-1* in skin tissue from the TDP1-EGF compared to the vehicle, *Arabidopsis*, and EGF groups, which showed no notable intergroup differences. Strikingly, TDP1-EGF surpassed EGF alone in upregulating lipid synthesis gene expression (Figure 5B). Primers sequences for RT-qPCR are provided in Supplementary Table S2. These results suggest that TDP1-EGF substantially enhances skin repair and regeneration by upregulating proteins involved in cell differentiation and lipid synthesis, an effect likely attributable to TPD1's enhancement of EGF's transdermal delivery within the fusion protein.

3.6 TDP1-EGF alleviates epidermal inflammation

To assess the impact of TDP1-EGF on the inflammatory response in epidermal barrier damage, mRNA expression of key pro-inflammatory cytokines (IL-1β, TNF-α, and IL-6) were quantified in skin tissue. Primers sequences for RT-qPCR are provided in Supplementary Table S2. RT-qPCR analysis demonstrated that the TDP1-EGF-treated group exhibited significantly reduced transcript levels of *IL-1β* and *TNF-α* compared to the vehicle and *Arabidopsis* groups, though no notable difference was observed between the TDP1-EGF and EGF

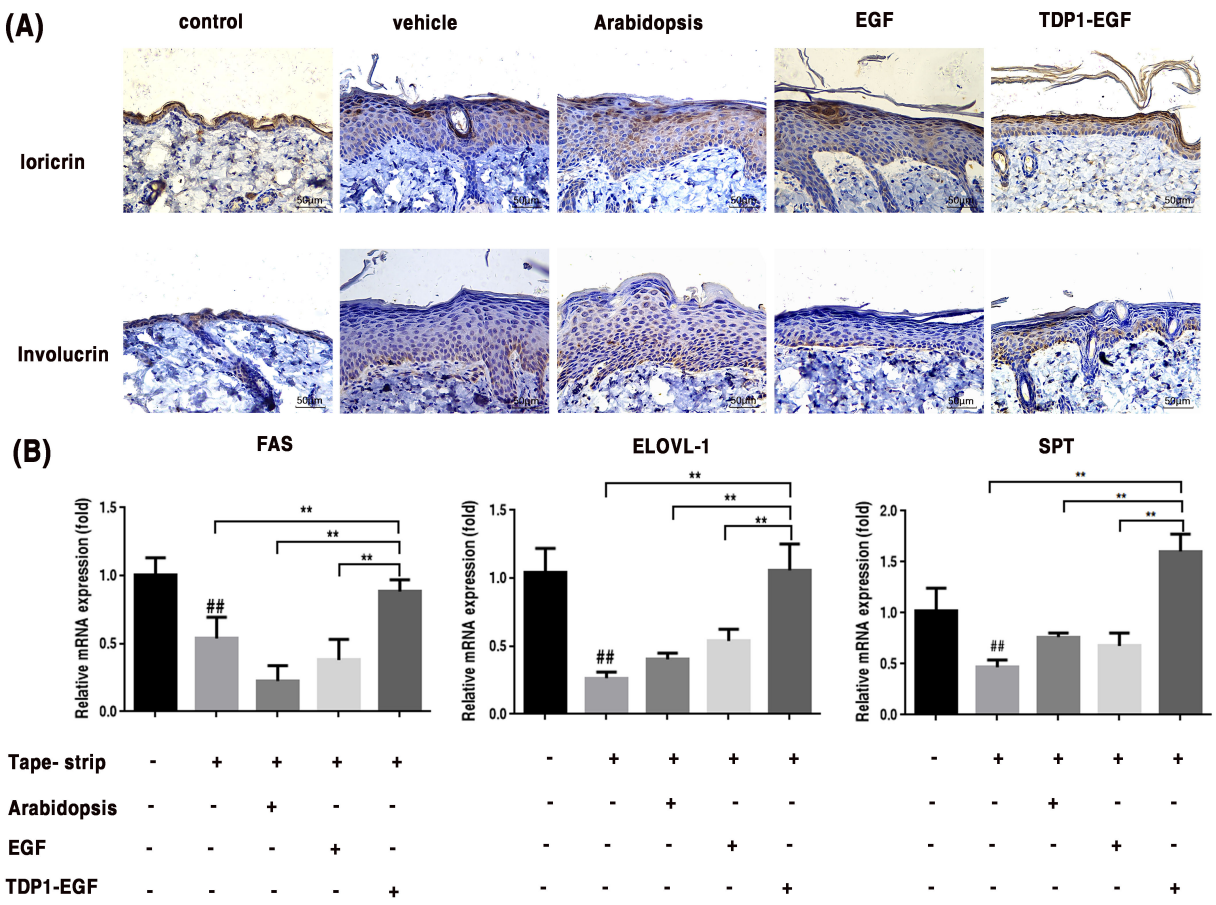

FIGURE 5
TDP1-EGF upregulates differentiation proteins and lipid synthesis genes to enhance skin barrier repair. **(A)** Expression levels of differentiation proteins involucrin and loricrin assessed via immunohistochemical analysis. **(B)** Transcript levels of lipid synthesis genes (*FAS*, *ELOVL-1*, and *SPT*) quantified by RT-qPCR. All graphical data are presented as mean ± SEM from four independent experiments. Statistical significance is denoted by '##' ($P < 0.01$ vs. control), '*' ($P < 0.05$ vs. vehicle), and '**' ($P < 0.01$ vs. vehicle).

groups (Figures 6A, B). Conversely, while *IL-6* expression showed no significant variation among the vehicle, *Arabidopsis* and EGF groups, the TDP1-EGF group displayed a pronounced downregulation of *IL-6* levels compared to all other experimental groups (Figure 6C). These results indicate that TDP1-EGF markedly suppresses the expression of inflammatory cytokines *IL-1β*, *TNF-α* and *IL-6*, exerting a more potent anti-inflammatory effect than EGF alone. This suggests that TDP1-EGF not only enhances epidermal barrier repair but also effectively modulates the inflammatory response associated with barrier damage.

4 Discussion

Epidermic growth factor is a protein known to promote wound closure and epidermal regeneration (Li et al., 2021). However, the effectiveness of topical application of EGF at the wound site can be hampered by the poor transdermal delivery of the protein into the skin tissue, primarily because of the size of EGF, which is greater than 6,000 Da, making it difficult to penetrate the corneal layer, which only allows molecules of less than 500 Da to readily pass through (Bos and Meinardi, 2000; Adamson and Rees, 1981). One approach to improve EGF's skin penetration is to fuse it with a highly efficient transdermal peptide. Given that this strategy entails the construction and expression of a recombinant protein, the expression system employed must prioritize product safety. While prokaryotic expression systems are well-established and widely utilized for exogenous protein production. Unfortunately, expressing exogenous proteins in a prokaryotic expression system such as the *E. coli* expression system may not be desirable if the expressed proteins are for human or animal usage since there is a risk of contamination by endotoxins, which pose a risk to health (Wakelin et al., 2006). Additionally, *E. coli*-based systems demand costly fermenters, stringent conditions, and offer limited scalability (Chaudhary et al., 2024). Thus, expressing exogenous proteins in a plant expression system would be more desirable (Chen et al., 2023; Huang and McDonald, 2012; Moustafa et al., 2016).

Currently, numerous plants are capable of enhancing the expression levels of foreign proteins through transient expression, thereby meeting commercial standards (Ruhlman et al., 2007). For stable nuclear transformation, optimizing expression vectors is widely acknowledged as an effective approach to enhance recombinant protein yields. For example, Ruggiero et al. (2000) demonstrated that incorporating an enhanced 35S promoter and 35S terminator in tobacco enabled the production of approximately 3 g of purified recombinant collagen per 100 kg of powdered plant material (Ruggiero et al., 2000). Similarly, Suo et al. (2006) reported substantially improved expression levels of bone morphogenetic protein 2 (BMP-2) in tobacco by employing the CaMV 35S promoter and codon optimization strategies (Suo et al., 2006). In our prior study, despite employing comparable optimization strategies, the expression level of the target protein was limited to 0.016% of total soluble protein, falling below commercial standard (Figure 1D). To achieve commercialization requirements, additional optimization approaches will be pursued, including optimizing *Arabidopsis thaliana* growth conditions, improving the post-translational stability of TDP1-EGF, and exploring co-expression with molecular cofactors. In a related study, Wirth et al. (2004) expressed hEGF in tobacco, targeting its accumulation to either the cytoplasm or the apoplast. Cytoplasmic accumulation resulted in a minimal expression level of 0.00001% of total soluble protein, whereas apoplast-targeted accumulation significantly elevated hEGF expression to 0.11% (Wirth et al., 2004). Similarly, Qiang et al. (2020) enhanced the stability and expression levels of a fusion protein by expressing oleosin-EGF in *Arabidopsis thaliana* seeds, with the highest expression level reaching 14.83 ng/μL (Qiang et al., 2020). These investigations offer valuable insights and approaches for further optimizing recombinant protein expression in plant-based systems.

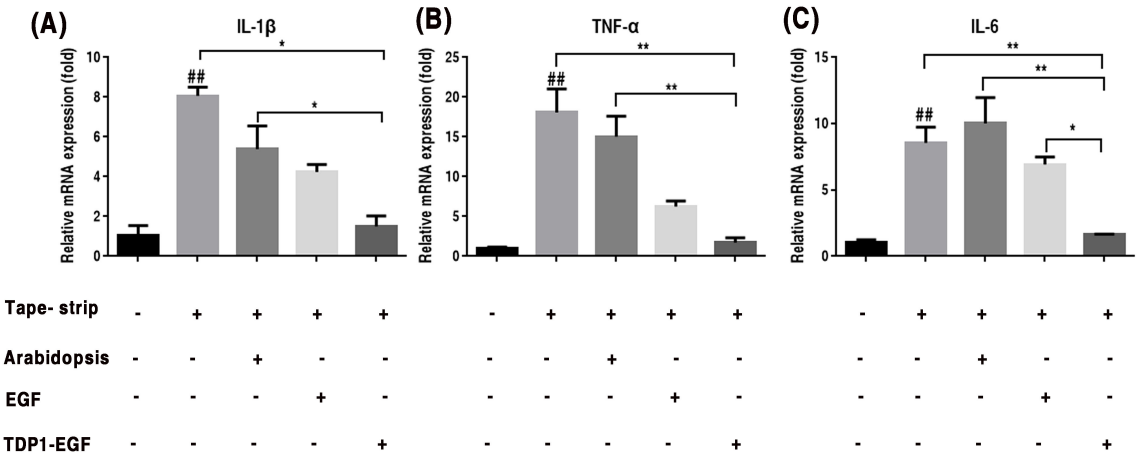

FIGURE 6
TDP1-EGF modulates inflammatory cytokine gene expression assessed by RT-qPCR. **(A)** To investigate the effect of TDP1-EGF on the expression levels of the inflammatory factor IL-1β. **(B)** To examine the effect of TDP1-EGF on the expression levels of the inflammatory factor TNF-α. **(C)** To assess the effect of TDP1-EGF on the expression levels of the inflammatory factor IL-6. Graphical data are presented as mean ±SEM from four independent experiments. Statistical significance is denoted by '##' ($P < 0.01$ vs. control), '*' ($P < 0.05$ vs. vehicle), and '**' ($P < 0.01$ vs. vehicle).

Our data demonstrate that TDP1-EGF is expressed across all *A. thaliana* tissues, including stems, roots, leaves, and flowers, as confirmed by RT-qPCR analysis, suggesting that *A. thaliana* serve as an effective bioreactor for the commercial production of TDP1-EGF (Figure 1B). Consequently, *A. thaliana* represents a promising plant-based bioreactor system for commercial applications. The transdermal peptide TDP1 can be linked to EGF via fusion expression or chemical coupling. Notably, EGF activity and TDP1 transdermal properties remained unaffected when expressed as the TDP1-EGF fusion protein (Supplementary Figure S4). Our findings revealed that the TDP1-EGF fusion protein reached peak accumulation during the second week of *A. thaliana* growth. Additionally, the fusion protein exhibited no impact on the phenotype or genetic patterns of *A. thaliana*, supporting the feasibility of fusing the transdermal peptide TPD1 with EGF. In experiments accessing epidermal barrier repair, hydrogel supplemented with total protein extracted from wild-type *A. thaliana* demonstrated superior repair promotion compared to hydrogel alone, suggesting that plant-derived compounds may enhance repair processes and potentially synergize with TDP1-EGF to improve epidermal barrier recovery. Taking into account both safety and efficacy, a wealth of current data has indicated that the optimal concentration of EGF is 1 μg per 30g (Fabi and Sundaram, 2014; Esquirol Caussa and Herrero Vila, 2015). Accordingly, the TDP1-EGF hydrogel was formulated with a protein-to-hydrogel ratio of 1μg per 30 g to attain the optimal concentration. After expression in *A. thaliana*, TDP1-EGF was extracted as the soluble protein fraction, incorporated into a hydrogel, and applied directly to the damaged skin. Its efficacy in skin repair was then compared with that of hydrogel alone and hydrogel containing standard EGF. The result demonstrated significantly accelerated recovery of the damaged skin with the TDP1-EGF hydrogel, indicating that fusing EGF with TDP1 substantially enhanced EGF's efficacy in skin repair. This improvement stemmed not from superior intrinsic activity of the fusion protein over EGF alone, but rather from TPD1-mediated enhancement of EGF's transdermal delivery (Figure 3A). The safety and efficacy of biological approaches to transdermal drug delivery have been consistently substantiated. For example, Rothbard et al. (2000) reported that the conjugation of Cyclosporine A with an arginine oligomer effectively penetrated the epidermal barrier and exerted anti-inflammatory effects (Rothbard et al., 2000). Similarly, Kim et al. (2006) successfully transduced Botulinum Neurotoxin (BoNT), an anti-aging compound, into mouse skin using the cell-penetrating peptide Pep-1 (Kim et al., 2006). To further assess the efficacy of transdermal peptides, multiple parameters were employed to evaluate TDP1-EGF 's effectiveness, and the collective dare underscore the benefits of fusing EGF with TDP1, positioning this approach as a promising enhancement for EGF application in treating damaged skin.

Our prior research has demonstrated that a healthy epidermal barrier is formed by the proliferation and differentiation of keratinocytes (Wikramanayake et al., 2014). Damage to the skin barrier leads to abnormal proliferation of keratinocytes, which in turn causes continuous deterioration of the barrier (Yang et al., 2020; Patrick et al., 2021). The key to repairing the barrier is to normalize the differentiation of abnormally proliferating keratinocytes. An important measure of epidermal barrier function is the TEWL value (Montero-Vilchez et al., 2022; Lodén et al., 1999). A growing body of research has established that EGF effectively promotes skin wound healing and epidermal regeneration, primarily by regulating proteins associated with cell proliferation, differentiation, and migration (Gibbs et al., 2000). Our results demonstrated that topical application of TDP1-EGF effectively promoted the recovery of epidermal barrier damage in the dorsal skin of mice, outperforming EGF alone, as evidenced by increased skin moisture levels observed via dermoscopy (Figures 3B, C). These findings confirmed our hypothesis that transdermal peptides, such as TPD1, facilitate the delivery of EGF to keratinocytes in the deeper epidermal layers, enabling precise exertion of its therapeutic effects. H&E staining revealed that, following tape stripping, the epidermis thickened due to injury; however, no significant difference in epidermal thickness was observed between the TDP1-EGF-treated group and the negative control group (Figure 4A). Collectively, these results indicate that TDP1-EGF treatment prevents aberrant keratinocyte proliferation.

EGF regulates differentiation, migration, proliferation, and other biological activities of keratinocytes through a mitogen-activated protein kinase (MAPK)-dependent mechanism and PI3K/AKT signal transduction (Haase et al., 2003; Chen et al., 2022a). TDP1-EGF was shown to modulate the expression of key differentiation markers, including involucrin and loricrin, thereby promoting orderly differentiation of stratum corneum cells to maintain skin barrier integrity (Figure 5A). Loricrin and involucrin are pivotal proteins in the differentiation of epidermal keratinocytes (Lee et al., 2014). Involucrin expression signals the onset of terminal differentiation in keratinocytes, with elevated levels closely linked to cellular flattening and keratinization (LaPres and Hudson, 1996). Research has demonstrated that the promoter region of the involucrin gene contains transcription factor binding sites that can be activated by the MAPK pathway, enabling EGF to enhance involucrin gene transcription by activating this pathway (Ghahary et al., 2001; Gibbs et al., 2000). Additionally, researchers have confirmed that EGF can upregulate involucrin expression in the A431 cell line and promote its differentiation process (Rosdy, 1988). To date, no direct evidence supports EGF-mediated regulation of loricrin expression. However, our prior research demonstrated that theTDP1-EGF fusion protein modulates the expression of differentiation proteins, including involucrin and loricrin, thus facilitating terminal keratinocyte differentiation. One plausible explanation for this finding is that EGF modulates the expression of differentiation proteins via well-established signaling pathways, including PI3K/AKT and MAPK. Ceramides and free fatty acids are critical components in sustaining normal epidermal barrier function. When the epidermal barrier is compromised, the synthesis of cholesterol, free fatty acids, and ceramides increases to facilitate the repair process of the epidermal barrier (Rosdy, 1988). Several studies have demonstrated that the expression of serine palmitoyltransferase (SPT) is significantly up-regulated during vascular repair, promoting ceramide synthesis and

thereby accelerating wound healing (Uhlinger et al., 2001). Additionally, ElovL-1 and fatty acid synthase (FAS) are pivotal in sustaining epidermal barrier integrity. ElovL-1, in particular, is recognized as a critical lipid synthetase indispensable for epidermal barrier function. Notably, mice deficient in ElovL-1 exhibit severe epidermal barrier defects and typically die shortly after birth (Sassa et al., 2013). Furthermore, ω-hydroxy-ceramide (ω-OH-Cer), anchored to the outer surface of the keratinocyte lipid envelope (CLE) and associated with involucrin, constitutes a vital lipid component of the stratum corneum (SC). The biosynthesis of ω-OH-Cer is closely linked to FAS activity, highlighting the interdependence of these pathways in maintaining epidermal barrier function (Ge et al., 2023). TDP1-EGF was found to upregulate the expression of lipid synthesis genes, including *ELOVLs, FAS*, and *SPT*, as evidenced by Figure 5B. Given that stratum corneum cell proliferation, differentiation, and migration are closely related to EGFR expression and lipid composition, this upregulation suggests that TDP1-EGF may initiate epidermal repair signaling by binding to EGFR. Future studies will further elucidate the mechanisms underlying TDP1-EGF's effects.

In addition to enhancing cell proliferation, differentiation, and migration, TDP1-EGF also mitigated inflammation resulting from damage to skin tissue. It has been reported that the abnormal proliferation of structural proteins and the abnormal expression of inflammatory factors are two important factors in the dysplasia of stratum corneum cells (Evtushenko et al., 2021; Jiao et al., 2022). PCNA and K16 are markers of abnormal cell proliferation, and these two markers can be used to estimate the extent of malignant lesions via histological analysis (Krecicki et al., 1999; Paladini and Coulombe, 1998). In this study, TDP1-EGF was found to downregulated the expression of PCNA and K16 proteins (Figure 4B). To date, no studies have demonstrated that EGF alone inhibits the expression of PCNA and K16. From another perspective, inflammatory factors, such as TNF-α and IL-1β can activate multiple intracellular signaling pathways, thereby promoting the expression of PCNA (Krecicki et al., 1999; Paladini and Coulombe, 1998). For instance, TNF-α has been shown to enhance PCNA gene transcription and expression by activating the NF-κB signaling pathway, which facilitates the nuclear translocation of NF-κB and its binding to the promoter region of the PCNA gene (Ji et al., 2016; De Simone et al., 2015; Niu et al., 2022). Furthermore, studies have indicated that inflammatory factors can induce a stress response in cells. In response to such stress, cells in the psoriatic epidermis may enhance the nuclear translocation of Nrf2. Once in the nucleus, Nrf2 can bind to the promoter region of the K16 gene, activate its transcription, and increase the expression of stress-related proteins such as K16 (Yang et al., 2017). Therefore, we hypothesize that the TDP1-EGF fusion protein may indirectly suppress the expression of proliferative proteins, such as PCNA and K16, by attenuating inflammatory cytokine levels in specific contexts, thereby ameliorating dysplasia in damaged regions of the murine epidermal barrier. Further validation confirmed that TDP1-EGF modulates inflammatory cytokine expression, with study results demonstrating significant downregulation of genes encoding IL-1β, TNF-α, and IL-6 in skin tissue following TDP1-EGF application, supporting its role in reducing inflammation (Figures 6A–C). This anti-inflammatory effect likely enhances TDP1-EGF's efficacy in repairing damaged epidermal barriers by mitigating inflammation-induced exacerbation of injury.

Although the development of genetically modified (GM) plants expressing skincare products holds considerable promise, several critical challenges impede its advancement. First, plant bioreactor technology lags behind prokaryotic expression systems in sophistication, resulting in lower protein yields and reduced market competitiveness (Law et al., 2025). Second, global regulatory frameworks governing the expression of pharmaceutical proteins in plants remain underdeveloped, lacking standardized guidelines (Turnbull et al., 2021). Regulatory policies differ markedly across countries, posing compliance challenges for companies. Moreover, therapeutic proteins derived from GM plants must satisfy stringent safety, efficacy, and quality control standards to qualify for clinical trials, a milestone achieved by only a handful of such proteins to date (Burnett and Burnett, 2020). Nevertheless, advancements in plant biotechnology, alongside ongoing refinements in regulatory frameworks and the intrinsic benefits of transgenic plants—including enhanced safety, cost-effective production, scalability, and broad applicability across diverse sectors—position plant-based expression systems as an emerging cornerstone for skincare product manufacturing.

5 Conclusion

This study demonstrates the feasibility of expressing the TDP1-EGF fusion protein in *Arabidopsis thaliana*, achieving a peak expression level of 142.05 ng/mL, which constitutes 0.016% of total soluble protein. Our results reveal that the transdermal absorption rate of TDP1-EGF fusion protein surpasses that of EGF alone. Significantly, this research provides the first evidence that *A. thaliana*-expressed TDP1-EGF fusion protein effectively ameliorates physically induced epidermal barrier damage through multiple mechanisms: (1) suppressing inflammation, (2) alleviating epidermal hyperplasia, (3) upregulating lipid synthesis, (4) enhancing keratinocyte differentiation, and (5) accelerating epidermal barrier repair. These findings lay a solid theoretical and practical foundation for leveraging *A. thaliana*-expressed TDP1-EGF fusion protein in medical and skincare applications, particularly for epidermal barrier repair. Moreover, this study offers valuable insights into the potential of plant-based bioreactors systems for advancing skin health solutions.

Data availability statement

All data supporting the findings of this study are available within the paper and its Supplementary Information.

Ethics statement

The animal study was approved by Experimental animal Welfare and Ethics Committee, Wenzhou University. The study was conducted in accordance with the local legislation and institutional requirements.

Author contributions

GY: Data curation, Project administration, Software, Writing – original draft. SL: Methodology, Project administration, Writing – review & editing. SG: Funding acquisition, Resources, Supervision, Writing – review & editing. CS: Investigation, Methodology, Writing – review & editing. FK: Investigation, Methodology, Resources, Writing – review & editing. JX: Data curation, Methodology, Writing – review & editing. XX: Data curation, Methodology, Writing – review & editing. XH: Methodology, Writing – review & editing. JW: Methodology, Software, Writing – review & editing. QC: Formal Analysis, Investigation, Validation, Writing – review & editing. NI: Data curation, Methodology, Project administration, Writing – review & editing. WZ: Formal Analysis, Project administration, Resources, Writing – review & editing. YW: Funding acquisition, Methodology, Project administration, Resources, Supervision, Writing – review & editing. NX: Funding acquisition, Investigation, Methodology, Project administration, Resources, Software, Supervision, Writing – review & editing.

Funding

The author(s) declare that financial support was received for the research and/or publication of this article. This work was supported by Grant Scientific and Technological Plan Project of Wenzhou (2023Y1819), Biological Breeding-Major Projects (2023ZD04062) and Ouhai District Key Scientific Research Projects (2024oh0002).

Acknowledgments

We thank Alan K. Chang from the College of Life and Environmental Sciences at Wenzhou University) for valuable discussion for his kind effort in revising the language of the manuscript.

Conflict of interest

Authors SG, JW and NX were employed by company Zhejiang Tianqu Beiben Instrument Technology Co., Ltd.

The remaining authors declare that the research was conducted in the absence of any commercial or financial relationships that could be construed as a potential conflict of interest.

Generative AI statement

The author(s) declare that no Generative AI was used in the creation of this manuscript.

Publisher's note

All claims expressed in this article are solely those of the authors and do not necessarily represent those of their affiliated organizations, or those of the publisher, the editors and the reviewers. Any product that may be evaluated in this article, or claim that may be made by its manufacturer, is not guaranteed or endorsed by the publisher.

Supplementary material

The Supplementary Material for this article can be found online at: https://www.frontiersin.org/articles/10.3389/fpls.2025.1573193/full#supplementary-material

References

Adamson, E. D., and Rees, A. R. (1981). Epidermal growth factor receptors. *Mol. Cell. Biochem.* 34, 129–152. doi: 10.1007/BF02359619

Bos, J. D., and Meinardi, M. M. H. M. (2000). The 500 Dalton rule for the skin penetration of chemical compounds and drugs. *Exp. Dermatol.* 9, 165–169. doi: 10.1034/j.1600-0625.2000.009003165.x

Burnett, M. J. B., and Burnett, A. C. (2020). Therapeutic recombinant protein production in plants: Challenges and opportunities. *PLANTS PEOPLE PLANET* 2, 121–132. doi: 10.1002/ppp3.10073

Candi, E., Schmidt, R., and Melino, G. (2005). The cornified envelope: a model of cell death in the skin. *Nat. Rev. Mol. Cell Biol.* 6, 328–340. doi: 10.1038/nrm1619

Chaudhary, S., Ali, Z., and Mahfouz, M. (2024). Molecular farming for sustainable production of clinical-grade antimicrobial peptides. *Plant Biotechnol. J.* 22, 2282–2300. doi: 10.1111/pbi.14344

Chen, J.-P., Gong, J.-S., Su, C., Li, H., Xu, Z.-H., and Shi, J.-S. (2023). Improving the soluble expression of difficult-to-express proteins in prokaryotic expression system via protein engineering and synthetic biology strategies. *Metab. Eng.* 78, 99–114. doi: 10.1016/j.ymben.2023.05.007

Chen, K., Li, Y., Zhang, X., Ullah, R., Tong, J., and Shen, Y. (2022a). The role of the PI3K/AKT signalling pathway in the corneal epithelium: recent updates. *Cell Death Dis.* 13, 513. doi: 10.1038/s41419-022-04963-x

Chen, L., Liu, Q., Liu, Z., Li, H., Liu, X., and Yu, H. (2022b). EGF protects epithelial cells from barrier damage in chronic rhinosinusitis with nasal polyps. *J. Inflammation Res.* 15, 439–450. doi: 10.2147/JIR.S345664

Chen, Y., Shen, Y., Guo, X., Zhang, C., Yang, W., Ma, M., et al. (2006). Transdermal protein delivery by a coadministered peptide identified via phage display. *Nat. Biotechnol.* 24, 455–460. doi: 10.1038/nbt1193

De Simone, V., Franzè, E., Ronchetti, G., Colantoni, A., Fantini, M. C., Di Fusco, D., et al. (2015). Th17-type cytokines, IL-6 and TNF-α synergistically activate STAT3 and NF-kB to promote colorectal cancer cell growth. *Oncogene* 34, 3493–3503. doi: 10.1038/onc.2014.286

Esquirol Caussa, J., and Herrero Vila, E. (2015). Epidermal growth factor, innovation and safety. *Med. Clin. (Barc)* 145, 305–312. doi: 10.1016/j.medcli.2014.09.012

Evtushenko, N. A., Beilin, A. K., Kosykh, A. V., Vorotelyak, E. A., and Gurskaya, N. G. (2021). Keratins as an inflammation trigger point in epidermolysis bullosa simplex. *Int. J. Mol. Sci.* 22 (22), 12446. doi: 10.3390/ijms222212446

Fabi, S., and Sundaram, H. (2014). The potential of topical and injectable growth factors and cytokines for skin rejuvenation. *Facial Plast. Surg.* 30, 157–171. doi: 10.1055/s-0034-1372423

Fusté, N. P., Guasch, M., Guillen, P., Anerillas, C., Cemeli, T., Pedraza, N., et al. (2019). Barley β-glucan accelerates wound healing by favoring migration versus proliferation of human dermal fibroblasts. *Carbohydr. Polym.* 210, 389–398. doi: 10.1016/j.carbpol.2019.01.090

Ge, F., Sun, K., Hu, Z., and Dong, X. (2023). Role of omega-hydroxy ceramides in epidermis: biosynthesis, barrier integrity and analyzing method. *Int. J. Mol. Sci.* 24, 5035. doi: 10.3390/ijms24055035

Ghahary, A., Marcoux, Y., Karimi-Busheri, F., and Tredget, E. E. (2001). Keratinocyte differentiation inversely regulates the expression of involucrin and transforming growth factor β1. *J. Cell. Biochem.* 83, 239–248. doi: 10.1002/jcb.1223

Gibbs, S., Silva Pinto, A. N., Murli, S., Huber, M., Hohl, D., and Ponec, M. (2000). Epidermal growth factor and keratinocyte growth factor differentially regulate epidermal migration, growth, and differentiation. *Wound Repair Regen.* 8, 192–203. doi: 10.1046/j.1524-475x.2000.00192.x

Goverman, J. (2014). Our natural defense: the skin! *Crit. Care Med.* 42, 1575–1577. doi: 10.1097/ccm.0000000000000356

Haase, I., Evans, R., Pofahl, R., and Watt, F. M. (2003). Regulation of keratinocyte shape, migration and wound epithelialization by IGF-1- and EGF-dependent signalling pathways. *J. Cell Sci.* 116, 3227–3238. doi: 10.1242/jcs.00610

Hänel, K. H., Cornelissen, C., Lüscher, B., and Baron, J. M. (2013). Cytokines and the skin barrier. *Int. J. Mol. Sci.* 14, 6720–6745. doi: 10.3390/ijms14046720

Harrison, S. J., Mott, E. K., Parsley, K., Aspinall, S., Gray, J. C., and Cottage, A. (2006). A rapid and robust method of identifying transformed Arabidopsis thaliana seedlings following floral dip transformation. *Plant Methods* 2, 19. doi: 10.1186/1746-4811-2-19

Huang, T. K., and McDonald, K. A. (2012). Bioreactor systems for *in vitro* production of foreign proteins using plant cell cultures. *Biotechnol. Adv.* 30, 398–409. doi: 10.1016/j.bioteChadv.2011.07.016

Ji, Y., Wang, Z., Li, Z., Zhang, A., Jin, Y., Chen, H., et al. (2016). Angiotensin II enhances proliferation and inflammation through AT1/PKC/NF-κB signaling pathway in hepatocellular carcinoma cells. *Cell. Physiol. Biochem.* 39, 13–32. doi: 10.1159/000445602

Jiao, Q., Yue, L., Zhi, L., Qi, Y., Yang, J., Zhou, C., et al. (2022). Studies on stratum corneum metabolism: function, molecular mechanism and influencing factors. *J. Cosmet. Dermatol.* 21, 3256–3264. doi: 10.1111/jocd.15000

Jing, R., Fu, M., Huang, Y., Zhang, K., Ye, J., Gong, F., et al. (2024). Oat β-glucan repairs the epidermal barrier by upregulating the levels of epidermal differentiation, cell-cell junctions and lipids via Dectin-1. *Br. J. Pharmacol.* 181, 1596–1613. doi: 10.1111/bph.16306

Joly-Tonetti, N., Ondet, T., Monshouwer, M., and Stamatas, G. N. (2021). EGFR inhibitors switch keratinocytes from a proliferative to a differentiative phenotype affecting epidermal development and barrier function. *BMC Cancer* 21, 5. doi: 10.1186/s12885-020-07685-5

Kim, D. W., Kim, S. Y., An, J. J., Lee, S. H., Jang, S. H., Won, M. H., et al. (2006). Expression, purification and transduction of PEP-1-botulinum neurotoxin type A (PEP-1-BoNT/A) into skin. *J. Biochem. Mol. Biol.* 39, 642–647. doi: 10.5483/bmbrep.2006.39.5.642

Koenig, D., and Weigel, D. (2015). Beyond the thale: comparative genomics and genetics of Arabidopsis relatives. *Nat. Rev. Genet.* 16, 285–298. doi: 10.1038/nrg3883

Kovinich, N., Kayanja, G., Chanoca, A., Riedl, K., Otegui, M. S., and Grotewold, E. (2014). Not all anthocyanins are born equal: distinct patterns induced by stress in Arabidopsis. *Planta* 240, 931–940. doi: 10.1007/s00425-014-2079-1

Krecicki, T., Jeleń, M., Zalesska-Krecicka, M., Rak, J., Szkudlarek, T., and Jeleń-Krzeszewska, J. (1999). Epidermal growth factor receptor (EGFR), proliferating cell nuclear antigen (PCNA) and Ki-67 antigen in laryngeal epithelial lesions. *Oral. Oncol.* 35, 180–186. doi: 10.1016/s1368-8375(98)00100-6

Labarrade, F., Bergeron, L., Serre, C., Lebleu, A., Busuttil, V., Botto, J. M., et al. (2015). Modulating the expression of survivin and other basal epidermal proteins protects human skin from UVB damage and oxidative stress. *J. Cosmet. Dermatol.* 14, 191–203. doi: 10.1111/jocd.12150

LaPres, J. J., and Hudson, L. G. (1996). Identification of a functional determinant of differentiation-dependent expression in the involucrin gene *. *J. Biol. Chem.* 271, 23154–23160. doi: 10.1074/jbc.271.38.23154

Law, J. D., Gao, Y., Wysocki, V. H., and Gopalan, V. (2025). Design of a yeast SUMO tag to eliminate internal translation initiation. *Protein Sci.* 34, e5256. doi: 10.1002/pro.5256

Lee, S. H., Jeong, S. K., and Ahn, S. K. (2006). An update of the defensive barrier function of skin. *Yonsei Med. J.* 47, 293–306. doi: 10.3349/ymj.2006.47.3.293

Lee, W. J., Park, K. H., Cha, H. W., Sohn, M. Y., Park, K. D., Lee, S.-J., et al. (2014). The expression of involucrin, loricrin, and filaggrin in cultured sebocytes. *Ann. Dermatol.* 26, 134–137. doi: 10.5021/ad.2014.26.1.134

Li, Y., Leng, Q., Pang, X., Shi, H., Liu, Y., Xiao, S., et al. (2021). Therapeutic effects of EGF-modified curcumin/chitosan nano-spray on wound healing. *Regener. Biomater.* 8, rbab009. doi: 10.1093/rb/rbab009

Lim, K.-M. (2021). Skin epidermis and barrier function. *Int. J. Mol. Sci.* 22, 3035. doi: 10.3390/ijms22063035

Liou, A., Elias, P. M., Grunfeld, C., Feingold, K. R., and Wood, L. C. (1997). Amphiregulin and nerve growth factor expression are regulated by barrier status in murine epidermis. *J. Invest. Dermatol.* 108, 73–77. doi: 10.1111/1523-1747.ep12285638

Lodén, M., Andersson, A. C., and Lindberg, M. (1999). Improvement in skin barrier function in patients with atopic dermatitis after treatment with a moisturizing cream (Canoderm). *Br. J. Dermatol.* 140, 264–267. doi: 10.1046/j.1365-2133.1999.02660.x

Ma, J. K. C., Drake, P. M. W., and Christou, P. (2003). The production of recombinant pharmaceutical proteins in plants. *Nat. Rev. Genet.* 4, 794–805. doi: 10.1038/nrg1177

Michalak, M. (2023). Plant extracts as skin care and therapeutic agents. *Int. J. Mol. Sci.* 24 (20), 15444. doi: 10.3390/ijms242015444

Montero-Vilchez, T., Cuenca-Barrales, C., Rodriguez-Pozo, J. A., Diaz-Calvillo, P., Tercedor-Sanchez, J., Martinez-Lopez, A., et al. (2022). Epidermal barrier function and skin homeostasis in atopic dermatitis: the impact of age. *Life (Basel)* 12 (1), 132. doi: 10.3390/life12010132

Montero-Vilchez, T., Segura-Fernández-Nogueras, M.-V., Pérez-Rodríguez, I., Soler-Gongora, M., Martinez-Lopez, A., Fernández-González, A., et al. (2021). Skin barrier function in psoriasis and atopic dermatitis: transepidermal water loss and temperature as useful tools to assess disease severity. *J. Clin. Med.* 10 , 359. doi: 10.3390/jcm10020359

Moustafa, K., Makhzoum, A., and Trémouillaux-Guiller, J. (2016). Molecular farming on rescue of pharma industry for next generations. *Crit. Rev. Biotechnol.* 36, 840–850. doi: 10.3109/07388551.2015.1049934

Niu, X., Song, H., Xiao, X., Yang, Y., Huang, Q., Yu, J., et al. (2022). Tectoridin ameliorates proliferation and inflammation in TNF-α-induced HFLS-RA cells via suppressing the TLR4/NLRP3/NF-κB signaling pathway. *Tissue Cell* 77, 101826. doi: 10.1016/j.tice.2022.101826

Oda, K., Matsuoka, Y., Funahashi, A., and Kitano, H. (2005). A comprehensive pathway map of epidermal growth factor receptor signaling. *Mol. Syst. Biol.* 1 (1), 2005-0010. doi: 10.1038/msb4100014

Paladini, R. D., and Coulombe, P. A. (1998). Directed expression of keratin 16 to the progenitor basal cells of transgenic mouse skin delays skin maturation. *J. Cell Biol.* 142, 1035–1051. doi: 10.1083/jcb.142.4.1035

Panzuti, P., Vidémont, E., Fantini, O., Fardouet, L., Noël, G., Cappelle, J., et al. (2020). A moisturizer formulated with glycerol and propylene glycol accelerates the recovery of skin barrier function after experimental disruption in dogs. *Vet. Dermatol.* 31, 344–e89. doi: 10.1111/vde.12859

Patrick, G. J., Archer, N. K., and Miller, L. S. (2021). Which way do we go? Complex interactions in atopic dermatitis pathogenesis. *J. Invest. Dermatol.* 141, 274–284. doi: 10.1016/j.jid.2020.07.006

Pozuelos, G. L., Rubin, M., Vargas, S., Ramirez, E., Bandaru, D., Sha, J., et al. (2022). Nicotine affects multiple biological processes in epiDermTM organotypic tissues and keratinocyte monolayers. *Atmosphere* 13 (5), 810. doi: 10.3390/atmos13050810

Purwantoro, A., Irsyadi, M. B., Sawitri, W. D., Fatumi, N. C., and Fajrina, S. N. (2023). Efficient floral dip transformation method using Agrobacterium tumefaciens on Cosmos sulphureus Cav. *Saudi J. Biol. Sci.* 30, 103702. doi: 10.1016/j.sjbs.2023.103702

Qiang, W., Gao, T., Lan, X., Guo, J., Noman, M., Li, Y., et al. (2020). Molecular pharming of the recombinant protein hEGF-hEGF concatenated with oleosin using transgenic arabidopsis. *Genes (Basel)* 11. doi: 10.3390/genes11090959

Ren, X., Wang, M., He, X., Li, Z., Zhang, J., Zhang, W., et al. (2018). Superoxide dismutase mimetic ability of Mn-doped ZnS QDs. *Chin. Chem. Lett.* 29, 1865–1868. doi: 10.1016/j.cclet.2018.12.007

Rosdy, M. (1988). Opposite effects of EGF on involucrin accumulation of A431 keratinocytes and a variant which is not growth-arrested by EGF. *In Vitro Cell. Dev. Biol.* 24, 1127–1132. doi: 10.1007/BF02620815

Rothbard, J. B., Garlington, S., Lin, Q., Kirschberg, T., Kreider, E., Mcgrane, P. L., et al. (2000). Conjugation of arginine oligomers to cyclosporin A facilitates topical delivery and inhibition of inflammation. *Nat. Med.* 6, 1253–1257. doi: 10.1038/81359

Ruggiero, F., Exposito, J. Y., Bournat, P., Gruber, V., Perret, S., Comte, J., et al. (2000). Triple helix assembly and processing of human collagen produced in transgenic tobacco plants. *FEBS Lett.* 469, 132–136. doi: 10.1016/S0014-5793(00)01259-X

Ruhlman, T., Ahangari, R., Devine, A., Samsam, M., and Daniell, H. (2007). Expression of cholera toxin B–proinsulin fusion protein in lettuce and tobacco chloroplasts – oral administration protects against development of insulitis in non-obese diabetic mice. *Plant Biotechnol. J.* 5, 495–510. doi: 10.1111/j.1467-7652.2007.00259.x

Sassa, T., Ohno, Y., Suzuki, S., Nomura, T., Nishioka, C., Kashiwagi, T., et al. (2013). Impaired epidermal permeability barrier in mice lacking elovl1, the gene responsible for very-long-chain fatty acid production. *Mol. Cell. Biol.* 33, 2787–2796. doi: 10.1128/MCB.00192-13

Segre, J. A. (2006). Epidermal barrier formation and recovery in skin disorders. *J. Clin. Invest.* 116, 1150–1158. doi: 10.1172/JCI28521

Suo, G., Chen, B., Zhang, J., Duan, Z., He, Z., Yao, W., et al. (2006). Effects of codon modification on human BMP2 gene expression in tobacco plants. *Plant Cell Rep.* 25, 689–697. doi: 10.1007/s00299-006-0133-6

Turnbull, C., Lillemo, M., and Hvoslef-Eide, T. A. K. (2021). Global regulation of genetically modified crops amid the gene edited crop boom - A review. *Front. Plant Sci.* 12. doi: 10.3389/fpls.2021.630396

Uhlinger, D. J., Carton, J. M., Argentieri, D. C., Damiano, B. P., and Dandrea, M. R. (2001). Increased expression of serine palmitoyltransferase (SPT) in balloon-injured rat carotid artery. *Thromb. Haemost.* 86, 1320–1326. doi: 10.1055/s-0037-1616067

Vasseur, F., Exposito-Alonso, M., Ayala-Garay, O. J., Wang, G., Enquist, B. J., Vile, D., et al. (2018). Adaptive diversification of growth allometry in the plant Arabidopsis thaliana. *Proc. Natl. Acad. Sci. U.S.A.* 115, 3416–3421. doi: 10.1073/pnas.1709141115

Wakelin, S. J., Sabroe, I., Gregory, C. D., Poxton, I. R., Forsythe, J. L., Garden, O. J., et al. (2006). Dirty little secrets"–endotoxin contamination of recombinant proteins. *Immunol. Lett.* 106, 1–7. doi: 10.1016/j.imlet.2006.04.007

Webster, D. E., and Thomas, M. C. (2012). Post-translational modification of plant-made foreign proteins; glycosylation and beyond. *Biotechnol. Adv.* 30, 410–418. doi: 10.1016/j.bioteChadv.2011.07.015

Wikramanayake, T. C., Stojadinovic, O., and Tomic-Canic, M. (2014). Epidermal differentiation in barrier maintenance and wound healing. *Adv. Wound Care* 3, 272–280. doi: 10.1089/wound.2013.0503

Wirth, S., Calamante, G., Mentaberry, A., Bussmann, L., Lattanzi, M., Barañao, L., et al. (2004). Expression of active human epidermal growth factor (hEGF) in tobacco plants by integrative and non-integrative systems. *Mol. Breed.* 13, 23–35. doi: 10.1023/B:MOLB.0000012329.74067.ca

Xu, H., Timares, L., and Elmets, C. A. (2019). "19 - Host Defenses in Skin," in *Clinical Immunology, Fifth Edition*. Eds. R. R. Rich, T. A. Fleisher, W. T. Shearer, H. W. Schroeder, A. J. Frew and C.M. Weyand (Elsevier, London). doi: 10.1016/B978-0-7020-6896-6.00019-3

Yang, L., Fan, X., Cui, T., Dang, E., and Wang, G. (2017). Nrf2 promotes keratinocyte proliferation in psoriasis through up-regulation of keratin 6, keratin 16, and keratin 17. *J. Invest. Dermatol.* 137, 2168–2176. doi: 10.1016/j.jid.2017.05.015

Yang, G., Seok, J. K., Kang, H. C., Cho, Y. Y., Lee, H. S., and Lee, J. Y. (2020). Skin barrier abnormalities and immune dysfunction in atopic dermatitis. *Int. J. Mol. Sci.* 21 (8), 2867. doi: 10.3390/ijms21082867

Yosipovitch, G., Misery, L., Proksch, E., Metz, M., Ständer, S., and Schmelz, M. (2019). Skin barrier damage and itch: review of mechanisms, topical management and future directions. *Acta Derm. Venereol.* 99, 1201–1209. doi: 10.2340/00015555-3296

Zhang, M.-P., Wang, M., and Wang, C. (2021). Nuclear transformation of Chlamydomonas reinhardtii: A review. *Biochimie* 181, 1–11. doi: 10.1016/j.biochi.2020.11.016

Zhang, Z., Xiao, C., Gibson, A. M., Bass, S. A., and Khurana Hershey, G. K. (2014). EGFR signaling blunts allergen-induced IL-6 production and Th17 responses in the skin and attenuates development and relapse of atopic dermatitis. *J. Immunol.* 192, 859–866. doi: 10.4049/jimmunol.1301062

frontiers | Frontiers in Plant Science

TYPE Original Research
PUBLISHED 19 June 2025
DOI 10.3389/fpls.2025.1565487

OPEN ACCESS

EDITED BY
Giuseppe Dionisio,
Aarhus University, Denmark

REVIEWED BY
Mercedes Diaz-Mendoza,
Complutense University of Madrid, Spain
Eliane Ferreira Noronha,
University of Brasilia, Brazil

*CORRESPONDENCE
Yongfeng Guo
guoyongfeng@caas.cn
Lingyan Li
lilingyan@qau.edu.cn

†These authors have contributed equally to this work and share first authorship

RECEIVED 23 January 2025
ACCEPTED 30 May 2025
PUBLISHED 19 June 2025

CITATION
Yang Y, Deng Z, Zhang Z, Yang Y, Pan X, Wu R, Liu T, Gao X, Li L and Guo Y (2025) Papain-like cysteine proteases in *Nicotiana benthamiana*: gene family members and their potential implications in recombinant protein expression. *Front. Plant Sci.* 16:1565487. doi: 10.3389/fpls.2025.1565487

Papain-like cysteine proteases in *Nicotiana benthamiana*: gene family members and their potential implications in recombinant protein expression

Yalun Yang[1,2,3†], Zhichao Deng[1,2†], Zhongqi Zhang[4], Yong Yang[4], Xiaolu Pan[1,2], Rongrong Wu[1,2], Tao Liu[1,2], Xiaoming Gao[1,2], Lingyan Li[1*] and Yongfeng Guo[2,3*]

[1]College of Agronomy, Qingdao Agricultural University, Qingdao, China, [2]Tobacco Research Institute, Chinese Academy of Agricultural Sciences, Qingdao, China, [3]Qingdao Municipal Key Laboratory of Plant Molecular Pharming, Tobacco Research Institute, Chinese Academy of Agricultural Sciences, Qingdao, China, [4]Vegetable and Landscape Gardening Institute, Heze Academy of Agricultural Sciences, Heze, China

Introduction: Papain-like cysteine proteases (PLCPs), characterized by a conserved cysteine residue at their active sites, play crucial roles in plant growth, development, and responses to biotic and abiotic stresses. While their importance in plants is well recognized, the characterization of the PLCP gene family in *Nicotiana benthamiana* (*NbPLCP*) and its involvement in biotic stress responses remains insufficiently studied. This study aims to identify *NbPLCP* genes in *N. benthamiana* and elucidate their roles in facilitating heterologous protein expression.

Methods: A comprehensive bioinformatics approach was employed to identify *NbPLCP* genes using *N. benthamiana* genomic data and homology with *Arabidopsis thaliana*. The analysis included examination of physicochemical properties, phylogenetic relationships, gene structures, conserved motifs, expression profiles, gene duplication events, and chromosomal distribution. Virus-induced gene silencing (VIGS) was utilized to screen for genes affecting heterologous protein expression in *N. benthamiana*.

Results: We identified and characterized 50 *NbPLCP* members. Phylogenetic analysis classified these *NbPLCPs* into nine subfamilies, with uneven distribution across 19 chromosomes. Comparative analysis revealed closer evolutionary relationships between *N. benthamiana* and *Solanum lycopersicum*, followed by *Arabidopsis thaliana*, while showing more distant relationships with *Oryza sativa*. Functional studies demonstrated that *NbPLCPs* likely participate in regulating plant growth, development, and biotic stress responses. Importantly, VIGS-mediated silencing of *NbXCP1*, *NbXCP2*, and *NbXCP3* significantly enhanced the expression of heterologous GFP protein.

Discussion: This study provides comprehensive insights into the PLCP family in *N. benthamiana*, highlighting their functional significance and potential in heterologous protein expression. Our findings establish a foundation for understanding the evolution and function of *NbPLCPs*, while demonstrating

their potential applications in plant biotechnology for enhancing disease resistance and improving recombinant protein production systems. These results underscore the importance of *PLCPs* in both plant physiology and biotechnological applications.

KEYWORDS

PLCP, *Nicotiana benthamiana*, biological stress, family analysis, gene expression patterns

1 Introduction

Proteases degrade substrate proteins by hydrolyzing peptide bonds. Based on the chemical nature of their catalytic sites, they can be classified into four categories: cysteine proteases, serine proteases, aspartic proteases, and metallo proteases (Zhang et al., 2023). Among them, cysteine proteases (CPs) rely on the cysteine residue at the active site as a nucleophilic group to catalyze reactions, a key subclass, papain-like cysteine proteases (PLCPs), is characterized by a conserved catalytic triad (Cys-His-Asn) at its core (Cen et al., 2019), by efficiently catalyzing reactions, they regulate plant growth and development, stress responses, and disease resistance processes (Liu et al., 2018; Li et al., 2025; Misas-Villamil et al., 2016; Rawlings et al., 2016). PLCPs are synthesized in the form of zymogens, with their precursors containing an N-terminal signal peptide, an autoinhibitory pro-domain, and a mature 25–35 kDa active protease domain. Some PLCPs also possess an unknown functional particle structure at the C-terminal (Zhang et al., 2023). These subfamilies include the CTB, ALP, RD19, SAG12, RD21, CEP, THI, XBCP, and XCP subfamilies (Kordis and Turk, 2009; Richau et al., 2012), Each subfamily achieves functional differentiation through specific structural domains, such as inhibitor-binding domains or substrate recognition regions (Long et al., 2025).

The activity of *PLCPs* is notably increased during the development and germination of seeds (Martinez et al., 2009), as well as in fruits (Lin et al., 1993) and various plant organs (van Wyk et al., 2014). In *Arabidopsis thaliana*, the gene *AtSAG12* exhibits a tightly regulated expression pattern associated with leaf senescence, and it has become a widely used molecular marker for studying leaf aging. Moreover, *AtRD21* and *AtRD19* serve as early-response marker genes for dehydration stress under drought and salt conditions, reflecting the role of PLCPs in the plant's response to abiotic stresses (Guo and Gan, 2014; Lohman et al., 1994). In *Oryza sativa*, PLCPs assist in pathogen defense by broadly activating signaling pathways and transcription factors that coordinate downstream responses. This includes the upregulation of various disease-related proteins and the biosynthesis of secondary metabolites, which contribute to resistance mechanisms (Nino et al., 2020). As a critical component of the proteolytic machinery, PLCPs are responsible for the degradation of intracellular proteins, playing an essential role in regulating programmed cell death (PCD). PCD is a highly regulated biological process that is integral to numerous aspects of plant development, as well as responses to both biotic and abiotic stressors (Liu et al., 2018). In the context of *Medicago truncatula*, *MtCP6* is induced during both developmental and stress-induced nodule senescence. Its early expression promotes nodule senescence, while *MtCP77* positively regulates root nodule aging by accelerating plant PCD and reactive oxygen species (ROS) accumulation (Deng et al., 2019; Pierre et al., 2014). Furthermore, PLCPs are closely associated with plant resistance to herbivory. For instance, papain, a well-known PLCP found in the latex exudate of papaya, plays a critical role in defending the plant against herbivorous insects, such as lepidopteran larvae (Konno et al., 2004). This highlights the multifaceted role of PLCPs in both plant development and stress response, emphasizing their importance in the regulation of cellular processes and interactions with environmental factors. Although the functional roles of PLCPs have been extensively investigated in other species, research on this family in *N. benthamiana* remains unexplored.

Tobacco (*Nicotiana benthamiana*), a model plant, is widely utilized in the study of plant innate immunity and defense signaling pathways. It is particularly suitable for virus-induced gene silencing and transient gene overexpression through Agrobacterium-mediated infiltration (Bally et al., 2018). In recent years, *N. benthamiana* has gained attention as a biological reactor for the production of vaccines and therapeutic proteins (Douglas, 2018). However, the expression of exogenous proteins in *N. benthamiana* can be influenced by a variety of factors. One such factor is the interference by endogenous proteases in *N. benthamiana*, which can reduce the accumulation of exogenous proteins (Jutras et al., 2020). Among the various protease inhibitors identified, the co-expression of four specific inhibitors, namely SICYS8, NbPR4, NbPot1, and human HsTIMP, has been shown to significantly enhance the expression levels of exogenous proteins when compared to controls (Grosse-Holz et al., 2018).The SICYS8 protease inhibitor targets papain-like cysteine proteases. Strong inhibition of nine distinct PLCPs in *N. benthamiana* leaves has been observed upon the expression of SICYS8, suggesting a direct and potent effect on PLCP activity (Jutras et al., 2019). Although several members of the PLCP family have been extensively studied in *N. benthamiana*, a comprehensive investigation into the phylogeny of the entire PLCP gene family has yet to be undertaken.

In this study, we utilized the latest genomic data to systematically identify and analyze the PLCP gene family in *N. benthamiana*. Our comprehensive analysis included the construction of a phylogenetic

tree, investigation of gene structures, identification of cis-regulatory elements, synteny analysis, expression profiling, and assessment of how specific PLCP family members influence the expression of the exogenous green fluorescent protein (GFP). These findings provide valuable insights into the evolutionary dynamics and functional roles of the PLCP gene family in *N. benthamiana*. Furthermore, this research contributes to a deeper understanding of *N. benthamiana* as a plant-based bioreactor, with potential applications in optimizing protein production within this species.

2 Materials and methods

2.1 Plant materials and growth conditions

The experimental materials used in this study were the *N. benthamiana* seeds kept by the Chinese Academy of Agricultural Sciences, and the designated tobacco seeds were sown on the soil matrix. After germination, the seedlings were transplanted to 25°C, 16 h/8 h (light/dark) photoperiod conditions to 6 to 8 leaf stage for Agrobacterium infiltration and inoculation.Samples were taken at 0h, 3 h, 12 h, 24 h, 36 h, 48 h and 72 h, and stored at -80°C after snap freezing in liquid nitrogen.

2.2 Identification and sequence analysis of the *NbPLCP* gene family

In order to search the members of the *PLCP* gene family, we downloaded the protein sequences of all the *Arabidopsis PLCP* family members from the TAIR (www.arabidopsis.org) *Arabidopsis* database, and analyzed these *PLCP* family members from the Pfam (http://pfam.xfam.org/) database, which showed that they generally possess the conserved domain of PF00112. Also we downloaded the genome and protein files of the NbeHZ1 version from the Nicomics (http://lifenglab.hzau.edu.cn/Nicomics/index.php) website. The hidden horse model file of PLCP gene family was found and downloaded through Pfam (http://pfam.xfam.org/) website using the hmmsearch program to set the E value of 1e-20 threshold; and the protein sequence of *AtPLCPs* family was Query to search the possible *NbPLCPs* sequence through BLAST search. The protein sequences obtained from both methods were removed after redundancy and uploaded to CDD (https://www.ncbi.nlm.nih.gov/Structure/bwrpsb/bwrpsb.cgi) and SMART (http://smart.embl.de/smart/set_mode.cgi?NORMAL=1) for domain validation to remove protein sequences without the PF000112 domain (Finn et al., 2014; Schultz et al., 1998).

By visiting the Expasy online platform (http://www.expasy.org/tools/protparam.html) and using its ProtParam tool, various physiochemical properties of NbPLCP protein members, including protein length, molecular weight, isoelectric point, aliphatic amino acid content and hydrophobicity index. The NbPLCP was named based on its chromosomal location (Gasteiger et al., 2003).

2.3 The evolutionary tree analysis of the *NbPLCPs* gene family members

The PLCP protein sequences of *Arabidopsis thaliana*, rice (*Oryza sativa*) and tomato (*Solanum lycopersicum*) can be downloaded from the Uniprot database (https://www.uniprot.org). A phylogenetic tree of these species and the PLCP proteins was constructed using MEGA11. Sequence ratios were performed using the ClustalW method, excluding non-conserved regions outside the aligned domains. A phylogenetic tree was constructed using a maximum likelihood method with a bootstrap value of 1000 (Kumar et al., 2018).

2.4 Analysis of gene structure, protein domains, and conserved motifs

Online tool MEME (http://meme-suite.org/) was used to predict conserved motifs in NbPLCP proteins, with motif lengths set to 6–100 with up to 10 motifs identified while maintaining default values for other parameters (Bailey et al., 2015). Using Batch CD-Search (https://www.ncbi.nlm.nih.gov/Structure/bwrpsb/bwrpsb.cgi) for the NbPLCP family, And the visualization of their protein-conserved domains using TBtools, Gene structure analysis based on the genomic DNA and CDS sequences of the NbPLCP gene family members, And using the online gene structure visualization server 2.0 (https://gsds.gao-lab.org/Gsds_help.php) for gene structure visualization.

2.5 Identification of cis-acting regulatory elements in the *PLCP* gene

From the 2000 bp region from the genome sequence file, the cis-regulatory elements (CAREs) of these promoter regions were then analyzed using PlantCARE software (http://bioinformatics.psb.ugent.be/webtools/plantcare/html/) (Lescot et al., 2002). Finally, tbtools presents all the identified elements of the promoter region of the *NbPLCP* gene as a heatmap.

2.6 Chromosomal localization and collinearity analysis

Information on the start and stop positions of *PLCPs* genes was extracted from the NbeHZ1 genome Gff3 file in TBtools software and mapped on the corresponding chromosome. For *NbPLCPs* analysis within species, TBtools software Fasta Tools and Blast tools, including chromosome length, gene location files and corresponding alignment files were used (Chen et al., 2020). *PLCPs* were analyzed using the One step MCScan X tool, and E value was set to 1e-5. The resulting Collinearity file was used for fragment duplication gene analysis and Tandem file was used for tandem repeat gene analysis (Wang et al., 2012). Use the

KaKs_Calculator 3.0 software to calculate the non-synonymous to synonymous substitution ratio (Ka/Ks) of homologous gene pairs within the *NbPLCP* gene family (Zhang, 2022).

2.7 Experimental processing and sampling

Synthesize the nucleic acid sequence of SICYS8 (Sainsbury et al., 2013) and construct the *pEAQ::SCYS8* overexpression vector using T4 ligation technology. Inject *pEAQ::SCYS8* and *TRBO::GFP* into one side of the leaves of 4-week-old *Nicotiana benthamiana*, and co-inject empty pEAQ vector and *TRBO::GFP* into the other side of the leaves as a control group. Take photos and collect samples 3 days later, extract total protein from the samples, and use it for subsequent Western Blot analysis to detect the expression level of green fluorescent protein (GFP).

Design transient silencing fragments of the NbRD21, NbCTB, NbRD19, NbXBCP, and NbCEP subfamilies using the VIGS TOOL, Based on the conservative sequences of the same subfamily members, several vectors were designed to simultaneously silence multiple genes the primers used are shown in Supplementary Table S1. The specific vectors include: *TRV2::NbRD21BD* (silencing *NbRD21B* and *NbRD21D*), *TRV2::NbRD21E* (silencing *NbRD21E*), *TRV2::NbXBCP17 (silencing NbXBCP1 and NbXBCP7*), *TRV2::NbXBCP345* (silencing *NbXBCP3*, *NbXBCP4*, and *NbXBCP5*), *TRV2::NbXBCP26* (silencing *NbXBCP2* and *NbXBCP6*), *TRV2::NbRD19ABC* (silencing *NbRD19A*, *NbRD19B*, and *NbRD19C*), *TRV2::NbRD19E* (silencing *NbRD19E*), *TRV2::NbCTB13* (silencing *NbCTB1* and *NbCTB3*), *TRV2::NbCTB2* (silencing *NbCTB2*), and *TRV2::NbXCP123* (silencing *NbXCP1*, *NbXCP2*, and *NbXCP3*).using homologous recombination technology. Construct the *TRV2::GUS* vector as a control. Co-inject Agrobacterium containing TRV2 experimental group with TRV1 into the leaves of 2-week-old Nicotiana benthamiana as the experimental treatment, and co-inject *TRV2::GUS* with TRV1 as the control. Fifteen days later, inject *TRBO::GFP* Agrobacterium into the T and CK groups, take photos, and collect samples 3 days later. Extract RNA and total protein from the samples for subsequent quantitative fluorescence analysis and Western Blot analysis to detect the expression level of green fluorescent protein (GFP).

2.8 Protein extraction and Western Blot detection

Nicotiana benthamiana leaves were ground in liquid nitrogen using a mortar and pestle, followed by the addition of Tris-HCl buffer (pH 8.0), 2.5 M NaCl (pH 8.0), EDTA (pH 8.0), glycerol, 100 mM PMSF, and ddH_2O. The samples were incubated on ice for 30 minutes and then centrifuged at 12,000 rpm for 10 minutes at 4°C. The supernatant was collected and mixed with 5× SDS-PAGE protein loading buffer (Solarbio P1040) at an appropriate ratio. The mixture was heated at 95°C for 10 minutes in a metal bath. Proteins were separated by 12.5% SDS-PAGE gel electrophoresis and transferred to a PVDF membrane using the Trans-Blot Turbo system (Bio-Rad, Hercules, CA). The membrane was blocked in TBS-T containing 5% non-fat milk and incubated with Anti-GFP antibody (1:8000; Abcam, ab6556) and goat anti-rabbit IgG H&L (HRP) secondary antibody (1:4000; Abcam, ab6721).

2.9 RNA extraction and quantitative real-time PCR analysis

Whole RNA of *N. benthamiana* from control and processing group extracted with an RNA extraction kit (Beijing Kangwei Century Company, CW0581M). The cDNA was reverse transcription kit (Nanjing Norzan Biotechnology Co., Ltd., R333-01). For real-time PCR (Real-time PCR) detection, 10-fold diluted cDNA was used as the reaction template and a set of specific PCR reaction process: at the starting stage, 3 minutes pre-denaturation at 95°C; then 40 PCR cycles with 10 seconds 95°C denaturation phase and 30 seconds 60°C extension phase; and the flow parameters were 15 seconds 95°C treatment, 60 seconds 60°C treatment, and finally 15 seconds 95°C treatment. Data were calculated and analyzed using the $2^{-\Delta\Delta CT}$ method (Rao et al., 2013), with *NbActin* as the reference gene. The results were compared and integrated with other data. Significance analysis was performed using the ANOVA method with a significance level set at 0.05. The specific primers applied in this trial are detailed in Supplementary Table S2, and three experimental replicates were performed for each sample.

3 Results

3.1 Identification and annotation of NbPLCPs

Using the HMMER search technique, a total of 50 PLCP family genes were successfully identified (Table 1). The corresponding proteins were analyzed using protein analysis tools to determine their physicochemical properties. The protein lengths ranged from 156 to 925 amino acids, with molecular weights ranging from 17,147.41 Da to 104,611.01 Da. The theoretical isoelectric points (pI) varied significantly, with NbRD19G showing the highest pI and NbTHI2 showing the lowest. NbXBCP6 exhibited the highest instability index, while NbRD19C had the lowest aliphatic index. These parameters enhanced our understanding of the characteristics of the NbPLCP family, providing deeper insights into their structure and physicochemical properties. Additionally, the subcellular localization of the proteins encoded by NbPLCP was predicted, and the results indicated that most family members are localized to vacuoles and the endoplasmic reticulum. Specifically, NbXBCP6, NbRD19C, and NbRD19F were predicted to be localized

TABLE 1 Physicochemical characterization of PLCP gene family members in *Nicotiana benthamiana*.

Group	Gene ID	Gene name	Number of amino acid	Molecular weight	Theoretical pI	Instability index	Aliphatic index	Gravy	Subcellular localization
RD21	*Nbe01g03680.1*	*NbRD21A*	240	27431.64	5.33	31.13	67.04	-0.59	Vacuole
	Nbe07g24350.1	*NbRD21B*	470	51539.07	5.58	30.16	67.43	-0.45	Vacuole
	Nbe12g22210.1	*NbRD21C*	465	51108.34	5.36	36.49	69.20	-0.4	Vacuole
	Nbe13g10990.1	*NbRD21D*	473	51786.26	5.76	30.09	65.54	-0.48	Vacuole
	Nbe15g02990.1	*NbRD21E*	465	51071.20	5.12	40.99	70.02	-0.39	Vacuole
	Nbe03g10470.1	*NbRDL1*	374	42365.55	7.10	35.17	68.77	-0.59	Vacuole
	Nbe04g29160.1	*NbRDL2*	374	42280.54	6.73	36.97	70.61	-0.54	Vacuole
CEP	*Nbe05g24660.1*	*NbCEP1*	361	40508.59	6.20	35.65	66.15	-0.6	Endoplasmic reticulum
	Nbe06g22830.1	*NbCEP2*	361	40558.46	5.78	36.28	65.60	-0.61	Endoplasmic reticulum
	Nbe13g08980.1	*NbCEP3*	357	39787.79	5.64	32.33	70.73	-0.47	Endoplasmic reticulum
	Nbe15g06380.1	*NbCEP4*	362	40565.54	6.04	29.74	67.07	-0.6	Endoplasmic reticulum
	Nbe16g15630.1	*NbCEP5*	362	40452.30	5.97	29.03	67.60	-0.59	Endoplasmic reticulum
	Nbe19g14710.1	*NbCEP6*	357	39762.79	5.91	35.26	68.54	-0.49	Endoplasmic reticulum
XCP	*Nbe07g17300.1*	*NbXCP1*	355	39907.19	5.64	26.23	78.54	-0.39	Vacuole
	Nbe12g34660.1	*NbXCP2*	355	39921.29	5.74	23.05	79.92	-0.36	Vacuole
	Nbe16g13040.1	*NbXCP3*	353	39725.80	5.39	39.50	73.48	-0.39	Vacuole
XBCP	*Nbe03g28930.1*	*NbXBCP1*	505	56728.90	5.31	48.98	63.15	-0.53	Vacuole
	Nbe03g28940.1	*NbXBCP2*	503	56274.89	5.26	50.14	72.68	-0.37	Vacuole
	Nbe07g20010.1	*NbXBCP3*	439	48169.12	5.38	39.46	71.03	-0.31	Vacuole
	Nbe13g14250.1	*NbXBCP4*	438	47859.87	5.59	39.33	70.30	-0.29	Vacuole
	Nbe17g00220.1	*NbXBCP5*	405	44255.53	5.73	41.07	64.72	-0.41	Vacuole
	Nbe18g28970.1	*NbXBCP6*	615	66994.26	5.39	80.87	59.90	-0.59	Nucleus/Vacuole
	Nbe18g28980.1	*NbXBCP7*	501	56188.28	5.36	47.34	65.21	-0.52	Vacuole
THI	*Nbe17g07020.1*	*NbTHI1*	205	22224.09	5.78	25.21	67.56	-0.36	Endoplasmic reticulum
	Nbe18g28670.1	*NbTHI2*	188	19998.55	4.57	24.15	88.14	0.09	Vacuole
	Nbe19g03320.1	*NbTHI3*	206	22295.99	4.99	23.12	67.72	-0.34	Endoplasmic reticulum

(Continued)

10.3389/fpls.2025.1565487

TABLE 1 Continued

Group	Gene ID	Gene name	Number of amino acid	Molecular weight	Theoretical pI	Instability index	Aliphatic index	Gravy	Subcellular localization
SAG12	*Nbe03g29120.1*	*NbSAG12A*	340	37474.88	5.06	23.13	67.47	-0.38	Vacuole
	Nbe16g10350.1	*NbSAG12B*	332	36623.07	5.29	17.51	67.38	-0.37	Vacuole
	Nbe17g18710.1	*NbSAG12C*	339	38061.05	6.55	14.76	72.21	-0.38	Vacuole
	Nbe18g19100.1	*NbSAG12D*	340	37952.64	6.67	24.11	63.71	-0.51	Vacuole
	Nbe18g28710.1	*NbSAG12E*	340	37140.68	6.61	20.97	65.76	-0.38	Endoplasmic reticulum
	Nbe18g28720.1	*NbSAG12F*	340	37129.60	5.76	19.56	66.62	-0.37	Endoplasmic reticulum
	Nbe18g28730.1	*NbSAG12G*	286	31339.30	6.60	13.45	70.66	-0.29	Vacuole
	Nbe18g28820.1	*NbSAG12H*	289	31816.93	6.89	25.41	65.16	-0.43	Vacuole
	Nbe17g18720.1	*NbPAP1*	324	36210.83	5.22	36.60	79.51	-0.37	Vacuole
	Nbe18g28680.1	*NbPAP2*	348	38704.14	4.96	29.26	72.59	-0.36	Vacuole
	Nbe18g28700.1	*NbPAP3*	201	22575.73	5.96	39.02	69.45	-0.31	Cell membrane/Vacuole
RD19	*Nbe01g01530.1*	*NbRD19A*	370	40804.10	6.01	32.56	78.54	-0.29	Vacuole
	Nbe02g13940.1	*NbRD19B*	370	40808.02	5.95	32.17	77.46	-0.28	Vacuole
	Nbe05g01930.1	*NbRD19C*	925	104611.01	8.43	50.63	55.63	-0.98	Nucleus
	Nbe06g32440.1	*NbRD19D*	387	42571.46	6.73	31.08	77.65	-0.21	Vacuole
	Nbe07g19880.1	*NbRD19E*	365	40284.39	6.13	29.43	75.95	-0.33	Vacuole
	Nbe08g09060.1	*NbRD19F*	156	17147.41	8.25	52.12	70.71	-0.4	Nucleus/Vacuole
	Nbe12g02110.1	*NbRD19G*	265	30432.11	9.01	31.97	79.89	-0.42	Vacuole
	Nbe14g32420.1	*NbRD19H*	238	26538.79	6.00	38.60	68.11	-0.57	Golgi/Vacuole
ALP	*Nbe09g10400.1*	*NbALP1*	359	39666.02	8.25	37.56	79.86	-0.25	Vacuole
	Nbe14g17540.1	*NbALP2*	360	39207.60	6.94	23.55	81.28	-0.13	Vacuole
CTB	*Nbe03g25810.1*	*NbCTB1*	862	95608.36	5.11	40.99	94.33	-0.11	Chloroplast/Vacuole
	Nbe03g25840.1	*NbCTB2*	357	39586.01	6.12	37.47	80.03	-0.22	Vacuole
	Nbe04g13100.1	*NbCTB3*	361	39876.46	6.00	37.69	83.77	-0.16	Vacuole

10.3389/fpls.2025.1565487

to the nucleus, NbRD19H was predicted to be localized to the Golgi apparatus, and NbPAP3 was predicted to be localized to the membrane, while NbCTB1 was predicted to be localized to both vacuoles and chloroplasts.

3.2 Phyloevolutionary analysis of the *NbPLCP* families

To further investigate the evolutionary relationships of *NbPLCP*, we constructed a phylogenetic tree using PLCP protein sequences from different species (Figure 1). Based on previous studies, PLCPs were classified into nine subfamilies: CTB, ALP, RD19, SAG12, CEP, THI, XBCP, XCP, and RD21. The *NbPLCP* family members are distributed across these nine subfamilies. The ALP subfamily contains the fewest *NbPLCP* members, with only two members; the CTB, THI, and XCP subfamilies each contain three members; the CEP subfamily has six members; the RD21 and XBCP subfamilies each have seven members; and the RD19 subfamily contains eight members. The SAG12 subfamily has the largest number of *NbPLCP* members, with eleven. Evolutionary analysis across different species indicates that the evolutionary mechanisms of the PLCP gene family are relatively conserved.

3.3 Conserved motifs, protein structure, and gene structure analysis of *NbPLCPs*

We analyzed the gene structure of *NbPLCPs*, and showed that these genes contained more than one exon, ranging from 1 to 20 (Figure 2), number of the same exons for the same members of the same subfamily.Such as the number of exons in the XCP subfamily, the XBCP subfamily, and the CEP subfamily. The member with the highest number of exons, *NbCTB1*, located in the CTB subfamily, has 20 exons. Although other subfamily members do not have uniform numbers of exons, they possess very close numbers of exons.

To further understand the structural and functional characteristics of NbPLCPs family members, 10 conserved motifs in NbPLCPs proteins were identified using MEME software (Figure 2), with only one Motif4 in NbRD19F and all members except NbRD19G without Motif4 having Motif4. Where Motif1 is

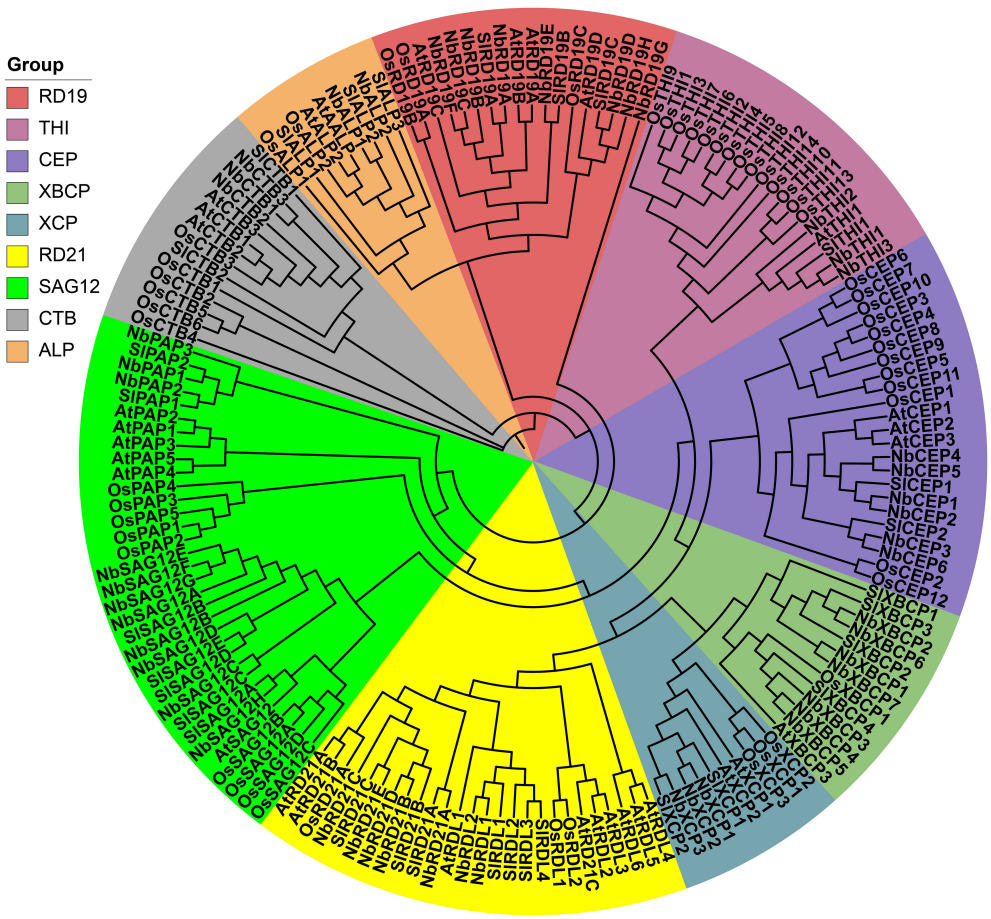

FIGURE 1
Evolutionary relationships of members of the NbPLCP family with *Arabidopsis*, tomato and rice.

10.3389/fpls.2025.1565487

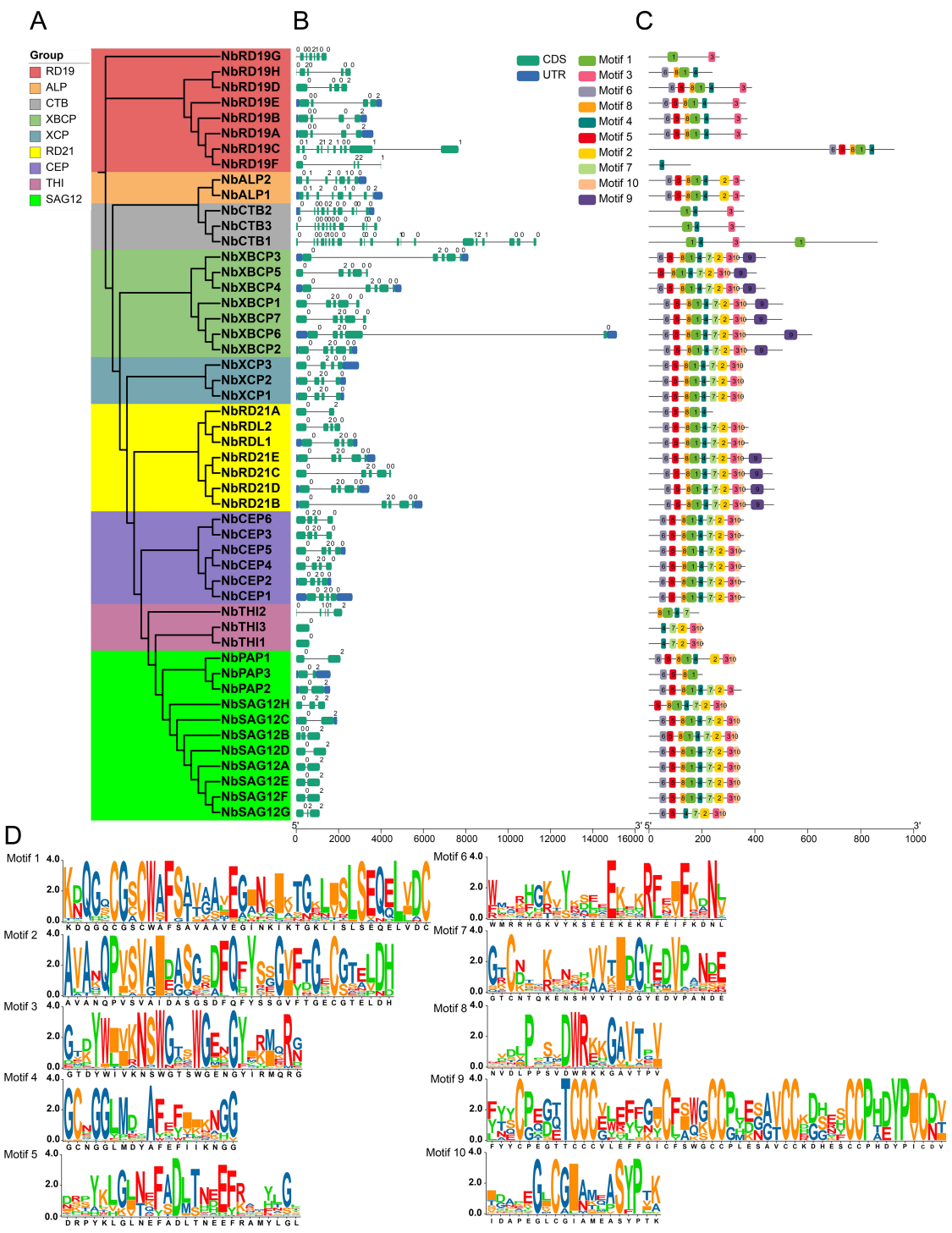

FIGURE 2
Structure and motif analysis of the *NbPLCPs* gene. **(A)** Phylogenetic tree of *NbPLCPs* constructed using MEGA. **(B)** A map of the exon structures displayed using the GSDS web site. **(C)** Analysis of 10 Motifs in the meme website construction. **(D)** Analysis of the conserved motifs.

present in other members except the four members, NbRD19F, NbTHI1, NbTHI3 and NbSAG12G. Combined with the phylogenetic tree, we shows that the protein structure of the members on the same branch is basically consistent, suggesting that the members on the same branch may continue their function. In summary, the analysis of conserved motifs, protein domains, and gene structure of gene family members provides strong evidence for the results of the phylogenetic analysis.

10.3389/fpls.2025.1565487

3.4 Gene duplication analysis and chromosomal distribution of *NbPLCPs*

In order to better understand the distribution of the *NbPLCP* gene family members across the genome, based on the current *N. benthamiana* genome, 50 *NbPLCP* genes are unevenly distributed across 17 of the 19 chromosomes (Figure 3). Chromosome 18 harbors the highest number of *NbPLCP* genes (10 genes), while chromosomes 2, 8, and 9 contain only one *NbPLCP* gene each. Two *NbPLCP* genes are located on chromosomes 1, 4, 5, 6, 14, 15, and 19 respectively,

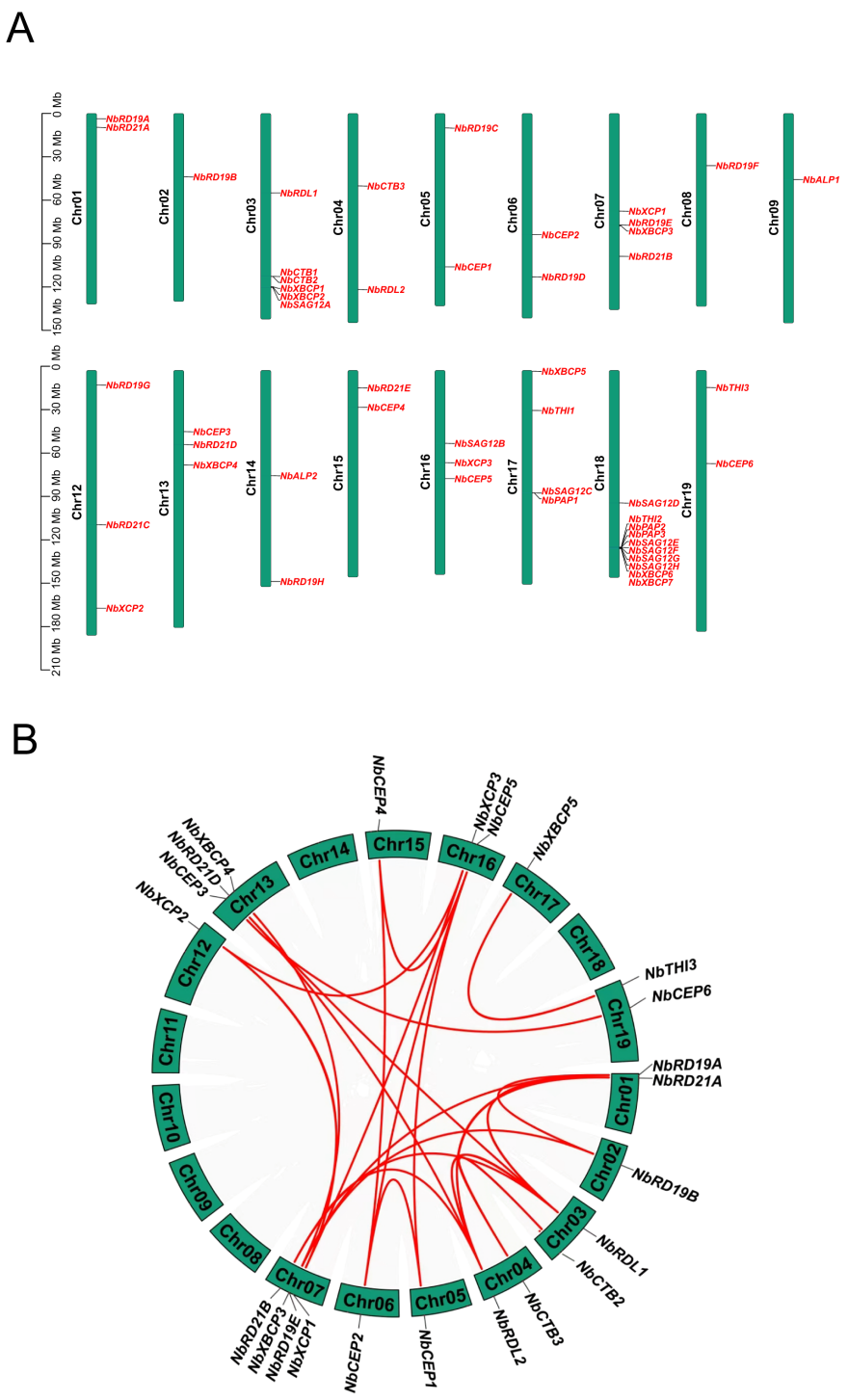

FIGURE 3
(A) Chromosome positioning is based on the location of 17 chromosomes (Mb), the proportion on the left is trillion 1 billion (Mb), and the number of chromosomes is located on the left of each chromosome. **(B)** The inter-genomic collinearity of PLCP genes in *N. benthamiana*. The red line represents the segmental duplication event among PLCP family members.

10.3389/fpls.2025.1565487

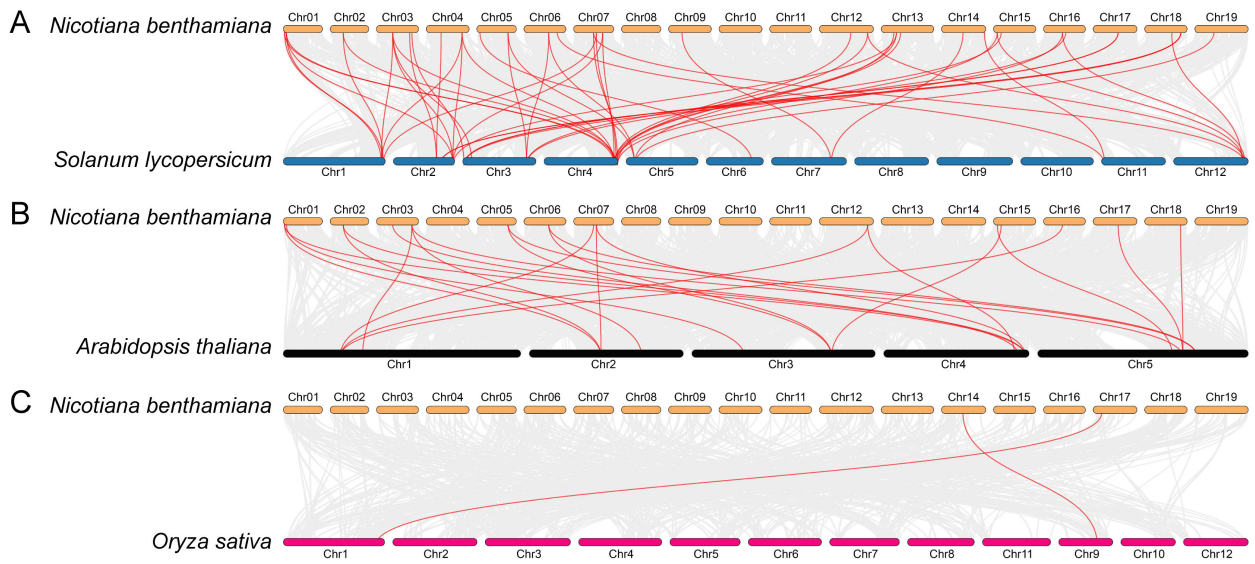

FIGURE 4
Synteny analysis between *Nicotiana benthamiana* and other species. Gray lines indicate all collinear relationships between different chromosomes, while colored lines represent collinear analysis specific to *NbPLCP* family genes. **(A)** Synteny analysis between *N. benthamiana* and *Solanum lycopersicum*. **(B)** Synteny analysis between *N. benthamiana* and *Arabidopsis thaliana*. **(C)** Synteny analysis between *N. benthamiana* and *Oryza sativa*.

whereas three *NbPLCP* genes are found on chromosomes 12, 13, and 16. Chromosomes 7 and 17 each possess four *NbPLCP* genes, and chromosome 3 accommodates six *NbPLCP* genes. Subsequent analyses identified 22 segmental duplication events among 23 *NbPLCP* genes, with the *NbXBCP5/NbTHI3* segmental duplication occurring across two subfamilies, while the remaining 21 segmental duplications occurred within the same subfamily. Notably, no tandem duplications were detected, suggesting that segmental duplications play a pivotal role in the evolution of the *NbPLCP* gene family. Additionally, the selection pressure analysis of the *NbPLCP* genes (Table 2) revealed that the Ka/Ks value for the *NbXBCP5/NbTHI3* gene pair (0.543), although less than 1, is greater than 0.5, indicating strong functional constraints on these genes during evolution, with certain sites undergoing adaptive changes.

3.5 Investigation of co-linear relationships between *N. benthamiana* and other species

In order to enhance our understanding of the evolutionary relationships within the *NbPLCP* gene family, we conducted a comparative analysis. This analysis examined the collinearity of *NbPLCP* genes in *N. benthamiana* with those from three other plant species (see Figure 4). The results indicated that there are 33, 15, and 2 *NbPLCP* genes exhibiting collinearity with the *NbPLCP* genes of tomato, Arabidopsis, and rice, respectively. Among these three species, the number of collinear gene pairs between *N. benthamiana* and each species was found to be 52, 23, and 2, respectively. Notably, the genes *NbRD19A, NbRD21A, NbRDL1, NbSAG12A, NbRDL2, NbCEP1*, and *NbXCP2* in *N. benthamiana* displayed consistent chromosomal positions with their homologous

TABLE 2 Ratios of nonsynonymous (Ka) and synonymous (Ks) of *NbPLCP* gene fragment duplication pairs in *Nicotiana benthamiana*.

Gene pairs	Ka	Ks	Ka/Ks
NbRD19A/NbRD19B	0.014	0.148	0.096
NbRD19A/NbRD19E	0.195	1.659	0.118
NbRD21A/NbRDL1	0.285	3.781	0.075
NbRD21A/NbRDL2	0.312	2.760	0.113
NbRD19B/NbRD19E	0.213	2.023	0.105
NbRDL1/NbRDL2	0.027	0.139	0.193
NbRDL1/NbRD21B	0.337	1.594	0.212
NbRDL1/NbRD21D	0.331	1.613	0.205
NbCTB2/NbCTB3	0.127	0.450	0.281
NbRDL2/NbRD21B	0.334	1.910	0.175
NbRDL2/NbRD21D	0.341	1.774	0.192
NbCEP1/NbCEP2	0.008	0.145	0.057
NbCEP1/NbCEP5	0.086	0.627	0.137
NbCEP2/NbCEP4	0.074	0.640	0.116
NbCEP2/NbCEP5	0.079	0.610	0.130
NbXCP1/NbXCP2	0.011	0.156	0.069
NbXCP1/NbXCP3	0.081	0.770	0.106
NbXBCP3/NbXBCP4	0.020	0.108	0.184
NbXCP2/NbXCP3	0.082	0.663	0.124
NbCEP3/NbCEP6	0.013	0.086	0.154

(Continued)

10.3389/fpls.2025.1565487

TABLE 2 Continued

Gene pairs	Ka	Ks	Ka/Ks
NbCEP4/NbCEP5	0.014	0.118	0.122
NbXBCP5/NbTHI3	0.027	0.049	0.543

genes in tomato, suggesting that these genes have maintained a similar genomic structure throughout evolution. In contrast, within the collinear gene pairs with *Arabidopsis*, only *NbCEP1* exhibited consistent chromosomal positioning with its homologous gene in *Arabidopsis*. The differences in ecological adaptability between *N. benthamiana* and rice reflect the distinct selective pressures they

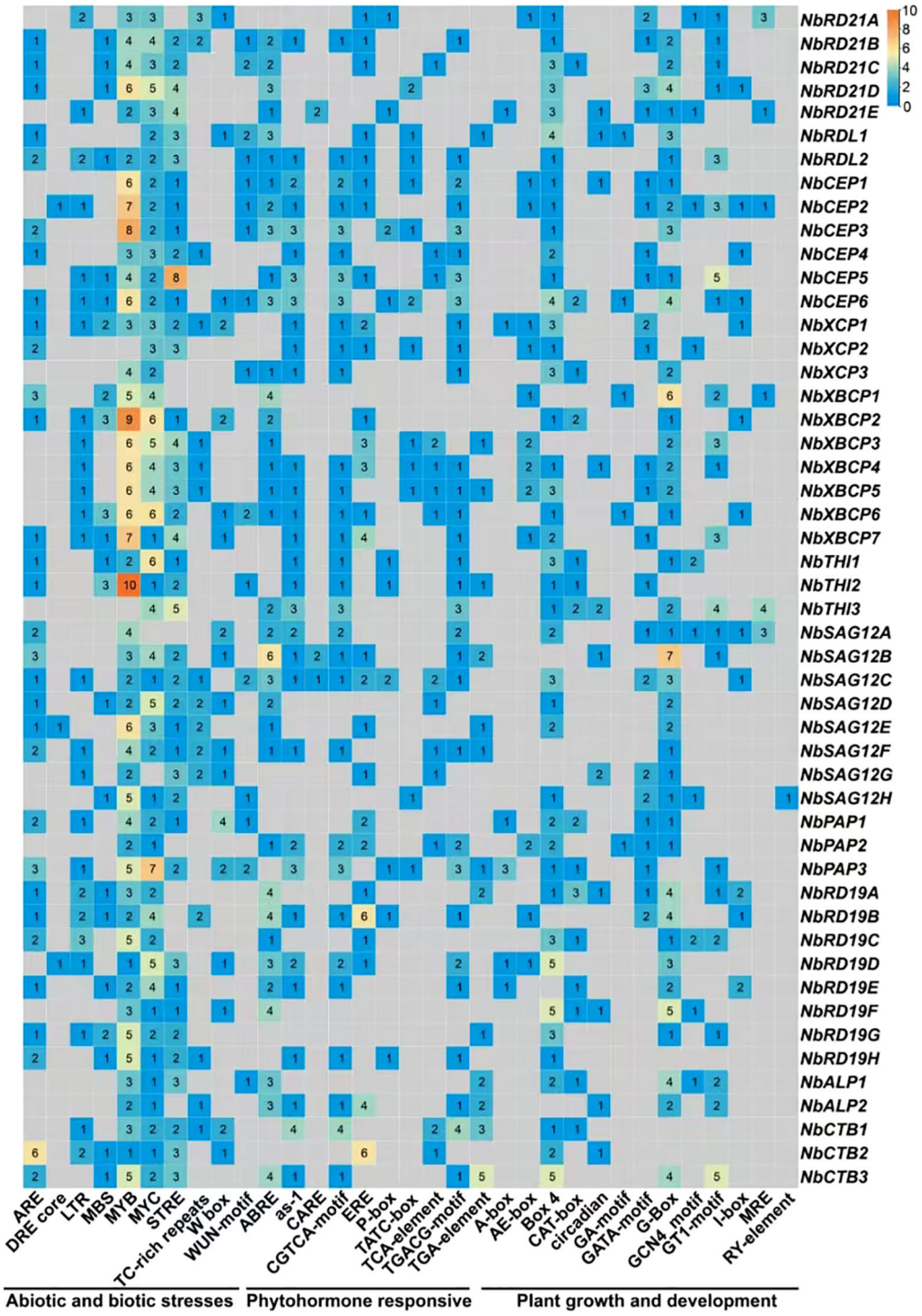

FIGURE 5
Analysis of promoter cis-acting elements in response to light signal, phytohormone, growth and development, and abiotic stress.

have encountered during evolution, leading to diversity in genomic structure and function. The comparative genomic data between *N. benthamiana*, tomato, *Arabidopsis*, and rice reveal significant insights into their evolutionary relationships, gene homology, and functional conservation, providing a foundational understanding of plant genetic diversity and evolutionary history.

3.6 Analysis of promoter cis-acting elements of *NbPLCP* gene

Research into *NbPLCP*'s potential involvement in stress responses necessitates a thorough analysis of the cis-acting elements within the promoter regions of these genes. This study

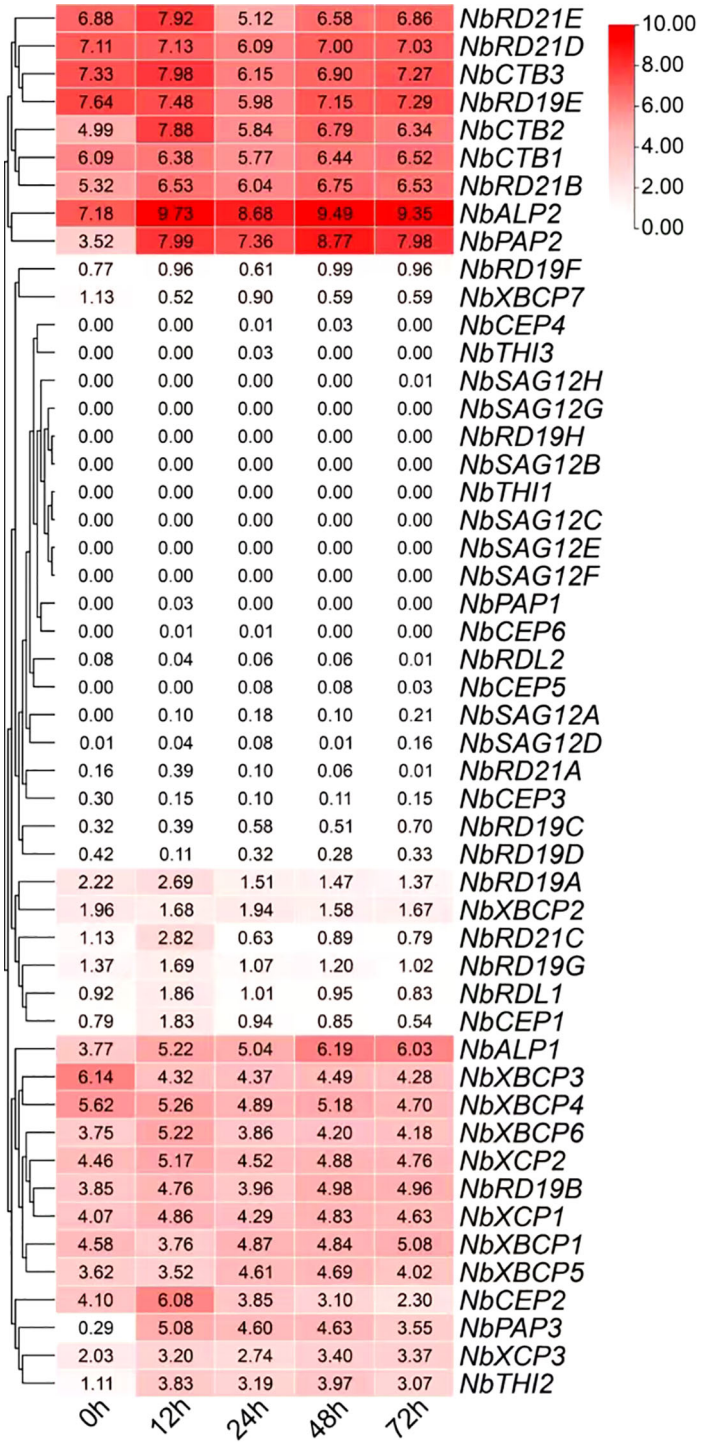

FIGURE 6
Analysis of *NbPLCP* gene expression patterns under viral infection treatment based on RNA-seq data. The legend represents the expression levels of *NbPLCP* genes, ranging from high expression (red) to low expression (white).

aims to uncover various elements associated with abiotic and biotic stresses, plant hormones, and growth and development (Figure 5), offering significant insights into the regulatory mechanisms of *NbPLCP* in response to environmental stimuli. Under abiotic and biotic stresses, genes in the *NbRD21* subfamily display diverse expression patterns under adverse conditions. Notably, *NbRD21D* possesses high binding capacities to promoter elements like DRE and MBS, highlighting its crucial role in drought and salt stresses. By modulating the expression of genes related to stress resistance, members of the *NbRD21* subfamily enhance the plant's adaptability to environmental pressures. *NbCEP2* shows maximum enrichment under cold and salt stresses, indicating its significance in adversity response. Moreover, *NbXCP1*'s high enrichment under oxidative stress suggests its link to plant antioxidative capabilities, potentially enhancing stress resistance through the modulation of relevant signaling pathways. Within the *NbSAG12* subfamily, increased enrichment of *NbSAG12B* on drought and high temperature regulatory elements suggests its key role in plant senescence and stress response. Additionally, changes in the enrichment of adversity cis-acting elements in members of the *NbALP* and *NbCTB* subfamilies also demonstrate their roles in plant growth and stress resistance. Particularly, the cold and saline-alkali stress elements of *NbCTB2* underscore its critical role in plant stress resistance. Finally, variations in multiple adversity elements in members of the *NbRD19* subfamily further emphasize the importance of promoter elements in regulating plant stress responses.

3.7 *NbPLCP* dynamic expression patterns in response to viral infection

To gain a better understanding of the role of the *NbPLCP* protease family in the *N. benthamiana* bioreactor, this study analyzed the dynamic expression patterns of *NbPLCP* in response to viral infection (Figure 6). Most members of this family responded to viral infection at varying degrees across different time points, with diverse time-dependent expression characteristics observed among different genes during the infection process, reflecting their potential roles in plant immune responses. Furthermore, some genes displayed stage-specific expression peaks, such as *NbRD21C*, which significantly increased after 12 hours of infection and then decreased, suggesting that it may have a key regulatory function at specific stages of infection. Similarly, the *NbXCP* and *NbRD19* subfamily genes exhibited coordinated expression changes, indicating that they may be regulated by a common regulatory network, potentially participating in the regulation of the same biological pathway or engaging in crosstalk between different immune signaling pathways. The synchronous expression observed within gene clusters further suggests the involvement of potential regulatory factors and co-regulatory mechanisms in driving their responses. For instance, *NbXCP1*, *NbXCP2*, and *NbXCP3* exhibited similar expression patterns, gradually increasing after infection, peaking at 48 hours, and then slightly declining thereafter. These findings highlight the intricate regulatory networks and diverse functional roles of *NbPLCP* family members in plant immunity.

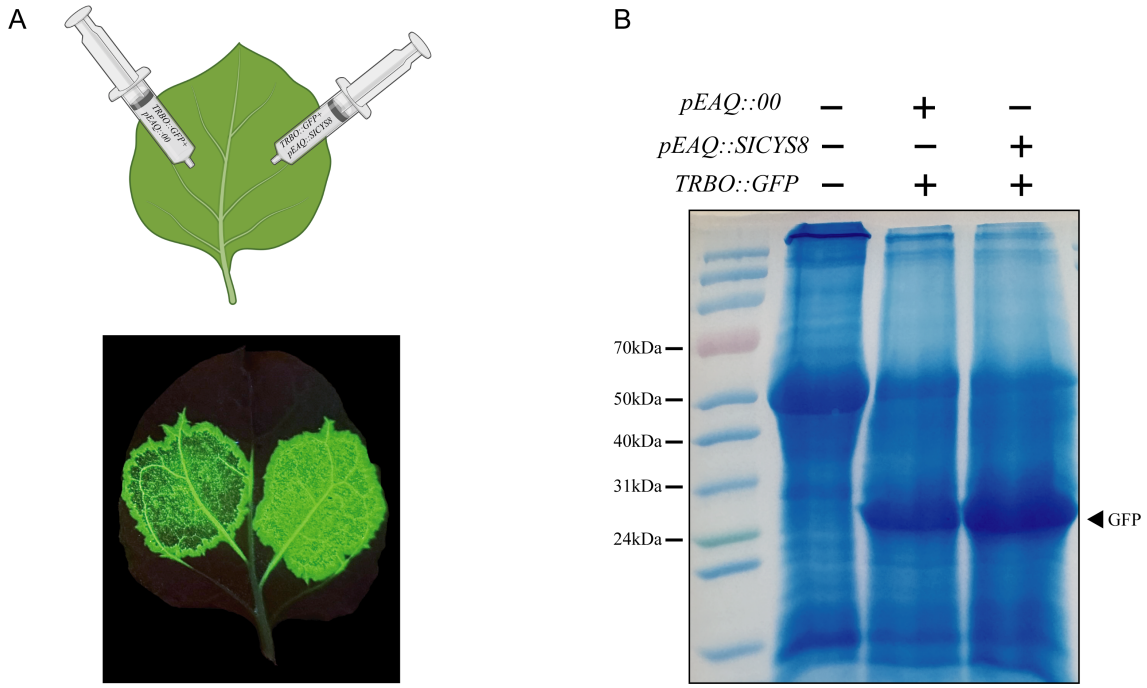

FIGURE 7
(A) Agroinfiltration of *Nicotiana benthamiana* leaves, with 35s::GFP infiltrated on the left side and a 1:1 mixture of 35s::GFP and 35s::SICYS8 infiltrated on the right side. **(B)** Western blot analysis of the samples from panel B, showing the detection results of GFP protein (molecular weight: 27 kDa).

3.8 The protease inhibitor SICYS8 enhances the expression of exogenous GFP protein

Previous studies have shown that the protease inhibitor SICYS8 inhibits the hydrolytic activity of the PLCP protease family, thereby increasing the expression of exogenous proteins in *N. benthamiana*. In this study, we transiently expressed GFP along with SICYS8 in *N. benthamiana* to investigate the impact of the NbPLCP protease inhibitor SICYS8 on the biological response of the *N. benthamiana* bioreactor. From the phenotype, it was observed that the green fluorescence intensity on the right side, where only GFP was expressed, was lower than on the left side, where both SICYS8 and GFP were co-expressed (Figure 7). Western blot analysis revealed that the GFP protein content was significantly higher in the samples co-expressing SICYS8 compared to the control group (Figure 7). This indicates that SICYS8 can enhance the expression of recombinant proteins in *N. benthamiana* by inhibiting the activity of proteinases.

3.9 The effect of PLCP family members on the expression of exogenous GFP in *Nicotiana benthamiana*

As shown in Figure 6, following infection with exogenous viruses, changes in the expression levels of PLCP family members are primarily concentrated in the NbRD21, NbCTB, NbRD19, NbXBCP, and NbCEP subfamilies. Based on the phylogenetic relationships of these subfamily members illustrated in Figure 2, we constructed ten transient silencing vectors: *TRV2::NbRD21BD, TRV2::NbRD21E, TRV2::NbXBCP17, TRV2::NbXBCP345, TRV2::NbXBCP26, TRV2::NbRD19ABC, TRV2::NbRD19E, TRV2::NbCTB13, TRV2::NbCTB2*, and *TRV2::NbXCP123*. Using transient silencing technology, these genes were knocked down. Following the knockdown, the plants were infected with green fluorescent protein (GFP), and the GFP expression level was observed and measured.

The results of the comparison showed that GFP fluorescence intensity in NbXCP123-silenced plants was higher than that in the control plants (Figure 8). As shown in Figure 8, the expression levels of three genes, *NbXCP1*, *NbXCP2*, and *NbXCP3*, were analyzed in Nicotiana benthamiana leaves infected with either GFP or an empty vector control over a three-day period. Compared to the control group, significant changes were observed in the GFP-infected plants after 24 hours. Specifically, the expression of *NbXCP1* and *NbXCP3* increased overall and stabilized after 24 hours, while *NbXCP2* showed an initial increase followed by a decrease. Figure 8 presents the results of a Western blot analysis of GFP expression in NbXCP123-silenced plants and control plants. The results indicate that GFP expression in the NbXCP123-silenced plants was higher than in the control plants. As shown in Figure 8, the three target genes, *NbXCP1*, *NbXCP2*, and *NbXCP3*, were significantly downregulated in NbXCP123-silenced plants compared to the control plants. These results demonstrate that the expression levels of XCP subfamily members in *Nicotiana benthamiana* were indeed altered after the infection with the exogenous GFP protein, showing a marked increase. Moreover, an obvious elevation in GFP expression was observed and detected in the transiently silenced plants.

4 Discussion

The PLCP (Papain-Like Cysteine Protease) family is one of the most abundant cysteine protease families in plants, participating in various life processes, including senescence, pollen development, fruit ripening, and seed germination (Liu et al., 2018). To date, systematic analyses of the PLCP family have been conducted in species such as *Arabidopsis thaliana* (Richau et al., 2012), rice (Nino et al., 2020), chili pepper (Chen et al., 2024), soybean (Yuan et al., 2020), grape (Kang et al., 2021), and papaya (Liu et al., 2018). In this study, we identified 50 members of the PLCP family in the genome of *N. benthamiana*. Phylogenetic analysis classified these genes into nine subfamilies, with members of the same subfamily showing similarities in gene structure and conserved motifs. The differences in amino acid length, molecular weight, isoelectric point, aliphatic amino acid ratio, hydrophobicity index, and chromosomal location of NbPLCP proteins suggest that these variations may be related to the functional diversity of these family members.

Gene structure analysis reveals significant differences in intron and exon compositions among the members of the *N. benthamiana PLCP* gene family. For example, members of the XCP, XBCP, and CEP subfamilies exhibit consistency in the number of exons, reflecting the conservation of these genes in specific biological functions. The lack of conserved motifs in some PLCP family members suggests potential functional diversification within the family, indicating that NbPLCP proteins may play diverse roles in various physiological processes. Members from the same evolutionary branch display highly consistent protein structures, pointing to functional conservation throughout evolution. By integrating conserved motif and gene structure analysis, the reliability of the phylogenetic tree is further validated, providing strong support for functional predictions of family members.

Additionally, 50 members of the *N. benthamiana* PLCP gene family are distributed across 17 chromosomes (Table 1, Figure 3). Among these, 22 pairs of segmental duplication genes were identified, involving 23 *NbPLCP* genes, while no tandem duplication gene pairs were detected. This contrasts with previous studies in other species, where tandem duplication gene pairs were more likely to occur than segmental duplications within the PLCP family members of grapevines (Kang et al., 2021). Similar findings were also observed in papaya (Liu et al., 2018). This suggests that segmental duplication plays a crucial role in the evolution of the *NbPLCP* gene family. Moreover, the Ka/Ks ratio for all gene pairs was less than 1, indicating that these gene pairs have undergone purifying selection to prevent the spread of harmful mutations. Comparative genomics analysis revealed 52 pairs of collinear genes between *N. benthamiana* and tomato, 23 pairs with *Arabidopsis*,

and 2 pairs with rice. These results highlight the significant evolutionary relationship, gene homology, and functional conservation between *N. benthamiana* and these species, providing fundamental insights into plant genetic diversity and evolutionary history.

This study provides an in-depth analysis of the phylogeny, gene structure, and the impact of *PLCP* genes on the expression of exogenous green fluorescent protein (GFP), revealing the importance of *PLCPs* in plant physiological processes and their potential applications in bioreactors. Previous studies have shown that PLCP protease families are common targets for pathogen effectors (Misas-Villamil et al., 2016), such as *XCP2* (Zhang et al., 2014) and *CEP2* (Mueller et al., 2013). The *VvRD21–1* gene plays a significant role in disease resistance in *Vitis vinifera L* (Kang et al., 2021). Similarly, in cotton, the orthologous gene *GhRD21–7* of *NbRD21D* in *N. benthamiana* has been shown to enhance resistance to *Verticillium dahliae* in overexpression plants (Zhang et al., 2019). The results indicate that PLCP family members exhibit significant expression changes during plant development and stress responses. We found that genes such as *NbTHI2* and *NbCEP1* are rapidly activated in the early stages of infection, exhibiting characteristics typical of acute response mechanisms, suggesting their involvement in the initiation of defense responses and signal transduction during the early stages of viral invasion. In contrast, genes such as *NbRD21D* and *NbALP2*

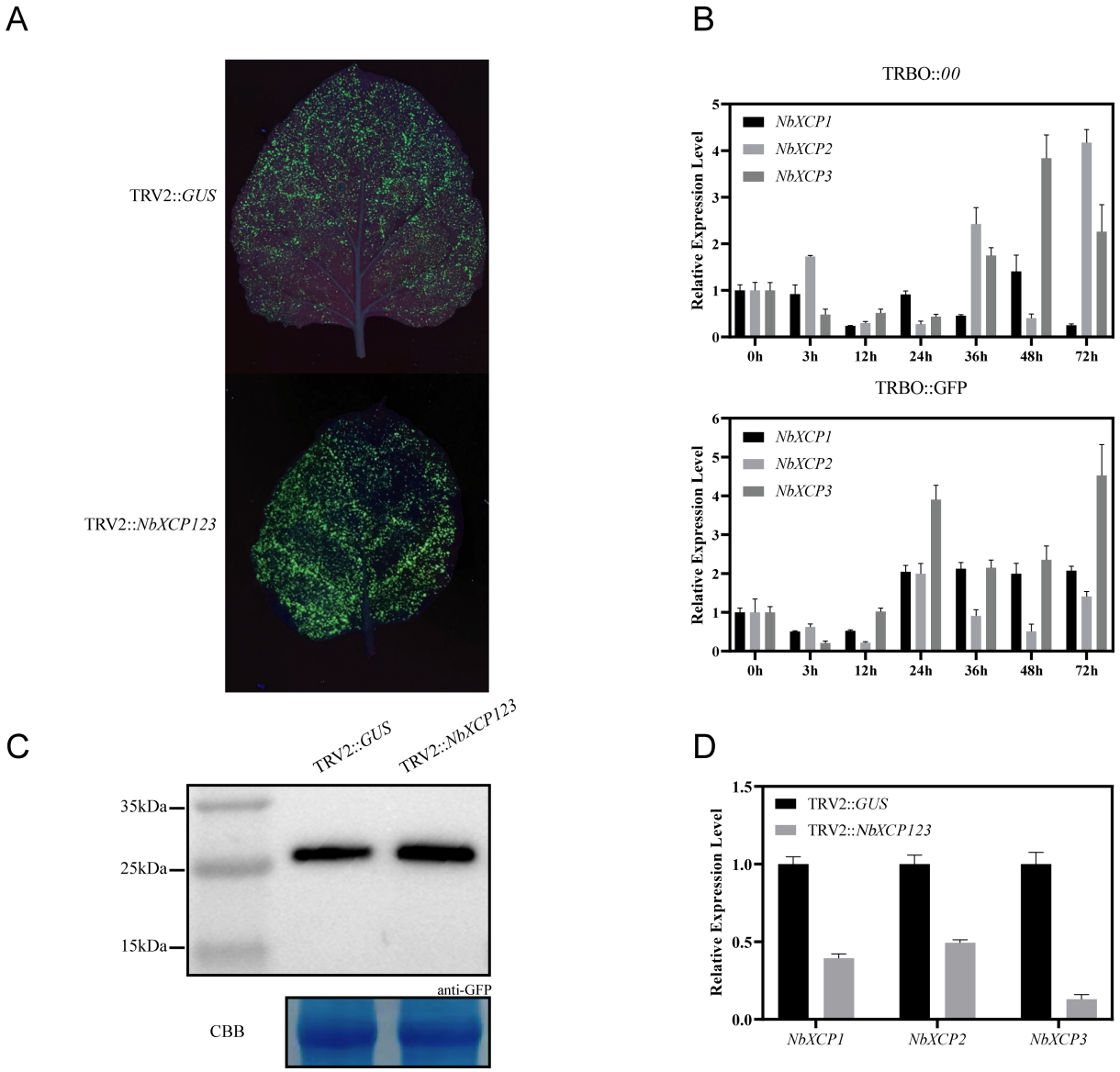

FIGURE 8
(A) Phenotypic comparison of *TRBO::GFP* infection in control plants and NbXCP123-silenced plants. **(B)** The expression levels of *NbXCP1*, *NbXCP2*, and *NbXCP3* in *Nicotiana benthamiana* infected with *TRBO::00* and *TRBO::GFP* were analyzed at 0 h, 3 h, 12 h, 24 h, 36 h, 48 h, and 72 (h) **(C)** Western blot analysis of GFP expression in control plants and NbXCP123-silenced plants. **(D)** Expression levels of *NbXCP1, NbXCP2*, and *NbXCP3* in control plants and NbXCP123-silenced plants.

maintain high expression levels throughout the infection process, suggesting they may play broader regulatory roles at multiple stages of the immune response. These findings suggest that silencing, knockout, or mutation of PLCP family members in plants makes them more susceptible to pathogen infection.

Through functional analysis of *PLCP* family members, we found that specific *PLCP* inhibitors (such as SICYS8) can significantly enhance the expression of exogenous GFP, indicating that the interference with endogenous proteases is a key factor affecting their accumulation. In the experiments, the GFP expression in plants with NbXCP123 silencing was significantly higher than in the control group, further validating the potential role of PLCPs in regulating exogenous protein expression. This finding provides a new strategy for optimizing N. benthamiana as a bioreactor, where the silencing or knockout of the genes *NbXCP1*, *NbXCP2*, and *NbXCP3* can potentially enhance the yield of vaccines and therapeutic proteins. Furthermore, the phylogenetic and gene structure analysis of the PLCP family lays the foundation for understanding its functional diversity. Although some PLCP members have been studied previously, this research fills the gap in phylogenetic analysis, revealing the conservation and specificity of PLCPs in different plant species. This work paves the way for future comparative functional studies of PLCPs in multiple plant species.

5 Conclusion

In summary, this study identified 50 members of the NbPLCP protease family through genome-wide analysis. The functional roles of the PLCP family in *N. benthamiana* and their importance in exogenous protein expression were thoroughly investigated, highlighting the potential of PLCP in plant physiology and biotechnological applications. Future research should further explore the regulatory mechanisms of PLCP and how these mechanisms can be leveraged to improve plant stress resistance and the efficiency of exogenous protein expression, thereby advancing the application of plant-based bioreactors.

Data availability statement

The datasets presented in this study can be found in online repositories. The names of the repository/repositories and accession number(s) can be found in the article/Supplementary Material.

Author contributions

YLY: Data curation, Formal Analysis, Writing – original draft, Writing – review & editing. ZD: Data curation, Writing – original draft. ZZ: Visualization, Writing – review & editing. YY: Funding acquisition, Writing – review & editing. XP: Data curation, Methodology, Writing – review & editing. RW: Investigation, Writing – review & editing. TL: Validation, Writing – review & editing. XG: Investigation, Writing – review & editing. LL: Data curation, Writing – original draft. YG: Data curation, Writing – original draft, Writing – review & editing.

Funding

The author(s) declare that financial support was received for the research and/or publication of this article. This work was supported by funds from the National Natural Science Foundation of China (No.32370374 and 32270332) and China National Tobacco Corporation Guizhou Branch Science and Technology Program Project (201911).

Conflict of interest

The authors declare that the research was conducted in the absence of any commercial or financial relationships that could be construed as a potential conflict of interest.

The authors declare that this study received funding from China National Tobacco Corporation Guizhou Branch Science and Technology Program Project. The funder was not involved in the study design, collection, analysis, interpretation of data, the writing of this article or the decision to submit it for publication.

Generative AI statement

The author(s) declare that no Generative AI was used in the creation of this manuscript.

Publisher's note

Supplementary material

The Supplementary Material for this article can be found online at: https://www.frontiersin.org/articles/10.3389/fpls.2025.1565487/full#supplementary-material

References

Bailey, T. L., Johnson, J., Grant, C. E., and Noble, W. S. (2015).). The meme suite. *Nucleic Acids Res.* 43, W39–W49. doi: 10.1093/nar/gkv416

Bally, J., Jung, H., Mortimer, C., Naim, F., Philips, J. G., Hellens, R., et al. (2018). The rise and rise of Nicotiana Benthamiana: a plant for all reasons. *Annu. Rev. Phytopathol.* 56, 405–426. doi: 10.1146/annurev-phyto-080417-050141

Cen, Y., Singh, W., Arkin, M., Moody, T. S., Huang, M., Zhou, J., et al. (2019). Artificial cysteine-lipases with high activity and altered catalytic mechanism created by laboratory evolution. *Nat. Commun.* 10, 3198. doi: 10.1038/s41467-019-11155-3

Chen, C., Chen, H., Zhang, Y., Thomas, H. R., Frank, M. H., He, Y., et al. (2020). Tbtools: an integrative toolkit developed for interactive analyses of big biological data. *Mol. Plant* 13, 1194–1202. doi: 10.1016/j.molp.2020.06.009

Chen, R., Wang, B., Huang, S., Chen, X., Tan, J., Zhang, H., et al. (2024). Genome-wide identification and male sterility-related expression analysis of papain - like cysteine protease gene family in capsicum annuum. *Horticulturae* 10, 892. doi: 10.3390/horticulturae10080892

Deng, J., Zhu, F., Liu, J., Zhao, Y., Wen, J., Wang, T., et al. (2019). Transcription factor bhlh2 represses cysteine protease77 to negatively regulate nodule senescence. *Plant Physiol.* 181, 1683–1703. doi: 10.1104/pp.19.00574

Douglas, A. E. (2018). Strategies for enhanced crop resistance to insect pests. *Annu. Rev. Plant Biol.* 69, 637–660. doi: 10.1146/annurev-arplant-042817-040248

Finn, R. D., Bateman, A., Clements, J., Coggill, P., Eberhardt, R. Y., Eddy, S. R., et al. (2014). Pfam: the protein families database. *Nucleic Acids Res.* 42, D222–D230. doi: 10.1093/nar/gkt1223

Gasteiger, E., Gattiker, A., Hoogland, C., Ivanyi, I., Appel, R. D., and Bairoch, A. (2003). Expasy: the proteomics server for in-depth protein knowledge and analysis. *Nucleic Acids Res.* 31, 3784–3788. doi: 10.1093/nar/gkg563

Grosse-Holz, F., Madeira, L., Zahid, M. A., Songer, M., Kourelis, J., Fesenko, M., et al. (2018). Three unrelated protease inhibitors enhance accumulation of pharmaceutical recombinant proteins in Nicotiana Benthamiana. *Plant Biotechnol. J.* 16, 1797–1810. doi: 10.1111/pbi.12916

Guo, Y., and Gan, S. S. (2014). Translational researches on leaf senescence for enhancing plant productivity and quality. *J. Exp. Bot.* 65, 3901–3913. doi: 10.1093/jxb/eru248

Jutras, P. V., Dodds, I., and van der Hoorn, R. A. (2020). Proteases of Nicotiana Benthamiana: an emerging battle for molecular farming. *Curr. Opin. Biotechnol.* 61, 60–65. doi: 10.1016/j.copbio.2019.10.006

Jutras, P. V., Grosse-Holz, F., Kaschani, F., Kaiser, M., Michaud, D., and van der Hoorn, R. (2019). Activity-based proteomics reveals nine target proteases for the recombinant protein-stabilizing inhibitor slcys8 in Nicotiana Benthamiana. *Plant Biotechnol. J.* 17, 1670–1678. doi: 10.1111/pbi.13092

Kang, J., Gong, P., Ge, M., Sadeghnezhad, E., Liu, Z., Zhang, M., et al. (2021). The plcp gene family of grapevine (vitis vinifera l.): Characterization and differential expression in response to plasmopara viticola. *BMC Plant Biol.* 21, 499. doi: 10.1186/s12870-021-03279-w

Konno, K., Hirayama, C., Nakamura, M., Tateishi, K., Tamura, Y., Hattori, M., et al. (2004). Papain protects papaya trees from herbivorous insects: role of cysteine proteases in latex. *Plant J.* 37, 370–378. doi: 10.1046/j.1365-313x.2003.01968.x

Kordis, D., and Turk, V. (2009). Phylogenomic analysis of the cystatin superfamily in eukaryotes and prokaryotes. *BMC Evol. Biol.* 9, 266. doi: 10.1186/1471-2148-9-266

Kumar, S., Stecher, G., Li, M., Knyaz, C., and Tamura, K. (2018). Mega x: molecular evolutionary genetics analysis across computing platforms. *Mol. Biol. Evol.* 35, 1547–1549. doi: 10.1093/molbev/msy096

Lescot, M., Dhais, P., Thijs, G., Marchal, K., Moreau, Y., Van de Peer, Y., et al. (2002). Plantcare, a database of plant cis-acting regulatory elements and a portal to tools for in silico analysis of promoter sequences. *Nucleic Acids Res.* 30, 325–327. doi: 10.1093/nar/30.1.325

Li, C., Li, S., Feng, L., Cheng, J., Xie, J., Lin, Y., et al. (2025). Arabidopsis otu2 deubiquitinates cysteine protease rd21a to enhance clubroot resistance. *Plant J.* 122, e70148. doi: 10.1111/tpj.70148

Lin, E., Burns, D. J., and Gardner, R. C. (1993). Fruit developmental regulation of the kiwifruit actinidin promoter is conserved in transgenic petunia plants. *Plant Mol. Biol.* 23, 489–499. doi: 10.1007/BF00019297

Liu, J., Sharma, A., Niewiara, M. J., Singh, R., Ming, R., and Yu, Q. (2018). Papain-like cysteine proteases in carica papaya: lineage-specific gene duplication and expansion. *BMC Genomics* 19, 26. doi: 10.1186/s12864-017-4394-y

Liu, H., Hu, M., Wang, Q., Cheng, L., and Zhang, Z. (2018). Role of papain-like cysteine proteases in plant development. *Front. Plant Sci.* 9, 1717. doi: 10.3389/fpls.2018.01717

Lohman, K. N., GAN, S. S., John, M. C., and Amasino, R. M. (1994). Molecular analysis of natural leaf senescence in arabidopsis thaliana. *Physiol. Plant* 92, 322–328. doi: 10.1111/j.1399-3054.1994.tb05343.x

Long, L., Meng, X., Yu, X., Wang, S., Wang, J., and Yang, M. (2025). Genome-wide identification of the papaya-like cysteine protease family in poplar and determination of the functional role of perd19a in conferring salt tolerance. *Int. J. Biol. Macromol* 294, 139361. doi: 10.1016/j.ijbiomac.2024.139361

Martinez, M., Cambra, I., Carrillo, L., Diaz-Mendoza, M., and Diaz, I. (2009). Characterization of the entire cystatin gene family in barley and their target cathepsin l-like cysteine-proteases, partners in the hordein mobilization during seed germination. *Plant Physiol.* 151, 1531–1545. doi: 10.1104/pp.109.146019

Misas-Villamil, J. C., van der Hoorn, R. A., and Doehlemann, G. (2016). Papain-like cysteine proteases as hubs in plant immunity. *New Phytol.* 212, 902–907. doi: 10.1111/nph.14117

Mueller, A. N., Ziemann, S., Treitschke, S., Assmann, D., and Doehlemann, G. (2013). Compatibility in the ustilago maydis-maize interaction requires inhibition of host cysteine proteases by the fungal effector pit2. *PloS Pathog.* 9, e1003177. doi: 10.1371/journal.ppat.1003177

Nino, M. C., Kang, K. K., and Cho, Y. G. (2020). Genome-wide transcriptional response of papain-like cysteine protease-mediated resistance against xanthomonas oryzae pv. Oryzae in rice. *Plant Cell Rep.* 39, 457–472. doi: 10.1007/s00299-019-02502-1

Pierre, O., Hopkins, J., Combier, M., Baldacci, F., Engler, G., Brouquisse, R., et al. (2014). Involvement of papain and legumain proteinase in the senescence process of medicago truncatula nodules. *New Phytol.* 202, 849–863. doi: 10.1111/nph.12717

Rao, X., Huang, X., Zhou, Z., and Lin, X. (2013). An improvement of the 2^(-delta delta ct) method for quantitative real-time polymerase chain reaction data analysis. *Biostat Bioinforma Biomath* 3, 71–85.

Rawlings, N. D., Barrett, A. J., and Finn, R. (2016). Twenty years of the merops database of proteolytic enzymes, their substrates and inhibitors. *Nucleic Acids Res.* 44, D343–D350. doi: 10.1093/nar/gkv1118

Richau, K. H., Kaschani, F., Verdoes, M., Pansuriya, T. C., Niessen, S., Stuber, K., et al. (2012). Subclassification and biochemical analysis of plant papain-like cysteine proteases displays subfamily-specific characteristics. *Plant Physiol.* 158, 1583–1599. doi: 10.1104/pp.112.194001

Sainsbury, F., Varennes-Jutras, P., Goulet, M., D'Aoust, M., and Michaud, D. (2013). Tomato cystatin sl cys8 as a stabilizing fusion partner for human serpin expression in plants. *Plant Biotechnol. J.* 11, 1058–1068. doi: 10.1111/pbi.12098

Schultz, J., Milpetz, F., Bork, P., and Ponting, C. P. (1998). Smart, a simple modular architecture research tool: identification of signaling domains. *Proc. Natl. Acad. Sci. U.S.A.* 95, 5857–5864. doi: 10.1073/pnas.95.11.5857

van Wyk, S. G., Du Plessis, M., Cullis, C. A., Kunert, K. J., and Vorster, B. J. (2014). Cysteine protease and cystatin expression and activity during soybean nodule development and senescence. *BMC Plant Biol.* 14, 294. doi: 10.1186/s12870-014-0294-3

Wang, Y., Tang, H., DeBarry, J. D., Tan, X., Li, J., Wang, X., et al. (2012). Mcscanx: a toolkit for detection and evolutionary analysis of gene synteny and collinearity. *Nucleic Acids Res.* 40, e49. doi: 10.1093/nar/gkr1293

Yuan, S., Ke, D., Li, R., Li, X., Wang, L., Chen, H., et al. (2020). Genome-wide survey of soybean papain-like cysteine proteases and their expression analysis in root nodule symbiosis. *BMC Plant Biol.* 20, 517. doi: 10.1186/s12870-020-02725-5

Zhang, Z. (2022). Kaks_calculator 3.0: calculating selective pressure on coding and non-coding sequences. *Genomics Proteomics Bioinf.* 20, 536–540. doi: 10.1016/j.gpb.2021.12.002

Zhang, C., Chen, Y., Wang, L., Liu, L., Zhong, X., Chu, P., et al. (2023). Genome-wide identification of papain-like cysteine protease family genes in cultivated peanut (arachis hypogaea l.) And functional characterization of ahrd21b in response to chilling stress. *Environ. Exp. Bot.* 209, 105272. doi: 10.1016/j.envexpbot.2023.105272

Zhang, B., Tremousaygue, D., Denance, N., van Esse, H. P., Horger, A. C., Dabos, P., et al. (2014). Pirin2 stabilizes cysteine protease xcp2 and increases susceptibility to the vascular pathogen ralstonia solanacearum in arabidopsis. *Plant J.* 79, 1009–1019. doi: 10.1111/tpj.12602

Zhang, S., Xu, Z., Sun, H., Sun, L., Shaban, M., Yang, X., et al. (2019). Genome-wide identification of papain-like cysteine proteases in gossypium hirsutum and functional characterization in response to verticillium dahliae. *Front. Plant Sci.* 10. doi: 10.3389/fpls.2019.00134

frontiers | Frontiers in Plant Science

TYPE Brief Research Report
PUBLISHED 11 July 2025
DOI 10.3389/fpls.2025.1605548

OPEN ACCESS

EDITED BY
Kevin Yueju Wang,
University of Pikeville, United States

REVIEWED BY
Lilya Kopertekh,
Julius Kühn-Institut, Germany
Md. Rezaul Islam Khan,
Michigan Technological University, United States

*CORRESPONDENCE
Christian Sievert
csievert@elevabiologics.com

RECEIVED 03 April 2025
ACCEPTED 05 June 2025
PUBLISHED 11 July 2025

CITATION
Jonner J, Fode B, Koch J, Boller S, Dabrowska-Schlepp P, Schaaf A and Sievert C (2025) Engineering the moss *Physcomitrium patens* to produce proteins with paucimannosidic glycans.
Front. Plant Sci. 16:1605548.
doi: 10.3389/fpls.2025.1605548

Engineering the moss *Physcomitrium patens* to produce proteins with paucimannosidic glycans

Jessica Jonner, Benjamin Fode, Jonas Koch, Sören Boller, Paulina Dabrowska-Schlepp, Andreas Schaaf and Christian Sievert*

Eleva GmbH, Freiburg, Germany

The moss *Physcomitrium patens* is an advantageous host for the production of biopharmaceutical proteins, particularly due to the ease of glyco-engineering. However, the ability to produce proteins with paucimannosidic (MM) glycans in this species currently depends solely on the nature of the product. MM glycans offer benefits for some therapeutic proteins by facilitating their import into target cells via a presumed mannose receptor. Here, we describe the use of *Spodoptera frugiperda* enzymes expressed in moss to produce recombinant human lysosomal acid α-glucosidase with mainly MM glycans. We tested the expression of mannosidase type III and a hexosaminidase by varying the promoter strength and protein localization. The parental line produced recombinant α-glucosidase with no detectable MM glycans at all, whereas the weak expression of mannosidase type III targeted to the medial Golgi produced 4% MM glycans. The strong expression of a hexosaminidase targeted to the extracellular space increased the MM glycan content to 43.5%. Unlike previous attempts to express proteins with MM glycans in plants, neither of our introduced modifications interfered with growth or recombinant protein production. Our data confirm that the finely tuned expression and cellular localization of the glycosylation machinery can improve the efficiency of glyco-engineering. We also exploit the assembly of DNA fragments *in vivo*, which overcomes the limitations of traditional knock-in methods and facilitates the screening of different genetic elements. Our combined methods therefore represent the first straightforward approach allowing the production of recombinant proteins with abundant MM glycans.

KEYWORDS

paucimannosidic glycans, glyco-engineering, lysosomal acid α-glucosidase, *Physcomitrium patens*, hexosaminidase

Introduction

The moss *Physcomitrium* (*Physcomitrella*) *patens* has unique advantages as a host for the production of biopharmaceuticals, including its amenity for glyco-engineering (Decker and Reski, 2020). The glycan profile of a therapeutic protein can influence its stability and functionality and is therefore a critical quality attribute in biopharmaceutical manufacturing (Strasser, 2023). Although glycosylation patterns tend to be more homogenous and stable in moss compared to other platforms, the specific glycan profile depends on the host strain and the product. For example, moss-derived human α-galactosidase A (Repleva AGAL, RPV-001), which has completed phase I clinical trials (Hennermann et al., 2019), features 57% paucimannosidic (MM) *N*-linked glycans (Shen et al., 2016). This facilitates the uptake of the drug by target cells, presumably via a yet unknown mannose receptor. In contrast, human lysosomal acid α-glucosidase (Repleva GAA, RPV-002) produced in the same host features mainly *N*-linked glycans terminating with *N*-acetylglucosamine (GlcNAc), giving the typical GnGn profile of most proteins expressed in moss (Hintze et al., 2020). It would be beneficial to develop engineered moss strains that produce GAA and other proteins with MM glycans to improve their uptake into target cells.

The GnGn profile generally found on moss proteins results from a stereotypical series of reactions in which the core Man_8 structure is pared back to Man_5 by mannosidase I (ManI), followed by the transfer of a GlcNAc residue by *N*-acetylglucosaminyltransferase I (GnT-I), the cleavage of two terminal mannose residues by ManII (yielding GnM), and a further transfer of GlcNAc by GnT-II (Supplementary Figure S1). Proteins such as AGAL that naturally display MM glycans in moss are presumed to have structures with a higher affinity for (and/or longer colocalization with) endogenous hexosaminidases, which cleave off terminal GlcNAc residues, potentially in addition to a lower affinity for GnT-II. In contrast, invertebrates such as the armyworm moth *Spodoptera frugiperda* are known for their dominant MM glycans (Shi and Jarvis, 2007), reflecting the presence of a unique ManIII that can cleave terminal mannose residues from Man_5 before GnT-I has attached GlcNAc, and is thus able to create MM glycans directly (Kawar et al., 2001). GlcNAc residues, which form due to competition for the substrate by GnT-I, can be cleaved by several hexosaminidases. These include the unique *fdl* gene product, which is found only in insects and specifically cleaves α3-branch GlcNAc residues, as well as broad-spectrum hexosaminidases involved in *N*-glycan and chitin degradation, which act on both GlcNAc branches (Geisler et al., 2008).

In an effort to increase the proportion of MM glycans in moss, we exploited the expression of ManIII to trim oligomannose structures, and hexosaminidase to remove unwanted GlcNAc residues. We found that the expression level and localization of both enzymes was a key determinant of efficiency, and that the fine tuning of expression was necessary to optimize the MM glycan content.

Materials and methods

Plant material and cultivation

All strains used in this study were glyco-engineered descendants of *Physcomitrium patens* (Hedw.) Mitt. ecotype "Gransden 2004" expressing recombinant human GAA and were cultivated on standard moss medium. Detailed strain description and cultivation conditions can be found in Text S1.

Cell line engineering

Transgenes were synthesized and transferred into our standard expression vector or assembled *in vivo*. Moss protoplasts were transformed via PEG-based method. Stably transformed moss clones were genotyped by PCR and transgene expression was quantified by real-time RT-PCR (qRT-PCR). Glycan profile was evaluated in 180-mL shake-flask cultures by high-performance liquid chromatography electrospray ionization mass spectrometry (HPLC-ESI-MS) analyses of in-gel digested GAA samples after sodium dodecylsulfate polyacrylamide electrophoresis (SDS-PAGE) separation of secreted proteins. For gel loading, GAA was quantified using an enzyme assay (Hintze et al., 2020). Additional details are included in Text S1.

Protein production and glycan analysis

We used 1-L cultures in a stirred-tank bioreactor to represent production conditions as previously described (Hintze et al., 2020). Moss culture, GAA enzyme activity assays to determine clonal productivity, SDS-PAGE under reducing conditions, column purification, and the analysis of *N*-glycans by hydrophilic interaction liquid chromatography (HILIC) were carried out as previously described (Hintze et al., 2020). Purified GAA was quantified by size-exclusion high-performance liquid chromatography (SE-HPLC). Briefly, GAA was loaded onto a Yarra SEC-3000 column in a 25 mM sodium phosphate running buffer (pH 6.5) with 100 mM NaCl. For isocratic elution, we applied a flow rate of 0.75 mL/min for 30 min. For quantification, the peak area was analyzed using freely available GAA (Myozyme) as a reference.

Results

We expressed *S. frugiperda* ManIII in the high-performance GAA-producing moss line Pp_P_GAA-1#007, which has been modified to eliminate the *xylT* and *fucT* gene products needed for the synthesis of plant-specific α-1,3-fucose and β-1,2-xylose residues (Koprivova et al., 2004) as well as GnT-I, thus yielding high-mannose *N*-linked glycans mainly with the structure Man_5 (Figure 1A). We expressed ManIII under the control of the strong

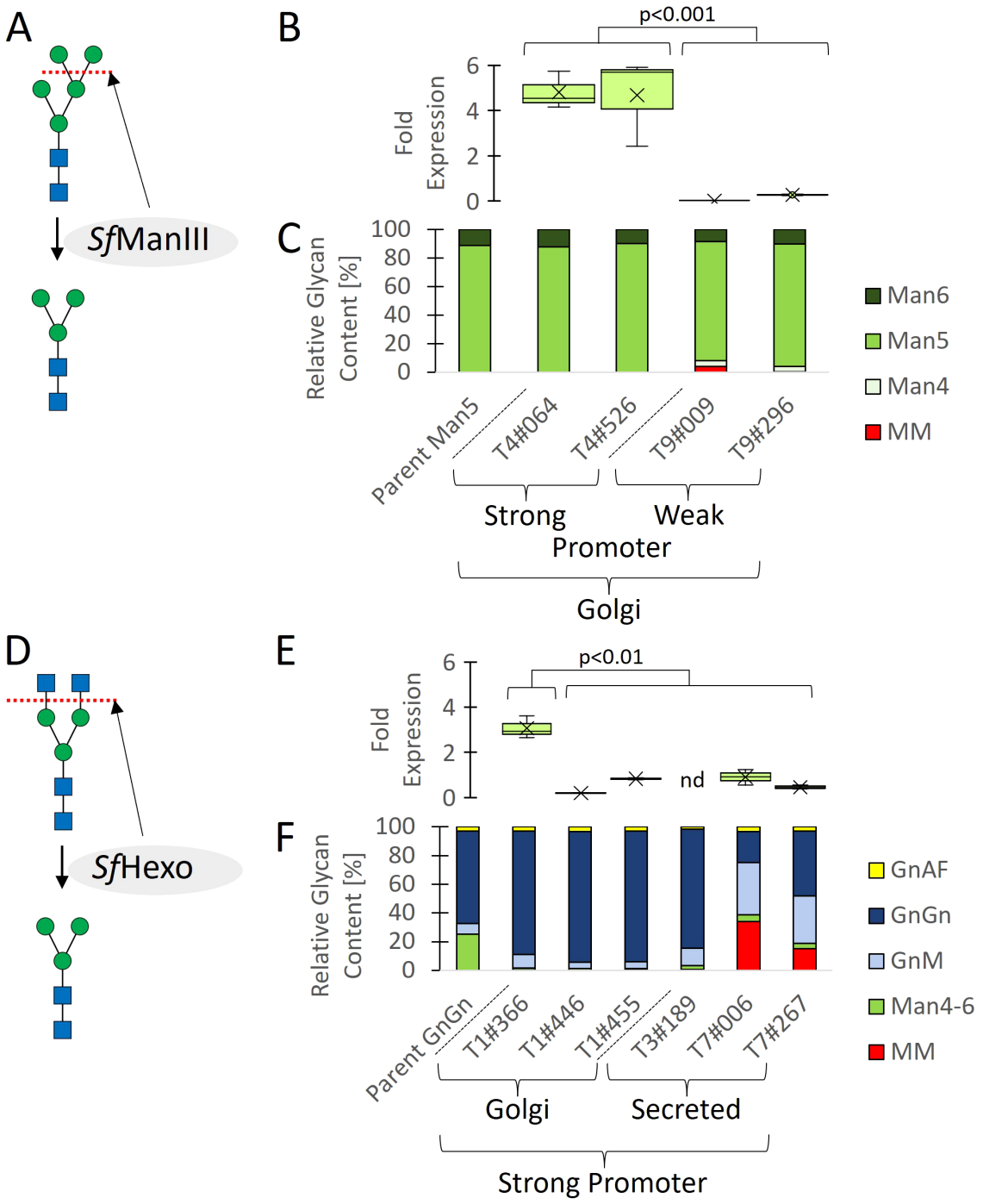

FIGURE 1
Cell line engineering, screening, and glycan profiling. Two parental lines expressing GAA with mainly GnGn (Pp_P_GAA-1#001) or Man_5 (Pp_P_GAA-1#007) glycans were glyco-engineered to favor MM glycans by expressing *Sf*ManIII or *Sf*Hexo under the control of strong or weak promoters, and with targeting to early or late Golgi vessels using a transmembrane domain, or without a domain fusion for secretion. **(A)** *Sf*ManIII was used to cleave Man residues from Man_5 glycans. **(B)** Transcript levels. **(C)** Proportions of different glycans. **(D)** *Sf*Hexo was used to cleave GlcNAc residues from GnGn glycans. **(E)** Transcript levels. **(F)** Proportions of different glycans. Transcript levels are shown as boxplots and are reported as $2^{-\Delta C_T}$ values (Schmittgen and Livak, 2008) representing the relative fold change related to endogenous *actin* mRNA (n = 4 including two technical and two biological replicates, nd = not detected; significance of difference between high and low transgene expression determined using a Mann–Whitney U-test; Text S1). Glycan proportions in **(C, F)** were determined by HPLC-ESI-MS for the quantification of glycosylated peptides.

endogenous moss *actin* promoter and fused it to the transmembrane domain of endogenous moss ManII for localization to the Golgi, where its substrate is found (Figures 2, S1). Having verified transgene integration and transcription (Supplementary Figures S3, 1B), we screened for MM glycans in GAA recovered from the supernatant of shake-flask cultures following protein separation by SDS-PAGE. However, HPLC-ESI-MS analysis did not detect any MM glycans (Figure 1C).

Overloading the protein secretion machinery can be detrimental (Torres et al., 2022), so we expressed the ManIII under the control of the weaker *fucT* promoter by using homologous recombination to create a single-copy knock-in strain at the disrupted *fucT* locus. To provide an expression cassette for the genetic transformation of moss cells, we delivered small PCR fragments, representing the required genetic elements and coding sequences (Supplementary Figure S2), into the cells and used the *in vivo* assembly capabilities of moss for stable genetic transformation. With this approach, we achieved a knock-in success rate of 15.8% (Supplementary Figure S4). Transcript analysis confirmed that the *SfManIII* transgene was expressed at a lower level when driven by the *fucT* promoter, verifying the knock-in strategy (Figure 1B). HPLC-ESI-MS analysis revealed the presence of a small quantity of MM glycans in clones T9#009 (4%) and T9#296 (0.1%), relative to the sum of all identified and glycosylated GAA peptides (Figure 1C).

We previously generated Repleva GAA with MM glycans by using the bacterial hexosaminidase β-*N*-acetylglucosaminidase S from *Streptomyces plicatus* (*Sp*Hexo) for the modification of purified GAA *in vitro* (Hintze et al., 2020). However, when we expressed *Sp*Hexo in the high-performance GAA-producing moss line Pp_P_GAA-1#001, which has been modified to eliminate the *xylT* and *fucT* genes (Koprivova et al., 2004) but retains GnT-I and therefore synthesizes mainly GnGn glycans (Figure 1D), we were unable to detect *Sp*Hexo transcription in any transgenic lines after several attempts to achieve stable transgene integration (data not shown). This suggests the product is toxic (Text S3). The addition of a signal peptide targeting the protein for secretion to avoid interference with Golgi-resident host proteins did not resolve this issue. We therefore expressed the broad-spectrum *S. frugiperda* hexosaminidase (*Sf*Hexo) in the same parent strain, this time fusing the protein to the transmembrane domain of FucT and following the same expression strategy as described above for *Sf*ManIII. We used the strong *actin* promoter for *Sf*Hexo and obtained clones with varying expression levels during screening (Figures 1E, S5), but again detected no MM glycans by HPLC-ESI-MS (Figure 1F). Localization within the late Golgi may prevent enzyme processing for activation or limit the colocalization of *Sf*Hexo with its substrate, so we expressed a soluble *Sf*Hexo without a transmembrane domain instead. This finally yielded two clones with 34.1% (T7#006) and 15.2% (T7#267) MM glycans, respectively (Figure 1F).

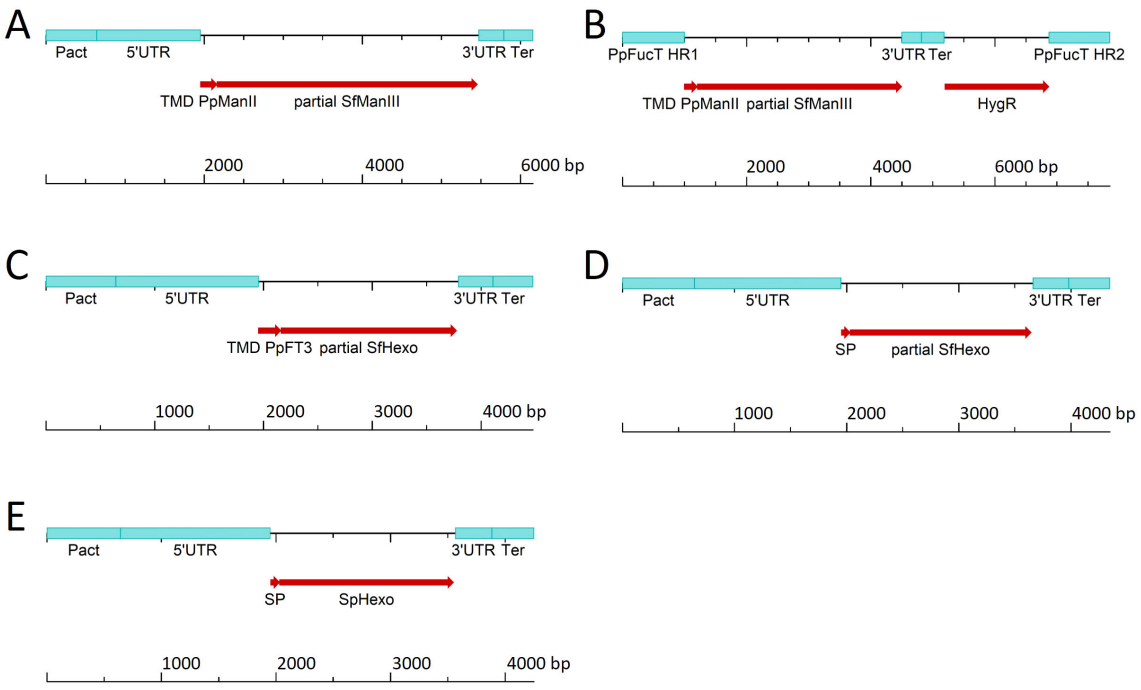

FIGURE 2
Linear DNA constructs used to express *Sf*ManIII under the control of **(A)** the strong *actin* promoter (P*act*) or **(B)** the weak fucosyltransferase promoter (*fucT*) and to target the *Sf*ManIII product to the *cis*-Golgi, to target *Sf*Hexo to **(C)** the *trans*-Golgi or **(D)** for secretion, and **(E)** to target *Sp*Hexo for secretion. All major elements are specified in Supplementary Table S1. HygR, hygromycin-resistance cassette; SP, signal peptide; Ter, terminator; TMD, transmembrane domain; UTR, untranslated region.

To quantify the portion of MM glycans in a production setting, we repeated the cultivation in a stirred-tank bioreactor using the best-performing strain (T7#006) along with the parent strain. During a 14-day cultivation experiment, both strains showed comparable morphology, growth and GAA production (Figures 3A-C). We extensively purified the GAA (Figure 4A, Text S2) to enable product-specific quantification of the cleaved glycans by HILIC, confirming that the GAA features up to 43.5% MM glycans (including methylated derivatives) and the GnGn content fell from 61.5% in the parental strain to 15.2% in the engineered line (Figures 4B, C).

Discussion

Glycosylated therapeutic proteins usually feature complex glycans terminated with GlcNAc or sialic acid residues (Kim et al., 2009; Shin et al., 2017). However, paucimannosidic (MM) *N*-glycans facilitate the uptake of proteins via mannose receptors, as shown for AGAL (Shen et al., 2016) and potentially for other lysosomal storage disease-associated proteins such as GAA (Platt et al., 2018). Recombinant proteins with MM glycans can be produced by cleaving off GlcNAc residues *in vitro* using a bacterial hexosaminidase, but this adds a process-related impurity that must be removed in a subsequent step, increasing costs (Hintze et al., 2020). The direct formation of MM glycans in the production host would be more elegant, as achieved when using the baculovirus expression system in Sf9 insect cells due to their prominent hexosaminidase activity (Bonten et al., 2004; Shi and Jarvis, 2007). Plant expression hosts typically produce complex-type *N*-linked glycans terminated with GlcNAc residues (Hanania et al., 2017; Hintze et al., 2020; Sariyatun et al., 2021; Tschongov et al., 2024), although MM is found more rarely (Shaaltiel et al., 2007; Shen et al., 2016). Strategies that favor MM glycans include directing recombinant proteins to the vacuole, which contains hexosaminidases (Tekoah et al., 2015), or using the Arabidopsis *alg3* mutant, which inhibits glycan maturation in the Golgi, although the latter induces ER stress and reduces overall yields (Sariyatun et al., 2021). We decided to equip our moss platform with the enzymes needed to produce MM glycans to expand our glyco-engineering toolbox and benefit from our previous achievements, i.e. efficient secretion of a recombinant protein lacking plant-specific xylose and fucose residues (Hintze et al., 2020). The hereby tested *in vivo* assembly approach offers a straightforward approach to facilitate cell line engineering (King et al., 2016; Text S3).

*Sf*ManIII was suitable for the production of recombinant GAA with MM glycans but it was important to tune the expression levels carefully to avoid overloading the secretion machinery (Torres et al., 2022). We fused *Sf*ManIII to the transmembrane domain of moss ManII to ensure localization in early Golgi vessels (Strasser et al., 2006) but detected only traces of the product. Glycosyltransferase activity is finely tuned by enzyme localization and multimerization (El-Battari et al., 2003). Given that *Sf*ManIII is a type II α-mannosidase that forms multimers (Kawar et al., 2001; Kuokkanen et al., 2007; Nemcovicova et al., 2013), overcrowding

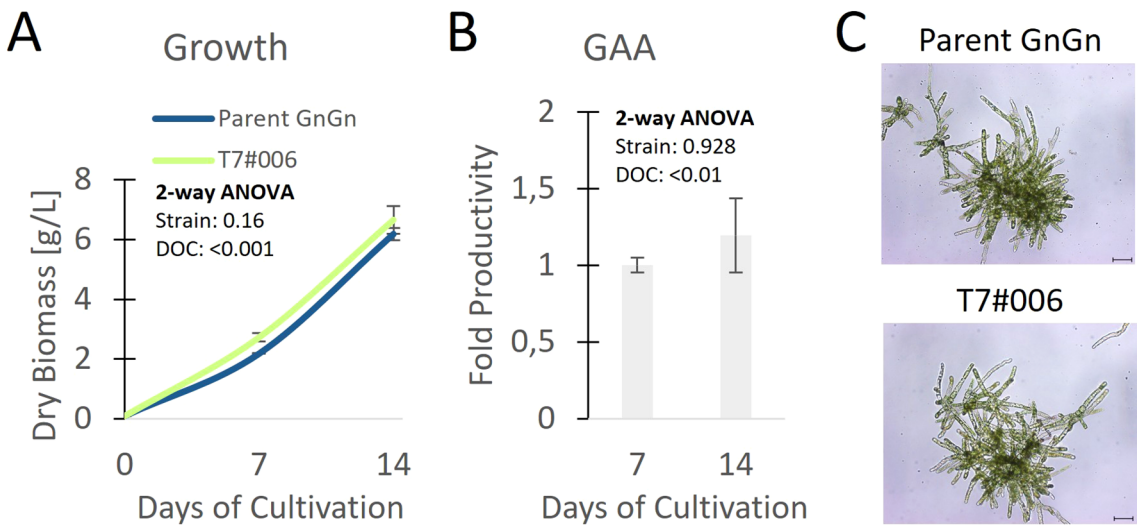

FIGURE 3
Clone with the highest proportion of MM glycans compared to the parental line showing **(A)** growth, **(B)** relative fold change of productivity related to parent, and **(C)** morphology on day 7 in a stirred-tank bioreactor (n = 3 technical replicates, error bars represent standard deviations). Statistical significance of differences between the parent strain and T7#006 on different days of cultivation (DOC) was determined by two-way ANOVA (Text S1); p values are for comparisons between strains and DOC. Scale bar represents 100 µm.

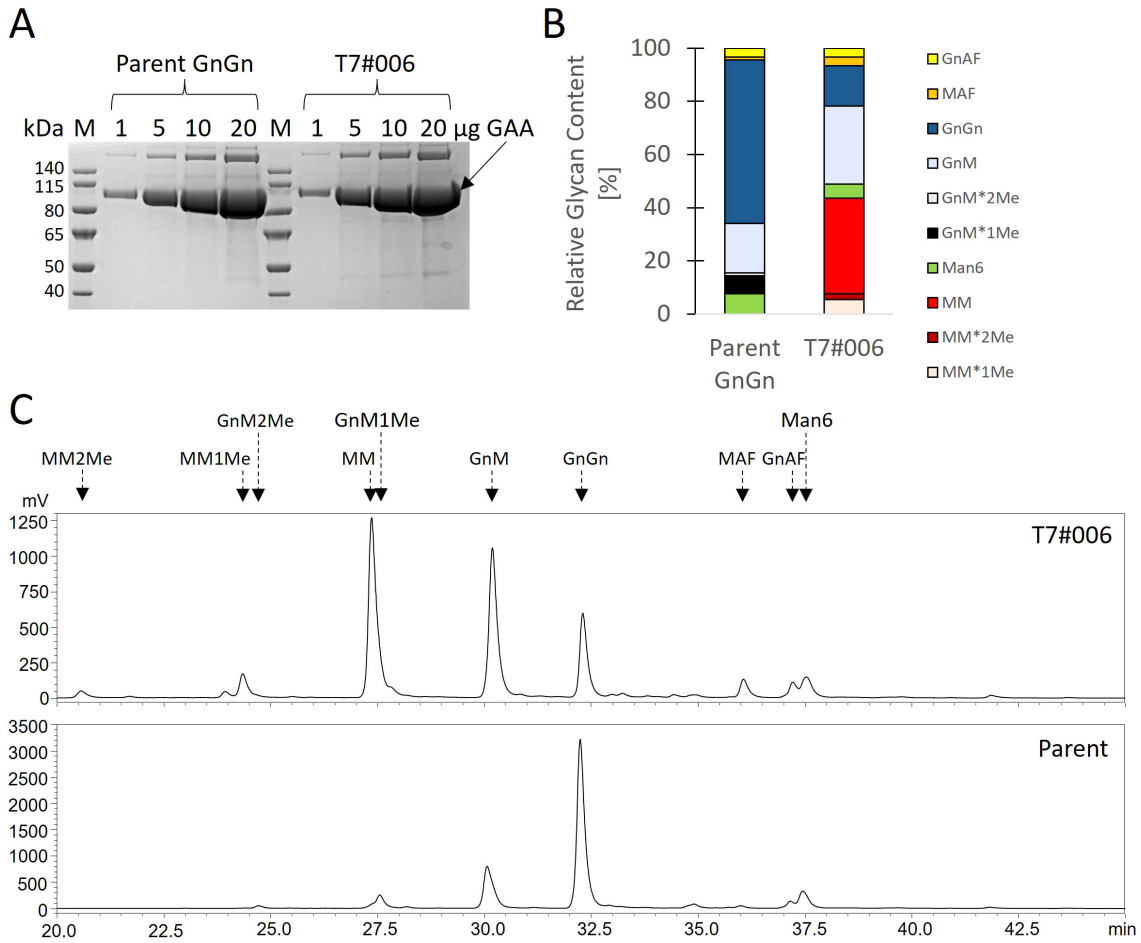

FIGURE 4
Glycan profile of GAA produced in a stirred-tank bioreactor. **(A)** SDS-PAGE showing amounts of purified GAA to estimate sample purity. **(B)** HILIC analysis and **(C)** proportions of cleaved glycans.

may reduce its activity by constraining interactions involving the transmembrane and lumenal domain by changing membrane curvature, reducing the lateral diffusion rate, and compressing the distance between subunits (Löwe et al., 2020; Welch and Munro, 2019).

We achieved the highest proportion of MM glycans by expressing *Sf*Hexo under the control of a strong promoter and secreting it to the extracellular space. When we targeted the late Golgi by fusing the lumenal domain of *Sf*Hexo to the transmembrane domain of FucT (Fitchette-Laine et al., 1994), we observed no activity at high or low expression levels. Native *Sf*Hexo is known to localize in secretory vesicles and outside the cell (Aumiller et al., 2006; Tomiya et al., 2006). We therefore cannot exclude the possibility that *Sf*Hexo exists as a pro-enzyme that must be processed as it moves through the secretory pathway to gain full activity (Tomiya et al., 2006). This is supported by our observation that only the secreted version of the enzyme was active. Another reason could be a prolonged co-localization of *Sf*Hexo with its secreted substrate GAA or a combination of both.

In conclusion, our results highlight the importance of appropriate expression levels and protein localization for components of the glycosylation machinery when optimizing the glyco-engineering of recombinant proteins (Strasser, 2023). Further engineering attempts, by testing other enzymes, different subcellular compartments and expression levels, may determine whether the MM content can be increased even more or if there is a maximum that moss can tolerate. Each attempt at glyco-engineering has the potential to alter host cell proteins and may negatively affect host physiology. However, the moss strain reported here shows no adverse changes in morphology, growth, or productivity, in agreement with many previous glyco-engineering experiments (Bohlender et al., 2020; Koprivova et al., 2004; Parsons et al.,

2012; Shen et al., 2016; Tschongov et al., 2024). This confirms the amenability of moss for glyco-engineering, as also reported in other plants such as tobacco (Kittur et al., 2020).

Data availability statement

The datasets presented in this study can be found in online repositories. The names of the repository/repositories and accession number(s) can be found in the article/Supplementary Material.

Author contributions

JJ: Investigation, Writing – review & editing. BF: Supervision, Writing – review & editing. JK: Supervision, Writing – review & editing. SB: Supervision, Writing – review & editing. PD-S: Conceptualization, Writing – review & editing. AS: Writing – review & editing, Conceptualization. CS: Writing – original draft, Writing – review & editing, Project administration, Conceptualization, Supervision.

Funding

The author(s) declare that financial support was received for the research and/or publication of this article. The work was funded by Eleva GmbH.

Acknowledgments

We acknowledge Prof. Friedrich Altmann and Dr. Clemens Grünwald-Gruber for HILIC and LC-ESI-MS analysis. We thank team Eleva for excellent technical assistance. We are grateful to Dr. Richard M. Twyman for language editing.

Conflict of interest

The authors are employed by Eleva GmbH. Data from this study have been included in patent application EP24186910.

Publisher's note

Supplementary material

The Supplementary Material for this article can be found online at: https://www.frontiersin.org/articles/10.3389/fpls.2025.1605548/full#supplementary-material

References

Aumiller, J. J., Hollister, J. R., and Jarvis, D. L. (2006). Molecular cloning and functional characterization of β-N-acetylglucosaminidase genes from Sf9 cells. *Protein Expr. Purif.* 47, 571–590. doi: 10.1016/j.pep.2005.11.026

Bohlender, L. L., Parsons, J., Hoernstein, S. N. W., Rempfer, C., Ruiz-Molina, N., Lorenz, T., et al. (2020). Stable protein sialylation in *Physcomitrella*. *Front. Plant Sci.* 11, 610032. doi: 10.3389/fpls.2020.610032

Bonten, E. J., Wang, D., Toy, J. N., Mann, L., Mignardot, A., Yogalingam, G., et al. (2004). Targeting macrophages with baculovirus-produced lysosomal enzymes: implications for enzyme replacement therapy of the glycoprotein storage disorder galactosialidosis. *FASEB J.* 18, 971–973. doi: 10.1096/fj.03-0941fje

Decker, E. L., and Reski, R. (2020). Mosses in biotechnology. *Curr. Opin. Biotechnol.* 61, 21–27. doi: 10.1016/j.copbio.2019.09.021

El-Battari, A., Prorok, M., Angata, K., Mathieu, S., Zerfaoui, M., Ong, E., et al. (2003). Different glycosyltransferases are differentially processed for secretion, dimerization, and autoglycosylation. *Glycobiology* 13, 941–953. doi: 10.1093/glycob/cwg117

Fitchette-Laine, A.-C., Gomord, V., Chekkafi, A., and Faye, L. (1994). Distribution of xylosylation and fucosylation in the plant Golgi apparatus. *Plant J.* 5, 673–682. doi: 10.1111/j.1365-313X.1994.00673.x

Geisler, C., Aumiller, J. J., and Jarvis, D. L. (2008). A *fused lobes* gene encodes the processing β-*N*-Acetylglucosaminidase in Sf9 cells. *J. Biol. Chem.* 283, 11330–11339. doi: 10.1074/jbc.M710279200

Hanania, U., Ariel, T., Tekoah, Y., Fux, L., Sheva, M., Gubbay, Y., et al. (2017). Establishment of a tobacco BY2 cell line devoid of plant-specific xylose and fucose as a platform for the production of biotherapeutic proteins. *Plant Biotechnol. J.* 15, 1120–1129. doi: 10.1111/pbi.2017.15.issue-9

Hennermann, J. B., Arash-Kaps, L., Fekete, G., Schaaf, A., Busch, A., and Frischmuth, T. (2019). Pharmacokinetics, pharmacodynamics, and safety of moss-aGalactosidase A in patients with Fabry disease. *J. Inher. Metab. Dis.* 42, 527–533. doi: 10.1002/jimd.2019.42.issue-3

Hintze, S., Limmer, S., Dabrowska-Schlepp, P., Berg, B., Krieghoff, N., Busch, A., et al. (2020). Moss-derived human recombinant GAA provides an optimized enzyme uptake in differentiated human muscle cells of Pompe disease. *Int. J. Mol. Sci.* 21, 2642. doi: 10.3390/ijms21072642

Kawar, Z., Karaveg, K., Moremen, K. W., and Jarvis, D. L. (2001). Insect cells encode a class II α-mannosidase with unique properties. *J. Biol. Chem.* 276, 16335–16340. doi: 10.1074/jbc.M100119200

Kim, Y. K., Kim, K. R., Kang, D. G., Jang, S. Y., Kim, Y. H., and Cha, H. J. (2009). Suppression of β-*N*-acetylglucosaminidase in the *N*-glycosylation pathway for complex glycoprotein formation in *Drosophila* S2 cells. *Glycobiology* 19, 301–308. doi: 10.1093/glycob/cwn138

King, B. C., Vavitsas, K., Ikram, N. K. B. K., Schrøder, J., Scharff, L. B., Hamberger, B., et al. (2016). *In vivo* assembly of DNA fragments in the moss, *Physcomitrella patens*. *Sci. Rep.* 6, 25030. doi: 10.1038/srep25030

Kittur, F. S., Hung, C.-Y., Zhu, C., Shajahan, A., Azadi, P., Thomas, M. D., et al. (2020). Glycoengineering tobacco plants to stably express recombinant human erythropoietin with different *N*-glycan profiles. *Int. J. Biol. Macromol.* 157, 158–169. doi: 10.1016/j.ijbiomac.2020.04.199

Koprivova, A., Stemmer, C., Altmann, F., Hoffmann, A., Kopriva, S., Gorr, G., et al. (2004). Targeted knockouts of *Physcomitrella* lacking plant-specific immunogenic *N*-glycans. *Plant Biotechnol. J.* 2, 517–523. doi: 10.1111/j.1467-7652.2004.00100.x

Kuokkanen, E., Smith, W., Mäkinen, M., Tuominen, H., Puhka, M., Jokitalo, E., et al. (2007). Characterization and subcellular localization of human neutral class II α-mannosidase cytosolic enzymes/free oligosaccharides/glycosidehydrolase family 38/M2C1/N-glycosylation. *Glycobiology* 17, 1084–1093. doi: 10.1093/glycob/cwm083

Löwe, M., Kalacheva, M., Boersma, A. J., and Kedrov, A. (2020). The more the merrier: effects of macromolecular crowding on the structure and dynamics of biological membranes. *FEBS J.* 287, 5039–5067. doi: 10.1111/febs.v287.23

Nemcovicova, I., Sestak, S., Rendic, D., Plskova, M., Mucha, J., and Wilson, I. B. H. (2013). Characterisation of class I and II α-mannosidases from *Drosophila melanogaster*. *Glycoconj. J.* 30, 899–909. doi: 10.1007/s10719-013-9495-5

Parsons, J., Altmann, F., Arrenberg, C. K., Koprivova, A., Beike, A. K., Stemmer, C., et al. (2012). Moss-based production of asialo-erythropoietin devoid of Lewis A and other plant-typical carbohydrate determinants. *Plant Biotechnol. J.* 10, 851–861. doi: 10.1111/j.1467-7652.2012.00704.x

Platt, F. M., d'Azzo, A., Davidson, B. L., Neufeld, E. F., and Tifft, C. J. (2018). Lysosomal storage diseases. *Nat. Rev. Dis. Primers* 4, 1–25. doi: 10.1038/s41572-018-0025-4

Sariyatun, R., Florence,, Kajiura, H., Ohashi, T., Misaki, R., and Fujiyama, K. (2021). Production of human acid-alpha glucosidase with a paucimannose structure by glycoengineered *Arabidopsis* cell culture. *Front. Plant Sci.* 12, 703020. doi: 10.3389/fpls.2021.703020

Schmittgen, T. D., and Livak, K. J. (2008). Analyzing real-time PCR data by the comparative CT method. *Nat. Prot.* 3, 1101–1108. doi: 10.1038/nprot.2008.73

Shaaltiel, Y., Bartfeld, D., Hashmueli, S., Baum, G., Brill-Almon, E., Galili, G., et al. (2007). Production of glucocerebrosidase with terminal mannose glycans for enzyme replacement therapy of Gaucher's disease using a plant cell system. *Plant Biotechnol. J.* 5, 579–590. doi: 10.1111/j.1467-7652.2007.00263.x

Shen, J.-S., Busch, A., Day, T. S., Meng, X.-L., Yu, C. I., Dabrowska-Schlepp, P., et al. (2016). Mannose receptor-mediated delivery of moss-made α-galactosidase A efficiently corrects enzyme deficiency in Fabry mice. *J. Inher. Metab. Dis.* 39, 293–303. doi: 10.1007/s10545-015-9886-9

Shi, X., and Jarvis, D. L. (2007). Protein *N*-glycosylation in the baculovirus–insect cell system. *Curr. Drug Targets* 8, 1116–1125. doi: 10.2174/138945007782151360

Shin, Y., Castilho, A., Dicker, M., Sadio, F., Vavra, U., Grünwald-Gruber, C., et al. (2017). Reduced paucimannosidic *N*-glycan formation by suppression of a specific β-hexosaminidase from *Nicotiana benthamiana*. *Plant Biotechnol. J.* 15, 197–206. doi: 10.1111/pbi.2017.15.issue-2

Strasser, R. (2023). Plant glycoengineering for designing next-generation vaccines and therapeutic proteins. *Biotechnol. Adv.* 67, 108197. doi: 10.1016/j.biotechadv.2023.108197

Strasser, R., Schoberer, J., Jin, C., Glössl, J., Mach, L., and Steinkellner, H. (2006). Molecular cloning and characterization of *Arabidopsis thaliana* Golgi α-mannosidase II, a key enzyme in the formation of complex N-glycans in plants. *Plant J.* 45, 789–803. doi: 10.1111/j.1365-313X.2005.02648.x

Tekoah, Y., Shulman, A., Kizhner, T., Ruderfer, I., Fux, L., Nataf, Y., et al. (2015). Large-scale production of pharmaceutical proteins in plant cell culture—the Protalix experience. *Plant Biotechnol. J.* 13, 1199–1208. doi: 10.1111/pbi.2015.13.issue-8

Tomiya, N., Narang, S., Park, J., Abdul-Rahman, B., Choi, O., Singh, S., et al. (2006). Purification, characterization, and cloning of a *Spodoptera frugiperda* Sf9 β-*N*-acetylhexosaminidase that hydrolyzes terminal *N*-acetylglucosamine on the *N*-glycan core. *J. Biol. Chem.* 281, 19545–19560. doi: 10.1074/jbc.M603312200

Torres, M., Hussain, H., and Dickson, A. J. (2022). The secretory pathway – the key for unlocking the potential of Chinese hamster ovary cell factories for manufacturing therapeutic proteins. *Crit. Rev. Biotechnol.* 43, 628–645. doi: 10.1080/07388551.2022.2047004

Tschongov, T., Konwar, S., Busch, A., Sievert, C., Hartmann, A., Noris, M., et al. (2024). Moss-produced human complement factor H with modified glycans has an extended half-life and improved biological activity. *Front. Immunol.* 15, 1383123. doi: 10.3389/fimmu.2024.1383123

Welch, L. G., and Munro, S. (2019). A tale of short tails, through thick and thin: investigating the sorting mechanisms of Golgi enzymes. *FEBS Lett.* 593, 2452–2465. doi: 10.1002/1873-3468.13553

frontiers | Frontiers in Plant Science

TYPE Original Research
PUBLISHED 21 July 2025
DOI 10.3389/fpls.2025.1631697

OPEN ACCESS

EDITED BY
Satomi Hayashi,
Queensland University of Technology, Australia

REVIEWED BY
Xiaoming Gao,
Chinese Academy of Agricultural Sciences, China
Chenliang Yu,
Zhejiang Agriculture and Forestry University, China

*CORRESPONDENCE
Kevin Wang
kevinwang@upike.edu
Nan Wang
wangnan@caas.cn

RECEIVED 20 May 2025
ACCEPTED 30 June 2025
PUBLISHED 21 July 2025

CITATION
Wang K, Mason H, Hall K, Slone E, Tackett K and Wang N (2025) Transient expression of full-length and mature nattokinase in Nicotiana benthamiana reveals early necrosis from full-length form and functional activity of the mature enzyme. *Front. Plant Sci.* 16:1631697. doi: 10.3389/fpls.2025.1631697

Transient expression of full-length and mature nattokinase in Nicotiana benthamiana reveals early necrosis from full-length form and functional activity of the mature enzyme

Kevin Wang[1*], Hugh Mason[2], Kylie Hall[1], Ethan Slone[1], Kylie Tackett[1] and Nan Wang[3*]

[1]Division of Math and Natural Sciences, University of Pikeville, Pikeville, KY, United States, [2]School of Life Sciences, Arizona State University, Tempe, AZ, United States, [3]Biotechnology Research Institute, Chinese Academy of Agriculture Sciences, Beijing, China

Nattokinase is a potent fibrinolytic enzyme widely used in the treatment of cardiovascular diseases for its ability to directly degrade fibrin and plasmin substrates, effectively dissolving blood clots. In this study, both full-length and mature forms of the nattokinase coding sequence were transiently expressed in *Nicotiana benthamiana* using a modified Bean Yellow Dwarf Virus (BeYDV) replicon system. Overexpression of the full-length (pre-pro) construct resulted in severe leaf necrosis within 2.5 days post-infiltration (dpi), with electrolyte leakage analysis indicating an 83.5% loss of membrane integrity by 3 dpi. In contrast, the mature form of nattokinase was successfully expressed without early cytotoxicity and exhibited strong caseinolytic and fibrinolytic activity, reaching 22,500 FU/g—comparable to commercial standards. These findings demonstrate the feasibility of producing biologically active nattokinase in plants and highlight the potential of plant-based expression systems as scalable, cost-effective platforms for therapeutic enzyme production.

KEYWORDS

plant transient expression, codon optimization, nattokinase, BEYDV, Nicotiana benthamiana

Introduction

Cardiovascular diseases (CVDs) remain a leading cause of mortality worldwide, often due to complications arising from blood clot formation. Nattokinase, a serine protease produced by *Bacillus subtilis* during natto fermentation, has attracted significant interest for its potent fibrinolytic activity (Granito et al., 2024; Yang et al., 2024). It directly degrades fibrin and plasmin substrates and has shown therapeutic potential in the prevention and

treatment of thrombosis, atherosclerosis, stroke, hypertension, and Alzheimer's disease (Chiu et al., 2024; Jensen et al., 2016; Tanikawa et al., 2024). Nattokinase (NK) is currently under Phase 4 clinical evaluation for oral administration (e.g., NCT02886507, NCT02913170, NCT00447434), with no significant adverse effects reported to date.

Commercial nattokinase is primarily produced through *B. subtilis* fermentation; however, residual impurities in these preparations may trigger allergic reactions, raising regulatory and safety concerns. Recombinant production in alternative microbial hosts such as *Escherichia coli* and yeast has been explored (Ni et al., 2016; Jain et al., 2024; Yan et al., 2021), but these systems often suffer from limitations including inclusion body formation, low yields, and reliance on toxic or tightly regulated inducers—factors that constrain scalability and cost-effectiveness.

In contrast to conventional expression platforms, plant-based platforms have emerged as promising alternatives for recombinant protein production, offering key advantages in scalability, safety, and cost (Eidenberger et al., 2023; Buyel, 2024; Akher et al., 2025; Shanmugaraj et al., 2025). Studies have demonstrated the enzymatic activity of plant-derived nattokinase. For example, Han et al. (2015) transiently expressed a full-length, codon-optimized nattokinase gene in melon, achieving a fibrinolytic activity of 79.30 U/mL. Similarly, Ni et al. (2023) reported *in vivo* thrombolytic efficacy in transgenic cucumber plants harboring an integrated full-length nattokinase gene. Among available plant hosts, *Nicotiana benthamiana* is widely used for transient expression due to its rapid growth, well-characterized genome (Chen et al., 2024; Golubova et al., 2024; Ranawaka et al., 2024), and ability to accumulate high levels of recombinant protein within 4–7 days. Akher et al. (2025) review advancements in viral vector-mediated transient expression systems in *N. benthamiana*, emphasizing their central role in rapid, scalable biopharmaceutical production and integration with hydroponics and controlled environment agriculture to support regulatory compliance and meet market demands.

However, challenges remain. In plant expression systems, overexpression of precursor or zymogen forms of proteins—especially those containing native prokaryotic signal peptides or pro-domains—often leads to endoplasmic reticulum (ER) stress, unfolded protein response (UPR), and hypersensitive response (HR)-like symptoms (Buono et al., 2019; Chen et al., 2023). These stress responses can culminate in localized cell death or systemic necrosis, particularly when the foreign protein is not efficiently processed or misfolds in the ER. Studies have shown that transient expression of proteases in plants can induce pronounced tissue damage characterized by necrotic lesions and compromised cell viability, ultimately leading to cell death (Dickey et al., 2017; Ma et al., 2019). In this study, we employed a modified Bean Yellow Dwarf Virus (BeYDV) replicon system (Diamos and Mason, 2019) to transiently express both the full-length (pre-pro) and mature forms of nattokinase in *N. benthamiana*. Enzymatic activity was evaluated using casein and fibrin degradation assays, while tissue integrity was assessed through visual inspection and electrolyte leakage analysis. Our findings revealed that expression of the full-length nattokinase triggered severe leaf necrosis as early as 2.5 dpi, consistent with early onset of BeYDV-driven gene expression. These results underscore the cytotoxic risks associated with overexpression of full-length proteases in plant systems and highlight the importance of using mature, pre-processed protein constructs to enable safe, functional, and sustainable production of therapeutic enzymes in plant-based platforms. Nonetheless, to achieve the full cost-effectiveness and commercial viability of plant-derived nattokinase, several upstream and downstream challenges must be addressed. As highlighted by Buyel (2024), key bottlenecks include variable protein yield, batch-to-batch consistency, regulatory alignment, and scalable purification. A unified, technology-driven framework that integrates optimized expression, extraction, and purification strategies will be essential to translating plant molecular farming into a commercially viable production system for enzymes like nattokinase.

Materials and methods

Plant expression constructs and leaf agroinfiltration

To design the nattokinase (*aprN*) expression constructs, a murine tobacco mosaic virus-specific monoclonal antibody heavy chain signal peptide (LPH: MECNWILPFILSVTSGAYS; Hiatt et al., 1989; Voss et al., 1995; Vaquero et al., 1999; Schiermeyer et al., 2005; Knödler et al., 2023) was fused to the N-terminus of both the full-length and mature forms of the *aprN* protein from *B. subtilis* MTCC (GenBank accession number: KJ174339.1). A hexahistidine tag (His_6) was added to the C-terminus to facilitate purification. These constructs, designated LPH-full-length-aprN-His_6 and LPH-mature-aprN-His_6, were codon-optimized for *N. benthamiana* using Invitrogen's GeneOptimizer® (Thermo Fisher Scientific, Waltham, MA, USA). The codon-optimized full-length *aprN* sequence has been deposited in GenBank under accession number PQ432224, which includes the signal peptide (residues 1–29), propeptide (residues 30–106), and the mature peptide (residues 107–381) (Weng et al., 2017).

To facilitate cloning, a XhoI–NbPsaK2!–5′–XbaI fragment was added to the 5′ end and a SacI site to the 3′ end of each construct. The complete cassettes—XhoI–NbPsaK2!–XbaI–LPH-full-length-aprN-His_6–SacI and XhoI–NbPsaK2!–XbaI–LPH-mature-aprN-His_6–SacI—were synthesized by Invitrogen's GeneArt® Gene Synthesis service and cloned into the XhoI and SacI sites of the pBYR2e-based vector (Diamos and Mason, 2019), generating the pBY!fNatto and pBY!mNatto constructs, respectively (Figure 1).

The plant expression vectors pBY!fNatto (full-length nattokinase) and pBY!mNatto (mature-length nattokinase) were validated by restriction enzyme digestion and PCR, then introduced into *Agrobacterium tumefaciens* strain EHA105 (GoldBio, St. Louis, MO, USA) via electroporation using a MicroPulser™ Electroporator (Bio-Rad, Hercules, CA, USA). Transformed *Agrobacterium* colonies were verified by PCR and plated on selective LB agar containing 50 mg/L kanamycin, followed by

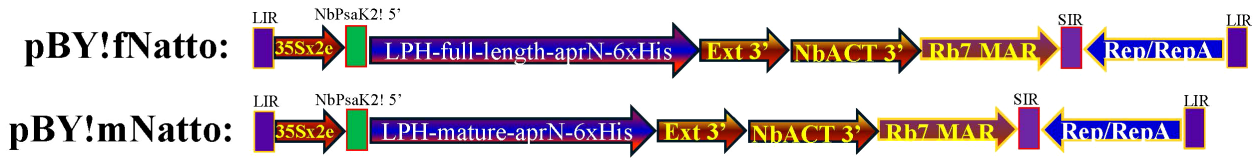

FIGURE 1
Schematic representation of the pBY!fNatto and pBY!mNatto expression vector for transient nattokinase expression in *N. benthamiana*. The plant expression vector pBY!fNatto (full-length nattokinase) and pBY!mNatto (mature-length nattokinase), utilized in this research, is based on the optimized BeYDV vector (Diamos and Mason, 2019) designed for high-level expression of a single target gene. The components of the vector include 35Sx2e, which is the 35S promoter from cauliflower mosaic virus enhanced with a duplicated enhancer region; NbPsaK2T! 5′, a truncated 5′ UTR from the *N. benthamiana* psaK gene; Ext 3′, a tobacco extensin terminator from which the intron has been removed; NbACT 3′, the 3′ UTR from the *N. benthamiana* ACT3 gene; Rb7 MAR, the tobacco Rb7 matrix attachment region; SIR, a short intergenic region from BeYDV; Rep/RepA, the replication proteins from BeYDV; and LIR, the long intergenic region from BeYDV. Additionally, the vector includes a plant codon-optimized murine monoclonal antibody heavy chain signal peptide (LPH) fused to the N-terminal of the codon-optimized nattokinase (aprN) sequence, with a hexahistidine (6xHis) tag at the C-terminal for Ni-NTA affinity purification.

incubation at ~30°C for 3 days. For agroinfiltration, bacterial cultures were harvested and resuspended in infiltration buffer (10 mM 2-(N-morpholino) ethanesulfonic acid (MES), 10 mM $MgSO_4$, pH 5.5) to an optical density at 600 nm (OD_{600}) of 0.2. The suspension was used to infiltrate the abaxial surface of 6- to 10-week-old *N. benthamiana* leaves using a 20 mL syringe without a needle. Leaf samples were collected at 4 dpi for subsequent protein extraction and purification.

Visualizing nattokinase-induced necrosis and electrolyte leakage assay

Tissue necrosis was assessed both visually and quantitatively using the electrolyte leakage (EL) assay, following the protocol described by Dickey et al. (2017). Leaf discs (5 mm diameter) were collected using a cork borer (5 mm diameter) from regions infiltrated with *A. tumefaciens* strain EHA105 alone, carrying either the pBY!fNatto or pBY!mNatto plasmid, or from untreated control leaves. On days 2.5, 3 and 4 post-infiltration (dpi), discs were briefly rinsed with deionized (DI) water to remove surface residues. Each disc was then placed into a 15 × 160 mm test tube containing 10 mL of DI water and incubated at room temperature on a shaker at 200 rpm for 1 hour. The initial conductivity (T_0) was measured using a conductivity meter (Bante Instruments, Sugar Land, TX, USA).

Following T_0 measurement, samples were boiled at 98°C for 2 hours in a water bath to release total electrolytes. After cooling, the volume was restored to 10 mL with DI water, and final conductivity (T_1) was measured. The extent of electrolyte leakage (% EL), representing the degree of tissue damage, was calculated using the formula:

$$\% \text{ EL} = 100 \times (T_0 - \text{DI})/(T_1 - \text{DI})$$

where DI is the conductivity of the water control.

Results were expressed as means ± standard error (SE) for n = 3 biological replicates and statistically analyzed using pairwise Student's t-tests.

Protein analysis and characterization by SDS-PAGE and western blot

All materials, kits, and reagents used for SDS-PAGE and Western blotting were obtained from Thermo Fisher Scientific Inc. (Waltham, MA, USA), unless otherwise specified. Total soluble proteins were extracted from approximately 150 mg of leaf tissue—using the Pierce™ Plant Total Protein Extraction Kit, following the manufacturer's protocol. Tissues were processed using either native lysis buffer supplemented with 0.1% Halt™ Protease Inhibitor Cocktail or denaturing lysis buffer, as appropriate for downstream applications.

For SDS-PAGE analysis, 20 µL of crude protein extract was mixed with 4X Bolt™ LDS Sample Buffer and 10X Bolt™ Reducing Agent. Deionized water was added to adjust the final volume to 40 µL. Samples were denatured at 70°C for 10 minutes prior to loading onto a Bolt™ Bis-Tris Plus Mini gel. Following electrophoresis, gels were stained with Imperial™ Protein Stain for visualization. His-tagged proteins were purified using HisPur™ Ni-NTA Spin Columns according to the manufacturer's instructions. The eluted fractions were subsequently desalted using Zeba™ Micro Spin Desalting Columns (7K MWCO) and concentrated using Pierce™ Protein Concentrators (10K MWCO). Protein yield was estimated by analyzing band intensity with ImageJ software, using BSA standard bands as internal loading controls. Western blotting was performed using the SuperSignal™ West HisProbe™ Kit according to the supplied protocol. Detection was carried out using SuperSignal® Working Solution, and the blots were imaged using a ChemiDoc™ XRS+ Imaging System (Bio-Rad, Hercules, CA, USA).

Casein hydrolysis test and fibrinolytic activity assay

Protease activity of recombinant nattokinase (rNK) was initially assessed using a casein plate assay as described by Zhang et al. (2021). A 0.5% agarose gel containing 1% casein (Sigma-Aldrich,

Allentown, PA, USA) was prepared in 1× phosphate-buffered saline (PBS) and poured into Petri plates to solidify. Wells (5 mm diameter) were created in the gel, and 3 µg of purified plant-derived rNK in 40 µL of 1× PBS was loaded into each well. Positive control wells received 3 µg of commercial nattokinase (AbMore BioScience Inc., Houston, TX, USA; Batch#: M2121-202401; Activity data: 22,500 FU/g), while negative control wells contained either PBS or crude supernatant from wild-type (non-infiltrated) leaves. Following a 5-hour incubation at 37°C, the gels were stained with Coomassie Brilliant Blue R-250 (Bio-Rad, Hercules, CA, USA) to visualize zones of casein degradation. Proteolytic activity was quantified by measuring the average of the long and short diameters of each clear zone, subtracting the original well diameter (5 mm). Results were expressed as means ± standard error (SE; $n = 3$) and statistical significance was evaluated using paired Student's *t*-tests.

Fibrinolytic activity was further assessed using a modified fibrin plate assay following the protocol of Dickey et al. (2017). Briefly, 0.2 g of agarose was dissolved in 40 mL of 1× PBS by microwave heating and cooled to approximately 40°C. Before the gel solidified, 30 mg of human fibrinogen (Sigma-Aldrich), 8 units of human plasminogen (rPeptide LLC, Bogart, GA, USA), and 8 units of human thrombin (Medix Biochemica Inc., St. Louis, MO, USA) were added with gentle mixing to prevent bubble formation. The mixture was poured into Petri dishes and allowed to solidify at room temperature. Wells (5 mm diameter) were then created in the gel, and 5 µg of purified rNK diluted in 40 µL of 1× PBS was added to each well. Commercial nattokinase (5 µg; Abmole Bioscience Inc., Houston, TX, USA; Batch#: M2121-202401; Activity data:22,500 FU/g) was used as a positive control, while PBS and eluates from wild-type leaf extracts were included as negative controls. Plates were incubated overnight at 37°C. The diameters of the clear halos, with the well diameter subtracted, were measured to determine fibrinolytic activity. Enzymatic activity was quantified relative to the commercial standard (22,500 FU/g) using methods described in Dickey et al. (2017). Results were reported as means ± SE ($n = 3$) and analyzed using paired Student's *t*-tests.

Results

Impact of full-length nattokinase expression on leaf necrosis and tissue integrity

The transient expression of full-length nattokinase in *N. benthamiana* resulted in pronounced necrosis and significant loss of tissue integrity. As shown in Figure 2, leaves infiltrated with the pBY!fNatto vector began showing abrupt stress responses at 2.5 dpi, coinciding with the onset of BeYDV-driven gene expression (as indicated by the onset of GFP fluorescence in Figure 2A). Early symptoms included yellowing, watery lesions, and marginal

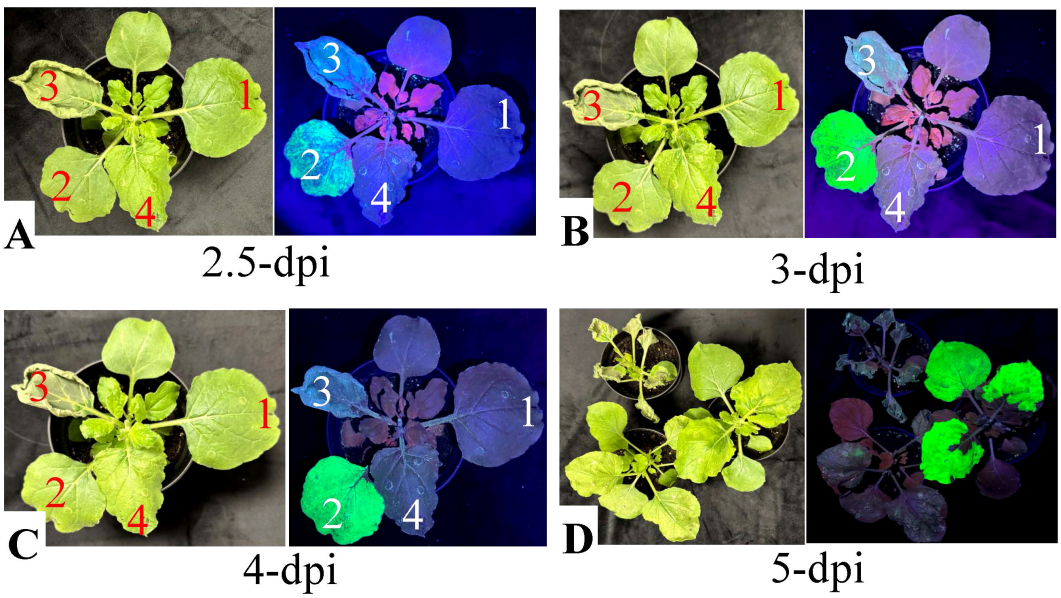

FIGURE 2
Evaluation of necrosis induced by nattokinase (NK) expression in *N. benthamiana* under normal and UV light. Fully expanded *N. benthamiana* leaves were infiltrated with *A.tumefaciens* strain EHA105 (1, negative control), or EHA105 carrying the vectors pBY!GFP (2), pBY!fNatto (3, full-length nattokinase), or pBY!mNatto (4, mature-length nattokinase). Plants were maintained under controlled growth conditions, and necrotic symptoms were documented at various time points. **(A)** Leaf images at 2.5 dpi under normal light. **(B)** Leaf images at 3 dpi. **(C)** Leaf images at 4 dpi under normal light. **(D)** Whole-plant images for treatments (2–4) captured under both normal and UV light at 5 dpi. Visible necrosis was evident under normal light, while UV imaging revealed reduced chlorophyll autofluorescence in necrotic areas. Leaves expressing full-length NK (pBY!fNatto) exhibited earlier onset and more severe necrosis compared to those expressing the mature form (pBY!mNatto), highlighting the greater cytotoxicity associated with full-length nattokinase expression.

curling—classic indicators of early necrotic onset. Under UV light, the affected regions appeared gray, signifying chlorophyll degradation and early cell death.

By 3 dpi, necrosis intensified. Infiltrated areas became brittle and desiccated, suggesting a substantial loss of turgor pressure and potential vascular collapse (Figure 2B). Other observable features included pale gray-green discoloration, leaf shrinkage, and curling at the edges, consistent with oxidative damage and membrane rupture. By 4 dpi, the damage had progressed to advanced necrosis. Leaves exhibited widespread dark gray discoloration, severe wilting, a dry, papery texture, and clear signs of tissue collapse (Figure 2C). These observations confirm the strong cytotoxic effect of full-length nattokinase expression in plant tissue, indicating that it actively induces cell death when overexpressed in plant-based expression systems.

In contrast, leaves infiltrated with pBY!GFP, pBY!mNatto (mature-length nattokinase), or *Agrobacterium* with no T-DNA remained visually healthy through 4 dpi, with no observable necrosis. These findings further support that the necrotic phenotype is specifically associated with the expression of the full-length nattokinase construct.

By 5 dpi, UV fluorescence imaging revealed gray patches in pBY!mNatto-infiltrated leaves, indicating delayed chlorophyll degradation and tissue damage (Figure 2D). The affected tissues exhibited a mosaic pattern of translucent and yellow lesions, consistent with progressive cellular degeneration associated with mature nattokinase expression. Mild yellowing was also occasionally observed in pBY!GFP-infiltrated controls, likely reflecting background stress from BeYDV vector replication, although no obvious necrotic symptoms were detected.

Full-length nattokinase expression significantly increases electrolyte leakage

Electrolyte leakage (EL), a proxy for cell death due to loss of membrane integrity, was measured to quantify tissue damage following transient expression of nattokinase. As shown in Figure 3, leaves infiltrated with pBY!fNatto exhibited a 52.1% loss of membrane integrity by 2.5 dpi, indicating significant early cell damage ($p < 0.0001$) compared to all control treatments (EHA105, pBY!GFP, and pBY!mNatto), which showed no statistically significant differences among themselves ($p > 0.1$). By 3 dpi, EL in pBY!fNatto-treated samples rose sharply to 83.5%, and by 4 dpi, it reached 93.4%, consistent with extensive tissue necrosis ($p < 0.0001$ at both time points). In contrast, pBY!GFP, pBY!mNatto, and EHA105 controls consistently maintained low EL levels across all time points, with no significant variation ($p > 0.1$). These results confirm that the observed loss of membrane integrity is specifically linked to the expression of full-length nattokinase, highlighting its cytotoxic effect in plant tissues.

Due to the rapid and severe necrosis caused by full-length nattokinase expression, all subsequent experiments in this study focused on the mature form, pBY!mNatto.

SDS-PAGE and western blot analysis of recombinant nattokinase

The total protein content from treated leaf areas was analyzed using SDS-PAGE and compared to the total soluble proteins from wild-type (WT) leaf tissue. At 4 dpi, leaves infiltrated with pBY!mNatto displayed a distinct ~28.4 kDa band (with C-terminal 6xHis tag) on SDS-PAGE gel (Figures 4A, B, Lane 2), consistent with the expected size of recombinant nattokinase (rNK). The band aligned with the predicted molecular weight of the nattokinase (NK) protein (27.7 kDa without his tag; Figure 4B, Lane 1). Western blotting using anti-His probe further confirmed the presence of rNK, showing a single band at ~28 kDa (Figure 4C). (Figure 4C). These findings confirm the successful expression of recombinant NK in the samples. The yield of NK was estimated to be approximately 370 μg/g leaf fresh weight (LFW), calculated using standard BSA as a reference and quantified with ImageJ software.

Measure the enzymatic activity of nattokinase by casein and fibrin plate assay

The casein plate assay (Figure 5) demonstrated that recombinant nattokinase effectively hydrolyzed casein, forming clear halos around the wells (Figure 5A). The mean diameters of the halos, calculated after subtracting the well diameter (5 mm), confirmed the proteolytic activity of the recombinant enzyme (Figure 5B). Statistical analysis showed no significant difference between recombinant nattokinase and the standard enzyme used as a positive control ($P = 0.635$, paired t-test). Negative controls, including PBS, exhibited no halo formation, further validating the specificity of nattokinase's protease activity. These results highlight the ability of plant-derived recombinant nattokinase to efficiently hydrolyze casein, consistent with its known enzymatic properties.

The fibrin plate assay (Figure 6) further demonstrated the fibrinolytic potential of recombinant nattokinase, providing a visual confirmation of enzyme activity through the formation of clear halos where fibrin was dissolved (Figure 6A). The diameters of the halos were measured to quantify fibrinolytic activity (Figure 6B). The results indicated no significant difference between the fibrinolytic activity of plant-derived recombinant nattokinase and the standard enzyme ($P = 0.643$, paired t-test). This suggests that the fibrinolytic potential of the plant-derived enzyme is comparable to that of the commercial standard reagent, which has a documented fibrinolytic activity of 22,500 FU/g. The comparable halo sizes validate the efficacy of using plant systems for producing functional nattokinase with therapeutic potential equivalent to commercially available products.

Discussion

Plants—particularly *N. benthamiana*—have demonstrated significant potential as platforms for heterologous protein

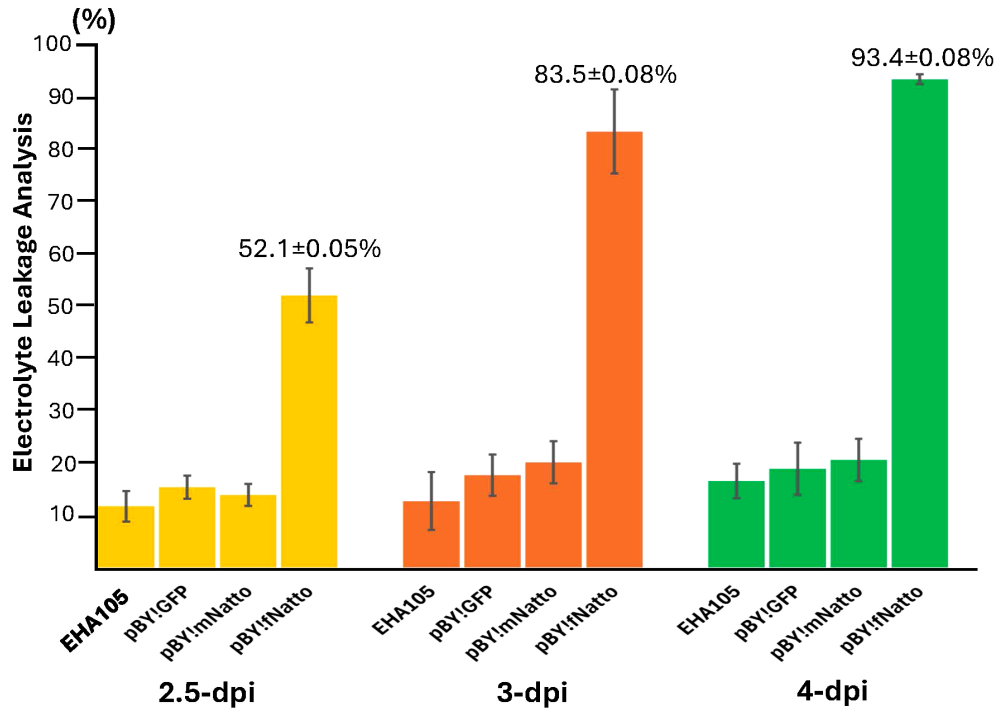

FIGURE 3
Electrolyte leakage (EL) analysis reveals significant tissue necrosis induced by Full-Length nattokinase Expression. Leaf discs were collected from *N, benthamiana* leaves infiltrated with pBY!fNatto (full-length nattokinase), pBY!mNatto (mature-length nattokinase), pBY!GFP (pBY), and *A. tumefaciens* strain EHA105 along (negative control). Samples were harvested at 2.5, 3, and 4 days post-infiltration (dpi). Conductivity was measured before and after heating, and EL percentages were calculated as the proportion of total electrolytes released prior to boiling. The results, presented as means ± SE (n = 3), show a significant ($p < 0.0001$) and progressive increase in electrolyte leakage in pBY!fNatto-treated samples compared to all control groups. Statistical analysis using pairwise Student's t-tests confirmed highly significant differences at each time point, indicating that expression of full-length nattokinase induces substantial loss of membrane integrity and cell viability.

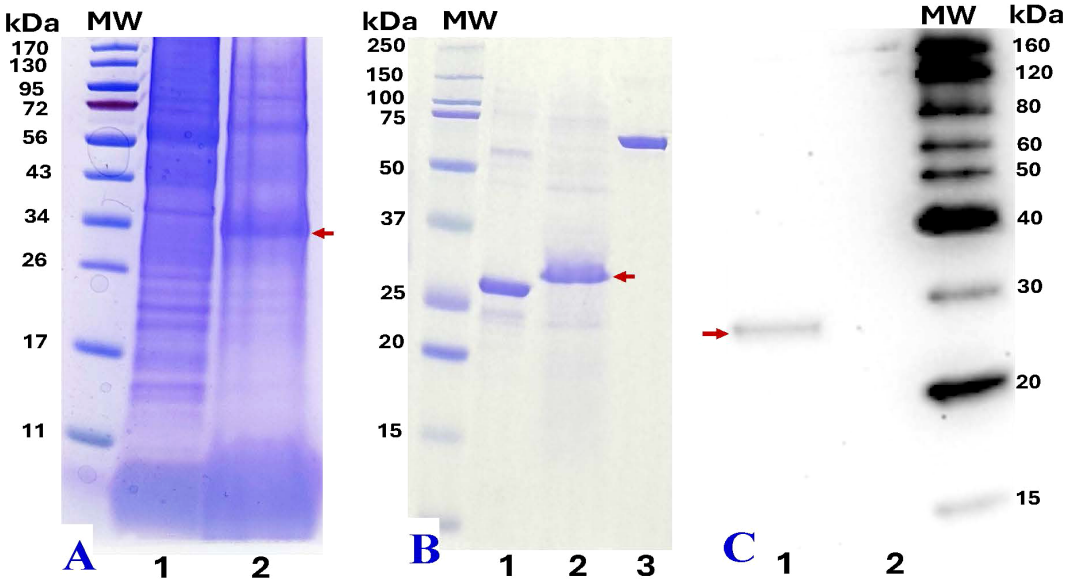

FIGURE 4
SDS-PAGE and western blot analysis of recombinant nattokinase (rNK). **(A)** SDS-PAGE analysis of crude protein extracts (20 µL) from wild-type leaves (Lane 1) and *N. benthamiana* leaves infiltrated with pBY!mNatto (mature-length nattokinase) at 4 dpi (Lane 2).**(B)** SDS-PAGE comparison of commercial nattokinase (3 µg, positive control, ~27.7 kDa, Lane 1), 6xHis-tag purified plant-derived rNK (~28.4 kDa, 10 µL, Lane 2), and BSA (2 µg, internal standard for ImageJ quantification, Lane 3). **(C)** Western blot analysis using anti-His probe detection: purified rNK (Lane 1) and His-tag eluate from non-infiltrated (wild-type) leaves (Lane 2). Molecular weight (MW) markers are shown alongside each gel for reference. Red arrows indicate the expected rNK protein bands at at ~28.4 kDa.

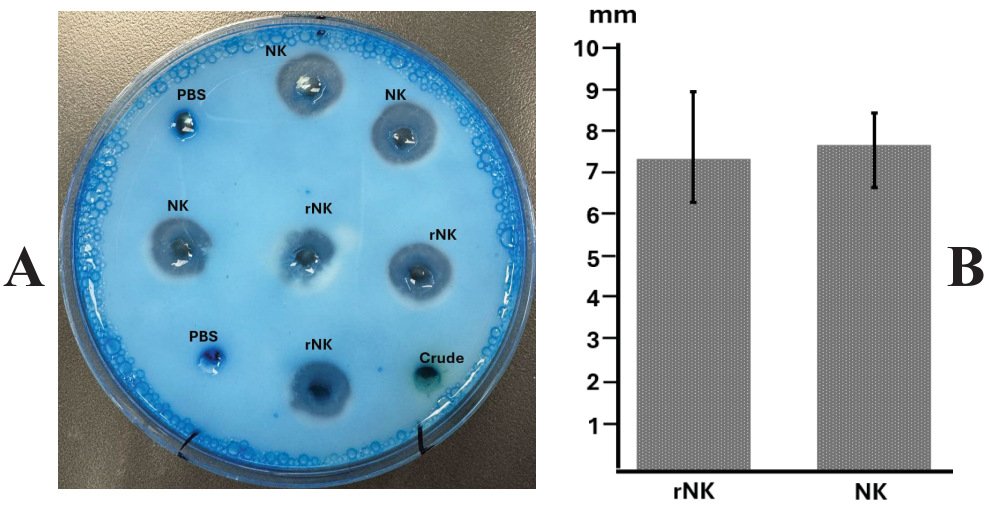

FIGURE 5
Assay of nattokinase activity on casein plate. **(A)** Representative image showing the hydrolysis halos produced by Nattokinase. **(B)** Quantification of lysis halo diameters (well diameter subtracted). PBS, Phosphate Buffered Saline, negative control; Crude, crude supernatant from wild-type leaves; NK: standard Nattokinase (AbMore BioScience Inc., Houston, TX, USA; Batch#: M2121-202401; Activity data:22,500 FU/g); rNK: plant-derived recombinant Nattokinase. Results show no significant difference between NK and rNK (P = 0.635, paired t-test, n = 3).

production (Buyel, 2024; Golubova et al., 2024; Kopertekh, 2024; Akher et al., 2025; Shanmugaraj et al., 2025). In this study, both the full-length and mature forms of nattokinase were transiently expressed in *N. benthamiana* to evaluate the plant-based system's ability to produce and process this fibrinolytic enzyme originally derived from *B. subtilis*.

Previous reports have shown successful expression of full-length nattokinase in transgenic cucumber (Ni et al., 2023) and through transient expression in melon (Han et al., 2015), with confirmed thrombolytic activity. Although full-length nattokinase (pre-pro form) is a zymogen—requiring signal peptide and propeptide cleavage for activation—these findings suggest that some plant species may possess endogenous proteases capable of processing the enzyme into its mature, active form.

The construct pBY!GFP, used as a control in this study, directed GFP to ER via the amylase signal peptide (Diamos and Mason, 2019). In parallel, previous studies have demonstrated that the LPH signal peptide promotes efficient ER targeting, secretion, and proper

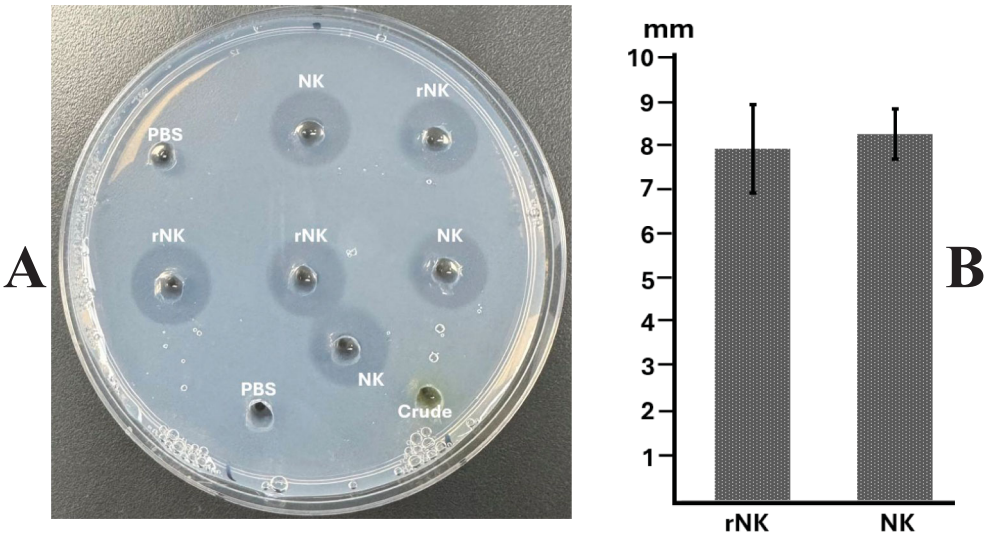

FIGURE 6
Assay of nattokinase activity on fibrin plate. **(A)** Representative image displaying the hydrolysis halos produced by Nattokinase. **(B)** Quantification of lysis halo diameters (well diameter subtracted). PBS, Phosphate Buffered Saline, negative control; Crude, crude supernatant from wild-type leaves; NK: standard Nattokinase (AbMore BioScience Inc., Houston, TX, USA; Batch#: M2121-202401; Activity data:22,500 FU/g); rNK: plant-derived recombinant Nattokinase. Results indicate no significant difference in activity between NK and rNK (P = 0.643, paired t-test, n = 3).

folding of recombinant proteins—including immunotoxins and GFP reporters—when transiently expressed in *N. benthamiana* (Knödler et al., 2023). In these studies, ER-targeted GFP expression did not induce visible tissue damage or necrosis, suggesting that ER localization itself is not intrinsically cytotoxic.

In contrast, BeYDV-driven expression of full-length nattokinase (pBY!fNatto) in *N. benthamiana* led to rapid and severe tissue necrosis. Necrotic symptoms appeared as early as 2.5 dpi (Figure 2A), corresponding with the onset of BeYDV-mediated gene expression (Diamos and Mason, 2019). By 3 dpi, extensive tissue collapse and desiccation were observed (Figure 2B), indicating proteolytic activity. Electrolyte leakage assays confirmed 83.5% loss of membrane integrity (Figure 3), highlighting the cytotoxic effects of unregulated protease activity in planta.

Previous studies have shown that the inclusion of a secretion signal peptide can significantly influence the subcellular localization and accumulation levels of recombinant proteins in plants. Targeting proteins to organelles such as the endoplasmic reticulum (ER) typically enhances folding, stability, and yield, whereas omission of the signal peptide often results in cytosolic retention, leading to increased susceptibility to misfolding and proteolytic degradation, ultimately reducing expression and activity (Liu and Timko, 2022). In this study, the LPH signal peptide was employed to direct recombinant nattokinase into the ER, facilitating its entry into the secretory pathway and supporting improved protein stability and accumulation (Voss et al., 1995; Vaquero et al., 1999; Schiermeyer et al., 2005; Knödler et al., 2023). However, in the case of the full-length construct, the combination of ER targeting via the LPH peptide and high-level expression driven by the BeYDV replicon likely induced acute ER stress. This stress was presumably caused by the accumulation of unfolded or misfolded proteins, which overwhelmed the plant's protein folding and quality control machinery (Wan and Jiang, 2016; Buono et al., 2019).

Improper full-length signal peptide or propeptide processing and unregulated or mislocalized protease activity may have further disrupted cellular homeostasis, while immune responses such as the hypersensitive response (HR) likely amplified the damage, culminating in rapid programmed cell death (Buono et al., 2019). It is highly plausible that the presence of both the eukaryotic ER signal peptide (LPH) and the retained prokaryotic signal peptide in the full-length nattokinase led to abnormal membrane anchoring or mislocalization of the protease. This misrouting likely exacerbated ER stress and contributed to activate plant defense signaling and leads to rapid program cell death (PCD) (Manghwar and Li, 2022; Chen et al., 2023). These observations underscore the importance of removing native bacterial targeting sequences when designing constructs for expression in eukaryotic systems. Collectively, these findings suggest that full-length nattokinase is unsuitable for high-level transient expression in *N. benthamiana* due to its incompatibility with host cellular machinery and its strong cytotoxic effects.

Foreign proteases can trigger necrosis in plant tissues due to their unregulated activity, which may interfere with endogenous proteins critical for maintaining cellular structure and function. Our previous work demonstrated that transient expression of another protease, Lumbrokinase, caused severe necrosis in *Nicotiana tabacum*, with electrolyte leakage exceeding 80% by 4 dpi and a relatively low recombinant protease yield of 20 μg/g fresh weight (Dickey et al., 2017). Similarly, Ma et al. (2019) reported that transient expression of bioactive recombinant Reteplase in *N. benthamiana* using the pJL-TRBO-G vector resulted in pronounced necrosis by 7 dpi, coinciding with peak foreign protein accumulation. These findings suggest that protease interactions with native plant proteins may disrupt essential cellular functions, triggering a cascade of degradation events and stress responses. Such necrotic outcomes likely reflect a plant defense mechanism—intended to contain damage, limit water loss, and redirect metabolic resources to enhance survival under proteolytic stress.

In contrast, the mature form of nattokinase—lacking the native signal peptide and propeptide—proved significantly more compatible with plant expression. Leaves infiltrated with pBY! mNatto remained visibly healthy through 4 dpi (Figure 2C), with only mild tissue damage observed by 5 dpi (Figure 2D). This delayed onset of necrosis may reflect the slower accumulation and more controlled activity of the mature enzyme, resulting in a less acute proteolytic environment and reduced cytotoxic stress on plant tissues. Additionally, the use of a modified BeYDV system, which enables separate and regulated expression of the BeYDV replication proteins Rep and RepA, likely contributed to reduced cell death during mature nattokinase expression (Diamos and Mason, 2019).

Functionally, the plant-derived mature nattokinase retained its biochemical activity, as confirmed by casein hydrolysis and fibrin degradation assays. Clear zones on casein-containing plates indicated robust protease activity, while transparent halos in fibrin plates were comparable in size to those formed by commercial nattokinase, validating its fibrinolytic potential. These findings indicate that the recombinant enzyme expressed in *N. benthamiana* retains functional proteolytic activity, suggesting it achieved a conformation compatible with substrate recognition and catalytic function.

Importantly, this activity was achieved without inducing significant tissue necrosis during the early expression period, supporting the feasibility of using plants for the functional production of proteolytic enzymes like nattokinase. The ability to replicate its native function—degrading fibrin, the key protein in blood clots—positions plant-produced nattokinase as a promising candidate for therapeutic or nutraceutical applications.

Conclusion

This study demonstrates that *N. benthamiana* is a viable host for the transient expression of biologically active mature nattokinase, while also revealing the severe cytotoxicity associated with overexpressing the full-length zymogen form. These findings highlight the importance of construct design in achieving functional and safe expression of nattokinase in plant systems. To enhance yield and reduce host tissue damage, future optimization

strategies—such as foliar application of ascorbic acid to suppress leaf stress (Nosaki et al., 2021), compartment-specific targeting (Adam, 1996), or co-expression of protease inhibitors—may prove beneficial. Beyond whole-plant agroinfiltration, Nattokinase could be scaled using plant cell suspension cultures, which provide sterile and controlled environments conducive to consistent recombinant protein production. Suspension cultures derived from fast-growing lines such as tobacco BY-2 cells (Karki et al., 2021) can be genetically engineered for either stable or transient expression of Nattokinase. Additionally, recent innovations—such as cell pack technology (Gengenbach et al., 2020) —have enhanced the scalability, throughput, and reproducibility of transient expression workflows, further supporting the potential of plant platforms for industrial-scale biomanufacturing. Together, these strategies support the development of efficient plant-based production platforms for therapeutic and industrial-grade nattokinase.

Data availability statement

The datasets presented in this study can be found in online repositories. The names of the repository/repositories and accession number(s) can be found in the article/supplementary material.

Author contributions

KW: Conceptualization, Data curation, Formal analysis, Funding acquisition, Investigation, Methodology, Project administration, Resources, Software, Supervision, Validation, Visualization, Writing – original draft, Writing – review & editing. HM: Methodology, Resources, Writing – review & editing. KH: Writing – review & editing. ES: Data curation, Methodology, Validation, Writing – review & editing. KT: Data curation, Methodology, Validation, Writing – review & editing. NW: Formal analysis, Funding acquisition, Resources, Supervision, Writing – original draft, Writing – review & editing.

Funding

The author(s) declare that financial support was received for the research and/or publication of this article. This publication was supported in part by the National Key Research and Development Program of China (grant numbers 2024YFD1200200 and 2024YFD1200205) and partially by grant P20GM103436-24 (KY INBRE) from the National Institute of General Medical Sciences, National Institutes of Health.

Conflict of interest

The authors declare that the research was conducted in the absence of any commercial or financial relationships that could be construed as a potential conflict of interest.

Generative AI statement

The author(s) declare that no Generative AI was used in the creation of this manuscript.

Publisher's note

References

Adam, Z. (1996). Protein stability and degradation in chloroplasts. *Plant Mol. Biol.* 32, 773–783. doi: 10.1007/BF00020476

Akher, S. A., Wang, K. Y., Hall, K., Hunpatin, O. S., Shan, M., Zhang, Z., et al. (2025). Harnessing transient expression systems with plant viral vectors for the production of biopharmaceuticals in *Nicotiana benthamiana*. *Int. J. Mol. Sci.* 26, 5510. doi: 10.3390/ijms26125510

Buono, R. A., Hudecek, R., and Nowack, M. K. (2019). Plant proteases during developmental programmed cell death. *J. Exp. Bot.* 0, 2097–2112. doi: 10.1093/jxb/erz072

Buyel, J. F. (2024). Towards a seamless product and process development workflow for recombinant proteins produced by plant molecular farming. *Biotechnol. Adv.* 75, 108403. doi: 10.1016/j.bioteChadv.2024.108403

Chen, X., Shi, C., He, M., Xiong, S., and Xia, X. (2023). Endoplasmic reticulum stress: molecular mechanism and therapeutic targets. *Sig Transduct Target Ther.* 8, 352. doi: 10.1038/s41392-023-01570-w

Chen, W., Yan, M., Chen, S., Sun, J., Wang, J., Meng, D., et al. (2024). The complete genome assembly of *Nicotiana benthamiana* reveals the genetic and epigenetic landscape of centromeres. *Nat. Plants.* 10, 1928–1943. doi: 10.1038/s41477-024-01849-y

Chiu, H. W., Chou, C. L., Lee, K. T., Shih, C. C., Huang, T. H., and Sung, L. C. (2024). Nattokinase attenuates endothelial inflammation through the activation of SRF and THBS1. *Int. J. Biol. Macromol* 268, 131779. doi: 10.1016/j.ijbiomac.2024.131779

Diamos, A. G., and Mason, H. S. (2019). Modifying the replication of geminiviral vectors reduces cell death and enhances expression of biopharmaceutical proteins in *Nicotiana benthamiana* leaves. *Front. Plant Sci.* 9. doi: 10.3389/fpls.2018.01974

Dickey, A., Wang, N., Cooper, E., Tull, L., Breedlove, D., Mason, H., et al. (2017). Transient expression of lumbrokinase (PI239) in tobacco (*Nicotiana tabacum*) using a geminivirus-based single replicon system dissolves fibrin and blood clots. *Evid Based Complement Alternat Med.* 2017, 6093017. doi: 10.1155/2017/6093017

Eidenberger, L., Kogelmann, B., and Steinkellner, H. (2023). Plant-based biopharmaceutical engineering. *Nat. Rev. Bioeng.* 1, 426–439. doi: 10.1038/s44222-023-00044-6

Gengenbach, B. B., Opdensteinen, P., and Buyel, J. F. (2020). Robot cookies - plant cell packs as an automated high-throughput screening platform based on transient expression. *Front. Bioeng Biotechnol.* 8. doi: 10.3389/fbioe

Golubova, D., Tansley, C., Su, H., and Patron, N. J. (2024). Engineering *Nicotiana benthamiana* as a platform for natural product biosynthesis. *Curr. Opin. Plant Biol.* 81, 102611. doi: 10.1016/j.pbi.2024.102611

Granito, M., Alvarenga, L., Ribeiro, M., Carvalhosa, P., Andrade, T., Mesquita, C. T., et al. (2024). Nattokinase as an adjuvant therapeutic strategy for non-communicable diseases: a review of fibrinolytic, antithrombotic, anti-inflammatory, and antioxidant effects. *Expert Rev. Cardiovasc. Ther.* 22, 565–574. doi: 10.1080/14779072.2024.2416663

Han, L., Zhang, L., Liu, J., Li, H., Wang, Y., and Hasi, A. (2015). Transient expression of optimized and synthesized nattokinase gene in melon (*Cucumis melo* L.) fruit by agroinfiltration. *Plant Biotechnol.* 32, 175–180. doi: 10.5511/plantbiotechnology.15.0430a

Hiatt, A., Cafferkey, R., and Bowdish, K. (1989). Production of antibodies in transgenic plants. *Nature* 342, 76–78. doi: 10.1038/342076a0

Jain, A., Sondhi, N., Singh, K., and Kaur, J. (2024). Heterologous expression of nattokinase in E. coli: biochemical characterization and functional analysis of fibrin binding residues. *Arch. Biochem. Biophys.* 757, 110026. doi: 10.1016/j.abb.2024.110026

Jensen, G. S., Lenninger, M., Ero, M. P., and Benson, K. F. (2016). Consumption of nattokinase is associated with reduced blood pressure and von Willebrand factor, a cardiovascular risk marker: results from a randomized, double-blind, placebo-controlled, multicenter North American clinical trial. *Integr. Blood Press Control* 9, 95–104. doi: 10.2147/IBPC.S99553

Karki, U., Fang, H., Guo, W., Unnold-Cofre, C., and Xu, J. (2021). Cellular engineering of plant cells for improved therapeutic protein production. *Plant Cell Rep.* 40, 1087–1099. doi: 10.1007/s00299-021-02693-6

Knödler, M., Frank, K., Kerpen, L., and Buyel, J. F. (2023). Design, optimization, production and activity testing of recombinant immunotoxins expressed in plants and plant cells for the treatment of monocytic leukemia. *Bioengineered* 14, 2244235. doi: 10.1080/21655979.2023.2244235

Kopertekh, L. (2024). Improving transient expression in *N. benthamiana* by suppression of the Nb-SABP2 and Nb-COI1 plant defense response-related genes. *Front. Plant Sci.* 15. doi: 10.3389/fpls.2024.1453930

Liu, H., and Timko, M. P. (2022). Improving protein quantity and quality-the next level of plant molecular farming. *Int. J. Mol. Sci.* 23, 1326. doi: 10.3390/ijms23031326

Ma, T., Li, Z., and Wang, S. (2019). Production of bioactive recombinant reteplase by virus-based transient expression system in *Nicotiana benthamiana*. *Front. Plant Sci.* 10. doi: 10.3389/fpls.2019.01225

Manghwar, H., and Li, J. (2022). Endoplasmic reticulum stress and unfolded protein response signaling in plants. *Int. J. Mol. Sci.* 23, 828. doi: 10.3390/ijms23020828

Ni, H., Guo, P. C., Jiang, W. L., Fan, X. M., Luo, X. Y., and Li, H. H. (2016). Expression of nattokinase in *Escherichia coli* and renaturation of its inclusion body. *J. Biotechnol.* 231, 65–71. doi: 10.1016/j.jbiotec.2016.05.034

Ni, Z. Z., Li, J. T., Zhang, S. M., Dong, Y. W., Liu, Q. Q., Li, M. G., et al. (2023). Construction and functional analysis of nattokinase-producing cucumber obtained by the CRISPR-Cas9 system. *Acta Alimentaria* 52, 121–131. doi: 10.1556/066.2023.00000

Nosaki, S., Kaneko, M. K., Tsuruta, F., Yoshida, H., Kato, Y., and Miura, K. (2021). Prevention of necrosis caused by transient expression in *Nicotiana benthamiana* by application of ascorbic acid. *Plant Physiol.* 186, 832–835. doi: 10.1093/plphys/kiab102

Ranawaka, B., An, J., Lorenc, M. T., Jung, H., Sulli, M., Aprea, G., et al. (2024). Author Correction: A multi-omic *Nicotiana benthamiana* resource for fundamental research and biotechnology. *Nat. Plants.* 0, 193. doi: 10.1038/s41477-024-01618-x

Schiermeyer, A., Schinkel, H., Apel, S., Fischer, R., and Schillberg, S. (2005). Production of Desmodus rotundus salivary plasminogen activator alpha1 (DSPAalpha1) in tobacco is hampered by proteolysis. *Biotechnol. Bioeng.* 89, 848–858. doi: 10.1002/bit.20410

Shanmugaraj, B., Ravi, K., and Baladevan, K. (2025). Plant molecular farming: a promising frontier for orphan drug production. *Biotechnol. Lett.* 47, 56. doi: 10.1007/s10529-025-03596-2

Tanikawa, T., Yu, J., Hsu, K., Chen, S., Ishii, A., and Kitamura, M. (2024). Effect of nattokinase in D-galactose- and aluminum chloride-induced Alzheimer's disease model of rat. *In Vivo* 38, 2672–2679. doi: 10.21873/invivo.13744

Vaquero, C., Sack, M., Chandler, J., Drossard, J., Schuster, F., Monecke, M., et al. (1999). Transient expression of a tumor-specific single-chain fragment and a chimeric antibody in tobacco leaves. *Proc. Natl. Acad. Sci. U. S. A.* 96, 11128–11133. doi: 10.1073/pnas.96.20.11128

Voss, A., Niersbach, M., Hain, H. J., Hirsch, R., Liao, Y. C., Kreuzaler, R., et al. (1995). Reduced virus infectivity in N. tabacum secreting a TMV-specific full-size antibody. *Mol. Breeding.* 1, 39–50. doi: 10.1007/BF01682088

Wan, S., and Jiang, L. (2016). Erratum to: Endoplasmic reticulum (ER) stress and the unfolded protein response (UPR) in plants. *Protoplasma* 253, 765. doi: 10.1007/s00709-015-0852-z

Weng, Y., Yao, J., Sparks, S., and Wang, K. Y. (2017). Nattokinase: An oral antithrombotic agent for the prevention of cardiovascular disease. *Int. J. Mol. Sci.* 18, 523. doi: 10.3390/ijms18030523

Yan, G., Shu, M., Shen, W., Ma, L., Zhai, C., Wang, Y., et al. (2021). Heterologous expression of nattokinase from B. subtilis natto using *Pichia pastoris* GS115 and assessment of its thrombolytic activity. *BMC Biotechnol.* 21, 49. doi: 10.1186/s12896-021-00708-4

Yang, X. Y., Wang, S. L., Xue, W. C., Zhang, Y. P., Li, L. L., Luo, Z. H., et al. (2024). Nattokinase's neuroprotective mechanisms in ischemic stroke: targeting inflammation, oxidative stress, and coagulation. *Antioxid Redox Signal.* 42 (5), 228–248. doi: 10.1089/ars.2023.0527

Zhang, X., Shuai, Y., Tao, H., Li, C., and He, L. (2021). Novel method for the quantitative analysis of protease activity: the casein plate method and its applications. *ACS Omega.* 6, 3675–3680. doi: 10.1021/acsomega.0c05192

frontiers | Frontiers in Plant Science

TYPE Original Research
PUBLISHED 02 September 2025
DOI 10.3389/fpls.2025.1652246

OPEN ACCESS

EDITED BY
Kevin Yueju Wang,
University of Pikeville, United States

REVIEWED BY
Muhammad Junaid Anwar,
Bahauddin Zakariya University, Pakistan
Tariq Alam,
Clemson University, United States

*CORRESPONDENCE
Fabian Schubert
fabian.schubert@boku.ac.at
Eva Stoger
eva.stoeger@boku.ac.at

RECEIVED 23 June 2025
ACCEPTED 30 July 2025
PUBLISHED 02 September 2025

CITATION
Schubert F, Arcalís E, Kyral M, Jeitler B, Raith M, Swoboda I and Stoger E (2025) Bio-encapsulation of allergen-derivatives for specific immunotherapy. *Front. Plant Sci.* 16:1652246. doi: 10.3389/fpls.2025.1652246

Bio-encapsulation of allergen-derivatives for specific immunotherapy

Fabian Schubert[1]*, Elsa Arcalís[1], Maximilian Kyral[1], Barbara Jeitler[2], Marianne Raith[2], Ines Swoboda[2] and Eva Stoger[1]*

[1]Institute of Plant Biotechnology and Cell Biology, Department of Biotechnology and Food Sciences, BOKU University, Vienna, Austria, [2]Research Center Molecular Biotechnoloy, The Molecular Biotechnology Section, University of Applied Sciences, Vienna, Austria

Allergen-specific oral immunotherapy is a disease-modifying treatment already established for respiratory allergies and tested for the treatment of several food allergies, with promising clinical and immunological outcomes. However, orally administered allergens must pass through the gastrointestinal tract, where they are exposed to proteolytic digestion. This study describes the design of multi-layered protein bodies (PBs) in *Nicotiana benthamiana* as a platform for allergen encapsulation, offering potential advantages for oral immunotherapy. By co-expression of three zein variants we generated multi-layered PBs with distinct core and shell structures containing derivatives of the major fish allergen parvalbumin. The specific layering and structural integrity of the PBs were confirmed by confocal microscopy. Correlative light and electron microscopy (CLEM), combined with immunolabelling, was then used to verify the exact position of the allergens in the different layers of the PBs. *In vitro* experiments simulating the gastrointestinal digestion process revealed a significantly increased, layer-specific resistance of PB-encapsulated allergens compared to soluble allergens. Additionally, the uptake of PBs by human intestinal epithelial cells was simulated using Caco-2 cells. Our work provides further insight into protein storage organelle formation and novel bioencapsulation strategies to produce customized delivery vehicles, whose compartments may offer increased protection against enzymatic degradation and support prolonged persistence upon oral administration.

KEYWORDS

molecular farming, bioencapsulation, recombinant pharmaceuticals, storage organelles, allergen, plant-based production

1 Introduction

Allergies, including food, seasonal, and skin allergies, affect a significant portion of the global population, with approximately 20-30% of people worldwide reporting at least one allergic condition (Alska et al., 2025). One major factor contributing to the development of allergies is the deregulation of immune tolerance. This initiates an exaggerated immune response (Baloh et al., 2022) to harmless substances such as food proteins, animal hair or pollen leading to allergic diseases (Maeda et al., 2019). Symptoms of allergic diseases range from sneezing, itching and other mild symptoms to severe consequences such as anaphylactic reactions (Deschildre and Lejeune, 2018). Allergic diseases tend to gradually worsen over time and develop into chronic conditions that can significantly impair a patient´s quality of life. Additionally, they place a considerable demand on the healthcare system, highlighting the crucial necessity for more effective therapeutic solutions (Cosme-Blanco et al., 2020; Fendrick and Baldwin, 2001). Traditional methods of allergy treatment focus primarily on allergen avoidance and symptom management through pharmacological intervention (Iweala et al., 2018; Tenero et al., 2023). However, these approaches fail to address the underlying causes of allergies and thus may not offer long-term improvement. This is why allergen-specific immunotherapy has been developed and remains the only disease-modifying therapy option for allergic diseases to date (Alvaro-Lozano et al., 2020). However, the standard subcutaneous allergen immunotherapy often has significant drawbacks (Incorvaia et al., 2023). These include the risk of local and systemic allergic reactions and the time-consuming nature of the therapy, which requires regular visits to a medical office over an extended period (Özdemir et al., 2023). Therefore, there is an increasing need to explore alternative routes of administration for allergens to enhance the convenience and safety of immunotherapy. One promising approach is oral allergen-specific immunotherapy (Jones et al., 2014). As an alternative to subcutaneous immunotherapy, oral administration of gradually increasing doses of allergens has shown considerable efficacy for achieving desensitization and immune tolerance (Iweala et al., 2018; Kulis et al., 2018). Additionally, oral administration can trigger a cascade where the interaction with antigen-presenting cells in the gastrointestinal tract induces regulatory T cells, leading to immunosuppression (Vickery et al., 2011). This process, known as oral tolerance, is facilitated by cytokines, which suppress inflammatory responses and prevent allergic reactions (Fu et al., 2006). Over time, repeated exposure to initially low-dose and gradually increasing amounts of the allergen can shift the immune response from an allergic Th2 profile to a more tolerogenic state, reducing hypersensitivity (Trogen et al., 2022). Beyond the exploration of alternative routes for allergen uptake, another critical focus for enhancing safety is the modification of allergens to create hypoallergenic variants. These variants are specifically designed to retain immunological activity while minimizing the potential to induce allergic reactions due to a reduced IgE binding capacity (Reginald et al., 2024). An example of this is the hypoallergenic version of parvalbumin, the major fish allergen (Swoboda et al., 2007). Although hypoallergenic parvalbumin offers the advantage of reducing allergic reactions, it also presents challenges. These include a reduced efficacy during oral immunotherapy, likely due to decreased stability (Freidl et al., 2020). This emphasizes the need for strategies to preserve the structural and functional integrity of orally administered allergens, especially during the gastrointestinal digestion phase. Encapsulating active components within protective matrices - such as liposomes, polymers, or protein-based carriers - mimic natural biological systems. One example is the structural protection of proteins within food matrices, which can enhance the stability and bioavailability of native allergens (Onwulata, 2012). A clinically relevant example is Palforzia®, an FDA-approved oral immunotherapy for peanut allergy. It consists of precisely dosed, defatted peanut flour administered with semi-solid food to promote immune tolerance through gradual allergen exposure while minimizing systemic allergic reactions (Berglund et al., 2017). In addition, encapsulation allows for more precise allergy management by enhancing allergen stability and potentially supporting prolonged persistence and exposure during gastrointestinal passage (Guo et al., 2021; Shutava and Lvov, 2012). It has been demonstrated with biopolymers that tailoring the structure and composition of the encapsulation matrix *in vitro* can influence the release kinetics and target specific sites within the body for allergen delivery (Drosou et al., 2017; Estevinho and Rocha, 2018). Therefore, the use of protective and biocompatible polymers may offer a useful strategy to improve the stability, safety and effectiveness of different oral delivery systems.

Zein, a prolamin protein, is the main storage protein in maize. The hydrophobic nature of zein promotes the formation of stable, self-assembled structures, called protein bodies (PBs). PBs have been successfully explored as drug carriers through *in vitro* loading (Lai and Guo, 2011; Liu et al., 2005). Due to its unique functional properties zein has also great potential for the encapsulation of allergens (Drosou et al., 2017; Schwestka et al., 2020). Various studies showed that zeins are resistant to digestion, indicating that the encapsulated allergens may remain intact until they reach target sites in the gastrointestinal immune system (Li et al., 2022; Zou and Gu, 2013). This slow and sustained release of allergens could be especially advantageous for oral immunotherapy, as it may help minimize the risk of systemic allergic reactions and increase the likelihood of uptake by gut-associated lymphoid tissues, which play a key role in inducing immune tolerance (Brayden et al., 2005). During normal biological processes, endogenous zein PBs form intracellularly in maize endosperm tissues, but ectopic PBs can also be induced in vegetative organs such as leaves (Llop-Tous et al., 2010). Given that plants are excellent production systems for recombinant therapeutic proteins and have the natural ability to form PBs, it is appealing to utilize plant hosts for *in vivo* microencapsulation. This can be done by directly incorporating recombinant proteins into protein storage organelles (Hofbauer et al., 2016; Whitehead et al., 2014). We have recently shown that the formation of multi-layered ectopic PBs in *N. benthamiana* leaves can be induced by selected combinations of zeins (Schwestka et al., 2023). In particular, the N-terminal part of 27-kDa-γ-zein, also known as Zera, directs the fused protein into the outer shell of the PBs, while the fusion to the 15-kDa-β-zein targets

it to the core (Schwestka et al., 2023). We speculate that the encapsulation of allergens within these specialized structures may add an innovative advantage to oral immunotherapy by increasing allergen stability and enabling prolonged persistence throughout the digestive tract.

In order to establish multi-layer zein PBs as an effective bio-encapsulation platform for allergens, it is important to clarify several key questions. These include whether allergens can be directed to distinct protein body layers (PB layers), how this affects their digestive stability during gastric and intestinal phases and whether multi-layered PBs are efficiently taken up by intestinal cells. In the present study, we employ *Nicotiana benthamiana* for in-planta bio-encapsulation of both wild-type and hypoallergenic (mutant) parvalbumin to enhance their persistence in the gastrointestinal tract. We demonstrate the incorporation of the allergens into two distinct PB layers and confirm their uptake into intestinal epithelial cells. Additionally, we evaluate the protective effect of layer-specific encapsulation through simulated digestion.

2 Materials and methods

2.1 Constructs for plant transformation

A synthetic sequence coding for carp parvalbumin Cyp c 1 wild-type (CW, accession number AJ292211), was ordered in a pUC57 vector backbone (GeneCust, Boynes, France). Mutations at amino acid positions 52 and 93, as well as 54 and 91 – previously identified as key substitutions for generating a hypoallergenic variant (Swoboda et al., 2007) – were introduced via site-directed mutagenesis using two rounds of PCR with mismatched primers. Primers 5′-AGG TCT CGT CTG CTG GAG ATG GCA AGA TTG GAG-3′ and 5′-AGG TCT CAC TTG GGC AAT GAC AGC AAA GGC CTT C-3′ were used to introduce mutations at codons 93 and 52, respectively. Similarly, primers 5′-AGG TCT CCC AAG CCA AGA GCG GCT TCA TTG AG-3′ and 5′-AGG TCT CAC AGA GGC TCC AGC TTT CAG GAA GGC-3′ were used to target codons 54 and 91.

The mutated sequences were digested with BsaI and ligated, forming a new plasmid containing the carp mutant (CM) sequence. Next, we utilized pre-existing zein-fluorophore fusion vectors containing the fusion proteins 15-kDa-β-zein-mCherry and the N-terminal part of 27-kDa-γ-zein also known as Zera-EGFP (Schwestka et al., 2023). These vectors were digested with Kpn2I and SalI to replace the fluorophore coding regions by the wild-type and mutated allergen sequences (Schwestka et al., 2023), resulting in the final constructs Zera-CWF (pTRA-Zera-CWF), Zera-CMF (pTRA-Zera-CMF), 15-kDa-β-zein-CWF (pTRA-bz15-CWF) and 15-kDa-β-zein-CMF (pTRA-bz15-CMF) (Supplementary Figure S1).

2.2 Biological material and transformation

N. benthamiana plants were grown in soil under a 16-hour photoperiod with 70% relative humidity and temperatures of 26°C during the day and 16°C at night. The plants were cultivated for a minimum of 4 weeks in this environment. Plant expression vectors were transferred into chemically competent *Rhizobium radiobacter* (commonly known and hereafter referred to as *Agrobacterium tumefaciens)* GV3101 containing the helper plasmid pMP90RK (Koncz and Schell, 1986). *A. tumefaciens* cultures containing the above-described constructs as well as cultures containing 15-kDa-β-zein-mCherry, 16-kDa-γ-zein-BFP and the N-terminal part of 27-kDa-γ-zein-EGFP (Zera-EGFP) (Schwestka et al., 2023), were inoculated from glycerol cryo-stocks and grown in Yeast Extract Beef Broth (YEB medium: 5 g/L beef extract, 1 g/L yeast extract, 5 g/L peptone, 5 g/L sucrose, 0.5 g/L MgSO4, sterilized by autoclaving) with 20 mg/L rifampicin and 50 mg/L carbenicillin at 28°C, shaking at 200 rpm. Subsequently, cultures were pelleted by centrifugation at 3000 x g for 10 minutes and washed twice with infiltration medium (10 mM MES pH 5.6, 10 mM $MgCl_2$, 100 µM acetosyringone). The following *A.tumefaciens* strains were adjusted to an OD_{600} of 0.1 and combined prior to infiltration: Zera-CWF/CMF, 16-kDa-γ-zein-BFP and 15-kDa-β-zein-mCherry (*shell encapsulation*) and Zera-EGFP, 16-kDa-γ-zein-BFP and 15-kDa-β-zein-CMF/CWF (*core encapsulation*) (Figure 1B).

2.3 Extraction of protein bodies

Leaves were harvested 7 days post-infiltration (dpi) and homogenized into a fine powder with liquid nitrogen. The homogenate was suspended in phosphate buffered saline (PBS) supplemented with 2% Triton X-100, centrifuged for 20 minutes at 4300 rpm and the resulting pellet was subjected to several washes with PBS. The suspension was then passed through nylon membranes with decreasing pore sizes (180, 120, 60, 30 and 10 µm, Merck Millipore Ltd. Nylon, Burlington, USA) and the resulting filtrate was pelleted and resuspended in PBS. PBs were subsequently purified according to Schwestka et al., 2020 and Schwestka et al., 2023. Finally, the resuspended PBs were sonicated and loaded onto a CsCl cushion (density 1.45 g/cm3). The top layer containing the PBs was recovered, washed twice with PBS, and the final pellet was resuspended in PBS for subsequent use in the digestion and uptake assays.

2.4 Protein immunoblot analysis

Leaf tissue was harvested 7 dpi from plants transiently expressing either carp wild-type parvalbumin (CWF) or the mutant version (CMF), immediately frozen and ground to a fine powder. The samples were extracted with four volumes (w/v) of chilled extraction buffer (2% Triton X-100 in PBS) and incubated on ice for 15 minutes. The supernatant was used for immunoblotting and the pellet was resuspended in 1.5x reducing Laemmli buffer, incubated at 37°C for 1 hour and centrifuged at 16,000 x g for 5 minutes prior to immunoblot analysis. A polyclonal antiserum against the flag-tag was used as a primary antibody at a 1:20,000 dilution, followed by an anti-rabbit-HRP antibody at the same dilution (Promega, Madison, USA). Samples were analyzed in three independent biological replicates.

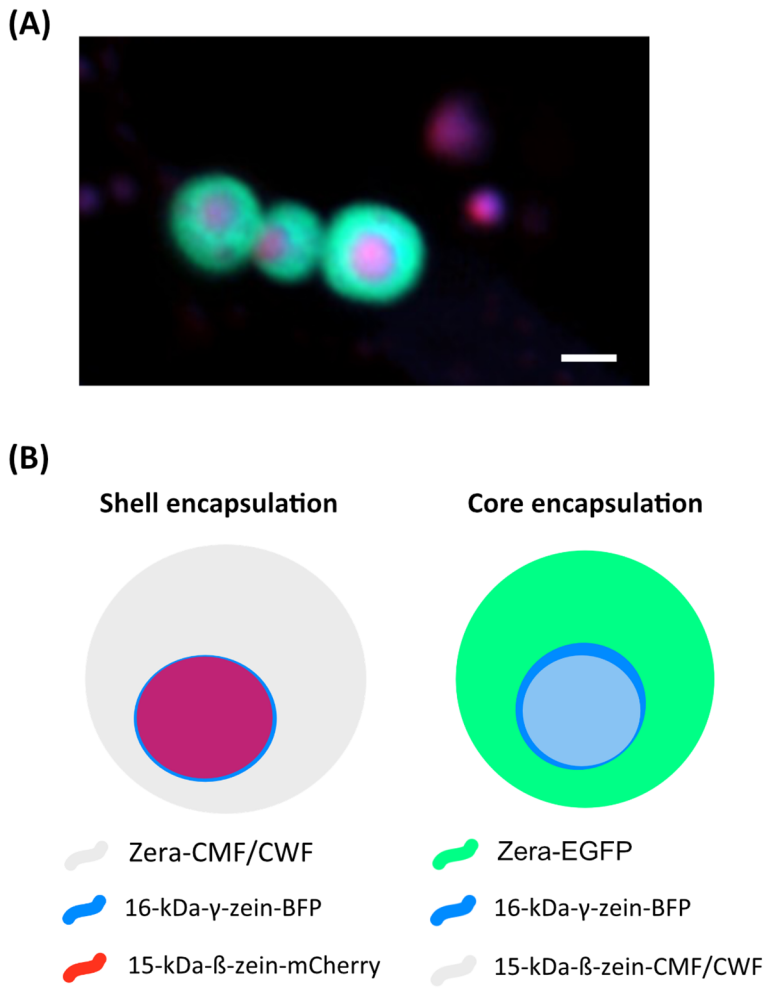

FIGURE 1
Encapsulation strategy of wild-type (CWF) and mutant parvalbumin fusions (CMF) in multilayered protein bodies. **(A)** Fluorescent protein bodies (Zera-EGFP, 16-kDa-γ-zein-BFP and 15-kDa-ß-zein-mCherry, as previously also described in Schwestka et al., 2023). The outer shell is indicated by GFP, while the core contains both BFP and mCherry. Notably, the BFP and mCherry signals do not fully co-localise. **(B)** Encapsulation strategies for CWF/CMF, derived from the setup shown in **(A)** Bar 1 µm.

For suspensions of isolated PB as described in 2.3, samples were mixed with 4x reducing Laemmli buffer and heated at 80°C for 5–10 minutes. Immunoblot analysis was performed according to standard protocols and as described previously (Schwestka et al., 2023). Rabbit antiserum raised against the carp parvalbumin mutant – produced according to the protocol described by Freidl et al., 2020 and manufactured by Charles River Laboratories, Miserey, France - was diluted 1:20,000 and used as the primary antibody, recognizing both the wild-type and the mutant forms of the allergen (Freidl et al., 2020). An anti-rabbit-HRP antibody diluted 1:20,000 (Promega, Madison, USA) was used as a secondary antibody. The analyses were performed in three biological replicates.

2.5 Flow cytometry

PBs were isolated from 16.8 g leaf material and resuspended in one mL of PBS. The particles were quantified using a flow cytometer (CytoFlex S; Beckman Coulter, Brea, USA) in a V-bottom 96-well plate, with 50,000 events recorded per sample. GFP and mCherry fluorescence were excited at 488 nm and 561 nm, respectively, and emissions were detected at 525 nm (GFP) and 610 nm (mCherry). Gain settings were configured to 25 for forward scatter, 4 for side scatter, 8 for GFP, and 41 for mCherry. Each sample was analyzed at three dilutions (1:10, 1:100, and 1:1000), with measurements performed in triplicates.

2.6 Confocal laser scanning microscopy

Live cell imaging was used to assess the expression and deposition of labelled proteins into PBs as previously described (Schwestka et al., 2023). Thus, purified PB suspension or small pieces of infiltrated leaves (7 dpi) were examined under a Leica SP8 or a Zeiss LSM980 confocal microscope. Representative images from at least three biological replicates were analyzed using the

softwares Leica LASX (Leica Microsystems, Wetzlar, Germany) or Zeiss ZEN lite (Carl Zeiss Microscopy, Jena, Germany).

2.6.1 Localization of encapsulated CWF/CMF

In order to investigate the localization of the allergen fusions in the *shell encapsulation*, immunofluorescence analysis was performed on fresh tissue. Small tissue sections were excised from infiltrated leaves (7 dpi) with a razor blade and fixed in 4% paraformaldehyde in cacodylate buffer (0.1 M, pH 7.4) for 2h at room temperature. After several washes in cacodylate buffer (0.1 M, pH 7.4), cross sections (120 µm) were obtained with a vibratome. Subsequently, sections were dehydrated and rehydrated through an ethanol series, washed in phosphate buffer (0.1 M, pH 7.6) and incubated in 2% (w/v) cellulase Onozuka R-10 (from *Trichoderma viride*) in phosphate buffer (0.1 M, pH 7.4) for 1 h at room temperature. Subsequently, the sections were incubated in 5% (w/v) BSA (Fraction V) in phosphate buffer to block non-specific binding sites, followed by overnight incubation at 4°C with a 1:200 dilution of serum from an immunized rabbit that recognizes both the wild-type and the mutant forms of the allergen (Freidl et al., 2020). The immunostaining was visualized using an Alexa Fluor 488-conjugated donkey anti-rabbit antibody (Thermo Fisher Scientific, Waltham, USA). Sections were then mounted in 50% glycerol in PBS and observed in a confocal laser scanning microscope LSM980-AiryScan2 (Carl Zeiss Microscopy, Jena, Germany).

For the *core encapsulation* of the allergen, a visualization strategy distinct from the one used for the shell encapsulation was employed, allowing access to the core of the purified PBs. The PBs were high pressure frozen and freeze substituted as described in Huber et al., 2024. Briefly, 100 µL of PB suspension were pelleted by centrifugation, and subsequently dried at room temperature for 1 hour before the pelleted material was placed into the wells of aluminum Type B carriers (Science Services, Munich, Germany), with 1-hexadecene as a cryoprotectant. The samples were then high pressure frozen and freeze substituted in 0.2% glutaraldehyde and 0.2% uranyl acetate in anhydrous acetone. Samples were further infiltrated and embedded in HM20 resin (Polysciences, Warrington, USA) and then polymerized under UV light. Sections showing silver interferences were collected onto formvar coated finder grids to facilitate the correlation of the regions of interest for correlative light and electron microscopy (CLEM).

To enable precise localization of the encapsulated allergen within these resin-embedded PBs, sections were subjected to immunogold labelling, as described in Schwestka et al., 2023. In short, sections were blocked with 5% (w/v) bovine serum albumin in 0.1M phosphate buffer (pH 7.4) and incubated with the rabbit antiserum raised against the carp parvalbumin mutant (Freidl et al., 2020). Gold-conjugated donkey-anti-rabbit antibodies were used for visualization.

For CLEM, grids were first examined under the confocal microscope as described by Chambaud et al., 2023 and several regions of interest were selected. Following, grids were carefully recovered, air dried and the previously selected regions of interest were imaged under a FEI Tecnai G2 transmission electron microscope (TEM). Natural landmarks such as shape and size of the PBs were used to correlate confocal and TEM images using the landmark correlation tool of ImageJ and the ec-CLEM plugin (Paul-Gilloteaux et al., 2017) of the Icy software (De Chaumont et al., 2012). Representative images showing GFP fluorescence and immunogold from 3 biological replicates are presented.

2.7 PB uptake into Caco-2 cells

To study cellular uptake of PBs, Caco-2 cells (HTB-37, ATCC, Manassas, USA) were utilized. Cells were cultured according to the standard procedure described by Wanes et al., 2021 on ACLAR® fluoropolymer foil (Science Service, Munich, Germany) pre-treated with UV light for 30 minutes to reduce potential contaminants. Approximately 70,000 PBs per cm^2, suspended in PBS and quantified by flow cytometry, were incubated with the cells for 24 hours. Following incubation, the medium was removed, and the cells were washed twice with PBS and subjected to confocal laser scanning microscopy (CLSM) or further prepared for electron microscopy. For confocal microscopy, cells were incubated in CellBrite® for 45 minutes and then fixed in 2% paraformaldehyde (PFA). Samples were washed twice in PBS prior to imaging under a Leica SP8 CLSM. For electron microscopy, Caco-2 cells growing on ACLAR® foil were fixed by cutting small pieces of foil (2x2 mm), immediately fixed in 2.5% glutaraldehyde and 2% paraformaldehyde in cacodylate buffer (0.15 M pH 7.4), and further processed as described in Arcalís et al., 2020. In short, double osmium impregnation was applied by post-fixing the cells in 2% osmium tetroxide added with 0.2% ruthenium red in 0.15 M cacodylate buffer, followed by thiocarbohydrazide solution (1% w/v in dH2O) and an additional incubation with 2% osmium tetroxide in dH2O. Subsequently, cells were incubated in UAR-EMS Uranyl Acetate Replacement Stain (1:4 v/v), followed by Walton's lead aspartate stain (20 mM lead nitrate in 30 mM L-aspartic acid solution). Next, samples were dehydrated through an ethanol series with a final step in pure acetone. Samples were then progressively infiltrated in LV Resin, embedded and polymerized at 60°C for 48 h. Resulting blocks were trimmed and sectioned. 200 nm sections were mounted on silicon wafers and an SEM stub prior to imaging under an Apreo SEM (Thermo Fisher Scientific, Waltham, USA), operating in Optiplan mode (2kV, 0.1 nA).

2.8 Digestion stability assay

To test the digestive stability of the encapsulated proteins, we adapted the protocol from Moreno et al., 2005 by scaling down the reaction volume from 2.2 mL to 1.6 mL. The soluble wild-type (CW) and mutant (CM) allergens were adjusted to a concentration of 1.59 mg/mL. To determine the amount of leaf tissue required to obtain comparable starting quantities of PB-encapsulated allergen, immunoblot analyses were performed. The results indicated that 20 mg of leaf tissue contained approximately 5 µg of PB-encapsulated allergen. Before starting the digestive stability assay, aliquots from CWF and CMF were taken to establish a reference value at timepoint 0 (G-0). The digestion procedure was carried out

under defined simulated gastric conditions (182 U Pepsin/mg protein in 1x simulated gastric fluid containing 0.15 M NaCl, pH 3) and simulated intestinal conditions (34.5 U trypsin/mg protein and 0.44 chymotrypsin/mg protein, 25 mM Bis-Tris and 9.2 mM CaCl2, pH 7). After stopping the digests, all aliquots were immediately frozen at -20°C until further analysis by immunoblotting. Detection was performed using a rabbit antiserum raised against mutant carp parvalbumin (Freidl et al., 2020) and a secondary anti-rabbit-HRP antibody. For the evaluation of the immunoblot results, band intensity profiles were analyzed using ImageLab software (Bio-Rad Laboratories, Inc, Hercules, USA). The signal intensity of each band was normalized to the reference band at G-0 and plotted against the total digestion time. Quantitative estimates were based on a minimum of three independent biological replicates (n = 3), and data were analyzed using GraphPad Prism (GraphPad Software, LLC, San Diego, USA). Statistical significance was assessed using two-way ANOVA followed by Dunnett´s multiple correction.

3 Results

3.1 Encapsulation of parvalbumin within multi-layered protein bodies

Based on previous studies by Schwestka et al., 2023, we employed a combination of 16-kDa-γ-zein, Zera (partial 27-kDa-γ-zein), and 15-kDa-β-zein to induce the *in vivo* formation of multi-layered protein bodies with distinct layers in *Nicotiana benthamiana*. To facilitate visual tracking, two of the zeins were fused to fluorescent proteins. The third (either 15-kDa-β-zein or Zera) was fused to carp parvalbumin variants, causing the incorporation of the fish allergen either in the core or the shell of the PBs (Figure 1).

In order to encapsulate the allergen within the core of insoluble protein bodies, wild-type parvalbumin (CWF) or its hypoallergenic version (CMF) were fused to 15-kDa-β-zein. To achieve incorporation in the PB shell, they were fused to Zera (Supplementary Figure S1). We then co-expressed each of the zein-allergen fusion proteins with the two fluorescently labelled complementary zeins to obtain multi-layered PBs. Seven days after infiltration of *N. benthamiana*, the crude leaf extract was separated into soluble and pellet fractions as described in Schwestka et al., 2023 and analyzed by immunoblot detection (Figure 2). Distinct allergen-containing bands at 25 kDa (Zera-CWF/CMF) and 30 kDa (15-kDa-β-zein-CMF/CWF), along with some higher molecular mass bands likely representing incompletely reduced polymers, appeared only in the PB-containing pellet fractions (Figure 2). In the supernatants, only faint bands could be detected, confirming the incorporation of the wild-type and mutant parvalbumin into the PBs. To further confirm these findings, immunoblot analysis was also performed with the enriched PB fractions. These fractions displayed a banding pattern similar to that observed in the crude extract, with strong signals for both the Zera- and 15-kDa-β-zein fusion proteins at the respective positions (Supplementary Figure S2).

The incorporation of the allergen within PBs was further investigated by correlative light and electron microscopy, taking advantage of the fluorescent protein tags. For the shell encapsulation of the allergen, PBs in the cytoplasm of *N. benthamiana* revealed a red and blue fluorescent core (≤1 µm in size), representing the 15-kDa-β-zein-mCherry and 16-kDa-γ-zein-BFP (Supplementary Figures S3, S4A). The presence of parvalbumin was determined via immunofluorescence (Figure 3), which revealed a ring-shaped distribution of the allergen surrounding the fluorescent core. This is consistent with the expected localization of a Zera-fused

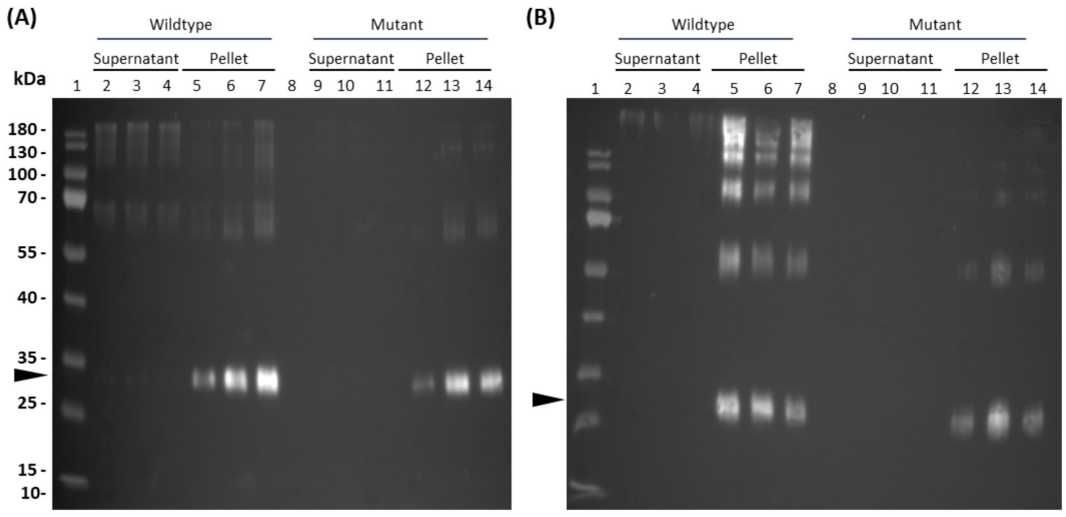

FIGURE 2
Detection of parvalbumin-derivatives from multilayered PBs of crude leaf extracts (7 dpi). Flag-tagged parvalbumin wild-type and mutant proteins were detected in immunoblots of crude leaf extracts using a polyclonal antibody against the flag-tag. **(A)** Core-encapsulation of the 15-kDa-β- zein-CWF (lanes 2-7) and 15-kDa-β- zein-CMF (lanes 9-14) fusion protein. **(B)** Shell-encapsulation of the Zera-CWF (2-7) and Zera-CMF (9-14) fusion protein. The arrows indicate the expected molecular mass of the fusion proteins 15-kDa-β- zein-CMF and 15-kDa-β- zein-CWF **(A)** and Zera-CWF and Zera-CMF **(B)**.

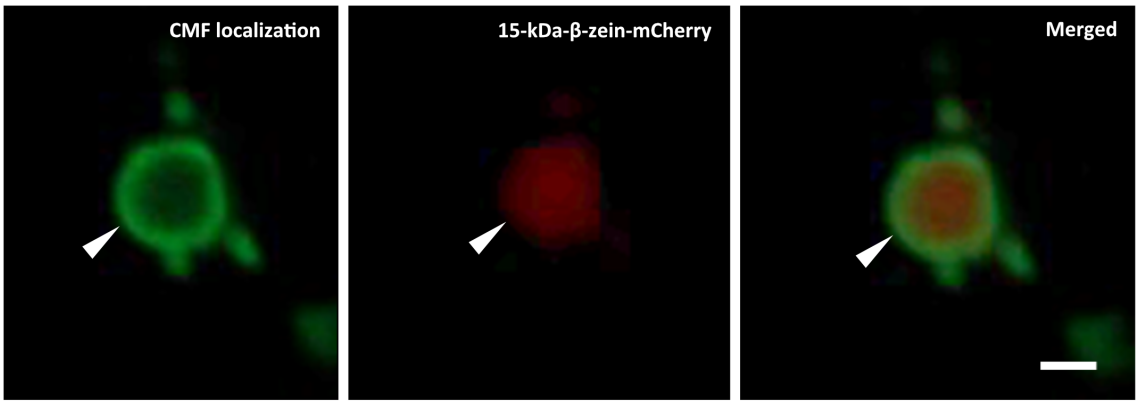

FIGURE 3
Shell encapsulation of mutant parvalbumin. Co-expression of Zera-CMF, 16-kDa-γ-zein-BFP, and 15-kDa-β-zein-mCherry. CMF localization was assessed by immunolocalization carried out on fixed vibratome sections. Rabbit serum recognizing both the wild-type and mutant form of the allergen served as primary antibody, followed by an Alexa Fluor 488-conjugated secondary antibody. First panel: Immunolocalization of CMF in the shell of the protein body completely surrounding the β-zein core; second panel: 15-kDa-β-zein-mCherry. Overlay images in the third panel reveal the spatial distribution of the signals within the PBs. CLSM images. Bar 1 µm.

protein within a multilayered PB measuring ≥1 µm in diameter (Figure 1A) (Schwestka et al., 2023). No significant differences in localization within the PB were observed between wild-type parvalbumin and its mutant variant (Supplementary Figure S4B). In the case of the core encapsulation, green fluorescent protein bodies (≥1 µm in size) were detected in the transformed leaf cells, showing a central void with a signal for 16-kDa-γ-zein-BFP (Figure 4A; Supplementary Figure S4C). For the localization of the allergen, we opted for immunogold labelling of thin sections of the enriched PB pellet followed by electron microscopy in order to gain access to the core of the PB. The preservation of GFP fluorescence after HPF-FS facilitated the identification of the protein bodies within the section. The central areas of the protein bodies were devoid of green fluorescence and showed abundant gold probes instead, indicating the presence of the allergen within the protein body core (Figure 4B). No co-localization with GFP was observed, confirming a precise distribution of the different components within the PB (Schwestka et al., 2023).

3.2 Simulated gastrointestinal digestion

To assess whether bio-encapsulation enhances allergen persistence under proteolytic conditions, we first used soluble wild-type (CW) and mutant parvalbumin (CM) as controls in a simulated digestion process. Following pepsin addition, protein levels declined rapidly within the first minute. The final detectable band for CW was observed after 20 minutes, at which point only about 2% of the protein remained (Supplementary Figure S5; Supplementary Table S1). For CM, the last detectable signal appeared after 6 minutes, with less than 1% of the protein remaining (Figures 5, S5; Supplementary Table S1). This highlights the difference in stability between wild-type and mutant parvalbumin (Freidl et al., 2020). Next, an equivalent amount of wild-type and mutant parvalbumin, encapsulated within the core of PBs, was subjected to simulated gastric digestion. As shown in Figure 5 and Supplementary Table S1, it took 90 minutes for core-encapsulated mutant parvalbumin to be fully digested, and core-encapsulated wild-type parvalbumin remained detectable for even longer. Thus, encapsulation in the PB-core prolonged the persistence of both the wild-type and mutant allergen, with average signal intensities of 80% and 40% remaining after 20 minutes of digestion, respectively. Even after 90 minutes, both allergen variants were still detectable (Supplementary Table S1). We also compared the persistence of the shell-encapsulated allergen in a simulated digestion process. In contrast to core encapsulation, in which the amount of allergen decreased steadily, the allergens incorporated in the shell exhibited a clear and sudden drop in abundance after about 20 minutes in the gastric phase. Nevertheless, the shell-incorporated wild-type and mutant allergens exhibited greater stability than their soluble counterparts, with an average of 47% and 26% of the signal remaining after 20 minutes, respectively (Figure 5, Supplementary Table S1).

3.3 Uptake of the PBs into Caco-2 cells

To investigate whether multi-layered PBs can be internalized by intestinal epithelial cells, we exposed Caco-2 cells to the different PBs. To analyze their uptake into Caco-2 cells we employed various staining and microscopy techniques. After incubation in a PB suspension (core encapsulation of wild-type parvalbumin), CellBrite® was used to visualize intracellular membranes. A fluorescent membrane surrounding the PB was visible (Figure 6A), suggesting PB uptake by endocytosis. Indeed, the fluorescence intensity profile of this region showed a green peak, originating from Zera-EGFP and defining the perimeter of the PB. It was flanked by two additional peaks corresponding to CellBrite® labelled membranes (Figure 6B). PB uptake could also be confirmed by electron microscopy. Cross sections of Caco-2 cell monolayer cultures showed PBs enclosed within a membrane and located inside the cells (Figure 6C).

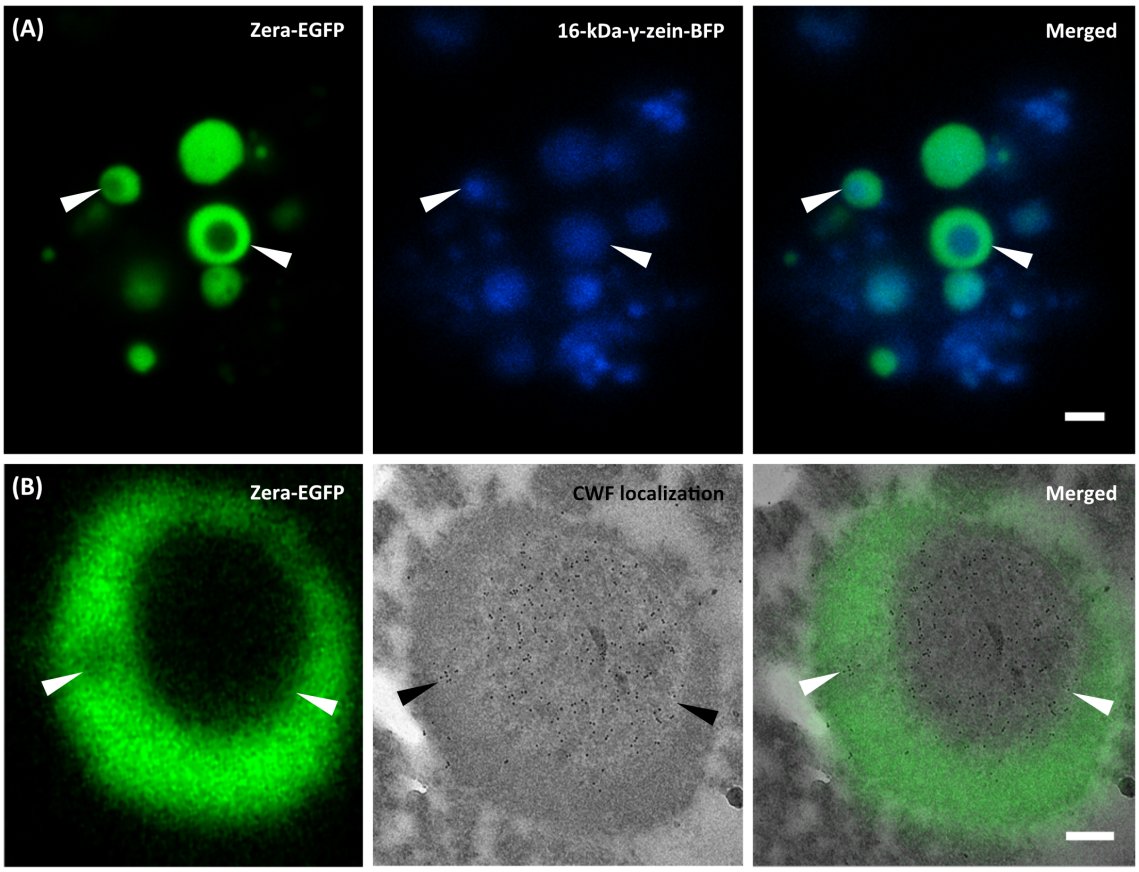

FIGURE 4
Core encapsulation of the wild-type parvalbumin. Co-expression of Zera-EGFP, 16-kDa-γ-zein-BFP, and 15-kDa-β-zein-CWF. **(A)** CLSM images of isolated PBs. First panel: Zera-EGFP; second panel: 16-kDa γ-zein-BFP; third panel: overlay of both channels. **(B)** First panel: CLSM image showing Zera-EGFP in resin-embedded PBs, prepared by high-pressure freezing and freeze substitution; second panel: CLEM image showing detection of wild-type parvalbumin via anti-parvalbumin antibody and 10 nm gold-labeled donkey anti-rabbit secondary antibodies. The third panel (overlay) reveals the spatial distribution of signals within the PBs. Bars 2 µm **(A)**, 0.25 µm **(B)**.

4 Discussion

This study presents the design of multi-layered PBs in *N. benthamiana* as a novel platform for allergen encapsulation. These structures offer promising advantages for oral immunotherapy, including enhanced control over allergen release and dosage, which may contribute to more effective and individualized allergy management. The successful generation of multi-layered PBs was achieved by the co-expression of three zeins: 16-kDa-γ-zein, Zera, and 15-kDa-β-zein, fused either to fluorescent tags or variants of the major fish allergen parvalbumin. As a result, PBs with distinct core and shell layers were formed, allowing precise allergen localization within the protein matrix. Confocal microscopy confirmed the clear layering of fluorescent labels, demonstrating the structural integrity of the PBs. Additionally, CLEM and immunofluorescence analysis showed the localization of the allergens in defined layers within the PBs. By combining high-resolution imaging, immunogold labelling and immunofluorescence, the exact positioning of the parvalbumins could be mapped, even in the absence of fluorescent labels.

One key finding of this study is the significantly increased resistance of PB-encapsulated parvalbumins to proteolytic degradation compared to their soluble counterparts. This characteristic is a critical factor for inducing robust and sustained oral tolerance (Freidl et al., 2020). We demonstrated that the soluble parvalbumin variants were no longer detectable after twenty minutes for the wild-type parvalbumin and after six minutes for the mutant parvalbumin during simulated gastric digestion. In contrast, core-encapsulated wild-type protein (CWF) remained detectable even after 60 minutes, and this was also observed for the core-encapsulated parvalbumin mutant (CMF), albeit to a lesser extent. Shell encapsulated parvalbumins demonstrated moderate stability, initially resisting proteolysis, but showing a sharp decline in abundance after twenty minutes. Nevertheless, even CMF remained detectable throughout the simulated gastric digestion. This enhanced protection against enzymatic gastric degradation is particularly important for oral administration, as the harsh conditions in the stomach often compromise the efficacy of protein therapeutics including mutant parvalbumin (Freidl et al., 2020; Han et al., 2024). Furthermore, the stability during the intestinal digestion phase was evaluated. While core encapsulation provided prolonged protection also against the simulated intestinal conditions, a gradual decrease in parvalbumin levels was observed over time, indicating the

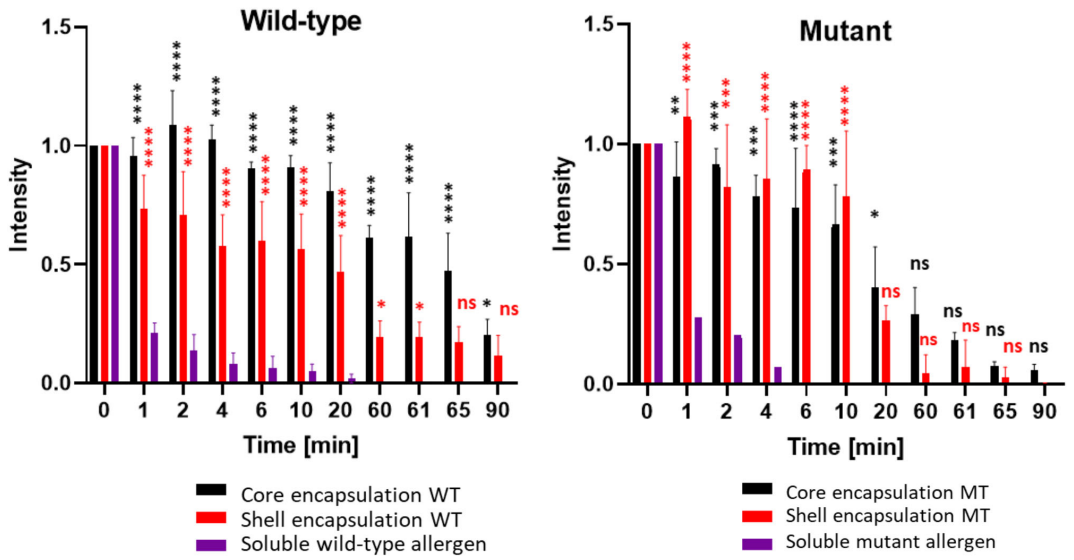

FIGURE 5
Encapsulated wild-type and mutant parvalbumins show higher resistance to simulated gastrointestinal digestion than the soluble proteins. The y-axis represents the relative signal strength compared to G-0 of the respective immunoblot. Detection was carried out using a rabbit antiserum recognizing both the mutant and wildtype carp parvalbumin. The x-axis represents the total digestion time in minutes. Gastric digestion was always started at G-0 by addition of pepsin to the samples (aliquots were taken after 1, 2, 4, 6, 10, 20, and 60 minutes). After 60 minutes, pepsin from the gastric phase was neutralized, and trypsin/chymotrypsin were added to the samples to initiate the intestinal phase (aliquots were taken after 61, 65 and 90 minutes). The values derived from three independent digests are shown (n = 3). A t-test to compare the allergen containing PBs with the soluble allergens was performed. Ns $p > 0.05$, *$p \leq 0.05$, **$p \leq 0.01$, ***$p \leq 0.001$, ****$p \leq 0.00001$.

progressive degradation of the protein. The continued persistence in both the gastric and intestinal phases highlights the potential of PBs as a delivery platform for therapeutic proteins requiring prolonged stability. The precise positioning of allergens within specific PB layers provides opportunities to fine-tune the release profile of encapsulated proteins. Thus, core encapsulation may support sustained release, while shell encapsulation might promote faster release.

Beyond stability, effective oral administration requires that the PBs are internalized by human intestinal epithelial cells, a key step for systemic absorption (Mohammed et al., 2022). This was simulated in our study by using Caco-2 cells, an established model for human intestinal epithelial cells (Bailey et al., 1996). Microscopy revealed that the PBs were surrounded by a fluorescently labelled membrane after internalization by Caco-2 cells, indicating uptake by endocytosis. Electron microscopy further confirmed that the PBs were present in intracellular vesicles within the Caco-2 cells. These results are in line with previous research that demonstrated the uptake of the peanut allergen Ara h1 into monocytes using microscopy, showing their internalization into vesicles that are likely part of the endolysosomal pathway (Price et al., 2017). This is a crucial step for antigen presentation and immune activation (van Kasteren and Overkleeft, 2014). While further studies are needed to understand the

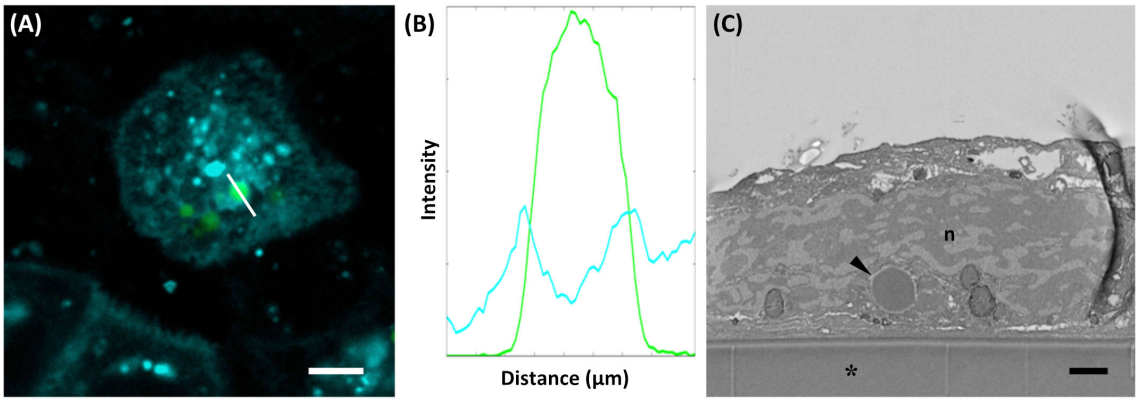

FIGURE 6
Uptake of PB by Caco-2-cells. **(A)** Cellbrite (cyan), visualizing intracellular membranes, and protein bodies (green). **(B)** Fluorescence intensity profile of the line indicated in **(A)**. Fluorescence intensity corresponds to the readout of the Leica LAS Software. **(C)** SEM cross section of a Caco-2 cell revealing protein bodies within the cytoplasm (arrowhead). Aclar foil (*), nucleus (n). Bars 5 µm **(A)**, 1 µm **(C)**.

mechanisms involved in the internalization of PBs by different cell types, the routing of PBs through the endolysosomal pathway supports their suitability for allergen immunotherapy.

Encapsulation of proteins for oral immunotherapy has proven advantageous in other studies using micro- or nanoparticles for this purpose (Jazayeri et al., 2021). Chimeric virus-like particles (VLPs), such as those based on hepatitis E (Jariyapong et al., 2013), Norwalk virus (Ball et al., 1998), HIV env (Takamura et al., 2004) and influenza (Serradell et al., 2019), have demonstrated protease resistance and strong immune responses after oral administration in animal models. Similarly, plant-made enveloped eBioparticles (eBPs) have been studied as an allergen expression platform in recent years. They are capable of inducing IgG responses and modulating dendritic cell activity in mice after administration (Busold et al., 2024; Gomord et al., 2020). In another study, eBPs carrying the peanut allergen Ara h 2 were produced in *N. bethamiana* with *A. tumefaciens*. After incubating sera from Ara h 2-sensitized patients with the eBPs, they measured a significant reduction in IgE binding potency and therefore an extensive decrease in the induction capacity of effector cell-driven allergic responses (Castenmiller et al., 2023). While VLPs have shown remarkable immunogenicity and some protection from gastrointestinal degradation (Serradell et al., 2019), PBs offer distinct advantages. PBs are fully plant-derived and self-assembled without the need for viral components, eliminating some biosafety concerns and simplifying downstream processing (Schwestka et al., 2023). Unlike VLPs, which often require complex multi-protein assembly and precise stoichiometry (Qin et al., 2023), PBs can form from a single fusion construct and are amenable to modular engineering (Hofbauer et al., 2016; Schwestka et al., 2023). Furthermore, PBs based on prolamin storage proteins such as zeins display natural resistance to digestive enzymes and acidic conditions, making them especially suitable for oral delivery (Luo et al., 2023). While VLPs and eBPs are well-established for injectable or mucosal applications, their production is often associated with challenges related to cost and regulatory complexity (Chen and Lai, 2013). PBs are based on cereal storage proteins that are part of the food chain and generally regarded as safe, and they can be rapidly produced in *N. benthamiana* by transient expression. Additionally, their multi-layered architecture offers new opportunities for tailoring antigen localization and release profiles.

PBs provide a particularly versatile platform for the *in planta* encapsulation of allergens. For example, endogenous PBs were utilized in a study where a hypoallergenic Bet v 1 tolerogen against birch pollen allergy was specifically expressed in the endosperm tissue of transgenic rice seeds (Wang et al., 2013). Fukuda et al., 2018 incorporated hypoallergenic forms of the major Japanese cedar pollen allergens into transgenic rice seed PBs. Oral immunotherapy in mice performed with such PBs led to the suppression of pollen-induced allergic conjunctivitis. Furthermore, these PBs even showed a protective effect against the development of allergic conjunctivitis, in experiments, where the transgenic rice was fed to mice prophylactically (Fukuda et al., 2018). Although the use of stable transgenic plants, particularly edible species, presents some advantages, their development remains a time-consuming and costly process. Moreover, the presence of endogenous storage proteins complicates the design of well-defined, multi-layered PBs. In contrast, transiently expressed PBs can be produced more rapidly and under controlled conditions, enabling the incorporation of the protein of interest either within the PB core or exposed on its surface. In addition, transient expression systems based on agroinfiltration are typically capable of achieving higher protein yields, rendering them well-suited for commercial production (Feng et al., 2022; Mardanova and Ravin, 2021; Nosaki et al., 2021; Suzaki et al., 2019).

Our study not only provides an advanced analysis of transiently expressed PBs for the encapsulation of allergens but also highlights several remaining issues. While our current findings are encouraging, they are based on *in vitro* analyses. Thus, *in vivo* studies using animal models are required to assess the efficacy, safety, and immunogenicity of PB-based delivery systems under physiological conditions. To further enhance their performance, the composition of PBs could also be optimized regarding stability and functionality. For example, incorporating alternative zein variants or fusion partners with suitable properties might additionally improve structural integrity under specific conditions. Furthermore, the development of stimuli-responsive PBs could also represent a future improvement towards producing adaptable PBs for diverse therapeutic applications. PB degradation could be triggered for example by certain environmental stimuli such as pH, temperature or enzymatic activity, potentially promoting allergen release under specific environmental conditions. However, for such advanced applications involving targeted delivery, a deeper understanding of the cellular mechanisms governing uptake, transport and degradation of PBs will be essential.

In conclusion, we have shown in this study that multi-layer PBs represent a robust and versatile system for the encapsulation of allergens. We were able to demonstrate precise localization of the major fish allergen derivatives, their enhanced stability during simulated gastric and intestinal digestion, and successful endocytic uptake. These findings highlight the potential of PBs as a delivery platform and provide a foundation for the further development of PB-based systems. Future animal studies using murine allergy models will be an essential next step to further evaluate the relevance of the platform for therapeutic strategies targeting allergic and other immune-related diseases.

Data availability statement

The original contributions presented in the study are included in the article/Supplementary Material. Further inquiries can be directed to the corresponding authors.

Ethics statement

Ethical approval was not required for the studies on animals in accordance with the local legislation and institutional requirements because only commercially available established cell lines were used.

Author contributions

FS: Conceptualization, Formal Analysis, Investigation, Methodology, Supervision, Visualization, Writing – original draft, Writing – review & editing. EA: Conceptualization, Writing – original draft, Writing – review & editing, Data curation, Formal Analysis, Investigation, Methodology, Validation, Visualization. MK: Data curation, Investigation, Methodology, Visualization, Writing – review & editing. BJ: Investigation, Methodology, Writing – review & editing. MR: Conceptualization, Data curation, Investigation, Methodology, Writing – review & editing. IS: Conceptualization, Data curation, Funding acquisition, Supervision, Writing – review & editing. ES: Conceptualization, Funding acquisition, Supervision, Validation, Writing – original draft, Writing – review & editing.

Funding

The author(s) declare financial support was received for the research and/or publication of this article. This research was funded in whole or in part by the Austrian Science Fund (FWF) (grant DOI: 10.55776/P34836 and 10.55776/DOC9173924). For open access purposes, the author has applied a CC BY public copyright license to any author-accepted manuscript version arising from this submission.

Acknowledgments

The authors would like to acknowledge technical support by the Institute of Colloid and Biointerface Science and the BOKU Core Facility for Multiscale Imaging.

Conflict of interest

The authors declare that the research was conducted in the absence of any commercial or financial relationships that could be construed as a potential conflict of interest.

The author(s) declared that they were an editorial board member of Frontiers, at the time of submission. This had no impact on the peer review process and the final decision.

Generative AI statement

The author(s) declare that no Generative AI was used in the creation of this manuscript.

Any alternative text (alt text) provided alongside figures in this article has been generated by Frontiers with the support of artificial intelligence and reasonable efforts have been made to ensure accuracy, including review by the authors wherever possible. If you identify any issues, please contact us.

Publisher's note

Supplementary material

The Supplementary Material for this article can be found online at: https://www.frontiersin.org/articles/10.3389/fpls.2025.1652246/full#supplementary-material

References

Alska, E., Doligalska, A., Napiórkowska-Baran, K., Dolina, M., Osińska, K., Pilichowicz, A., et al. (2025). Global burden of allergies: mechanisms of development, challenges in diagnosis, and treatment. *Life* 15, 878. doi: 10.3390/life15060878

Alvaro-Lozano, M., Akdis, C. A., Akdis, M., Alviani, C., Angier, E., Arasi, S., et al. (2020). EAACI allergen immunotherapy user's guide. *Pediatr. Allergy Immunol.* 31, 1–101. doi: 10.1111/pai.13189

Arcalís, E., Hörmann-Dietrich, U., Zeh, L., and Stoger, E. (2020). 3D electron microscopy gives a clue: maize zein bodies bud from central areas of ER sheets. *Front. Plant Sci.* 11. doi: 10.3389/fpls.2020.00809

Bailey, C. A., Bryla', P., and Malick, A. W. (1996). The use of the intestinal epithelial cell culture model, Caco-2, in pharmaceutical development. *Advanced Drug Delivery Rev.* 22 (1-2), 85-103. doi: 10.1016/S0169-409X(96)00416-4

Ball, J. M., Hardy, M. E., Atmar, R. L., Conner, M. E., and Estes, M. K. (1998). Oral immunization with recombinant norwalk virus-like particles induces a systemic and mucosal immune response in mice. *J. OF Virol.* 72, 1345-1353. doi: 10.1128/jvi.72.2.1345-1353.1998

Baloh, C. H., Huffaker, M. F., and Laidlaw, T. (2022). Biomarkers and mechanisms of tolerance induction in food allergic patients drive new therapeutic approaches. *Front. Immunol.* 13. doi: 10.3389/fimmu.2022.972103

Berglund, J. P., Szczepanski, N., Penumarti, A., Beavers, A., Kesselring, J., Orgel, K., et al. (2017). Preparation and analysis of peanut flour used in oral immunotherapy clinical trials. *J. Allergy Clin. Immunology: In Pract.* 5, 1098–1104. doi: 10.1016/j.jaip.2016.11.034

Brayden, D. J., Jepson, M. A., and Baird, A. W. (2005). Keynote review: Intestinal Peyer's patch M cells and oral vaccine targeting. *Drug Discov. Today*. 10 (), 1145-1157. doi: 10.1016/S1359-6446(05)03536-1

Busold, S., Aglas, L., Menage, C., Desgagnés, R., Faye, L., Fitchette, A. C., et al. (2024). Plant-produced Der p 2-bearing bioparticles activate Th1/Treg-related activation patterns in dendritic cells irrespective of the allergic background. *Clin. Exp. Allergy*. doi: 10.1111/cea.14456

Castenmiller, C., Stigler, M., Kirpas, M. E., Versteeg, S., Akkerdaas, J. H., Pena-Castellanos, G., et al. (2023). Plant-based enveloped Ara h 2 bioparticles display exceptional hypo-allergenicity. *Clin. Exp. Allergy*. 53, 577-581. doi: 10.1111/cea.14294

Chambaud, C., Cookson, S. J., Ollat, N., Bernard, A., and Brocard, L. (2023). Targeting Ultrastructural Events at the Graft Interface of Arabidopsis thaliana by A Correlative Light Electron Microscopy Approach. *Bio Protoc.* 13 (2), e4590. doi: 10.21769/BioProtoc.4590

Chen, Q., and Lai, H. (2013). Plant-derived virus-like particles as vaccines. *Hum. Vaccines&Immunotherapy*. 9 (1), 26-49. doi: 10.4161/hv.22218

Cosme-Blanco, W., Arroyo-Flores, E., and Ale, H. (2020). Food allergies. *Pediatr. Rev.* 41, 403–415. doi: 10.1542/pir.2019-0037

De Chaumont, F., Dallongeville, S., Chenouard, N., Hervé, N., Pop, S., Provoost, T., et al. (2012). Icy: An open bioimage informatics platform for

extended reproducible research. *Nat. Methods*. 9 (7), 690–696. doi: 10.1038/nmeth.2075

Deschildre, A., and Lejeune, S. (2018). How to cope with food allergy symptoms? *Curr. Opin. Allergy Clin. Immunol.* 18, 234–242. doi: 10.1097/ACI.0000000000000447

Drosou, C. G., Krokida, M. K., and Biliaderis, C. G. (2017). Encapsulation of bioactive compounds through electrospinning/electrospraying and spray drying: A comparative assessment of food-related applications. *Drying Technol.* 35 (2), 139-162. doi: 10.1080/07373937.2016.1162797

Estevinho, B. N., and Rocha, F. (2018). "Chapter 7 - Application of Biopolymers in Microencapsulation Processes," in *Handbook of Food Bioengineering, Biopolymers for Food Design*. Eds. A. M. Grumezescu and A. M. Holban (Academic Press), 191–222. doi: 10.1016/B978-0-12-811449-0.00007-4

Fendrick, A. M., and Baldwin, J. L. (2001). Allergen-induced inflammation and the role of immunoglobulin E (IgE). *Am. J. Ther.* 8, 291–297. doi: 10.1097/00045391-200107000-00011

Feng, Z., Li, X., Fan, B., Zhu, C., and Chen, Z. (2022). Maximizing the production of recombinant proteins in plants: from transcription to protein stability. *Int. J. Mol. Sci.* 23, 13516. doi: 10.3390/ijms232113516

Freidl, R., Gstöttner, A., Baranyi, U., Swoboda, I., Stolz, F., Focke-Tejkl, M., et al. (2020). Resistance of parvalbumin to gastrointestinal digestion is required for profound and long-lasting prophylactic oral tolerance. *Allergy: Eur. J. Allergy Clin. Immunol.* 75, 326–335. doi: 10.1111/all.13994

Fu, C. L., Ye, Y. L., Lee, Y. L., and Chiang, B. L. (2006). Effects of overexpression of IL-10, IL-12, TGF-β and IL-4 on allergen induced change in bronchial responsiveness. *Respir. Res.* 7, 72. doi: 10.1186/1465-9921-7-72

Fukuda, K., Ishida, W., Harada, Y., Wakasa, Y., Takagi, H., Takaiwa, F., et al. (2018). Efficacy of oral immunotherapy with a rice-based edible vaccine containing hypoallergenic Japanese cedar pollen allergens for treatment of established allergic conjunctivitis in mice. *Allergology Int.* 67, 119–123. doi: 10.1016/j.alit.2017.06.006

Gomord, V., Stordeur, V., Fitchette, A. C., Fixman, E. D., Tropper, G., Garnier, L., et al. (2020). Design, production and immunomodulatory potency of a novel allergen bioparticle. *PloS One* 15 (12), e0242867. doi: 10.1371/journal.pone.0242867

Guo, Y., Qiao, D., Zhao, S., Zhang, B., and Xie, F. (2021). Starch-based materials encapsulating food ingredients: Recent advances in fabrication methods and applications. *Carbohydr Polym.* 270, 118358. doi: 10.1016/j.carbpol.2021.118358

Han, R., He, H., Lu, Y., Lu, H., Shen, S., and Wu, W. (2024). Oral targeted drug delivery to post-gastrointestinal sites. *J. Controlled Release*. 370, 256-276. doi: 10.1016/j.jconrel.2024.04.047

Hofbauer, A., Melnik, S., Tschofen, M., Arcalis, E., Phan, H. T., Gresch, U., et al. (2016). The encapsulation of hemagglutinin in protein bodies achieves a stronger immune response in mice than the soluble antigen. *Front. Plant Sci.* 7. doi: 10.3389/fpls.2016.00142

Huber, S., Hörmann-Dietrich, U., Kapusi, E., Stöger, E., and Arcalis, E. (2024). Correlative microscopy - illuminating the endomembrane system of plant seeds. *J. Cell Sci.* 137 (20), jcs262251. doi: 10.1242/jcs.262251

Incorvaia, C., Cavaliere, C., Schroeder, J. W., Leo, G., Nicoletta, F., Barone, A., et al. (2023). Safety and adverse reactions in subcutaneous allergen immunotherapy: a review. *Acta Biomedica*. 94 (4). doi: 10.23750/abm.v94i4.14239

Iweala, O. I., Choudhary, S. K., and Commins, S. P. (2018). Food allergy. *Curr. Gastroenterol. Rep.* 20, 17. doi: 10.1007/s11894-018-0624-y

Jariyapong, P., Xing, L., van Houten, N. E., Li, T. C., Weerachatyanukul, W., Hsieh, B., et al. (2013). Chimeric hepatitis E virus-like particle as a carrier for oral-delivery. *Vaccine* 31, 417–424. doi: 10.1016/j.vaccine.2012.10.073

Jazayeri, S. D., Lim, H. X., Shameli, K., Yeap, S. K., and Poh, C. L. (2021). Nano and microparticles as potential oral vaccine carriers and adjuvants against infectious diseases. *Front. Pharmacol.* 12. doi: 10.3389/fphar.2021.682286

Jones, S. M., Burks, A. W., and Dupont, C. (2014). State of the art on food allergen immunotherapy: Oral, sublingual, and epicutaneous. *J. Allergy Clin. Immunol.* 133, 318–323. doi: 10.1016/j.jaci.2013.12.1040

Koncz, C., and Schell, J. (1986). The promoter of TL-DNA gene 5 controls the tissue-specific expression of chimaeric genes carried by a novel type of Agrobacterium binary vector. *Mol. Gen. Genet.* 204, 383–396. doi: 10.1007/BF00331014

Kulis, M. D., Patil, S. U., Wambre, E., and Vickery, B. P. (2018). Immune mechanisms of oral immunotherapy. *J. Allergy Clin. Immunol.* 141, 491–498. doi: 10.1016/j.jaci.2017.12.979

Lai, L. F., and Guo, H. X. (2011). Preparation of new 5-fluorouracil-loaded zein nanoparticles for liver targeting. *Int. J. Pharm.* 404, 317–323. doi: 10.1016/j.ijpharm.2010.11.025

Li, W., Zhang, X., Tan, S., Li, X., Gu, M., Tang, M., et al. (2022). Zein enhanced the digestive stability of five citrus flavonoids via different binding interaction. *J. Sci. Food Agric.* 102, 4780–4790. doi: 10.1002/jsfa.11838

Liu, X., Sun, Q., Wang, H., Zhang, L., and Wang, J. Y. (2005). Microspheres of corn protein, zein, for an ivermectin drug delivery system. *Biomaterials* 26, 109–115. doi: 10.1016/j.biomaterials.2004.02.013

Llop-Tous, I., Madurga, S., Giralt, E., Marzabal, P., Torrent, M., and Ludevid, M. D. (2010). Relevant elements of a Maize γ-zein domain involved in protein body biogenesis. *J. Biol. Chem.* 285, 35633–35644. doi: 10.1074/jbc.M110.116285

Luo, X., Wu, S., Xiao, M., Gu, H., Zhang, H., Chen, J., et al. (2023). Advances and prospects of prolamine corn protein zein as promising multifunctional drug delivery system for cancer treatment. *Int. J. Nanomedicine.* 18, 2589-2621. doi: 10.2147/IJN.S402891

Maeda, K., Caldez, M. J., and Akira, S. (2019). Innate immunity in allergy. *Allergy: Eur. J. Allergy Clin. Immunol.* 74, 1660-1674. doi: 10.1111/all.13788

Mardanova, E. S., and Ravin, N. V. (2021). Transient expression of recombinant proteins in plants using potato virus X based vectors, in: Methods in Enzymology. *Acad. Press Inc.* 660, 205–222. doi: 10.1016/bs.mie.2021.05.013

Mohammed, Y., Holmes, A., Kwok, P. C. L., Kumeria, T., Namjoshi, S., Imran, M., et al. (2022). Advances and future perspectives in epithelial drug delivery. *Adv. Drug Delivery Rev.* n, 114293. doi: 10.1016/j.addr.2022.114293

Moreno, F. J., Mellon, F. A., Wickham, M. S. J., Bottrill, A. R., and Mills, E. N. C. (2005). Stability of the major allergen Brazil nut 2S albumin (Ber e 1) to physiologically relevant *in vitro* gastrointestinal digestion. *FEBS J.* 272, 341–352. doi: 10.1111/j.1742-4658.2004.04472.x

Nosaki, S., Hoshikawa, K., Ezura, H., and Miura, K. (2021). Transient protein expression systems in plants and their applications. *Plant Biotechnol.* 38 (3), 297-304. doi: 10.5511/plantbiotechnology.21.0610a

Onwulata, C. I. (2012). Encapsulation of new active ingredients. *Annu. Rev. Food Sci. Technol.* 3, 183–202. doi: 10.1146/annurev-food-022811-101140

Özdemir, P. G., Sato, S., Yanagida, N., and Ebisawa, M. (2023). Oral immunotherapy in food allergy: where are we now? *Allergy Asthma Immunol. Res.* 15 (2), 125-144. doi: 10.4168/aair.2023.15.2.125

Paul-Gilloteaux, P., Heiligenstein, X., Belle, M., Domart, M. C., Larijani, B., Collinson, L., et al. (2017). EC-CLEM: Flexible multidimensional registration software for correlative microscopies. *Nat. Methods*. 14, 102-103. doi: 10.1038/nmeth.4170

Price, D., Ackland, M. L., and Suphioglu, C. (2017). Identifying Epithelial Endocytotic Mechanisms of the Peanut Allergens Ara h 1 and Ara h 2. *Int. Arch. Allergy Immunol.* 172, 106–115. doi: 10.1159/000451085

Qin, C., Xiang, Y., Liu, J., Zhang, R., Liu, Z., Li, T., et al. (2023). Precise programming of multigene expression stoichiometry in mammalian cells by a modular and programmable transcriptional system. *Nat. Commun.* 14, 1500. doi: 10.1038/s41467-023-37244-y

Reginald, K., Nadeem, K., Yap, E. Z. Y., and Latiff, A. H. A. (2024). Diving deep into fish allergen immunotherapyCurrent knowledge and future directions. *Asian Pac J. Allergy Immunol.* 42 (1), 1-13. doi: 10.12932/ap-030923-1687

Schwestka, J., Tschofen, M., Vogt, S., Marcel, S., Grillari, J., Raith, M., et al. (2020). Plant-derived protein bodies as delivery vehicles for recombinant proteins into mammalian cells. *Biotechnol. Bioeng* 117, 1037–1047. doi: 10.1002/bit.27273

Schwestka, J., Zeh, L., Tschofen, M., Schubert, F., Arcalis, E., Esteve-Gasent, M., et al. (2023). Generation of multi-layered protein bodies in N. benthamiana for the encapsulation of vaccine antigens. *Front. Plant Sci.* 14. doi: 10.3389/fpls.2023.1109270

Serradell, M. C., Rupil, L. L., Martino, R. A., Prucca, C. G., Carranza, P. G., Saura, A., et al. (2019). Efficient oral vaccination by bioengineering virus-like particles with protozoan surface proteins. *Nat. Commun.* 10, 361. doi: 10.1038/s41467-018-08265-9

Shutava, T. G., and Lvov, Y. M. (2012). "Encapsulation of natural polyphenols with antioxidant properties in polyelectrolyte capsules and nanoparticles," in *Natural Compounds as Inducers of Cell Death*. Eds. M. Diederich and K. Noworyta (Springer Netherlands), 215–235. doi: 10.1007/978-94-007-4575-9_9

Suzaki, T., Tsuda, M., Ezura, H., Day, B., and Miura, K. (2019). Agroinfiltration-based efficient transient protein expression in leguminous plants. *Plant Biotechnol.* 36, 119–123. doi: 10.5511/plantbiotechnology.19.0220b

Swoboda, I., Bugajska-Schretter, A., Linhart, B., Verdino, P., Keller, W., Schulmeister, U., et al. (2007). A recombinant hypoallergenic parvalbumin mutant for immunotherapy of igE-mediated fish allergy 1. *J. Immunol.* 57, 94-96. doi: 10.4049/jimmunol.178.10.6290

Takamura, S., Niikura, M., Li, T.-C., Takeda, N., Kusagawa, S., Takebe, Y., et al. (2004). DNA vaccine-encapsulated virus-like particles derived from an orally transmissible virus stimulate mucosal and systemic immune responses by oral administration. *Gene Ther.* 11, 628–635. doi: 10.1038/sj.gt.3302193

Tenero, L., Vaia, R., Ferrante, G., Maule, M., Venditto, L., Piacentini, G., et al. (2023). Diagnosis and management of allergic rhinitis in asthmatic children. *J. Asthma Allergy*. 16, 45-57. doi: 10.2147/JAA.S281439

Trogen, B., Jacobs, S., and Nowak-wegrzyn, A. (2022). Early introduction of allergenic foods and the prevention of food allergy. *Nutrients*. doi: 10.3390/nu14132565

van Kasteren, S. I., and Overkleeft, H. S. (2014). Endo-lysosomal proteases in antigen presentation. *Curr. Opin. Chem. Biol.* 23, 8-15. doi: 10.1016/j.cbpa.2014.08.011

Vickery, B. P., Scurlock, A. M., Jones, S. M., and Burks, A. W. (2011). Mechanisms of immune tolerance relevant to food allergy. *J. Allergy Clin. Immunol.* 127 (3), 576-584. doi: 10.1016/j.jaci.2010.12.1116

Wanes, D., Naim, H. Y., and Dengler, F. (2021). Proliferation and differentiation of intestinal caco-2 cells are maintained in culture with human platelet lysate instead of fetal calf serum. *Cells*. 10, 3038. doi: 10.3390/cells10113038

Wang, S., Takahashi, H., Kajiura, H., Kawakatsu, T., Fujiyama, K., and Takaiwa, F. (2013). Transgenic rice seeds accumulating recombinant hypoallergenic birch pollen allergen bet v 1 generate giant protein bodies. *Plant Cell Physiol.* 54, 917–933. doi: 10.1093/pcp/pct043

Whitehead, K. A., Dorkin, J. R., Vegas, A. J., Chang, P. H., Veiseh, O., Matthews, J., et al. (2014). Degradable lipid nanoparticles with predictable *in vivo* siRNA delivery activity. *Nat. Commun.* 5, 4277. doi: 10.1038/ncomms5277

Zou, T., and Gu, L. (2013). TPGS emulsified zein nanoparticles enhanced oral bioavailability of daidzin: *In vitro* characteristics and *in vivo* performance. *Mol. Pharm.* 10, 2062–2070. doi: 10.1021/mp400086n

frontiers | Frontiers in Plant Science

TYPE Original Research
PUBLISHED 06 October 2025
DOI 10.3389/fpls.2025.1678814

OPEN ACCESS

EDITED BY
Kevin Yueju Wang,
University of Pikeville, United States

REVIEWED BY
Kai Wang,
Shenzhen University of Advanced Technology, China
Nan Wang,
Chinese Academy of Agricultural Sciences, China

*CORRESPONDENCE
Iryna Gerasymenko
gerasymenko@bio.tu-darmstadt.de

RECEIVED 03 August 2025
ACCEPTED 15 September 2025
PUBLISHED 06 October 2025

CITATION
Gerasymenko I, Sheludko YV, Schmidts V and Warzecha H (2025) Efficient accumulation of new irregular monoterpene malonyl glucosides in *Nicotiana benthamiana* achieved by co-expression of isoprenyl diphosphate synthases and substrate-producing enzymes. *Front. Plant Sci.* 16:1678814. doi: 10.3389/fpls.2025.1678814

Efficient accumulation of new irregular monoterpene malonyl glucosides in *Nicotiana benthamiana* achieved by co-expression of isoprenyl diphosphate synthases and substrate-producing enzymes

Iryna Gerasymenko[1]*, Yuriy V. Sheludko[1], Volker Schmidts[2] and Heribert Warzecha[1]

[1]Plant Biotechnology and Metabolic Engineering, Technical University of Darmstadt, Darmstadt, Germany, [2]Clemens-Schöpf-Institute for Organic Chemistry and Biochemistry, Technical University of Darmstadt, Darmstadt, Germany

Irregular monoterpenes have limited natural sources but possess unique activities applicable in medicine and agriculture. To enable sustainable plant-based production of these compounds, we established a transient expression procedure to enhance the biosynthetic flux in *Nicotiana benthamiana* toward dimethylallyl diphosphate (DMAPP), a substrate for isopentenyl diphosphate synthases (IDSs) that generate irregular monoterpene skeletons. Considering the benefits of glycosylation for accumulating and storing monoterpenes in extractable form, we focused on developing a platform for the production of non-volatile glycosylated irregular monoterpenes using three IDS that form branched and cyclic structures. The analysis of methanolic leaf extracts from transiently transformed *N. benthamiana* plants revealed six major new components, 6-*O*-malonyl-β-D-glucopyranoside and 6-*O*-malonyl-β-D-glucopyranosyl-(1→2)-β-D-glucopyranoside derivatives of chrysanthemol, lavandulol and cyclolavandulol, five of which are novel compounds. Alleviating two bottlenecks in the DMAPP formation in plastids by co-expressing 1-deoxyxylulose 5-phosphate synthase and isopentenyl diphosphate isomerases increased the yield of chrysantemyl and lavandulyl glucosides produced by plant-derived IDS to 1.7 $\pm$ 0.4 µmol g^{-1} FW and 1.4 $\pm$ 0.3 µmol g^{-1} FW, respectively. A bacterial cyclolavandulyl diphosphate synthase operated efficiently in chloroplasts and cytoplasm. The highest irregular monoterpene concentrations were achieved in cytoplasm by co-expression of

hydroxymethylglutaryl-CoA reductase, the bottleneck enzyme of the mevalonate pathway for DMAPP biosynthesis. The mean level of cyclolavandulyl glucosides reached 3.9 ± 1.5 µmol g^{-1} FW; the top-performing plants contained 6.6 µmol g^{-1} FW. This yield represents the highest amount of irregular monoterpenes produced in plant systems.

KEYWORDS

irregular monoterpenes, lavandulol, cyclolavandulol, chrysanthemol, *Nicotiana benthamiana*, DMAPP biosynthetic pathway engineering

1 Introduction

Terpenoids form the largest group of natural products, with over 80000 different structures identified (Christianson, 2017). Approximately three-quarters of all known terpenes have been isolated from plants (Li et al., 2024), where they serve various functions, including defensive, communicative, and stress-protective roles. The terpene scaffold is a common structural feature found in many natural and synthetic compounds that have pharmaceutical, cosmetic, and agrochemical applications, often playing a crucial role in their biological activity. In pharmacology, these molecules are substantial contributors to six major classes of drugs: steroids, tocopherols, taxanes, artemisinins, ingenanes, and cannabinoids (Jansen and Shenvi, 2014; Yang et al., 2020).

Biosynthesis of terpenes proceeds through the formation of C5 isoprenyl diphosphate isomers, isopentenyl diphosphate (IPP) and dimethylallyl diphosphate (DMAPP), which undergo condensation to yield various groups of terpenes. This reaction, catalyzed by isoprenyl diphosphate synthases (IDS), typically starts with the head-to-tail (1'-4) coupling of IPP and DMAPP, resulting in the linear monoterpene scaffolds with *trans*- or *cis*-configuration. The chain can be further elongated through either additional head-to-tail or head-to-head (1'-1) linkages. The initial linear skeletons can be cyclized and further modified by terpene synthases and other enzymes, e.g. cytochromes P450 (Boutanaev et al., 2015). Most terpenes are formed using this mechanism and are classified as regular terpenes. In contrast, a limited number of so called irregular terpenes are produced by the head-to-middle linkage of two DMAPP molecules, which results in the direct formation of branched or cyclized structures with specific biological activities. For example, compounds with branched lavandulyl (Figure 1A) or various cyclic structures often function as insect pheromones and are promising candidates for developing sustainable pest control strategies (Zou and Millar, 2015; Rizvi et al., 2021). Natural pyrethrins, derivatives of the irregular monoterpene chrysanthemyl diphosphate with a cyclopropane skeleton (Figure 1B), along with chemically produced pyrethroids serve as highly effective insecticides. They are typically harmless to animals and are known for their rapid biodegradation (Lybrand et al., 2020). Cyclolavandulyl moiety is a part of several types of pharmaceutically valuable compounds, e.g. phenazine-derived meroterpenoids, such as lavanducyanin (Figure 1C), exhibiting cytotoxic and antibiotic activities, and neuroprotective carbazole alkaloid lavanduquinocin (Shin-Ya et al., 1995; Baumgartner and McKinnie, 2024).

Although significant progress has been made in the chemical synthesis of various terpenes (Kanwal et al., 2022), the production of irregular monoterpenes often remains inefficient and may involve hazardous reagents. For example, synthesizing achiral β-cyclolavandulol from a commercial precursor through a 5-step chemical route yielded 33-50% (Kinoshita et al., 1995; Knölker and Fröhner, 1998). In a stereodivergent total synthesis of lavandulol, the process involved 11–16 reaction steps and resulted in an overall yield of 6-26% (Bhosale and Waghmode, 2017). As an environmentally friendly alternative, biocatalytic methods are developed, e.g. preparing enantiomerically pure (*R*)-lavandulol by the enzyme-catalyzed resolution of racemic mixtures (Zada and Dunkelblum, 2006).

Multiple attempts have been made to produce regular terpenes using microbial biofactories. Extensive metabolic engineering aimed at increasing the precursor supply and inhibiting competing pathways combined with the optimization of fermentation conditions resulted in impressive sesquiterpene titers reaching up to 140 g/l farnesene (Meadows et al., 2016) and more than 40 g/l amorphadiene in yeast (Westfall et al., 2012). For monoterpenes, the accumulation levels are significantly lower (Yang et al., 2025) due to their volatility and toxicity to the host cells. An effective way of alleviating these problems is *in situ* product extraction (Brennan et al., 2012) or conversion into less volatile and toxic molecules. For geraniol, esterification to geranyl acetate increased the product accumulation in *E. coli* systems to 10.4 and 19 g/l (Wang et al., 2022b; Shukal et al., 2024), while the highest reported level of free alcohol for this chassis is 2.1 g/l (Wang et al., 2021). Further development of this strategy allowed for recovery of geraniol at concentration of 13.2 g/l by hydrolysis of geranyl acetate (Wang et al., 2022a). The microbial production of irregular monoterpenes has been rarely reported. Recently, engineered *Saccharomyces cerevisiae* achieved a yield of 309 mg/l of lavandulol through fed-batch fermentation in a 5 liter bioreactor (Nie et al., 2025).

More research on biotechnological production of irregular monoterpenes has been carried out using plants as hosts. Plant cells

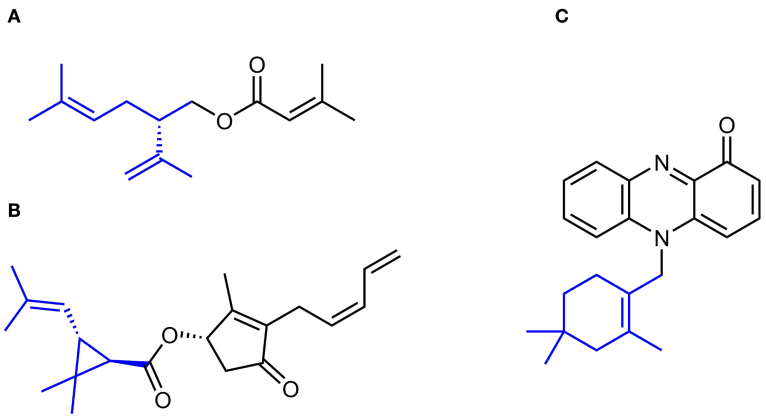

FIGURE 1
Examples of irregular monoterpene motifs in the structures of biologically active small molecules. **(A)** (S)-(+)-Lavandulyl senecioate, the sex pheromone of vine mealybug, *Planococcus ficus*. **(B)** Pyrethrin I, a natural irregular monoterpene known for its potent insecticidal activity. **(C)** Lavanducyanin, a phenazine-derived meroterpenoid exhibiting cytotoxic and antibiotic properties.

offer access to precursor flux through either the mevalonic acid (MVA) pathway in the cytoplasm or the methylerythritol phosphate (MEP) pathway in the plastids (Bergman et al., 2024), with the ability to localize enzymes in different cell compartments. Efforts to engineer terpenoid metabolism in plants to enhance the accumulation of native irregular monoterpenes or to produce heterologous compounds have involved stable genetic transformation of tobacco (Yang et al., 2014; Matáeos-Fernández et al., 2023), as well as host species that naturally produce high levels of terpenoids, such as *Chrysanthemum morifolium* (Hu et al., 2018), *Lavandula×intermedia* (Munoz-Bertomeu et al., 2006) and *Solanum lycopersicum* (Xu et al., 2018a).

A convenient platform for the rapid production of recombinant proteins and manipulating plant metabolism is transient expression (Gerasymenko et al., 2019; Nosaki et al., 2021). Advantages of this strategy include a high level of recombinant protein accumulation, which can exceed that of nuclear transformed plants by several times. Additionally, it offers flexibility in testing various gene combinations and allows for the restriction of expression products to certain plant organs. This capability enables temporary accumulation of potentially toxic products at concentrations that would be harmful to the entire plant. There is particular interest in using plants for the transient biosynthesis of small molecules with valuable activities, employing combinations of heterologous enzymes directed to specific compartments within the plant cell. The development of such a platform offers a source of inexpensive material for *in planta* or whole-cell biocatalysis as transient expression protocols are easily scalable from analytical to preparative and manufacturing levels. However, it requires adaptation of foreign proteins to the plant's intracellular environment and optimization of intrinsic metabolic fluxes. The transient expression of genes encoding irregular IDS enzymes, lavandulyl and chrysanthemyl diphosphate synthases (LDS and CDS), was reported in *N. benthamiana* (Xu et al., 2018b; Matáeos-Fernández et al., 2023). This approach was used for proving the functionality of IDS enzymes and enzymes that oxidizes *trans*-chrysanthemol to chrysanthemic acid, but no experiments on increasing the yield of heterologous irregular monoterpenes by expanding the supply of precursors were attempted.

In this study, we endeavored to improve the performance of plants as production system for irregular monoterpenes by enlarging the pool of DMAPP, the substrate for IDS performing the irregular coupling. To enhance the metabolic flux through the MEP and MVA pathways, the corresponding bottleneck enzymes were overexpressed. In addition, the enzymes producing DMAPP from dimethylallyl phosphate and IPP were introduced (Figure 2). Previous research has shown that the major part of heterologous terpenoids in transgenic plants underwent glucosylation (Lucker et al., 2001; Hu et al., 2018; Xu et al., 2018a, 2018), a common modification allowing for sequestration and storage of hydrophobic and often toxic monoterpenes in plant cells (Dudareva and Pichersky, 2008). Therefore, we focused on the accumulation of non-volatile forms of irregular monoterpenes that can be easily extracted from the harvested plant material unlike volatile metabolites requiring continuous trapping techniques. We identified six major components of methanolic extracts from *N. benthamiana* plants expressing irregular IDS enzymes, five of them being previously unknown substances (Figure 2, compounds 1-6), and achieved the yield of the products in the range of 1.4 – 3.9 µmol g^{-1} FW representing the highest reported concentrations of irregular monoterpenes produced in a plant system.

2 Materials and methods

2.1 Analytical instruments and assays

LC-ESI-MS analysis was performed on a 1260 Infinity HPLC system coupled to a G6120B quadrupole mass spectrometry detector (Agilent, USA). The separation was carried out on a

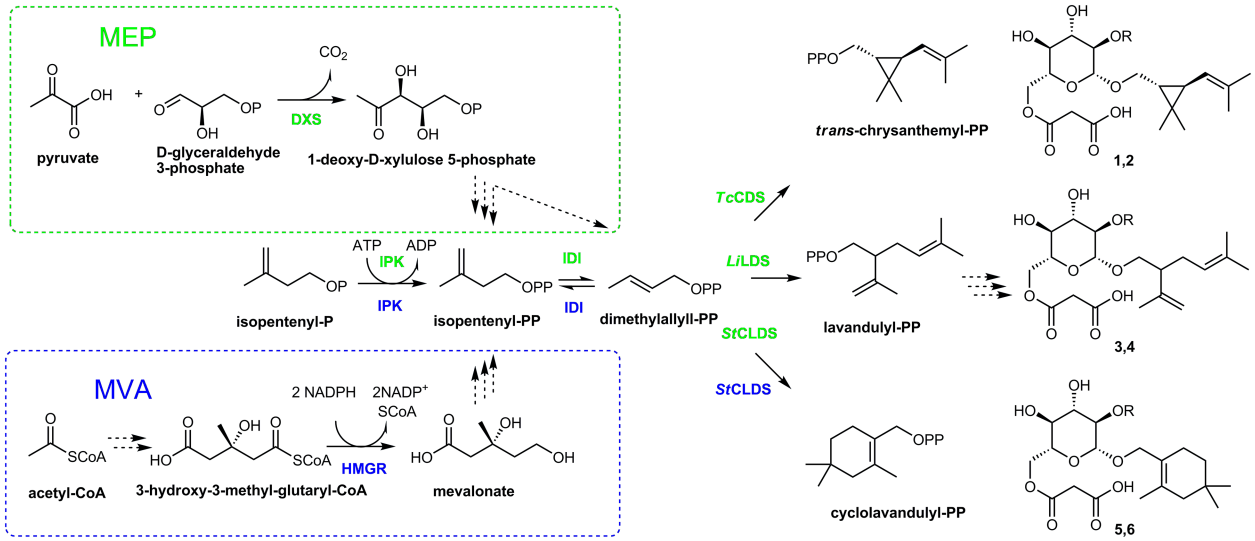

FIGURE 2
Selected steps of the metabolic pathway for irregular monoterpene malonyl glucoside biosynthesis in *N. benthamiana*. Solid arrows indicate the reactions catalized by the enzymes heterologously expressed in this study. 1-deoxy-D-xylulose 5-phosphate synthase (DXS), chrysanthemyl diphosphate synthase (*Tc*CDS), and lavandulyl diphosphate synthase (*Li*LDS) were localized to chloroplasts (highlighted in green); 3-hydroxy-3-methyl-glutaryl-CoA reductase (HMGR) operated in cytoplasm (highlighted in blue); cyclolavandulyl diphosphate synthase (CLDS), isopentenyl phosphate kinase (IPK), and isopentenyl diphosphate isomerases (IDI) were expressed with and without chloroplast targeting peptide. Structures 1, 3, 5, R = H; 2, 4, 6, R = Glu. Abbreviation: Glu, glucopyranose; CoA, coenzyme A; MEP, methylerythritol phosphate pathway; MVA, mevalonate pathway; PP, diphosphate; P, phosphate.

Zorbax Extend-C18 (4.6 x 150 mm, 3.5 µm) column (Agilent, USA), according to the protocol described by Nagel (Nagel et al., 2012). The detection of C10 prenyl glycosides was performed in a negative total ion current and a single ion mode.

An Impact II system (Bruker Daltonik, Germany) was used for recording ESI-HR-MS spectra.

HPLC analysis was performed using a 1260 Infinity system connected to a Zorbax Eclipse Plus C18 column, 4.6 × 250 mm, 5 µm (Agilent, USA), and the mobile phase consisted of 50 mM ammonium acetate (pH 4.5) (A) and 70:30 (v/v) acetonitrile:50 mM ammonium acetate (pH 4.5) (B) (Sun et al., 2010) with the binary gradient elution program (% B): 20–50 within 25 min; 50–100 within 1 min. The column was flushed with 100% B for 3 min and re-equilibrated with 20% B for an additional 3 min. The flow rate was set to 1.0 ml/min and detection was at 256 nm.

^{1}H and ^{13}C NMR, CLIP-COSY (25 Hz mixing (Koos et al., 2016), NOESY (500 ms mixing), ^{1}H -^{13}C multiplicity-edited HSQC and ^{1}H -^{13}C HMBC, TOCSY and DOSY (stimulated echo, bipolar gradient pairs, $\delta/2$ = 1 ms, Δ = 60 ms, 16 gradient steps linearly spaced between 2% and 98%) spectra were recorded in DMSO-d_6 using an AVANCE III HD instrument (Bruker, USA) equipped with a 5 mm QCI CryoProbe (^{1}H/^{19}F-^{31}P/^{13}C/^{15}N/^{2}H with a z-gradient coil with maximum amplitude of 53 G/cm) at 700 MHz (^{1}H) and 176 MHz (^{13}C). All measurements were carried out at 300 K. Bruker TopSpin 3.5pl7 was used for data acquisition using pulse sequences as provided by the vendor library. Default parameter values were used unless noted otherwise.

2.2 Genetic vectors and transient expression

Genes of IDS and auxiliary enzymes used in this study (Table 1) were either synthesized or amplified as described in the Supplementary Materials (S1.2). Gene *GFP* served as a physiologically neutral control. The cloned or synthetic genes were inserted into genetic vectors using the Golden Braid modular cloning system (Sarrion-Perdigones et al., 2013).

The transcriptional units (TUs) for all genes were assembled in alpha-level vectors and included 35S CaMV promoter and nopaline synthase gene terminator from *A. tumefaciens*. For protein transport into chloroplasts, the sequence encoding an artificial chloroplast transit peptide from the pICH13688 plasmid (ICONGenetics, Halle, Germany, GenBank accession number AM888351.1) was added to the TUs for CLDS, IDIs and IPK. The TUs for IDS genes were combined in omega-level vectors with the TU for p19 suppressor of post-transcriptional gene silencing from the tomato bushy stunt virus. The TUs for auxiliary genes were either expressed from alpha-level vectors or combined in omega-level vectors as shown in Supplementary Table S1.1. The vectors were introduced into the *A. tumefaciens* EHA105 strain. The transient expression was performed in plants of *N. benthamiana* as described earlier (Gerasymenko et al., 2019). For co-expression, the bacterial suspensions carrying corresponding vectors were mixed in equal volumes before infiltration (Supplementary Table S1.1). The biomass was collected six days after infiltration.

TABLE 1 Enzymes used in experiments on the biosynthesis of irregular monoterpene malonyl glucosides in *N. benthamiana*.

Enzyme	Acronym	Origin	UniProt or NCBI Acc. No.	Reference
Chrysanthemyl diphosphate synthase	*Tc*CDS	*Tanacetum cinerariifolium*	P0C565	(Rivera et al., 2001)
Lavandulyl diphosphate synthase	*Li*LDS	*Lavandula x intermedia*	M4QSY7	(Demissie et al., 2013)
Cyclolavandulyl diphosphate synthase	CLDS	*Streptomyces* sp. CL190	X5IYJ5	(Ozaki et al., 2014)
1-Deoxyxylulose 5-phosphate synthase	DXS	*Solanum lycopersicum*, DXS2	NP_001332799.1	(Di and Rodriguez-Concepcion, 2023)
Hydroxymethylglutaryl-CoA reductase, the N-truncated soluble version of HMGR1	tHMGR	*Saccharomyces cerevisiae*, HMGR1	P12683 (Δ1-553, membrane-binding region)	(Polakowski et al., 1998)
Isopentenyl diphosphate isomerase	*At*IDI *Ec*IDI *Bl*IDI	*Arabidopsis thaliana*, IDI1 *E. coli* *Bacillus licheniformis*	Q38929 (Δ1-53, chloroplast targeting peptide) WP_001192814.1 Q65I10	(Phillips et al., 2008) (Hahn et al., 1999) (Rad et al., 2012)
Isopentenyl phosphate kinase	IPK	*Arabidopsis thaliana*	Q8H1F7	(Henry et al., 2015)

2.3 Quantification of monoterpene malonyl glucosides

The leaf explants (130 ± 10 mg) were frozen in liquid nitrogen, ground and extracted with 200 µl of 80% methanol in an ultrasound bath filled with water/ice slurry during 30 min. After centrifugation (10 min, 17000 x g), the supernatants were transferred in new Eppendorf tubes and centrifuged once more for 10 min at 17000 g. The supernatants after the second centrifugations were used for LC-ESI-MS as described in 2.1.

The calibration lines were build using the purified samples prepared as described in 2.4. The content of glucosylated monoterpenes was calculated either as µg of each derivative, mono- and diglucoside, per g of plant fresh weight (FW) or as a sum of molar quantities of both derivatives (µmol/g FW). The results are presented as box plots. Within each box, horizontal lines denote median values and square dots show mean values; boxes extend from the 25th to the 75th percentile of each group's distribution of values; bars represent standard deviation; round dots illustrate individual measurements. The sample sizes are shown in the figure legends.

A one-way ANOVA and Tukey's HSD test were performed using the calculator retrieved from https://www.socscistatistics.com/tests/anova/default2.aspx.

2.4 Isolation of irregular monoterpene malonyl glucosides

For the preparative isolation of irregular monoterpene malonyl glucosides (1-6), the plant material from the various experiments on the expression of the corresponding IDS gene was combined. The infiltrated leaves (20–25 g) were frozen in liquid nitrogen, ground and extracted with 80% (v/v) methanol (40 ml) in an ultrasound bath filled with water/ice slurry during 30 min. After centrifugation (10 min, 12500 x g), the supernatant was filtered through filter paper, dried on a rotary evaporator and taken up in 20 ml methanol. After the second centrifugation (10 min, 12500 x g), the supernatant was filtered through filter paper, dried on the rotary evaporator and dissolved in 2 ml methanol. HPLC-MS analysis displayed that the extract contained the corresponding monoterpene malonyl mono- and diglucosides in different proportions. For normal phase chromatography, the column (18 mm id) was packed with silica gel (40–60 µm, 230–400 mesh, 10 g) equilibrated in ethyl acetate. After extract application, the column was washed with 50 ml ethyl acetate, and the fractions of 10 ml were collected during elution with 150 ml ethyl acetate:methanol 4:1 mixture followed by 150 ml ethyl acetate: methanol 35:15 mixture and 50 ml methanol. The fractions were analysed by HPLC-MS and those containing monoterpene malonyl mono- and diglucosides were pooled (typically fractions 4–13 eluted with acetate:methanol 4:1 mixture for monoglucosides and fractions 14–28 eluted with acetate:methanol 35:15 mixture for diglucosides). After drying on a rotary evaporator, the combined fractions were dissolved in 1 ml 5 mM ammonium bicarbonate (ABC) and subjected to reverse phase chromatography on a Sep-Pak C18–1 cc Vac Cartridge (Waters, USA) activated with acetonitrile and equilibrated with ABC. The cartridge was washed with 3 ml ABC, and elution was performed with an acetonitrile:ABC 95:5 mixture (10–12 ml) collecting 1 ml fractions. After LC-MS analysis, the fractions containing monoterpene malonyl mono- or diglucosides were combined, dried on a rotary evaporator, dissolved in methanol, and separated on ALUGRAM® Xtra SIL G/UV254 TLC plates (0.2 mm silica gel layer, Macherey-Nagel (Germany)) using ethyl acetate: methanol 1:1 mixture as a mobile phase. After the plates were resolved and dried, a 1.5 cm strip was cut from one side and developed using a potassium permanganate stain. The silica gel from the area corresponding to the position of the main compound in the stained section was extracted with methanol which yielded 2–5 mg of material. The obtained samples were dissolved in DMSO-d_6 (99.8 atom%D, Roth (Germany)) for NMR analysis.

Chrysanthemyl-1-*O*-(6-*O*-malonyl)-β-D-glucopyranoside (1): amorphous solid; ESIMS m/z 357.2 [M - COOH] $^-$; HRESIMS m/

z 803.3721 [2M - H] $^-$ (calcd for $C_{38}H_{59}O_{18}$, 803.3707; Δmass 1.7 ppm); m/z 401.1833 [M - H] $^-$ (calcd for $C_{19}H_{29}O_9$, 401.1817; Δmass 4.0 ppm); m/z 357.1937 [M - COOH] $^-$ (calcd for $C_{18}H_{29}O_7$, 357.1919; Δmass 5.0 ppm); ^{1}H-NMR (700 MHz, DMSO-d_6) δ (ppm): 4.86 (d, J = 8.2 Hz, 1H), 4.16 – 4.05 (m, 2H), 4.13 (d, J = 7.9 Hz, 1H), 3.82 (dd, 1H, J = 11, 8.7 Hz), 3.43 (dd, 1H, J = 11, 5.7 Hz), 3.31 – 3.27 (m, 1H), 3.14 (t, J = 9.4, 8.9 Hz, 1H), 3.09 (t, J = 9.3, 8.9 Hz, 1H), 2.96 (t, J = 9.4, 7.9 Hz, 1H), 1.65 (s, 3H), 1.62 (s, 3H), 1.10 – 1.07 (m, 1H), 1.07 (s, 3H), 0.99 (s, 3H), 0.75 (dt, J = 8.5, 5.6 Hz, 1H); ^{13}C-NMR (176 MHz, DMSO-d_6) δ (ppm): 169.19, 168.43, 131.71, 123.91, 102.27, 76.41, 73.69, 73.36, 70.10, 68.56, 63.51, 45.61, 31.8, 27.56, 25.43, 21.79, 22.37, 21.22, 18.12; (Supplementary Material, Supplementary Table S1.2, Supplementary Figure S2.2-S2.9).

Chrysanthemyl-1-*O*-(6-*O*-malonyl)-*β*-D-glucopyranosyl-(1→2)-*β*-D-glucopyranoside (**2**): amorphous solid; ESIMS m/z 519.3 [M - COOH] $^-$; HRESIMS m/z 563.2366 [M - H] $^-$ (calcd for $C_{25}H_{39}O_{14}$, 563.2345; Δmass 3.7 ppm); m/z 519.2452 [M - COOH] $^-$ (calcd for $C_{18}H_{29}O_7$, 519.2447; Δmass 1.0 ppm); ^{1}H-NMR (700 MHz, DMSO-d_6) δ (ppm): 4.86 (d, J = 8.2 Hz, 1H), 4.40 (d, J = 7.9 Hz, 1H), 4.31 (d, J = 7.7 Hz, 1H), 4.14 – 4.10 (m, 1H); 4.07 (d, J = 11.6 Hz, 1H), 3.79 (t, J = 10.7, 8.1 Hz, 1H), 3.62 (d, J = 11.9 Hz, 1H), 3.51 – 3.47 (m, 2H), 3.38 (t, a = 9.1 Hz, 1H), 3.36 – 3.33 (m, 1H), 3.30 – 3.26 (m, 1H), 3.16 – 3.13 (m, 1H), 3.10 – 3.16 (m, 2H), 3.06 – 3.03 (m, 1H), 2.99 (t, J = 8.3 Hz, 2H), 2.92 – 2.88 (m, 2H), 1.65 (s, 3H), 1.63 (s, 3H), 1.11 – 1.08 (m, 1H), 1.07 (s, 3H), 0.98 (s, 3H), 0.81 – 0.77 (m, 1H); ^{13}C-NMR (176 MHz, DMSO-d_6) δ (ppm): 169.72, 167.19, 131.49, 123.94, 103.9, 101.02, 81.68, 77.02, 76.06, 75.51, 74.92, 73.71, 69.76, 69.72, 68.83, 63.29, 60.72, 45.98, 31.64, 27.62, 25.42, 22.36, 21.53, 21.14, 18.14; (Supplementary Material; Supplementary Table S1.2; Supplementary Figure S2.10-S2.17). The sample used for NMR analyses contained impurities that hindered the direct identification of carbon resonance positions in the ^{13}C NMR spectrum. The corresponding signal values were retrieved from HSQC and HMBC spectra.

Lavandulyl-1-*O*-(6-*O*-malonyl)-*β*-D-glucopyranoside (3): amorphous solid; ESIMS m/z 357.2 [M - COOH] $^-$; HRESIMS m/z 803.3716 [2M - H] $^-$ (calcd for $C_{38}H_{59}O_{18}$, 803.3707; Δmass 1.1 ppm); m/z 401.1837 [M - H] $^-$ (calcd for $C_{19}H_{29}O_9$, 401.1817; Δmass 5.0 ppm); m/z 357.1937 [M - COOH] $^-$ (calcd for $C_{18}H_{29}O_7$, 357.1919; Δmass 5.0 ppm); ^{1}H-NMR (700 MHz, DMSO-d_6) δ (ppm): 5.02 (t, 1H, J = 7.0 Hz), 4.73 (s, 1H), 4.69 (s, 1H), 4.14 (d, J = 7.8 Hz, 1H), 4.08-4.12 (m, 2H), 3.63 (dd, 1H, J = 9.8, 7.1 Hz), 3.44 (dd, 1H, J = 9.8, 6.6 Hz), 3.30 (m, 1H), 3.14 (t, J = 8.9 Hz, 1H), 3.09 (t, J = 10.6, 9.3 Hz, 1H), 2.95 (t, J = 9.3, 7.8 Hz, 1H), 2.92 – 2.88 (m, 2H), 2.3 (m, 1H), 2.2 (dt, J = 13.5, 6.4 Hz, 1H), 1.98 (m, 1H), 1.64 (s, 3H), 1.63 (s, 3H), 1.56 (s, 3H); ^{13}C-NMR (176 MHz, DMSO-d_6) δ (ppm): 169.7, 167.63, 145.49, 131.36, 122.48, 111.81, 102.92, 76.33, 73.75, 73.4, 70.8, 70, 63.43, 46.45, 45.86, 28.21, 25.63, 20.12, 17.77; (Supplementary Table S1.2; Supplementary Figure S2.18-S2.25).

Lavandulyl-1-*O*-(6-*O*-malonyl)-*β*-D-glucopyranosyl-(1→2)-*β*-D-glucopyranoside (4): amorphous solid; ESIMS m/z 519.3 [M - COOH] $^-$; HRESIMS m/z 563.2351 [M - H] $^-$ (calcd for $C_{25}H_{39}O_{14}$, 563.2345; Δmass 0.9 ppm); m/z 519.2435 [M - COOH] $^-$ (calcd for $C_{18}H_{29}O_7$, 519.2447; Δmass 2.2 ppm); ^{1}H-NMR (700 MHz, DMSO-d_6) δ (ppm): 5.02 (t, 1H, J = 7.1 Hz), 4.73 (s, 1H), 4.68 (s, 1H), 4.38 (d, J = 7.7 Hz, 1H), 4.31 (d, J = 7.6 Hz, 1H), 4.16 – 4.06 (m, 2H), 3.66 (dd, 1H, J = 9.4, 7.4 Hz), 3.61 (d, J = 11.5 Hz, 1H), 3.50 – 3.48 (m, 1H), 3.44 (dd, 1H, J = 9.4, 6.2 Hz), 3.39 (t, J = 9.0 Hz, 1H), 3.37 – 3.34 (m, 2H), 3.31 – 3.27 (m, 1H), 3.19 – 3.16 (m, 1H), 3.17 – 3.10 (m, 2H), 3.03 – 3.00 (m, 1H), 2.98 (t, J = 8.4 Hz, 1H), 2.95 – 2.90 (m, 2H), 2.29 (m, 1H), 2.2 (dt, J = 13.7, 6.4 Hz, 1H), 1.99 (m, 1H), 1.64 (s, 3H), 1.63 (s, 3H), 1.56 (s, 3H); ^{13}C-NMR (176 MHz, DMSO-d_6) δ (ppm): 169.6, 168.15, 145.58, 131.22, 122.57, 111.68, 104.11, 101.36, 81.4, 77.1, 76.01, 75.58, 75.1, 73.53, 70.74, 69.87, 69.77, 63.33, 60.75, 46.54, 45.69, 28.14, 25.62, 20.19, 17.78; (Supplementary Table S1.2, Supplementary Figure S2.26-S2.33).

β-Cyclolavandulyl-1-*O*-(6-*O*-malonyl)-*β*-D-glucopyranoside (**5**): amorphous solid; ESIMS m/z 357.2 [M - COOH] $^-$; HRESIMS m/z 803.3701 [2M - H] $^-$ (calcd for $C_{38}H_{59}O_{18}$, 803.3707; Δmass 0.8 ppm); m/z 401.1814 [M - H] $^-$ (calcd for $C_{19}H_{29}O_9$, 401.1817; Δmass 0.9 ppm); m/z 357.1917 [M - COOH] $^-$ (calcd for $C_{18}H_{29}O_7$, 357.1919; Δmass 0.5 ppm); ^{1}H-NMR (700 MHz, DMSO-d_6) δ (ppm): 4.23 (d, J = 11.4 Hz, 1H), 4.18 (dd, J = 11.8, 1.8 Hz, 1H), 4.06 (dd, J = 11.8, 6.9 Hz, 1H), 4.03 (d, J = 7.9 Hz, 1H), 3.97 (d, J = 11.4 Hz, 1H), 3.24 (ddd, J = 8.9, 6.9, 1.8 Hz, 1H), 3.11 (t, J = 9.4, 8.8 Hz, 1H), 3.07 (t, J = 9.4, 8.8 Hz, 1H), 2.97 (t, J = 9.1, 8.0 Hz, 1H), 2.96 – 2.94 (m, 2H), 2.14 (d, J = 17.4 Hz, 1H); 1.95 (d, J = 17.4 Hz, 1H), 1.73 (s, 2H), 1.62 (s, 3H), 1.28 (t, J = 6.6 Hz, 2H), 0.86 (s, 3H), 0.86 (s, 3H); ^{13}C-NMR (176 MHz, DMSO-d_6) δ (ppm): 169.31, 168.08, 130.76, 124.58, 100.43, 76.47, 73.89, 73.22, 70.2, 66.73, 63.58, 45.58, 45.32, 35.12, 28.77, 28.12, 28.08, 24.95, 18.82; (Supplementary Material; Supplementary Table S1.2; Supplementary Figure S2.34-S2.41).

β-Cyclolavandulyl-1-*O*-(6-*O*-malonyl)-*β*-D-glucopyranosyl-(1→2)-*β*-D-glucopyranoside (6): amorphous solid; ESIMS m/z 519.3 [M - COOH] $^-$; HRESIMS m/z 563.2342 [M - H] $^-$ (calcd for $C_{25}H_{39}O_{14}$, 563.2345; Δmass 0.7 ppm); m/z 519.2463 [M - COOH] $^-$ (calcd for $C_{18}H_{29}O_7$, 519.2447; Δmass 3.1 ppm); ^{1}H-NMR (700 MHz, DMSO-d_6) δ (ppm): 4.39 (d, J = 7.8 Hz, 1H), 4.24 (d, J = 7.7 Hz, 1H), 4.15 (d, J = 11.6 Hz, 0H), 4.13 – 4.08 (m, 2H), 4.09 (dd, J = 11.6, 6.5 Hz, 1H), 3.60 (d, J = 11.6 Hz, 1H), 3.51 – 3.47 (m, 1H), 3.41 – 3.35 (m, 1H), 3.34 – 3.31 (m, 1H), 3.31 – 3.28 (m, 1H), 3.18 – 3.14 (m, 1H), 3.17 – 3.11 (m, 1H), 3.15 – 3.11 (m, 1H), 3.05 – 3.02 (m, 1H), 2.98 (t, J = 8.3 Hz, 1H), 2.94 – 2.90 (m, 2H), 2.14 (d, J = 17.2 Hz, 1H), 2.01 (d, J = 17.2 Hz, 1H), 1.71 (s, 2H), 1.60 (s, 3H), 1.27 (t, J = 6.5 Hz, 2H), 0.85 (s, 6H); ^{13}C-NMR (176 MHz, DMSO-d_6) δ (ppm): 169.54, 168.13, 129.85, 124.99, 104.01, 99.69, 81.51, 77.01, 76.01, 75.76, 75.07, 73.63, 69.99, 69.72, 67.35, 63.3, 60.8, 45.63, 45.58, 35.16, 28.74, 28.25, 28.02, 24.68, 18.87; (Supplementary Material; Supplementary Table S1.2; Supplementary Figure S2.42-S2.49).

2.5 Acid hydrolysis and derivatization with 3-methyl-1-phenyl-5-pyrazolone

Compounds 1-6 (2–5 mg of each) were incubated with 2 ml of 2 M trifluoroacetic acid in locked Eppendorf tubes at 105 °C for six

hours. After incubation, the mixtures were cooled and centrifuged. The supernatants were then diluted with 10 ml of methanol and evaporated under vacuum. The resulting residues were dissolved in 100-200 µl of deionized water, and 5-10 µl of 3 M NaOH was added to neutralize the residual acid. Reference samples were prepared as 50 mM solutions of monosaccharides.

Derivatization was performed according to the method described by Sun et al. (2010) with minor modifications. For derivatization, 20 µl of the hydrolyzed glycoside solution or reference sample was mixed with 180 µl of acetonitrile, along with 20 µl of a 0.5 M MPP solution in methanol and 10 µl of a 25% ammonium hydroxide solution. The samples were incubated for 25 minutes at 70 °C, then cooled and diluted with 760 µl of acetonitrile before HPLC analysis.

The relative configuration of the sugar moiety in compounds 1–6 was confirmed by comparing the retention times of the derivatized carbohydrates to that of a reference sample of D-glucose (t_R = 19.6 min).

3 Results

3.1 Transient expression of heterologous IDS enzymes in *N. benthamiana*

We applied *trans*- and *cis*-IDS enzymes of plant origin performing irregular coupling, chrysanthemyl diphosphate synthase from *Tanacetum cinerariifolium* (*Tc*CDS) and lavandulyl diphosphate synthase from *Lavandula x intermedia* (*Li*LDS), catalyzing the formation of a cyclopropane ring (Rivera et al., 2001) and a branched moiety (Demissie et al., 2013), respectively. Additionally, we included a prokaryotic cyclolavandulyl diphosphate synthase (CLDS), a *cis*-IDS derived from *Streptomyces* sp. capable of head-to-trunk 1'-2 condensation which is followed by the creation of a six-carbon ring through 4-3' bond closure (Ozaki et al., 2014). The *Tc*CDS and *Li*LDS enzymes were expressed with their native chloroplast transit peptides (Supplementary Figure S2.1). The bacterial CLDS was examined in its native form lacking identifiable targeting signals and in fusion with an artificial chloroplast targeting peptide.

To monitor terpene glucoside accumulation, we extracted the plant material with 80% methanol on the 6th day post infiltration and analyzed it using LC-MS. Transient expression of each irregular IDS enzyme in *N. benthamiana* resulted in the detection of two major new compounds in the leaf methanolic extracts (Figure 3). These metabolites were identified as 6-*O*-malonyl-*β*-D-glucopyranoside and 6-*O*-malonyl-*β*-D-glucopyranosyl-(1→2)-*β*-D-glucopyranoside derivatives of chrysanthemol, lavandulol and cyclolavandulol (compounds 1-6; Figure 2). Among these substances, only chrysanthemyl-1-*O*-(6-*O*-malonyl)-*β*-D-glucopyranoside (1) was characterized previously (Yang et al., 2014; Hu et al., 2018). In this report, we provide a detailed elucidation of the structures of new molecules based on one- and two-dimensional NMR assays. The original NMR spectra, along with the CLIP-COSY, HMBC, and NOESY correlations are available in the Supplementary Materials (Supplementary Table S1.2, Supplementary Figure S2.2-S2.49).

3.2 Structure elucidation of irregular monoterpene malonyl glycosides

3.2.1 Monoglucosylated derivatives (6-*O*-malonyl-*β*-D-glucopyranosides) of chrysanthemyl, lavandulyl and cyclolavandulyl (1, 3, and 5)

ESI-HRMS analysis of 1, 3, and 5 in negative mode revealed base peak with *m/z* values of 803.3721, *m/z* 803.3716, and *m/z* 803.3701, respectively. This suggests a molecular formula of $C_{38}H_{59}O_{18}$ for each compound. Additionally, the spectra displayed ions with *m/z* values of 401.1833, *m/z* 401.1837, and *m/z* 401.1814, respectively, corresponding to the molecular formula $C_{19}H_{29}O_9$ ($[M–H]^-$) and indicating that the base peak is likely an adduct $[2M–H]^-$.

TOCSY spectra of 1, 3, and 5 revealed two distinct networks of protons coupled within a spin system. One group of signals was specific to each compound and corresponded to the protons associated with the respective monoterpene moiety. The other group consisted of six protons that exhibited similar NMR shift values across all three molecules, characteristic of a pyranose ring, particularly glucopyranose (Brito-Arias, 2007). The anomeric proton H-1' appeared as a doublet at δ 4.1 – 4.0 ppm with a coupling constant (*J*) of 7.9-7.8 Hz, indicating an axial-axial interaction with H-2' and β-glycosidic linkage. The chemical shifts of the C-1' carbon in compounds 1, 3, and 5 fell within the range of δ 102.9 – 100.4 ppm, which is characteristic of a glycosidic bond. Three triplets at δ 3.2 – 3.0 ppm, with a coupling of 9–10 Hz, were assigned to the protons H-2' through H-4' of D-pyranoses in a $^4C_1$ conformation. A multiplet (ddd) at δ 3.3 – 3.2 was assigned to H-5', which was coupled to two H-6' protons.

The signals for H-6' in all three compounds were shifted downfield (δ 4.2 – 4.1 ppm), along with the corresponding carbon resonances detected at δ 63.6 – 63.4 ppm. These shifts suggest derivatization of the hydroxyl group at C-6', which was confirmed by ^{1}H -^{13}C HMBC analysis. In the HMBC spectra of compounds 1, 3, and 5, we observed correlations between the H-6' protons and a quaternary carbon at δ 169.7 – 169.2. Additionally, two protons in the range of δ 3.0 – 2.9 ppm also interacted with this carbon, as well as with another quaternary carbon having a chemical shift in the range of δ 168.4 – 167.6 ppm. These correlations suggest the presence of two carboxylic groups linked by a methylene carbon, indicating malonylation of the glucopyranose ring at the C-6 position.

In substances 1, 3, and 5, the sugar component was identified as glucose through HPLC analysis following acid hydrolysis and MPP derivatization. The retention time of the derivatized hydrolysis product matched that of the reference sample of D-glucose (Supplementary Figure S2.50) in the HPLC system designed for separating MPP-derivatized reductive monosaccharides (Sun et al., 2010). While none of the techniques used can definitively determine

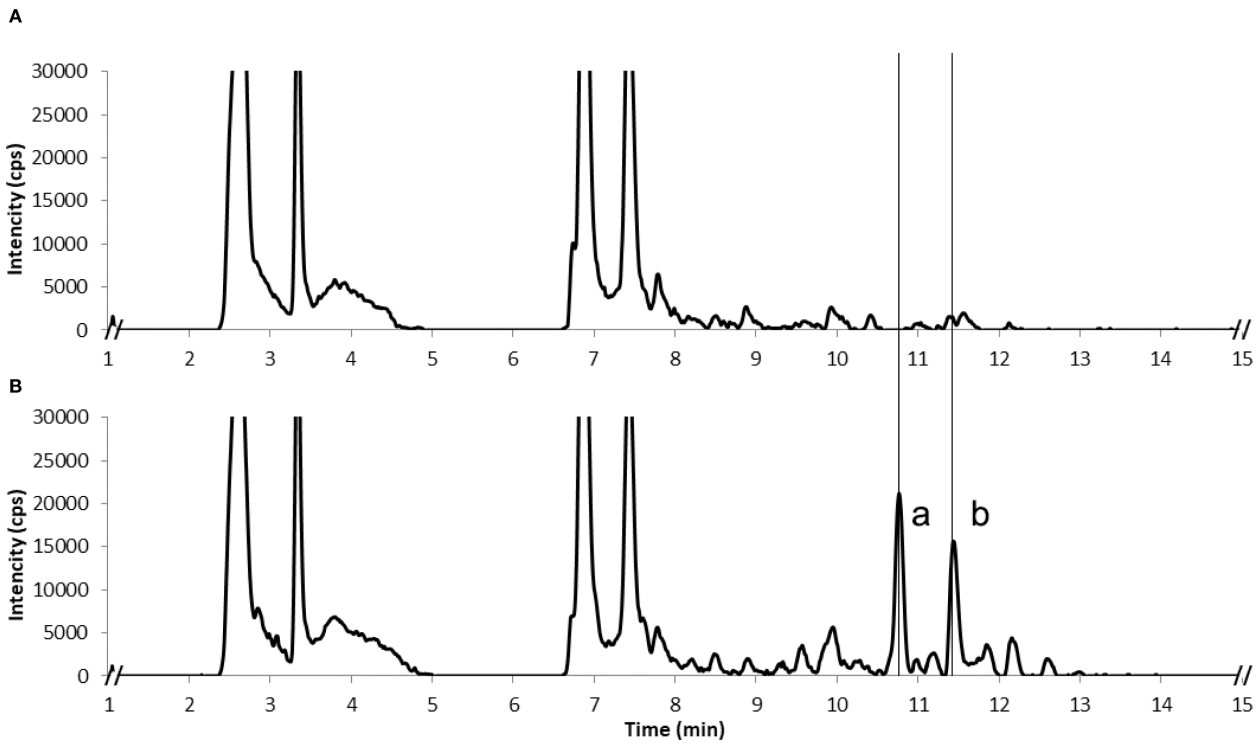

FIGURE 3
LC-ESI-MS chromatograms of methanolic extracts from *N. benthamiana* plants expressing GFP as a negative control **(A)** and an irregular IDS enzyme, chloroplast-targeted CLDS **(B)**. Detection in negative ion mode; two new peaks were identified as 6-*O*-malonyl-*β*-D-glucopyranoside (compound 5, b) and 6-*O*-malonyl-*β*-D-glucopyranosyl-(1→2)-*β*-D-glucopyranoside (compound 6, a) derivatives of cyclolavandulyl.

the absolute configuration of the glucose enantiomer in the terpene derivatives, the absence of L-glucose in higher living organisms leads us to conclude that the compounds investigated are D-glucosides.

The proton and carbon chemical shifts of the monoterpene moiety in substances 1, 3, and 5 were consistent with the literature data for the corresponding irregular monoterpene alcohols (Kim et al., 2011; Ozaki et al., 2014; Bergmann et al., 2019, respectively). The exception was the resonance positions at the glycosidic bond, which were shifted downfield. The assignments of these signals were confirmed using 2D NMR experiments. The HMBC spectra for all substances displayed correlations between C-1 of the monoterpene part and the H-1' proton of the sugar. This data revealed that substances 1, 3, and 5 contain chrysanthemyl, lavandulyl, and cyclolavandulyl moieties, respectively, linked to a 6-*O*-malonyl-glucopyranose via a 1-*O*-*β*-D-glycosidic bond.

Based on the obtained data, we identified the structures of substances 1, 3, and 5 as follows: chrysanthemyl-1-*O*-(6-*O*-malonyl)-*β*-D-glucopyranoside, lavandulyl-1-*O*-(6-*O*-malonyl)-*β*-D-glucopyranoside, and β-cyclolavandulyl-1-*O*-(6-*O*-malonyl)-*β*-D-glucopyranoside, respectively.

To determine the relative stereochemistry of the chrysanthemyl cyclopropane ring in compounds 1 and 2, we considered the biosynthesis of chrysanthemol by *Tc*CDS from *T. cinerariifolium*, which produces the *trans*-(1*R*,3*R*)-isomer of the molecule (Yang et al., 2014; Hu et al., 2018; Xu et al., 2018a). The NOESY experiment (Supplementary Figure S2.9 and S2.17) showed similar intensity signals between H-4 and H-2, H-3, 3H-7, and 3H-9. Analyzing this data with 3D models of energy-optimized conformers of both *cis*- and *trans*-1 supports the assignment of a *trans* configuration for the molecule. In this configuration, the distances between all interacting protons are within 3 Å, with the distance between protons H-4 and H-2 measuring 2.4 Å. In contrast, the calculated distance between H-4 and H-2 protons in the *cis* configuration increases to 3.6 Å, which would significantly weaken the correlation. The high conformational flexibility of the alkyl chain in compound 3 and 4 prevents a similar NOE-based assignment of the relative configuration of the lavandulyl derivatives.

Regarding the native stereoselectivity of the enzyme *Tc*CDS, data of the NOESY experiment and a single set of signals in the NMR spectra, we can assume a *trans*-(1*R*,3*R*)-configuration for the isolated chrysanthemol glucosides 1 and 2.

3.2.2 Diglucosylated derivatives (6-*O*-malonyl-*β*-D-glucopyranosyl-(1→2)-*β*-D-glucopyranosides) of chrysanthemyl, lavandulyl and cyclolavandulyl (2, 4, and 6)

Compared to compounds 1, 3, and 5, the ESI-HRMS data for substances 2, 4, and 6 revealed an increase in the $[M - H]^-$ peak by 162 mass units with the molecular formula $C_{25}H_{39}O_{14}$, indicating the addition of a hexose moiety.

NMR analysis of compounds 2, 4, and 6 showed the presence of the same monoterpene residues as those in compounds 1, 3, and 5, which are bound to a 6-*O*-malonyl hexopyranose. The data from

TOCSY, CLIP-COSY, and HMBC confirmed the presence of an additional isolated group of spin-coupled protons associated with a second hexopyranose ring. The coupling constants of 7.9-7.7 Hz for the anomeric protons in both hexoses suggest that β-glycoside linkages are present.

In compounds 2, 4, and 6, the secondary glycosylation occurred at the 2-O' position, resulting in the deshielding of the C-2' by approximately 8 ppm compared to compounds 1, 3, and 5. In all three diglycosides, the C-2' signal appeared between δ 81.7 – 81.4 ppm, while the anomeric C-1'' signal, linked at O-2', was also shifted downfield and observed at δ 104.1 – 103.9 ppm. This behavior is consistent with observations for di- and triterpene-*β*-D-glucopyranosyl-(1→2)-*β*-D-glycosides (Mizutani et al., 1984). No significant shifts in the signals for C-3 and C-4 atoms in any of the sugar moieties were observed. Additionally, the absence of a deshielding effect from the malonyl group resulted in an upfield shift of the C-6'' resonances (δ 60.8 – 60.7) and a downfield shift of C-5'' (δ 77.1 – 77.0).

The hydrolysis of compounds 2, 4, and 6, followed by MPP derivatization, confirmed that both hexapyranose residues are glucose (Supplementary Figure S2.50). Consequently, we assigned the following structures: compound 2 is chrysanthemyl-1-*O*-(6-*O*-malonyl)-*β*-D-glucopyranosyl-(1→2)-*β*-D-glucopyranoside; compound 4 is lavandulyl-1-*O*-(6-*O*-malonyl)-*β*-D-glucopyranosyl-(1→2)-*β*-D-glucopyranoside; and compound 6 is β-cyclolavandulyl-1-*O*-(6-*O*-malonyl)-*β*-D-glucopyranosyl-(1→2)-*β*-D-glucopyranoside. To the best of our knowledge, these compounds have not been previously reported and represent a new subgroup of natural irregular monoterpene glycosides.

3.3 Accumulation of non-volatile forms of irregular monoterpenes after transient expression in *N. benthamiana*

For all three irregular monoterpene skeletons, the ratios of malonyl mono- to diglucosides varied considerably among samples. To facilitate a clear comparison across experiments, the product yields are represented as a sum of the molar amounts of both glucosylated derivatives for each irregular monoterpene. The expression of *Tc*CDS and *Li*LDS with the native chloroplast targeting peptides resulted in comparable amounts of irregular terpene glucosides 1-4. Chrysanthemyl glucosides accumulated at the concentration of 0.9 ± 0.3 µmol g^{-1} FW (288 ± 102 µg g^{-1} FW of 1 and 77 ± 44 µg g^{-1} FW of 2); the content of lavandulyl glucosides was determined as 0.6 ± 0.3 µmol g^{-1} FW (161 ± 74 µg g^{-1} FW of 3 and 122 ± 100 µg g^{-1} FW of 4). Cytoplasmic CLDS formed higher amounts of irregular structures, 1.1 ± 0.3 µmol g^{-1} FW (299 ± 89 µg g^{-1} FW of 5 and 195 ± 98 µg g^{-1} FW of 6). When CLDS was translocated into chloroplasts, the yield of these products significantly increased ($p < 0.01$), reaching 1.9 ± 0.6 µmol g^{-1} FW (527 ± 176 µg g^{-1} FW of 5 and 330 ± 111 µg g^{-1} FW of 6) (Figure 4).

3.4 Supporting irregular monoterpene production in chloroplasts

The common approach to enhancing terpene accumulation in plants involves the overexpression of the enzymes that act as bottlenecks in the biosynthesis pathways for C5 precursors. For the MEP pathway in plastids, metabolic control analysis indicated that the major controlling enzyme is 1-deoxyxylulose 5-phosphate synthase (DXS) (Wright et al., 2014). DXS was repeatedly shown to be the most effective co-expression partner for increasing the biosynthesis of heterologous regular terpenoids in chloroplasts of transiently transformed *N. benthamiana*, e.g. for formation of mono- (Park et al., 2022), sesqui- (Li et al., 2019), and diterpenes (Forestier et al., 2021). Overexpression of DXS was successfully employed also for enhancing the production of native components of essential oil in transgenic lavender (Munoz-Bertomeu et al., 2006). However, when the DXS enzyme was co-expressed with the chloroplast-localized *Tc*CDS, we did not observe a statistically significant increase in glucoside accumulation ($p > 0.05$).

The next limiting factor in biosynthesis of irregular terpenes may be the unfavorable ratio of DMAPP to IPP. While the MEP pathway produces both isoprenyl diphosphate isomers, IPP is the predominant product, and the MVA pathway ends in IPP only. The overexpression of isopentenyl diphosphate isomerases (IDI), which interconvert C5 precursors, was beneficial even for the formation of regular terpenes that result from the joining of IPP and DMAPP (Chen et al., 2012). We hypothesized that this reaction may be particularly essential for enhancing the irregular coupling involving two DMAPP units. Indeed, a significant improvement in product formation was achieved by simultaneously alleviating two bottlenecks in DMAPP formation, the DXS reaction and shifting the ratio between IPP and DMAPP by an IDI activity. In our experiments, we utilized three IDIs. Two of these enzymes, *Ec*IDI1 from *E. coli* and *At*IDI1 from *A. thaliana*, belong to the widespread type I of the IDI family. The third enzyme, *Bl*IDI2 from *B. licheniformis*, is classified as type II, which is primarily found in thermophilic bacterial and archaeal species and differs significantly in structure from the type I (Berthelot et al., 2012). For all three applied IDI enzymes, we found that co-expressing a chloroplast-targeted isomerase with DXS and *Tc*CDS resulted in a significant increase ($p < 0.01$) in chrysanthemyl glucoside accumulation when compared to *Tc*CDS expressed alone or in combination with DXS. Co-expressing *Tc*CDS with IDIs alone did not produce any change in product levels ($p > 0.05$). Additionally, we observed no effect on product accumulation when *Tc*CDS was co-expressed with HMGR, a bottleneck enzyme in the cytoplasmic mevalonate pathway of precursor biosynthesis, whether or not it was combined with IDI (Figure 5).

A possibility of increasing the DMAPP pool by recycling monophosphate DMAP by isopentenyl phosphate kinase (IPK) was considered. This activity has been reported in *Arabidopsis*, and overexpressing *At*IPK has led to increased levels of native and

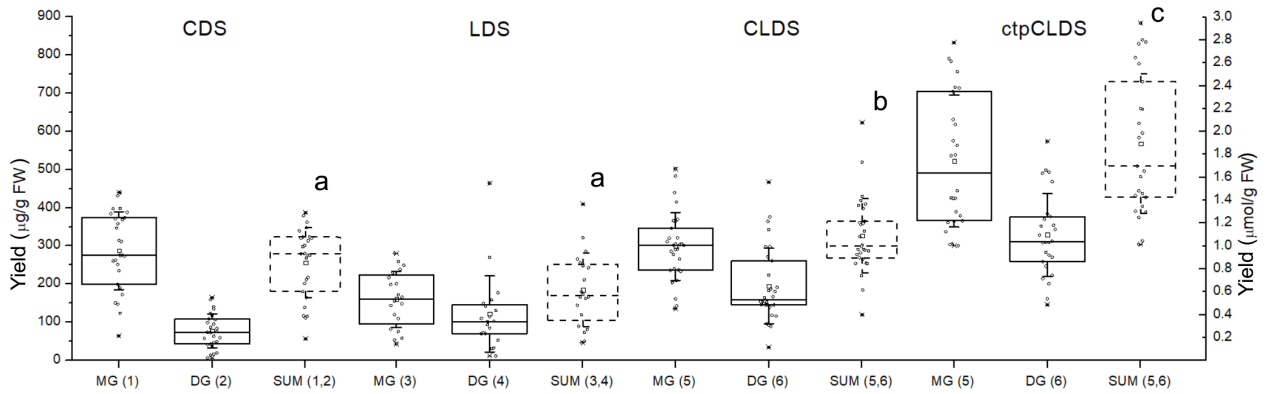

FIGURE 4
The concentration of monoterpene malonyl-glucosides in leaf biomass after transient expression of heterologous IDS in *N. benthamiana*. MG – malonyl-monoglucoside, µg/g FW; DG – malonyl-diglucoside, µg/g FW; SUM – total molar concentration of both glucosylated derivatives, µmol/g FW; the numbers in brackets refer to the structures. Different letters indicate significant differences at $p < 0.01$; n = 20–30 repeats.

heterologous terpenes (Henry et al., 2015; Gutensohn et al., 2021). However, the co-expressed chloroplast-targeted *At*IPK did not significantly enhance *Tc*CDS product accumulation, whether used alone or in combination with DXS or both DXS and IDI (Figure 5).

The co-expression of DXS and IDI resulted in a statistically significant increase ($p < 0.01$) in the accumulation of lavandulyl glucosides, too. However, it did not lead to a significant improvement ($p > 0.05$) in the levels of cyclolavandulyl glucosides produced by the chloroplast-targeted CLDS (Figure 6). This outcome may be attributed to the initially higher levels of irregular terpene glucoside accumulation following the expression of ctpCLDS.

3.5 Improving cyclolavandulyl skeleton formation in cytoplasm

The accumulation of MVA-pathway derived heterologous regular sesqui- (Park et al., 2022) and triterpenes (Reed et al., 2017) by transient expression of cytoplasmic enzymes was most effectively supported by co-expression of hydroxymethylglutaryl-CoA reductase (HMGR), particularly the N-truncated soluble version of HMGR1 enzyme from *S. cerevisiae* (tHMGR) (Polakowski et al., 1998). We utilized tHMGR to improve the productivity of CLDS in cytoplasm. Unlike DXS co-expression, inclusion of tHMGR alone resulted in a statistically significant increase ($p < 0.01$) in the levels of cyclolavandulyl malonyl-glucosides (5, 6). The addition of IDI or IPK activities did not further enhance the product accumulation. The activity of CLDS in the cytoplasm was not significantly improved ($p > 0.05$) by the overexpression of bottleneck enzymes of MEP pathway in chloroplasts, such as DXS alone or in combination with ctp*At*IDI (Figure 7).

It is important to note that co-expressing CLDS and tHMGR often caused necrosis in the leaf tissue (Supplementary Figure S2.51). This phenomenon occurred only in experiments involving tHMGR and cytoplasmic CLDS, with or without additional enzymes. Approximately half of the leaves expressing CLDS in conjunction with tHMGR developed severe necrosis and showed negligible levels of cyclolavandulyl glucosides. These samples were excluded from the calculations of monoterpene glucoside levels presented in Figure 7.

4 Discussion

Considering the benefits of monoterpene glycosylation for easier accumulation and storage in extractable forms within plant cells, we focused our study on developing a platform for producing non-volatile glycosylated irregular monoterpenes in the leaves of *N. benthamiana* after the transient expression of the corresponding IDS genes. Glycosylation is the enzymatic process in which a sugar residue from an activated nucleotide sugar is attached to an acceptor molecule. This process is widely found throughout the plant kingdom. Numerous enzymes, glycosyl transferases and glycosidases, have been identified to facilitate the synthesis and hydrolysis of glycosides. Glycosylation plays several important metabolic roles, such as providing structural support, enabling transport, offering protection, and serving storage functions. For secondary metabolites, many of which are toxic, glucosylation facilitates their transport and storage in vacuoles in an inactive form. Later, through enzymatic hydrolysis, an active aglycone can be released (Kytidou et al., 2020).

Plants produce a wide variety of glycosylated secondary metabolites. Within the monoterpene group, nearly 400 glycosides have been isolated and identified from various plant species over the past few decades (Dembitsky, 2006; Soni et al., 2025). Notably, only 1-2% of these glycosides feature a glucose moiety decorated with a malonyl group. The aglycone portions of these malonyl glycosides consist of regular cyclic monoterpene structures (Yamada et al., 2010; Selenge et al., 2014). These compounds have been isolated from *Dracocephalum foetidum* and *Monarda punctata*, both belonging to the Lamiaceae family, along with various other groups of glycosylated metabolites (Yamada

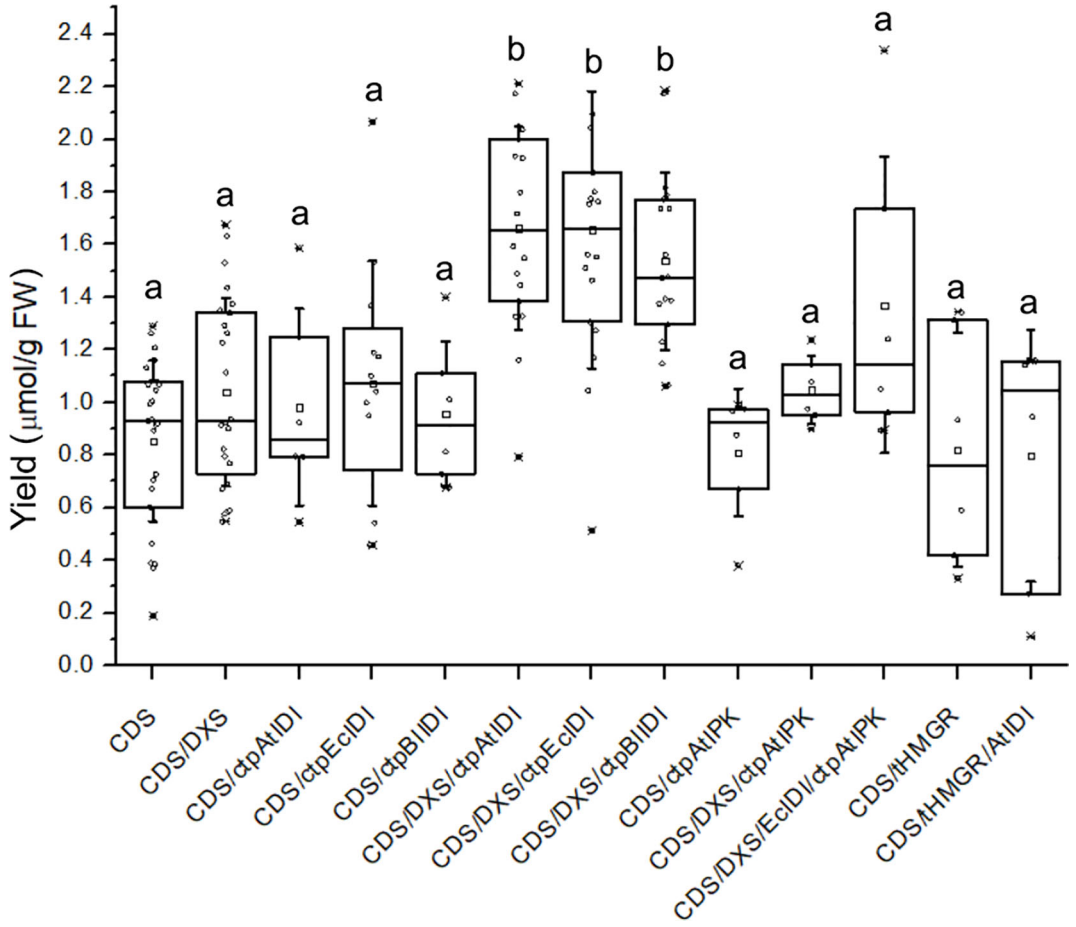

FIGURE 5
The total concentration of chrysanthemyl-malonyl-glucosides **(1, 2)** in leaf biomass following transient expression of *Tc*CDS and auxiliary genes in *N. benthamiana*. Different letters indicate significant differences at $p < 0.01$; $n = 6–27$ repeats.

et al., 2010; Selenge et al., 2014). To date, no native malonylated glycosides have been reported in tobacco. Systematic screening of glycosides in tobacco leaf extracts using HPLC-MS has revealed 64 glycosylated structures, which include 39 monosaccharide-linked glycosides, 18 diglycosides, and 7 triglycosides. The aglycone components include flavonoids, coumarins, ionone-related molecules, and sesquiterpene structures (Ding et al., 2015).

The investigation of transgenic tobacco expressing heterologous regular and irregular IDS and terpene synthase genes resulted in a significant increase in the total levels of volatile monoterpenes emitted from the flowers and leaves (Lucker et al., 2004; Yang et al., 2014; Matáeos-Fernández et al., 2023). In one of the early studies, Lucker et al. (2004) found no evidence of heterologous monoterpene glycosylation in tobacco cells. However, a later study by Yang et al. (2014) demonstrated the presence of malonyl-glucoside derivatives of chrysanthemol and chrysanthemic acid in *N. tabacum* (Yang et al., 2014; Xu et al., 2018b). When the pathway for synthesis of geranic acid was introduced in maize, the most dominant new compound was identified as geranoyl-6-*O*-malonyl-β-D-glucopyranoside. It is noteworthy, that this metabolite was not detected in control plants which contained other geraniol derivatives, although at relatively low levels (Yang et al., 2011).

For many monoterpenes, the accumulation of glycosylated forms predominated over that of aglycones. In *Petunia hybrida* plants transformed with linalool synthase, as well as in transgenic *Chrysanthemum morifolium* expressing the *Tc*CDS gene, the synthesized monoterpenes were almost entirely converted and stored in glucosylated form (Lucker et al., 2001; Hu et al., 2018). In transgenic *S. lycopersicum* or *N. benthamiana* that transiently expressed *Tc*CDS along with two oxidoreductases, approximately two-thirds of the produced *trans*-chrysanthemic acid were glycosylated (Xu et al., 2018a, 2018).

In our experiments, the concentration of terpene monoglucosides prevailed over that of diglucosides, but the ratio varied for different monoterpene moieties, ranging from 3.7 for the compounds 1 and 2 to 1.3 and 1.6 for the compounds 3 and 4 and 5 and 6, respectively. Notably, the ratio for the compounds 5 and 6 did not differ between cytoplasm and chloroplast-localized IDS, being 1.6 and 1.5, respectively. The variability in glycoside accumulation among different plant hosts may be influenced by the species-specific

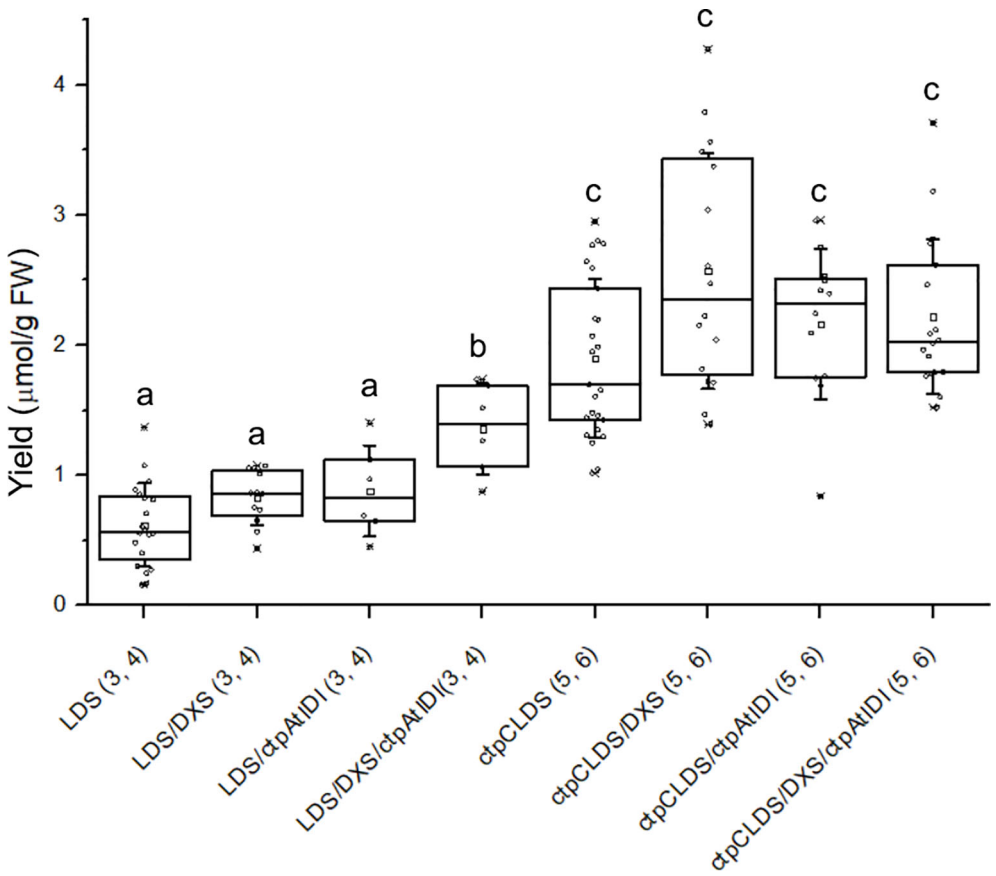

FIGURE 6
The total concentration of lavandulyl-malonyl-glucosides (3, 4) and cyclolavandulyl-malonyl-glucosides (5, 6) in leaf biomass following transient expression of *Li*LDS or chloroplast-targeted CLDS and auxiliary genes in *N. benthamiana*. Different letters indicate significant differences at $p < 0.01$; $n = 6–23$ repeats.

activity of glycosylation enzymes. This activity can, in turn, be regulated by the concentration of heterologous monoterpenes and the rate of their biosynthesis. An analysis of the terpenoid database (TPCN) showed a positive correlation between the levels of terpenoids in various plant species and their glycosylation levels (Li et al., 2024). From a plant physiology perspective, glycosylation enhances the water solubility and stability of terpenoids. This process facilitates the transfer and storage of terpenoids in vacuoles and reduces their toxicity to plant cells. During transient expression, the rapid synthesis of heterologous IDS, followed by an intensive formation of products, may stimulate intracellular mechanisms related to metabolite transport and detoxification, further promoting glycosylation.

The reported concentrations of heterologous non-volatile monoterpenes in the tissues of transgenic plants range from 0.07 to 0.7 µmol g^{-1} FW (10 to 121 µg g^{-1} FW) (Lucker et al., 2001; Yang et al., 2011; Xu et al., 2018a). Transient expression of *Tc*CDS, in combination with two oxidoreductases, led to the accumulation of *trans*-chrysanthemic acid in esterified forms, including malonylated glucosides, at a level of 1.1 µmol g^{-1} FW (190 µg g^{-1} FW) which constituted 58% of the total monoterpene content (Xu et al., 2018b). In our experiments, transient co-expression of plant-derived naturally plastid-targeted *Li*LDS and *Tc*CDS with auxiliary substrate-producing enzymes DXS and IDI resulted in accumulation of lavandulyl and chrysanthemyl glycosides at levels of 1.4 ± 0.3 and 1.6 ± 0.4 µmol g^{-1} FW, respectively. Prokaryotic CLPS fused with an artificial chloroplast-targeting peptide allowed for the accumulation of 2.2 ± 0.7 µmol g^{-1} FW of cyclolavandulol in the form of non-volatile mono- and diglucosides. Initially higher level of the latter compound was not statistically significantly increased further by enhancing the metabolic flux through the MEP pathway and intensifying the isomerization of IPP to DMAPP by overexpression of DXS and IDI. Subsequent experiments on cytoplasmic formation of irregular monoterpenes have indicated that the observed product concentrations approach the tolerance threshold for plant cells regarding these compounds.

Co-expression of CLDS and tHMGR in the cytoplasm led to the highest concentration of cyclolavandulyl glucosides in the tissue. Significantly better performance of the MVA pathway for terpene production has been repeatedly demonstrated in microbial hosts. Not only in eukaryotic chassis, e.g. *S. cerevisiae*, the highest titers were achieved by engineering the native MVA pathway, but the most effectively producing bacterial strains were constructed by introducing the heterologous enzymes of the MVA route (Yang et al., 2025). In plants, the overexpression of the enzymes of both pathways increases the terpene production (Park et al., 2022).

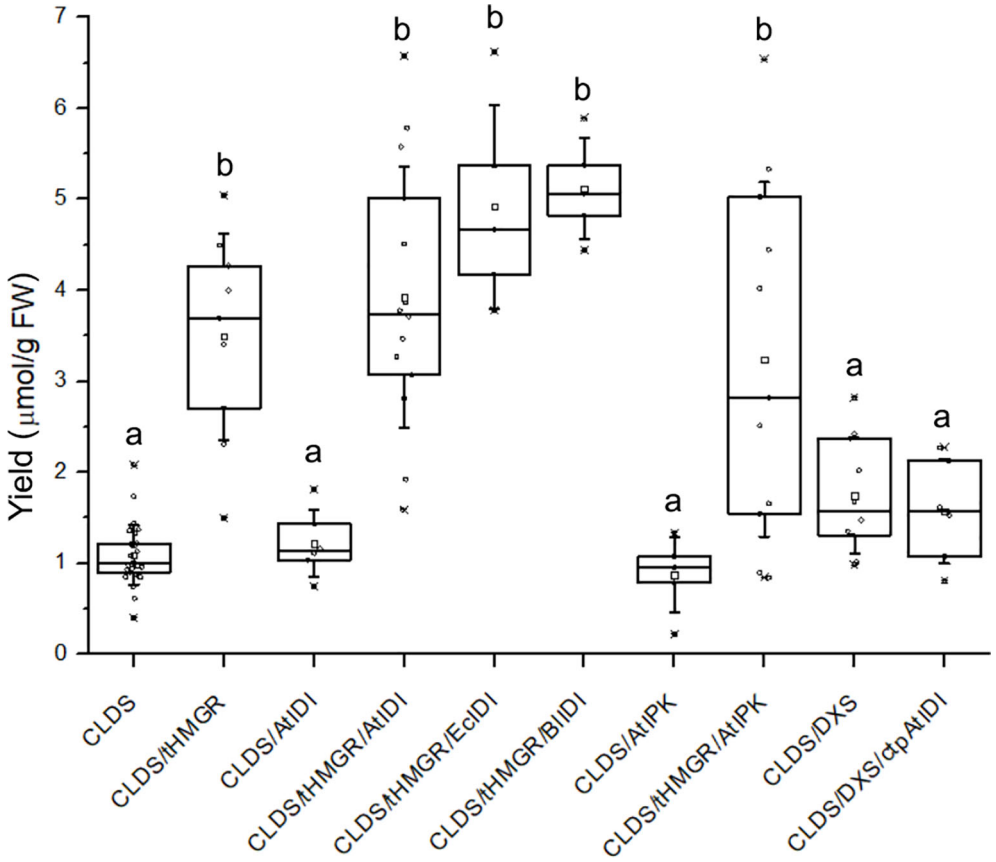

FIGURE 7
The total concentration of cyclolavandulyl-malonyl-glucosides (5, 6) in leaf biomass following transient expression of CLDS and auxiliary genes in *N. benthamiana*. Different letters indicate significant differences at $p < 0.01$; n = 5–30 repeats.

Investigation of substrate availability in plastids and cytoplasm of tomato fruit cell revealed that MVA-derived sesquiterpenes were formed in considerably less amounts than monoterpenes originated from MEP. However, the overexpression of HMGR elevated the product level more efficiently than DXS (Gutensohn et al., 2021). In our experiments, the co-expression of HMGR with CLDS often caused leaf necrosis which was not observed for each of these enzymes alone or for any other protein combination. We assume that either the amount of produced monoterpenes surpasses the capacities of the glycosylation system leading to the accumulation of toxic free alcohols or the malonyl glucosides are also toxic at high concentrations. The mean level of cyclolavandulyl glucosides after co-expression of CLDS and HMGR reached 3.9 ± 1.5 µmol g^{-1} FW; the best samples contained 6.6 µmol g^{-1} FW of these compounds. These values represent the highest reported concentrations of irregular monoterpenes isolated from a plant system. The obtained compounds can either be tested for biological activities in the glucosylated form or used to obtain the aglycones that can be converted into known valuable derivatives. For example, lavandulyl senecioate and cyclolavandulyl butyrate serve as signaling molecules for insects (Hinkens et al., 2001; Tabata et al., 2011) and can be implemented into environmental-friendly plant pest control strategies (Rizvi et al., 2021). On the other hand, it has been shown that chrysanthemyl-6-*O*-malonyl-*β*-D-glucopyranoside has a deterring effect on aphids (Hu et al., 2018), so the glucosylated derivatives of chrysanthemol may be applied for plant protection directly.

5 Conclusions

To promote sustainable plant-based production of irregular monoterpenes, we established a transient procedure to enhance the biosynthetic flux in *Nicotiana benthamiana* toward DMAPP by coexpressing IDS genes and the genes of substrate-producing enzymes of MEP or MVA pathways. That allowed the accumulation of substantial amounts of non-volatile glucosylated derivatives of irregular monoterpenes. We identified five new metabolites of lavandulol, cyclolavandulol and chrysanthemol in addition to the previously described chrysanthemyl-6-*O*-malonyl-*β*-D-glucopyranoside. Alleviating the bottlenecks in the biosynthesis of the substrate for the key enzymes resulted in the highest yields of irregular monoterpenes reported for the plant systems.

Data availability statement

The raw data supporting the conclusions of this article will be made available by the authors, without undue reservation.

Author contributions

IG: Conceptualization, Investigation, Methodology, Validation, Writing – original draft, Writing – review & editing. YS: Investigation, Methodology, Validation, Writing – original draft, Writing – review & editing. VS: Methodology, Writing – review & editing. HW: Funding acquisition, Project administration, Writing – review & editing.

Funding

The author(s) declare financial support was received for the research and/or publication of this article. The research was supported by the European Research Area Cofund Action 'ERACoBioTech' under Horizon 2020, the project SUSPHIRE (Sustainable Production of Pheromones for Insect Pest Control in Agriculture). The financial support from the German Federal Ministry of Education and Research (BMBF), grant number 031B0605, and from the German Research Foundation (DFG), grant number INST 163/444-1 FUGG (QTOF MS) is highly appreciated. YS acknowledges the support by DFG, grant number 516587177.

Acknowledgments

The authors are grateful to the mass spectrometry core facility team of the Chemistry Department at the Technical University of Darmstadt for measurements of the ESI/APCI spectra. The authors thank Prof. Christina M. Thiele, Technische Universität Darmstadt, for measurement time on the 700 MHz NMR spectrometer.

Conflict of interest

The authors declare that the research was conducted in the absence of any commercial or financial relationships that could be construed as a potential conflict of interest.

Generative AI statement

The author(s) declare that no Generative AI was used in the creation of this manuscript.

Any alternative text (alt text) provided alongside figures in this article has been generated by Frontiers with the support of artificial intelligence and reasonable efforts have been made to ensure accuracy, including review by the authors wherever possible. If you identify any issues, please contact us.

Publisher's note

Supplementary material

The Supplementary Material for this article can be found online at: https://www.frontiersin.org/articles/10.3389/fpls.2025.1678814/full#supplementary-material

References

Baumgartner, J. T., and McKinnie, S. M. K. (2024). Regioselective halogenation of lavanducyanin by a site-selective vanadium-dependent chloroperoxidase. *Organic Lett.* 26, 5725–5730. doi: 10.1021/acs.orglett.4c01869

Bergman, M. E., Kortbeek, R. W. J., Gutensohn, M., and Dudareva, N. (2024). Plant terpenoid biosynthetic network and its multiple layers of regulation. *Prog. Lipid Res.* 95, 101287. doi: 10.1016/j.plipres.2024.101287

Bergmann, J., Tapia, J., Bravo, M., Zaviezo, T., and Flores, M. F. (2019). Synthesis of citrophilus mealybug sex pheromone using chrysanthemol extracted from Pyrethrum (*Tanacetum cinerariifolium*). *Nat. Prod. Res.* 33, 303–308. doi: 10.1080/14786419.2018.1446136

Berthelot, K., Estevez, Y., Deffieux, A., and Peruch, F. (2012). Isopentenyl diphosphate isomerase: A checkpoint to isoprenoid biosynthesis. *Biochimie* 94, 1621–1634. doi: 10.1016/j.biochi.2012.03.021

Bhosale, V. A., and Waghmode, S. B. (2017). An efficient total synthesis of (-)-(R), (+)-(S)-lavandulol pheromones and their derivatives through proline catalyzed asymmetric α-aminooxylation and [3,3] claisen rearrangement. *Chemistryselect* 2, 1262–1266. doi: 10.1002/slct.201601890

Boutanaev, A. M., Moses, T., Zi, J., Nelson, D. R., Mugford, S. T., Peters, R. J., et al. (2015). Investigation of terpene diversification across multiple sequenced plant genomes. *Proc. Natl. Acad. Sci. U. S. A.* 112, E81–E88. doi: 10.1073/pnas.1419547112

Brennan, T. C., Turner, C. D., Kromer, J. O., and Nielsen, L. K. (2012). Alleviating monoterpene toxicity using a two-phase extractive fermentation for the bioproduction of jet fuel mixtures in Saccharomyces cerevisiae. *Biotechnol. Bioeng.* 109, 2513–2522. doi: 10.1002/bit.24536

Brito-Arias, M. (2007). "Nuclear magnetic resonance of glycosides," in *Synthesis and Characterization of Glycosides*. Ed. M. Brito-Arias (Springer US, Boston, MA), 314–329.

Chen, R., Harada, Y., Bamba, T., Nakazawa, Y., and Gyokusen, K. (2012). Overexpression of an isopentenyl diphosphate isomerase gene to enhance trans-polyisoprene production in Eucommia ulmoides Oliver. *BMC Biotechnol.* 12, 78. doi: 10.1186/1472-6750-12-78

Christianson, D. W. (2017). Structural and chemical biology of terpenoid cyclases. *Chem. Rev.* 117, 11570–11648. doi: 10.1021/acs.chemrev.7b00287

Dembitsky, V. M. (2006). Astonishing diversity of natural surfactants: 7. Biologically active hemi- and monoterpenoid glycosides. *Lipids* 41, 1–27. doi: 10.1007/s11745-006-5065-y

Demissie, Z. A., Erland, L. A., Rheault, M. R., and Mahmoud, S. S. (2013). The biosynthetic origin of irregular monoterpenes in Lavandula: isolation and biochemical characterization of a novel cis-prenyl diphosphate synthase gene, lavandulyl diphosphate synthase. *J. Biol. Chem.* 288, 6333–6341. doi: 10.1074/jbc.M112.431171

Di, X., and Rodriguez-Concepcion, M. (2023). Exploring the deoxy-D-xylulose-5-phosphate synthase gene family in tomato (Solanum lycopersicum). *Plants* 12, 3886. doi: 10.3390/plants12223886

Ding, L., Wang, X., Wang, S., Yu, J., Qin, Y., Zhang, X., et al. (2015). Systematic screening and characterization of glycosides in tobacco leaves by liquid chromatography with atmospheric pressure chemical ionization tandem mass spectrometry using neutral loss scan and product ion scan. *J. Sep Sci.* 38, 4029–4035. doi: 10.1002/jssc.201500760

Dudareva, N., and Pichersky, E. (2008). Metabolic engineering of plant volatiles. *Curr. Opin. Biotechnol.* 19, 181–189. doi: 10.1016/j.copbio.2008.02.011

Forestier, E. C. F., Czechowski, T., Cording, A. C., Gilday, A. D., King, A. J., Brown, G. D., et al. (2021). Developing a Nicotiana benthamiana transgenic platform for high-value diterpene production and candidate gene evaluation. *Plant Biotechnol. J.* 19, 1614–1623. doi: 10.1111/pbi.13574

Gerasymenko, I., Sheludko, Y., Frabel, S., Staniek, A., and Warzecha, H. (2019). Combinatorial biosynthesis of small molecules in plants: Engineering strategies and tools. *Methods Enzymol.* 617, 413–442. doi: 10.1016/bs.mie.2018.12.005

Gutensohn, M., Henry, L. K., Gentry, S. A., Lynch, J. H., Nguyen, T. T. H., Pichersky, E., et al. (2021). Overcoming bottlenecks for metabolic engineering of sesquiterpene production in tomato fruits. *Front. Plant Sci.* 12. doi: 10.3389/fpls.2021.691754

Hahn, F. M., Hurlburt, A. P., and Poulter, C. D. (1999). Escherichia coli open reading frame 696 is idi, a nonessential gene encoding isopentenyl diphosphate isomerase. *J. Bacteriol.* 181, 4499–4504. doi: 10.1128/JB.181.15.4499-4504.1999

Henry, L. K., Gutensohn, M., Thomas, S. T., Noel, J. P., and Dudareva, N. (2015). Orthologs of the archaeal isopentenyl phosphate kinase regulate terpenoid production in plants. *Proc. Natl. Acad. Sci. U.S.A.* 112, 10050–10055. doi: 10.1073/pnas.1504798112

Hinkens, D. M., Mcelfresh, J. S., and Millar, J. G. (2001). Identification and synthesis of the sex pheromone of the vine mealybug. *Tetrahedron Lett.* 42, 1619–1621. doi: 10.1016/S0040-4039(00)02347-9

Hu, H., Li, J., Delatte, T., Vervoort, J., Gao, L., Verstappen, F., et al. (2018). Modification of chrysanthemum odour and taste with chrysanthemol synthase induces strong dual resistance against cotton aphids. *Plant Biotechnol. J.* 16, 1434–1445. doi: 10.1111/pbi.12885

Jansen, D. J., and Shenvi, R. A. (2014). Synthesis of medicinally relevant terpenes: reducing the cost and time of drug discovery. *Future Med. Chem.* 6, 1127–1146. doi: 10.4155/fmc.14.71

Kanwal, A., Bilal, M., Rasool, N., and Zubair, M. (2022). Total synthesis of terpenes and their biological significance: A critical review. *Pharmaceuticals* 15, 1392. doi: 10.3390/ph15111392

Kim, H. J., Su, L., Jung, H., and Koo, S. (2011). Selective deoxygenation of allylic alcohol: stereocontrolled synthesis of lavandulol. *Organic Lett.* 13, 2682–2685. doi: 10.1021/ol200779y

Kinoshita, Y., Watanabe, H., Kitahara, T., and Mori, K. (1995). Concise construction of N-alkylated phenazinone skeletons: synthesis of lavanducyanin (WS-9659A). *Synlett* 1995, 186–188. doi: 10.1055/s-1995-4905

Knölker, H.J., and Fröhner, W. (1998). Transition metal complexes in organic synthesis.: Part 42.: First total synthesis of the potent neuronal cell protecting substance (±)-lavanduquinocin iron- and nickel-mediated coupling reactions. *Tetrahedron Lett.* 39, 2537-2540. doi: 10.1016/S0040-4039(98)00340-2

Koos, M. R. M., Kummerlöwe, G., Kaltschnee, L., Thiele, C. M., and Luy, B. (2016). CLIP-COSY: A clean in-phase experiment for the rapid acquisition of COSY-type correlations. *Angewandte Chemie Int. Edition* 55, 7655–7659. doi: 10.1002/anie.201510938

Kytidou, K., Artola, M., Overkleeft, H. S., and Aerts, J. (2020). Plant glycosides and glycosidases: A treasure-trove for therapeutics. *Front. Plant Sci.* 11, 357. doi: 10.3389/fpls.2020.00357

Li, W. Q., Chen, Y. L., Yang, R. F., Hu, Z. L., Wei, S. Z., Hu, S., et al. (2024). A terpenoids database with the chemical content as A novel agronomic trait. *Database* 2024, baae027. doi: 10.1093/database/baae050

Li, J., Mutanda, I., Wang, K., Yang, L., Wang, J., and Wang, Y. (2019). Chloroplastic metabolic engineering coupled with isoprenoid pool enhancement for committed taxanes biosynthesis in Nicotiana benthamiana. *Nat. Commun.* 10, 4850. doi: 10.1038/s41467-019-12879-y

Lucker, J., Bouwmeester, H. J., Schwab, W., Blaas, J., van der Plas, L. H., and Verhoeven, H. A. (2001). Expression of Clarkia S-linalool synthase in transgenic petunia plants results in the accumulation of S-linalyl-beta-D-glucopyranoside. *Plant J.* 27, 315–324. doi: 10.1046/j.1365-313x.2001.01097.x

Lucker, J., Schwab, W., Van Hautum, B., Blaas, J., van der Plas, L. H., Bouwmeester, H. J., et al. (2004). Increased and altered fragrance of tobacco plants after metabolic engineering using three monoterpene synthases from lemon. *Plant Physiol.* 134, 510–519. doi: 10.1104/pp.103.030189

Lybrand, D. B., Xu, H. Y., Last, R. L., and Pichersky, E. (2020). How plants synthesize pyrethrins: safe and biodegradable insecticides. *Trends Plant Sci.* 25, 1240–1251. doi: 10.1016/j.tplants.2020.06.012

Matáeos-Fernández, R., Vacas, S., Navarro-Fuertes, I., Navarro-Llopis, V., Orzáez, D., and Gianoglio, S. (2023). Assessment of tobacco (Nicotiana tabacum) and N. benthamiana as biofactories of irregular monoterpenes for sustainable crop protection. *Ind. Crops Prod.* 206, 117634. doi: 10.1016/j.indcrop.2023.117634

Meadows, A. L., Hawkins, K. M., Tsegaye, Y., Antipov, E., Kim, Y., Raetz, L., et al. (2016). Rewriting yeast central carbon metabolism for industrial isoprenoid production. *Nature* 537, 694–697. doi: 10.1038/nature19769

Mizutani, K., Hayashi, A., Kasai, R., Tanaka, O., Yoshida, N., and Nakajima, T. (1984). N.M.R.-spectral studies of 2-linked glycosides: 2-O-glycosylation shifts of 2-O-glycosylated α- and β-l-arabinopyranosides. *Carbohydr. Res.* 126, 177–189. doi: 10.1016/0008-6215(84)85376-8

Munoz-Bertomeu, J., Arrillaga, I., Ros, R., and Segura, J. (2006). Up-regulation of 1-deoxy-D-xylulose-5-phosphate synthase enhances production of essential oils in transgenic spike lavender. *Plant Physiol.* 142, 890–900. doi: 10.1104/pp.106.086355

Nagel, R., Gershenzon, J., and Schmidt, A. (2012). Nonradioactive assay for detecting isoprenyl diphosphate synthase activity in crude plant extracts using liquid chromatography coupled with tandem mass spectrometry. *Anal. Biochem.* 422, 33–38. doi: 10.1016/j.ab.2011.12.037

Nie, S., Chen, R., Ge, M., Qu, Y., Liu, X., Ruan, C., et al. (2025). Biosynthesis of irregular monoterpene lavandulol in Saccharomyces cerevisiae. *Synth. Syst. Biotechnol.* 10, 1267-1274. doi: 10.1016/j.synbio.2025.06.001

Nosaki, S., Hoshikawa, K., Ezura, H., and Miura, K. (2021). Transient protein expression systems in plants and their applications. *Plant Biotechnol. (Tokyo)* 38, 297–304. doi: 10.5511/plantbiotechnology.21.0610a

Ozaki, T., Zhao, P., Shinada, T., Nishiyama, M., and Kuzuyama, T. (2014). Cyclolavandulyl skeleton biosynthesis via both condensation and cyclization catalyzed by an unprecedented member of the isoprenyl diphosphate synthase superfamily. *J. Am. Chem. Soc.* 136, 4837–4840. doi: 10.1021/ja500270m

Park, S., Mani, V., Kim, J. A., Lee, S. I., and Lee, K. (2022). Combinatorial transient gene expression strategies to enhance terpenoid production in plants. *Front. Plant Sci.* 13, 1034893. doi: 10.3389/fpls.2022.1034893

Phillips, M. A., D'auria, J. C., Gershenzon, J., and Pichersky, E. (2008). The Arabidopsis thaliana type I Isopentenyl Diphosphate Isomerases are targeted to multiple subcellular compartments and have overlapping functions in isoprenoid biosynthesis. *Plant Cell* 20, 677–696. doi: 10.1105/tpc.107.053926

Polakowski, T., Stahl, U., and Lang, C. (1998). Overexpression of a cytosolic hydroxymethylglutaryl-CoA reductase leads to squalene accumulation in yeast. *Appl. Microbiol. Biotechnol.* 49, 66–71. doi: 10.1007/s002530051138

Rad, S. A., Zahiri, H. S., Noghabi, K. A., Rajaei, S., Heidari, R., and Mojallali, L. (2012). Type 2 IDI performs better than type 1 for improving lycopene production in metabolically engineered E. coli strains. *World J. Microbiol. Biotechnol.* 28, 313–321. doi: 10.1007/s11274-011-0821-4

Reed, J., Stephenson, M. J., Miettinen, K., Brouwer, B., Leveau, A., Brett, P., et al. (2017). A translational synthetic biology platform for rapid access to gram-scale quantities of novel drug-like molecules. *Metab. Eng.* 42, 185–193. doi: 10.1016/j.ymben.2017.06.012

Rivera, S. B., Swedlund, B. D., King, G. J., Bell, R. N., Hussey, C. E. Jr., Shattuck-Eidens, D. M., et al. (2001). Chrysanthemyl diphosphate synthase: isolation of the gene and characterization of the recombinant non-head-to-tail monoterpene synthase from Chrysanthemum cinerariaefolium. *Proc. Natl. Acad. Sci. U. S. A.* 98, 4373–4378. doi: 10.1073/pnas.071543598

Rizvi, S., George, J., Reddy, G. V. P., Zeng, X., and Guerrero, A. (2021). Latest developments in insect sex pheromone research and its application in agricultural pest management. *Insects* 12, 484. doi: 10.3390/insects12060484

Sarrion-Perdigones, A., Vazquez-Vilar, M., Palaci, J., Castelijns, B., Forment, J., Ziarsolo, P., et al. (2013). GoldenBraid 2.0: a comprehensive DNA assembly framework for plant synthetic biology. *Plant Physiol.* 162, 1618–1631. doi: 10.1104/pp.113.217661

Selenge, E., Murata, T., Tanaka, S., Sasaki, K., Batkhuu, J., and Yoshizaki, F. (2014). Monoterpene glycosides, phenylpropanoids, and acacetin glycosides from. *Phytochemistry* 101, 91–100. doi: 10.1016/j.phytochem.2014.02.007

Shin-Ya, K., Shimizu, S., Kunigami, T., Furihata, K., Furihata, K., and Seto, H. (1995). A new neuronal cell protecting substance, lavanduquinocin, produced by Streptomyces viridochromogenes. *J. Antibiot (Tokyo)* 48, 574–578. doi: 10.7164/antibiotics.48.574

Shukal, S., Ong, L., Rehka, T., Chen, X. X., and Zhang, C. Q. (2024). Microaerobic fermentation enables high-titer biosynthesis of the rose monoterpenes geraniol and geranyl acetate in. *ACS Sustain. Chem. Eng.* 12, 3921–3932. doi: 10.1021/acssuschemeng.3c06030

Soni, M., Singh, I. P., and Lal, U. R. (2025). Naturally occurring monoterpene glycosides of plant origin. *Flavour Fragrance J.* 40, 613–637. doi: 10.1002/ffj.3862

Sun, Z. W., Song, C. H., Xia, L., Wang, X. Y., Suo, Y. R., and You, J. M. (2010). Comprehensive comparisons between 1-phenyl-3-methyl-5-pyrazolones, 1-(4-methoxyphenyl)-3-methyl-5-pyrazolones and 1-(2-naphthyl)-3-methyl-5-pyrazolones as labeling reagents used in LC-DAD-ESI-MS-MS analysis of neutral aldoses and uronic acids. *Chromatographia* 71, 789–797. doi: 10.1365/s10337-010-1570-5

Tabata, J., Teshiba, M., Hiradate, S., Tsutsumi, T., Shimizu, N., and Sugie, H. (2011). Cyclolavandulyl butyrate: an attractant for a mealybug parasitoid, (Hymenoptera: Encyrtidae). *Appl. Entomol. Zool.* 46, 117–123. doi: 10.1007/s13355-010-0012-z

Wang, X., Chen, J., Zhang, J., Zhou, Y., Zhang, Y., Wang, F., et al. (2021). Engineering Escherichia coli for production of geraniol by systematic synthetic biology approaches and laboratory-evolved fusion tags. *Metab. Eng.* 66, 60–67. doi: 10.1016/j.ymben.2021.04.008

Wang, X., Xiao, L. J., Zhang, X. Y., Zhang, J., Zhang, Y., Wang, F., et al. (2022a). Combined bioderivatization and engineering approach to improve the efficiency of geraniol production. *Green Chem.* 24, 864–876. doi: 10.1039/D1GC03419G

Wang, X., Zhang, X. Y., Zhang, J., Xiao, L. J., Zhou, Y. J. J., Zhang, Y., et al. (2022b). Genetic and bioprocess engineering for the selective and high-level production of geranyl acetate in. *ACS Sustain. Chem. Eng.* 10, 2881–2889. doi: 10.1021/acssuschemeng.1c07336

Westfall, P. J., Pitera, D. J., Lenihan, J. R., Eng, D., Woolard, F. X., Regentin, R., et al. (2012). Production of amorphadiene in yeast, and its conversion to dihydroartemisinic acid, precursor to the antimalarial agent artemisinin. *Proc. Natl. Acad. Sci. U. S. A.* 109, E111–E118. doi: 10.1073/pnas.1110740109

Wright, L. P., Rohwer, J. M., Ghirardo, A., Hammerbacher, A., Ortiz-Alcaide, M., Raguschke, B., et al. (2014). Deoxyxylulose 5-phosphate synthase controls flux through the methylerythritol 4-phosphate pathway in arabidopsis. *Plant Physiol.* 165, 1488–1504. doi: 10.1104/pp.114.245191

Xu, H., Lybrand, D., Bennewitz, S., Tissier, A., Last, R. L., and Pichersky, E. (2018a). Production of trans-chrysanthemic acid, the monoterpene acid moiety of natural pyrethrin insecticides, in tomato fruit. *Metab. Eng.* 47, 271–278. doi: 10.1016/j.ymben.2018.04.004

Xu, H., Moghe, G. D., Wiegert-Rininger, K., Schilmiller, A. L., Barry, C. S., Last, R. L., et al. (2018b). Coexpression analysis identifies two oxidoreductases involved in the biosynthesis of the monoterpene acid moiety of natural pyrethrin insecticides in tanacetum cinerariifolium. *Plant Physiol.* 176, 524–537. doi: 10.1104/pp.17.01330

Yamada, K., Murata, T., Kobayashi, K., Miyase, T., and Yoshizaki, F. (2010). A lipase inhibitor monoterpene and monoterpene glycosides from Monarda punctata. *Phytochemistry* 71, 1884–1891. doi: 10.1016/j.phytochem.2010.08.009

Yang, W. Q., Chen, X., Li, Y. L., Guo, S. F., Wang, Z., and Yu, X. L. (2020). Advances in pharmacological activities of terpenoids. *Natural Prod. Commun.* 15. doi: 10.1177/1934578X20903555

Yang, T., Gao, L., Hu, H., Stoopen, G., Wang, C., and Jongsma, M. A. (2014). Chrysanthemyl diphosphate synthase operates in planta as a bifunctional enzyme with chrysanthemol synthase activity. *J. Biol. Chem.* 289, 36325–36335. doi: 10.1074/jbc.M114.623348

Yang, D., Liang, H., Li, X., Zhang, C., Lu, Z., and Ma, X. (2025). Unleashing the potential of microbial biosynthesis of monoterpenes via enzyme and metabolic engineering. *Biotechnol. Adv.* 79, 108525. doi: 10.1016/j.biotechadv.2025.108525

Yang, T., Stoopen, G., Yalpani, N., Vervoort, J., De Vos, R., Voster, A., et al. (2011). Metabolic engineering of geranic acid in maize to achieve fungal resistance is compromised by novel glycosylation patterns. *Metab. Eng.* 13, 414–425. doi: 10.1016/j.ymben.2011.01.011

Zada, A., and Dunkelblum, E. (2006). A convenient resolution of racemic lavandulol through lipase-catalyzed acylation with succinic anhydride:: simple preparation of enantiomerically pure (R)-lavandulol. *Tetrahedron-Asymmetry* 17, 230–233. doi: 10.1016/j.tetasy.2005.12.021

Zou, Y., and Millar, J. G. (2015). Chemistry of the pheromones of mealybug and scale insects. *Nat. Prod. Rep.* 32, 1067–1113. doi: 10.1039/C4NP00143E

frontiers | Frontiers in Plant Science

TYPE Original Research
PUBLISHED 26 November 2025
DOI 10.3389/fpls.2025.1727190

OPEN ACCESS

EDITED BY
Kevin Yueju Wang,
University of Pikeville, United States

REVIEWED BY
Kathleen L Hefferon,
Cornell University, United States
Luca Marchetti,
University of Tartu, Estonia

*CORRESPONDENCE
Linda Avesani
linda.avesani@univr.it
Nico Betterle
nico.betterle@univr.it

RECEIVED 17 October 2025
ACCEPTED 03 November 2025
PUBLISHED 26 November 2025

CITATION
Ljumović K, Rosa A, Raneri A, Ballottari M, Avesani L and Betterle N (2025) An innovative infection method for the accumulation of viral nanoparticles in *Nicotiana benthamiana*. *Front. Plant Sci.* 16:1727190. doi: 10.3389/fpls.2025.1727190

An innovative infection method for the accumulation of viral nanoparticles in *Nicotiana benthamiana*

Kristina Ljumović[1], Anthony Rosa[2], Alessia Raneri[1], Matteo Ballottari[1], Linda Avesani[1*] and Nico Betterle[1*]

[1]Department of Biotechnology, University of Verona, Verona, Italy, [2]Diamante SB srl, Verona, Italy

Tomato Bushy Stunt Virus (TBSV) naturally infects tomato plants, although it can also infect other plant species, such as *Nicotiana benthamiana*, a known model system in plant molecular farming. In the presented work, a novel system for TBSV infection of *Nicotiana benthamiana* plants, designed to produce nanomaterials, was developed and optimized based on a simple foliar spray, without the use of surfactants. Up to now, the standard procedures for the viral infection have been syringe or vacuum infiltration, which are a time-consuming manual procedure or requiring expensive machinery, respectively. The spraying method was chosen because it could be implemented in industrial conditions, such as vertical farms, where spraying systems are already present or can be easily installed at a low cost. In this work, as a proof of concept, a wild type and a modified version of TBSV construct, which generated a viral nanoparticle (VNP) exposing a small 12 aa-domain Liprin alpha 1 protein (Lip1) on each capsid protein, were successfully expressed in *Nicotiana benthamiana* plants. Specifically, VNP displaying Lip1 is a candidate for the treatment of rheumatoid arthritis. After 7 days of incubation, signs of viral infection were visible in the infected plants, while prolonged incubation time to 8 days significantly increased the accumulation of VNPs. The infection method described here offers straightforwardness and scalability of plant molecular farming, representing an efficient solution for the complexity of the conventional infection process.

KEYWORDS

***Nicotiana benthamiana*, plant molecular farming, TBSV, viral nano particles, transient expression, hydroponic, spraying infection**

1 Introduction

Viruses are infectious agents programmed to deliver their nucleic acids into the hosts, such as plants, humans, and animals, enabling their replication and production of new viral copies. This strategy has several properties that can be further applied in various fields, including biotechnology, agriculture, medicine, and nanotechnology (Wen and Steinmetz,

2016; Nkanga and Steinmetz, 2021). Auto-assembly of one or more protein subunits forms viral capsids, establishing VNPs that are homogenous in shape and dimension. On the capsid subunits, it is possible to attach peptides of interest both via genetic engineering and via chemical reactions (Sánchez et al., 2013). VNPs can be based on bacteriophages, mammalians, and plant viruses. In particular, plant VNPs have all the characteristics mentioned above and are not pathogenic to mammals such as humans.

The production of plant VNPs can be achieved by molecular farming, which consists in the production of recombinant proteins or secondary metabolites of interest using plants as biofactories. To date, plant VNPs have been developed for the production of therapeutic agents and immunostimulants (Rybicki, 2020), as well as for applications in bioimaging and cancer therapies (Zhou et al., 2023). Specifically in the case of immunostimulants, applications of recombinant plant VNPs consisted in the surface exposure of immunodominant peptides associated with autoimmune diseases.

Rheumatoid arthritis is a systemic disease that comprises progressive synovial inflammation (Majithia and Geraci, 2007). Recently, it has been shown that Lip1 peptide is immunodominant in patients with Rheumatoid Arthritis (Bason et al., 2021). Such a peptide, composed of 12 amino acids, was successfully expressed on the surface of TBSV Tomato Bushy Stunt Virus (TBSV) capsid (Zampieri et al., 2020). Specifically, Lip1 was fused to the viral coat proteins, yielding TBSV.pLip. TBSV usually infects tomato plants, but successful infection of *Nicotiana benthamiana* plants has also been reported (Zampieri et al., 2020).

Tomato bushy stunt virus (TBSV), a member of the Tombusvirus genus, is a non-enveloped plant virus approximately 30 nm in diameter, composed of 180 identical copies of its coat protein (CP). While wild-type TBSV is not known to infect humans or other mammals, it is pathogenic to a range of plant species, including tomato and various horticultural crops. The virus has a broad geographic distribution, having been reported in Western and Central Europe, North Africa, Argentina, Canada, and Mexico (Tomlinson et al., 1982).

TBSV transmission occurs primarily through mechanical means, including direct inoculation and grafting. It can also be transmitted via seed at low frequencies and potentially through pollen-mediated pathways, although it is not spread by simple plant-to-plant contact. Notably, TBSV can persist in soil environments, from which it may be taken up by susceptible host plants (Martelli et al., 1988). Its use for biotechnological applications is conducted under strict biological containment, by maintaining and propagating the virus in laboratory Escherichia coli strains that are non-pathogenic to humans and plants. Biological containment also involves limiting environmental transmission by treating soil material as infectious waste. An additional strategy to prevent horizontal transmission is to inhibit flowering in infected plants, thereby reducing the risk of pollen- and seed-mediated spread.

The ability of TBSV to infect *N. benthamiana* is due to the presence of CP and p19 protein. The CP protein can be modified to attach a peptide of interest to its C-terminus (Marchetti et al., 2023). The presence of p19 protein is required to suppress virus-induced gene silencing in plants, allowing the virus to systemically infect the host (Qu and Morris, 2002).

Conventional techniques for the transient expression of heterologous proteins in plants rely on the use of *Agrobacterium tumefaciens* and manual or automated infiltration methods (Zampieri et al., 2020). Manual methods include syringe infiltration of individual leaves; this methodology is time- and labor-consuming, and it is also prone to technical errors. Conversely, automated methods use expensive machinery to simultaneously infect a large number of plants (eg. vacuum pumps for infiltration). These processes have a significant impact on the capital investment and operational costs of the molecular farming facility (Huebbers and Buyel, 2021). Moreover, an experienced workforce is needed for these operations, which can further increase operational costs. Considering these challenges, there was a need for the development of innovative and less expensive infection methods.

In this work, a novel approach to produce VNPs of interest in *Nicotiana benthamiana* is presented. Such an approach relies on spraying viral sap on top of the plant biomass, simplifying the process of plant infection with the TBSV virus. The latter was either wild-type or TBSV.pLip. Several tests were conducted to optimize the accumulation of viral coat proteins in plant biomass. In conclusion, this work describes an alternative to time-consuming manual infiltration methods, which are currently considered as gold standard in plant molecular farming. Furthermore, the spraying infection method offers the opportunity for automation of the production system, leading to a potential decrease in operational costs.

2 Materials and methods

2.1 Plant material and growth conditions

N. benthamiana plants were grown hydroponically using the formulation Idrofill Base (https://k-adriatica.it/eng/products/hydroponics/idrofill-base; K-Adriatica, Italy), ~2 g/L, supplemented with 50 mg/L Sequifill 6.0T SS, a Fe-EDDHA-based product, as an iron source (https://k-adriatica.it/eng/products/meso-and-microelements/sequifill-6.0t-ss; K-Adriatica, Italy). The electrical conductivity (EC) of the hydroponic solution (HS) was set at 2.4 mS/cm and the pH was adjusted at ~5.5. These two parameters were measured using a DiST4 EC tester and a Checker pHmeter (Hanna Instrument, USA). The nutrient solution of the plants kept in the growth chamber was refilled every week, and mild air bubbling was supplied to ensure oxygenation of the HS.

The seeds of *N. benthamiana* plants were put on plastic plates with wet paper towels for germination. Such plates were kept for 4 days at 25 °C in dark conditions. After germination, seedlings were placed in plastic plugs containing inert jute (Holland BioProducts, The Netherlands) as support for plant rooting. Such plugs were then put in specific metal grids and trays for hydroponic cultivation (Ono Exponential Farming, Italy) (Supplementary Figure S1). The

growth trays containing the seedlings were placed under light at ~200 μmol*$m^{-2}s^{-1}$, with a humidity of ~60% and a temperature of ~23 °C. The jute supports were moisturized daily with a nutrient solution to prevent them from drying out. 400 plants/m^2 were cultivated, and the hydroponic solution was added on demand to prevent plant dehydration during lab-scale hydroponic cultivation in a controlled chamber. The volume of nutrient solution used in the trays was ~4 L. Plants were cultivated for an average of 30 days.

2.2 Infection methods

A fine mist sprayer (Supplementary Figure S2) was used to infect the plants, and two middle leaves of a ~25-day-old plant (leaf length 5–6 cm) were sprayed with ~400 μL of viral sap or purified particles each. Viral sap consists of sap from homogenized TBSV-infected plants containing VNPs (Esteves et al., 2021). Viral sap was obtained by homogenizing plant biomass in a buffer solution. Such biomass was prepared starting from previously infected plant material, which was stored at -80 °C. The homogenization occurred in 50 mM PBS buffer pH 7.4, using an ice-cold mortar, with a 1:5 or 1:10 ratio (g/mL) of plant biomass to buffer solution. The supernatant was collected after centrifugation and used for the infection.

In the case of the positive control samples, the leaf surface was covered with celite (Merck Life Science, Italy), causing first mechanical damage, and then 40 μl of viral sap was spread over the leaf. After the infection, plants were immediately placed in an incubation chamber for the required incubation time. Plant material was collected after 7-, 8-, 9-, and 10-days post-infection (dpi).

In all the infection tests, second-generation leaf material provided by Diamante SB srl (Italy) was used as a starting viral sap. Specifically, first-generation leaf material was obtained by introducing the DNA construct harboring viral genes into the plant through agroinfiltration. Consequently, second-generation plants were infected with viral sap extracted from the leaves of first-generation plants.

2.3 Extraction and purification of TBSV

For the extraction of TBSV, 200 μg of infected plant material was used, while the purification was done using 1 g of material. The extraction and purification of viral particles were adapted from previous literature (Grasso et al., 2013). Briefly, plant material was ground and homogenized with an extraction buffer consisting of 50 mM Na-acetate pH 5.3, 1% ascorbic acid, and protease inhibitors. Plant material was homogenized with 3 mL/g in case of VNPs purification and 2 mL/g in case of VNPs extraction for quantification in agarose gels (Section 2.4). After incubation on ice for 1 hour, followed by filtration using filters with a porosity of 0.8 μm, the extract was centrifuged at 8,000 g for 15 minutes at 4°C. The supernatant was used for the quantification of VNPs in agarose gels. For further VNPs purification, the supernatant was additionally centrifuged at 90,000 g for 1 hour at 4 ˚C to finally precipitate the viral particles. The pellet was resuspended in 0.7% NaCl and centrifuged for the last time at 8,000 g for 15 minutes at 4°C. Protein content in the supernatant was quantified by Bradford method (Bradford, 1976) and used for the infection of plants with purified TBSV viral particles (VNPs).

2.4 Gel electrophoresis and quantification of viral particles

The method used for detecting and visualizing VNPs was adopted from recent literature (Pivotto et al., 2025). Briefly, viral particles were extracted from infected leaf material as described in Section 2.3 and then mixed with loading buffer (50 mM Tris-HCl pH 6.8, 10% glycerol, 18 mg bromophenol blue, 6X stock) added before protein electrophoresis in a 1% agarose-TAE buffered gel to quantify VNPs. As a reference, a known amount of purified TBSV.pLip particles was used. Electrophoresis was conducted in a TAE buffer at 120 V for 1 hour. Overnight staining with Quick Coomassie Stain (Neo-Biotech, France) was used for the visualization of protein bands, and their quantification was done by densitometric analysis using ImageLab software (Bio-Rad, USA).

Quantification of VNPs in viral sap was done similarly to the procedure described above. Infected plant material was homogenized directly in PBS instead of the extraction buffer and loaded with the same loading buffer previously mentioned. After the quantification, different amounts of VNPs were used to infect *N. benthamiana*. The quantities of VNPs tested were 31, 62.5, 125, 250, and 500 μg per plant. A total of six plants per condition were infected *via* spray. As a positive control, two *N. benthamiana* plants for each amount were infected *via* method described in section 2.2.

2.5 Statistics

The statistical significance of the amount of accumulated VNPs in sampled plant material (sample consists of 6 plants ground together, and the positive control includes 2 plants ground together, both with 3 replicates) was evaluated by comparing the results obtained in the same experiment, running Tukey-Kramer multiple comparison tests. Statistically significant variations with a p-value <0.05 are marked with different letters.

3 Results

3.1 Optimization of infection method

N. benthamiana is a well-known system used for approaches of plant molecular farming, and it can be inoculated with viral vectors by using spraying methods (Monroy-Borrego and Steinmetz, 2022). Recently, an engineered TBSV virus was used to infect *N. benthamiana* for the production of VNPs displaying the immunodominant peptide Lip1 (Zampieri et al., 2020). It is worth

considering that plants showed signs of infection on apical leaves 4 days after TBSV inoculation, while after 10 to 14 days they were completely necrotic (Dildabek et al., 2021).

To develop a TBSV infection process of *N. benthamiana* that can be easily implemented in an indoor cultivation system, the possibility of infecting the plants with a simple sprayer was investigated. The spraying method was developed without the use of surfactants (Figure 1A), utilizing a viral sap derived from previously infected plants. The tested plants were infected as previously described, and untreated plants were used as controls (Figure 1B, left). No major phenotypic differences were observed comparing *N. benthamiana* plants infected via the spraying method (Figure 1B, middle) or the conventional viral infiltration method, with the latter used as a positive control (Figure 1B, right). Figure 1C shows where the infected plants were kept in the incubation phase for VNPs accumulation.

The efficiency of infection with only spraying of viral sap was assessed with different spraying solutions (Supplementary Figure S3), such as spraying a mix of viral sap and celite, spraying first a dilution of celite in PBS and then sap, or using viral sap for infection. The dilutions of viral sap used in this infection test were 1:10. As controls, two methods of infection were used, namely a conventional method of infection where celite was used for mechanical damage before application of viral sap, and a second one where celite and viral sap were applied on the leaf surface together as a mixed solution. The results presented in Supplementary Figure S3 show the accumulation of 2.7 ± 0.3 mg/g FW of VNPs using the conventional procedure of infection. Anyway, VNPs were also significantly accumulated in plants sprayed with the sap solution. In more detail, spraying only viral sap without celite resulted in the accumulation of 1.4 ± 0.05 mg/g FW of VNPs, the highest among the two different spraying

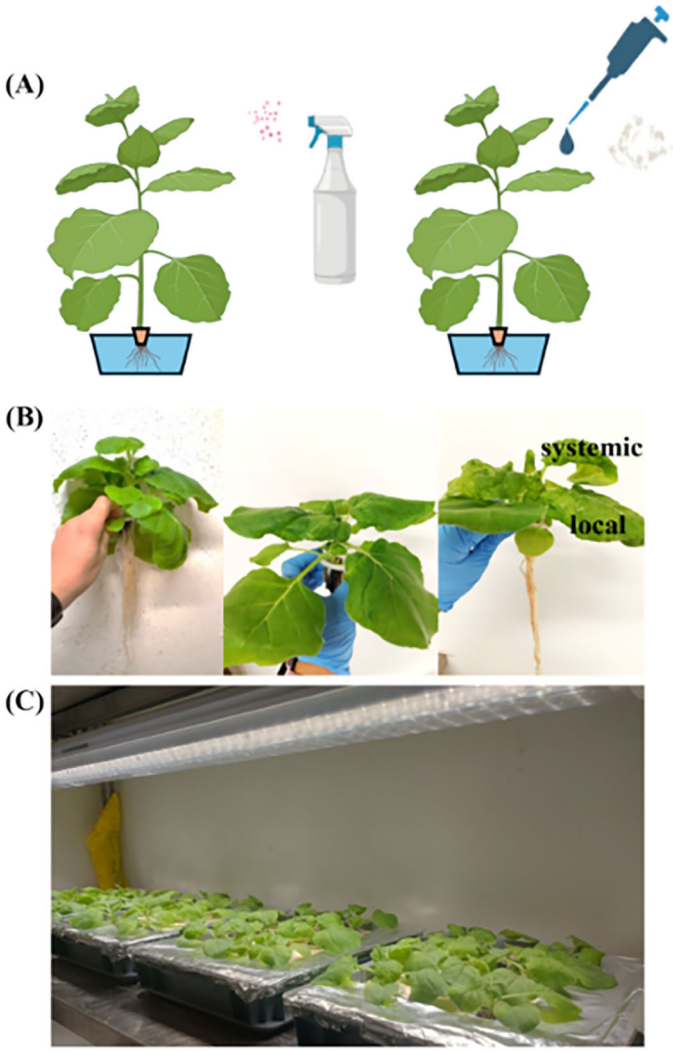

FIGURE 1
Spraying and conventional method using celite (diatomaceous earth) for the infection of *N. benthamiana*, respectively. Picture created with https://Biorender.com **(A)**. Phenotypic traits of infection with TBSV virus in hydroponic *N. benthamiana* with representation of local and systemic infection **(B)**. Specifically, from left to right: not infected *N. benthamiana*, infected via spray with TBSV WT, positive control plant infected with TBSV WT. Picture of the incubation chamber for infected hydroponic plants **(C)**.

methods, potentially due to the blockage of the virus entrance when celite is applied but not spread evenly on the leaf surface. Furthermore, accumulation of VNPs in control plants was higher when celite was separately applied before viral sap than when it was spread as a mixture on the leaf. Thus, the method in which celite was first spread on the leaf surface, followed by the sap application, was used in the further tests as a positive control. Conversely, only viral sap was applied for the infection *via* spray.

3.2 TBSV infection with quantified particles

The relationship between the amount of VNPs used for the infection and their final accumulation in infected plant material was investigated (Supplementary Figure S4). Specifically, the infection of the plants was performed using VNPs purified from previously infected plant material. A positive correlation was observed between the VNPs used for the infection and the particles accumulated during the 7-day incubation period. Anyway, this correlation was only observed in control plants (Supplementary Figure S4A), which were infected using 2, 10 and 50 µg of VNPs. Conversely, VNPs-sprayed plants showed infection symptoms; however, the accumulation of viral particles was too low and under the limit of detection of the Bradford assay (Supplementary Figure S4B).

To tackle the problem of quantification and detection of VNPs, an innovative protocol, recently described in literature (Pivotto et al., 2025), was used. Figure 2 presents the detection capacity and sensitivity of agarose gel electrophoresis used for the separation of native VNPs extracted in acidic buffer from plants infected by spraying and then visualized with commercial Coomassie stain. Using this protocol, it was possible to detect only one band that referred to TBSV VNPs; conversely, non-infected plants (negative control) showed no bands after staining.

To investigate the correlation between the quantity of VNPs used for infection and the amount accumulated in infected plant material, an infection test was conducted using sap containing a known amount of TBSV WT. Figure 3 and Supplementary Figure S5 indicate that the accumulation of VNPs in plants after 7-dpi was positively correlated with the amounts of particles used for infection in the samples containing 31, 62.5, and 125 µg of VNPs. Surprisingly, when the two highest quantities of VNPs were used for infection (250 and 500 µg), lower amounts of VNPs were detected after 7-dpi. Specifically, the excessive use of particles might have caused the lower accumulation of VNPs in the infected plants. This was likely due to the viral infection mechanisms, in which di-RNAs (defective interfering RNAs) can alter the replication of the virus and consequently its accumulation in the host cell (Havelda et al., 2005; Pathak and Nagy, 2009). Additionally, it was also shown that an excessive amount of infectious agent decreased the expression efficiency of the protein of interest in the plant host (Jin et al., 2015).

3.3 *N. benthamiana* infection with TBSV WT and TBSV.pLip viral sap

The infection tests with purified particles, where positive correlation was observed only in control plants (Supplementary Figure S4A), steered the experimental approach to avoid the costly and time-consuming purification of VNPs, instead using ground and homogenized material with PBS buffer, without VNPs enrichment. Moreover, the evidence of higher accumulation of VNPs in plants treated with the conventional procedure

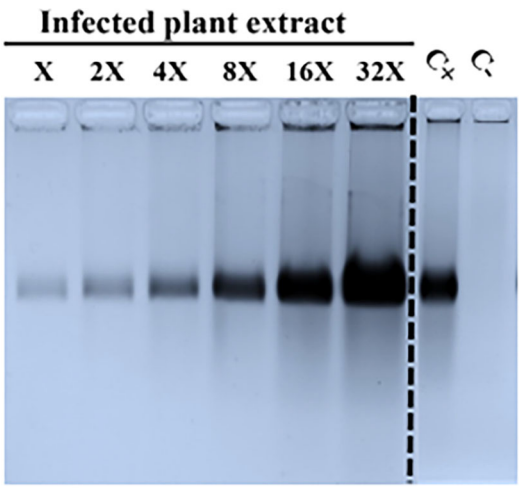

FIGURE 2
Sensitivity detection method for TBSV particles extracted from sprayed plants for TBSV infection. Extraction of VNPs was done in an acidic extraction buffer; for every 200 mg of fresh leaf material, 400 µL of extraction buffer was added. Different volumes (X = 0.47 µL) of infected plant material (TBSV WT) were loaded on the gel and stained with Coomassie staining. Infected plant material showed only one band, corresponding to the VNPs, as shown in a representative extract from infected plants (sample), while no bands were detected in the negative control.

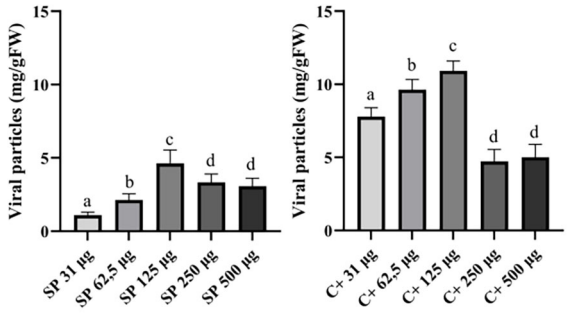

FIGURE 3
Accumulation of VNPs (mg/gFW) in *N. benthamiana* plants infected with viral sap containing a known amount of TBSV WT. The leaf material was collected after 7-dpi. Amounts of viral particles used for the infection per plant are: 31, 62.5, 125, 250, and 500 µg. Infection methods: *via* spray (left) or celite (control, right), as described in M&M. Data shown are based on quantification of the bands observed in Coomassie-stained agarose gel and analyzed by densitometric analysis. Error bars are reported as standard deviation (n = 3, mean ± SD, statistical significance is expressed with different letters according to Tukey-Kramer test, p <0.05).

compared to the sprayed plants (Figure 3) suggested that the infection in the latter might be delayed due to a late entry of the virus into the plant inner sections. Thus, different incubation times were evaluated to increase the accumulation of particles in sprayed plants. To this end, TBSV WT and TBSV.pLip viral sap were utilized, with the latter being a promising therapeutic technology for rheumatoid arthritis (Zampieri et al., 2020). The saps in PBS buffer were used at dilution of 1:5 and 1:10 (ratio g fresh biomass/mL solvent) and sprayed on *N. benthamiana* plants. Leaf material was collected after a 7- or 8-dpi, and the accumulation of viral particles was evaluated. It is worth mentioning that the collected leaf samples were locally and systemically infected due to the possibility of TBSV to move through the plant tissue (Qu and Morris, 2002). As a proof of concept, Figure 4 shows the infection with TBSV WT viral sap in 1:5 and 1:10 PBS buffer and the accumulation of VNPs after 7- and 8-dpi. Significant differences were observed between the accumulation in samples collected on days 7 and 8 (Supplementary Figure S6), meaning that the accumulation of VNPs can be increased with longer incubation time. Control plants still show the highest accumulation among all treatments.

As TBSV WT was used as proof of concept for the development of spraying and quantification methods, the same experiment was also conducted using the TBSV.pLip construct expressing the peptide of interest. Moreover, incubations longer than 8-dpi were also evaluated to reach high accumulation in sprayed samples.

To this aim, *N. benthamiana* plants were sprayed with a 1:5 dilution of TBSV.pLip-viral sap in PBS and collected after 7-, 8-, 9- and 10-dpi (Figure 5). It was observed that sprayed samples collected at 8-dpi or longer had comparable accumulation of VNPs to samples infected with the conventional approach (Supplementary Figure S7), where the entrance of the virus in plant tissue was facilitated with celite ($p<0.05$). Sprayed plants at 9-dpi accumulated 1.6 ± 0.19 mg/gFW of VNPs, while control plants reached 1.9 ± 0.33 mg/gFW at 7-dpi. The accumulation of VNPs in plants at 10-dpi showed a large variability, possibly due to the occurring necrosis in the leaf biomass.

As evidenced in Figure 5, the higher accumulation of particles at 8-dpi was confirmed. Moreover, it was observed that the best accumulation of VNPs occurred with post-infection incubation time between 8 and 9 days, resulting in ~1.55 and 1.65 mg/gFW, respectively. Supplementary Figure S8 shows that there are no major changes in phenotype between the plants at 8, 9, and 10 dpi. This agrees with the lack of statistical difference in the accumulation of VNPs in plants collected at these time points. Control plants are always collected after 7-dpi, as a longer period was not possible due to leaf necrosis. Although it has been reported that necrosis in plants can be postponed with anti-necrotic substances (Norkunas et al., 2018), such as lipoic acid, ascorbic acid, and polyvinylpyrrolidone (PVP), these substances were not used in this work due to the efforts to keep the infection process as simple as possible and lower the costs of an already costly system.

In this work, the growth of *N. benthamiana* was tested at a lab-scale using a hydroponic system at a density of 400 plants/m^2, with controlled environmental conditions such as light intensity, temperature, and humidity (Supplementary Figure S1). A single plant weighed ~10g, resulting in the growth of up to ~4 kg/m^2. Considering that a) out of the whole plant only local and systemic

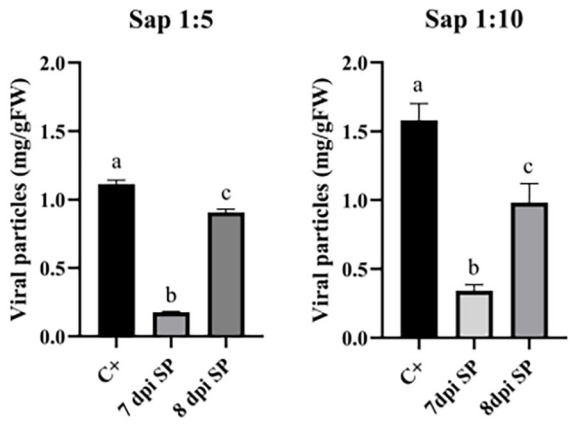

FIGURE 4
Accumulation of VNPs (mg/gFW) in *N. benthamiana* plants infected with TBSV WT viral sap in dilutions of 1:5 and 1:10 with PBS buffer. The leaf material was collected after 7 days for the C+ sample, whereas 7- and 8-dpi were evaluated for SP (sprayed) samples. Data shown are based on quantification of the bands observed in Coomassie-stained agarose gel and analyzed by densitometric analysis. Error bars are reported as standard deviation (n = 3, mean ± SD, statistical significance is expressed with different letters according to Tukey-Kramer test, $p < 0.05$).

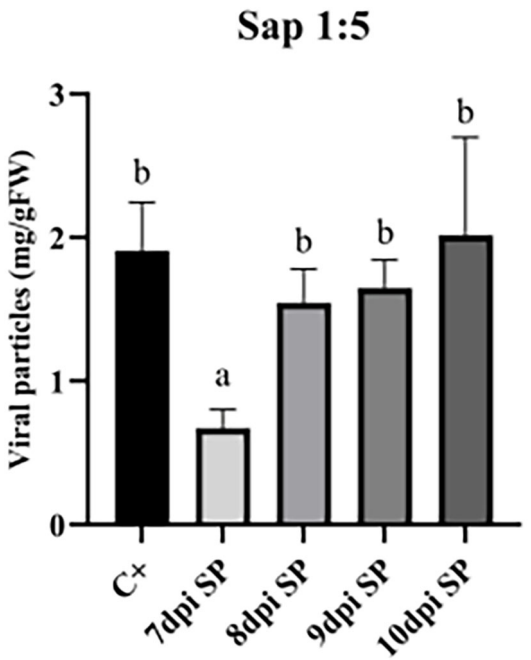

FIGURE 5
Accumulation of VNPs (mg/gFW) in *N. benthamiana* plants infected with TBSV.pLip viral sap in dilution of 1:5 with PBS. The leaf material was collected after 7-, 8-, 9- and 10-dpi. Data shown are based on quantification of the bands observed in Coomassie-stained agarose gel and analyzed by densitometric analysis. Error bars are reported as standard deviation (n = 3, mean ± SD), and the statistical significance is expressed with different letters according to Tukey-Kramer test ($p < 0.05$).

leaves were collected (Figure 1), with the biomass of ~1.3 g/plant (systemic + local), b) *N. benthamiana* took 4 weeks to grow from seeds to the plant of desired size in the tested conditions, and c) a year had 49 operational weeks, and 3 weeks dedicated to maintenance and possible breaks in production, it was possible to hypothesize 12 cycles of cultivation per year, including the infection stage. Thus, the leaf biomass yearly production yield reached around ~6.25 kg/m^2. Considering the accumulation of VNPs per fresh weight (Figure 5), such yearly biomass production leads to a potential VNPs yearly production of ~12.5 g/m^2.

4 Discussion

Efforts presented in this work had a final goal to be implemented on a larger scale. The control method for the TBSV infection, based on the use of celite, showed the best result in terms of VNPs accumulation compared to other treatments (Figure 3). However, this traditional infection system is manageable only at lab-scale conditions and not easily implementable in an industrial setting. Thus, any pretreatment of plants or the use of a conventional method of infection will be excluded to obtain the simplicity needed for industrial applications.

Several successful studies have been conducted in the field of molecular farming for the production of plant-made therapeutics (Diamos et al., 2020; Rybicki, 2020; Chung et al., 2022). Notably, agroinfiltration is the most used method for further production of recombinant molecules, as it is a well-established technique for the transient infection of plants (Leuzinger et al., 2013; Norkunas et al., 2018).

Molecular farming systems that rely on the use of viruses instead of *A. tumefaciens* simplify operational processes, as there is no need to maintain bacterial culture cultivation as previously described (Monroy-Borrego and Steinmetz, 2022). Specifically, viral sap can be obtained directly from infected leaf material, and the spraying method also contributes to the system's straightforwardness. Another advantage of using the virus compared to *Agrobacterium*-based inoculation methods is the absence of LPS (lipopolysaccharide). The latter must be removed from the final product for many applications, particularly in human therapies (Monroy-Borrego and Steinmetz, 2022). Even though *A. tumefaciens* can be sprayed on plants too, it requires adding surfactants such as Silwet-77 (Hahn et al., 2015; Jibrin et al., 2021) to facilitate the entrance of bacteria into the plant cells. Instead, as shown in this work, such surfactants are not necessary to produce the molecule of interest using TBSV. Although further research is needed, especially in the relationship between the amount of viral material used for the infection and accumulation of VNPs post-infection, this approach can be implemented in the scale-up production of pharmaceutical molecules. It has been demonstrated that the use of high-pressure spraying systems in combination with various mechanical aids, such as celite or beads, improved the transmission of plant viruses in plant material (Laidlaw, 1986; Fahim et al., 2012). However, this technology requires higher investments in terms of costs and technology compared to a fine mist sprayer, which can be easily implemented in an automated indoor system.

As mentioned in the Results section, systemically and locally infected leaves were collected, mimicking the harvesting that could be performed in an automated system such as vertical farming modules. In such modules, all the processes, from sowing seeds through infection to the collection of leaf material, are executed by automated machines (Holtz et al., 2015; Buyel, 2019). Figure 6 describes a scheme of an indoor system used for plant molecular farming. After cultivation in the growth chamber, the plants are transferred to an infection chamber where infection is done by spraying the TBSV virus. This section must be separated from the growth room to prevent viral contamination of the growing non-infected plants. Furthermore, the infection chamber can be separated from the incubation chamber. In particular, the infection chamber is a tunnel with a conveyor track, where trays with plants are sprayed with the virus. Then plants are kept in the incubation chamber for VNP accumulation. The harvesting of locally and systemically infected leaves can be done after 7–9 days, depending on the VNP accumulation and the health state of plants. Next steps include VNP extraction/purification and quantification to obtain the peptide of interest. A significant part of the process being automated can help reduce production costs, which are already very high for indoor systems, as reported in literature (Tusé et al., 2014; McNulty et al., 2020).

Considering that the cultivation system showed a fresh leaf biomass productivity of ~6.25 kg/m^2/year at lab scale, and that ~2 mg/gFW of VNPs were produced in the mentioned lab-scale settings (Figure 5, 9-dpi), it is possible to estimate a productivity ~1 g of VNPs per m^2 and ~12.5 g of VNPs per m^2/year. From such 12.5 g of VNPs, it could be possible to extract ~0.4 g/m^2/year of highly-pure Lip1, taking into account that 50µg of VNPs have 4*10^{12} individual particles and 1.6 µg of Lip1 peptide. Monroy-Borrego reported a yield of 0.3-0.5 mg/gFW of TMV (Tobacco mosaic virus) particles when *N. benthamiana* plants were infected with the spraying method, while slightly lower yield (0.17-0.28 mg/gFW) was obtained when TMV-Lys mutant was used for spray infection of plants (Monroy-Borrego and Steinmetz, 2022).

Additionally, to ensure that the process produces the highest quality VNPs, the entire production process must comply with current Good Manufacturing Practices (cGMP), even though the upstream process is allowed to be non-GMP (Schillberg and Finnern, 2021). Overall, the upstream and downstream processes require additional testing and monitoring systems.

In conclusion, the presented work aimed to simplify the production process of VNPs derived from TBSV host in *Nicotiana benthamiana*. The conventional infiltration method is time-consuming and requires qualified personnel to perform the infection, whereas the method developed by spraying viral sap can be easily and simultaneously performed by automated machines on a large number of plants. Automation of the process can reduce the number of workers needed to perform infiltration, and it further decreases operational costs, as sprayers are cost-effective devices and usually already present in indoor cultivation systems. Overall, the results obtained in this work showed that infection by spray

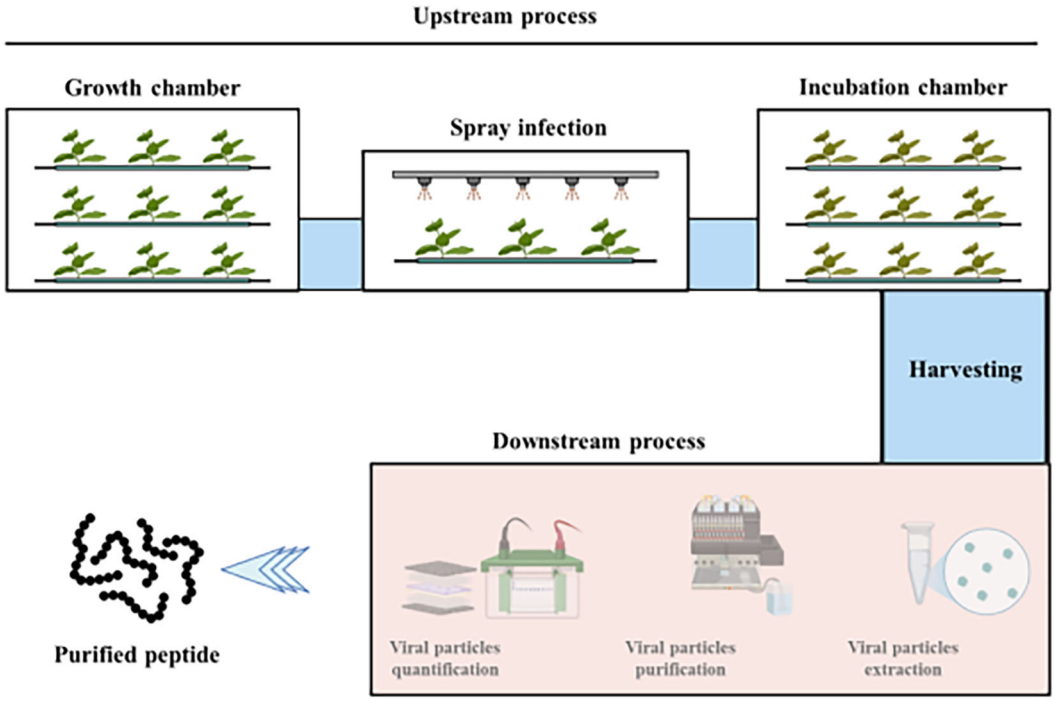

FIGURE 6
Schematic representation of an indoor system for the hydroponic cultivation of *N. benthamiana*. The plants are then infected with viral vectors for the production of recombinant proteins. Plants are first grown in a specific growth chamber until reaching the desired size. At this point, the mature plants are moved into a tunnel where they are sprayed with the viral sap. Then, the protein constructs of interest accumulate in the plant biomass kept in a specific incubation chamber. Finally, the desired protein constructs are purified from the plant material and quantified. The scheme was done using BioRender.

initiated later compared to the conventional method due to the delayed entrance of the virus; on the other hand, it can reach an accumulation of VNPs similar to that obtained in control plants, if the cycle is prolonged by just one or two days. The lower time efficiency presented here can compensate for the complexity and time consuming of the conventional process. Moreover, it can be easily scaled to increase the production yield of the system, especially when performed in a controlled environment, such as a vertical farming system.

Data availability statement

The original contributions presented in the study are included in the article/Supplementary Material. Further inquiries can be directed to the corresponding authors.

Author contributions

KL: Conceptualization, Data curation, Investigation, Methodology, Writing – original draft, Writing – review & editing. ARo: Investigation, Methodology, Supervision, Writing – original draft, Writing – review & editing. ARa: Writing – original draft, Writing – review & editing, Investigation, Methodology. MB: Funding acquisition, Resources, Supervision, Visualization, Writing – original draft, Writing – review & editing, Conceptualization, Project administration. LA: Conceptualization, Funding acquisition, Resources, Supervision, Visualization, Writing – original draft, Writing – review & editing, Project administration. NB: Conceptualization, Investigation, Methodology, Project administration, Supervision, Writing – original draft, Writing – review & editing.

Funding

The author(s) declare that financial support was received for the research and/or publication of this article. This research was funded by CARIVERONA FOUNDATION (Grant No. 2019.0419.2019) to MB and by the EIC 2024 Accelerator program, specifically through the Diamante SB srl project under grant agreement number 101189019. NB acknowledges PRIN2022PNRR-SAME-P2022TXEBF grant by MUR.

Acknowledgments

Authors thank Roberta Zampieri from Diamante SB srl and Denise Pivotto from University of Verona for useful discussions. Thomas Ambrosi from ONO EXPONENTIAL FARMING srl is also thanked for providing material for the plant cultivation system.

Conflict of interest

The authors declare that this study received support from the company ONO EXPONENTIAL FARMING srl San Giovanni Lupatoto, Verona, Italy, providing material for the plant cultivation. The company ONO EXPONENTIAL FARMING srl was not involved in the study design, collection, analysis, interpretation of data, the writing of this article, or the decision to submit it for publication.

MB is a member of the Advisory Board of ONO EXPONENTIAL FARMING srl company San Giovanni Lupatoto, Verona, Italy. LA is a co-founder of Diamante SB srl. ARo is employee of Diamante SB srl.

The remaining authors declare that the research was conducted in the absence of any commercial or financial relationships that could be construed as a potential conflict of interest.

The author(s) declared that they were an editorial board member of Frontiers, at the time of submission. This had no impact on the peer review process and the final decision.

Generative AI statement

The author(s) declare that no Generative AI was used in the creation of this manuscript.

Any alternative text (alt text) provided alongside figures in this article has been generated by Frontiers with the support of artificial intelligence and reasonable efforts have been made to ensure accuracy, including review by the authors wherever possible. If you identify any issues, please contact us.

Publisher's note

All claims expressed in this article are solely those of the authors and do not necessarily represent those of their affiliated organizations, or those of the publisher, the editors and the reviewers. Any product that may be evaluated in this article, or claim that may be made by its manufacturer, is not guaranteed or endorsed by the publisher.

Supplementary material

The Supplementary Material for this article can be found online at: https://www.frontiersin.org/articles/10.3389/fpls.2025.1727190/full#supplementary-material

References

Bason, C., Barbieri, A., Martinelli, N., Olivieri, B., Argentino, G., Bartoloni, E., et al. (2021). Identification of a novel serological marker in seronegative rheumatoid arthritis using the peptide library approach. *Front. Immunol.* 12. doi: 10.3389/fimmu.2021.753400

Bradford, M. M. (1976). A rapid and sensitive method for the quantitation of microgram quantities of protein utilizing the principle of protein-dye binding. *Anal. Biochem.* 72, 248–254. doi: 10.1016/0003-2697(76)90527-3

Buyel, J. F. (2019). Plant molecular farming – Integration and exploitation of side streams to achieve sustainable biomanufacturing. *Front. Plant Sci.* 9. doi: 10.3389/fpls.2018.01893

Chung, Y. H., Church, D., Koellhoffer, E. C., Osota, E., Shukla, S., Rybicki, E. P., et al. (2022). Integrating plant molecular farming and materials research for next-generation vaccines. *Nat. Rev. Mater.* 7, 372–388. doi: 10.1038/s41578-021-00399-5

Diamos, A. G., Hunter, J. G. L., Pardhe, M. D., Rosenthal, S. H., Sun, H., Foster, B. C., et al. (2020). High level production of monoclonal antibodies using an optimized plant expression system. *Front. Bioeng. Biotechnol.* 7. doi: 10.3389/fbioe.2019.00472

Dildabek, A. B., Stamgaliyeva, Z. B., Ilyasova, B. B., Tleukulova, Z. B., Madirov, A. A., Kassenova, S. M., et al. (2021). Superinoculation of nicotiana benthamiana promotes the development of immunity to tomato bushy stunt virus. *Russ. J. Plant Physiol.* 68, 883–889. doi: 10.1134/S102144372104004X

Esteves, E., Locatelli, G., Bou, N. A., and Ferrarezi, R. S. (2021). Sap analysis: A powerful tool for monitoring plant nutrition. *Hortic* 7, 426. doi: 10.3390/horticulturae7110426

Fahim, M., Mechanicos, A., Ayala-Navarrete, L., Haber, S., and Larkin, P. J. (2012). Resistance to Wheat streak mosaic virus– a survey of resources and development of molecular markers. *Plant Pathol.* 61, 425–440. doi: 10.1111/j.1365-3059.2011.02542.x

Grasso, S., Lico, C., Imperatori, F., and Santi, L. (2013). A plant derived multifunctional tool for nanobiotechnology based on Tomato bushy stunt virus. *Transgenic Res.* 22, 519–535. doi: 10.1007/s11248-012-9663-6

Hahn, S., Giritch, A., Bartels, D., Bortesi, L., and Gleba, Y. (2015). A novel and fully scalable Agrobacterium spray-based process for manufacturing cellulases and other cost-sensitive proteins in plants. *Plant Biotechnol. J.* 13, 708–716. doi: 10.1111/pbi.12299

Havelda, Z., Hornyik, C., Válóczi, A., and Burgyán, J. (2005). Defective interfering RNA hinders the activity of a tombusvirus-encoded posttranscriptional gene silencing suppressor. *J. Virol.* 79, 450–457. doi: 10.1128/JVI.79.1.450-457.2005

Holtz, B. R., Berquist, B. R., Bennett, L. D., Kommineni, V. J. M., Munigunti, R. K., White, E. L., et al. (2015). Commercial-scale biotherapeutics manufacturing facility for plant-made pharmaceuticals. *Plant Biotechnol. J.* 13, 1180–1190. doi: 10.1111/pbi.12469

Huebbers, J. W., and Buyel, J. F. (2021). On the verge of the market – Plant factories for the automated and standardized production of biopharmaceuticals. *Biotechnol. Adv.* 46, 107681. doi: 10.1016/j.bioteChadv.2020.107681

Jibrin, M. O., Liu, Q., Jones, J. B., and Zhang, S. (2021). Surfactants in plant disease management: A brief review and case studies. *Plant Pathol.* 70, 495–510. doi: 10.1111/ppa.13318

Jin, T., Wang, J., Zhu, X., Xu, Y., Zhou, X., and Yang, L. (2015). A new transient expression system for large-scale production of recombinant proteins in plants based on air-brushing an Agrobacterium suspension. *Biotechnol. Rep.* 6, 36–40. doi: 10.1016/j.btre.2015.01.004

Laidlaw, W. M. R. (1986). Mechanical aids to improve the speed and sensitivity of plant virus diagnosis by the biological test method. *Ann. Appl. Biol.* 108, 309–318. doi: 10.1111/j.1744-7348.1986.tb07652.x

Leuzinger, K., Dent, M., Hurtado, J., Stahnke, J., Lai, H., Zhou, X., et al. (2013). Efficient agroinfiltration of plants for high-level transient expression of recombinant proteins. *J. Vis. Exp.* 77, 50521. doi: 10.3791/50521

Majithia, V., and Geraci, S. A. (2007). Rheumatoid arthritis: diagnosis and management. *Am. J. Med.* 120, 936–939. doi: 10.1016/j.amjmed.2007.04.005

Marchetti, L., Simon-Gracia, L., Lico, C., Mancuso, M., Baschieri, S., Santi, L., et al. (2023). Targeting of tomato bushy stunt virus with a genetically fused C-end rule peptide. *Nanomater* 13, 1428. doi: 10.3390/nano13081428

Martelli, G. P., Gallitelli, D., and Russo, M. (1988). "Tombusviruses," in: *The Plant Viruses* Koenig, R. (eds) The Viruses. Boston, MA: Springer. doi: 10.1007/978-1-4613-0921-5_2

McNulty, M. J., Gleba, Y., Tusé, D., Hahn-Löbmann, S., Giritch, A., Nandi, S., et al. (2020). Techno-economic analysis of a plant-based platform for manufacturing antimicrobial proteins for food safety. *Biotechnol. Prog.* 36, e2896. doi: 10.1002/btpr.2896

Monroy-Borrego, A. G., and Steinmetz, N. F. (2022). Three methods for inoculation of viral vectors into plants. *Front. Plant Sci.* 13. doi: 10.3389/fpls.2022.963756

Nkanga, C. I., and Steinmetz, N. F. (2021). The pharmacology of plant virus nanoparticles. *Virology* 556, 39–61. doi: 10.1016/j.virol.2021.01.012

Norkunas, K., Harding, R., Dale, J., and Dugdale, B. (2018). Improving agroinfiltration-based transient gene expression in Nicotiana benthamiana. *Plant Methods* 14, 1–14. doi: 10.1186/s13007-018-0343-2

Pathak, K. B., and Nagy, P. D. (2009). Defective interfering RNAs: foes of viruses and friends of virologists. *Viruses* 1, 895–919. doi: 10.3390/v1030895

Pivotto, D., Rosa, A., Elsheikh, A. M., Gecchele, E., Zampieri, R., Raneri, A., et al. (2025). Clinical-grade Plant-made nanomaterials: from Process Design to the construction of a Manufacturing facility. *bioRxiv*. doi: 10.1101/2025.10.14.682267

Qu, F., and Morris, T. J. (2002). Efficient Infection of Nicotiana benthamiana by Tomato bushy stunt virus Is Facilitated by the MPMI Coat Protein and Maintained by p19 Through Suppression of Gene Silencing. *MPMI* 15, 193–202. doi: 10.1094/MPMI.2002.15.3.193

Rybicki, E. P. (2020). Plant molecular farming of virus-like nanoparticles as vaccines and reagents. *Wiley Interdiscip. Rev. Nanomedicine Nanobiotechnology* 12, e1587. doi: 10.1002/wnan.1587

Sánchez, F., Sáez, M., Lunello, P., and Ponz, F. (2013). Plant viral elongated nanoparticles modified for log-increases of foreign peptide immunogenicity and specific antibody detection. *J. Biotechnol.* 168, 409–415. doi: 10.1016/j.jbiotec.2013.09.002

Schillberg, S., and Finnern, R. (2021). Plant molecular farming for the production of valuable proteins – Critical evaluation of achievements and future challenges. *J. Plant Physiol.* 258–259, 153359. doi: 10.1016/j.jplph.2020.153359

Tomlinson, J. A., Faithfull, E., Flewett, T. H., and Beards, G. (1982). Isolation of infective tomato bushy stunt virus after passage through the human alimentary tract. *Nature* 300, 637–638. doi: 10.1038/300637a0

Tusé, D., Tu, T., and McDonald, K. A. (2014). Manufacturing economics of plant-made biologics: case studies in therapeutic and industrial enzymes. *BioMed. Res. Int.* 2014, 256135. doi: 10.1155/2014/256135

Wen, A. M., and Steinmetz, N. F. (2016). Design of virus-based nanomaterials for medicine, biotechnology, and energy. *Chem. Soc Rev.* 45, 4074–4126. doi: 10.1039/C5CS00287G

Zampieri, R., Brozzetti, A., Pericolini, E., Bartoloni, E., Gabrielli, E., Roselletti, E., et al. (2020). Prevention and treatment of autoimmune diseases with plant virus nanoparticles. *Sci. Adv.* 6, eaaz0295. doi: 10.1126/sciadv.aaz0295

Zhou, Y., Li, Q., Wu, Y., Li, X., Zhou, Y., Wang, Z., et al. (2023). Molecularly stimuli-responsive self-assembled peptide nanoparticles for targeted imaging and therapy. *ACS Nano* 17, 8004–8025. doi: 10.1021/acsnano.3c01452

frontiers | Frontiers in Plant Science

TYPE Original Research
PUBLISHED 12 December 2025
DOI 10.3389/fpls.2025.1701668

OPEN ACCESS

EDITED BY
Kevin Wang,
University of Pikeville, United States

REVIEWED BY
Jelli Venkatesh,
International Atomic Energy Agency, Austria
Pu Yuan,
The Ohio State University, United States

*CORRESPONDENCE
Okjae Koo
okjae.koo@gmail.com
Geung-Joo Lee
gjlee@cnu.ac.kr

†PRESENT ADDRESS
Okjae Koo,
Hanwha Solutions, Seoul, Republic of Korea

RECEIVED 08 September 2025
REVISED 10 November 2025
ACCEPTED 17 November 2025
PUBLISHED 12 December 2025

CITATION
Kaur C, Song H, Lee M, Kim S-Y, Seo D-H, Kang H, Sohn E-J, Ran Y, Koo O and Lee G-J (2025) Multiplex CRISPR/Cas9-mediated editing of seven glycosyltransferase homologs in *Nicotiana benthamiana* to produce stable, Cas9-free, glycoengineered plants. *Front. Plant Sci.* 16:1701668. doi: 10.3389/fpls.2025.1701668

Multiplex CRISPR/Cas9-mediated editing of seven glycosyltransferase homologs in *Nicotiana benthamiana* to produce stable, Cas9-free, glycoengineered plants

Chetan Kaur[1], Hayoung Song[1], Myungjin Lee[1], Seo-Young Kim[1], Dong-Hoon Seo[2], Hyangju Kang[3], Eun-Ju Sohn[3], Yidong Ran[4], Okjae Koo[5*†] and Geung-Joo Lee[1,2*]

[1]Department of Horticulture, Chungnam National University, Daejeon, Republic of Korea, [2]Department of Smart Agriculture Systems, Chungnam National University, Daejeon, Republic of Korea, [3]BioApplications Inc., Pohang, Republic of Korea, [4]Qi Biodesign, Beijing, China, [5]Department of Veterinary Medicine, Kyungpook National University, Daegu, Republic of Korea

Introduction: Plant-based systems hold great potential for producing therapeutic proteins, but differences in N-glycosylation pathways between plants and mammals present major technical and regulatory barriers. In particular, plant-specific α-1,3-fucosylation and β-1,2-xylosylation can generate immunogenic glycan structures, necessitating genome engineering to humanize plant glycosylation profiles.

Methods: We applied multiplex CRISPR/Cas9 genome editing in Nicotiana benthamiana to simultaneously target five α-1,3-fucosyltransferase genes and two β-1,2-xylosyltransferase genes. Resulting T_0 transformants were genotyped to assess mutagenesis, and subsequent T1 and T2 generations were screened to identify Cas9-free, homozygous plants. Growth and morphological characteristics were evaluated across germination, flowering, and seed production stages.

Results: Two T_0 lines (HL40 and HL64) exhibited successful edits in all seven target genes, with mutations consisting of single-base insertions and deletions up to 26 bp. In later generations, we identified stable Cas9-free homozygous lines containing mutations across all targeted loci. Three T_1 transformants with the highest number of homozygous alleles were selected to generate T_2 progeny. Heterozygous alleles segregated into homozygous genotypes in the T_2 generation, accompanied by confirmed loss of enzymatic activity. T_2 plants showed no detectable morphological or growth differences compared with wild-type plants, indicating no adverse phenotypic effects. Ultimately, we generated 12 independent Cas9-free, glycoengineered, homozygous lines.

Discussion: This work establishes the first *N. benthamiana* lines that are fully Cas9-free and homozygously edited at all seven key glycosyltransferase loci. These glycoengineered lines provide a stable and versatile genetic platform for future plant-based glycoengineering efforts and the production of recombinant therapeutic proteins.

KEYWORDS

multiplex CRISPR-Cas9 editing, homozygous gene knockouts, agrobacterium-mediated transformation, glycoengineered plants, plant molecular farming, *Nicotiana benthamiana*

Introduction

Plant molecular farming is emerging as a leading contender for sustainable and affordable biopharmaceutical production (Yao et al., 2015; Shanmugaraj et al., 2020). Plants harness photosynthesis to generate their own energy, thereby significantly reducing overall production costs. Plant systems also exhibit a lower risk of contamination by human pathogens than animal systems. This inherent safety feature stems from the inability of human pathogens to effectively replicate within plant cells (Sil and Jha, 2014). Despite their advantages over alternative expression systems, plant-based expression systems are not without limitations. A major hurdle in plant-based protein production is the incompatibility between plant and animal protein glycosylation (Brooks et al., 2014). Glycosylation is a post-translational modification involving the enzymatic addition of sugar chains to specific amino acid residues of proteins. These covalent linkages alter protein folding, morphology, stability, and half-life, consequently influencing protein activity, signaling, and intercellular interactions (Castilho and Steinkellner, 2012; Strasser, 2016). Two types of glycosylation pathways exist: N-glycosylation and O-glycosylation. During N-glycosylation, a glycan forms a covalent bond with the nitrogen atom of an asparagine (Asn) residue. O-glycosylation, on the other hand, attaches a sugar molecule to the hydroxyl side chain of either serine (Ser) or threonine (Thr) residues. The specific pattern of N-glycosylation on a medicinal protein significantly impacts its functionality and therapeutic efficacy (Barolo et al., 2020).

Plants and animals share a conserved N-glycosylation pathway that initiates in the endoplasmic reticulum (ER). However, the later stages of N-glycan maturation differ substantially between them, as these steps are catalyzed by distinct sets of glycosyltransferases. Plant N-glycans typically contain β-1,2-xylose and α-1,3-fucose residues, whereas mammalian N-glycans possess β-mannose and α-1,6-fucose (Pattison and Amtmann, 2009). These structural differences can elicit immune responses in humans, limiting the use of plant based systems for producing therapeutic glycoproteins (Gomord et al., 2010; Rup et al., 2017). The addition of β-1,2-xylose and α-1,3-fucose residues in plants is catalyzed by β-1,2-xylosyltransferase (*XylT*) and α-1,3-fucosyltransferase (*FucT*), respectively. *Nicotiana benthamiana* contains five *XylT* and two *FucT* homologs, thus complicating complete suppression through single-gene RNAi approaches (Strasser et al., 2008). Six glycosyltransferase genes were previously targeted using CRISPR/Cas9 genome editing; however, one *FucT* homolog (*FucT5*) was omitted, and the resulting plants retained the Cas9 transgene, thus maintaining their transgenic status (Jansing et al., 2019). Cas9 free lines are required to meet biosafety and regulatory standards for the production of molecular farming crops, as transgene presence can raise concerns about off-target editing and transgene remobilization (Ahmad et al., 2024). Developing Cas9-free plants addresses both scientific and regulatory challenges. Removing Cas9 stabilizes the edits and prevents further nuclease activity. It also brings the edited plants closer to conventional breeding standards, easing regulatory evaluation and public acceptance. For these reasons, producing Cas9-free lines has become an important step toward practical CRISPR applications in agriculture. In addition to generating Cas9-free lines, it is important to fully modify the pathway to eliminate all plant specific glycosylation. Although Jansing et al. reported the absence of detectable α-1,3-fucose despite omitting *FucT5*, the functional status of this homolog remains unresolved. Given the redundancy within the *FucT* family and the polyploid genome of N. benthamiana, the possibility of residual or conditional *FucT5* activity cannot be fully ruled out.

Here, we address both limitations by targeting all seven glycosyltransferase homologs, including *FucT5*, using multiplex CRISPR/Cas9 editing to generate stable, homozygous, and Cas9 free *N. benthamiana* lines. Through genetic screening, we isolated plants carrying homozygous mutations in all target loci and confirmed complete segregation of the Cas9 transgene by the T_2 generation. This strategy not only validates the comprehensive removal of plant-specific glycosylation but also establishes a regulatory compliant platform for scalable production of recombinant proteins with fully humanized N-glycan structures.

Materials and methods

Plant material and growth conditions

Forty days after germination, *Nicotiana benthamiana* seedlings were grown *in vitro* in a growth chamber under a 16-h light/8-h

dark photoperiod, 140 µmol m^{-2} s^{-1} light intensity, and a temperature of 25 °C. Seeds from T_0 transgenic plants were collected, and subsequent generations were propagated by seed harvesting and sowing. The regenerated T_1 and T_2 seedlings were grown in a controlled growth chamber. The chamber maintained a 16-hour light/8-hour dark photoperiod, a temperature range of 22-26°C and, a relative humidity of 40-60%.

Cas9/sgRNA plasmid construction

Sequence information for two β-1,20-xylosyltransferase (*XylT*) genes and five α-1,3-fucosyltransferase (*FucT*) genes was obtained from the *N. benthamiana* genome data registered on the Sol Genomics Network (https://solgenomics.net). Conserved domain search was done using NCBI conserved domain database. These sequences were further compared using CLUSTAL Omega (EMBL-EBI, UK) to identify the conserved motif regions between homologous genes. gRNAs were designed using CRISPOR (http://crispor.tefor.net/; accessed March 2022) and selected based on on-target efficiency, off-target mismatch count (≥ 3 mismatches to minimize off-target cleavage < 3 %), and frame-shift probability. Each sgRNA cassette was placed downstream of the *Arabidopsis U6* promoter and assembled into the pGenovo111 binary CRISPR/Cas9 vector (Genovo Bio, Tianjin, China) using Golden Gate cloning with BsaI-HFv2 and T4 DNA ligase (37 °C 5 min / 16 °C 5 min, 25 cycles). Constructs were confirmed by Sanger sequencing and introduced into *Agrobacterium tumefaciens* strain EHA105 by electroporation. Transformation followed the Agrobacterium-mediated leaf-disc procedure: 40-day-old seedlings were inoculated with *A. tumefaciens suspension* (OD_{600} = 0.6–0.8) and co-cultivated for 3 days at 25 °C on shoot-induction medium containing 200 µM acetosyringone, 1.0 mg/L BAP, 0.1 mg/L IAA, and 0.3 % Gelrite. Shoots were selected on MS medium with 20 µg/mL hygromycin and 150 mg/L Timentin, elongated on 0.3 mg/L BAP + 0.1 mg/L IAA, and rooted on ½ MS medium with 15 µg/mL hygromycin. Regenerated plants were transferred to soil and grown under 16 h light/8 h dark at 20–24 °C and 40–60 % RH. Seeds were obtained by self pollination for segregation and homozygosity analysis Song et al., 2022).

DNA isolation and analysis of gene modifications

The leaves of the regenerated plants were used to extract the total genomic DNA using a Deasy Plant Mini Kit (QIAGEN, Hilden, Germany). Fragments spanning each of the seven target loci (*NbFucT1–5*, *NbXylT1*, *NbXylT2*) were amplified by PCR using gene-specific primers (Supplementary Table S1). PCR products were analyzed for mutations using Sanger sequencing first, followed by targeted next-generation sequencing (NGS) for more comprehensive coverage. For NGS, three successive high fidelity PCR amplifications were performed to enrich the target region while minimizing amplification bias. Each 25 µL reaction contained 50 ng genomic DNA, 0.5 µM primers, 200 µM dNTPs, 1× Phusion HF buffer, and 0.5 U Phusion High-Fidelity DNA Polymerase (Thermo <ns/>F530L). The second and third PCR reactions used 1/10 and 1/100 dilutions of the previous reaction as templates, without intermediate purification. Amplicons (~350 bp) were pooled, purified with AMPure XP beads (Beckman Coulter), and dual indexed libraries were prepared using the NEBNext Ultra II DNA Library Prep Kit (New England Biolabs). Libraries were sequenced on an Illumina MiSeq platform. Raw reads were demultiplexed and quality-trimmed (Phred > 30) using Trimmomatic v0.39, and low-quality reads were discarded. Clean reads were aligned to the *N. benthamiana* reference genome and analyzed using the CRISPR RGEN Cas-Analyzer pipeline to quantify insertions, deletions, and single-nucleotide variants within ± 10 bp of each Cas9 cleavage site. Mutations were classified as homozygous when identical alleles accounted for ≥ 80 % of reads and as bi-allelic when two distinct alleles each exceeded 30 % frequency.

Total protein N-glycan analysis by Western blot

Total soluble protein was extracted from 100 mg of *N. benthamiana* leaf tissue by grinding in two volumes of ice cold PBS (137 mM NaCl, 2.7 mM KCl, 8.1 mM Na_2HPO_4, 1.5 mM KH_2PO_4, pH 7.4). The homogenate was centrifuged at 16,100 × g for 10 min at 4 °C, and 10 µg of total protein per lane was resolved by SDS–PAGE (100 V, 90 min) and transferred to a nitrocellulose membrane (Thermo Fisher Scientific, MA, USA) using Towbin transfer buffer (25 mM Tris, 192 mM glycine, 20% methanol) for 1 h at 100 V, following the general workflow of Jansing et al (Jansing et al., 2019). Membranes were blocked for 1 h in 5% skim milk in TBS–T (20 mM Tris, 150 mM NaCl, 0.05% Tween-20, pH 7.5) and briefly rinsed. Blots were incubated with primary antibodies from Agrisera AB (Umeå, Sweden): anti-β-1,2-xylose (AS07 267, 1:5000) or anti-α-1,3-fucose (AS07 268, 1:10000), diluted in standard or high-salt TBS-T (20 mM Tris, 500 mM NaCl, 0.1% Tween-20), respectively. The two glycan specific blots were performed on separate membranes. Following primary incubation, membranes were washed three times (5 min each) in the corresponding TBS-T buffer and probed for 1 h with alkaline-phosphatase-conjugated goat anti-rabbit IgG (H + L) secondary antibody (AS09 607, Agrisera, 1:10000), pre-adsorbed against wild-type *N. benthamiana* extract to reduce non-specific binding. After three final washes, membranes were developed in BCIP/NBT substrate (Thermo Fisher Scientific) for 5–15 min in the dark, rinsed in distilled water, and air dried.

Validation of Cas9 integration

The presence of Cas9 within the transformants was verified using Cas9 gene-specific genomic PCR. Each 20 µL reaction contained 1 µL genomic DNA (30–50 ng), 1 µL each of Cas9 forward and reverse

primers (10 pmol/μL), 1 μL each of *NbActin* control primers (10 pmol/μL), 10 μL of 2× PCR premix (Takara Ex Taq, Japan), and 7 μL nuclease-free water. PCR was performed with an initial denaturation at 94°C for 5 min; 32 cycles of 94°C for 30 s, 58°C for 30 s, and 72°C for 30 s; followed by a final extension at 72°C for 7 min. PCR products were visualized using a gel documentation system under UV light. The expected product sizes were 1448 bp for *Cas9* and 267 bp for *NbActin* (primer sequences listed in Supplementary Table S1).

Results

Design and assembly of Cas9/sgRNA constructs for generating multiple knockout transformants

Sequence information of the two *XylT* genes (Niben101Scf04551: *NbXylT1*, Niben101Scf04205: *NbXylT2*) and five *FucT* genes (Niben101Scf01272:*NbFucT1*, Niben101Scf02631:*NbFucT2*, Niben101Scf05494: *NbFucT3*, Niben101Scf17626: *NbFucT4*, Niben101Scf05447: *NbFucT5)* present in *N. benthamiana* were aligned and analyzed to identify conserved motifs and domains (Figures 1A, B). The *XylT* genes consisted of a conserved domain, belonging to the Glycosyltransferase 61 domain family, and the *FucT* genes consisted of a conserved domain belonging to the Glycosyltransferase 10 domain family. Notably, PFAM/HMMER analysis identified this canonical GT10 domain in *FucT5* (E = 2.16 × 10^{-29}), identical to the catalytic domain found in *FucT1–4*. Reciprocal BLASTP comparisons further revealed high sequence identity and similarity among *FucT1–5*. These results indicate that *FucT5* retains the conserved catalytic core characteristic of functional α-1,3-fucosyltransferases. Based on the conserved motifs of each gene, three sgRNAs were designed to simultaneously target seven genes: sgRNA-Xyl1,2 targets *NbXylT1* and *NbXylT2*, and sgRNA-Fuc1–4 targets *NbXylT1*, *NbXylT2*, *NbXylT3*, and *NbXylT4* (Figure 1). Additionally, sgRNA-Fuc5 was designed to target *NbFucT5* to increase the target specificity due to a polymorphism in the 5th sequence from the PAM site. As for *NbXylTs*, reverse sgRNAs were designed by referring to the 100%-matching conserved sequences identified on exon 1 of *NbXylT1* and *NbXylT2* (Figure 1B). Three gRNAs targeting the five *NbFucT* and two *NbXylT* genes were inserted into the Cas9-containing plasmid (Figure 1C). Agrobacterium-mediated transformation was used to deliver the designed Cas9 containing DNA constructs (pk-NbFUCT-XYLT) into plant cells, resulting in a successful generation of transformants.

Evaluation and characterization of the mutations induced by multiplexed Cas9 targeting of the *XylT* and the *FucT* genes

Mutations resulting from the editing of the five *NbFucT* and two *NbXylT* genes were identified by Sanger sequencing of the target gene fragment (Figure 2A). Among these transformants, two plant lines, HL40 and HL64, were selected, each of which exhibited mutations in all seven genes (Table 1). The transformant line HL40 exhibited bi-

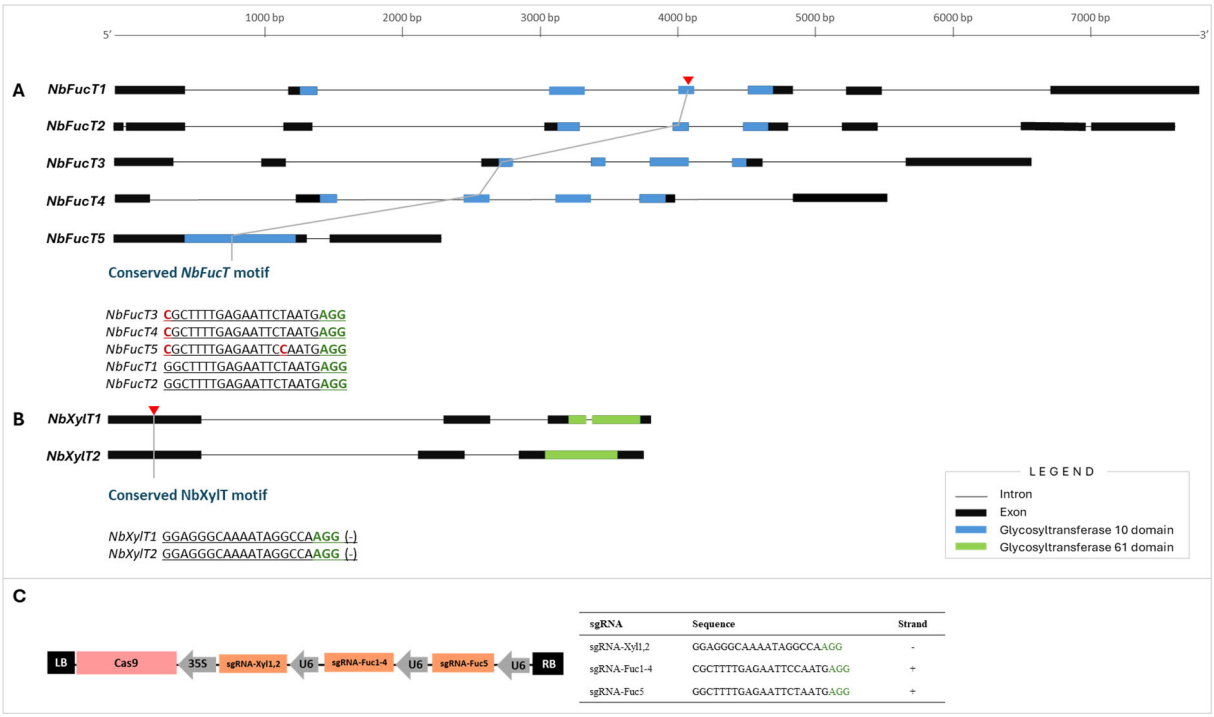

FIGURE 1
Selection of target sites for multiplexed genome editing to knockout in five *NbFucT* and two *NbXylT* genes using CRISPR-Cas9. Target sites in **(A)** *NbFucT* and **(B)** *NbXylT* genes. **(C)** Schematic diagram of the Cas9-sgRNA construct. The black boxes indicate exons, and the underlined sequences correspond to the sgRNA. The red and green nucleotides represent SNPs and PAM sequences, respectively. .

10.3389/fpls.2025.1701668

A

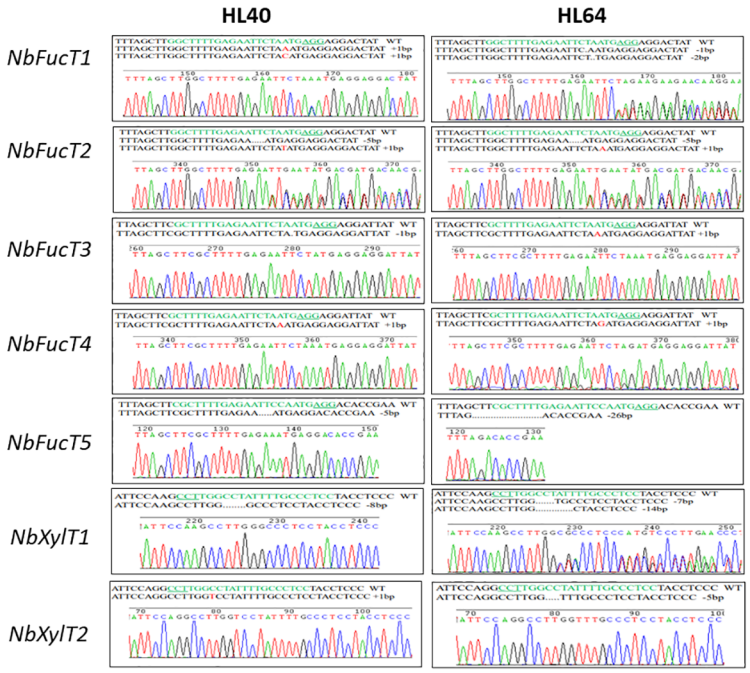

B

Plant ID			Target gene						
			NbFucT1	*NbFucT2*	*NbFucT3*	*NbFucT4*	*NbFucT5*	*NbXylT1*	*NbXylT2*
T_0	HL40	Mutation	+1/+1	+1/-5	WT/-1	WT/+1	-1/-5	+1/-8	+1/-3
		Zygosity	Bi-allele	Bi-allele	Heterozygote	Heterozygote	Bi-allele	Bi-allele	Bi-allele
	HL64	Mutation	-1/-2	+1/-5	WT/+1	WT/+1	-26	-7/-14	-5/-9
		Zygosity	Bi-allele	Bi-allele	Heterozygote	Heterozygote	homozygote	Bi-allele	Bi-allele

FIGURE 2
Mutations induced in *N. benthamiana* by the CRISPR/Cas9 system. **(A)** Results of mutation analysis of 7 target sites identified in HL40 and HL60 T_0 transgenic plants. **(B)** Genotype and zygosity analysis of T_0 transformants.

allelic mutations at five target gene sites which included one base insertion in *NbFucT1*, one base insertion or five base deletions in *NbFucT2*, one base deletion or five base deletions in *NbFucT5*, one base insertion or eight base deletions in *NbXylT1*, and one base insertion or three base deletions in *NbXylT2* (Figure 2B). Heterozygous mutations were identified in the target regions on *NbFucT3* and *NbFucT4* with one base deletion and one base insertion, respectively. In the transformant line HL64, bi-allelic mutations were identified at four target sites: one- or two-base deletions in *NbFucT1*, one- or five-base deletions in *NbFucT2*, seven- or fourteen-base deletions in *NbXylT1*, and five- or nine-base deletions in *NbXylT2*. The target sites *NbFucT3* and *NbFucT4* in HL64 exhibited heterozygous mutations with one base insertion each. Additionally, a deletion of 26 bases was observed in the HL64 *NbFucT5* target site (Figure 2B).

Identification of T_1 *FucT* and *XylT* knockout lines

T_0 plants of lines HL40 and HL64 were self-pollinated to produce T_1 generation plants. Two screening strategies were applied to identify transformants among T_1 generation plants: PCR analysis to select lines free of the Cas9 transgene, and Western blotting with fucose and xylose antibodies to confirm the absence of α-1,3-fucose and β-1,2-xylose residues, indicating targeted gene silencing. Western blot analysis of the T_1 transformants revealed no fucose residues in line HL40–4 and no xylose residues in lines HL40-11, HL40-14, HL40-18, HL40-20, HL64-15, and HL64-17 (Supplementary Figure S2). In HL64-19, neither fucose nor xylose residues were detected (Supplementary Figure S2B). Eight T_1 transformants displaying loss-of-function of the target gene were selected for sequencing.

Additional screening of the Cas9-free T_1 transformants lacking the target genes was performed using primers specifically designed to amplify the Cas9 and sgRNA fragments within the engineered plasmid. (Supplementary Table S1, Supplementary Figure S3). Five T_1 lines lacking the amplification products for both sets of primers were selected: HL40-48, HL40-219, HL40-379, HL-40-591, and HL64-512 (Supplementary Figure S3). As a result of these two screening processes, 13 T_1 transformants were selected for further analysis of the genotypes and segregation patterns of the mutations using targeted deep sequencing (Supplementary Table S2).

The T_1 transformant HL40-4, which lacked α-1,3-fucose residues, inherited the same heterozygous mutations from the T_0-HL40 parent, in the target sites *NbFucT5*, *NbXylT1*, *NbXylT2*,

TABLE 1 Characterization of mutations in the target genes of the T2 transformant plant lines. (*Cas9 free plants).

CRISPR/Cas9-induced mutations											
Generation	T0	T1	T2		NbFUCT1	NbFUCT2	NbFUCT3	NbFUCT4	NbFUCT5	NbXYLT1	NbXYLT2
Plant IDs	HL40			Mutation	+1(A)/+1(C)	+1/-5	WT/-1	WT/+1	-1/-5	+1/-8	+1/-3
				Zygosity	Bi-allele	Bi-allele	Heterozygote	Heterozygote	Bi-allele	Bi-allele	Bi-allele
		HL40-48*		Mutation	+1bp(A)	-+1/-5	-1	+1	-5	-8	+1
				Zygosity	Homozygote	Bi-allele	Homozygote	Homozygote	Homozygote	Homozygote	Homozygote
			HL40-48-1*	Mutation	+1bp(A)	-5bp	-1bp	+1bp	-5bp	-8bp	+1bp
				Zygosity	Homozygote	Homozygote	Homozygote	Homozygote	Homozygote	Homozygote	Homozygote
			HL40-48-2*	Mutation	+1bp(A)	-5bp	-1bp	+1bp	-5bp	-8bp	+1bp
				Zygosity	Homozygote	Homozygote	Homozygote	Homozygote	Homozygote	Homozygote	Homozygote
			HL40-48-3*	Mutation	+1bp(A)	+1bp	-1bp	+1bp	-5bp	-8bp	+1bp
				Zygosity	Homozygote	Homozygote	Homozygote	Homozygote	Homozygote	Homozygote	Homozygote
			HL40-48-4*	Mutation	+1bp(A)	+1bp/-5bp	-1bp	+1bp	-5bp	-8bp	+1bp
				Zygosity	Homozygote	Bi-allele	Homozygote	Homozygote	Homozygote	Bi-allele	Homozygote
		HL40-219*		Mutation	+1bp(C)	-5bp	-1bp	+1bp	-1bp/-5bp	+1bp	+1bp
				Zygosity	Homozygote	Homozygote	Homozygote	Homozygote	Bi-allele	Homozygote	Homozygote
			HL40-219-1*	Mutation	+1bp(C)	-5bp	-1bp	+1bp	-1bp/-5bp	+1bp	+1bp
				Zygosity	Homozygote	Homozygote	Homozygote	Homozygote	Bi-allele	Homozygote	Homozygote
			HL40-219-2*	Mutation	+1bp(C)	-5bp	-1bp	+1bp	-1bp/-5bp	+1bp	+1bp
				Zygosity	Homozygote	Homozygote	Homozygote	Homozygote	Bi-allele	Homozygote	Homozygote
			HL40-219-3*	Mutation	+1bp(C)	-5bp	-1bp	+1bp	-5bp	+1bp	+1bp
				Zygosity	Homozygote	Homozygote	Homozygote	Homozygote	Homozygote	Homozygote	Homozygote
			HL40-219-4*	Mutation	+1bp(C)	-5bp	-1bp	+1bp	-1bp/-5bp	+1bp	+1bp
				Zygosity	Homozygote	Homozygote	Homozygote	Homozygote	Bi-allele	Homozygote	Homozygote
	HL64			Mutation	-1bp/-2bp	+1bp/-5bp	WT/+1bp	WT/+1bp	-26bp	-7bp/-14bp	-5bp/-9bp
				Zygosity	Bi-allele	Bi-allele	Heterozygote	Heterozygote	Homozygote	Bi-allele	Bi-allele
		HL64-512*		Mutation	-1/-2	+1	+1	+1	-26	-7/-14	-5
				Zygosity	Bi-allele	Homozygote	Homozygote	Homozygote	Homozygote	Bi-allele	Homozygote

(Continued)

10.3389/fpls.2025.1701668

10.3389/fpls.2025.1701668

TABLE 1 Continued

Generation	T0	T1	T2		CRISPR/Cas9-induced mutations						
					NbFUCT1	NbFUCT2	NbFUCT3	NbFUCT4	NbFUCT5	NbXYLT1	NbXYLT2
			HL64-512-1*	Mutation	-2bp	+1bp	+1bp	+1bp	-26bp	-7bp	-5bp
				Zygosity	Homozygote	Homozygote	Homozygote	Homozygote	Homozygote	Homozygote	Homozygote
			HL64-512-2*	Mutation	-1bp/-2bp	+1bp	+1bp	+1bp	–26bp	-7bp	-5bp
				Zygosity	Bi-allele	Homozygote	Homozygote	Homozygote	Homozygote	Homozygote	Homozygote
			HL64-512-3*	Mutation	-1bp	+1bp	+1bp	+1bp	-26bp	-7bp	-5bp
				Zygosity	Homozygote	Homozygote	Homozygote	Homozygote	Homozygote	Homozygote	Homozygote
			HL64-512-4*	Mutation	-1bp/-2bp	+1bp	+1bp	+1bp	-26bp	-7bp-14bp	-5bp
				Zygosity	Bi-allele	Homozygote	Homozygote	Homozygote	Homozygote	Bi-allele	Homozygote

* Cas-9 Free Plants.

whereas all the other target genes inherited the mutation in a homozygous pattern. Another T_1 transformant lacking the α-1,3-fucose residues; HL64-19, inherited the heterozygous mutation pattern from the T_0-HL64 parent in the target sites NbFucT1, *NbXylT1*. All the other target genes showed inheritance of the mutation in a homozygous pattern (Supplementary Table S2). Sequencing of the T_1 transformants HL40-11, HL40-14, HL40-18, and HL40–20 revealed the presence of a wild-type allele in the target regions of *NbFucT3* and *NbFucT4*. Western blot analysis revealed the absence of β1,2-xylose residues but the presence of α-1,3-fucose residues in these transformants. This suggests that a complete knockout of the α-1,3-fucose phenotype, as evidenced by the lack of fucose residues, likely requires the absence of the wild-type allele in both *NbFucT3* and *NbFucT4* genes. In HL40-4, β1,2-xylose residues were detected despite the absence of the wild-type allele in either of the *NbXylT* target genes. In contrast, HL40-20, which lacked β1,2-xylose residues, shared the same heterologous mutation at the *NbXylT1* target site as HL40–4 but inherited only one base homologous insertion at the *NbXylT2* target site. Consequently, it can be inferred that the three-base deletion in the *NbXylT2* site did not significantly affect the β-1,2-xylosyltransferase activity. All lines selected through PCR screening (HL40-48, HL40-219, HL40-379, HL-40-591, and HL64-512) lacked the wild-type allele, whereby it could be anticipated that the mutation pattern in these lines would result in loss of function of all *NbFucT* and *NbXylT* target genes.

Generation of Cas9-free, stable FucT and XylT knockout T_2 plants

Of the five Cas9-free T_1 plants, three T_1 transformants (HL40-48, HL40-219, and HL64-512) were selected for the production of T_2 plants because these lines showed the highest number of homozygous mutations. In particular, these selected transformants, HL40-48, HL40-219, and HL64-512, showed six homozygous mutations and one heterozygous mutation in NbFucT2, NbFucT5, and NbXylT2, respectively. To obtain stable homozygous mutant lines for F-KO and X-KO, individuals from these lines were cultivated and sequencing of the target sites was performed. The morphology and growth rate of the T_2 plants were also observed to detect the side effects of the mutations. No significant differences were observed between T_0 and T_2 generation plants compared to wild-type plants in terms of external morphological characteristics, from germination to flowering, and seed production (Figure 3A). Sequence analysis revealed the segregation of heterozygous alleles into homozygous genotypes in the T_2 generation. Among the T_2 plants derived from the HL-40–48 T_1 line, the plants identified as HL40-48-1, HL 40-48-2, and HL40-48–3 exhibited homozygous genotypes in all seven target regions (Table 1). Similarly, T_2 plants HL40-219-3, HL64-512-1, and HL64-512–3 were confirmed to have homozygous mutations in the seven target genes (Table 1). Furthermore, T_2 plants HL40-48-1~4, HL40-219-1~4, and HL64-512-1~4 were all Cas9-free (Figure 3B).

Western blot analysis on selected T2 lines provided final confirmation of functional enzyme loss for all seven targeted genes. This analysis revealed the absence of both β1,2-xylose and

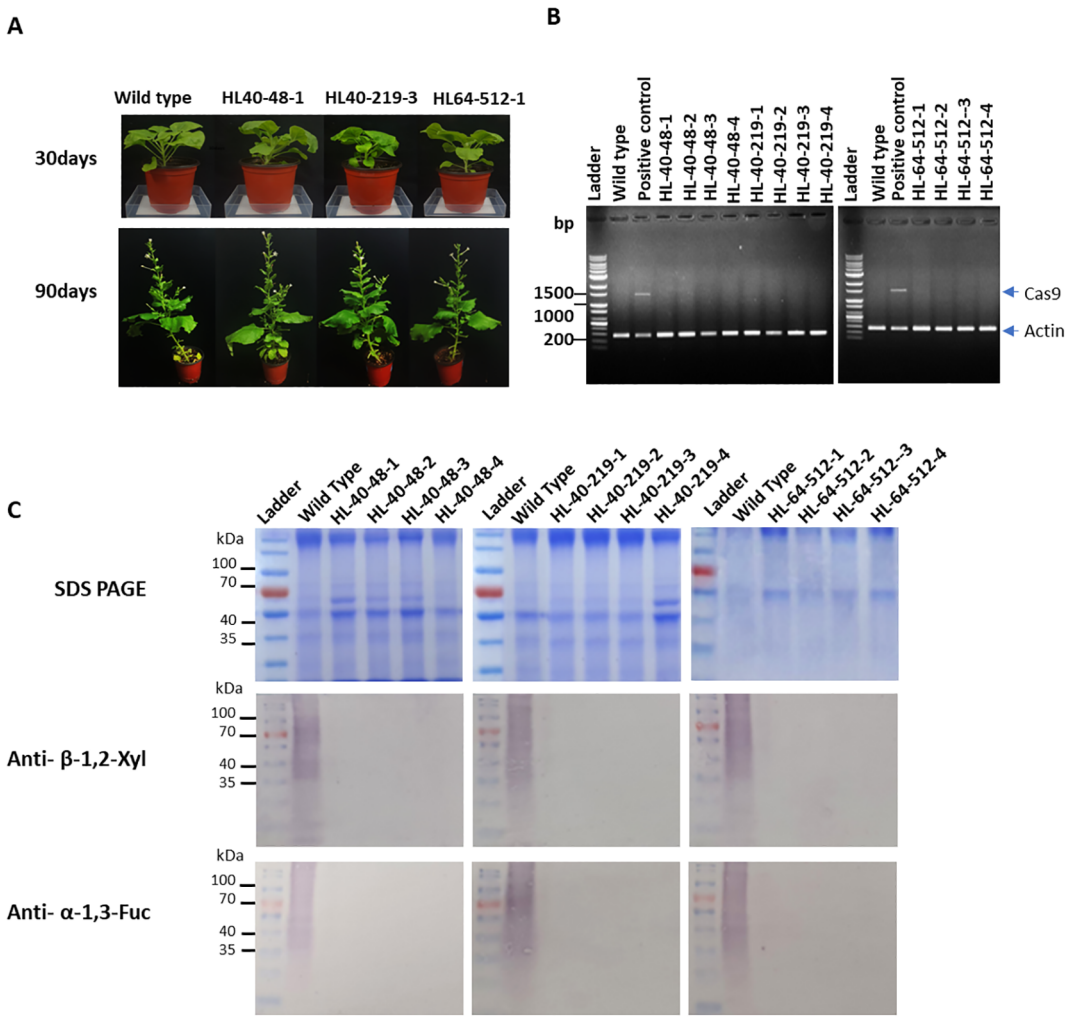

FIGURE 3
Phenotypic comparison and molecular characterization of transformants. **(A)** Morphological comparison of T_2 generation plants throughout their growth stages. Plants were photographed 30 and 90 days after sowing. **(B)** PCR-based reconfirmation of absence of Cas9 in T_2 transformants. Wild type *N. benthamiana* was used as negative control. HL-64–19 T_1 plant was used as positive control. HL40-48-1~4, HL40-219-1~4, HL64-512-1~4 T2 plants were Cas9-free. Actin amplification product size: 267 bp, Cas9 amplification product size:1448 bp. **(C)** Western blot analysis for comparison of α-1,3-fucose and β-1,2-xylose residues in *NbFucT* and *NbXylT* transformants and wild-type. Wild-type tobacco was used as positive control. Results of anti- β-1,2-XylT is β-1,2-xylosyltransferase antibody reaction results.

α-1,3-fucose residues in the T2 transformants, solidifying the successful knockout of all seven target genes (Figure 3C).

Discussion

Harnessing plants as factories for therapeutic proteins holds immense promise for enhancing and optimizing the synthesis of proteins that are crucial for treating and preventing diseases in humans and animals. There are significant advantages to using this strategy; however, successful implementation requires addressing technical and regulatory hurdles. Although several vaccines, antibiotics, and therapeutic proteins have been developed in plants (Obembe et al., 2011), the generation of mutants lacking the activity of key enzymes (e.g., β-1,2-xylosyltransferase and α-1,3-fucosyltransferase) prevents the formation of certain epitopes on plant N-glycans. The effectiveness of this approach was validated by generating *Arabidopsis thaliana* knockout mutants, including a triple knockout line that displayed normal plant development under standard growth conditions (Strasser et al., 2004).

N. benthamiana has shown promise as a potential host for producing recombinant glycoproteins with customized N- and O-glycan modifications (Strasser et al., 2008; Jansing et al., 2019). Random mutagenesis studies using EMS demonstrated that a 4- or 5-fold knockout of exclusively the fucosyltransferase genes resulted in a decrease in fucose levels but unexpectedly led to an increase in xylose levels in plants (Nagels et al., 2011). This indicates a compensatory mechanism in glycan synthesis, where the absence of fucose may trigger an upregulation of xylose incorporation. A complete disruption of both fucose and xylose biosynthetic pathways is necessary to significantly alter the glycan profile. Therefore, a 7-fold knockout of fucosyltransferase and

xylosyltransferase genes is more effective in disrupting glycan synthesis than a 4- or 5-fold knockout. This is likely due to the elimination of redundant pathways, the suppression of compensatory mechanisms, and the synergistic effect of targeting both types of genes, resulting in a greater reduction of fucose and xylose levels in the plant. The advent of techniques like multiplex gene editing, base editing, prime editing and Cas12a/CPpf1 have accelerated the progress in plant glycoengineering Abdelrahman et al., 2021). Recent advances in gene editing, including base editing, prime editing and multiplex CRISPR strategies, have expanded the toolkit for precise genome manipulation in plants. Base editing and prime editing offer powerful options for targeted nucleotide substitutions, small insertions or corrections, and motif-level refinements without introducing double-strand breaks (Molla et al., 2021). These tools are especially useful for fine tuning enzyme function, modifying catalytic residues and generating allelic variants with subtle but biologically meaningful changes. However, their current delivery limitations, lower efficiency in several crop species and complexities in multiplexing make them less suited for large-scale gene family knockouts. Multiplex CRISPR/Cas9 gene editing remains the most efficient and practical strategy for simultaneously disrupting several homologous genes to completely abolish their function, especially in systems in which multiple paralogs act redundantly within the same biochemical pathway.

Building on our previous work targeting *NbXylT1* and *NbFucT2* to characterize mutation nature and inheritance, we expanded our approach to achieve near complete elimination of *FucT* and *XylT* activity by simultaneously targeting all seven genes Song et al., 2022). This represents, to our knowledge, the first successful multiplex CRISPR/Cas9 editing of all seven glycosyltransferase homologs in *N. benthamiana*, addressing limitations of previous studies that excluded the *FucT5* homolog. We employed Agrobacterium-mediated CRISPR/Cas9 to achieve targeted editing of all homologous *NbXylT* and *NbFucT* genes. A systematic analysis of mutation rates, types, and genetic trends was performed on the transformed sample. Two T0 transformants were identified that successfully carried mutations in all seven target genes, HL40 and HL64. Analysis of the mutational characteristics in the selected T0 mutants revealed deletions and insertions as the most frequent types of induced edits. Notably, insertions were predominantly single nucleotide additions, while deletions spanned a wider range, from one to twenty-six nucleotides. The *NbFucT3* and *NbFucT4* genes showed heterozygous mutations carrying the wild-type allele in both the HL40 and HL64 transformants, whereas the other target gene mutations were bi-allelic or homozygous. Despite the expected segregation of alleles, a few plants in the T1 generation retained the wild-type allele, which has been the case for many other plant edits using CRISPR/Cas9 (Pan et al., 2016; Cheng et al., 2019). From the three T1-Cas9 free plants, which carried homozygous mutations

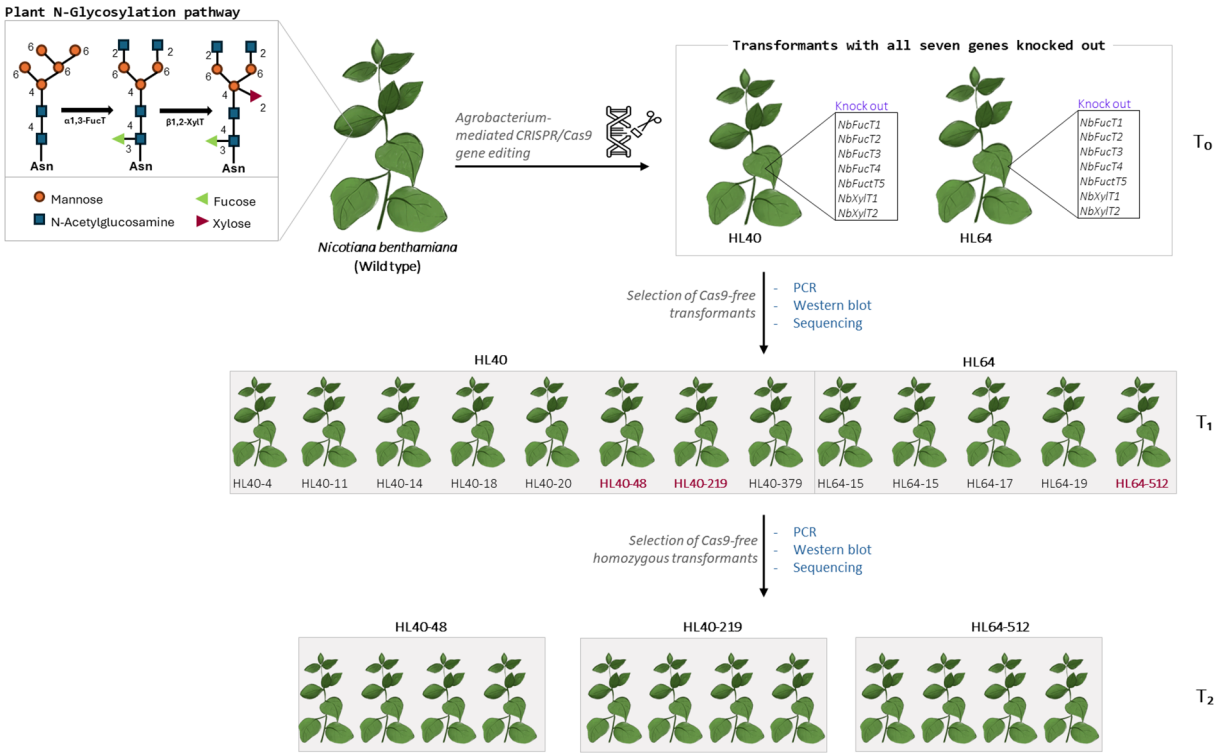

FIGURE 4
Summary of CRISPR/Cas9 mediated knockout of seven N-glycosylation genes in *Nicotiana benthamiana* and selection of Cas9-free homozygous transformants in the consecutive generations (T1 and T2).

in all but one target gene site, we generated T2 transformant lines that carried a stable mutation in all seven target genes and were Cas-9 free (Figure 3). Loss of enzymatic activity for both *NbFucT* and *NbXylT* was confirmed in all T2 transformants. The external morphology and growth of T2 plants remained largely similar to those of T0 and wild-type plants throughout development, providing preliminary evidence of minimal side effects induced by the mutations (Figure 3A). The lack of observable morphological or growth defects in T2 plants suggests these multiplex gene edits do not impair plant viability or development, which is essential for their use as production platforms. Overall, this study provides a solid genetic platform for glycoengineering in *N. benthamiana*, overcoming prior limitations by achieving full knockout of all seven glycosyltransferase homologs in stable, Cas9-free lines. In addition to achieving Cas9-free edited lines, our approach ensures complete pathway coverage by including *FucT5*, which was previously omitted. Sequence and domain analyses confirm that *FucT5* contains the GT10 catalytic core and shares high sequence similarity with other *NbFucT* homologs, supporting its potential functionality. This comprehensive targeting strategy prevents residual or context-dependent α-1,3-fucosylation and provides a more reliable foundation for downstream biopharmaceutical protein production. The study has been graphically summarized in Figure 4.

Data availability statement

The datasets presented in this study can be found in online repositories. The names of the repository/repositories and accession number(s) can be found in the article/Supplementary Material.

Author contributions

CK: Investigation, Methodology, Software, Writing – original draft, Writing – review & editing. HS: Investigation, Methodology, Writing – original draft. ML: Investigation, Writing – review & editing. S-YK: Investigation, Writing – review & editing. D-HS: Investigation, Writing – review & editing. HK: Data curation, Software, Writing – review & editing. E-JS: Conceptualization, Resources, Supervision, Writing – review & editing. YR: Investigation, Writing – review & editing. OK: Conceptualization, Supervision, Writing – review & editing. G-JL: Conceptualization, Resources, Supervision, Writing – review & editing.

Funding

The author(s) declared financial support was received for this work and/or its publication. This research was funded by the New Breeding Technologies Development Program (RS-2024-00322302), Rural Development Administration, Republic of Korea.

Conflict of interest

Author HK and E-JS were employed by the company BioApplications Inc. Author YR was employed by company Qi Biodesign.

The remaining authors declare that the research was conducted in the absence of any commercial or financial relationships that could be construed as a potential conflict of interest.

Generative AI statement

The author(s) declare that no Generative AI was used in the creation of this manuscript.

Any alternative text (alt text) provided alongside figures in this article has been generated by Frontiers with the support of artificial intelligence and reasonable efforts have been made to ensure accuracy, including review by the authors wherever possible. If you identify any issues, please contact us.

Publisher's note

Supplementary material

The Supplementary Material for this article can be found online at: https://www.frontiersin.org/articles/10.3389/fpls.2025.1701668/full#supplementary-material

References

Abdelrahman, M., Wei, Z., Rohila, J. S., and Zhao, K. (2021). Multiplex genome-editing technologies for revolutionizing plant biology and crop improvement. *Front. Plant Sci.* 12, 721203. doi: 10.3389/fpls.2021.721203

Ahmad, A., Abd-Elsalam, K. A., Ali, M., Majeed, H. N., Arif, A., Munir, A., et al. (2024). "Regulatory triggers of CRISPR-edited crops," in *Global regulatory outlook for CRISPRized plants* (Academic Press: Elsevier), 91–112.

Barolo, L., Abbriano, R. M., Commault, A. S., George, J., Kahlke, T., Fabris, M., et al. (2020). Perspectives for glyco-engineering of recombinant biopharmaceuticals from microalgae. *Cells* 9, 633. doi: 10.3390/cells9030633

Brooks, C., Nekrasov, V., Lippman, Z. B., and Van Eck, J. (2014). Efficient gene editing in tomato in the first generation using the clustered regularly interspaced short palindromic repeats/CRISPR-associated9 system. *Plant Physiol.* 166, 1292–1297. doi: 10.1104/pp.114.247577

Castilho, A., and Steinkellner, H. (2012). Glyco-engineering in plants to produce human-like N-glycan structures. *Biotechnol. J.* 7, 1088–1098. doi: 10.1002/biot.201200032

Cheng, Y., Zhang, N., Hussain, S., Ahmed, S., Yang, W., and Wang, S. (2019). Integration of a FT expression cassette into CRISPR/Cas9 construct enables fast generation and easy identification of transgene-free mutants in Arabidopsis. *PloS One* 14, e0218583. doi: 10.1371/journal.pone.0218583

Gomord, V., Fitchette, A. C., Menu-Bouaouiche, L., Saint-Jore-Dupas, C., Plasson, C., Michaud, D., et al. (2010). Plant-specific glycosylation patterns in the context of therapeutic protein production. *Plant Biotechnol. J.* 8, 564–587. doi: 10.1111/j.1467-7652.2009.00497.x

Jansing, J., Sack, M., Augustine, S. M., Fischer, R., and Bortesi, L. (2019). CRISPR/Cas9-mediated knockout of six glycosyltransferase genes in Nicotiana benthamiana for the production of recombinant proteins lacking β-1, 2-xylose and core α-1, 3-fucose. *Plant Biotechnol. J.* 17, 350–361. doi: 10.1111/pbi.12981

Molla, K. A., Sretenovic, S., Bansal, K. C., and Qi, Y. (2021). Precise plant genome editing using base editors and prime editors. *Nat. Plants* 7, 1166–1187. doi: 10.1038/s41477-021-00991-1

Nagels, B., Van Damme, E. J., Pabst, M., Callewaert, N., and Weterings, K. (2011). Production of complex multiantennary N-glycans in Nicotiana benthamiana plants. *Plant Physiol.* 155, 1103–1112. doi: 10.1104/pp.110.168773

Obembe, O. O., Popoola, J. O., Leelavathi, S., and Reddy, S. V. (2011). Advances in plant molecular farming. *Biotechnol. Adv.* 29, 210–222. doi: 10.1016/j.biotechadv.2010.11.004

Pan, C., Ye, L., Qin, L., Liu, X., He, Y., Wang, J., et al. (2016). CRISPR/Cas9-mediated efficient and heritable targeted mutagenesis in tomato plants in the first and later generations. *Sci. Rep.* 6, 24765. doi: 10.1038/srep24765

Pattison, R. J., and Amtmann, A. (2009). N-glycan production in the endoplasmic reticulum of plants. *Trends Plant Sci.* 14, 92–99. doi: 10.1016/j.tplants.2008.11.008

Rup, B., Alon, S., Amit-Cohen, B.-C., Brill Almon, E., Chertkoff, R., Tekoah, Y., et al. (2017). Immunogenicity of glycans on biotherapeutic drugs produced in plant expression systems—The taliglucerase alfa story. *PloS One* 12, e0186211. doi: 10.1371/journal.pone.0186211

Shanmugaraj, B., Bulaon, C. J. I., and Phoolcharoen, W. (2020). Plant molecular farming: A viable platform for recombinant biopharmaceutical production. *Plants* 9, 842. doi: 10.3390/plants9070842

Sil, B., and Jha, S. (2014). Plants: The future pharmaceutical factory. *Am. J. Plant Sci.* 5, 319–327. doi: 10.4236/ajps.2014.53044

Song, H., Ahn, J.-Y., Yan, F., Ran, Y., Koo, O., and Lee, G.-J. (2022). Genetic dissection of CRISPR-Cas9 mediated inheritance of independently targeted alleles in tobacco α-1, 3-Fucosyltransferase 1 and β-1, 2-Xylosyltransferase 1 Loci. *Int. J. Mol. Sci.* 23, 2450. doi: 10.3390/ijms23052450

Strasser, R. (2016). Plant protein glycosylation. *Glycobiology* 26, 926–939. doi: 10.1093/glycob/cww023

Strasser, R., Altmann, F., Mach, L., Glössl, J., and Steinkellner, H. (2004). Generation of Arabidopsis thaliana plants with complex N-glycans lacking β1, 2-linked xylose and core α1, 3-linked fucose. *FEBS Lett.* 561, 132–136. doi: 10.1016/S0014-5793(04)00150-4

Strasser, R., Stadlmann, J., Schähs, M., Stiegler, G., Quendler, H., Mach, L., et al. (2008). Generation of glyco-engineered Nicotiana benthamiana for the production of monoclonal antibodies with a homogeneous human-like N-glycan structure. *Plant Biotechnol. J.* 6, 392–402. doi: 10.1111/j.1467-7652.2008.00330.x

Yao, J., Weng, Y., Dickey, A., and Wang, K. Y. (2015). Plants as factories for human pharmaceuticals: applications and challenges. *Int. J. Mol. Sci.* 16, 28549–28565. doi: 10.3390/ijms161226122

frontiers | Frontiers in Plant Science

TYPE Original Research
PUBLISHED 02 January 2026
DOI 10.3389/fpls.2025.1724810

OPEN ACCESS

EDITED BY
Kevin Wang,
University of Pikeville, United States

REVIEWED BY
Cong Vu,
NanoSoils Bio, Australia
VÕ Khoa,
Gachon University, Republic of Korea
Daria Rutkowska,
Council for Scientific and Industrial Research (CSIR), South Africa

*CORRESPONDENCE
Linda Avesani
linda.avesani@univr.it

RECEIVED 14 October 2025
REVISED 03 December 2025
ACCEPTED 05 December 2025
PUBLISHED 02 January 2026

CITATION
Pivotto D, Rosa A, Elsheikh AM, Gecchele E, Zampieri R, Raneri A, Garonzi V and Avesani L (2026) Clinical-grade plant-made nanomaterials: from process design to the construction of a manufacturing facility. *Front. Plant Sci.* 16:1724810. doi: 10.3389/fpls.2025.1724810

Clinical-grade plant-made nanomaterials: from process design to the construction of a manufacturing facility

Denise Pivotto[1], Anthony Rosa[2], Aya Maged Elsheikh[2], Elisa Gecchele[2], Roberta Zampieri[2], Alessia Raneri[1], Valentina Garonzi[2] and Linda Avesani[1]*

[1]Department of Biotechnology, University of Verona, Verona, Italy, [2]Diamante SB Srl, Verona, Italy

Plant-made nanomaterials are proteinaceous elements that are emerging as multi-purpose and versatile tools in the therapeutic landscape. In the context of autoimmune diseases, Tomato Bushy Stunt Virus (TBSV) has been previously explored as a platform for inducing immune tolerance by displaying disease-specific immunodominant peptides—offering a potential path toward disease remission. In this study, we developed a dedicated facility and a Good Manufacturing-compliant Process for producing TBSV-based nanoparticles engineered to display peptides relevant to specific autoimmune disorders. Data collected from multiple non-consecutive pilot-scale production batches were used to build a simplified techno-economic model of the process. The process is readily scalable and offers opportunities for further improvements, supporting the potential to meet market demands for early-stage therapeutic interventions in autoimmune diseases. Additionally, a preliminary Environmental, Health, and Safety (EHS) assessment of the process showed a highly favorable environmental output index and minimal associated risks, reinforcing the platform's sustainability. These results support the viability of plant-based manufacturing for therapeutic nanomaterials and highlight TBSV's potential as a novel platform for tolerance-inducing treatments in autoimmune diseases.

KEYWORDS

nanobiotechnology, peptide Liprin (pLip), plant molecular farming, rheumatoid arthritis, TBSV, tolerance induction, viral nanoparticles

Introduction

Plant Molecular Farming, which includes the production of recombinant proteins and nanomaterials using plant biotechnology, could provide a steep change in improving health outcome, especially in developing countries and in pandemic contexts, due to its scalability, safety and speed.

The first current Good Manufacturing Process (cGMP) facility producing Plant-Made Pharmaceuticals was designed by Large Scale Biology Corporation (LSBC) in Owensboro, KY, USA (now Kentucky BioProcessing) and opened in the year 1999, using the plant-virus transient expression system Geneware® (Pogue et al., 2002, 2010). Ever since, PMF has developed as a safe, easily scalable and cost-effective technology to produce biopharmaceuticals, when compared to other cell-based systems. Canadian former enterprise Medicago, now acquired by Aramis Biotechnology, was one of the pioneers in the industry. Founded in 1999, its focus was the production of Virus-Like Particles (VLPs) as vaccines, reaching phase III clinical studies with their product Covifenz®, a vaccine candidate for the treatment of SARS-CoV2, before announcing their sudden closure in 2023.

Within this continuous framework and thanks to ongoing efforts in basic research, various emerging applications now rely on plant-made nanomaterials, primarily derived from or inspired by viral structures, as promising tools for addressing multiple human diseases. These materials represent a natural progression in the application of plant biotechnology to create innovative solutions for a range of human diseases.

Viruses are excellent examples of naturally occurring nanoparticles that can serve as ideal platforms for the development of new biomedical applications. Plant viruses, in general, are non-enveloped structures, and they can assume a spherical/icosahedral or filamentous/tubular shape. Plant virus capsids are formed through the self-assembly of repeating protein subunits, providing a high degree of multivalency. Their repetitive structure support their function as adjuvants and provide an ideal scaffold for the display of peptides and delivery of drugs (Chung et al., 2020; Santoni et al., 2020). As plant viruses they also have an inherent safety profile in humans.

Tomato Bushy Stunt Virus (TBSV) is a virus of the Tombusvirus family, characterized by an icosahedral capsid of ~ 32 nm in diameter made up of 180 subunits of the coat protein (CP). TBSV Nanoparticles (NPs) can either encapsulate or present small molecules and polypeptides on the surface (Grasso et al., 2013) and are not toxic or teratogenic (Blandino et al., 2015). When intravenously injected into mice, these NPs do not induce alterations of tissues/organs (Lico et al., 2016).

We recently demonstrated the potential of plant-made nanoparticles for preventing and curing autoimmune diseases such as Type 1 Diabetes (T1D) and Rheumatoid Arthritis (RA) (Zampieri et al., 2020). Indeed, the immense potential of nanomaterials as tolerogenic agents to be used in the context of diverse immunological diseases such as autoimmune diseases, allergies and transplants has been extensively demonstrated (Kusumoputro et al., 2023); however, plant viruses have never before been employed for such applications prior to our study.

For RA, we demonstrated that the use of plant-made nanoparticles was able to induce regulatory T cells by diverting the autoimmune response to a tolerogenic setting that reversed the clinical score of the disease with outcomes comparable to golden standard treatments based on immunosuppressants (Zampieri et al., 2020). We used the TBSV genome as a vector of expression and exploited the TBSV Coat Protein for the display of the peptide Liprin (pLip) on the external surface of the capsid.

TBSV NPs manufacturing in plants relies on the use of transient viral expression in *Nicotiana benthamiana*, widely used as a bioreactor for the production of biopharmaceuticals, due to its versatility and susceptibility to plant pathogens. Besides acting as vectors that regulate gene expression (Bally et al., 2018), plant viruses can be genetically engineered to incorporate non-native peptides into their CPs. The modified viruses are then propagated in host plant leaves, which are subsequently harvested and processed for purification (Pogue et al., 2002).

In this sense, once harvested after infection, the plant leaves can be processed to obtain a purified virus that presents a target peptide. This whole NP represents the final Active Pharmaceutical Ingredient (API). Being a plant pathogen, the use of these NPs for therapeutical purposes is entirely safe for humans, due to the absence of specific receptors for viral recognition and penetration into host cells (Nikitin et al., 2016).

While there is currently no clinically approved plant-based nanomedicine in the market, several are undergoing preclinical development while some systems are poised to enter translational development. Given our promising preclinical evidence, we made a concerted effort to spin-out the project from an academic setting by establishing a GMP-grade manufacturing facility, enabling the production of NPs under GMP conditions for use in human clinical studies.

Here, we describe the manufacturing process overseeing the production of TBSV NPs within a small-scale laboratory setting, meant to be GMP-compliant and designed to produce quantities sufficient for toxicological pre-clinical studies and Phase 1 clinical trials in humans. All projections presented throughout the article are based on a hypothetical API dosage of 2 mg per patient/year, aimed at achieving the desired clinical outcome of tolerance induction in RA patients.

Materials and methods

Host plant species selection and biomass production

In the described experimental setup, *N. benthamiana* plants are cultivated indoors under controlled environmental conditions, maintaining a constant temperature of 24°C ± 3°C and relative humidity between 50% and 60%, with a photoperiod of 16 hours light and 8 hours dark. Seeds are initially sown and allowed to germinate for up to 10 days, after which the plantlets are moved into larger pots to accommodate growth and are redistributed across trays. Plants are irrigated every 2–3 days for a period of 18 days, until they reach optimal biomass. At this stage, the average leaf fresh weight (LFW) per plant is approximately 8.2 g. Five-week-old *N. benthamiana* plants are then ready for infection, initiating the manufacturing workflow, which is divided into upstream and downstream processing phases.

Upstream process

Primary infection

N. benthamiana plants used in the process are grown under the conditions described above.

In vitro transcription is used to produce TBSV.pLip infectious RNAs (Grasso et al., 2013), of which 4 µg per plant are used for the manual infection of two leaves in *N. benthamiana* with the aid of an abrasive powder (Celite®). After 6 days, leaves displaying local and systemic infection symptoms are harvested, pooled and checked for recombinant virus RNA by reverse transcription polymerase chain reaction (RT-PCR). The collected leaves are homogenized in 1X Phosphate Buffered Saline (PBS), composed of 151 mM NaCl, 8.4 mM $Na_2HPO_4 \times 12\ H_2O$, 1.86 mM $NaH_2PO_4 \times H_2O$, adjusted to pH 7.2), at a ratio of 1:10 (g LFW/mL buffer), resulting in a suspension containing virions, which is used in the next step.

Secondary infection

Forty microliters of sap, a solution containing infectious plant material, are used to infect one leaf, for a total of two leaves per plant, with the same rubbing procedure described above; once again, the state of the infection is monitored by phenotypical assessment, then, 6 days post infection, the leaves are harvested and homogenized with 1X PBS to obtain another infectious suspension to proceed analogously with the infection of a third batch, for the third step of the process named tertiary infection.

Tertiary infection

The plant biomass originating from this phase represents the starting material to be processed for final product purification. The necessary quality controls are performed during all phases, to ensure structural integrity of the virus and presence of the peptide of interest. These include RNA extraction for RT-PCR and sequencing, as well as Western blot and Coomassie staining on a native agarose gel for TBSV.p.Lip NPs quantification.

For RT-PCR, total RNA is extracted using protocols provided by the manufacturer of the TRIzol™ reagent (Invitrogen). Following RNA extraction, cDNA is synthesized, and PCR is carried out using primers TBSV_CP_For (TGCAACTGGTACGTTTGTCATATC) and TBSV_2_Back (AAGATCCAAGGACTCTGTGC). RNA extraction is the only part of the process that uses a small amount of hazardous chemicals, due to extraction with Trizol™ agent, such as chloroform and lithium chloride, but it is an essential step for quality control, and for which other commercially available extraction kits are under evaluation, to lower the environmental impact on production.

Western blot analysis is performed using a 1% agarose, 38 mM glycine gel run under native electrophoretic conditions. After addition of the 6X loading dye (for 10 ml: 6 ml glycerol 100%, 1 ml Tris-HCl 0.5 M pH 6.8 and 18 mg bromophenol blue) to the samples, they are loaded onto the agarose gel, and electrophorized at 100 V for 45 minutes. Following electrophoresis, proteins are transferred onto a nitrocellulose membrane and the presence of TBSV is detected using 1:3000 anti-TBSV primary antibody (TBSV-CO – Prime Diagnostic) and horseradish peroxidase-conjugated anti-rabbit polyclonal antibody diluted 1:3000 (Clinisciences). The signal development is obtained on washed membranes by enhanced chemiluminescence (Amersham Biosciences, Amersham, UK) and the images acquired through ChemiDoc Imaging System (Biorad). For Coomassie staining, the gel is run in the same conditions and then stained with 30 mL Quick Coomassie Stain (Clinisciences).

Downstream process

The downstream purification process begins with the collection of the infected leaves obtained from the tertiary cycle of infection. The biomass is first weighed to determine the leaf fresh weight and then homogenized accordingly with 3 volumes of extraction buffer (sodium acetate 50 mM pH 5.3, 1% ascorbic acid) (plant-to-buffer ratio, weight in mg to volume in ml) using a steel blender, then filtered using four layers of Miracloth®. After this step, the homogenate undergoes a sedimentation process overnight at 4°C, to help precipitate debris and plant components. The precipitate is then consolidated with a first super-centrifuge step at 8,000 g for 15 minutes at 4°C, after which the clarified supernatant is collected and undergoes an ultra-centrifugation round at 90,000 g for 1h, 4°C. Both centrifugation steps are performed with an Avanti JXN26 Centrifuge (Beckman Coulter). The pellet obtained after ultracentrifugation is resuspended in 0.7% physiological buffer solution (NaCl in Water for Injection), centrifuged once again at 8,000g for 15 minutes at 4°C and filter sterilized: this represents the final product, which then undergoes all quality control steps, as described below. At the end of both primary and secondary infection, the product undergoes RT-PCR, sequencing and a Western blot for confirmation, respectively, of RNA and coat protein identity. After the tertiary infection, the API is produced and the following controls are performed: SDS-PAGE, Western blot, DAS-ELISA for quantification, Dynamic Light Scattering (DLS), and an LAL test as described by the manufacturer to assess endotoxin content (Gen Script).

For SDS-PAGE analysis, TBSV.pLip NPs sample is supplemented with 0.5 volume of R buffer (for 10 ml: 3 ml of Tris-HCl 0.5 M pH 6.8, 2.4 ml glycerol 100%, 1.6 ml SDS 10%, 1 ml Bromophenol blue in TE, 300 µl EDTA 15 mM, 1.7 ml H_2O; 6.25% of 2-mercaptoethanol freshly added). After the addition of R buffer, samples are incubated at room temperature for 3 minutes and vortexed, then heated at 60°C for 1 minute, vortexed again, and kept on ice until electrophoresis performed with a SurePAGE™, Bis Tris, 12% gel (Genscript). TBSV.pLip NPs are then visualized using silver staining, following the manufacturer's instructions (Pierce™ Silver Stain Kit, Thermo Scientific).

The Western blot is performed as described in the upstream process using a 1% agarose, 38mM glycine gel run under native electrophoretic conditions.

DAS-ELISA is used to determine TBSV.pLip NPs concentration in solution. Briefly, 150 µl of sample diluted in diluent solution (0.2% BSA - PBS-Tween 0.05% pH 7.4) are distributed in ELISA Maxisorp plates (NUNC) previously coated with 150 µl of primary

antibody TBSV-Co (Prime Diagnostic) diluted 1:1000 in carbonate buffer (Na_2CO_3 1.59 g/L, $NaHCO_3$ 2.93 g/L pH 9.6). The presence and quantity of TBSV.pLip NPs is determined by adding 150 µl secondary alkaline phosphatase conjugated antibody TBSV-AP (Prime Diagnostic) diluted 1:1000 in diluent solution and 100 µl p-Nitrophenyl Phosphate (pNPP) substrate (Kementec). The reaction is stopped using 100 µl of 0.1 M NaOH. Plate is read using a Tecan Infinite 200 PRO plate reader at 405 nm. To quantify NPs, the ELISA test includes a calibration curve ranging from 30.02 to 0.06 nanograms of TBSV.pLip.

For DLS analysis, 0.4–0.5 mg/mL of TBSV NPs are analyzed three times using a Zetasizer instrument. Each measurement represents the mean of 12 repetitions.

Manufacturing facility

The facility described was designed for the production of a GMP-compliant biopharmaceutical, with manufacturing volumes suitable to support Phase 1 Clinical Studies and toxicological studies. In all laboratory rooms air is filtered using High Efficiency Particulate Air (HEPA) filters, to avoid any source of contamination. Following the laboratory rooms, an isolating door grants access to the production and downstream chamber areas. All areas of production are subject to pressurization, with the three main chambers (growth, infection and downstream chambers) presenting a higher pressure than the adjacent corridors, which in turn present a higher pressure than the outside laboratories. This allows for air to flow from production towards the outside environment, thus avoiding the entry of external contaminations. Prior to entering the infection and downstream chambers, the use of proper Personal Protective Equipment (PPE) and specific dressing is mandatory, as well as removal of PPE is necessary prior to exiting. Irrigation of the plants is performed manually and to achieve optimal plant growth, the LED system has been designed to comprise three light channels: red (660 nm), blue (450 nm) and white (prevalently in the region between 500 and 600 nm). All LED have a certified degree of protection IP65, and an efficiency of 3.15 µmoles/J. Each LED is 100 cm long and four of them are meant to fit a 200 cm x 60 cm shelf, arranged for plants growth, and four shelves compose a rack, for a total capacity of 1024 plants in both the growth room and the infection room.

Results

Process and facility design

In Diamante SB, *N. benthamiana* is used as a self-building, single-use, biodegradable bioreactor to produce a therapeutic nanomaterial named TBSV.pLip NPs. The company facility has

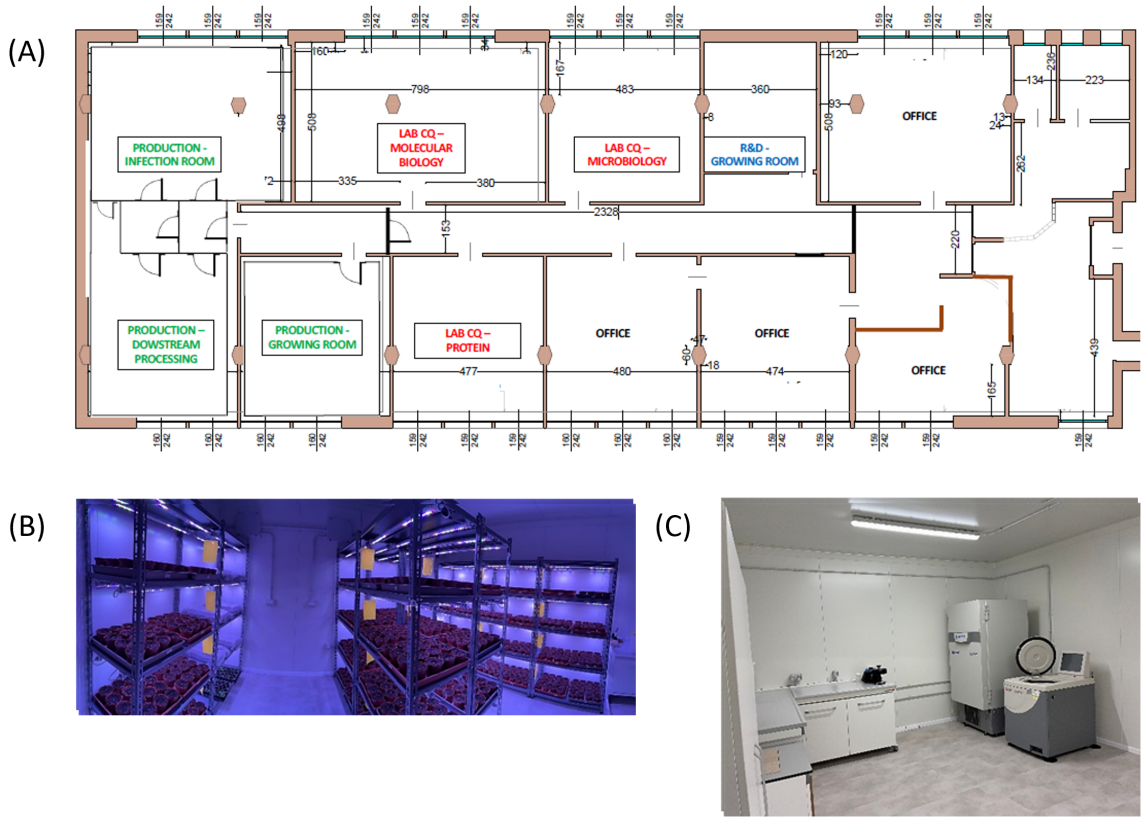

FIGURE 1
Overview of the facility. **(A)** Facility floor plan. **(B)** Production - growing room: together with the infection room, where the upstream process takes place. **(C)** Production – downstream processing dedicated room.

been carefully designed to accomplish this purpose, mindful of the active use of plant viruses in the production process. The equipment used for quality control and production is cGMP compliant. The laboratory rooms in the facility are equipped to perform all quality control analyses of the product. The current production process is controlled and monitored during working hours by working personnel. The high presence of manual operations during the production process, such as plant handling, plant-material extraction and centrifuge runs, at the moment do not allow for a more automated process, but remote monitoring is currently being implemented. Specific equipment like the -80°C freezer, used to stock material, and the general ventilation system are controlled remotely, allowing for tracking and fast intervention at any time.

An overview of the facility is shown in Figure 1.

Manufacturing of TBSV.pLip nanoparticles

TBSV.pLip NPs are produced using a process that can be summarized as described in Figure 2. The upstream process is divided into three subsequential sections, beginning with the primary infection, as described previously (Lico et al., 2021). Once symptomatic leaves are harvested, they are extracted to produce sap as starting material for a secondary infection. The same process is repeated with leaves collected from this second step, to continue with a tertiary infection, after which leaves are harvested and directly processed in the downstream phase. This last phase ends with collection of TBSV.pLip NPs. DAS-ELISA assay is used to correctly quantify the API. It has been estimated that the average total production yield for one batch of plants is 71 mg/kg. This was calculated in relation to the plants used for all the production phases, as summarized in Table 1.

TABLE 1 Starting material and process yields from the four phases described.

Phase	Starting material	Nr of plants infected	Yield
1	4 ug of RNA	1	1.4 g LFW
2	860 mg of SAP	107	150 g LFW
3	8.2 g of SAP	1024	1.4 kg LFW
4	1.4 Kg LFW	–	99.4 mg TBSV ± 22%

LFW. leaf fresh weight.

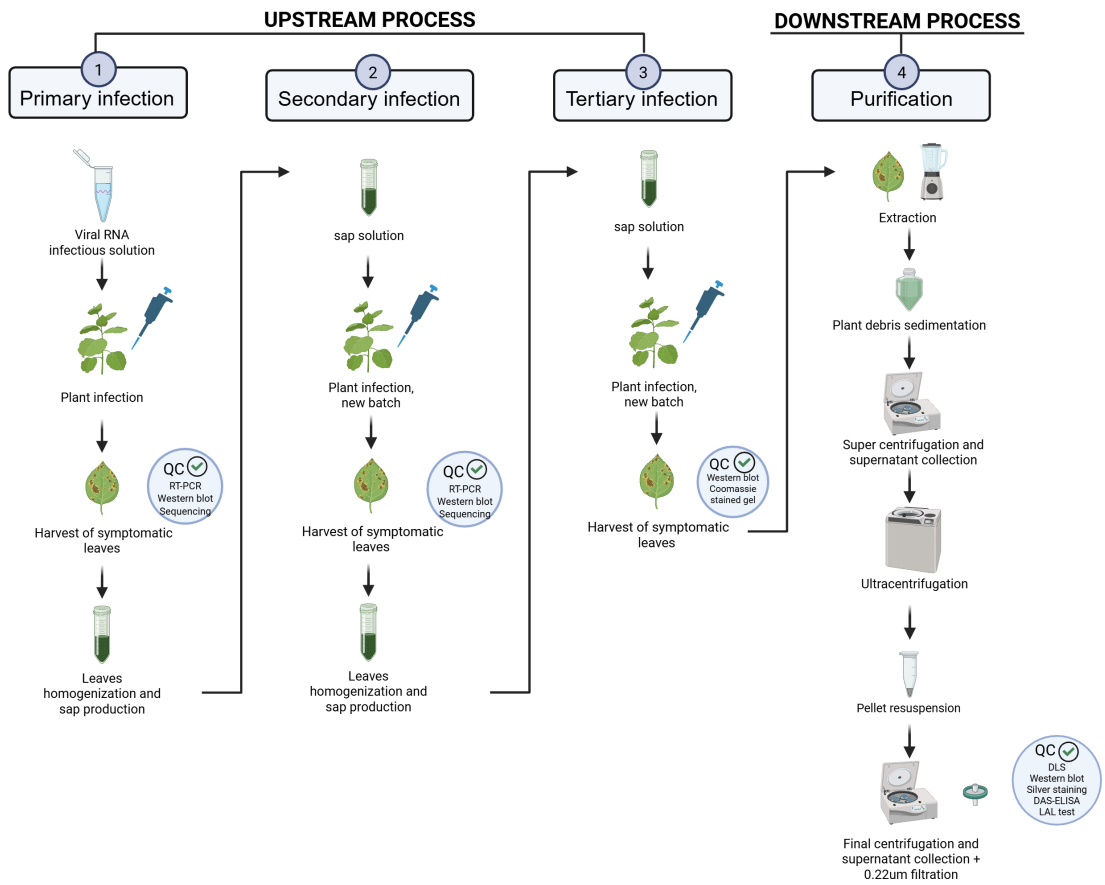

FIGURE 2
Process overview. The initial phase of the process, referred to as the upstream stage, is subdivided into three successive infection steps: primary, secondary, and tertiary. Following the tertiary infection, the product undergoes purification through the downstream processing phase.

For each stage of the process *N. benthamiana* leaves are collected only when symptomatic. Typical symptoms of virus presence in a plant include curling of the leaves and chlorosis (Figure 3). It is only these leaves that are processed to obtain the final product.

During each step of the process, the necessary quality controls are performed to ensure NPs integrity: RT-PCR, Western blot, Coomassie stained agarose gels and sequencing are part of the upstream phase, whereas in the downstream phase, the controls comprise SDS-PAGE, Western blot, DAS-ELISA, DLS and LAL Test (Figure 4; Table 2).

Economic analysis of TBSV production costs

The production system in the current facility allows for the annual cultivation and processing of 13 full batches, each comprising of 1,024 plants: each batch is housed in vertically stacked racks under high-efficiency LED lights, and it grows over the course of 6 days and yields a total of 1.4 kilograms (LFW) of biomass. Due to the capacity of the available ultracentrifuge, which is the primary bottleneck in downstream processing, a maximum of 256 plants can be processed per day. As a result, each full batch is processed over four consecutive days, in sub-batches of 256 plants per day. The processing of a single sub-batch yields approximately 24.9 mg of TBSV.pLip NPs. Therefore, the total yield per full batch is 99.6 mg of TBSV.pLip NPs. Given the production of 13 batches per year, the estimated annual yield is approximately 1.3 grams of TBSV.pLip NPs. To obtain 1 gram of TBSV.pLip TBSV NPs, 10 full batches are required. The API is manufactured in *N. benthamiana* using TBSV genome as a vector of expression and exploiting the TBSV Coat Protein for the display of the peptide Liprin (pLip) on the external surface of the capsid.

A comprehensive economic analysis was conducted to assess the operational expenditure (OPEX) associated with the production of 1 gram of TBSV and it is reported in Table 3 with the corresponding graphical illustration in Figure 5. This analysis is based on current small-scale batch production data and includes both direct and indirect costs, while capital expenditures (CAPEX) such as facility depreciation, equipment amortization, and long-term investments are excluded from the present assessment.

FIGURE 3
Plant infection. Example of symptomatic *N. benthamiana* plants infected with TBSV.

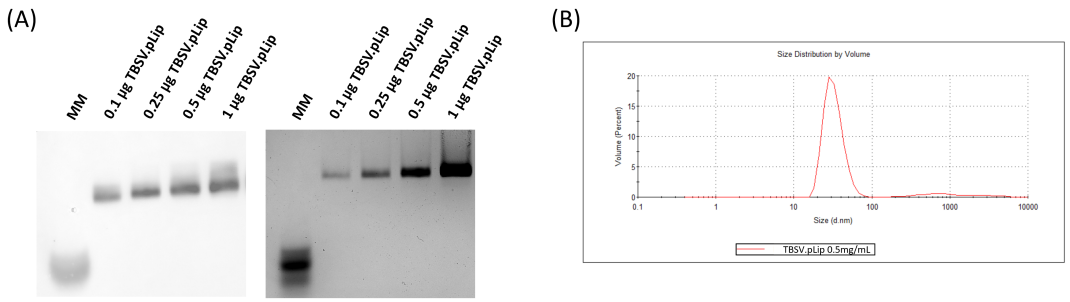

FIGURE 4
Analyticals overview. **(A)** 1% agarose gel transferred to a nitrocellulose membrane and blotted against an anti-TBSV antibody and 1% agarose gel stained with Coomassie Quick Stain show a calibration curve with increasing quantities of TBSV.pLip; **(B)** DLS profile of TBSV.pLip sample concentration 0.5 mg/mL, indicating distribution by volume: the peak indicates that most of the population is in the range of 30 nm, which is the molecular size of the virus. This graph shows the mean value obtained from three separate measurements on the same sample, each of which is the mean of 12 measurements. The standard deviation of the three measurements is 0.65.

10.3389/fpls.2025.1724810

TABLE 2 Quality control of the API.

Phase	Analysis	Purpose	Acceptance criteria
Upstream	RT-PCR	Amplification of the viral genome from plant extracts	Primer-specific band
	Sequencing	Peptide conformity check	<3 silent mutations
	Western blot	VNP assembly check and identification	Positive identification
	Native gel-coomassie staining	Quantification of VNPs	TBD
Downstream	DLS	VNP size and poly-dispersity index	Size 30 ± 5nm PDI: <0.3
	Western blot	VNP assembly check and identification	Positive identification
	SDS-PAGE Silver staining	Purity of the preparation	> 99%
	qDAS-ELISA	Quantification of the virus	> 0.5mg/mL
	LAL test	Quantification of endotoxin levels	< 1EU/mL

TABLE 3 Breakdown of the process cost per category, including direct and indirect costs. All cost values reported here reflect the aggregate expenses incurred to produce 1 gram of TBSV, inclusive of upstream (US) and downstream (DS) operations, as well as quality control (QC) and managerial oversight.

Component	Percentage	Component	Percentage
Direct costs			
Raw Materials & Consumables	1%	Materials & Consumables	5%
QC Materials & Consumables	4%		
Production Labor Cost	14%	Labor Cost	40%
Production Manager Cost	11%		
QC Labor Cost	6%		
QC Manager Cost	9%		
Indirect costs			
Electricity	5%	Utilities	8%
Water	1%		
Heating	2%		
Rent	40%	Facility-Related Costs	47%
Building Maintenance	3%		
Cleaning Services	5%		
Total	100%	Total	100%

The results highlight that labor-related costs constitute the most significant portion of the annual operational direct cost, representing 40% of total OPEX. This includes both production labor (€ 10991.63 - 14%), QC labor (€ 5054.14 - 6%), and their respective managerial roles (€ 8462.52 - 11% for production management, € 6891.95 - 9% for QC management). These findings reflect the labor-intensive nature of the process, especially under small-scale conditions requiring high oversight and manual handling. Facility-related expenses emerged as the second major cost component, contributing € 37100.00, corresponding to 47% of total OPEX. The largest element within this category is facility rent, which alone accounts for € 31500.00 corresponding to 40%, followed by cleaning services (3600.00 € - 5%) and building maintenance (€ 2000.00 - 3%). These are fixed costs that remain constant regardless of output volume, thereby exerting a strong influence on cost per unit at limited production scales. Utilities, including electricity (€ 3938.34 - 5%), water (€ 501.38 - 1%), and heating (€ 1969.17 - 2%), together contribute 8% (€ 6408.89) of total OPEX. These costs are primarily associated with machinery operation and climate control, particularly during downstream processing steps. In contrast, materials and consumables represent only € 4276,48 corresponding to 5% of the total OPEX. This includes raw materials (€ 994.89 - 1%) and quality control reagents and consumables (€ 3281.59 - 4%). Despite being essential to the production process, these inputs have minimal economic impact compared to labor and infrastructure costs.

Upstream *vs*. downstream cost distribution

In the upstream phase, including cultivation, infiltration, and incubation, the dominant costs are labor-related. Production labor and its associated management constitute a combined 22.6% of the total OPEX, while QC labor and materials used during in-process checks contribute an additional approximately 2%. The use of raw materials in upstream operations accounts for a modest 1% of the total operational budget. In the downstream phase, comprising tissue harvesting, clarification, ultracentrifugation, and product release testing, labor remains the primary cost driver. QC labor and QC management represent a combined 12%, reflecting the intensive resource demands of analytical validation and batch release procedures. Production labor associated with downstream extraction amounts to less than 1%, while QC materials and consumables contribute to 3%. The cost of raw materials used in this phase is negligible (<1%).

Spatial productivity and vertical farming integration in plant-based TBSV production

An essential parameter for evaluating the scalability of plant-based production platforms is spatial productivity, commonly expressed as yield per unit area. In the current system, the TBSV.pLip NPs yield has been estimated at 6.2 mg per square meter of cultivation area per batch. Assuming 12 months of active

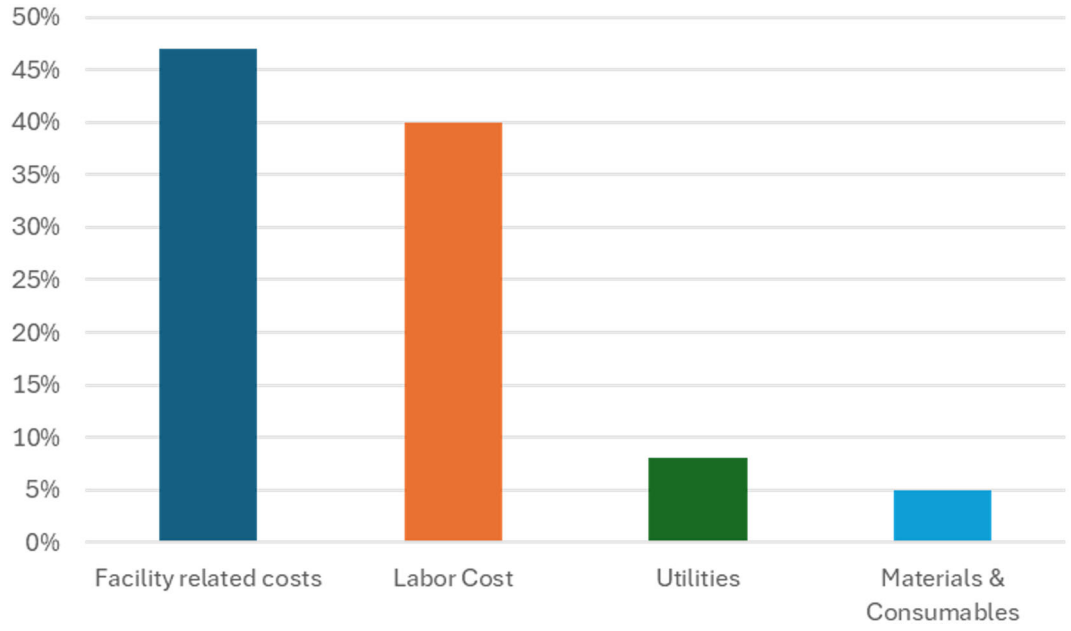

FIGURE 5
Breakdown of the percentage contribution of each cost category to the total production cost.

production per year, this corresponds to an annual yield of approximately 80.6 mg per square meter per year. Assuming an annual therapeutic dose of 2 mg of TBSV.pLip per patient (a dosage that remains to be validated for clinical studies based on the delivery of 4 injections of 500µg of TBSV.pLip per patient), this production rate allows one square meter of cultivation space to support treatment for approximately 40 patients per year. To meet a therapeutic demand of 5,000 patients per year, an estimated 125 square meters of cultivation area would be required. This requirement increases proportionally with treatment demand, reaching 1,250 square meters and 25,000 square meters for 50,000 and 1,000,000 patients, respectively (Table 4). To optimize land use efficiency and reduce the physical footprint of the production facility, a vertical farming system should be adopted (Figure 6). By incorporating five levels of vertically stacked shelving, the required floor area is effectively reduced by a factor of five. Accordingly, the floor area needed to treat 5,000, 50,000, and 1,000,000 patients per year is reduced to 25 m^2, 250 m^2, and 5,000 m^2, respectively (Table 4).

TABLE 4 scalability of TBSV.pLip NPs production by using vertical farming.

Target patients/year	Required floor area	Floor area - vertical farming (5 levels)
5,000	125 m^2	25 m^2
50,000	1,250 m^2	250 m^2
1,000,000	25,000 m^2	5,000 m^2

Materials hazardness and environmental impact

The workflow described includes the use of a limited number of hazardous chemicals, such as Trizol®, chloroform, hydrochloric acid, and lithium chloride. Importantly, these substances are utilized in minute quantities—typically in microliters per batch—and their contribution to the overall environmental footprint is negligible. Strict adherence to laboratory safety and waste management protocols further mitigates their risk.

One potential concern unique to our system is the use of TBSV as a vector. While TBSV is a plant-specific virus with no known risk to humans or animals, its presence in biomass waste could raise biosafety considerations, particularly in open-field or large-scale settings. We recognize this challenge and are currently investigating strategies to inactivate the virus post-harvest, ensuring that the final biomass is free of viable viral particles before disposal or downstream use. In summary, the combination of (i) low-volume reagent usage, (ii) elimination of persistent organic solvents, (iii) the biodegradable nature of plant material, and (iv) ongoing viral inactivation efforts, reinforces the environmental advantages of our production method.

Discussion

Despite the recent closure of Medicago following the withdrawal of investment by its parent company, the global landscape of plant-based biotechnology companies remains dynamic. Notable examples include Protalix Therapeutics (Israel),

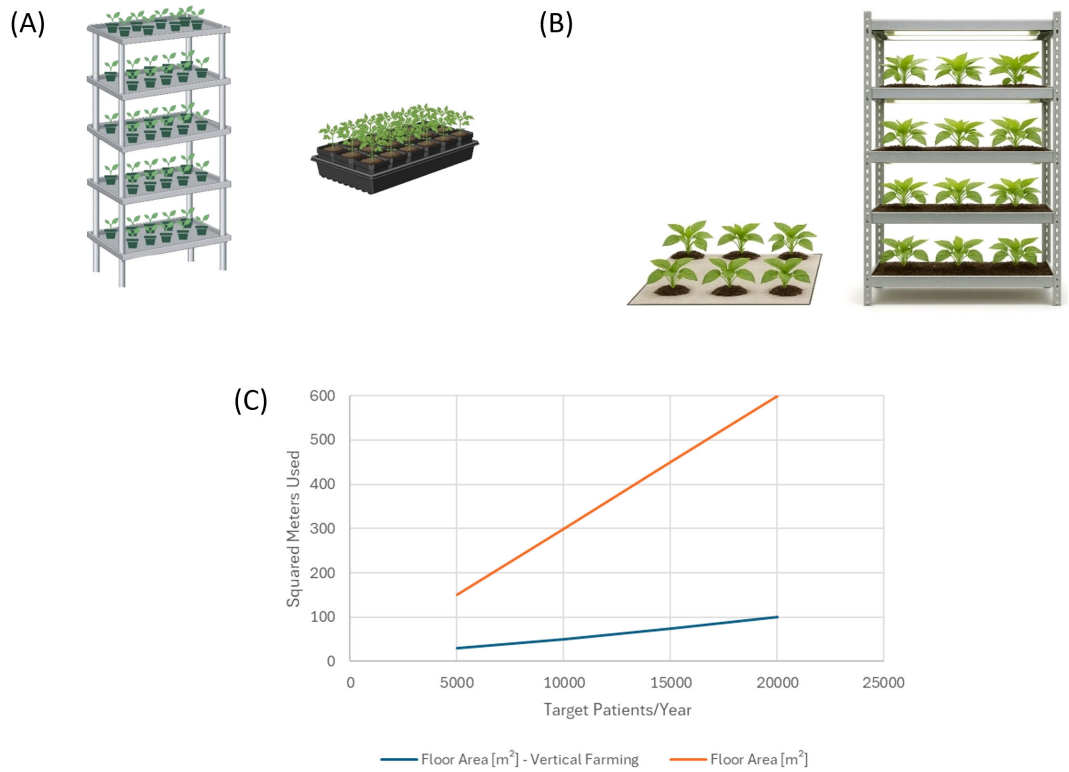

FIGURE 6
(A, B) The advantage of vertical farming versus traditional plant cultivation. The use of shelves allows to take advantage of the entire room area, extending cultivation in vertical layers and optimizing the space **(C)**.

with two marketed products—Elelyso® and Elfabrio®; BioApp (South Korea), developer of the HERBAVAC™ pig vaccine; KBio (USA), focused on various recombinant proteins; Eleva (Germany), advancing a moss-derived therapeutic for Fabry disease; InVitria (USA), producing technical-grade proteins; ORF Genetics (Iceland), supplying growth factors and cytokines for cosmetics and research; Agrenvec (Spain) and Baiya Phytopharm (Thailand), both targeting applications in cultivated meat and cosmetics; and CapeBio (South Africa), developing medical diagnostic solutions.

In this vibrant and dynamic scenario, Diamante SB, founded in 2016 as a spin-off of the University of Verona with support from European public funding programs such as Bio-based innovation for sustainable goods and services with the project PharmaFactory and the EIC accelerator, has successfully transitioned from an academic setting to an industrial reality. The company is focusing on the development of a platform for autoimmune disease treatment with the first therapeutic application in Rheumatoid Arthritis. Here we report a basic techno-economic analysis from laboratory data collected in the first year of work in the new lab-setting meant to obtain GMP certification disclosing the production process of the therapeutic TBSV.pLip NPs meant for Rheumatoid Arthritis treatment.

Plant-based biomanufacturing of therapeutic viral proteins represents a relatively novel platform with few commercial-scale facilities currently in operation. However, it provides several advantages, including linear production scalability, simplified upstream processes, shorter time to market, and the potential for reduced capital and operational expenditures.

The facility described here annually produces 1.3 g of TBSV.pLip NPs, the API, from 18.2 kg LFW *N. benthamiana* leaves. The plant, selected for its productivity and host of TBSV infection, is inherently more sustainable than traditional production platforms, largely due to its biodegradable nature and its low-impact cultivation requirements. In general, plants serve as renewable, carbon-sequestering bioreactors, and their post-harvest waste can often be composted or disposed of with minimal environmental burden (Buyel, 2019).

Furthermore, *N. benthamiana* is familiar to European Medical Agency (EMA) and Food and Drug Administration (FDA) thus facilitating its acceptance in regulation-compliant manufacturing (Streatfield and Howard, 2003; McCormick et al., 2008; Bendandi et al., 2010; Tusé, 2011; Plant Viral Vectors for Delivery by Agrobacterium, 2013).

13 batches are seeded and grown annually, with one batch reaching harvest every 28 days. Expression rate of 355 mg of TBSV.pLip NPs per kilogram of biomass (fresh weight) and a downstream recovery of 20% give a yield of 71 mg of TBSV.pLip NPs per kilogram of harvested biomass. This corresponds to 6.2 mg of TBSV.pLip NPs per square meter of cultivation area per batch, the combination of this approach with spatial modularity offered by

vertical farming solutions offers a clear advantage for scalable models, enabling increased productivity per unit footprint and facilitating expansion without the need for large horizontal land allocations. When combined with the inherent flexibility of plant-based systems, vertical farming provides a strategically efficient pathway for transitioning toward larger-scale, economically sustainable production of biopharmaceuticals such as TBSV.pLip NPs.

The economic feasibility of TBSV production at small scale was conducted by analyzing direct operating expenditures (OPEX), which include labor, materials, and utilities in both upstream and downstream processes. Capital expenditures (CAPEX) were excluded to focus on recurrent, process-dependent costs. As detailed in the Results section, labor and facility-related costs dominated the cost structure, accounting for 40% and 47% of total OPEX, respectively, while materials and consumables contributed only 5%.

Based on the annual yield of approximately 1.3 grams, the direct OPEX per mg of TBSV.pLip was estimated at €27.61. This cost reflects the fixed-intensive nature of the process and highlights the potential for improvement through economies of scale. Increasing batch numbers or optimizing facility use would reduce per-unit costs significantly.

Moreover, the labor-heavy profile suggests that selective automation, especially in routine handling and monitoring, could reduce manual workload, improve consistency, and support future scale-up.

However, it is important to highlight that a critical point in the described production of TBSV.pLip NPs is the potential environmental risk associated with the particles, which are currently treated as infectious material. This classification significantly impacts disposal costs and logistics. At present, viral inactivation strategies are being evaluated, which will require confirmation through preclinical studies to ensure therapeutic efficacy. Previous work in oncology (Mao et al., 2021) has shown that when using virus nanoparticles genetic material inactivation can negatively affect therapeutic performance, making this validation step essential.

Together, these strategies represent key opportunities to enhance the economic sustainability of TBSV-based production, a platform that may be explored for diverse tolerance induction applications simply changing the peptide displayed by virus nanoparticles.

Finally, it is important to note that in addition to the conventional cost of goods, Life Cycle Assessment accounting for the costs of the environmental footprint of manufacturing should be addressed, even in the field of biopharmaceuticals.

When comparing our process with standard methods used for the chemical synthesis of peptides, the core therapeutic agent, the footprint of the plant-based upstream process is negligible when compared to the volumes of organic solvents used in traditional solid-phase peptide synthesis (SPPS). In contrast, SPPS is well-documented for its environmental burden, primarily due to its reliance on toxic, non-biodegradable solvents (e.g., dimethylformamide, dichloromethane) and repetitive washing steps, which generate significant chemical waste. The cumulative impact of these solvents not only raises health and safety concerns but also requires energy-intensive waste treatment and solvent recovery systems.

This approach represents a meaningful step toward greener, safer, and more scalable biomanufacturing when compared with traditional peptide synthesis platforms and it could be used as a platform for the production of nanomaterials meant for tolerance induction in the framework of autoimmune diseases.

Conclusion

This study demonstrates the potential of a plant-based platform for nanoparticle production, with a disruptive impact on therapies for autoimmune diseases. Although the described facility and processes still require optimization in certain areas, they can be implemented within a compact space and, with a relatively modest investment, to effectively support Phase I clinical trials.

Data availability statement

The raw data supporting the conclusions of this article will be made available by the authors, without undue reservation.

Author contributions

DP: Writing – review & editing, Investigation, Software, Methodology, Writing – original draft, Formal analysis. ARo: Validation, Methodology, Writing – review & editing. AE: Data curation, Formal analysis, Writing – review & editing. EG: Writing – review & editing, Formal analysis, Methodology. RZ: Data curation, Validation, Writing – review & editing, Supervision. ARa: Writing – review & editing, Formal analysis, Investigation. VG: Resources, Funding acquisition, Writing – review & editing. LA: Funding acquisition, Writing – original draft, Conceptualization, Writing – review & editing, Resources, Project administration, Supervision.

Funding

The author(s) declared financial support was received for this work and/or its publication. This work has been co-funded by the EIC 2024 Accelerator program, specifically through the “Diamante” project under grant agreement number 101189019. Authors acknowledge CPT (Centro Piattaforme Tecnologiche) of the University of Verona for the access and support to the DLS equipment. Part of the work has been supported by ‘Finanziamento dell’Unione Europea-Next Generation EU, Missione 4, Componente 1 CUP B53D23024740001’.

Conflict of interest

LA, VG and RZ were founders of Dimante SB srl. AR, EG, VG, RZ and AME were employees of Diamante SB srl. The process here described has been patented in U.S. as Provisional Application Serial No. 63/898,154.

The remaining author(s) declared that this work was conducted in the absence of any commercial or financial relationships that could be construed as a potential conflict of interest.

Generative AI statement

The author(s) declare that Generative AI was not used in the creation of this manuscript.

Any alternative text (alt text) provided alongside figures in this article has been generated by Frontiers with the support of artificial intelligence and reasonable efforts have been made to ensure accuracy, including review by the authors wherever possible. If you identify any issues, please contact us.

Publisher's note

References

Bally, J., Jung, H., Mortimer, C., Naim, F., Philips, J. G., Hellens, R., et al. (2018). The rise and rise of *nicotiana benthamiana* : A plant for all reasons. *Annu. Rev. Phytopathol.* 56, 405–426. doi: 10.1146/annurev-phyto-080417-050141

Bendandi, M., Marillonnet, S., Kandzia, R., Thieme, F., Nickstadt, A., Herz, S., et al. (2010). Rapid, high-yield production in plants of individualized idiotype vaccines for non-Hodgkin's lymphoma. *Ann. Oncol.* 21, 2420–2427. doi: 10.1093/annonc/mdq256

Blandino, M., Marinaccio, F., Ingegno, B. L., Pansa, M. G., Vaccino, P., Tavella, L., et al. (2015). Evaluation of common and durum wheat rheological quality through Mixolab® analysis after field damage by cereal bugs. *Field Crops Res.* 179, 95–102. doi: 10.1016/j.fcr.2015.04.014

Buyel, J. F. (2019). Plant molecular farming – integration and exploitation of side streams to achieve sustainable biomanufacturing. *Front. Plant Sci.* 9. doi: 10.3389/fpls.2018.01893

Chung, Y. H., Cai, H., and Steinmetz, N. F. (2020). Viral nanoparticles for drug delivery, imaging, immunotherapy, and theranostic applications. *Adv. Drug Deliv. Rev.* 156, 214–235. doi: 10.1016/j.addr.2020.06.024

Grasso, S., Lico, C., Imperatori, F., and Santi, L. (2013). A plant derived multifunctional tool for nanobiotechnology based on Tomato bushy stunt virus. *Transgenic Res.* 22, 519–535. doi: 10.1007/s11248-012-9663-6

Kusumoputro, S., Au, C., Lam, K. H., Park, N., Hyun, A., Kusumoputro, E., et al. (2023). Liver-targeting nanoplatforms for the induction of immune tolerance. *Nanomaterials* 14, 67. doi: 10.3390/nano14010067

Lico, C., Giardullo, P., Mancuso, M., Benvenuto, E., Santi, L., and Baschieri, S. (2016). A biodistribution study of two differently shaped plant virus nanoparticles reveals new peculiar traits. *Colloids Surf. B Biointerfaces* 148, 431–439. doi: 10.1016/j.colsurfb.2016.09.019

Lico, C., Tanno, B., Marchetti, L., Novelli, F., Giardullo, P., Arcangeli, C., et al. (2021). Tomato bushy stunt virus nanoparticles as a platform for drug delivery to shh-dependent medulloblastoma. *Int. J. Mol. Sci.* 22, 10523. doi: 10.3390/ijms221910523

Mao, C., Beiss, V., Fields, J., Steinmetz, N. F., and Fiering, S. (2021). Cowpea mosaic virus stimulates antitumor immunity through recognition by multiple MYD88-dependent toll-like receptors. *Biomaterials* 275, 120914. doi: 10.1016/j.biomaterials.2021.120914

McCormick, A. J., Cramer, M. D., and Watt, D. A. (2008). Changes in photosynthetic rates and gene expression of leaves during a source–sink perturbation in sugarcane. *Ann. Bot.* 101, 89–102. doi: 10.1093/aob/mcm258

Nikitin, N. A., Trifonova, E. A., Karpova, O. V., and Atabekov, J. G. (2016). Biosafety of plant viruses for human and animals. *Mosc. Univ. Biol. Sci. Bull.* 71, 128–134. doi: 10.3103/s0096392516030081

Plant Viral Vectors for Delivery by Agrobacterium (2013). *Current topics in microbiology and immunology* (Berlin, Heidelberg: Springer Berlin Heidelberg), 155–192. doi: 10.1007/82_2013_352

Pogue, G. P., Lindbo, J. A., Garger, S. J., and Fitzmaurice, W. P. (2002). M AKING AN A LLY FROM AN E NEMY : plant virology and the new agriculture. *Annu. Rev. Phytopathol.* 40, 45–74. doi: 10.1146/annurev.phyto.40.021102.150133

Pogue, J., Thabane, L., Devereaux, P., and Yusuf, S. (2010). Testing for heterogeneity among the components of a binary composite outcome in a clinical trial. *BMC Med. Res. Methodol.* 10. doi: 10.1186/1471-2288-10-49

Santoni, M., Zampieri, R., and Avesani, L. (2020). Plant virus nanoparticles for vaccine applications. *Curr. Protein Pept. Sci.* 21, 344–356. doi: 10.2174/1389203721666200212100255

Streatfield, S. J., and Howard, J. A. (2003). Plant-based vaccines. *Int. J. Parasitol.* 33, 479–493. doi: 10.1016/s0020-7519(03)00052-3

Tusé, D. (2011). Safety of plant-made pharmaceuticals: Product development and regulatory considerations based on case studies of two autologous human cancer vaccines. *Hum. Vaccin.* 7, 322–330. doi: 10.4161/hv.7.3.14213

Zampieri, R., Brozzetti, A., Pericolini, E., Bartoloni, E., Gabrielli, E., Roselletti, E., et al. (2020). Prevention and treatment of autoimmune diseases with plant virus nanoparticles. *Sci. Adv.* 6, eaaz0295. doi: 10.1126/sciadv.aaz0295

frontiers | Frontiers in Plant Science

TYPE Brief Research Report
PUBLISHED 02 January 2026
DOI 10.3389/fpls.2025.1721928

OPEN ACCESS

EDITED BY
Kevin Wang,
University of Pikeville, United States

REVIEWED BY
Eva Stoger,
University of Natural Resources and Life Sciences Vienna, Austria
Lilya Kopertekh,
Julius Kühn-Institut, Germany
Andrea Pompa,
University of Urbino Carlo Bo, Italy

*CORRESPONDENCE
Mauro Miguel Morgenfeld
mmorgenfeld@ingebi-conicet.gov.ar

†These authors have contributed equally to this work and share first authorship

RECEIVED 10 October 2025
REVISED 02 December 2025
ACCEPTED 05 December 2025
PUBLISHED 02 January 2026

CITATION
Vater CF, Pérez Sáez JM, Stupirski JC, Massaro M, Mirkin FG, Bravo-Almonacid FF, Rabinovich GA and Morgenfeld MM (2026) Production of functional human galectin-1 in transplastomic tobacco and simplified recovery via batch-mode purification. *Front. Plant Sci.* 16:1721928. doi: 10.3389/fpls.2025.1721928

Production of functional human galectin-1 in transplastomic tobacco and simplified recovery via batch-mode purification

Catalina Francisca Vater[1,2†], Juan Manuel Pérez Sáez[3†], Juan Carlos Stupirski[3], Mora Massaro[3], Federico Gabriel Mirkin[1], Fernando Félix Bravo-Almonacid[1,4], Gabriel Adrián Rabinovich[2,3,5] and Mauro Miguel Morgenfeld[1,2*]

[1]Laboratorio de Biotecnología Vegetal, Instituto de Investigaciones en Ingeniería Genética y Biología Molecular "Dr. Héctor N. Torres" (INGEBI-CONICET), Ciudad Autónoma de Buenos Aires, Argentina, [2]Facultad de Ciencias Exactas y Naturales, Universidad de Buenos Aires, Ciudad Autónoma de Buenos Aires, Argentina, [3]Laboratorio de Glicomedicina, Programa de Glicociencias, Instituto de Biología y Medicina Experimental (IBYME-CONICET), Ciudad Autónoma de Buenos Aires, Argentina, [4]Departamento de Ciencia y Tecnología, Universidad Nacional de Quilmes, Buenos Aires, Argentina, [5]Laboratory of Glycoimmunology, Caixa Research Institute, Barcelona, Spain

Plant molecular farming has established itself as a transformative technology for the cost-effective and sustainable production of biopharmaceuticals, offering scalable solutions to meet growing global demand. Among the different stable plant expression systems, plastid-based platforms are particularly attractive due to their high recombinant protein accumulation potential, genetic stability, and reduced risk of transgene escape. Human Galectin-1 (hGAL1) is a β-galactoside-binding lectin with potent immunomodulatory properties, positioning it as a promising therapeutic candidate for autoimmune and inflammatory diseases. Preserving its native conformation and carbohydrate-binding capacity is essential to keep its biological activity, and both properties may be compromised under suboptimal expression or purification conditions. Here, we demonstrate the relevance of chloroplast transformation in *Nicotiana tabacum* as a platform for producing functional hGAL1, which accumulated up to 5.67 mg per kg of leaf tissue, corresponding to ~0.05% of total soluble protein (TSP). Using a simplified batch-mode purification strategy, intact hGAL1 retaining carbohydrate-binding activity was obtained and functional properties as shown by its ability to induce T cell apoptosis in a dose-dependent manner. These results highlight the potential of a transplastomic tobacco platform to deliver biologically active human lectins with therapeutic relevance, while minimizing downstream processing complexity, supporting their use in cost-effective biopharmaceutical production.

KEYWORDS

batch mode purification, biopharmaceutical production, chloroplast transformation, human galectin-1, plant molecular farming, transplastomic tobacco

Introduction

Plant molecular farming (PMF) has emerged as a versatile and sustainable strategy for the production of high-value recombinant proteins. In some cases PMF offers certain advantages of scalability, reduced costs, and improved endotoxin-free biosafety compared to conventional microbial and mammalian cell systems (Burnett and Burnett, 2020; Buyel, 2019). At the moment there are many examples of human proteins expressed in plant cells that retain their activity indicating that folding occurs correctly as hIDO1, hFGF or hEGF (Bellucci et al., 2021; Wang et al., 2023; Müller et al., 2024). Moreover, this strategy has enabled the production of vaccines, therapeutic antibodies, and enzymes, some of which have functional folding reached clinical trials or market authorization (Schillberg and Finnern, 2021), including Elelyso® and Elfabrio® (Protalix Biotherapeutics) and Covifenz® (Medicago). Within PMF platforms, chloroplast transformation, also known as transplastomic plants, stands out as a robust expression system due to the exceptional levels of protein accumulation achievable in plastids (Bock, 2015; Maliga and Bock, 2011; Daniell et al., 2021).

The plastid genome is highly polyploid with thousands of genome copies per cell (Shaver et al., 2006), which enables massive accumulation of heterologous proteins when transgenes are integrated by homologous recombination. Moreover, chloroplast transformation bypasses the gene silencing effects typical of nuclear transformation and supports polycistronic transcription units resembling operons (Scotti et al., 2013; Barkan and Goldschmidt-Clermont, 2000). Additional advantages include stable maternal inheritance that limits transgene flow via pollen and genetic stability across generations (Lal et al., 2020). As a result, heterologous protein accumulation in plastids has reached levels exceeding 70% of total soluble protein (Oey et al., 2009; Castiglia et al., 2016). Our group and others have contributed to expanding this field by developing plastid-based expression of antigens, growth factors, and therapeutic proteins in *Nicotiana tabacum* (Morgenfeld et al., 2020; Müller et al., 2024). These achievements highlight the enormous potential of transplastomic plants as factories for biopharmaceuticals.

Nevertheless, several challenges still constrain the industrial application of plastid biotechnology. Expression levels vary widely depending on the protein of interest, and reliable predictive rules for accumulation efficiency are still lacking (Ahmad et al., 2016). Furthermore, plastids lack glycosylation and other complex post-translational modifications, which can limit the expression of proteins requiring them for functionality (Lehtimäki et al., 2015). In contrast, proteins that are soluble, stabilized by disulfide bonds and non-glycosylated represent excellent candidates for plastid expression. Finally, downstream processing is considered the major economic bottleneck, often accounting for up to 80% of total manufacturing costs (Buyel, 2015). Traditional chromatography steps are expensive, time-consuming, and prone to clogging due to plant secondary metabolites, stressing the need for simplified purification strategies compatible with large-scale deployment (Buyel, 2024).

Human Galectin-1 (hGAL1) is a prototype member of the galectin family. It forms homodimers composed of ~14.5 kDa subunits, each carrying a conserved carbohydrate recognition domain (CRD) that preferentially binds to N-acetyllactosamine motifs (Troncoso et al., 2023; Porciúncula-González et al., 2021). hGAL1 is expressed in multiple immune and stromal cell compartments, where it regulates apoptosis, angiogenesis, and immune tolerance (Perillo et al., 1995; Rabinovich et al., 1997; Rabinovich et al., 1999; Rabinovich, 2005). Extensive studies have established its therapeutic relevance, demonstrating anti-inflammatory and immunomodulatory effects in diverse models of chronic inflammation, autoimmunity, and neurodegeneration. In fact, this lectin reduces disease severity in murine models of rheumatoid arthritis, colitis, diabetes, uveitis, multiple sclerosis, and Sjögren disease, largely by promoting apoptosis of activated T cells and skewing immune responses toward Th2 and regulatory T (Treg) cell profiles (Rabinovich et al., 1999; Perone et al., 2006; Santucci et al., 2003; Toscano et al., 2006; Starossom et al., 2012; Toscano et al., 2018; Martínez Allo et al., 2020; Morosi et al., 2021; Sundblad et al., 2021; Rabinovich et al., 2025). Additionally, hGAL1 shows neuroprotective effects after cerebral ischemia and alleviates atopic dermatitis in mice, highlighting its potential as a versatile therapeutic agent (Qu et al., 2011; Corrêa et al., 2017). Interestingly, recent studies demonstrated the ability of GAL1 to reprogram myeloid cells toward an immunosuppressive phenotype (Blidner et al., 2025), suggesting the ability of this lectin to control both lymphoid and myeloid cell compartments in a myriad of pathologic conditions.

Recombinant Human Galectin-1 has been produced as research reagent in several conventional heterologous expression systems. Bacterial expression in *Escherichia coli* is the most widely used approach, enabling high-yield production of recombinant hGAL1 that is properly folded and biologically active after purification (Rabinovich et al., 1999; Toscano et al., 2006). Yeast platforms, including *Pichia pastoris*, have also been explored for lectin production and offer advantages in secretion and scalability, although the hyperglycosylating nature of yeast can be incompatible with proteins—such as hGAL1—that require precise disulfide bond formation but do not undergo N-glycosylation. Mammalian cell expression (e.g., CHO or HEK293) provides native folding and post-translational processing and has been used to obtain recombinant galectins with immunomodulatory activity, but these systems are substantially more expensive, require complex infrastructure, and typically yield lower amounts of purified protein. In this context, plant-based platforms—and particularly plastid transformation—represent an attractive complementary strategy, combining the ability to fold cysteine-rich proteins in an oxidizing environment with agricultural scalability and inherent endotoxin-free biosafety. From a biochemical perspective, hGAL1 is a soluble protein stabilized by three intrachain disulfide bonds and does not require glycosylation for folding or activity (Guardia et al., 2014). This makes it particularly well-suited for plastid expression, as the chloroplast stroma supports oxidative folding and disulfide bond formation (Wittenberg and Danon, 2008).

In this work, we evaluated the potential of *N. tabacum* chloroplasts as a platform for hGAL1 production. Transplastomic lines were generated and confirmed to be homoplasmic, accumulating hGAL1 predominantly in the soluble protein fraction. To address downstream challenges, we implemented a simplified batch-mode lactosyl-Sepharose affinity capture. Compared with an equivalent column-based affinity protocol using the same resin, the batch mode purification procedure simplified the purification workflow increasing protein recovery, avoiding resin clogging and demonstrating scalability to larger biomasses. The enriched hGal1 fraction obtained was suitable for downstream functional assays Plant-derived hGAL1 preserved its carbohydrate-binding activity and induced apoptosis in Jurkat T cells, confirming its biological properties. Although the pro-apoptotic potency is lower than observed for bacterially-produced hGAL1, the results demonstrate that chloroplasts can produce functional lectins of therapeutic relevance.

Altogether, our findings provide proof-of-concept for the stable expression and simplified purification of biologically active hGAL1 in tobacco plastids. This approach addresses two central challenges of molecular farming: the production of correctly folded human proteins and the development of cost-efficient purification methods. Future research should focus on enhancing expression yields, exploring stabilizing formulations, and refining purification strategies to fully exploit the potential of chloroplast biotechnology for the scalable production of human lectins and other therapeutic proteins.

Materials and methods

Chloroplast transformation vector

The human GAL1 coding sequence (NCBI #3956) was excised from pGem-hGAL1 and inserted into the plastid transformation vector pBSWUTR, previously developed in our laboratory (Wirth et al., 2006). Cloning was carried out using *NdeI* and *XbaI* restriction sites, and the construct was validated by Sanger sequencing. The expression cassette included the psbA promoter/5′UTR, the *aadA* selectable marker, and plastid recombination flanks corresponding to the rrn16 and trnI-trnA regions. The schematic representation of the pBSW5'UTRhGAL1 vector is shown in Figure 1A.

Tobacco plastid transformation and plant regeneration

Plastid transformation was performed in *N. tabacum* cv. Petite Havana by biolistic delivery using a PDS-1000/He device (Bio-Rad), following adapted protocols previously reported (Maliga, 2004). Expanded leaves were bombarded with gold particles (0.6 µm, 50 µg) coated with 10 µg plasmid DNA under 1,100 psi helium pressure. Spectinomycin-resistant shoots were selected on RMOP medium (Svab et al., 1990) containing 500 mg/L spectinomycin and subsequently transferred to MS medium (Murashige and Skoog, 1962) containing 500 mg/L spectinomycin for root development. To achieve homoplasmy, putative transformants underwent three cycles of regeneration under selection before transfer to soil. Transgene integration was initially screened in primary regenerants (T0) by PCR using primers CloroFw (5′-GTATCTGGGGAATAAGCATCGG-3′) and CloroRv (5′-CGATGACGCCAACTACCTCTG-3′), which yield a 1,450 bp product.

Plant cultivation

Seeds from the first progeny (T1) confirmed transplastomic lines were surface-sterilized (10% bleach or sodium hypochlorite vapor), germinated on MS medium supplemented with spectinomycin, and grown under a 16 h light/8 h dark photoperiod at 25°C. For greenhouse cultivation, plants were maintained at 20–25°C with a 16 h light cycle until 14–18 weeks of age, when leaves were harvested for analyses.

Molecular analyses (southern and northern blot)

Blot analyses were performed using the DIG system (Roche) following the manufacturer's instructions. Total DNA was isolated from T1 plants by the CTAB method (Allen et al., 2006) and digested with *NcoI* prior to electrophoresis and transfer to nylon membranes. 1 µg of digested DNA was loaded per lane. Hybridization with a DIG-labeled trnI/A probe was used to assess site-specific integration and homoplasmy. For transcript analysis, total RNA was purified from T1 plants with TRIzol (Invitrogen), separated on denaturing agarose gels (1 µg of total RNA per lane), and hybridized with DIG-labeled probes specific for *hGAL1* and *aadA*. Signals were visualized by chemiluminescence using CSPD as substrate.

Protein extraction and western blot analysis

For total protein extraction, 50 mg of leaf tissue of T1 plants were ground directly in 200 µl of 1X Laemmli buffer (Laemmli, 1970) and boiled at 99°C for 10 min. For solubility analysis, 0.2 g of leaf tissue of T1 plants was ground in liquid nitrogen and homogenized in 1 ml PBS (137 mM NaCl, 2.7 mM KCl, 10 mM Na2HPO4, 1.8 mM KH2PO4, pH 7.4) containing 4 mM β-mercaptoethanol to preserve thiol groups and prevent aggregation. Extracts were clarified by centrifugation (21,000 × g,

Abbreviations: hGAL1, Human galectin-1; hGAL1st, Recombinant human galectin 1 expressed in *E. coli* as standard reference; *hGAL1*, hGAL1 coding sequence; G1 A-C, transplastomic *N. tabacum* lines expressing hGAL1; NT, Non-transformed *N. tobacum* plants.

10.3389/fpls.2025.1721928

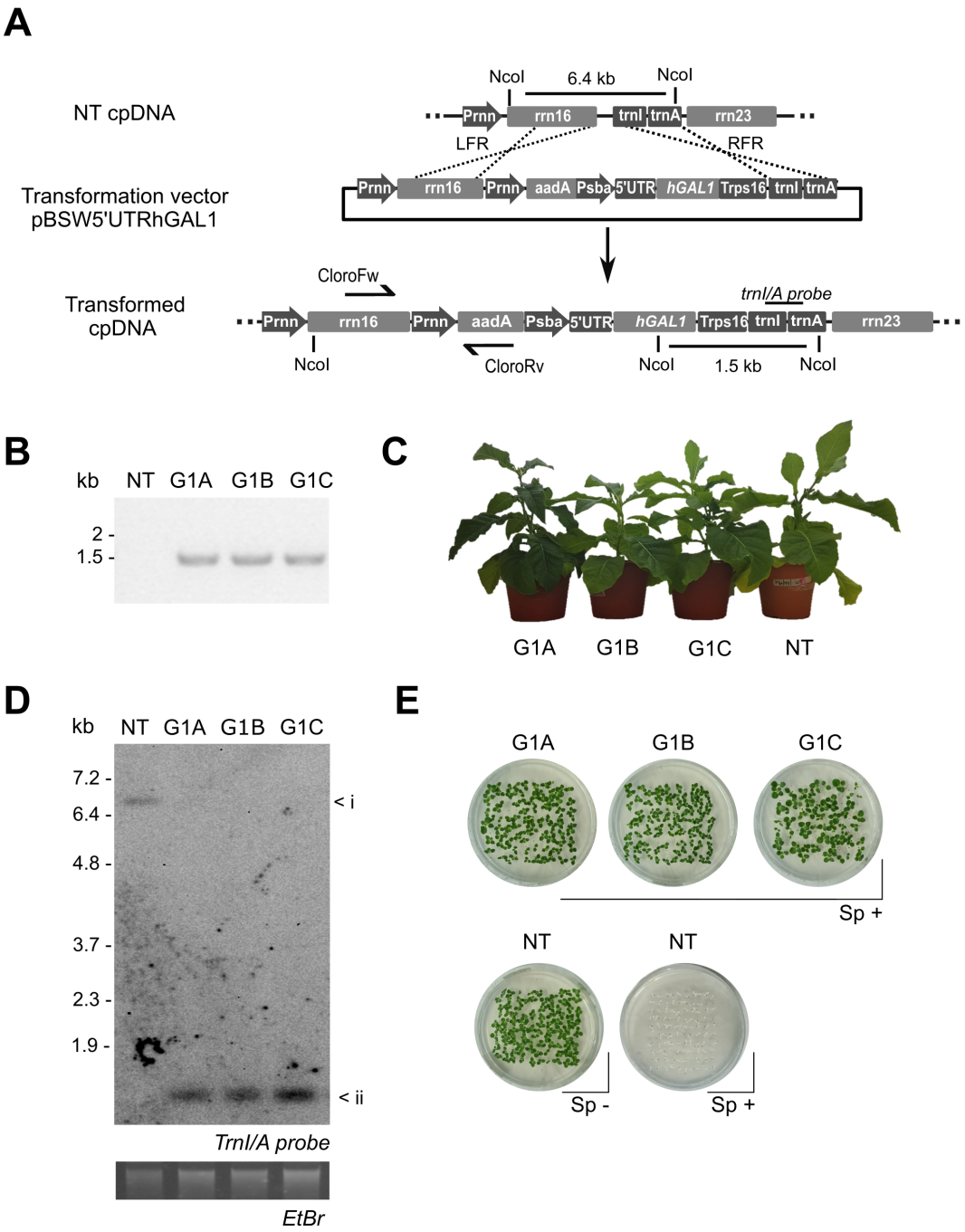

FIGURE 1
Generation and molecular characterization of transplastomic *Nicotiana tabacum* lines. **(A)** Schematic representation of the chloroplast transformation vector pBSW5'UTRhGAL1 (upper panel) and its targeted integration into the plastid genome (lower panel). The expression cassette comprises the *hGAL1* and the *aadA* selectable marker, flanked by homologous recombination sequences: the 3′ region of rrn16 (LFR) and the *trnI-trnA* intergenic region (RFR). Locations of PCR primers (CloroFw/Rv), *NcoI* restriction sites, and probe for Southern blot analysis are indicated. **(B)** PCR confirmation of transgene integration in primary regenerants (T0) corresponding to independent G1 A–C lines (expected amplicon size: 1.5 kb). **(C)** Phenotypic appearance of greenhouse-grown plants at 15 weeks post-germination. **(D)** Southern blot analysis of 1 µg NcoI-digested genomic DNA using a trnI–trnA probe. Expected fragment sizes: NT (6.5 kb), G1 A–C (1.5 kb). Ethidium bromide-stained gel is shown as a loading control. **(E)** Germination assay on selective medium. Upper panel: 100 T1 seeds from each transplastomic line (G1 A, G1 B, G1 C) germinated in MS with spectinomycin as selector agent (Sp^+, 500 mg/L). Lower panel: 100 NT seeds were germinated in MS medium with or without spectinomycin (Sp^-). Photo was taken after 7 days.

20 min, 4°C) and separated into soluble (supernatant) and insoluble (pellet) fractions. Two volumes of each fraction were mixed with one volume of 3X Laemmli buffer, heated at 99°C for 10 min. Proteins were separated on 15% polyacrylamide gels, stained with Coomassie Brilliant Blue, or transferred to nitrocellulose membranes, with transfer quality verified by Ponceau S staining. Membranes were blocked with 5% (w/v) non-fat dry milk in 1× TTBS (20 mM Tris-HCl, 150 mM NaCl, 0.1% Tween-20, pH 7.5) and incubated with a rabbit α -hGAL1 IgG (1:7000), followed by an alkaline phosphatase–conjugated secondary antibody (1:2000). Detection was performed in alkaline phosphatase buffer using BCIP/NBT as chromogenic substrates.

Protein quantification

Soluble protein extracts from T1 plants were obtained from 0.2 g of leaf tissue (fourth leaf from the top) in 1 mL PBS (pH 7.4) containing 4 mM β-mercaptoethanol, centrifuged twice (20,000 × g, 20 min). Total soluble protein (TSP) was determined by BCA assay, and ELISA plates were loaded based on TSP equivalence (1–7 µg TSP/mL for G1 and 14–28 µg TSP/mL for NT samples), using 1X PBS; 0,05% Tween-20; BSA 1% as diluyent and assay blank. Detection was performed as previously described in Croci et al., 2012, using rabbit α-hGAL1 IgG as capture antibody and biotinylated α-hGAL1 IgG followed by HRP–streptavidin/TMB for revelation. Purified recombinant *E. coli* hGAL1 0.5–9 ng/mL was used to generate the standard curve.

Purification of hGAL 1

Recombinant hGAL1 was purified from soluble protein extracts by lactose-Sepharose affinity capture, exploiting the carbohydrate recognition domain of galectins (Guardia et al., 2014). Preliminary column affinity purification was performed as described (Roldán-Montero et al., 2022). To avoid clogging commonly associated with plant extracts in column-based methods, purification was implemented in batch mode. Soluble fractions extracted from 240 mg of leaf tissue (600 ml) were incubated with 13 ml of lactose-Sepharose resin (Sigma Aldrich) for 1 h at 4°C under agitation. The resin was recovered by centrifugation, washed with 120 ml PBS containing 4 mM β-mercaptoethanol, and eluted with 200 mM lactose (60 ml). Eluates were sterile filtered (0.22 µm) and buffer-exchanged to 1X PBS pH 7,4 containing 4 mM β-mercaptoethanol (0.7-1.3 ml). Similar process was applied to protein extracts of non-transformed plants and to purificate hGal1 from *E. Coli* culture (300ml) after sonication. Fractions were evaluated by SDS-PAGE and Western blot.

Carbohydrate-binding activity

Glycan-binding activity of hGAL1 was assessed in solid-phase binding assays (Rapoport et al., 2010; Cagnoni et al., 2024). Microplates coated with asialofetuin (ASF) were incubated with purified hGAL1 (from batch mode) or hGal1st in the presence of serial dilutions of lactose (Sigma Aldrich) or N-acetyllactosamine (Elicityl). Bound protein was detected with a biotinylated α-hGAL1 antibody, streptavidin-HRP, and TMB/H_2O_2, with absorbance measured at 450 nm. Half maximal inhibitory concentration (IC_{50}) values were calculated (mean ± SD, n = 3).

Induction of T cell apoptosis

The immunoregulatory activity of plastid-derived hGAL1 was evaluated by its ability to induce T cell apoptosis of Briefly. Jurkat T cells were incubated with increasing concentrations of purified hGAL1 (from batch mode) or hGal1st in presence or absence of 20 mM lactose as a competitive inhibitor. As a negative control, an extract obtained from non-transformed plants and purified under identical conditions was included. After 6 h, early and late apoptosis was determined by Annexin V-FITC and propidium iodide staining followed by flow cytometry.

Statistical analysis

All analyses were performed in R using RStudio. Linear mixed-effects models were applied to ELISA data, and two-way ANOVA to apoptosis assays. Pairwise comparisons were conducted with the emmeans package using Tukey or Sidak adjustment; differences were considered significant at $p < 0.05$.

Results

Generation and molecular characterization of transplastomic lines

The hGAL1 coding sequence was sub cloned into the chloroplast transformation vector pBSWUTR previously developed in our laboratory (Wirth et al., 2006). The transgene was inserted downstream of the promoter and 5' untranslated region (5´UTR) of the *psbA* gene (Fernández-San Millán et al., 2003; Eibl et al., 1999). The vector pBSWUTR hGAL1 contains a selectable marker gene (*aadA)* that confers spectinomycin resistance to transplastomic shoots. This vector mediates site-specific integration of transgenes into the *rrn* operon of the plastome, in the intergenic region located between the ribosomal *16 s* and the *trnI* genes (Figure 1A). Biolistic transformation of tobacco leaves with the pBSWUTR hGAL1 plasmid yielded multiple spectinomycin-resistant shoots after 4–6 weeks of regeneration. Initial PCR screening confirmed transgene integration (Figure 1B). G1A, G1B and G1C positive plants were subjected to additional regeneration rounds in spectinomycin-containing medium to obtain homoplasmy. Plants from the third regeneration cycle were transferred to soil and grown to maturity. The phenotypic appearance of the transplastomic and non-

transformed plants was indistinguishable after 15 weeks of growth under greenhouse conditions (Figure 1C). No differences were observed when comparing growth rate, flowering time and germination rate between the transplastomic lines and non-transformed type plants.

Southern blot analysis was performed to confirm transgene integration and assess the homoplasmy in regenerated lines. Total leaf DNA was extracted, digested with *NcoI* restriction enzyme and separated by electrophoresis. Blot was hybridized with a probe specific for the trnI-trnA region. The expected 1.5 kb fragment size was detected in transformed lines confirming correct site-specific integration of the *hGAL1* cassette (Figure 1D). In contrast, NT plants exhibited the diagnostic 6.5 kb band. The absence of the 6.5 hybridization fragment in transplastomic lines indicated the elimination of residual non-transformed plastomes copies following successive regeneration cycles under antibiotic selection.

Homoplasmy was further analyzed by germination assay on MS medium supplemented with spectinomycin. All progeny from G1 lines displayed complete resistance, whereas NT seeds germinated only in the absence of the antibiotic (Figure 1E). These results confirmed stable integration of the transgene, reinforcing the conclusion that G1A, G1B, and G1C lines had achieved homoplasmy.

Analysis of transgene transcription

Transgene transcription in transplastomic lines was assessed by Northern blot. For this purpose, total RNA was extracted from leaves and subjected to electrophoretic separation. Three types of transcripts were observed after hybridization with the *human hGAL1* probe in the transplastomic lines but not in the NT plants. The revealed pattern included monocistronic transcripts corresponding to transgene sequence transcribed from the *psbA* promoter (present in the 5′*psbA* sequence), bicistronic transcripts transcribed from the *rrn* promoter (*Prrn*) included in the cassette, and a larger transcript generated by read-through transcription from the endogenous promoter of the *rrn* operon (Figure 2A). The identity of bicistronic and polycistronic transcripts was confirmed by hybridization with the *aadA* probe. The electrophoretic mobility for each transcript was consistent with the expected sizes of the three transplastomic lines analyzed confirming *hGAL1* transgene expression.

Recombinant hGAL1 accumulation in plants

Recombinant protein accumulation in transplastomic lines was verified by Western blot using a polyclonal antibody against hGAL1. Analysis of total protein extracts from leaf tissue revealed a band of the expected size (~14.5 kDa) in the three transplastomic lines (Figure 2B). The absence of additional bands of higher or lower molecular weight suggests that no detectable aggregation, proteolysis, or other post-translational modifications occurred in the recombinant hGAL1 expressed in chloroplasts. Furthermore, hGAL1 expression was analyzed in leaves at different developmental stages, revealing an increase in accumulation correlated with plant age (Supplementary Figure S1A). Mature leaves accumulated higher protein levels than younger leaves, and hGAL1 remained stable in senescent tissue. Interestingly, plants grown under dark conditions showed enhanced hGAL1 accumulation (Supplementary Figure S1B).

Western blot analysis revealed the expected band of ~14.5 kDa in the total protein sample and the soluble fraction but not in the insoluble fraction confirming that plastid-produced hGAL1 was fully soluble (Figure 2C). hGAL1 accumulation was quantified by ELISA.

Transplastomic lines produced soluble hGAL1 at average yield of 5.67 mg per kilogram of leaf tissue corresponding to approximately 0.05% of total soluble protein (TSP) (Supplementary Figure S2, Supplementary Table S1).

Batch-mode purification of hGAL1

Recombinant hGAL1 is commonly purified by α-lactose Sepharose affinity chromatography. To adapt this approach for plant extracts, we developed a simplified purification procedure that avoided resin clogging typically observed during column chromatography. This protocol was implemented in batch mode, to streamline the workflow and reduce downstream costs (Figure 3A).

Analysis of the elution fractions by SDS-PAGE followed by Coomassie Blue staining showed a clear enrichment of a protein band corresponding to the expected molecular mass of hGAL1 (~14.5 kDa). Traces of co-eluting proteins were only detectable when the loaded sample was concentrated more than 100-fold (Figure 3B). Western blot analysis confirmed that no signal was detected with the α-hGAL1 antibody in the percolate (P), indicating efficient retention of hGAL1 on the affinity matrix. No evidence of proteolysis or higher– or lower–molecular-weight species was observed in the elution fraction or in the final preparation.

The final preparation was sterile and directly suitable for downstream applications. When processing 240 g of leaf tissue, this procedure reached higher yields than those obtained using affinity columns, while reducing purification time (Supplementary Table S2). For the functional evaluation assays, the purification procedure was also carried out using extracts from non-transformed plants and from *E. coli* expressing hGAL1 (Supplementary Figure S3).

Biochemical validation: carbohydrate-binding activity of plastid-derived hGAL1

Carbohydrate-binding activity, a prerequisite for the biological function of hGAL1, was evaluated by solid-phase binding assays using asialofetuin (ASF)-coated microplates. Lactose and N-acetyllactosamine were tested as competitive inhibitors of

10.3389/fpls.2025.1721928

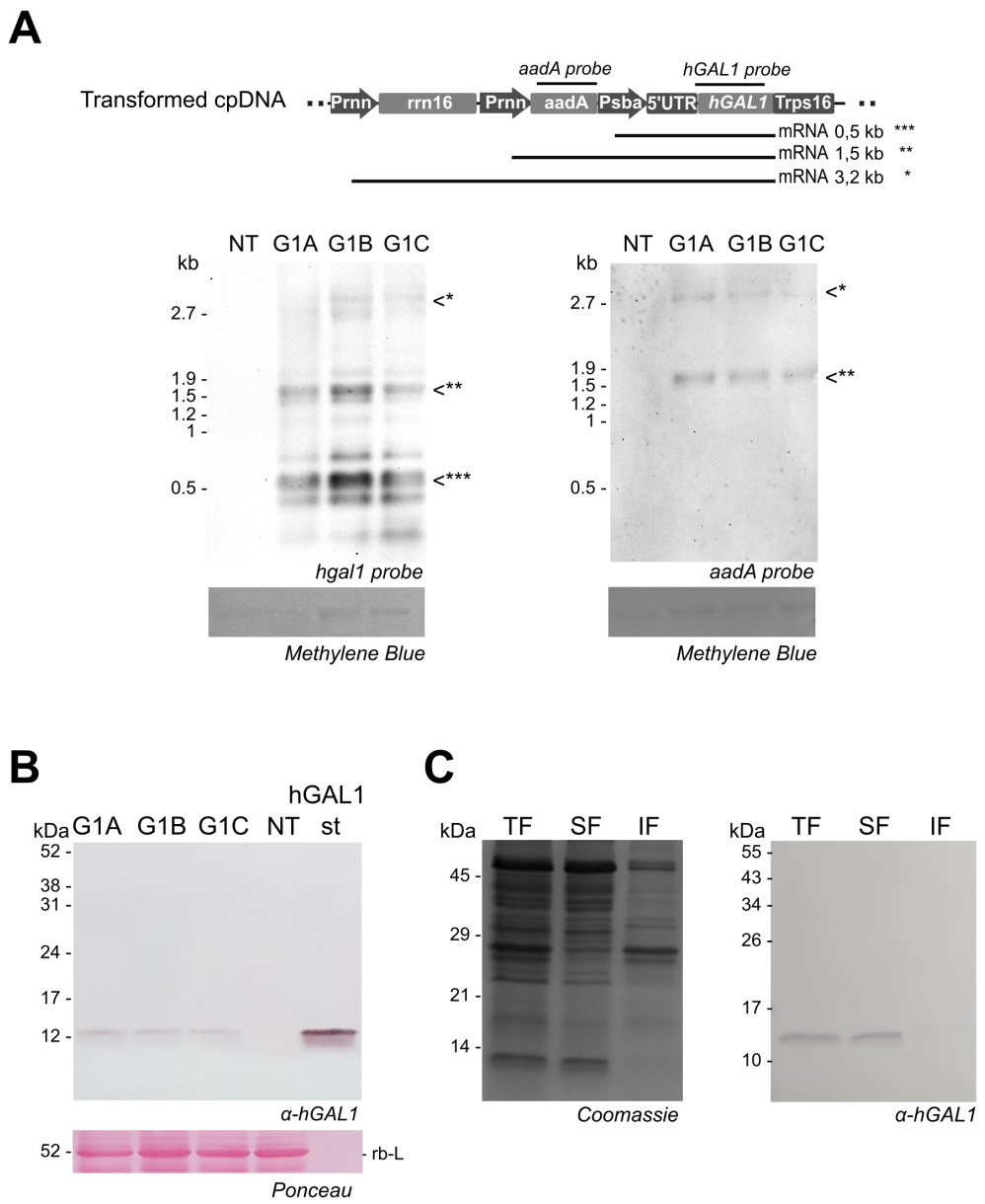

FIGURE 2
hGAL1 expression in transplastomic lines. **(A)** Northern blot of 1 µg total RNA from G1 A–C and NT plants, hybridized with *hGAL1* (left) and *aadA* (right) probes. Equal RNA loading was verified by methylene blue staining of the ribosomal RNA (rRNA) bands in the membrane. The upper panel shows a schematic representation of the probe locations and the expected mRNA transcripts, indicated as *, **, and *** in the blots. The position of 23S (2.9 kb) and 16S (1.5 kb) rRNA is indicated on the left. **(B)** Western blot analysis of total leaf protein from G1 A–C and NT plants (4.5 mg of leaf tissue) using α-hGAL1 antibodies. RuBisCO large subunit (rb-L) stained with Ponceau S serves as a loading control. hGAL1st: 200 ng of purified recombinant human galectin 1 expressed in *E. coli*. **(C)** Solubility profile of hGAL1 in G1 line (5 mg of leaf tissue) in PBS containing β-mercaptoethanol. The SDS-PAGE gel stained with Coomassie is shown on the left, and an equal Western blot detected with α-hGAL1 antibodies is shown on the right. TF, total fraction; SF, soluble fraction; IF, insoluble fraction.

interaction between hGAL1 and ASF, and IC_{50} values were calculated for each compound. The binding profile comparison between plastid hGAL1 and the recombinant hGAL1 from *E. coli* utilized as standard reference hGAL1st, showed no significant difference within both ligands (Figure 4A; Supplementary Table S3). These findings indicate preservation of the native carbohydrate recognition domain and confirm that chloroplast expression in chloroplasts does not compromise the lectin's ability to recognize specific glycans.

Functional validation: induction of apoptosis of Jurkat T cells

To assess the biological activity of the hGAL1 produced in tobacco chloroplasts, its immunomodulatory capacity was evaluated by analyzing apoptosis induction in Jurkat T cells. Cells were incubated with different concentrations of plastid hGAL1 or the standard hGAL1, in the presence or absence of lactose as a competitive inhibitor. Results revealed a dose-dependent induction

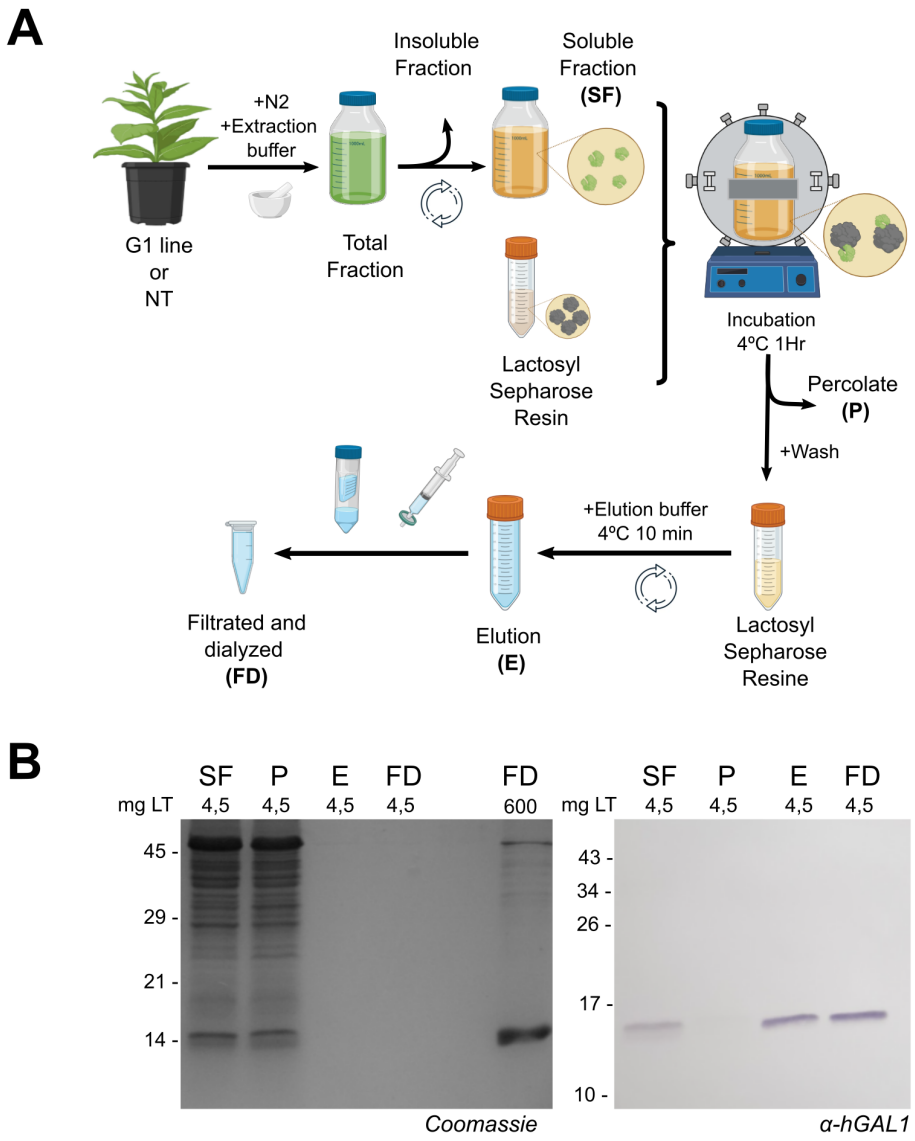

FIGURE 3
Batch purification. **(A)** Schematic representation of the purification workflow using Lactosyl Sepharose resin, including sequential precipitation and concentration steps. **(B)** Purification profile from 240 g of pooled leaf tissue from G1 plants. Protein fractions analyzed by SDS PAGE stained with Coomassie Blue (left) and equal Western blot using α-hGAL1 antibodies (right). SF, Soluble fraction incubated with the resin; P, percolate; E, elution; FD, filtered and dialyzated fraction. mg LT: leaf tissue mass corresponding to the sample.

of apoptosis (Figure 4B; Supplementary Table S4). Treatment with plastid hGAL1 showed a significant increase in apoptosis only at the highest concentration tested (120 µg hGal1/ml), reaching an average of 48.8 ± 2.2% apoptotic cells. In contrast, bacterial hGAL1 induced apoptosis in a dose-dependent manner, reaching 73 ± 1.3% apoptotic cells at 120 µg hGal1/ml. The pro-apoptotic potency of plant-derived hGAL1 was approximately 70% of that observed for the bacterial counterpart.

Co-incubation with lactose significantly reduced apoptosis induced in both plant- and bacteria-derived hGAL1 at all concentrations tested. In the presence of lactose, apoptosis levels remained below 15%, similar to unstimulated controls. Control purifications from non-transformed plants (Supplementary Figure S3) did not show binding activity in the carbohydrate-recognition assays nor pro-apoptotic activity in Jurkat cells (Figure 4; Supplementary Table S4), indicating that endogenous lectins—if present—did not contribute detectable background signals. These findings confirm the specificity of hGAL1-mediated T cell ted apoptosis, demonstrating that this effect occurred through its carbohydrate-binding activity.

Discussion

Chloroplast transformation in *Nicotiana tabacum* proved suitable for producing soluble and functional hGAL1. Three aspects were central to this proof-of-concept: stable transgene integration, accumulation of a structurally competent protein, and

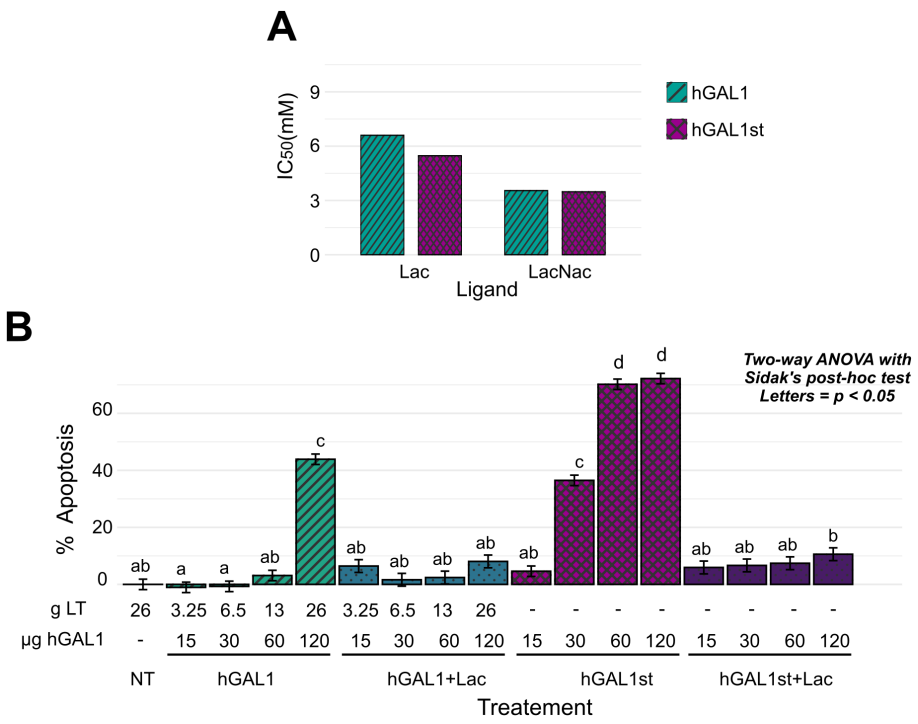

FIGURE 4
Biological activity of plastid expressed hGAL1. **(A)** Solid-phase binding assay (SPA) assessing hGAL1 affinity for lactose (Lac) and N-acetyllactosamine (LacNac) using asialofetuin (ASF) as ligand. Inhibition curves generated from serial dilutions of Lac or LacNac. Half maximal inhibitory concentration (IC_{50}) values (mean, n = 3) are showed for plant-derived (hGAL1) and *E. coli* derived hGAL1 (hGAL1st) used as positive control. **(B)** Induction of apoptosis in Jurkat T cells following 6 h exposure to increasing concentrations of hGAL1 (15–120 µg), with or without 20 mM lactose (Lac). Apoptosis was quantified by Annexin V staining and analyzed with a two-factor linear model (treatment × dose) using lm(), followed by estimated marginal means comparisons with the *emmeans* package and Sidak correction; different letters indicate significant differences ($p < 0.05$), n=3. g LT, leaf tissue mass corresponding to the extract used in each treatment; µg hGAL1, mass of purified hGAL1 applied per treatment; NT, extract from non-transformed plants processed under identical purification conditions.

implementation of a simplified purification workflow compatible with plant extracts.

Expression and folding environment in plastids

The successful generation of homoplasmic lines that express hGAL1 without evident phenotypic penalties indicates that hGAL1 acumulation imposes minimal metabolic burden on the plastid compartment. In contrast, other proteins expressed in plastids has led to chlorosis or growth delay (Müller et al., 2024; Castiglia et al., 2016). The transcriptional pattern observed by Northern blot analysis revealed the expected transcript diversity—monocistronic, bicistronic, and polycistronic—driven by the *psbA* and *rrn* promoters (Maliga, 2004; Bock, 2015). This profile demonstrates efficient recognition of regulatory plastid elements and hGal1 sequence by plastid transcriptional machinery. Together, these data confirm that the chloroplast provides a compatible environment for hGAL1 expression.

The solubility of plastid-produced hGAL1 is particularly relevant. The absence of soluble aggregates - within the detection limits of our western blot assays- suggests that plastid hGAL1 remained soluble. In contrast, preliminary results from our laboratory showed that hGAL1 transiently expressed in the tobacco apoplast accumulates in an insoluble form. Importantly, the elimination of the need for refolding steps constitutes a major advantage of plastid expression, which provides a favorable folding environment for hGAL1 (Bally et al., 2008).

Accumulation levels and physiological modulation

Although the accumulation level (~0.05% TSP) is modest relative to the highest-yielding plastid-expressed proteins (De Cosa et al., 2001; Oey et al., 2009), it falls within the broad range reported for transplastomic systems (Ahmad et al., 2016). The observed influence of leaf developmental stage and photoperiod suggests that hGAL1 accumulation is sensitive to plastid redox and metabolic state, mirroring effects previously described for other cysteine-rich plastid-derived proteins (Staub et al., 2000; Wirth et al., 2006; Zhang et al., 2013). This effect is in line with the six cysteine residues in hGAL1, which form three intramolecular disulfide bonds in their oxidized state (Cys2–Cys130, Cys16–Cys88, and Cys42–Cys60) (Guardia et al., 2014), suggesting that plastid redox conditions influence hGAL1 folding and stability, and that cultivation strategies and molecular approaches can be optimized to improve yields.

Purification constraints and simplified batch-mode recovery

Downstream processing is a major bottleneck in plant molecular farming (Buyel, 2019; Shanmugaraj et al., 2020). Although α-lactose–Sepharose affinity chromatography is standard for galectin purification (Dey et al., 2023), plant extracts often hinder column flow due to clogging and non-specific interactions. Here we show that a simplified batch-mode procedure enables efficient recovery of functional hGAL1 while avoiding filtration problems and reducing processing time compared with column formats.

Because plant tissues contain diverse soluble proteins, we evaluated whether endogenous β-galactoside-binding proteins could co-elute with hGAL1. However, control purifications from non-transformed plants displayed neither glycan-binding signals nor apoptotic activity indicating that endogenous lectins—if present—did not contribute to detectable background signals. The resulting eluates, although not fully purified, were highly enriched in hGAL1, sterile, and suitable for downstream analyses. This streamlined workflow fits with ongoing efforts to develop cost-effective, chromatography-light purification strategies (Buyel, 2019; Shanmugaraj et al., 2020). Recovering functional hGAL1 in a single affinity step strengthens the economic feasibility of plastid-based systems. Future work should aim to integrate batch capture with scalable unit operations to progress toward production-grade purification.

Functional activity and comparison with bacterial hGAL1

Plastid-derived hGAL1 retained glycan-binding specificity and induced specific apoptosis in T cells, confirming functional integrity. However it showed reduced pro-apoptotic potency relative to *E. coli*-derived hGAL1st. A plausible explanation for the reduced pro-apoptotic potency of plastid-derived hGAL1 is the intrinsic redox sensitivity of this lectin (Rabinovich et al., 1999; Toscano et al., 2006). hGAL1 requires the correct formation of intrachain disulfide bonds and an appropriate monomer–dimer equilibrium to reach full biological activity (Stowell et al., 2009). These parameters are strongly influenced by protein concentration. In our plant extracts, hGAL1 is present at relatively low concentrations (~0.05% TSP), where partial oxidation or shifts in the dimerization state are more likely to occur during extraction or handling. In contrast, *E. coli* expression yields substantially higher protein concentrations, which favor structural stability and preserve dimeric active species. These differences in concentration-dependent stability provide a mechanistic rationale for the higher doses required to elicit apoptosis with the plastid-derived preparation, without implying a loss of intrinsic carbohydrate-binding specificity or folding competence.

Implications and future directions

The ability to obtain active hGAL1 directly from leaf tissue broadens the toolkit of plastid-produced human proteins. Given the therapeutic potential of hGAL1 therapeutic potential of hGAL1 in inflammation and autoimmunity (Toscano et al., 2006; Rabinovich et al., 2025; Corrêa et al., 2017), the plastid platform may help overcome persistent challenges in producing stable, active lectins at scale. Future work should focus on increasing accumulation via codon optimization, alternative UTRs, fusion tags or relocalization (Morgenfeld et al., 2014; De Marchis et al., 2012), improving stability through optimized extraction and storage conditions, and integrating batch affinity with other low-cost purification technologies. Ultimately, validation in animal models will be required to determine equivalence to bacterially produced protein.

Concluding remarks

In summary, plastid transformation enables production of soluble, correctly folded hGAL1 and supports a simplified recovery process yielding functional protein. While yields and potency remain below those of *E. coli*, plastids offer unique advantages in biosafety, folding environment, and scalability. With further optimization and process engineering, plastid biotechnology may provide an economically competitive route for producing hGAL1 and related therapeutic lectins.

Data availability statement

The original contributions presented in the study are included in the article/Supplementary Material. Further inquiries can be directed to the corresponding author.

Author contributions

CV: Methodology, Writing – review & editing, Conceptualization, Investigation, Validation, Writing – original draft, Formal Analysis, Visualization. JMPS: Writing – review & editing, Methodology, Conceptualization, Writing – original draft, Formal Analysis, Visualization, Funding acquisition, Validation. JS: Resources, Data curation, Methodology, Formal Analysis, Writing – review & editing. MM: Methodology, Formal Analysis, Data curation, Resources, Writing – review & editing. FM: Writing – review & editing, Methodology. FB: Investigation, Conceptualization, Writing – review & editing, Resources, Project administration, Funding acquisition. GAR: Visualization, Project administration, Supervision, Funding acquisition, Resources, Conceptualization, Investigation, Writing – review & editing, Validation. MM: Resources, Formal Analysis, Writing – original draft, Funding acquisition, Writing – review & editing, Supervision, Visualization, Project administration, Methodology, Data curation, Conceptualization, Validation, Investigation.

Funding

The author(s) declared that financial support was received for this work and/or its publication. This research was funded by the

Agencia Nacional de Promoción de Ciencia y Tecnología (ANPCYT, grant: PICT2017-1379) and the Consejo Nacional de Investigaciones Científicas y Técnicas (CONICET, grant: PIP 2017-2019, 11220170100290CO). Work in GR's lab is funded by Secretaría de Ciencia, Tecnología e Innovación (Redes Federales de Alto Impacto; Argentina) and the Sales, Baron, and Lounsbery Foundations.

Acknowledgments

The authors are grateful to Marina Fumagalli for her valuable technical support in greenhouse cultivation and handling of tobacco plants. We thank the Ferioli, Ostry, Caraballo, and Alfonzo families for kind donations for GR's lab.

Conflict of interest

JMPS and GAR are co-founders of GALTEC.

The remaining author(s) declared that this work was conducted in the absence of any commercial or financial relationships that could be construed as a potential conflict of interest.

Generative AI statement

The author(s) declared that generative AI was not used in the creation of this manuscript.

Any alternative text (alt text) provided alongside figures in this article has been generated by Frontiers with the support of artificial intelligence and reasonable efforts have been made to ensure accuracy, including review by the authors wherever possible. If you identify any issues, please contact us.

Publisher's note

Supplementary material

The Supplementary Material for this article can be found online at: https://www.frontiersin.org/articles/10.3389/fpls.2025.1721928/full#supplementary-material

SUPPLEMENTARY FIGURE 1
Optimization of hGAL1 expression in transplastomic plants. **(A)** Effect of leaf age on hGAL1 accumulation G1 transplastomic plants. Leaves were numbered from top (1) to bottom (8). Left panel: total protein extracts from leaves 1–8. Right panel: total (TF), soluble (SF), and insoluble (IF) protein fractions from leaves 3, 5, and 8. Total protein was stained with Ponceau Red. Non-transformed (NT) plant extract was use as negative control. **(B)** Effect of photoperiod on hGAL1 accumulation. Left panel: total protein extracts from G1 plants sampled at 2 and 5 days. Middle panel: fractionation into TF, SF, and IF in PBS containing β-mercaptoethanol. Right panel: independent experiment sampled at 2, 5, 8, and 12 days. At each time point, tissue was collected from the same fourth leaf from T1 G1 plants. Total protein extract obtained from 4 mg of plant tissue was loaded per lane. Bar graphs show relative hGAL1 abundance (mean ± SE), calculated as the ratio of hGAL1 to RbcL band intensity from three independent replicates quantified with ImageJ. Loading control: RbcL stained with Ponceau Red. L/D, 16 h light/8 h dark; Dark, continuous darkness; d, days of treatment.

SUPPLEMENTARY FIGURE 2
Determination of hGAL1 accumulation in transplastomic tobacco plants. hGAL1 in soluble protein extracts from G1 lines (fourth leaf from the top) was measured by ELISA using rabbit α-hGAL1 antibodies and recombinant *E. coli* hGAL1 as standard. Acumulation expressed as mg hGAL1 per kilogram of leaf tissue (mg hGAL1/kg LT, upper panel) and %hGAL1/TSP (lower panel). Data were analyzed in R using a linear mixed-effects model on log-transformed values (upper panel) and a beta model (lower panel), with Line (G1 A, B, C) as a fixed effect and assay day (1–4) as a random effect. Pairwise comparisons were performed with the emmeans package and Tukey adjustment; estimated marginal means (back-transformed) are shown ± 95% CI. NT plants showed no detectable signal. Data represent four independent ELISA assays (n = 4), each including four plants (NT, G1A, G1B, and G1C). For each plant, hGAL1 accumulation was estimated from 3–4 extract concentrations measured in duplicate.

SUPPLEMENTARY FIGURE 3
Control purifications from *E. coli* and non-transformed (NT) plants. *E. coli* hGAL1 corresponds to recombinant hGAL1 expressed in *E. coli* and purified by lactose-affinity chromatography, used as positive control in biological assays. The NT profile represents the same purification protocol performed from non-transformed *N. tabacum* extract, included as a negative control in apoptosis assay. Fractions were analyzed by SDS-PAGE (Coomassie staining) and Western blot (α-hGAL1). SF, soluble fraction; P, percolate; E, elution; FD, filtered and dialyzed fraction.

SUPPLEMENTARY TABLE 1
hGAL1 accumulation in transplastomic tobacco lines G1 A-C measured by ELISA from soluble protein extracts. The table shows the assay day (Day), transplastomic line (Line), hGAL1 concentration expressed as mg hGAL1 per kilogram of leaf tissue (mg/kg LT), and as percentage of total soluble protein (%hGAL1/TSP). Data corresponds to those presented in Supplementary Figure S2.

SUPPLEMENTARY TABLE 2
Values of purification yields of hGAL1 from transplastomic tobacco plants. The table summarizes the amount of leaf tissue processed, the final extract volume, the concentration of hGAL1 in the soluble fraction, the recovered hGAL1 per kilogram of leaf tissue, and the overall purification yield (%), calculated as the mass of purified hGAL1 recovered at the end of the purification process relative to the total hGAL1 content in the corresponding soluble extract at the start of the purification process. Mean and standard deviation (SD) values are reported.

SUPPLEMENTARY TABLE 3
IC_{50} values from solid-phase binding assay (SPA) shown in Figure 4A, assessing hGAL1 affinity for lactose (Lac) and N-acetyllactosamine (LacNAc). Columns indicate the ligand, protein, and corresponding IC_{50} value. hGAL1st refers to recombinant human Galectin 1 expressed in *E. coli* as standard reference.

SUPPLEMENTARY TABLE 4
Values from the apoptosis induction experiment shown in Figure 4B, in Jurkat T cells treated with plastid hGAL1 and the standard hGAL1st, in the absence or presence of lactose (Lac). Columns indicate treatment, protein dosage (µg hGAL1), equivalent fresh leaf tissue (g LT), and percentage of apoptosis (%). % Apoptosis was calculated from Annexin V/PI staining as (%Annexin V^+PI^+ in treated – %Annexin V^+PI^+ in untreated)/(%Annexin V^-PI^- in untreated) × 100.

References

Ahmad, N., Michoux, F., Lössl, A. G., and Nixon, P. J. (2016). Challenges and perspectives in commercializing plastid transformation technology. *J. Exp. Bot.* 67, 5945–5960. doi: 10.1093/jxb/erw360

Allen, G. C., Flores-Vergara, M. A., Krasynanski, S., Kumar, S., and Thompson, W. F. (2006). A modified protocol for rapid DNA isolation from plant tissues using cetyltrimethylammonium bromide. *Nat. Protoc.* 1, 2320–2325. doi: 10.1038/nprot.2006.384

Bally, J., Paget, E., Droux, M., Job, C., Job, D., and Dubald, M. (2008). Both the stroma and thylakoid lumen of tobacco chloroplasts are competent for the formation of disulphide bonds in recombinant proteins. *Plant Biotechnol. J.* 6, 46–61. doi: 10.1111/j.1467-7652.2007.00298.x

Barkan, A., and Goldschmidt-Clermont, M. (2000). Participation of nuclear genes in chloroplast gene expression. *Biochimie* 82, 559–572. doi: 10.1016/S0300-9084(00)00602-7

Bellucci, M., Pompa, A., De Marcos Lousa, C., Panfili, E., Orecchini, E., Maricchiolo, E., et al. (2021). Human indoleamine 2,3-dioxygenase 1 (IDO1) expressed in plant cells induces kynurenine production. *Int. J. Mol. Sci.* 22, 5102. doi: 10.3390/ijms22105102

Blidner, A. G., Bach, C. A., García, P. A., Merlo, J. P., Cagnoni, A. J., Bannoud, N., et al. (2025). Glycosylation-driven programs coordinate immunoregulatory and pro-angiogenic functions of myeloid-derived suppressor cells. *Immunity* 58, 1553–1571.e8. doi: 10.1016/j.immuni.2025.04.027

Bock, R. (2015). Engineering plastid genomes: methods, tools, and applications in basic research and biotechnology. *Annu. Rev. Plant Biol.* 66, 211–241. doi: 10.1146/annurev-arplant-050213-040212

Burnett, M. J. B., and Burnett, A. C. (2020). Therapeutic recombinant protein production in plants: challenges and opportunities. *Plants People Planet* 2, 121–132. doi: 10.1002/ppp3.10073

Buyel, J. F. (2015). Process development strategies in plant molecular farming. *Curr. Pharm. Biotechnol.* 16, 966–982. doi: 10.2174/1389201016111509021154l3

Buyel, J. F. (2019). Plant molecular farming – integration and exploitation of side streams to achieve sustainable biomanufacturing. *Front. Plant Sci.* 9. doi: 10.3389/fpls.2018.01893

Buyel, J. F. (2024). Towards a seamless product and process development workflow for recombinant proteins produced by plant molecular farming. *Biotechnol. Adv.* 75, 108403. doi: 10.1016/j.bioteChadv.2024.108403

Cagnoni, A. J., Massaro, M., Cutine, A. M., Gimeno, A., Pérez-Sáez, J. M., Manselle Cocco, M. N., et al. (2024). Exploring galectin interactions with human milk oligosaccharides and blood group antigens identifies BGA6 as a functional galectin-4 ligand. *J. Biol. Chem.* 300, 107573. doi: 10.1016/j.jbc.2024.107573

Castiglia, D., Sannino, L., Marcolongo, L., Ionata, E., Tamburino, R., and De Stradis, A. (2016). High-level expression of thermostable cellulolytic enzymes in tobacco transplastomic plants and their use in hydrolysis of an industrially pretreated Arundo donax L. biomass. *Biotechnol. Biofuels* 9, 154. doi: 10.1186/s13068-016-0569-z

Corrêa, M. P., Andrade, F. E. C., Gimenes, A. D., and Gil, C. D. (2017). Anti-inflammatory effect of galectin-1 in a murine model of atopic dermatitis. *J. Mol. Med.* 95, 1005–1015. doi: 10.1007/s00109-017-1566-9

Croci, D. O., Salatino, M., Rubinstein, N., Cerliani, J. P., and Cavallin, L. E.. (2012). Disrupting galectin-1 interactions with N-glycans suppresses hypoxia-driven angiogenesis and tumorigenesis in Kaposi's sarcoma. *J. Exp. Med.* 209, 1985–2000. doi: 10.1084/jem.20111665

Daniell, H., Jin, S., Zhu, X. G., Gitzendanner, M. A., Soltis, D. E., and Soltis, P. S. (2021). Green giant—a tiny chloroplast genome with mighty power to produce high-value proteins: history and phylogeny. *Plant Biotechnol. J.* 19, 430–447. doi: 10.1111/pbi.13556

De Cosa, B., Moar, W., Lee, S. B., Miller, M., and Daniell, H. (2001). Overexpression of the Bt cry2Aa2 operon in chloroplasts leads to formation of insecticidal crystals. *Nat. Biotechnol.* 19, 71–74. doi: 10.1038/83559

De Marchis, F., Pompa, A., and Bellucci, M. (2012). Plastid proteostasis and heterologous protein accumulation in transplastomic plants. *Plant Physiol.* 160, 571–581. doi: 10.1104/pp.112.203778

Dey, C., Palm, P., and Elling, L. (2023). Characterization of galectin fusion proteins with glycoprotein affinity columns and binding assays. *Molecules* 28, 1054. doi: 10.3390/molecules28031054

Eibl, C., Zou, Z., Beck, A., Kim, M., Mullet, J., and Koop, H. U. (1999). *In vivo* analysis of plastid psbA, rbcL and rpl32 UTR elements by chloroplast transformation: tobacco plastid gene expression is controlled by modulation of transcript levels and translation efficiency. *Plant J.* 19, 333–345. doi: 10.1046/j.1365-313X.1999.00543.x

Fernández-San Millán, A., Mingo-Castel, A., Miller, M., and Daniell, H. (2003). A chloroplast transgenic approach to hyper-express and purify human serum albumin, a protein highly susceptible to proteolytic degradation. *Plant Biotechnol. J.* 1, 71–79. doi: 10.1046/j.1467-7652.2003.00008.x

Guardia, C. M., Caramelo, J. J., Trujillo, M., Méndez-Huergo, S. P., Radi, R., Estrin, D. A., et al. (2014). Structural basis of redox-dependent modulation of galectin-1 dynamics and function. *Glycobiology* 24, 428–441. doi: 10.1093/glycob/cwu008

Laemmli, U. K. (1970). Cleavage of structural proteins during the assembly of the head of bacteriophage T4. *Nature* 227, 680–685. doi: 10.1038/227680a0

Lal, M., Bhardwaj, E., Chahar, N., Dangwal, M., and Das, S. (2020). "(Trans)gene flow: mechanisms, biosafety concerns and mitigation for containment," in *Reproductive ecology of flowering plants: patterns and processes*. Eds. R. Tandon, K. R. Shivanna and M. Koul (Springer, Singapore), 321–346. doi: 10.1007/978-981-15-4210-7_15

Lehtimäki, N., Koskela, M. M., and Mulo, P. (2015). Posttranslational modifications of chloroplast proteins: an emerging field. *Plant Physiol.* 168, 768–775. doi: 10.1104/pp.15.00117

Maliga, P. (2004). Plastid transformation in higher plants. *Annu. Rev. Plant Biol.* 55, 289–313. doi: 10.1146/annurev.arplant.55.031903.141633

Maliga, P., and Bock, R. (2011). Plastid biotechnology: food, fuel, and medicine for the 21st century. *Plant Physiol.* 155, 1501–1510. doi: 10.1104/pp.110.170969

Martínez Allo, V. C., Hauk, V., Sarbia, N., Pinto, N. A., Croci, D. O., Dalotto-Moreno, T., et al. (2020). Suppression of age-related salivary gland autoimmunity by glycosylation-dependent galectin-1-driven immune inhibitory circuits. *Proc. Natl. Acad. Sci. United States America* 117, 6630–6639. doi: 10.1073/pnas.1922778117

Morgenfeld, M., Lentz, E., Segretin, M. E., Alfano, E. F., and Bravo-Almonacid, F. (2014). Translational fusion and redirection to thylakoid lumen as strategies to enhance accumulation of human papillomavirus E7 antigen in tobacco chloroplasts. *Mol. Biotechnol.* 56, 1021–1031. doi: 10.1007/s12033-014-9781-x

Morgenfeld, M. M., Vater, C. F., Alfano, E. F., Boccardo, N. A., and Bravo-Almonacid, F. F. (2020). Translocation from the chloroplast stroma into the thylakoid lumen allows expression of recombinant epidermal growth factor in transplastomic tobacco plants. *Transgenic Res.* 29, 295–305. doi: 10.1007/s11248-020-00199-7

Morosi, L. G., Cutine, A. M., Cagnoni, A. J., Manselle-Cocco, M. N., Croci, D. O., Merlo, J. P., et al. (2021). Control of intestinal inflammation by glycosylation-dependent lectin-driven immunoregulatory circuits. *Sci. Adv.* 7, eabf8630. doi: 10.1126/sciadv.abf8630

Müller, C., Budnik, N., Mirkin, F. G., Vater, C. F., Bravo-Almonacid, F. F., Perez-Castro, C., et al. (2024). Production of biologically active human basic fibroblast growth factor (hFGFb) using Nicotiana tabacum transplastomic plants. *Planta* 260, 28. doi: 10.1007/s00425-024-04456-5

Murashige, T., and Skoog, F. (1962). A revised medium for rapid growth and bio assays with tobacco tissue cultures. *Physiol. Plant* 15, 473–497. doi: 10.1111/j.1399-3054.1962.tb08052.x

Oey, M., Lohse, M., Kreikemeyer, B., and Bock, R. (2009). Exhaustion of the chloroplast protein synthesis capacity by massive expression of a highly stable protein antibiotic. *Plant J.* 57, 436–445. doi: 10.1111/j.1365-313X.2008.03702.x

Perillo, N. L., Pace, K. E., Seilhamer, J. J., and Baum, L. G. (1995). Apoptosis of T cells mediated by galectin-1. *Nature* 378, 736–739. doi: 10.1038/378736a0

Perone, M. J., Bertera, S., Tawadrous, Z. S., Shufesky, W. J., Piganelli, J. D., Baum, L. G., et al. (2006). Dendritic cells expressing transgenic galectin-1 delay onset of autoimmune diabetes in mice. *J. Immunol.* 177, 5278–5289. doi: 10.4049/jimmunol.177.8.5278

Porciúncula-González, C., Cagnoni, A. J., Fontana, C., Mariño, K. V., Saenz-Méndez, P., Giacomini, C., et al. (2021). Structural insights in galectin-1-glycan recognition: relevance of the glycosidic linkage and the N-acetylation pattern of sugar moieties. *Bioorganic Medicinal Chem.* 44, 116309. doi: 10.1016/j.bmc.2021.116309

Qu, W. S., Wang, Y. H., Ma, J. F., Tian, D. S., Zhang, Q., Pan, D. J., et al. (2011). Galectin-1 attenuates astrogliosis-associated injuries and improves recovery of rats following focal cerebral ischemia. *J. Neurochemistry* 116, 217–226. doi: 10.1111/j.1471-4159.2010.07095.x

Rabinovich, G. A. (2005). Galectin-1 as a potential cancer target. *Br. J. Cancer* 92, 1188–1192. doi: 10.1038/sj.bjc.6602493

Rabinovich, G. A., Hershkoviz, R., Hirabayashi, J., Kasai, K., and Lider, O. (1999). Specific inhibition of T-cell adhesion to extracellular matrix and proinflammatory cytokine secretion by human recombinant galectin-1. *Immunology* 97, 100–106. doi: 10.1046/j.1365-2567.1999.00746.x

Rabinovich, G. A., Modesti, N. M., Castagna, L. F., Landa, C. A., Riera, C. M., and Sotomayor, C. E. (1997). Specific inhibition of lymphocyte proliferation and induction of apoptosis by CLL-I, a beta-galactoside-binding lectin. *J. Biochem.* 122, 365–373. doi: 10.1093/oxfordjournals.jbchem.a021762

Rabinovich, G. A., Rademacher, C., Schattner, M., and Macauley, M. S. (2025). Glycan-binding proteins in immunity. *Annu. Rev. Immunol.* doi: 10.1146/annurev-immunol-083024-030822

Rapoport, E. M., Pochechueva, T. V., Kurmyshkina, O. V., Pazynina, G. V., Severov, V. V., Gordeeva, E. A., et al. (2010). Solid-phase assays for study of carbohydrate specificity of galectins. *Biochem. (Moscow)* 75, 310–319. doi: 10.1134/S0006297910030077

Roldán-Montero, R., Pérez-Sáez, J. M., Cerro-Pardo, I., Oller, J., Martinez-Lopez, D., Nuñez, E., et al. (2022). Galectin-1 prevents pathological vascular remodeling in atherosclerosis and abdominal aortic aneurysm. *Sci. Adv.* 8, eabm7322. doi: 10.1126/sciadv.abm7322

Santucci, L., Fiorucci, S., Rubinstein, N., Mencarelli, A., Palazzetti, B., Federici, B., et al. (2003). Galectin-1 suppresses experimental colitis in mice. *Gastroenterology* 124, 1381–1394. doi: 10.1016/S0016-5085(03)00267-1

Schillberg, S., and Finnern, R. (2021). Plant molecular farming for the production of valuable proteins: critical evaluation of achievements and future challenges. *J. Plant Physiol.* 258–259, 153359. doi: 10.1016/j.jplph.2020.153359

Scotti, N., Bellucci, M., and Cardi, T. (2013). "The chloroplast as platform for recombinant protein production," in *Translation in mitochondria and other organelles*. Ed. A. M. Duchêne (Springer, Berlin). doi: 10.1007/978-3-642-39426-3_10

Shanmugaraj, B., Bulaon, C. J. I., and Phoolcharoen, W. (2020). Plant molecular farming: a viable platform for recombinant biopharmaceutical production. *Plants* 9, 842. doi: 10.3390/plants9070842

Shaver, J. M., Oldenburg, D. J., and Bendich, A. J. (2006). Changes in chloroplast DNA during development in tobacco, Medicago truncatula, pea, and maize. *Planta* 224, 72–82. doi: 10.1007/s00425-005-0195-7

Starossom, S. C., Mascanfroni, I. D., Imitola, J., Cao, L., Raddassi, K., Hernandez, S. F., et al. (2012). Galectin-1 deactivates classically activated microglia and protects from inflammation-induced neurodegeneration. *Immunity* 37, 249–263. doi: 10.1016/j.immuni.2012.05.023

Staub, J. M., Garcia, B., Graves, J., Hajdukiewicz, P. T. J., Hunter, P., Nehra, N., et al. (2000). High-yield production of a human therapeutic protein in tobacco chloroplasts. *Nat. Biotechnol.* 18, 333–338. doi: 10.1038/73796

Stowell, S. R., Cho, M., Feasley, C. L., Arthur, C. M., Song, X., Colucci, J. K., et al. (2009). Ligand reduces galectin-1 sensitivity to oxidative inactivation by enhancing dimer formation. *J. Biol. Chem.* 284, 4989–4999. doi: 10.1074/jbc.M808925200

Sundblad, V., Garcia-Tornadu, I. A., Ornstein, A. M., Martínez Allo, V. C., Lorenzo, R., Gatto, S. G., et al. (2021). Galectin-1 impacts on glucose homeostasis by modulating pancreatic insulin release. *Glycobiology* 31, 908–915. doi: 10.1093/glycob/cwab040

Svab, Z., Hajdukiewicz, P., and Maliga, P. (1990). Stable transformation of plastids in higher plants. *Proc. Natl. Acad. Sci. U.S.A.* 87, 8526–8530. doi: 10.1073/pnas.87.21.8526

Toscano, M. A., Commodaro, A. G., Ilarregui, J. M., Bianco, G. A., Liberman, A., Serra, H. M., et al. (2006). Galectin-1 suppresses autoimmune retinal disease by promoting concomitant Th2- and T regulatory-mediated anti-inflammatory responses. *J. Immunol.* 176, 6323–6332. doi: 10.4049/jimmunol.176.10.6323

Toscano, M. A., Martínez Allo, V. C., Cutine, A. M., Rabinovich, G. A., and Mariño, K. V. (2018). Untangling galectin-driven regulatory circuits in autoimmune inflammation. *Trends Mol. Med.* 24, 348–363. doi: 10.1016/j.molmed.2018.02.008

Troncoso, M. F., Elola, M. T., Blidner, A. G., Sarrias, L., Espelt, M. V., and Rabinovich, G. A. (2023). The universe of galectin-binding partners and their functions in health and disease. *J. Biol. Chem.* 299, 105400. doi: 10.1016/j.jbc.2023.105400

Wang, Y., Fan, J., Wei, Z., and Xing, S. (2023). Efficient expression of fusion human epidermal growth factor in tobacco chloroplasts. *BMC Biotechnol.* 23, 1. doi: 10.1186/s12896-022-00771-5

Wirth, S., Segretin, M. E., Mentaberry, A., and Bravo-Almonacid, F. (2006). Accumulation of hEGF and hEGF-fusion proteins in chloroplast-transformed tobacco plants is higher in the dark than in the light. *J. Biotechnol.* 125, 159–172. doi: 10.1016/j.jbiotec.2006.02.012

Wittenberg, G., and Danon, A. (2008). Disulfide bond formation in chloroplasts. *Plant Sci.* 175, 459–466. doi: 10.1016/j.plantsci.2008.05.011

Zhang, Q., Yu, H., Zhang, F., and Shen, Z. (2013). Expression and purification of recombinant human serum albumin from selectively terminable transgenic rice. *J. Zhejiang Univ. Sci. B* 14, 867–874. doi: 10.1631/jzus.B1300090

Frontiers in
Plant Science

Cultivates the science of plant biology and its applications

The most cited plant science journal, which advances our understanding of plant biology for sustainable food security, functional ecosystems and human health.

Discover the latest Research Topics

See more →

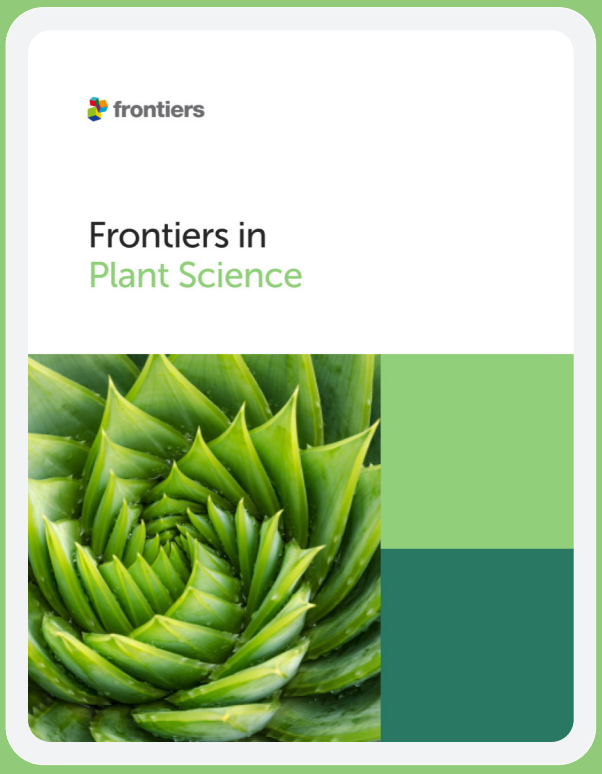

Frontiers

Avenue du Tribunal-Fédéral 34
1005 Lausanne, Switzerland
frontiersin.org

Contact us

+41 (0)21 510 17 00
frontiersin.org/about/contact